Journal of Geophysics Zeitschrift für Geophysik

Volume 47 1980

Springer International

Journal of Geophysics – Zeitschrift für Geophysik

This journal was founded by the Deutsche Geophysikalische Gesellschaft on the initiative of L. Mintrop in 1924 as the Zeitschrift für Geophysik and edited by G. Angenheister from Vol. 1–18 (1944). It reappeared in 1954 edited by B. Brockamp from Vol. 19–26 (1960), and edited by W. Dieminger and J. Untiedt from Vol. 27 (1961). After Vol. 40 (1970) the title was changed to Journal of Geophysics – Zeitschrift für Geophysik.

Published: Vols. 19–39 by Physica-Verlag, Würzburg, from Vol. 40 by Springer Berlin, Heidelberg, New York.

Springer-Verlag Berlin Heidelberg New York

Printed in Germany by Universitätsdruckerei H. Stürtz AG Würzburg

Iceland

Evolution, Active Tectonics, and Structure

Edited by
W. Jacoby, A. Björnsson, and D. Möller

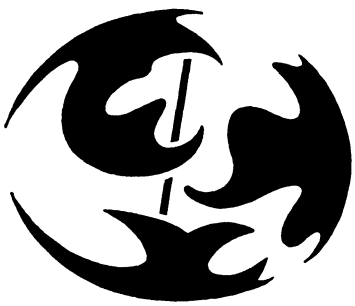

Inter-Union Commission on Geodynamics
Scientific Report No. 59

Author Index

Subject Index

Journal of Geophysics Zeitschrift für Geophysik

Volume 47 Numbers 1–3 1980

Iceland

Evolution, Active Tectonics, and Structure

Edited by
W. Jacoby, A. Björnsson, and D. Möller

Inter-Union Commission on Geodynamics
Scientific Report No. 59

Springer International

Journal of Geophysics – Zeitschrift für Geophysik

Edited for the **Deutsche Geophysikalische Gesellschaft** by **W. Dieminger and J. Untiedt**

This journal was founded by the Deutsche Geophysikalische Gesellschaft on the initiative of L. Mintrop in 1924 as the Zeitschrift fur Geophysik and edited by G. Angenheister from Vol. 1–18 (1944). It reappeared in 1954 edited by B. Brockamp from Vol. 19–26 (1960), and edited by W. Dieminger and J. Untiedt from Vol. 27 (1961). After Vol. 40 (1970) the title was changed to Journal of Geophysics – Zeitschrift fur Geophysik.

Published: Vols. 19–39 by Physica-Verlag, Wurzburg, from Vol. 40 by Springer Berlin, Heidelberg, New York.

Manuscripts may be addressed to any of the Editors. For addresses see last cover page. Manuscripts should conform with the journal's accepted practice as described in the Instructions to Authors.

The Journal accepts

- Review Articles (invited by the Editors)
- Original Papers
- Short Communications
- Letters to the Editors
- Book Reviews

in the field of Geophysics and Space Physics.

The Geodynamics Project is an international program of research on the dynamics and dynamic history of the earth with emphasis on deep-seated foundations of geological phenomena. This includes investigations related to movements and deformations, past and present, of the lithosphere, and all relevant properties of the earth's interior and especially any evidence for motions at depth. The program is an interdisciplinary one, coordinated by the Inter-Union Commission on Geodynamics (I.C.G.) established by I.C.S.U. at the request of I.U.G.G., and I.U.G.S., with rules providing for the active participation of all interested I.C.S.U. Unions and Committees.

Das Heft enthalt eine Beilage des Springer-Verlages Berlin Heidelberg New York

Springer International

Subscription Information

Volumes 47+48 [3 issues each totalling about 246 pages (due to a larger format)] will appear in 1980. The price of a volume is DM 143,– or $80.00. Prices for backvolumes are available on request. In addition, we also offer microform editions in 16 mm and 35 mm microform and microfiche. Correspondence concerning subscriptions should be addressed to the publisher.

Changes of Address: Allow six weeks for all changes to become effective. All communications should include both old and new addresses (with Zip Codes) and should be accompanied by a mailing label from a recent issue.

Members. Members of the Deutsche Geophysikalische Gesellschaft are entitled to purchase the Journal for their own use at a privilege price of DM 98,— payable with the Membership dues. Orders should be sent to the Society's office at the following address: Postfach 230, D-3392 Clausthal-Zellerfeld.

North America. Subscription rate: $169.00, including postage and handling. Subscriptions are entered with prepayment only. Orders should be addressed to: Springer-Verlag New York Inc., Service Center Secaucus, 44 Hartz-Way, Secaucus, N.J. 07094, USA, Tel. (201) 348-4033, Telex 0023-125994.

Japan. Subscription rate: DM 314,— including postage (surface airmail lifted) and handling. Orders can either be placed with your bookdealer or sent directly to: Springer-Verlag, Heidelberger Platz 3, D-1000 Berlin 33, Tel. (030) 8207-1, Telex 01-83319.

All Other Countries. Subscription rate: DM 286,—, plus postage and handling. Orders can either be placed with your bookdealer or sent directly to: Springer-Verlag, Heidelberger Platz 3, D-1000 Berlin 33, Tel. (030) 8207-1, Telex 01-83319.

Offices

Springer-Verlag, Heidelberger Platz 3, D-1000 Berlin 33, Tel. (030) 8207-1, Telex 01-83319.

Springer-Verlag, Journal Production Department II, Postfach 105280, D-6900 Heidelberg 1, Tel. (06221) 487-1, Telex 04-61690.

Springer-Verlag New York Inc., 175 Fifth Avenue, New York, N.Y. 10010, USA, Tel. (212) 477-8200, Telex 0023-23223.

Responsible for Advertisements:

G. Sternberg, Kurfürstendamm 237, D-1000 Berlin 15, Tel. (030) 8821031, Telex 01-85411.

Printed in Germany by Universitätsdruckerei H. Stürtz AG, Wurzburg

J. Geophys. 47, 1–6, 1980

Journal of Geophysics

Iceland: Evolution, Active Tectonics, and Structure. A Preface

W.R. Jacoby[1], A. Björnsson[2], and D. Möller[3]

[1] Institut für Meteorologie und Geophysik, Universität, Feldbergstr. 47, D-6000 Frankfurt 1, Federal Republic of Germany
[2] Orkustofnun, Grensásvegur 9, Reykjavík, Iceland
[3] Institut für Vermessungskunde, Technische Universität, Pockelsstr. 4, D-3300 Braunschweig, Federal Republic of Germany

Introduction: Iceland and Wegener

Iceland is a unique phenomenon, land raised high where ocean should be. Neither Wegener's concept of continental drift nor its modern version of sea-floor spreading and plate tectonics leave space for a large land mass in the middle of the North Atlantic. This problem and the promise it offers to the study of the earth presented themselves to Wegener (1915, 1920, 1922, 1929) when he attempted to reconstruct the pre-drift positions of the continents, but then his thinking on Iceland was already influenced by the vexing problem of the drift mechanism. Earlier, when he first (1912a and b) published the arguments for drift, he did not mention Iceland, but it seems worthwhile to remember some of his early thinking which, indeed, sounds very modern.

Although Wegener considered the evidence for drift more important than an understanding of the mechanism, which would come with time, he nevertheless allowed himself some speculation on that subject. We cannot resist the temptation to quote a whole paragraph from Wegener's 1912a paper (pp. 305, 306):

'Weiter scheint mir aber jetzt eine Möglichkeit vorzuliegen, die Unterschiede der Meerestiefen zu erklären. Da wir für größere Gebiete doch auch am Boden der Tiefsee isostatische Kompensation annehmen müssen, so besagt der Unterschied, daß die nach unserer Auffassung alten Tiefseeböden spezifisch schwerer sind als die jungen. Nun ist der Gedanke wohl nicht von der Hand zu weisen, daß frisch entblößte Simaflächen, wie der Atlantik oder westliche Teil des Indik, noch lange Zeit hindurch nicht nur eine geringere Riegheit, sondern auch eine höhere Temperatur (vielleicht um 100° im Mittel der obersten 100 km) bewahren als die alten, schon stark ausgekühlten Meeresböden. Und eine solche Temperaturdifferenz würde, wenn sie auch, wie früher erwähnt, zur Erklärung der Gewichtsdifferenz zwischen kontinentalem und ozeanischem Material bei weitem nicht ausreicht, doch wahrscheinlich genügen, um die relativ geringfügigen Niveaudifferenzen der großen ozeanischen Becken untereinander zu erklären. Diese scheinen es auch nahezulegen, die mittelatlantische Bodenschwelle als diejenige Zone zu betrachten, in welcher bei der noch immer fortschreitenden Erweiterung des Atlantischen Ozeans der Boden desselben fortwährend aufreißt und frischem, relativ flüssigem und hoch temperiertem Sima aus der Tiefe Platz macht.'

(Freely translated: Further, I now believe I can explain the differences in ocean depth. Since we must assume isostatic compensation for the ocean floors, it follows that old (in our view) sea floor is denser than that which is younger. It is likely that recently uncovered sima, as the Atlantic and the western Indic, long preserves lower rigidity and higher temperatures (perhaps 100° C on the average for the uppermost 100 km) than old, considerably cooled sea floor. Although not sufficient to explain the density difference between continental and oceanic material, such temperature differences could adequately explain the minor differences in depth between the great ocean basins. These differences also seem to indicate that the Mid-Atlantic Ridge is that zone in which the floor of the Atlantic in its progressive spreading is rifting open and making space for fresh, relatively fluid, high-temperature sima rising from depth.)

Of course, a large body of new data on bathymetry, magnetics, and heat flow of the oceans was needed to substantiate such speculations (Vine and Matthews, 1963, Sclater and Francheteau, 1970). To be sure, Wegener never quite gave them up (e.g., 1922, p. 96; 1929, p. 211), but he could not see their significance for lack of data and perhaps because he was distracted by the 'new' model of the continents sailing in the sima like icebergs in the sea. His fascination with rheology may have played a role here; consider that the model involved strong (possessing strength), though fragile continents floating in viscous, though hard sima, like cork floating up in cold tar; and remember that Wegener was in need of a convincing model in view of the mounting opposition to continental drift. In contrast to some of his opponents, however, Wegener was never dogmatic about the mechanism.

Returning now to the subject of this volume, we conjecture that Wegener's thinking on mechanisms might have taken a different course, had he known Iceland better. Actually, in 1912 he did travel by pony from Akureyri in the north to, and across, Vatnajökull in the southeast (Koch, 1912), but he probably did not see conspicuous fissures and may have been preoccupied by the preparations for the Greenland expedition (Schwarzbach, 1979). Otherwise his ideas on rifting and spreading might have been strengthened since they are so obviously demonstrated in Iceland as a part of the Mid-Atlantic Ridge. Instead, the ridge more and more became a continental relic from the original splitting (1922, p. 42) and Iceland came to have originated between a double rift (p. 41) or to be held up by molten sial rising beneath it from under the receding continents (p. 40). In this at least there is a surprising affinity with those who contest continental drift altogether and wish Iceland to have a stable continental basement (Belousov, 1970; Belousov and Milanovsky, 1976).

Wegener died in Greenland during the winter 1930/1931, but his ideas remained alive and were heatedly discussed. The majority of earth scientists rejected them, and we must admit today that there were many open questions. The picture of Iceland in particu-

0340-062X/80/0047/0001/$01.20

lar was confusing, indeed; this has, however, not impeded geodynamic research there, and may have rather stimulated it. Probably the first to link the tectonic and volcanic style of Iceland to Wegener's drift hypothesis was the Danish geomorphologist and geologist N. Nielsen (1930, 1933), and S. Thorarinsson (1937) concluded his study of the 1934 Dalvik earthquake in North Iceland by suggesting that also seismotectonics supports the hypothesis.

In this situation several German geodesists, geophysicists, and geologists felt that it was most important to prove or disprove continental drift by direct geodetic observation in Iceland. Wegener (1912, pp. 307–309; 1922, pp. 77–82; 1929, pp. 22–34) himself had often stressed the importance of geodetic proof (but he had thought that the drift between Greenland and Europe is fast enough to be observable, and in fact was successfully measured, by longitude determinations). The choice of Iceland suggests that Wegener's early ideas as quoted above were seriously considered a possibility. The neovolcanic zone in North Iceland was chosen under geologic advice, probably for its simple shape and its conspicuous fissures. The working group consisted of O. Niemczyk, E. Ansel, F. Bernauer, E. Emschermann, and A. Schleusener. An account of their 1938 expedition to Iceland was given by Niemczyk (1943) who argued (p. 1) that even if the inner young volcanic zone 'flows' apart, the behaviour of the rigid Tertiary basalt massifs on both sides must give evidence for or against the expected horizontal drift, and that this evidence could be obtained by setting up a network for repeated measurements of distance, elevation, and gravity. Fortunately, the network could be largely recovered after the war; in 1964/1965 it was remeasured for the first time and extended by K. Gerke (1967, 1974), H. Spickernagel (1966), and A. Schleusener and W Torge (1971) with assistance from E. Tryggvason. Surprisingly, the 1965-1938 comparison demonstrated no significant extension across the rift zone. This might have been taken as evidence against Wegener's hypothesis, but at the time these results became known, sea-floor spreading had already been convincingly inferred from the marine magnetic anomalies (Vine and Matthews, 1963) and the concept of plate tectonics was just being formulated to explain seismological data (McKenzie and Parker, 1967; Morgan, 1968, Isacks et al., 1968). Thus the geodetic observations in North Iceland were most puzzling, raising more questions than they answered.

Work Reported

The choice of North Iceland for measuring drift, after all, has turned out to be an extremely fortunate one. It was in this zone that an episode of rifting started in 1975 (Björnsson et al., 1977, 1979) which continues to the day of writing. The 1938 and 1965 measurements cross this zone and now serve as the necessary reference for the horizontal and vertical motions as well as the gravity changes along an E-W line more than 100 km long. Several papers in this volume (Möller and Ritter, Pelzer and Gerstenecker, Tryggvason, Spickernagel, Sigurdsson, Torge and Kanngieser, Johnsen et al.) are devoted to this subject. The rifting event may be the first one to be observed and certainly is the best documented. It is thus extremely important to our understanding of the process. The observation of magma movement through a dyke by its related seismicity (Einarsson and Brandsdóttir) during this event is therefore particularly valuable. Two of the geodetic studies (Tryggvason, Johnsen et al.) focus on the vicinity of the Krafla magma chamber, continuously inflated from below, but occasionally deflated rapidly by outflow into dykes; three (Möller and Ritter, Spickernagel, Torge and Kanngieser) present accurate measurements of the regional deformation; two (Sigurdsson, Pelzer and Gerstenecker) look at the effects of the rifting on the fissure swarm some 50 km north of Krafla where seismicity has also been studied (Einarsson and Brandsdóttir).

Although less spectacular than in N-Iceland, activity in the southwest is obvious and manifests itself in earthquakes (Foulger and Einarsson). Their relation with the state of stress is, however, complicated (Voight et al.). For the region of current rifting in N-Iceland, strain and stress measurements are not yet available, but such measurements are in progress. The comparison with large-scale deformation (Möller and Ritter, Spickernagel, Torge and Kanngieser) would shed light on the driving forces (long-distance tension versus push from dyke intrusions).

Another important question is that of the history of tectonicsm and magmaticsm activity in Iceland. The very different appearance of the Tertiary flood basalt regions (Fig. 1) and that of the neovolcanic zones (Fig. 2) made many people believe that there had been a hiatus between Tertiary and Pleistocene volcanic activity. Statistics offers no evidence for any variation during historical time (Gudmundsson and Saemundsson) and theoretical modelling of crustal generation (Pálmason) suggests that the different character of old and young regions is not in conflict with a continuing, more or less steady process. This is supported by work on paleomagnetism (Kristjansson et al., Schweitzer and Soffel) and magnetic anomalies (Becker); a side-line is the clarification of the history of glaciations. Even more directly revealing the tectonic history are the marine magnetic anomalies from the regions south (Voppel and Rudloff) and north of Iceland (Vogt et al.); these studies continue a well known tradition in the region (Vine and Matthews, 1963; Heirtzler et al., 1966) and pose new questions as to the interaction of 'normal' sea-floor spreading and the action of a deep 'Iceland plume' In discussing models of such an interaction it is helpful to compare Iceland with related geotectonic phenomena such as Hawaii (Wyss).

There is no doubt that Iceland is part of the Mid-Atlantic Ridge and that it is an anomalous part. Iceland cannot be understood without looking at the surrounding sea floor (Johnson and Pálmason, Jacoby, Bram), but we can also learn much about the oceans by studying Iceland, which is a much more convenient place for many kinds of observations than the sea floor. We must, however, use caution before making any generalization one way or the other. Detailed data on sea-floor morphology (Vogt et al., Jacoby) and heat flow (Bram) north and south of Iceland will be important information on the transition from the Iceland anomaly to normal ocean. Some of the differences between Iceland and the surrounding sea floor, to be sure, are simply the expression of the different environments (submarine versus subaerial volcanism). The Icelandic plateau basalts and ash layers smear out the magnetic anomaly strips so typical for the ocean, where dyke injection dominates the magmatic processes. For the same reasons the bulk mechanical properties of Iceland and ocean crust may be different, Iceland being more ductile; the lack of clear transform faults, expected from the spreading geometry, may be explained this way, but also simply by frequent burial under flood basalts and ash layers. Thus, it is not easy to distinguish direct and secondary effects of the anticipated cause in the deep mantle.

The question what Iceland really is, has been controversial and is still in the very centre of current geodynamic research it is that of vertical versus horizontal (plate) tectonics and also that of deep-mantle plumes. The question, of course, cannot be answered without some more direct information on the structure, state, and composition of the crust and upper mantle beneath Iceland and the North Atlantic. Seismic methods using earth-

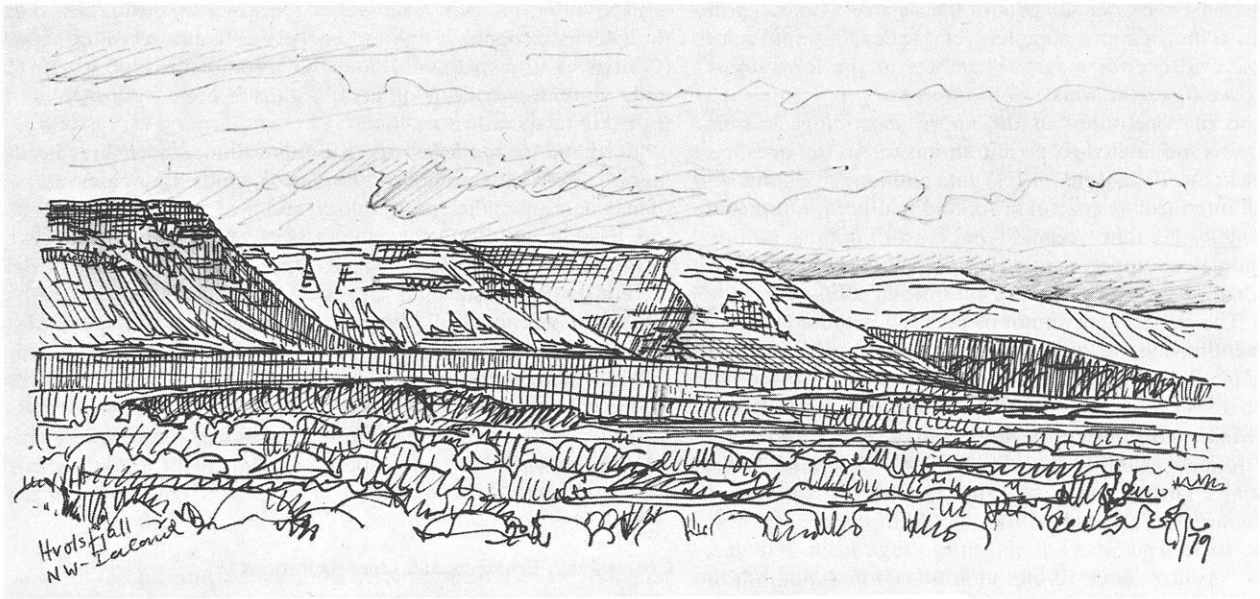

Fig. 1. Flood basalts of NW-Iceland: Hvolsfjall across Gilsfjördur in September 1979

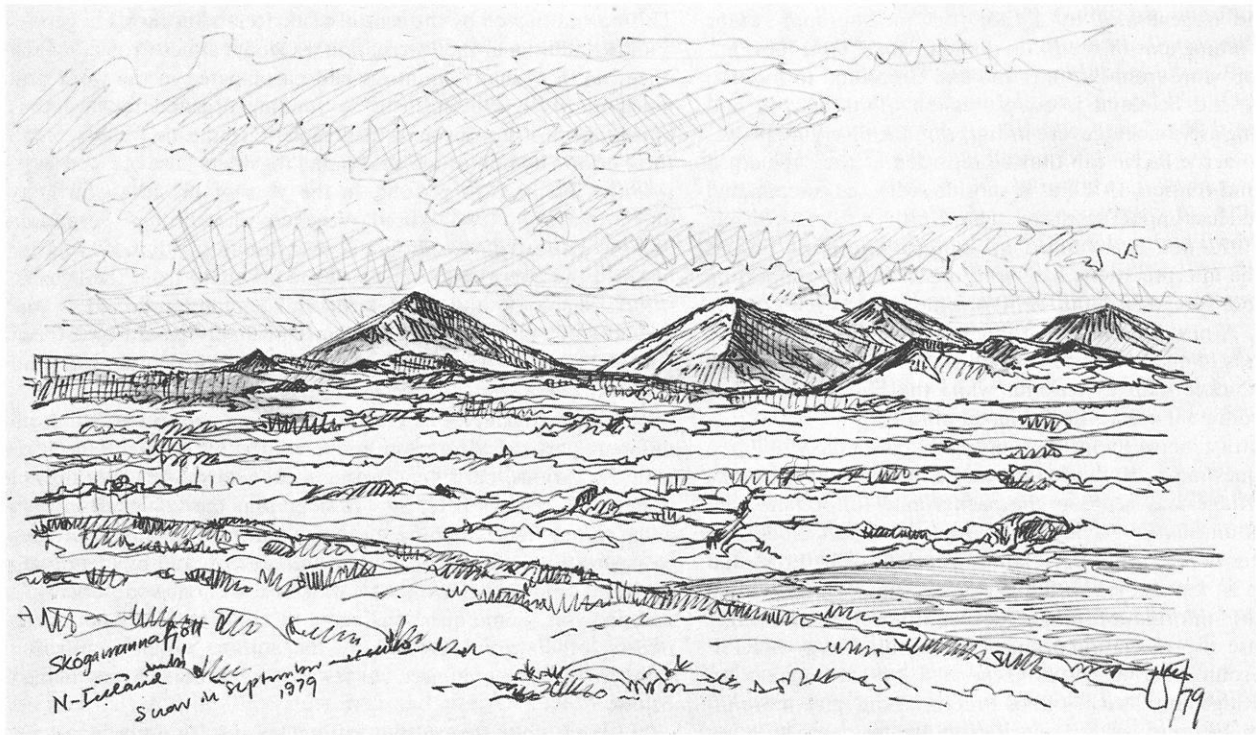

Fig. 2. The neovolcanic zone of N-Iceland: Skógarmannafjöll east of Mývatn across post-Pleistocene flood basalts (Búrfellshraun) under partial snow cover (September 1979)

quakes and/or explosions yield the most detailed and least ambiguous information on structure, but less on temperature and composition; with magneto-tellurics the opposite is true, thus complementing the former; gravity is useful in giving a broad picture of the effects of the dynamic processes on mass balance and isostasy.

Considerable efforts have been made in all these fields, and one of the purposes of the present volume is to assemble many of the results. Earlier crustal refraction profiles of Pálmason (1971) have been re-interpreted with the aid of synthetic seismograms (Flóvenz), with the result that the Icelandic crust now looks more like oceanic crust (Bunch, Goldflam et al.). Two extensive wide-angle reflection surveys have been carried out recently in the active rift zones and the adjacent plateau basalts of Iceland (2 papers by Zverev et al.) resulting in the most detailed picture of the crust so far obtained in such zones; Pálmason's model predictions

are confirmed in their essential points, but as one would expect the structure is much more complex; of particular importance is the seismic evidence for magma chambers in the lower crust under the active fissure swarms.

The depth of penetration in the above short-range seismic experiments was too limited to permit an answer to the question of crustal thickness. Pálmason's (1971) data and long-range refraction, without intermediate control in Iceland had been interpreted as to either indicate a thin 'Iceland-type' crust of oceanic affinity above an anomalous upper mantle (Pálmason, 1971, Bott, 1974) or a more than 50-km-thick crust of continental affinity (Zverev et al., 1976). The controversy cannot be resolved without a refraction experiment having the longest range and tightest intermediate control possible. Such an experiment was carried out by an international group in 1977; it involved a multiple refraction profile of 800 km length along the southeast flank of Reykjanes Ridge and across Iceland (RRISP Working Group; Gebrande et al., Goldflam et al.). There seems to be a sharp transition from typical oceanic crust and upper mantle of 10 Ma old lithosphere at Reykjanes Ridge, to Iceland where P velocities range from 7 to less than 8 km/s between about 10 and at least 60 km depth, which is atypical for both continental and oceanic upper mantle; it may be termed 'Iceland-type upper mantle' which according to magneto-telluric observations (Beblo and Björnsson) is hot and probably partially molten.

If Iceland is generated by a 'hot' or 'melting spot' at or near the spreading axis of the Mid-Atlantic Ridge, then the Thulean basalt province from Baffin Island and Greenland to Iceland, the Faeroes, and Scotland is an expression of its activity and the connecting aseismic ridges are its traces on the diverging plates; the Iceland-Faeroe Ridge can thus be regarded as the submerged part of Iceland (Nilsen, 1978), as it subsides with the surrounding sea floor and cooling lithosphere. The North Atlantic Seismic Project in 1972 had been aimed at studying the crust of this ridge, but the interpretations had been controversial, supporting either sea-floor spreading (Bott, 1974) or a more fixist view (Zverev et al., 1976). A new more detailed interpretation (Bott and Gunnarsson) leads to the conclusion that the crust is of the 'Iceland type', but thicker than in Iceland, while the Faeroe block has a distinctly different crust of continental affinity.

The contrast between Iceland and the adjacent ocean is an important question in studying the crust and upper mantle. The Reykjanes Ridge may serve as the background for Iceland, but this ridge is unusual in having a conspicuous crestal block and shallow water depth, probably related to Iceland. The crust and its evolution is best studied with explosion seismology (Goldflam et al., Bunch); information on the deeper lithosphere is meager partly because of propagation problems of seismic energy (RRISP Working Group). Surface waves generated by earthquakes on Reykjanes Ridge and Charlie-Gibbs Fracture Zone give more information on average seismic velocities at greater depth than on detailed vertical structure (Keen et al., Jacoby and Girardin). Nevertheless, a rather detailed picture of lithospheric evolution has come forth from the above studies: very thin lithosphere near the crest (Keen et al.) traps rising melt below 20 km depth after a few million years of existence; this is evident in an upper low-velocity layer, before the lithosphere-asthenosphere transition at 60 km depth is clearly established at 10 Ma age, or so (Jacoby and Girardin). By this time the crust is fully developed (Bunch, Goldflam et al.).

Finally, there is the question why slow spreading ridges generally have a crestal rift while Reykjanes Ridge, similar to the fast spreading East Pacific Rise, has a positive crestal block which is itself rifted, at least near 62° N (Jacoby). A model study of the viscous response of the asthenosphere to the receding plates (Collette et al.) explains this and the accompanying gravity field quite convincingly with different asthenospheric viscosities and probably temperatures.

We have arranged the papers in this volume under three headings: (1) Tectonic Framework, Evolution (studied by observations of magnetic anomalies, morphology, and heat flow and by theoretical modelling); (2) Deformation, Stress, Seismicity, i.e., active tectonics (studied by geodetic, gravity, and seismological methods); (3) Crustal and Upper Mantle Structure (studied by seismic or seismological, magneto-telluric, and gravity methods). Not all papers have found an entirely satisfactory place in this scheme. This introductory paper is meant to serve as a guide to the contents of the volume. Finally, the most recent reviews of geophysical work on Iceland include: Björnsson (1967), Kristjansson (1974), Pálmason and Saemundsson (1974), Jacoby (1979).

Conclusions: Problems and Open Questions

When the idea was formed to publish an Iceland Volume, it was intended as a common platform for new results from the large amount of work done in and around Iceland in recent years. This was motivated by the central place Iceland occupies in geodynamics and thus in the International Geodynamics Project. Many scientists from many countries had participated in the work and much money has been spent by funding organizations; it thus appeared most appropriate to demonstrate the usefulness of all these efforts by publishing the results together. Last but not least, it is the intention to honour, in the year of his 100th birthday on November 1, 1980, Alfred Wegener, who died in the middle of his work nearly 50 years ago. We venture to say that, if Wegener had had the opportunity to see all the new data from the oceans, from seismology, and from structural geology collected in the second half of this century, he most probably would have been one of the first to understand the New Global Tectonics and to throw overboard his old idea of the sailing continents.

Most importantly, this volume is to bring together results from different parts of the region and obtained by different methods with the various, partly conflicting ideas and models. We do not attempt a synthesis here, but we hope that the volume itself will advance our understanding of geodynamics by opening our eyes to aspects and relationships hitherto unnoticed, and by identifying problems and questions to be attacked with new observations and analyses. Some questions come to mind by just reading the papers, others are expressed by the authors taking conflicting views of the same subject. A few of the problems are named below.

1. How does the current rifting episode fit into long-term spreading? A synthesis of the various geodetic and other observations, both local and regional is called for with information on inter-episode deformation. It is also most important to continue the local and regional observation of deformation through the whole rifting event and beyond to study how the deformation spreads through the lithosphere.

2. What is the driving mechanism of the rifting event? Is magma squeezed in gravitationally (buoyantly) pushing the sides into compression or is regional tension from plate divergence released in fissures tearing open and making space for the magma? The regional deformation of the area (Möller and Ritter) can be interpreted either way. Strain/stress measurements by overcor-

ing or hydrofracturing in North Iceland could discriminate between the two models by means of the 'absolute' stress.

3. How does the suspected Iceland plume interact with sea-floor spreading? Two somewhat conflicting views are expressed, one concerning the regional stress field in and around Iceland (Wyss), the other concerning the obliquely spreading Reykjanes Ridge subject to both regional (plate) tectonic and thermal stresses (Jacoby).

4. Several seismic models of the crust and upper mantle of Reykjanes Ridge are presented (Bunch, RRISP Working Group, Goldflam et al., Keen et al., Jacoby and Girardin) which are not in perfect agreement with each other. The lithospheric low-velocity layer is clearly evident only in one surface wave study (Jacoby and Girardin). Is it real? If so, is it a special feature of Reykjanes Ridge close to Iceland or a property of all spreading ridges? In the first case, does it record a transient influence of the 'Iceland plume' or a steady-state process of lithosphere evolution? A promising exercise for the immediate future is to synthesize all the new and old data to establish a consistent model of Reykjanes Ridge.

5. For Iceland and the Iceland-Faeroe Ridge a special 'Iceland-type' crust has been demonstrated (RRISP Working Group, Bott and Gunnarsson), but at the Iceland-Faeroe Ridge it is distinctly thicker. Why is this so? Is it the result of aging or of temporal variation in crustal generation?

6. Will the controversy about the nature of the Iceland crust and upper mantle be finally settled or shall we continue to disagree?

7. Several different seismic anisotropy models are discussed in this volume (e.g., RRISP Working Group, Goldflam et al., Keen et al.). Each is connected to different dynamic processes under Reykjanes Ridge. A discrimination between the models therefore has interesting consequences. Which model is correct?

These are only some of the questions which will be asked.

At this point we wish to thank all those whose work and efforts have brought about this volume: the authors, the referees, the Journal editor, the publisher, and Deutsche Forschungsgemeinschaft. Several referees reviewed more than one manuscript. R.I. Walcott, C. Kisslinger, H. Illies, and J. Untiedt gave their advice on such editorial questions as to how to formulate the title of the volume and many others. B. Geidel patiently put up with author's special requests and the inadequacies of the coordinating editor of this volume. G. Jung-Jacoby supported him in this work actively. Professor H. Illies first proposed to the National Committee of the International Geodynamics Commission and to the editor of the Journal of Geophysics that an Iceland Volume should be put together.

This is also the proper place to remind the reader that the original work reported here was made possible by many funding organizations and by the cooperation and efforts of many scientists, technicians, ships' crews, administrators and others, not named anywhere in the volume. One organisation, however, should be named here: the National Research Council of Iceland, representing the Iceland science community, that has given permission and support to the work in Icelandic Territory. Last but not least, a large unnamed group often forgotten are the scientists' companions who put up with them going to the field and writing papers till late at night.

M. Schwarzbach, D. Voppel, and K. Gerke supplied important information on Alfred Wegener and the early studies; H. Illies, J. Untiedt, B. Higgs, G. Ranalli, and J.G. Dennis assisted in clarifying the contents and the English style of this article. We thank all of them.

References

Belousov, V V Against the hypothesis of sea-floor spreading. Tectonophysics **9**, 489–511, 1970

Belousov, V V., Milanovsky, Y Y On the tectonics and tectonic position of Iceland. Greinar **5**, 96–120, 1976

Björnsson, A., Johnsen, G., Sigurdsson, S., Thorbergsson, G., Tryggvason, E.: Rifting of the plate boundary in North Iceland 1975–1978. J. Geophys. Res. **84**, 3029–3038, 1979

Björnsson, A., Saemundsson, K., Einarsson, P., Tryggvason, E., Grönvold, K. Current rifting episode in North Iceland. Nature **266**, 318–323, 1977

Björnsson, S. (ed.): Iceland and Mid-Ocean Ridges. Reikjavík: Leittur, 1967

Bott, M.H.P. Deep structure, evolution, and origin of the Icelandic transverse ridge. In. Geodynamics of Iceland and the North Atlantic Area, L. Kristjansson, ed., Dordrecht: Reidel 1974

Gerke, K. Ein Beitrag zur Bestimmung rezenter Erdkrustenbewegungen. In: Festschrift zum 70. Geburtstag von Professor Dr. Walter Großmann. pp. 66–78. Stuttgart: Wittwer 1967

Gerke, K. Crustal movements in the Mývatn- and in the Thingvallavatn-area, both horizontal and vertical. In: Geodynamics of Iceland and the North Atlantic Area, L. Kristjansson ed.: pp. 263–275. Dordrecht: Reidel 1974

Heirtzler, J.R., LePichon, X., Baron, J.G. Magnetic anomalies over the Reykjanes Ridge. Deep-Sea Res. **13**, 427–443, 1966

Isacks, B., Oliver, J., Sykes, L.R. Seismology and the New Global Tectonics. J. Geophys. Res. **73**, 5855–5899, 1968

Jacoby, W.R. Iceland and the North Atlantic: a review. Geojournal **3**, 253–262, 1979

Koch, J.P. Die Reise durch Island 1912. Petermanns Geogr. Mitt. **58**, 185–189, 1912

Kristjansson, L. (ed.): Geodynamics of Iceland and the North Atlantic Area. Dordrecht. Reidel 1974

McKenzie, D.P., Parker, D.L. The North Pacific: an example of tectonics on a sphere. Nature **216**, 1276–1280, 1967

Morgan, W.J. Rises, trenches, great faults, and crustal blocks. J. Geophys. Res. **73**, 1959–1982, 1968

Nielsen, N. Contributions to the physiography of Iceland. Danske Vidensk. Selsk. Skr., Naturv. Math. Afd. 9. Raekke, IV.5. Kopenhagen 1933

Nielsen, N. Tectonik und Vulkanismus Islands unter Berücksichtigung der Wegener-Hypothese. Geol. Rundsch. **21**, 347–349, 1930

Niemczyk, O.: Spalten auf Island. Stuttgart: Wittwer 1943

Nilsen, T.H. Lower Tertiary laterite on the Iceland-Faeroe Ridge and the Thulean land bridge. Nature **274**, 786–788, 1978

Pálmason, G. Crustal structure of Iceland from explosion seismology. Soc. Sci. Islandica, Rit **40**, 1971

Pálmason, G., Saemundsson, K. Iceland in relation to the Mid-Atlantic Ridge. Annu. Rev. Earth Planet. Sci. **2**, 25–50, 1974

Schleusener, A., Torge, W.: Investigations of secular gravity variations in Iceland. Z. Geophys. **37**, 679–701, 1971

Schwarzbach, M. Alfred Wegener. Große Naturforscher. Bd. 42. Stuttgart: Wiss. Verlagsges. in press, 1979

Sclater, J.G., Francheteau, J. The implications of terrestrial heat flow observations on current tectonic and geochemical models

of the crust and upper mantle of the earth. Geophys. J. R. Astron. Soc. **20**, 509–542, 1970

Spickernagel, H. Höhenmessungen in Nord-Island. Mitt. Markscheidewesen **73**, 139–152, 1966

Thorarinsson, S. Das Dalvík-Beben in Nordisland, 2. Juni 1934. Geogr. Ann. Svensk. Sällsk. Antropol. Geogr. **19**, 232–277, 1937

Vine, F.J., Matthews, D.H. Magnetic anomalies over oceanic ridges. Nature **199**, 947–949, 1963

Wegener, A. Die Entstehung der Kontinente. Petermanns Geogr. Mitt. **58**, 185–195, 253–257, 305–309, 1912a

Wegener, A.. Die Entstehung der Kontinente. Geol. Rundschau **3**, 276–292, 1912b

Wegener, A.: Die Entstehung der Kontinente und Ozeane. Braunschweig: Vieweg [1]1915, [2]1920, [3]1922, [4]1929

Zverev, S.M., Kosminskaya, I.P., Krasilstchikova, G.A., Mikhota, G.G. The crustal structure of Iceland and the Iceland-Faeroe-Shetland region. Greinar **5**, 72–95, 1976

J. Geophys. 47, 7–18, 1980

Journal of Geophysics

Tectonic Framework, Evolution

A Continuum Model of Crustal Generation in Iceland; Kinematic Aspects

G. Pálmason

Orkustofnun, Grensásvegi 9, Reykjavík, Iceland

Abstract. A steady-state plate-tectonic kinematic model of crustal accretion in Iceland is presented. It describes quantitatively the overall time-averaged movements of solid crustal elements during the accretion process, and correlates accretion parameters in the axial zone (width of lava deposition zone, total lava production rate, width of horizontal strain zone, spreading velocity, normal faulting) with structural properties in the Tertiary lava pile (lava dips, lava deposition rate, dyke fraction). The model is used, firstly, to predict the accretion parameters of the Tertiary volcanic zone on the basis of observed structural properties in the Tertiary lava pile; secondly, to predict possible structures of the lower crust in terms of a lava/intrusion ratio; thirdly, the model may be used to calculate the crustal temperature field caused by intrusions, but this application is outside the scope of the present paper. The model is essentially a further development of a previous one presented earlier by the author. The analysis, in terms of the model, of various published structural observations indicates that the width of lava deposition and the spreading rate in the Tertiary volcanic zone were consistent with the corresponding properties in the present-day volcanic zone. This may suggest a certain uniformity in the volcanic processes during the last 10–15 Ma. The visible Tertiary lava pile was, according to the model, deposited outside the innermost 50-km-wide central part of the volcanic zone, which may explain the difference in appearance between the two main volcanic regions of Iceland, i.e., the active volcanic zone and the Tertiary flood basalts. Furthermore, an analysis of possible structures of the lower crust, consistent with various surface observations, indicates a gradual rather than a sharp transition from an upper lava-dominated crust to a lower intrusion-dominated crust.

Key words: Iceland – Mid-ocean ridges – Crustal accretion model – Lava dip – Dykes – Normal faults.

Introduction

In recent years a considerable amount of radiometric age data from the Icelandic basalt pile has been published (e.g. McDougall et al., 1977; Watkins and Walker, 1977). They show a remarkably constant rate of deposition of lavas which may be taken to indicate a certain uniformity in the intensity of the volcanic processes during the time interval since Iceland began to be formed. Other kinds of data on the regional structure of the Tertiary lava pile, such as dips of lavas and dyke volume fraction, also testify to the processes that originally formed the lava pile. The lavas generally dip gently towards the zone of rifting and volcanism, with the dip increasing with depth in the lava pile. The dyke fraction generally increases downwards in the crust, but laterally there are large variations in the dyke fraction. The first systematic study of these relationships was made by Walker (1959, 1960) in eastern Iceland. He interpreted his observations in terms of a sagging process associated with lava deposition in an active volcanic zone. This process was further elaborated by Bodvarsson and Walker (1964).

The present day volcanic zone of Iceland differs in appearance from the Tertiary flood basalt areas. In part this difference is due to the wet environment of the Pleistocene volcanism, but apart from that, the sheer number of visible volcanic vents and faults and fissures is much greater in the axial zone than can be observed in the Tertiary flood basalt pile. The inference is not unnatural that the present day volcanic zone represents a separate episode of volcanism, distinct from that which formed the Tertiary lava pile.

To clarify the relationships between the present day volcanic and tectonic processes in the axial zone and the structure of the Tertiary lava pile, a model is needed which describes the volcanic and tectonic processes taking place. In the present paper such a model will be discussed. It is based on plate tectonics concepts, and is in agreement with the processes envisaged by Bodvarsson and Walker (1964). It is essentially a further development of a model previously presented by the author (Pálmason, 1973). The main modification is that the processes of lava deposition and strain by dyke injection are assumed to have a normal distribution across the volcanic zone instead of a truncated one.

As is well known the active volcanic zone forms a rather complicated pattern through Iceland, with parallel branches and a possible shifting of the zone between two or more locations. Under these circumstances a simple steady-state model can at best only be a rough approximation. When only regional properties are considered, such a model may still be of help in clarifying relationships between various observable properties.

In this paper only the kinematic aspects of the model will be considered, while the thermal aspects will be considered in another paper. It should be noted that the model is intended to describe only the solid or semi-solid crust, but not the underlying two phase flow at temperatures in the melting range. The lower boundary of the model will thus be outlined by isotherms, deduced by calculations of the thermal state of the crust.

0340-062X/80/0047/0007/$02.40

The Model

The assumptions involved in the model were discussed in a previous paper (Pálmason, 1973) and will not be repeated here in detail. The model is essentially a kinematic one, describing the overall time-averaged movement of solid crustal elements during the accretion process. A flow field is constructed in such a way that it fits certain boundary conditions. It is characterized by several parameters that may be varied to fit observations of various structural properties of the lava pile in Iceland. The divergence of the flow velocity field is equal to the intensity of the emplacement of magma in the crust. Specifying the flow field thus makes possible calculation of the thermal state of the crust.

In the model the discontinuous processes of lava extrusion, dyke intrusion and tectonic movements are treated as continuous processes representing the average behaviour over a long time. A disadvantage of this point of view is that the details of the volcanic and tectonic processes, such as individual central volcanic complexes, dykes, and faults, are lost in the model. An advantage is, on the other hand, that analytical descriptions of the regional movement of crustal material are easily made, as well as calculations of the thermal state of the crust. Another approach to the modeling where the volcanic and tectonic processes were treated statistically, was made by Daigniéres et al. (1975).

The Flow Field

The model is a two-dimensional one. The boundary conditions for the flow field are the following:

(a) At the surface of the crust lava is deposited at a certain average rate which varies with the distance from the axis. For a steady-state process the downward movement of the solid crustal elements must be equal to the deposition rate.

(b) At the axis the horizontal component of the flow must be zero for reasons of symmetry.

(c) The distant lithosphere moves horizontally as a 'rigid' body with a constant velocity. The movement is assumed to be perpendicular to the axis.

A flow field satisfying these boundary conditions can be set up in many ways, but perhaps the simplest way is to assume that both velocity components are independent of depth, but vary with the horizontal coordinate only. If furthermore the horizontal strain rate associated with the increase in horizontal velocity from zero at the axis to a final value V_d in the distant lithosphere, is assumed to have a normal distribution with standard deviation σ_1, and the lava deposition rate is also assumed to have a normal distribution with a standard deviation σ_2, the two velocity components may be written, assuming the density to be constant:

$$v_x = \int_0^x \frac{dv_x}{dx} \cdot dx = V_d \frac{\sqrt{2}}{\sqrt{\pi} \cdot \sigma_1} \cdot \int_0^x \exp\left(-\frac{x^2}{2\sigma_1^2}\right) dx$$

$$= V_d \cdot \operatorname{erf}\left(\frac{x}{\sqrt{2} \cdot \sigma_1}\right) \tag{1a}$$

$$v_z = \frac{q}{\sqrt{2\pi} \cdot \sigma_2} \cdot \exp\left(-\frac{x^2}{2\sigma_2^2}\right) \tag{1b}$$

where q is the rate of lava deposition per unit length of the axial zone, but integrated across the width of the zone. The four parameters V_d, q, σ_1, and σ_2 characterize the simple model. Later on, when discussing the effects of normal faulting, two additional parameters will be introduced. In that case the velocity components do not depend only on the horizontal coordinate, but on the depth as well.

The flow field described by these velocities does not conserve material:

$$\operatorname{div} \bar{v} = \frac{\sqrt{2} \cdot V_d}{\sqrt{\pi} \cdot \sigma_1} \cdot \exp\left(-\frac{x^2}{2\sigma_1^2}\right). \tag{2}$$

This is the horizontal strain rate associated with the spreading process and gives the volume rate of emplacement of magma intrusions per unit volume in the crust which in this case depends only on the horizontal coordinate. It is assumed that the magma is emplaced instantaneously from the underlying source zone of partial melting, which is equivalent to saying that the time taken for the movement of the magma to its destination in the crust is short on the time scale of movements of the crust. Some of the magma reaches the surface where it solidifies as lava.

In the flow field above the axial topography is assumed to be a plane surface. This is not a critical assumption, and an irregular but steady-state topography, e.g., a rift valley, would do just as well, but would make the calculations more cumbersome.

For a given flow field it is possible to compute various properties of interest in the solid crust by methods that were described in the previous paper (Pálmason, 1973). Trajectories and isochrons of lava elements, regional dip of lavas, and the lava fraction in the crust can all be computed. In this paper the lava fraction L will be used as much as the dyke fraction D which was used in the previous paper ($L = 1 - D$). The thermal state of the crust can also be computed, but this is outside the scope of the present paper.

The isochrons are the loci of lavas of constant age in the crust. As long as the lavas deform by bending in the axial zone during the accretion process, the dip of the isochrons is the same as the regional dip of the lavas. This will probably be the case for the uppermost part of the frozen crust. At greater depth the lavas will be more broken by faults and dyke intrusions. In that case the dip of the isochrons will not necessarily be the same as the dips of the lavas.

It is convenient when discussing the flow field to use dimensionless variables for the horizontal and vertical coordinates and the time (age of lavas). They will be defined as follows:

$$\xi = \frac{x}{\sqrt{2}\sigma_2}; \quad \eta = \frac{2V_d}{q} \cdot z; \quad \tau = \frac{V_d}{\sqrt{2}\sigma_2} \cdot t;$$

The trajectories of lava elements from their origin of deposition at the surface in the axial zone may in the present case be written as follows (Pálmason, 1973):

$$\eta = \frac{2}{\sqrt{\pi}} \cdot \int_{\xi(0)}^{\xi} \frac{\exp(-s^2)\,ds}{\operatorname{erf}\left(\frac{\sigma_2}{\sigma_1} \cdot s\right)} \tag{3}$$

where $\xi(0)$ is the horizontal coordinate of the point of origin at the surface, and s is a variable of integration. The ratio σ_1/σ_2 crustal strain/lava deposition standard deviations can be expect-

ed to lie in the interval 0–1. The two limiting values give the following trajectories:

$$\begin{aligned} &\text{I.} \quad \sigma_1/\sigma_2 = 0 \qquad \eta = \operatorname{erf}(\xi) - \operatorname{erf}[\xi(0)] \\ &\text{II.} \quad \sigma_1/\sigma_2 = 1 \qquad \eta = \ln\left[\frac{\operatorname{erf}(\xi)}{\operatorname{erf}(\xi(0))}\right] \end{aligned} \tag{4}$$

The difference between the trajectories in the two limiting cases is small at shallow depths in the crust, but increases with increasing depth.

The time parameter, or age of the lavas from the time of their deposition at the surface, may be calculated from the following formulas (Pálmason, 1973):

$$\tau = \int_{\zeta(0)}^{\zeta} \frac{ds}{\operatorname{erf}\left(\frac{\sigma_2}{\sigma_1} \cdot s\right)} \tag{5}$$

where the integral is along a trajectory originating at the surface position $\xi(0)$.

The lava fraction L may be calculated from the equation of continuity for lavas within the crust.

$$\frac{\partial L}{\partial t} + \operatorname{div}(L \cdot \bar{v}) = 0. \tag{6}$$

This may also be written:

$$\frac{dL}{L} = -\frac{\operatorname{div} \bar{v}}{v} \cdot ds = -\frac{\operatorname{div} \bar{v}}{v_x} \cdot dx$$

or

$$\ln L = -\int_{x(0)}^{x} \frac{\operatorname{div} \bar{v}}{v_x} dx \tag{7}$$

where the integral is along a trajectory originating at the surface position $x(0)$.

In the special case where $\bar{v}$ depends only on the horizontal coordinate, the expression for the lava fraction reduces to:

$$L = \frac{v_x(x(0))}{v_x(x)}. \tag{8}$$

In general the isochrons and the lava fraction may be calculated numerically from the above equations. In the limiting case $\sigma_1/\sigma_2 = 0$ (zero width of crustal strain zone) the trajectory $\eta = \operatorname{erf}(\xi)$ forms the sharp boundary between 100% lavas (above) and 100% intrusions (below). The isochrons in the lava pile can in this case be expressed as follows:

$$\eta = \operatorname{erf}(\xi) - \operatorname{erf}(\xi - \tau). \tag{9}$$

Although this expression applies strictly only for $\sigma_1/\sigma_2 = 0$, it can still be considered a good approximation to the isochrons in the uppermost part of the crust, for other values of σ_1/σ_2. This is because the structure of the uppermost crust, where the dyke fraction is small, is largely independent of σ_1/σ_2. Thus the above relationship can be expected to be a good approximation to the isochrons in the visible Tertiary lava pile of Iceland. The lava trajectories and isochrons for this case are shown in Fig. 1.

The case $\sigma_1/\sigma_2 = 0$ was discussed by Cann (1974) using graphical methods. As shown by Kidd (1977) this is the only case which with the present assumptions can approximate the relatively sharp transition between pillow lavas and sheeted dyke complexes, which is observed in ophiolite complexes, e.g., in the Troodos Massif in Cyprus. Later in this paper other possibilities will be discussed which can also lead to a relatively sharp transition between lavas and intrusions.

For the other limiting case $\sigma_1/\sigma_2 = 1$ (crustal strain and lava deposition standard deviations equal) the trajectories and isochrons are shown in Fig. 2. The lava fraction L in the crust is here dependent only on the η coordinate, and is given by

$$L = e^{-\eta} \quad (\text{or } D = 1 - e^{-\eta}). \tag{10}$$

The Standard Deviations σ_1 of Crustal Strain Rate and σ_2 of Lava Deposition Rate

It is of some importance for the usefulness of the model that the standard deviations σ_1 and σ_2, and in particular their ratio, can be estimated from field data.

If the distribution of lava deposition rate from a single linear vent is normal with a standard deviation σ_3, and the distribu-

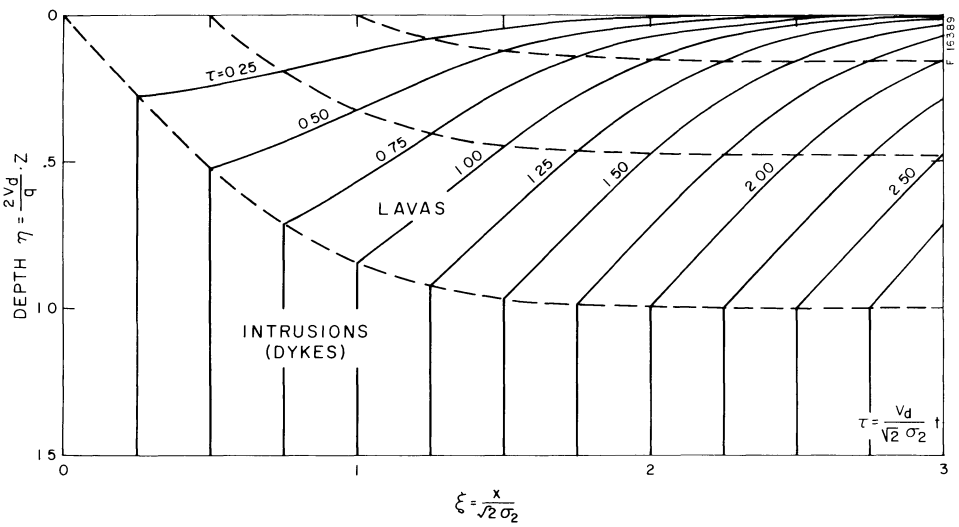

Fig. 1. Dimensionless lava isochrons *(solid lines)* and trajectories *(dashed)* in the model crust for $\sigma_1/\sigma_2 = 0$ (crustal strain/lava deposition standard deviations)

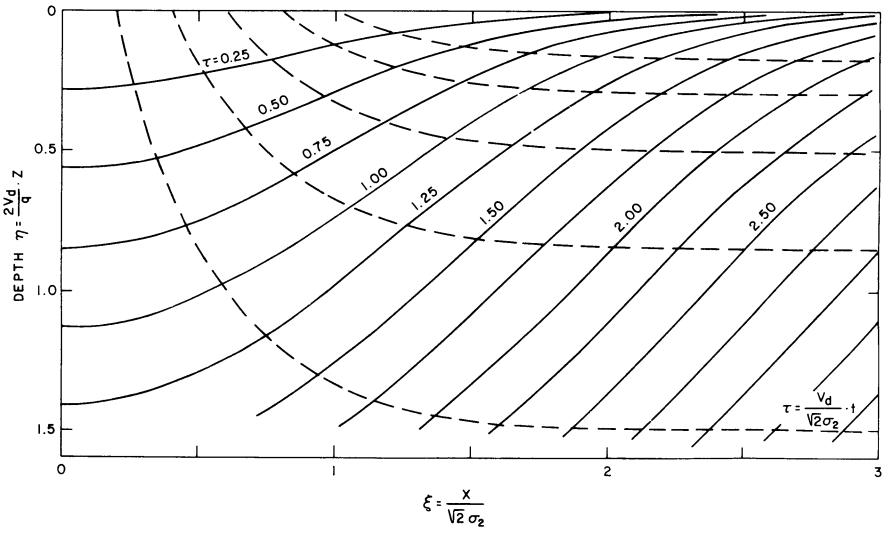

Fig. 2. Dimensionless lava isochrons *(solid lines)* and trajectories *(dashed)* in the model crust for $\sigma_1/\sigma_2 = 1$ (crustal strain/lava deposition standard deviations)

tion of the linear vents around the axis is also normal with a standard deviation σ_1, it may be shown that

$$\sigma_2^2 = \sigma_1^2 + \sigma_3^2 \tag{11}$$

provided the two distributions are independent of each other.

For the mid-ocean ridges, estimates based on the magnetic anomaly pattern indicate strain zone values of a few km for σ_1 (Matthews and Bath, 1967; Harrison, 1968), while no estimates seem to exist for σ_2 of deposition. From the above relation it seems natural to assume that σ_2 is greater than σ_1. The ridge crest topography may, however, play a decisive role in controlling the ratio σ_1/σ_2.

For the Iceland segment of the Mid-Atlantic Ridge the volcanic activity occurs over a considerably wider zone than usually postulated for the mid-ocean ridges. On the basis of the areal distribution of lavas erupted in Iceland during the last 10,000 years, a rough estimate may be obtained for the present-day value of σ_2. An effective width W_e, that is comparable to the width of the zone of Postglacial lavas, will be defined in such a way that at its edge the deposition rate is 1 lava in 10,000 years. The width W_e is then related to σ_2 by Eq. (1b).

$$v_z = \frac{q}{\sqrt{2\pi}\cdot\sigma_2}\cdot\exp\left(-\frac{W_e^2}{8\sigma_2^2}\right)$$

For two values of v_z, corresponding to lava thicknesses of 2 and 5 m, the following relationships are obtained between W_e and σ_2 (with $q = 4/3\times10^{-4}\,\mathrm{km^2/a}$.):

Table 1

	$v_z = 2\times10^{-7}$ km/a	5×10^{-7} km/a
σ_2 km	W_e km	W_e km
5	28.2	24.7
10	51.2	43.5
15	71.9	59.4
20	91.0	73.1
25	108.7	85.1
30	125.3	95.5

The width of the zone of Postglacial lavas is quite variable but mostly in the range 50–100 km. From the table we may then infer that the corresponding σ_2 values are likely to be in the range 10–30 km. It should be noted that the lava thicknesses (or v_z) chosen have a relatively small effect on the relationship between σ_2 and W_e. There is a second set of σ_2 values consistent with Eq. (1b) for given values of v_z and W_e, but this gives a much wider distribution of lavas with $\sigma_2 > W_e$, and is not likely to be consistent with the conditions in the volcanic zone of Iceland.

A considerably lower value is indicated for the strain value, σ_1, probably in the range of 5–15 km. The standard deviations probably reach maximum values near central Iceland, where according to Jakobsson (1972) the lava deposition rate is highest, and decrease towards the north and southwest along the ridge.

In the following, a few estimates will be made of σ_2 for lava deposition from the Tertiary lava pile, and compared with the above estimate from the present day volcanic zone.

Model Parameters and the Structure of the Tertiary Lava Pile in Iceland

The Tertiary basalt areas on both sides of the axial zone in Iceland provide an opportunity for a comparison with the model. The deeply incised basalt pile in eastern, northern and western Iceland gives in some areas structural information to a depth of 1–1.5 km from the original top of the pile.

The structural properties which are of particular importance for comparison with the model are (a) the relative dyke volume fraction, (b) the regional dip of the lavas, and (c) the deposition rate of lavas. All these properties vary with depth, and it is therefore necessary to have a method of estimating the depth of observation from the original surface of the lava pile, since the uppermost part of the pile has been eroded away. Walker (1960) used the zeolite zoning of the uppermost crust together with the dyke fraction and its vertical variation. Following Walker we will assume that the top of the analcite zone lies at a depth of 600 m from the original top of the lava pile in other parts of Iceland. This assumption implies that the maximum surface thermal gradient in the crust, which controls the level of the zeolite zones, was the same in other parts of Iceland as in eastern Iceland.

Before going into a detailed comparison of the model with field observations from the Tertiary basalt pile in Iceland, the model

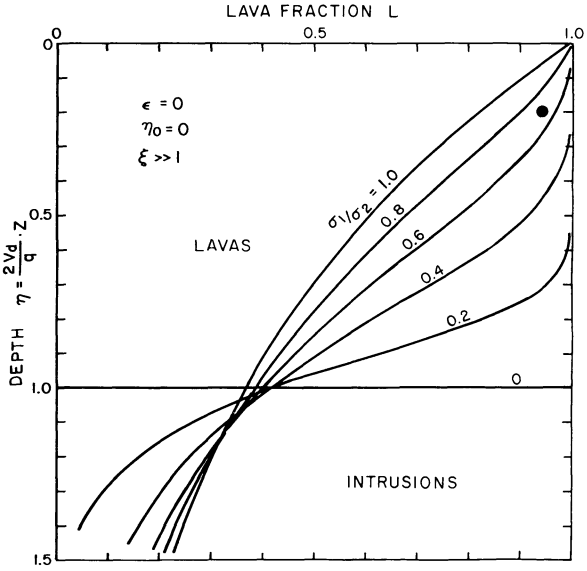

Fig. 3. Lava fraction vs. dimensionless depth in the distant model crust, for various values of the ratio σ_1/σ_2 (crustal strain/lava deposition standard deviations). The normal fault parameters ε and η_0 are discussed in a later section. The *black dot* denotes the average conditions at sea-level in the eastern Iceland lava pile (with $q = 4/3 \times 10^{-4}$ km^2/a and $V_d = 1$ cm/a)

relationships needed for this purpose will be derived. The three structural properties mentioned above, i.e., the dip of the lavas, the deposition rate and the dyke fraction, can all be expressed as functions of depth in the crust, and of the parameters of the model, i.e., V_d, q, σ_1 and σ_2. It turns out that for a constant depth the structural properties depend more ome of the model parameters than on others. The sensitivity of the structural properties to variations in the model parameters will be discussed in some detail. This sensitivity is important when an attempt is made to put constraints on the model parameters from observations of the structural properties in the lava pile.

For the purpose of comparison with the Tertiary lava pile in Iceland we will look only at the structure of th model crust well outside the accretion zone, i.e., for $\xi \gg 1$.

The structural properties can be expressed as functions of the parameter $\xi(0)$, i.e., the horizontal coordinate of the point of origin of a lava trajectory which reaches a depth η in the frozen-in crust. The relationship between η and $\xi(0)$ is given by Eq. (3) with $\xi \gg 1$. This equation gives $\eta = \eta(\xi(0), \sigma_1/\sigma_2)$ and thus contains the ratio σ_1/σ_2 as a parameter, i.e., the crustal strain/lava deposition standard deviations ratio.

The lava fraction in the crust is expressed by Eq. (7). When the velocities v_x and v_z depend only on x this equation reduces to:

$$L = \frac{v_x(x(0))}{v_x(x_1)} = \frac{\operatorname{erf}\left(\frac{\sigma_2}{\sigma_1} \cdot \xi(0)\right)}{\operatorname{erf}\left(\frac{\sigma_2}{\sigma_1} \cdot \xi\right)} \simeq \operatorname{erf}\left(\frac{\sigma_2}{\sigma_1}\ \xi(0)\right). \tag{8a}$$

This formula, together with Eq. (3), thus gives $L = L(\eta, \sigma_1/\sigma_2)$. A family of curves for this relationship is given in Fig. 3. This diagram gives, for an observed value of L at a certain depth z, a relationship between possible values of V_d/q (spreading velocity/total lava deposition rate) and σ_1/σ_2.

The regional dip of the lavas (isochrons) in the upper crust is given by the following formula [Pálmason, 1973; p. 458 Eq. (7a)], assuming that both velocity components depend only on x:

$$\left(\frac{dz}{dx}\right)_t = -\frac{v_z(x(0)) - v_z(x)}{v_x(x)}. \tag{12}$$

In the distant crust well away from the accretion zone ($\xi \gg 1$) this may be written as follows, using the dimensionless variables and the expressions for v_z and v_x.

$$\left(\frac{d\eta}{d\xi}\right)_\tau = -\frac{2}{\sqrt{\pi}} \cdot \exp(-\xi(0)^2). \tag{13}$$

As before, $\xi(0)$ is related to η by Eq. (3). This expression thus gives $(d\eta/d\xi)_\tau$ as a function of η and σ_1/σ_2 (the ratio of standard deviations of crustal strain and lava deposition). In Fig. 4 this relationship is shown for the two limiting cases $\sigma_1/\sigma_2 = 0$ and 1. It is evident that the dip depends little on σ_1/σ_2 in the upper part of the crust. The diagram in Fig. 4 gives, for an observed value of the dip $(dz/dx)_t$ at a certain depth z, a relationship between possible values of V_d/q and σ_2. This relationship depends slightly but not significantly on the ratio σ_1/σ_2.

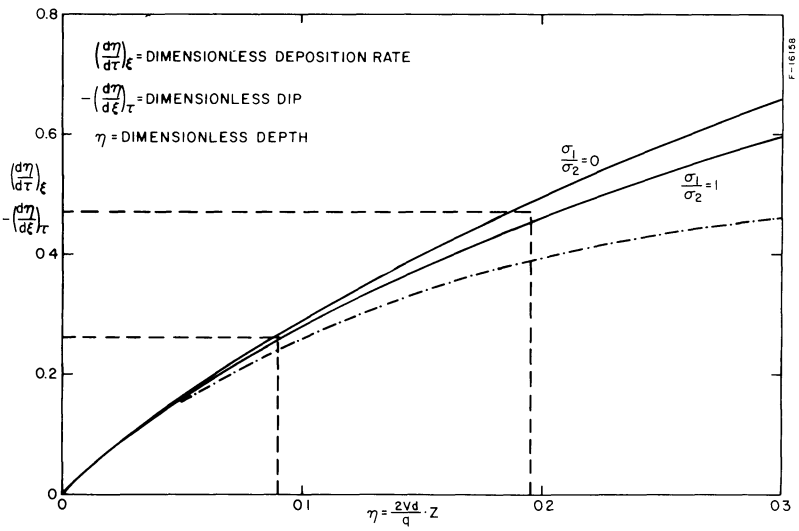

Fig. 4. Dimensionless deposition rate and dip in the distant model crust. The *solid curves* show the range of variation with σ_1/σ_2 (crustal strain/lava deposition standard deviations). The *dot-dashed curve* shows the lower boundary of variation with the normal fault parameters ε and η_0 discussed in a later section

The last structural property, the lava deposition rate $(dz/dt)_x$, may be deduced from equations given by Pálmason (1973). A simple way to find this is to use the mathematical relationship

$$\left(\frac{d\eta}{d\tau}\right)_\xi = -\left(\frac{d\eta}{d\xi}\right)_\tau \left(\frac{d\xi}{d\tau}\right)_\eta \tag{14}$$

Noting that by the definitions of ξ and τ:

$$\left(\frac{d\xi}{d\tau}\right)_\eta = 1, \quad \text{since } \left(\frac{dx}{dt}\right)_z = V_d, \quad (\xi \gg 1)$$

it follows that

$$\left(\frac{d\eta}{d\tau}\right)_\xi = -\left(\frac{d\eta}{d\xi}\right)_\tau = +\frac{2}{\sqrt{\pi}} \cdot \exp(-\xi(0)^2). \tag{15}$$

Thus the same relationship is found between $(d\eta/d\tau)_\xi$ and η as was previously found between $-(d\eta/d\xi)_\tau$ and η, and both are shown by the curves in Fig. 4. In the case of the deposition rate, however, the diagram gives, for an observed value of the deposition rate $(dz/dt)_x$ at a certain depth z, a relationship between possible values of V_d/q and σ_2/V_d.

The curves in Fig. 4 allow constraints to be placed on the model parameters on the basis of observed values of regional dip and deposition rate at certain depths in the lava pile. In this connection it is important to realize that the curves constrain some of the parameters more than others. This is perhaps best seen by imagining that the functions in Fig. 4 were straight lines instead of being slightly curved. Then an observation of the dip at a certain depth in the lava pile would give a unique determination of σ_2, independently of both spreading velocity, V_d, and lava deposition rate per unit length, q. In the same way an observation of the deposition rate at a certain depth would give a unique determination of σ_2/V_d, independently of q. The relatively slight curvature of the functions in Fig. 4 means that they constrain the parameters σ_2 and σ_2/V_d much more than they do the parameter q. The significance of this is that it is possible to make more meaningful statements about possible values of σ_2 and σ_2/V_d on the basis of observations of the dip and deposition rate respectively, than one can make about possible values of q. The parameter q can vary within wide limits with only a small effect on the dip and deposition rate as measured at a certain depth in the lava pile.

It is worth noting finally that the two observable quantities, the regional dip of lavas and the rate of deposition, are closely related to each other. One of them can be deduced from the other if the spreading rate for the particular section of the lava pile is known. Alternatively, the spreading rate can be deduced if these two quantities are both known. This follows from the mathematical relationship mentioned earlier [Eq. (14)]:

$$-\left(\frac{dz}{dt}\right)_x \Big/ \left(\frac{dz}{dx}\right)_t = \left(\frac{dx}{dt}\right)_z \quad (= V_d \text{ for } \xi \gg 1). \tag{16}$$

The model relationships derived above and shown in Figs. 3 and 4 will in the following be used to put some constraints on the model parameters on the basis of structural observations in the Tertiary lava pile of Iceland.

An Estimate of σ_1/σ_2 From the Tertiary Lava Pile in Eastern Iceland

According to the studies of Walker (1959, 1960, 1974) in eastern Iceland of the dyke fraction at various levels in the Tertiary lava pile the average value of D at sea level is about 0.06. The sea level corresponds to a depth of about 1.3 km from the original top of the lava pile according to studies of secondary mineral zones and the upwards decrease of dyke fraction in the pile (Walker, 1960). The diagram in Fig. 3 then gives a relationship between possible values of q/V_d (lava deposition rate per unit length/spreading velocity) and of σ_1/σ_2 (crustal strain/lava deposition standard deviations). If we assume the parameter q/V_d to have had the same value during the formation of the eastern Iceland lava pile, as is indicated at the present time,

$$q = \tfrac{4}{3} \times 10^{-4}\,\text{km}^2/\text{a}, \qquad V_d = 10^{-5}\,\text{km/a},$$

the diagram gives a value of about 0.69 for σ_1/σ_2. The main uncertainty in this estimate with the present model assumptions is in the value of the lava production rate q, since for V_d a relatively steady spreading rate for the Iceland area during the last 47.5 Ma may be deduced from the magnetic anomaly pattern on the Reykjanes Ridge (Herron and Talwani, 1972). A greater lava production rate would give a higher estimate for σ_1/σ_2 and vice versa.

Later on, where a more elaborate version of the model will be discussed, it will be shown that the dyke observations in eastern Iceland cannot constrain the ratio σ_1/σ_2 more than within the range 0.69–1.0.

Three Estimates of the Standard Deviation of Lava Deposition Rate, σ_2, From the Tertiary Lava Pile in Eastern and Western Iceland

The relationships deduced earlier (Fig. 4) between the structural properties and the model parameters will now be used to place constraints on the model parameters on the basis of observations of dip and deposition rate. We will use (a) Walker's observations on the regional dip at sea level in the eastern Iceland Tertiary lava pile, (b) the results of McDougall et al. (1977) on the deposition rate in the Tertiary lavas of central western Iceland, and (c) the results of Watkins and Walker (1977) on the deposition rate in Tertiary lavas in eastern Iceland.

(a) According to Walker (1959, 1960, 1974) the regional dip at sea level of the Tertiary lavas in eastern Iceland is in the range 6–8°. The sea level is at a depth of about 1.3 km from the original top of the lava pile (Walker, 1960). From Fig. 4 we may then deduce a relationship between possible values of σ_2 and q/V_d, according to the model. If we assume that the ratio q/V_d had the same value at the time of formation of the eastern Iceland lavas as it has today, a value of 0.195 is obtained for η. The curves in Fig. 4 then give $(d\eta/d\xi)_\tau = 0.47$, assuming $\sigma_1/\sigma_2 \simeq 0.5$. From the definitions of the dimensionless variables ξ and η we find:

$$\sigma_2 = \frac{z}{\sqrt{2}\left(\frac{dz}{dx}\right)_t} \cdot \frac{\left(\frac{d\eta}{d\xi}\right)_\tau}{\eta}$$

from which we obtain:

$\sigma_2 = 21.1$ km for a dip of 6°

$\sigma_2 = 15.8$ km for a dip of 8°

It may be seen from the above expression for σ_2 that a variation of the other model parameters V_d and q has a relatively small effect on

the value obtained for σ_2. This is because the ratio $(d\eta/d\xi)_\tau/\eta$ changes slowly when η is varied by changing the value of q/V_d. Multiplying the value of q/V_d by 2 gives $\sigma_2 = 18.8$–25.1 km instead of 15.8–21.1 km. Dividing it by 2 gives $\sigma_2 = 12.3$–16.5 km. Thus multiplying or dividing q/V_d by 2 gives a variation in σ_2 of about $\pm 20\,\%$.

(b) In the second example we will estimate σ_2, or rather the ratio σ_2/V_d, from the lava deposition rate $(dz/dt)_x$, as deduced from a study of McDougall et al. (1977) of a lava succession 2–7 Ma old from Borgarfjördur in western Iceland, which has been mapped in detail by Jóhannesson (1975). The samples for K-Ar datings were taken from a 32-km-long profile, at levels ranging mostly ± 200 m around the boundary between the chabazite-thomsonite zone and the analcite zone of secondary mineralization. In order to estimate the depth range of the samples from the original top of the lava pile, it will be assumed that the top of the analcite zone is at a depth of about 600 m, i.e., the same depth as was deduced by Walker (1960) for the lava pile in eastern Iceland. The samples thus are mainly from the depth range 400–800 m. The average rate of lava deposition given by McDougall et al. (1977) was 730 m/Ma, and we will assume for the purpose of calculation that this applies for a depth of 600 m.

With the above values for the lava deposition rate and depth we may use Fig. 4 to deduce a relationship between possible values of σ_2/V_d and q/V_d. If we assume that the ratio q/V_d had the same value at the time of formation of the Borgarfjördur lavas as it has today, a value of 0.09 is obtained for η. The curves in Fig. 4 then give $(d\eta/d\tau)_\xi = 0.261$, assuming $\sigma_1/\sigma_2 \simeq 0.5$. From the definitions of the dimensionless variables ξ and η we find:

$$\frac{\sigma_2}{V_d} = \frac{z}{\sqrt{2}\cdot\left(\frac{dz}{dt}\right)_x}\cdot\frac{\left(\frac{d\eta}{d\tau}\right)_\xi}{\eta}$$

and with inserted values:

$$\frac{\sigma_2}{V_d} = 1.69\ \text{Ma}.$$

With $V_d = 1$ cm/a this gives for the standard deviation:

$$\sigma_2 = 16.9\ \text{km}.$$

As before, the value of σ_2/V_d is rather insensitive to moderate variations in q/V_d. Varying q by a factor of 2, leads to σ_2/V_d values in the range 1.43–1.94 Ma or a variation of about $\pm 15\,\%$. Varying V_d on the other hand leads to an approximately proportionate variation in σ_2. Thus, observations of the deposition rate of lavas constrain primarily the ratio σ_2/V_d, while q can vary within much wider limits and still be consistent with the observations.

The influence of a possible error in the depth value of 600 m can easily be estimated. For a ± 100 m variation in the depth, i.e., 500–700 m, a range of 14.7–19.1 km is obtained for the standard deviation σ_2, assuming $V_d = 1$ cm/a.

(c) In the third example we will estimate σ_2, or σ_2/V_d, from the results of Watkins and Walker (1977) on the deposition rate of lavas in eastern Iceland. The authors deduced an average lava deposition rate of 620 m/Ma at the top of the analcite zone (assumed to be at a depth of 600 m from the original top of the pile) for a lava sequence 2.0–13.6 Ma old. Corrections were made to take into account that the samples for radiometric dating originated from various depths in the range of about 200–1600 m in the lava pile. The data used included those of McDougall et al. (1976a and b). Some variation in the deposition rate was deduced from the data but this was greatly reduced when the corrections for depth were applied.

Applying the diagram in Fig. 4 to the deposition rate in the same manner as before gives the following:

$$\sigma_2/V_d = 1.98\ \text{Ma}$$

or, with $V_d = 1$ cm/a, $\sigma_2 = 19.8$ km. Allowing for a variation by a factor of 2 in q gives σ_2 values in the range 16.9–22.8 km.

In the three examples discussed above, similar values of σ_2 are obtained, based on data from different localities and crustal sections of partly different age. The values of 14–25 km for σ_2 predicted by the model for the Tertiary lava pile in eastern and western Iceland is in rather good agreement with the situation in the present day zone of rifting and volcanism of Iceland, where postglacial lavas are distributed over a zone some 50–100 km wide. These results may indicate a rather uniform intensity of volcanism in the Icelandic zone for the past 10–15 Ma. It should be emphasized, however, that the deposition rate and the regional dip at a certain depth in the Tertiary lava pile depend only very weakly on q, the total lava production rate per unit length of the axial zone. This is perhaps somewhat unexpected but may easily be ascertained from the curves in Fig. 4. On the other hand, both quantities are rather strongly dependent on the standard deviation σ_2, and in addition the deposition rate is also strongly dependent on the spreading velocity V_d. The conclusion that may be drawn is that it is not possible to infer from measurements of deposition rate and dip about past variations in q. Measurements of dip give primarily information on σ_2, and measurements of deposition rate give primarily information on σ_2/V_d.

Determination of the Spreading Rate From Observations of Regional Dip and Lava Deposition Rate

We will now use Eq. (16) to estimate the spreading velocity from two areas in Iceland where measurements of dip and deposition rate have been made at the same level in the Tertiary lava pile.

As the first example we will take the western Iceland (Borgarfjördur) section of McDougall et al. (1977) discussed earlier. According to the authors the regional dips in the section are in the range 2°–8° towards southeast. Taking the average 5° as a representative value, and the deposition rate 730 m/Ma, we obtain for the spreading velocity

$$V_d = \frac{0.073}{0.087} = 0.84\ \text{cm/a}.$$

In the second example we will take the data on dip and deposition rate given by Watkins and Walker (1977) for a section in eastern Iceland. A mean dip at the top of the analcite zone is 3.9° while the mean deposition rate is 620 m/Ma. This gives for the spreading velocity:

$$V_d = \frac{0.062}{0.068} = 0.91\ \text{cm/a}.$$

Direct measurement of the spreading velocity on the same profile with the $^{40}Ar/^{39}Ar$ method gives according to Ross and Mussett (1976) a value of 'not less than 0.8 cm/a'.

The above estimates of spreading velocities from the Tertiary lava pile on both sides of the axial zone in Iceland are in reasonably good agreement with the spreading rates deduced from magnetic anomalies on the Reykjanes Ridge (Herron and Talwani, 1972).

The Origin of the Visible Tertiary Basalt Pile in Iceland Relative to the Axis of the Accretion Zone

The trajectories of lava elements erupted at the surface in the axial zone give the average paths of such elements from their place of origin at the surface to a final depth in the distant crust. The volcanic products erupted near the axis are buried deep into the crust while those erupted farther from the axis remain closer to the surface (cf. Figs. 1 and 2). The model permits a simple evaluation of the origin with respect to the axis of lavas reaching a certain depth in the crust, provided the model parameters are known.

At the relatively shallow depth in the crust, which we are concerned with here, there is little difference between the trajectories calculated for $\sigma_1/\sigma_2=0$ and $\sigma_1/\sigma_2=1$ as discussed earlier. In Eq. (4) we may put $\xi \gg 1$ for the distant crust, and obtain for the trajectories:

$$\begin{aligned} &\text{I.} \quad \sigma_1/\sigma_2=0; \quad \operatorname{erf}(\xi(0))=1-\eta \\ &\text{II.} \quad \sigma_1/\sigma_2=1, \quad \operatorname{erf}(\xi(0))=\exp(-\eta). \end{aligned} \tag{4a}$$

From these formulas we will estimate the distance from the axis corresponding to the origin of the deepest (sea-level) visible parts of the lava pile in eastern Iceland, assuming the same values of q and V_d as before. The sea level corresponds to a depth of about 1.3 km, which gives $\eta=0.195$. This gives for $x(0)$:

$$\begin{aligned} &\text{I.} \quad \xi(0)=0.916; \quad x(0)=1.30 x \sigma_2 \\ &\text{II.} \quad \xi(0)=0.970; \quad x(0)=1.37 x \sigma_2. \end{aligned}$$

The standard deviation σ_2 has earlier been estimated to be in the range 14–25 km. Taking 20 km as a representative value gives $x(0)$ in the range 26–27 km. This means, according to the model, that the visible eastern Iceland basalt pile was originally deposited outside an axial zone some 50–55 km wide. The lavas deposited within this zone have been buried to depths in the crust which are below sea level and are thus not accessible to direct observation in the fjords of eastern Iceland.

This result is of considerable interest when comparing the visible structure and surface topography of the Tertiary flood basalt areas with the present-day active volcanic zone. It is well known that there is a conspicuous difference in appearance between the two areas. In the active zone volcanic vents of various forms abound. While some of the topography of the axial zone is no doubt due to the controlling influence of an ice cover during the last glacial period on the behaviour of magma erupted at the surface, it is nevertheless likely that the sheer number and distribution of vents is a more permanent feature of the zone and largely independent of an ice cover. The Tertiary flood basalt areas on the other hand are characterized by a relatively smooth horizontal surface at its highest levels, underlain by horizontal lava flows. Deeper down in the basalt pile signs of eruptive vents become more frequent, dyke swarms and extinct central volcanic complexes begin to appear. At the same time the regional dip of the lava sections increases.

The difference in the appearance of the two main volcanic regions of Iceland is easily understood in terms of the model, and no major change in the behaviour of the volcanic processes in Iceland is required to account for this difference. Assuming that the density of volcanic vents is distributed normally across the accretion zone with the same standard deviation σ_1 as the horizontal strain rate one may easily calculate what fraction of volcanic vents, produced in the axial zone, will be visible in the uppermost 1,300 m of the crust, e.g., in the eroded fjords of eastern Iceland. With $\sigma_1/\sigma_2=0.7$ this is found to be 5.4%, and with $\sigma_1/\sigma_2=1.0$ the fraction is 17.7%. The first value is likely to be more realistic since $\sigma_1/\sigma_2=1$ is a limiting case not likely to correspond to the real situation. In any case, the fraction of the volcanic vents produced in the accretion zone, which would be visible in the uppermost 1,300 m of the crust is small, probably well within 10% of the total produced in the axial zone. The remaining 90% disappear below sea level. This explains the relative scarcity of such vents in the Tertiary flood basalts, not only in eastern Iceland but in other parts of Iceland as well.

Further Modification of the Model. The Effect of Normal Faults

So far only the simplest assumptions have been made regarding the flow field of lava elements in the model. Both the horizontal strain rate dv_x/dx and the vertical velocity v_z have been assumed to be independent of the depth coordinate. This may prove to be an oversimplification, if the intrusive activity associated with the horizontal strain varies with depth. In particular normal faults may take up some of the horizontal strain in the upper part of the crust.

Although normal faults are of relatively minor importance in the structure of the visible Tertiary basalt pile of Iceland (Bodvarsson and Walker, 1964), this should not be taken as an indication that they were uncommon in the axial zone of those times. For the same reason as discussed before for the volcanic vents, most traces of normal faults in the axial zone would have been buried to depths below sea level and thus not be accessible to observation. Normal faults are quite conspicuous in some parts of the present day axial zone in Iceland, in particular in the Thingvellir area in southwest Iceland, and at Tjörnes along the western margin of the active zone in northeast Iceland. The observation of Saemundsson (1967) that the vertical displacements along some of these faults is greater where they cut through older rocks than where they cross younger rocks shows that these faults have been active over a long time, perhaps moving episodically during rifting events such as is taking place in northern Iceland at present (Björnsson et al., 1977). The relative exposure of the normal faults along the axial zone may be related to short term variations in the rate of deposition of lavas along the zone.

In the axial zones of the mid-ocean ridges normal faults appear to be quite common, at least where an axial rift valley is well developed. The normal faults then show up in the topography across the valley (Atwater and Mudie, 1973; Needham and Francheteau, 1974; Tapponnier and Francheteau, 1978; Atwater, 1979).

An attempt will be made to incorporate the normal faults into the model by treating them as a continuous process of horizontal strain and an associated subsidence. It will be assumed that the horizontal strain rate associated with the normal faults is highest at the surface and decreases with increasing depth where dykes and other intrusions take up a larger fraction of the horizontal strain. It is necessary to introduce two new

parameters to describe this process. One of them is the fraction ε of the total horizontal strain rate at the surface that is taken up by normal faults. The other, z_0, describes how this part of the strain rate decreases with depth, as will be discussed below.

The volume strain rate associated with the emplacement of intrusions in the crust is given by the divergence of the velocity vector $\bar{v}$ of lava elements. Using the parameters described above this will be assumed to be of the form.

$$\operatorname{div}\bar{v}=\frac{\sqrt{2}\cdot V_d}{\sqrt{\pi}\cdot\sigma_1}\cdot\exp\left(-\frac{x^2}{2\sigma_1^2}\right)\cdot\left(1-\varepsilon\cdot\exp\left(-\frac{z}{z_0}\right)\right). \tag{2a}$$

The function in the second parenthesis takes into effect the influence of the normal faults. Its form is chosen mainly for reasons of convenience. The parameter ε is the fraction of the total horizontal strain rate at the surface that is taken up by the normal faults, while the parameter z_0 represents the decrease with depth of the influence of the normal faults. For $\varepsilon=0$ the expression reduces to that given earlier [Eq. (2)].

It will furthermore be assumed that the total horizontal strain rate dv_x/dx has the same form as before and depends only on x:

$$\frac{dv_x}{dx}=\frac{\sqrt{2}\cdot V_d}{\sqrt{\pi}\cdot\sigma_1}\cdot\exp\left(-\frac{x^2}{2\sigma_1^2}\right);\qquad v_x=V_d\cdot\operatorname{erf}\left(\frac{x}{\sqrt{2}\sigma_1}\right). \tag{1a}$$

Then $\frac{\partial v_z}{\partial z}=\operatorname{div}\bar{v}-\frac{\partial v_x}{\partial x}$, from which it is found by integration that

$$v_z(x,z)=v_z(x,0)-\frac{\sqrt{2}\cdot V_d}{\sqrt{\pi}\cdot\sigma_1}\cdot\varepsilon z_0\cdot \cdot\exp\left(-\frac{x^2}{2\sigma_1^2}\right)\cdot\left(1-\exp\left(-\frac{z}{z_0}\right)\right). \tag{17}$$

The vertical velocity component at the surface is assumed to have the same form as before:

$$v_z(x,0)=\frac{q}{\sqrt{2\pi}\cdot\sigma_2}\cdot\exp\left(-\frac{x^2}{2\sigma_2^2}\right). \tag{1b}$$

Using the dimensionless variables and introducing the dimensionless velocities

$$U_x=v_x/V_d\quad\text{and}\quad U_z=2\sqrt{2}\cdot\sigma_2\cdot v_z/q$$

the flow field components may be written:

$$U_x=\operatorname{erf}\left(\frac{\sigma_2}{\sigma_1}\cdot\xi\right) \tag{18a}$$

$$U_z=\frac{2}{\sqrt{\pi}}\cdot\exp(-\xi^2)-\frac{2}{\sqrt{\pi}}\cdot\frac{\sigma_2}{\sigma_1}\cdot \cdot\varepsilon\eta_0\exp\left(-\xi^2\cdot\left(\frac{\sigma_2}{\sigma_1}\right)^2\right)\cdot(1-\exp(-\eta/\eta_0)). \tag{18b}$$

This flow field is consistent with the boundary conditions at the surface, at the axis, and in the distant crust. The introduction of the two new parameters ε and η_0 gives the flow field new properties which were not present in the previously discussed case, where $\varepsilon=0$. In particular the vertical velocity, which is a function of both ξ and η, can now become zero for certain values of ξ and negative at greater depth. The physical explanation for this is that the lava supply from the surface which makes up the crust has been exhausted at a certain depth, and material from below is brought up to form the lower crust.

The properties of this flow field are perhaps most clearly shown by considering the special case $\varepsilon=1$ and $\eta_0\to\infty$. This is an extreme case where all the horizontal strain rate in the upper crust is taken up by normal faults. In this case the vertical velocity component is:

$$U_z=\frac{2}{\sqrt{\pi}}\cdot\exp(-\xi^2)-\frac{2}{\sqrt{\pi}}\cdot\frac{\sigma_2}{\sigma_1}\cdot\eta\cdot\exp\left(-\xi^2\left(\frac{\sigma_2}{\sigma_1}\right)^2\right). \tag{18c}$$

At the axis $U_z=0$ for $\eta=\frac{\sigma_1}{\sigma_2}$. The trajectory leading from this point on the axis into the crust approaches asymptotically a depth of $\eta=1$ in the distant crust. This trajectory forms in this special case a sharp boundary between 100% lavas and material brought up from below (intrusions). This is thus another case, in addition to the one mentioned earlier, $\sigma_1/\sigma_2=0$, that gives a sharp boundary between lavas and intrusive rocks.

In the less extreme cases where ε and η_0 have lower values, the boundary between predominantly lavas and predominantly intrusions becomes blurred. Lava trajectories, lava isochrons and lava fraction may be calculated numerically as was done for the simpler cases discussed earlier. As an example, the isochrons in the distant crust ($\xi\gg1$) for the case $\sigma_1/\sigma_2=1$ and $\eta_0\to\infty$ may be calculated from the following equations deduced from Eqs. (5), (18), and (A7) in the Appendix:

$$\eta=\frac{1}{\varepsilon}(1-\operatorname{erf}(\xi(0))^{\varepsilon})\qquad\text{Trajectories}$$

$$-\left(\frac{d\eta}{d\xi}\right)_\tau=\frac{2}{\sqrt{\pi}}\cdot\exp(-\xi(0)^2)\cdot(1-\varepsilon\eta)\qquad\text{Isochrons.}$$

The form of the lava isochrons in the distant crust for this case, with $\varepsilon=1$, is shown in Fig. 5.

The variation of the lava fraction L with depth and its dependence on the parameters ε, η_0, and σ_1/σ_2 is of particular interest for comparison with observations in the Tertiary lava pile of Iceland. The three sets of curves in Figs. 3 and 6 are calculated for the distant crust ($\xi\gg1$) from formulas derived from Eqs. (7) and (18). The black dots inserted show average conditions in the eastern Iceland lava pile according to Walker (1960) (with $q=\frac{4}{3}\times10^{-4}\,\mathrm{km^2/a}$, $V_d=1\,\mathrm{cm/a}$).

On the basis of the model curves in Figs. 3 and 6 it is possible to put some constraints on possible model parameters that are compatible with Walker's observations of the dyke fraction in eastern Iceland. Assuming $q=4/3\times10^{-4}\,\mathrm{km^2/a}$ and $V_d=1\,\mathrm{cm/a}$, the following constraints are obtained:

(i) $0.69<\sigma_1/\sigma_2<1$. This is valid regardless of the values of ε and η_0. The lower limit $\sigma_1/\sigma_2=0.69$ is obtained for $\varepsilon=\eta_0=0$.

(ii) for $\sigma_1/\sigma_2=1$ the following limits are found for ε and η_0: $0.74<\varepsilon<1$ and $0.35<\eta_0<\infty$. The value $\varepsilon=0.74$ corresponds to $\eta_0=\infty$, and $\eta_0=0.35$ corresponds to $\varepsilon=1$. For each value of σ_1/σ_2 there is a minimum value of ε corresponding to $\eta_0=\infty$, and a minimum value of η_0 corresponding to $\varepsilon=1$.

From Figs. 3 and 6 it may be seen that the normal fault parameters ε and η_0 together with the ratio σ_1/σ_2, have a very pronounced effect on the dyke fraction in the upper part of the

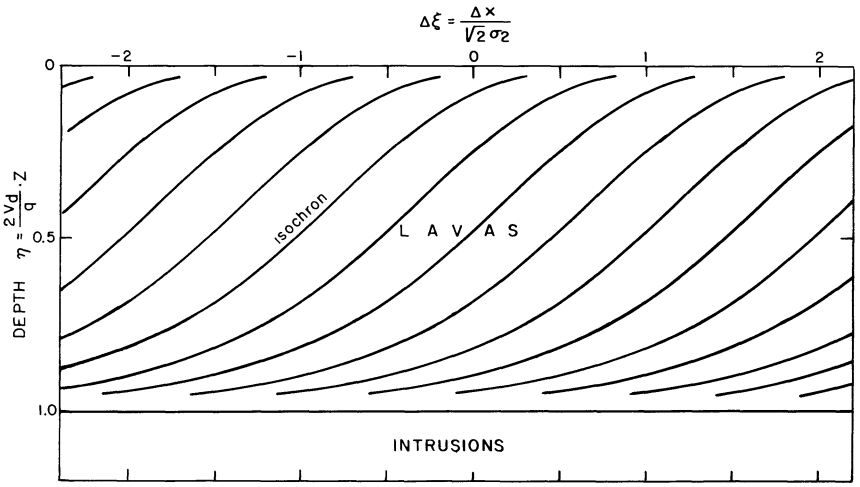

Fig. 5. Lava isochrons in the distant model crust for the extreme case $\sigma_1/\sigma_2 = 1$, $\varepsilon = 1$, $\eta_0 = \infty$. A sharp boundary is obtained between the upper lava layer and the underlying intrusive layer. ($\varepsilon =$ relative influence of normal faulting on total crustal strain rate at surface; $\eta_0 =$ depth constant of this influence)

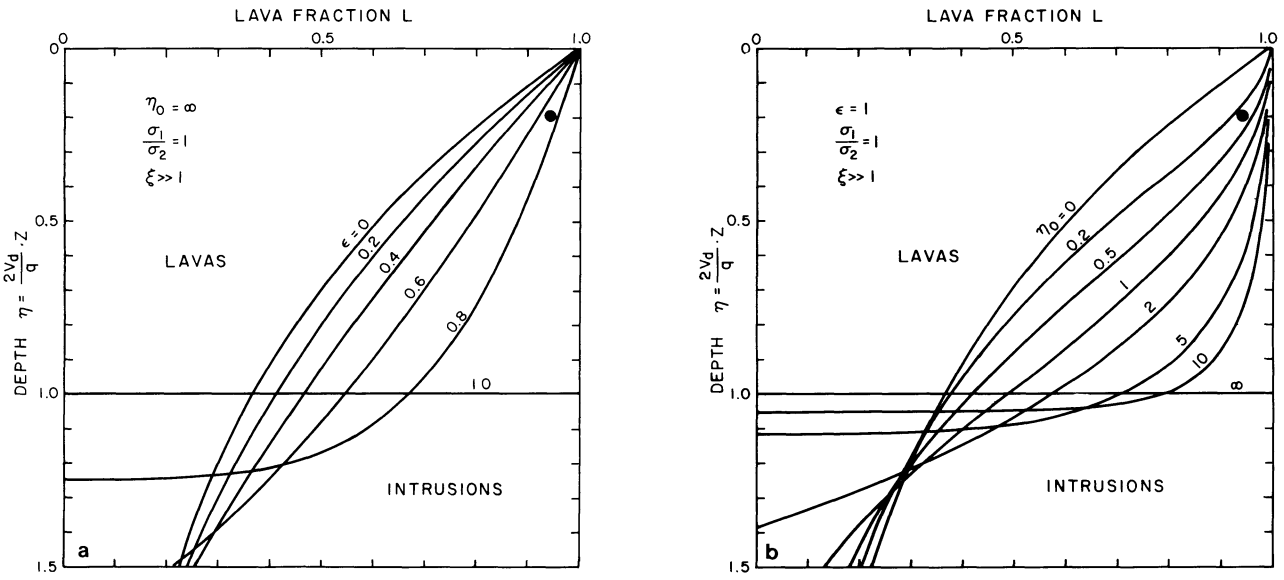

Fig. 6a and b. Lava fraction vs. dimensionless depth in the distant model crust, for various values of the normal fault parameters (**a**) ε and (**b**) η_0. The *black dots* denote the average conditions at sea-level in the eastern Iceland lava pile (with $q = 4/3 \times 10^{-4}$ km^2/a and $V_d = 1$ cm/a). (ε, η_0 see caption of Fig. 5)

model crust. Therefore, only rather broad conclusions regarding the values of individual parameters can be drawn from observations of the dyke fraction in the Tertiary lava pile of Iceland.

Finally, one may ask how the normal fault parameters ε and η_0 will affect the earlier conclusion, that the dip and deposition rate at a certain depth in the upper part of the distant crust (corresponding to the Tertiary lava pile in Iceland) depend mainly on the parameters σ_2 and σ_2/V_d, and only weakly on q. Referring to Fig. 4, the lowest curve (dot-dashed) is obtained for the extreme case $\varepsilon = 1$, $\eta_0 = \infty$ and $\sigma_1/\sigma_2 = 1$. Between this curve and the one labeled $\sigma_1/\sigma_2 = 0$ is the possible range of variation. Considering that the probable range of variation is much smaller, it is evident that the above conclusion regarding the dip and deposition rate remains largely valid. It also follows that the earlier derivations of the parameters σ_2 and σ_2/V_d from the dips and deposition rate measured in various parts of Iceland would not be affected significantly by taking into account the probable range of values for the normal fault parameters ε and η_0.

The normal fault parameters have a major effect on the thermal state of the model crust. This is because extension by dykes implies a strong heat source, while extension by normal faults does not. The detailed discussion of the thermal state of the model crust is, however, outside the scope of this paper.

Discussion

In Iceland regional structural data from two distinct geological environments, the active zone of rifting and volcanism, and the Tertiary flood basalt areas on both sides, can be brought to bear on the process of crustal accretion. A major objective of the present paper has been to analyse such data from both areas in terms of a common model of crustal accretion, to investigate whether they can be fitted to a single kinematic model with a common set of parameters, which would indicate that the accretion process had been going on more or less continuously in the same way it is today, since Iceland began to be formed.

The observational data include regional dips, lava deposition rate, and dyke fraction in the Tertiary areas, width, total lava production rate, and faulting in the active volcanic zone. The analysis in terms of the model shows that from the regional dips (isochrons) of lavas and the local deposition rate of lavas one can obtain estimates of the width of the Tertiary volcanic zone (in terms of the standard deviation σ_2) and the spreading rate. The standard deviation σ_2 is estimated to be in the range 14–25 km, compared to an estimated 10–30 km for its present day value. There is thus no indication that the width of the volcanic zone has changed in a significant way during the last 10–15 Ma. Another result of the analysis is that from measurements of the local deposition rate in the Tertiary lava pile, no conclusions can be drawn about the total lava production rate per unit length of the volcanic zone. This can vary within wide limits without being detected in the uppermost crust. Evidence of volcanic and tectonic processes in the central part of the active zone disappears gradually into the deeper part of the distant crust, where it can not be observed directly. An estimate based on the model indicates that the eastern Iceland visible Tertiary lava pile, some 1,300 m thick, was formed outside a 50–55-km-wide central part of the Tertiary volcanic zone.

An analysis of the factors influencing the dyke fraction in the upper crust, and its variation with depth, indicates that this is influenced both by the ratio σ_1/σ_2 and by the relative importance of dyke injection and normal faulting in the extensional process of the axial zone. Therefore, only rather wide constraints can be put individually on the three parameters describing these processes, from observations of the dyke fraction in the eastern Iceland lava pile.

The same parameters which govern the dyke fraction in the upper crust, also control the transition from an upper lava-dominated layer to a lower intrusion-dominated layer. This transition can be a sharp one, e.g., for $\sigma_1/\sigma_2=0$, as discussed by Kidd (1977). But it is also possible to produce a sharp boundary between lavas and intrusions by a wider extensional zone ($\sigma_1>0$), where normal faults take up the horizontal strain instead of dykes. Both these possibilities should be considered in discussing the relatively sharp boundary observed in some ophiolite sequences. In the Iceland case, likely model parameters would give a gradual transition from the lava layer to the intrusion layer (cf. Fig. 6).

Although the kinematic model appears to correlate fairly well with some regional properties in the active volcanic zone and in the Tertiary flood basalts, care should be taken not to carry the model analogy too far. The simple geometry of the model contrasts rather strongly with the complicated pattern of the present volcanic zones, parts of which have shifted or jumped from one location to another during the geological history of the Iceland area. Structural complications resulting from such jumps are of course not incorporated into the model in its present form. It appears that a volcanic accretion zone has to be active for several million years in the same location to develop the steady-state properties described by the model.

Appendix

A general expression for the isochrons in the model crust may be derived in the following way. A trajectory of lava elements originating at the surface position $\xi(0)$ can be written

$$\eta=\eta(\xi,\xi(0)) \tag{A1}$$

and the time variable (age of lavas) along the trajectory

$$\tau=\tau(\xi,\xi(0)). \tag{A2}$$

Taking the differentials

$$d\eta=\left(\frac{\partial\eta}{\partial\xi}\right)_{\xi(0)}d\xi+\left(\frac{\partial\eta}{\partial\xi(0)}\right)_{\xi}d\xi(0) \tag{A3}$$

$$d\tau=\left(\frac{\partial\tau}{\partial\xi}\right)_{\xi(0)}d\xi+\left(\frac{\partial\tau}{\partial\xi(0)}\right)_{\xi}d\xi(0). \tag{A4}$$

From (A4): $$\left(\frac{d\xi(0)}{d\xi}\right)_{\tau}=-\frac{\left(\frac{\partial\tau}{\partial\xi}\right)_{\xi(0)}}{\left(\frac{\partial\tau}{\partial\xi(0)}\right)_{\xi}}. \tag{A5}$$

From (A3) and (A5):

$$\left(\frac{d\eta}{d\xi}\right)_{\tau}=\left(\frac{\partial\eta}{\partial\xi}\right)_{\xi(0)}-\left(\frac{\partial\eta}{\partial\xi(0)}\right)_{\xi}\cdot\frac{\left(\frac{\partial\tau}{\partial\xi}\right)_{\xi(0)}}{\left(\frac{\partial\tau}{\partial\xi(0)}\right)_{\xi}}. \tag{A6}$$

This is the general differential equation for the isochrons in the model crust. In the distant crust, i.e., $\xi\gg1$, we have

$$\left(\frac{\partial\tau}{\partial\xi}\right)_{\xi(0)}=1 \quad \text{and} \quad \left(\frac{\partial\eta}{\partial\xi}\right)_{\xi(0)}=0,$$

and (A6) reduces to:

$$\left(\frac{d\eta}{d\xi}\right)_{\tau}=-\frac{\left(\frac{\partial\eta}{\partial\xi(0)}\right)_{\xi}}{\left(\frac{\partial\tau}{\partial\xi(0)}\right)_{\xi}}. \tag{A7}$$

References

Atwater, T.: Constraints from the FAMOUS area concerning the structure of the oceanic section. In: Deep Drilling Results in the Atlantic Ocean: Ocean Crust, (M. Talwani, C.G. Harrison, D.E. Hayes, eds.) Am. Geophys. Union, Maurice Ewing Series **2**, 33–42, 1979

Atwater, T., Mudie, J.D.: Detailed near-bottom geophysical study of the Gorda Rise. J. Geophys. Res. **78**, 8665–8686, 1973

Björnsson, A., Saemundsson, K., Einarsson, P., Tryggvason, E., Grönvold, K.: Current rifting episode in north Iceland. Nature **266**, 318–322, 1977

Bodvarsson, G., Walker, G.P.L.: Crustal drift in Iceland. Geophys. J.R. Astron. Soc. **8**, 285–300, 1964

Cann, J.R.: A model for the oceanic crustal structure developed. Geophys. J.R. Astron. Soc. **39**, 169–187, 1974

Daigniéres, M., Courtillot, V., Bayer, R., Tapponnier, P.: A model for the evolution of the axial zone of mid-ocean ridges as suggested by Icelandic tectonics. Earth Planet. Sci. Lett. **26**, 222–232, 1975

Harrison, C.G.A.: Formation of magnetic anomaly patterns by dyke injection. J. Geophys. Res. **73**, 2137–2142, 1968

Herron, E.M., Talwani, M.: Magnetic anomalies on the Reykjanes Ridge. Nature **238**, 390–392, 1972

Jakobsson, S.P.: Chemistry and distribution pattern of Recent basaltic rocks in Iceland. Lithos **5**, 365–386, 1972

Jóhannesson, H.: Structure and petrochemistry of the Reykjadalur central volcano and the surrounding areas, midwest Iceland. Ph.D. Thesis. Durham University, 273 pp., 1975

Kidd, R.G.W.: A model for the process of formation of the upper oceanic crust. Geophys. J.R. Astron. Soc. **50**, 149–183, 1977

Matthews, D.H., Bath, J.: Formation of magnetic anomaly pattern of mid-Atlantic ridge. Geophys. J.R. Astron. Soc. **13**, 349–357, 1967

McDougall, I., Saemundsson, K., Jóhannesson, H., Watkins, N.D., Kristjánsson, L.: Extension of the geomagnetic polarity time scale to 6.5 m.y.: K-Ar dating, geological and paleomagnetic study of a 3,500 m lava succession in western Iceland. Geol. Soc. Am. Bull. **88**, 1–15, 1977

McDougall, I., Watkins, N.D., Kristjánsson, L.: Geochronology and paleomagnetism of a Miocene-Pliocene lava sequence at Bessastadaá, eastern Iceland. Am. J. Sci. **276**, 1078–1095, 1976a

McDougall, I., Watkins, N.D., Walker, G.P.L., Kristjánsson, L.: Potassium-argon and paleomagnetic analysis of Icelandic lava flows: Limits on the age of anomaly 5. J. Geophys. Res. **81**, 1505–1512, 1976b

Needham, H.D., Francheteau, J.: Some characteristics of the rift valley in the Atlantic Ocean near 36° 48′ north. Earth Planet. Sci. Lett. **22**, 29–43, 1974

Pálmason, G.: Kinematics and heat flow in a volcanic rift zone, with application to Iceland. Geophys. J.R. Astron. Soc. **33**, 451–481, 1973

Ross, J.G., Mussett, A.E.: $^{40}Ar/^{39}Ar$ dates for spreading rates in eastern Iceland. Nature **259**, 36–38, 1976

Saemundsson, K.: Vulkanismus und Tektonik des Hengill-Gebietes in SüdwestLIsland. Acta Nat. Isl. **II** (7), 195 pp., 1967

Tapponnier, P., Francheteau, J.: Necking of the lithosphere and the mechanics of slowly accreting plate boundaries. J. Geophys. Res. **83**, 3955–3970, 1978

Walker, G.P.L.: Geology of the Reydarfjördur area, eastern Iceland. Q. J. Geol. Soc. London **114**, 367–391, 1959

Walker, G.P.L.: Zeolite zones and dyke distribution in relation to the structure of the basalts in eastern Iceland. J. Geol. **68**, 515–528, 1960

Walker, G.P.L.: The structure of eastern Iceland. In: Geodynamics of Iceland and the North Atlantic Area, L. Kristjánsson, ed.: pp. 177–188. Dordrecht: Reidel 1974

Watkins, N.D., Walker, G.P.L.: Magnetostratigraphy of eastern Iceland. Am. J. Sci. **227**, 513–584, 1977

Received March 19, 1979; Revised Version September 10, 1979

J. Geophys. 47, 19–22, 1980

Journal of Geophysics

Hawaiian Rifts and Recent Icelandic Volcanism: Expressions of Plume Generated Radial Stress Fields

M. Wyss

Cooperative Institute for Environmental Sciences, University of Colorado, Boulder, Colorado 80309, USA

Abstract. Hawaiian volcanoes have two to three major rift zones which radiate in three preferred azimuths of 82°, 201°, and 322° These three principal rift arms form angles of about 120° with each other and one of them is oriented approximately parallel to the youngest part of the Hawaiian Island chain. I propose that these three rift systems are plume generated, and after they are removed from the hotspot they could be considered triple junctions of aulacogens. In Iceland the idea of sea floor spreading is apparently contradicted by the distribution of recent volcanism. The Snaefellsnes volcanic zone for instance strikes EW in contrast to all other volcanic zones in the Atlantic and it terminates abruptly without being transformed by a fault into a plate boundary. The eastern volcanic zone of Iceland strikes approximately NS and also terminates without a transform fault at its southern end which is represented by Surtsey. Interpreting the Icelandic recent volcanic zones (with the exception of the Reykjanes zone) as representing the three rift arms of a hotspot removes all contradiction with the sea floor spreading hypothesis in the area.

Key words: Iceland – Hawaii – Stress – Rift – Triple junction – Plume.

Introduction

Triple-arm tear patterns (Mercedes star-like) are often observed radiating from geological features. The dimensions of these range from meters (lava and salt domes) to 100 km (mantle plumes). Usually the angle between the three tear arms is close to 120° Most often this phenomenon is interpreted as caused by radially symmetrical updoming of a brittle layer, due to the upwelling of a cylindrical or plume-like mass from below. The radial symmetry of the triple-arm pattern indicates that the stress field causing the tears is radially compressive and tangentially extensive in the horizontal plane around the center of the pattern. In addition to doming, this type of pattern could be caused by gravitational forces in a cone or thermal stresses caused by radial cooling.

Burke and Dewey (1973) proposed that plumes generate triple junctions. The conjecture is that plumes pushing through the lithosphere from below will cause a concentric uplift of the surface. Tangential stresses will then tear the crust and perhaps the lithosphere in three radial rifts which will be oriented symetrically at approximately 120° to each other. Three rifts are usually observed presumably because three rifts allow for the largest opening with the minimum rupture area, i.e., the minimum work required. Dewey and Burke (1974) further proposed that continental break-ups are initiated by chains of hotspots, the rifts of which connect to each other and thus create the jagged outlines of the resulting continental boundaries. In this scheme two rifts of each hotspot connect to the next plumes along the chain and become active spreading axes, whereas the third one becomes a failed arm or aulacogen. Hoffman et al. (1974) illustrated this point by an extinct and a currently active hotspot-generated triple junction. The Afar hotspot represents their concept of the typical case of a current plume-generated triple junction. The Red Sea and the Gulf of Aden are the active rifts with the Ethiopian rift showing minor activity, which invites the suggestion that it will cease spreading in the future and become a failed arm. One of the best documented paleo-aulacogens is the Niger delta depression. As shown by Hoffman et al. (1974) the plumegenerated triple junction that produced this failed arm also produced the sharp eastern point of South America that, with its fit into Africa's Bay of Guinea, suggested to Wegener (1924) that these continents were once joined. The characteristics of failed arms are that the initial stage of graben type normal faulting and volcanism occurred synchronously with the beginning of rifting along the successful arms and that tectonic activity will be terminated and followed by stability once the location has drifted away from the plume.

Hawaii

One of the best known hotspots is Hawaii. Wilson (1963) proposed that the Pacific plate moves rapidly to the NW over a relatively stationary mantle plume (a concept further developed by Morgan, 1971, 1972) and that therefore the Hawaiian volcanic islands are continuously removed from the plume location. Thus, a long island and seamount chain deposited on the moving lithosphere is created in the wake of the hotspot. The most active volcano is located at the southeastern-most island above the plume. Today this is Kilauea, on the island of Hawaii. Figure 1 shows the rift zones of the 5 major volcanoes on Hawaii. Macdonald (1956) recognized that these rifts and those on other Hawaiian islands (Fig. 2) form radial patterns with respect to the volcanoe summits. Fiske and Jackson (1972) combined the major rifts of the Hawaiian islands (Fig. 2) in a rose diagram of rifts radiating from the hot spot (Fig. 3). The rose diagram shows a clear pattern with three preferred directions being mapped by the longest rifts and by the largest number of rifts. Clockwise from N these directions are approximately 82°, 201°, and 322° The angles between these major rifting directions are close to 120° The clearest single example of the typical symetrical three arm system is shown by the rifts of Haleakala on Maui (Fig. 2).

0340-062X/80/0047/0019/$01.00

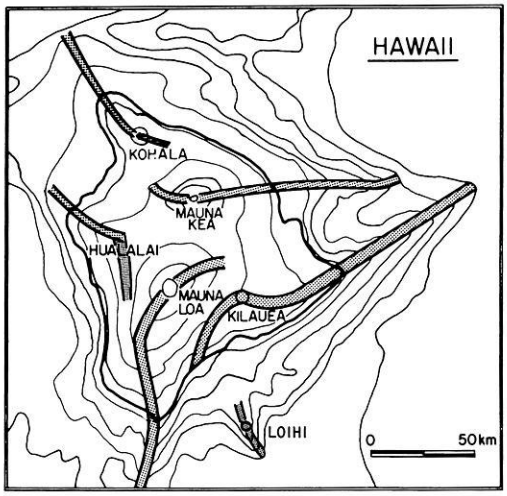

Fig. 1. Topographic map of the island of Hawaii and vicinity. Stippled pattern marks the rift zones of volcanoes. (After Fiske and Jackson, 1972)

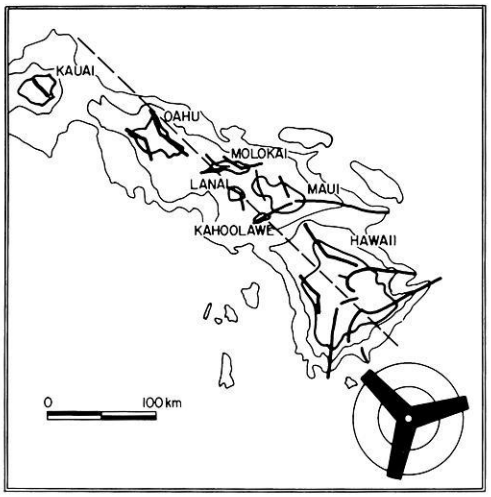

Fig. 2. Topographic map of the southeastern part of the Islands of Hawaii, Rift zones of major volcanoes from Fiske and Jackson (1972) are heavy lines. The dashed line is an approximation of the azimuthal trend of the islands shown. The shematic plume-generated triple rift zone SE of Hawaii represents the expected tectonic structure of the next island that will be generated by this hotspot

The opening and maintaining of the rift zones may be understood as huge hydrofracture experiments. The injections of magma originate from the shallow summit chamber. While the summit deflates, magma is propagating laterally at a few kilometers depth below the rift, opening cracks against the least compressive horizontal stress, with the crack (rift) propagating in the direction of the greatest principal horizontal stress. The orientation of the greatest and least principal horizontal stresses in the crust have been mapped on the basis of the strike of dike and rift systems. For instance, Nakamura et al. (1977) used the major dikes of Aleutian volcanoes to map the direction of the greatest principal stress in the horizontal plane, which was found to be oriented parallel to the local slip vector of the Pacific relative to American plate.

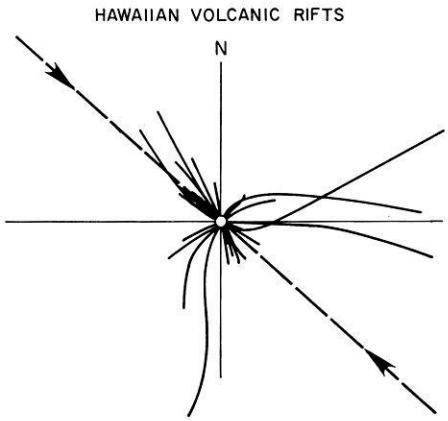

Fig. 3. Rose diagram showing 33 Hawaiian rift segments radiating from a single imaginary hotspot center (from Fiske and Jackson, 1972). The dashed line is the strike of that segment of the Hawaiian Island chain shown in Fig. 2, which is the segment where the rifts are located

From the orientation of Hawaiian rifts (Figs. 1–3), I conclude that the stress field in the Hawaiian crust is characterized by compression pointing radially away from Hawaiian volcanoe summits, with extension oriented tangentially to circles around these summits. Endo and Rogers (1980) showed that earthquakes at approximately 40-km depth below the island of Hawaii also exhibit the same pattern of radially oriented *P*-axies. It is clear, therefore, that the stress field in the crust and lithosphere below the Hawaiian islands does not find its origin in dynamic forces acting on the whole Pacific plate as proposed by Jackson and Shaw (1975). Rather the radial stress field around each volcanic center must have been generated by forces at the hot spot. In a wide sense the stress field is plume-generated. As more high quality focal mechanisms become available for crustal earthquakes it is expected that the radial Hawaiian stress field will be mapped in more detail.

In addition to the radial nature of the stress field, Fig. 3 shows that Hawaiian rifts exhibit a triple-arm pattern, which remained constant in its orientation over the last few million years (the age of the island in Fig. 2). This triple-arm pattern is not commonly found in the andesitic volcanoes of subduction zones (e.g., Nakamura et al., 1977), but it is typical for the triple junctions described by Burke and Dewey (1973).

In the part of the island chain from which the data were taken the azimuth of the chain is 315° in the average, and 326° for the best data on the youngest islands (Fig. 2). The overall strike (294°) of the island-seamount chain, including the portion not represented by the rift data, was inappropriately used by Fiske and Jackson (1972) for comparison. Since the recent island chain direction is within a few degrees the same as one of the preferred major rift azimuths (322°), I conclude that the island chain controls the directions of the three arms by a mechanism which is demonstrated by the newly emerging volcano Loihi southeast of Hawaii (Moore et al., 1979).

From the submarine topography I conclude that Loihi is located at the center of a crack which built up a rift in the direction NNW-SSE (Fig. 1). This direction closely parallels the radial compressive stress field due to the active volcanoes Kilauea and Mauna Loa. Since the rifts of these volcanoes extend to distances away

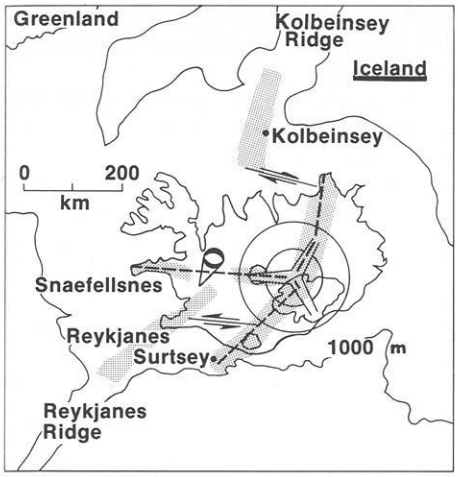

Fig. 4. Map of Iceland and mid-Atlantic rift system and 1000-m depth contour (After Sigurdsson, 1970). Shaded areas represent the neo-volcanic zones with focal mechanism from Einarsson et al. (1977). The approximate location of the plume center and its conjectured three rift arms are sketched in. It is postulated that the actual trend of two of the arms (*dashed*) is due to the dominance of the extensional stress field perpendicular to the mid-Atlantic spreading axis

from the summits beyond the location of Loihi (Fig. 1) I conclude that at Loihi magma was injected into a crust which is located within the radial stress fields of Kilauea and Mauna-Loa. If each new volcano originates in the stress field of the last ones but is located to the southeast, in accordance with the Pacific plate motion, one would expect that the initial rift will develop in the island chain direction approximately. After a new volcano like Loihi grows to be the major focus of the hot spot, it will create its own radial stress field. Then it will change from a one-crack volcano to one with the triple-arm pattern. In this way new islands with rift systems as shown schematically in Fig. 2 will be created in the distant future.

This model of the origin of Hawaiian rifts and their orientation differs from that of Fiske and Jackson (1972), who proposed that the rift orientations are controlled by local topography. I contend that on the contrary as rifts develop they orient themselves according to the local stress field and subsequently build up, by repeated fissure eruptions, the ridge topography found along them. This process is demonstrated by the Loihi rift which developed on the lowest part and beyond the gently sloping edifice of Hawaii (i.e., at oceanic depths exceeding 4,500 m). I suggest that when Loihi originally developed there was no local ridge to dictate the orientation of its rift, as required by the mechanism proposed by Fiske and Jackson (1972). Instead, the rift oriented itself according to the radial stress field of Kilauea, and then gradually a ridge was built up by eruptions along the rift.

The Hawaiian rifts show curvature and directions deviating locally from the directions expected from an ideal three-arm system generated by a plume. These deviations reflect local perturbations of the crustal stress field. The major source for such deviations are probably the proximity and buttressing of older volcanoes which existed at the time newer ones started to develop. For instance, the simultaneous activity of Mauna Loa will influence the stress field around the newer volcano Kilauea (Fiske and Jackson, 1972).

Iceland

Iceland is a major hotspot located on an actively spreading ridge in contrast to the Hawaiian hot spot. The shallow banks connecting Iceland to Greenland and Europe are taken to be the traces left by the hot spot on the respective plates. The distribution of recent volcanism in Iceland has been the subject of controversy (Pálmason and Saemundsson, 1974). The Reykjanes Ridge continues on land in Southwest Iceland in the form of the 'western volcanic zone' (Fig. 4). However, half way through Iceland this zone terminates, or turns into a neo-volcanic zone with an easterly trend to meet the 'eastern volcanic zone'. The latter crosses Iceland from Surtsey in the south to Tjörnes in the north, were a transform fault connects it to the Kolbeinsey Ridge (Saemundsson, 1974; 1978). In addition, the central EW volcanic zone is continued to the west in the Snaefellsnes volcanic zone. Opponents of the sea floor spreading idea have taken this distribution of neo-volcanic zones to indicate that spreading is not taking place in Iceland. The major facts unexplained by sea floor spreading are the transverse volcanic zone in central Iceland and Snaefellsnes, as well as the lack of a transform connection to the Atlantic spreading axis at the southern termination of the eastern volcanic zone at Surtsey. The transform fault proposed by Ward (1971) is located north of Surtsey and Heimaey along the southern coast of the main island.

If the center of the Iceland hot spot is assumed to be located as indicated in Fig. 4, one finds that the east-west volcanic zone and the northern half of the eastern volcanic zone almost perfectly fit the expected relative directions of two rift arms. The southern part of the eastern volcanic zone (terminating at Surtsey) may be the third arm. However, its direction does not match the expected direction. Instead of indicating a radially symetrical stress field of tangential tensional stress surrounding the center of the hot spot, the rifts that should run in azimuths of NNE and SE orient themselves N and SW instead. We note that these latter directions are those of the closest parts of the Atlantic spreading ridge to the N and S of Iceland, respectively. Drastic deviations of dike orientation from radial can be explained by superposition of a regional tectonic stress field and the radial stress field of a volcanic center (Muller and Pollard, 1977). In analogy, I postulate that the extensional stress field perpendicular to the spreading Reykjanes Ridge caused the arm that should have trended SE to turn into a southwestern direction so that intrusive dikes opened against the regional least compressive stress. The rift-arm orientation suggests that the regional tectonic stress field due to the mid-Atlantic ridge dominated over the plume induced stress field. This interpretation implies that the extensional stress field of oceanic ridges is still strongly extensional in the plates at distances of 200 km from the sea floor spreading centers.

The northern part of the Reykjanes Ridge deviates to the east from the trend in the southern part of the ridge, and the mid-Atlantic spreading direction is not perpendicular to the northern Reykjanes Ridge. This peculiarity can be explained by speculating that the Iceland plume-generated radial stress field is perturbing the mid-Atlantic spreading stress field enough to change the direction of the crack which can open easiest against the least compressive stress.

The same explanation can be offered for the deviating trend of the southern Kolbeinsey ridge. While the northern part of this ridge strikes NNE, its southern part swings around to a N-S direction pointing more towards the plume center.

Several authors have interpreted the Snaefellsnes and the central valcanic zone as a right-lateral fracture zone and transform

fault (e.g., Sigurdsson, 1970; Schäfer, 1972). However, Einarsson et al. (1977) found focal mechanisms in the Borgarfjordur area which indicated NS extension (Fig. 4). This observation strongly supports the idea that the Snaefellsnes volcanic zone is the third plume-generated rift arm. Einarsson et al. (1977) and Einarsson (1979) offered the hypothesis of a plume-related origin of the Snaefellsnes volcanic zone as one of the two most likely explanations. Based on the fact that the center of the plume identified here is almost identical with that suggested by geochemical data (Sigvaldason et al., 1974), and that there is a close resemblance between Iceland and Hawaiian rift systems, I believe that the distribution of Icelandic volcanism represents the three rift arms of the Icelandic hot spot.

Conclusions

The geometrical similarity of the three-rift-arm pattern between Iceland and Hawaii is striking (Figs. 2 and 4). However, there are also some differences: In Iceland at least one rift arm is strongly deflected in its direction by the regional stress field which evidently is extensional perpendicular to the Reykjanes ridge. Also the Iceland hotspot is much larger than the Hawaiian one. Within the three Icelandic rift arms there are volcanoes of the size of Kilauea which seem to have their own feeder systems and which cause their own rifting episodes (e.g., Björnsson et al., 1977). To what extent a volcano like Krafla can be compared with craters within, say, Kilauea's rifts is beyond the scope of this paper. While the dominating forces creating the stress fields may be different at plate boundaries from those at intra-plate hot spots, it seems of interest to point out that the over-all patterns of rifting in Iceland and Hawaii are similar to each other and closely resemble the three-rift-arm pattern commonly associated with plumes.

Acknowledgements. I thank K. Nakamura, P. Einarsson, F. Klein, and D. McKenzie for helpful criticisms. This work was supported by NSF grant No. EAR 78–03633.

References

Björnsson, A., Saemundsson, D., Einarsson, P., Tryggvasson, E., Grönvold, K.: Current rifting episode in north Iceland. Nature **266**, 318, 1977

Burke, K., Dewey, J.F.: Plume generated triple junctions. J. Geol. **81**, 406, 1973

Dewey, J.F., Burke, F.: Hot spots and continental break-up: Implications for collisional orogeny. Geology **2**, 57, 1974

Einarsson, P., Klein, F.W., Björnsson, S.: The Borgarfjördur earthquakes of 1974 in west Iceland. Bull. Seismol. Soc. Am. **67**, 187, 1977

Einarsson, P.: Seismicity and earthquake focal mechanisms along the Mid-Atlantic plate boundary between Iceland and the Azores. Tectonophysics, in press, 1979

Endo, E.T., Rogers, D.B.: Focal mechanisms for upper-mantle earthquakes and flexure of the lithosphere near Hawaii. J. Geophys. Res., in press, 1980

Fiske, R.S., Jackson, E.D.: Orientation and growth of Hawaiian volcanic rifts: The effect of regional structure and gravitational stress. Proc. R. Soc. London, Ser. A: **329**, 299, 1972

Hoffman, P., Dewey, J.F., Burke, K.: Aulacogens and their genetic relation to geosynclines, with a proterozoic example from Great Slave Lake, Canada. Soc. Econ. Paleontol. Mineral. Spec. Publ. 1974

Jackson, E.D., Shaw, H.R.: Stress fields in central portions of the Pacific Plate: delineated in time by linear volcanic chains. J. Geophys. Res. **80**, 1861, 1975

Macdonald, G.A.: The structure of Hawaiian volcanoes. Nederlands Geol. Mijnbouwkundig. Genootschap. Verhandelingen **16**, 274, 1956

Moore, J.G., Normark, W.R., Lipman, P.: Loihi Seamount – a young submarine Hawaiian volcano. Hawaii Symp. on Intraplate and Submarine Volcanism, in press, 1979

Morgan, W.J.: Convection plumes in the lower mantle. Nature **230**, 42, 1971

Morgan, W.J.: Plate motions and deep mantle convection. Geol. Soc. Am. Mem. **132**, 7, 1972

Muller, O.H., Pollard, D.D.: The stress strate near Spanish Peaks, Colorado, determined from a dike pattern. Pure Appl. Geophys. **115**, 69, 1977

Nakamura, K., Jacobs, K.H., Davies, J.N.: Volcanoes as possible indicators of tectonic stress orientation – Aleutians and Alaska. Pure Appl. Geophys. **115**, 87, 1977

Pálmason, G., Saemundsson, K.: Iceland in relation to the Mid-Atlantic Ridge. Annu. Rev. Earth Planet. Sci. **2**, 25–50, 1974

Saemundsson, K.: Evolution of the axial rifting zone in northern Iceland and the Tjörnes fracture zone. Bull. Geol. Soc. Am. **85**, 459–506, 1974

Saemundsson, K.: Fissure swarms and central volcanoes of the neovolcanic zones of Iceland. Geol. J. Spec. Iss. **10**, 415–432, 1978

Schäfer, K.: Transform faults in Iceland. Geol. Rundsch. **61**, 942, 1972

Sigurdsson, H.: Structural origin and plate tectonics of the Snaefellsnes volcanic zone, western Iceland. Earth Planet. Sci. Lett. **10**, 129, 1970

Sigvaldason, G.E., Steinthorsson, S., Oskarsson, N., Insland, P.: Compositional variation in recent Icelandic tholeites and the Kverkfjöll hot spot. Nature **251**, 579, 1974

Ward, P.L.: New interpretation of the geology of Iceland. Geol. Soc. Am. Bull. **82**, 2991, 1971

Wegener, A.: The origin of continents and oceans. London: Methuen 1924

Wilson, J.T.: A possible origin of the Hawaiian Islands. Can. J. Phys. **41**, 863, 1963

Received May 29, 1979; Revised Version August 13, 1979

J. Geophys. 47, 23–30, 1980

Journal of Geophysics

Observations of the Morphology and Structure of the Sea Floor South and West of Iceland

G.L. Johnson[1] and G. Pálmason[2]

[1] Office of Naval Research, Arlington, Virginia 22217, USA
[2] National Energy Authority, Reykjavik, Iceland

Abstract. Two submarine canyons with well developed levees are present on the insular margin of southern Iceland. In response to the Coriolis force the western levee predominates, except near the source region. Active redistribution of bottom sediment is apparent in the Denmark Strait, and also along the flanks of the Reykjanes Ridge. Data from a multi-channel seismic reflection line may be interpreted to indicate rocks of recent volcanic origin present on the shelf west of Snaefellsnes peninsula. An anomalous flat reflector on the eastern flanks of the Reykjanes Ridge may represent extrusive basaltic layers.

Key words: Iceland – Insular margin – Seafloor morphology – Submarine canyons – Sediment ridges – Shelf structure.

Introduction

Iceland is geographically part of the mid-ocean ridge; however, it is anomalous in that it is subaerial, although it may be no more atypical than other segments of the ridge. Volcanic and tectonic activity on Iceland distributed over a broad complex zone does, however, depart from the simplicity of the typical Mid-Oceanic Ridge. This has led to speculation that Iceland sits astride a hot spot in the Earth's asthenosphere. As a classic example of the geodynamic processes, a plethora of scientific articles have appeared about various aspects of the geology/geophysics of Iceland and environs in the last decade. Rather than cite a long list of notable articles, the reader is referred to Kristjánsson (1974) and Pálmason and Saemundsson (1974).

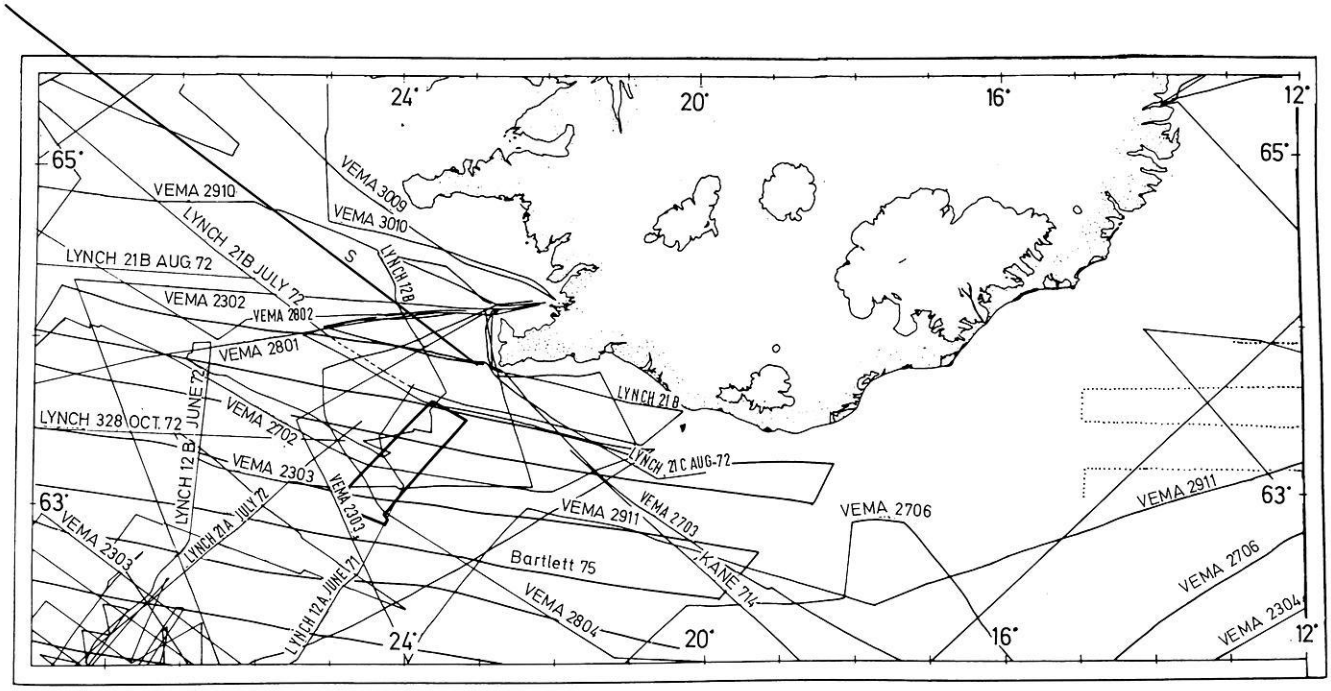

Fig. 1. Seismic records taken in the vicinity of Iceland which were utilized in this study. *Dotted lines* are KEATHLEY data (Johnson and Tanner, 1971). *Boxed area* is detailed study (Jakobsson and Johnson, in preparation). *Heavy line*, marked 'S', denotes location of Fig. 8

0340-062X/80/0047/0023/$01.60

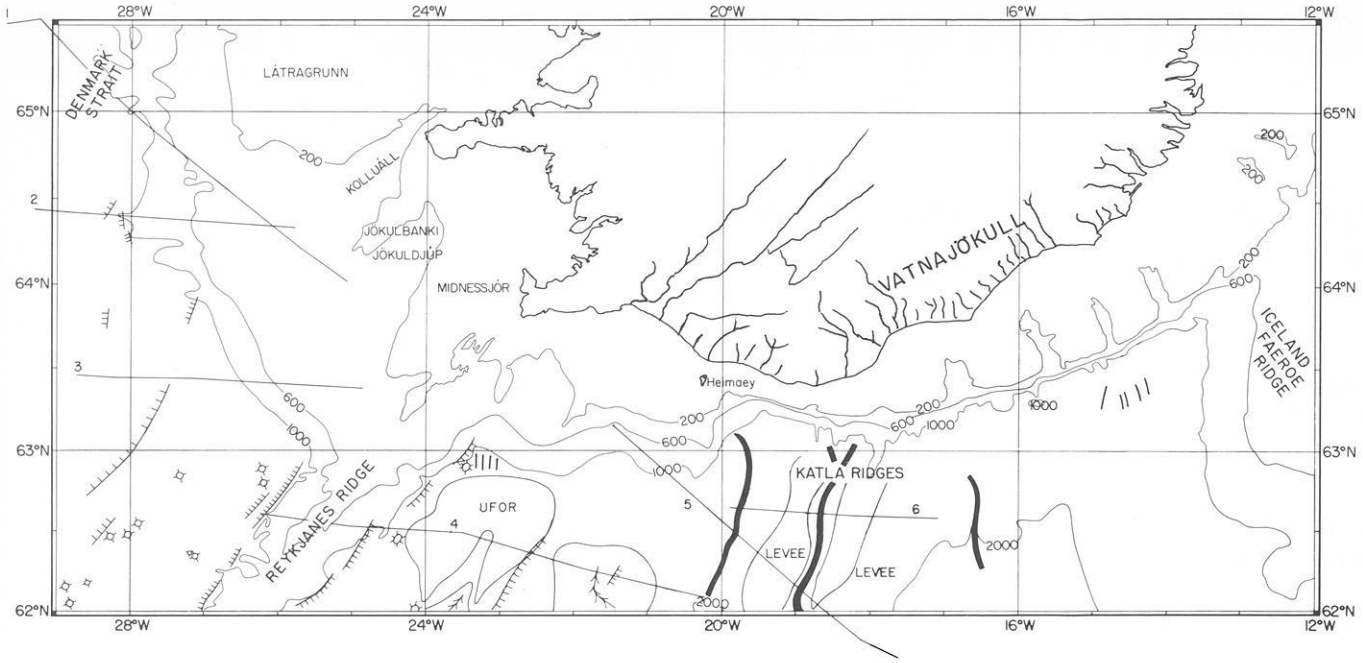

Fig. 2. Location of seismic lines shown in Figs. 3, 4, 6, and 7 and physiographic and structural features mentioned in the text. Submarine canyons are shown by *solid black lines*, sedimentary drifts by connected inverted v's to delineate axes. *UFOR* denotes areas of ultra-flat opaque reflectors

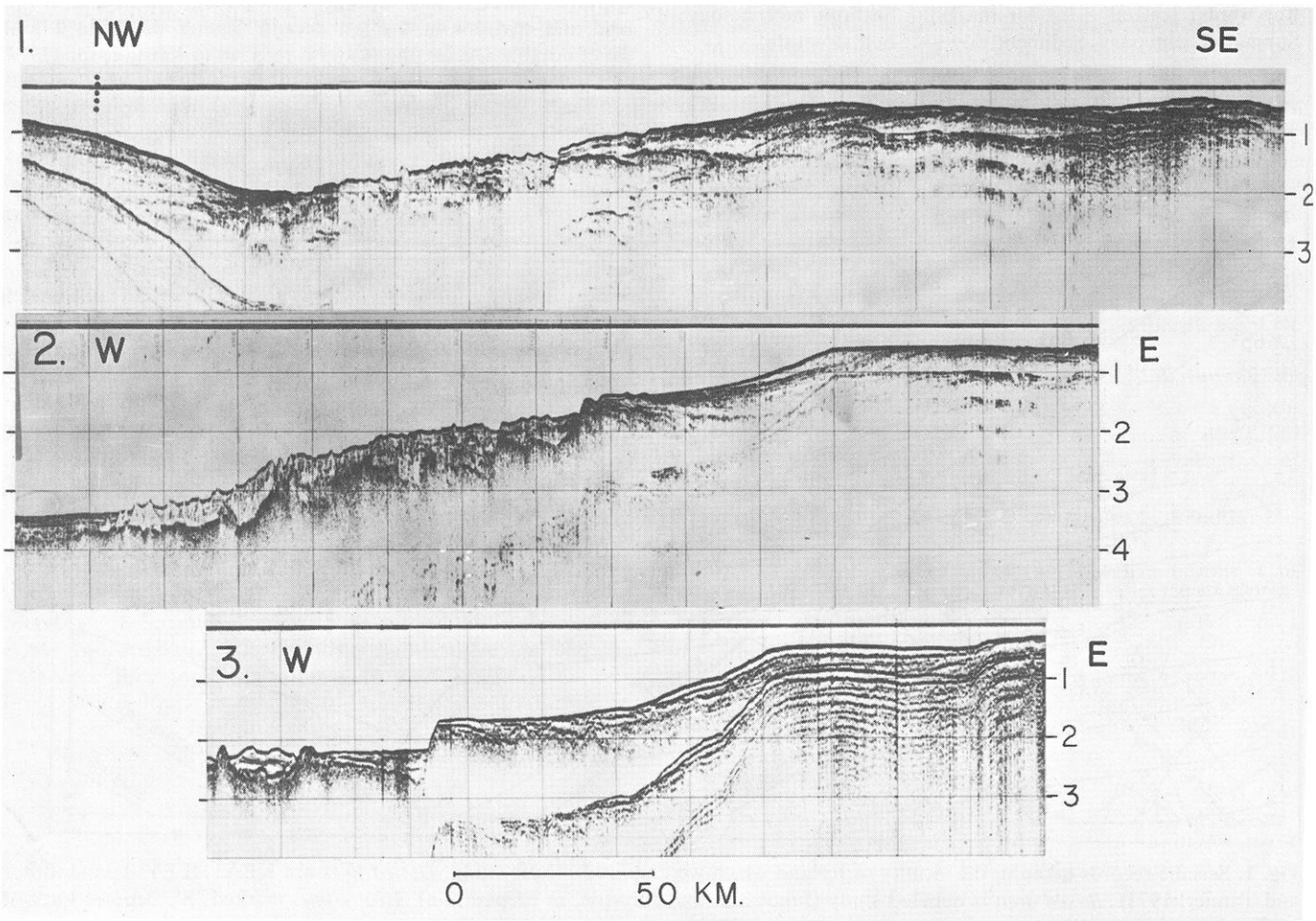

Fig. 3. Seismic reflection lines crossing the southwestern insular margin of Iceland. One second of travel time equals about 1 km. See Fig. 2 for index

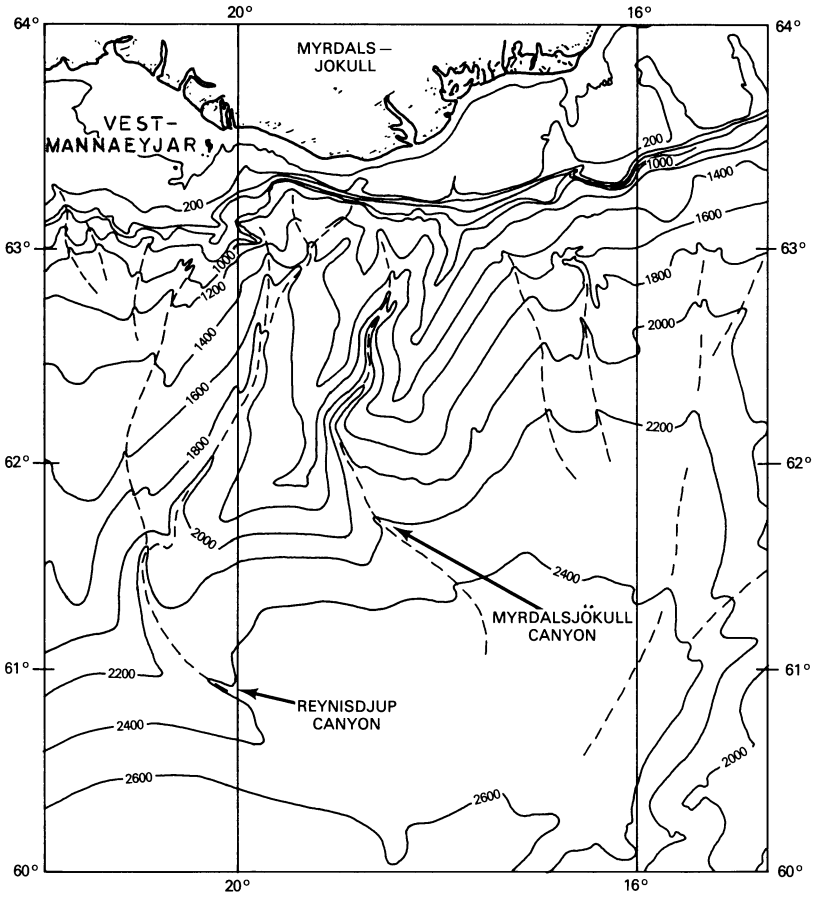

Fig. 4. Bathymetric contour chart of the southern insular margin. Basic chart courtesy of J. Gilg, U.S. Naval Oceanographic Office. Depths in meters

The purpose of this paper is to examine the insular margin of Iceland (with emphasis on its southern margin) and its evolution and relationship to the adjacent island and sea floor. Figure 1 shows some ship tracks in the area. In addition, a survey of the shelf to a distance of about 100 km from the coast was made in 1972–1973 with a line spacing of about 10 km.

Morphology

Shelf and Slope

Iceland is surrounded by a shelf of shallow depth, mostly 100–300 m, with an area larger than that of Iceland itself. The shelf is in some places relatively narrow, especially in the south where its width is 15 km. The bathymetry is more complicated where the crest of the Mid-Atlantic Ridge enters the shelf and a series of *en echelon* elongate topographic highs are present. In some parts of the shelf shallow, wide valleys are found with a relief of 100–150 m, many of them located in front of the main present-day rivers on the shore (Fig. 2). The insular slope is steep on the southeast margin averaging 1·15. This may be a reflection of swift bottom currents scouring the sea bed. The slope to the west is more gentle averaging 1 120 which is gentler than defined continental slopes (Profiles 1–3, Fig. 3), (Heezen et al. 1959). An extensive study of the continental shelf and environs based on seismic reflection data is found in Egloff and Johnson (1979).

The southeastern insular slope and rise are dissected by an extensive submarine canyon system which is of interest.

Submarine Canyons

The Maury Channel is the major sea floor canyon system in the Northeast Atlantic (Ruddiman et al. 1972). The northern continuation of Maury Channel is a broad trough (with two deep axes) which contains Maury Fan. One axis points northeast toward the Faeroe Bank Channel. The second deep axis turns north-northwest toward large youthful canyons cut into the southeast slope of Iceland.

This study reinforces the suggestion by Davies and Laughton (1972) that probably the major headwater canyon is presently incised into the insular slope and rise of southern Iceland. This canyon (Mýrdalsjökull) has a subsidary yazoo canyon (Reynisdjúp) along the base of its western levee (Figs. 4–6). Numerous smaller canyons are also present on the insular rise (Fig. 3), all of which contribute turbidite debris to the Maury Fan. These are the tributaries of the Maury Channel system which disperses Icelandic sediment, introduced mainly by subaerial and subglacial eruptions (jökulhlaups) as far as the Iberian Basin. Ruddiman et al. (1972) have suggested that the total volume of Maury Channel and Fan sediments is over 30,000 km^3, excluding sediment which has been carried south to the Biscay Abyssal Plain.

The major canyon is named Mýrdalsjökull Canyon, after an ice cap on the shore which covers the central volcano Katla. Katla has probably erupted about twenty times since the settlement of Iceland, the last eruption in 1918 causing discharges of water estimated to have reached a maximum of 100,000–200,000 m^3/s (Einarsson, 1978). Such enormous discharges are believed to be the prime source of this major submarine canyon.

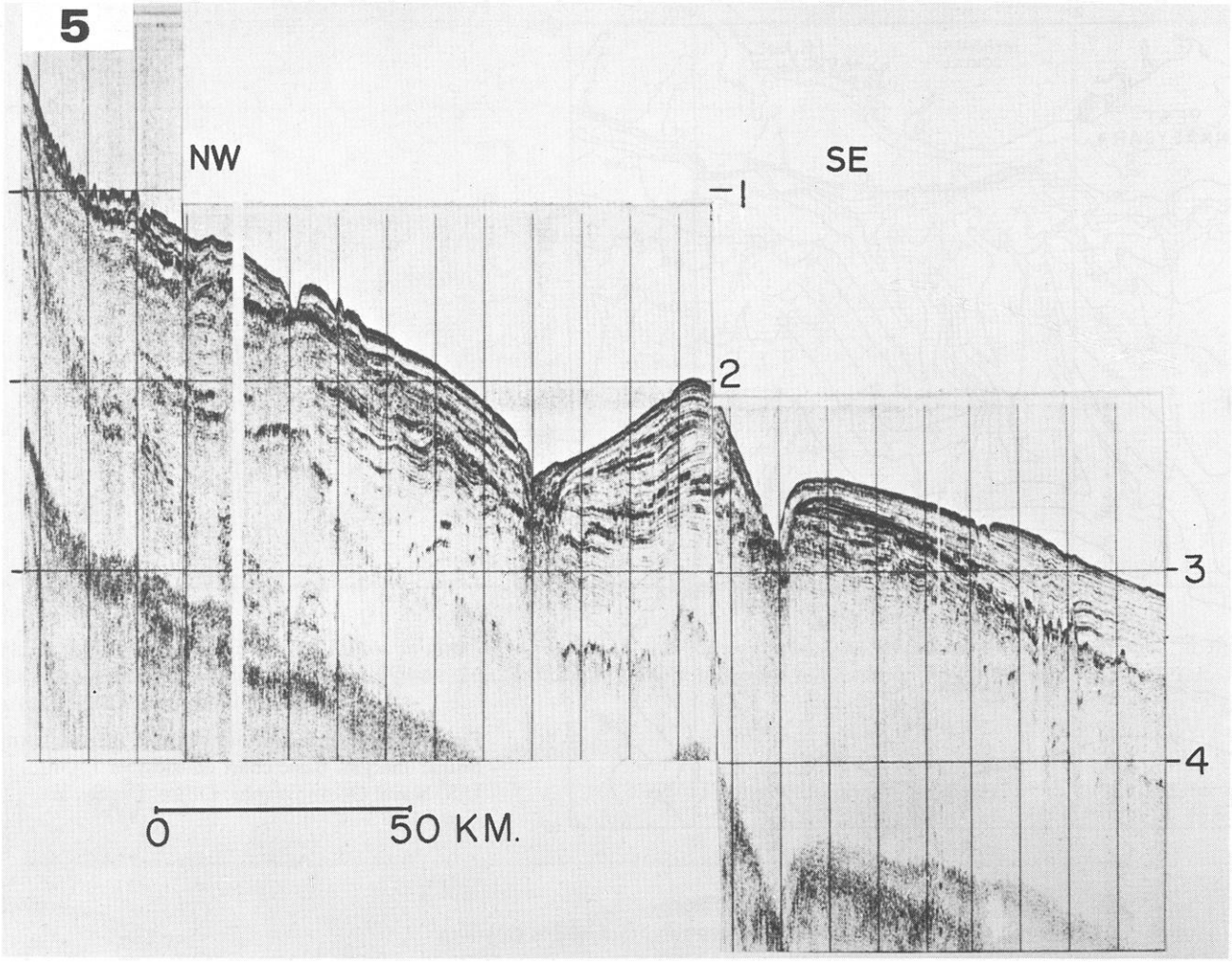

Fig. 5. Seismic reflection line across Mýrdalsjökull and Reynisdjúp Canyons. One second of travel time equals about 1 km. West is on the left. See Fig. 2 for index

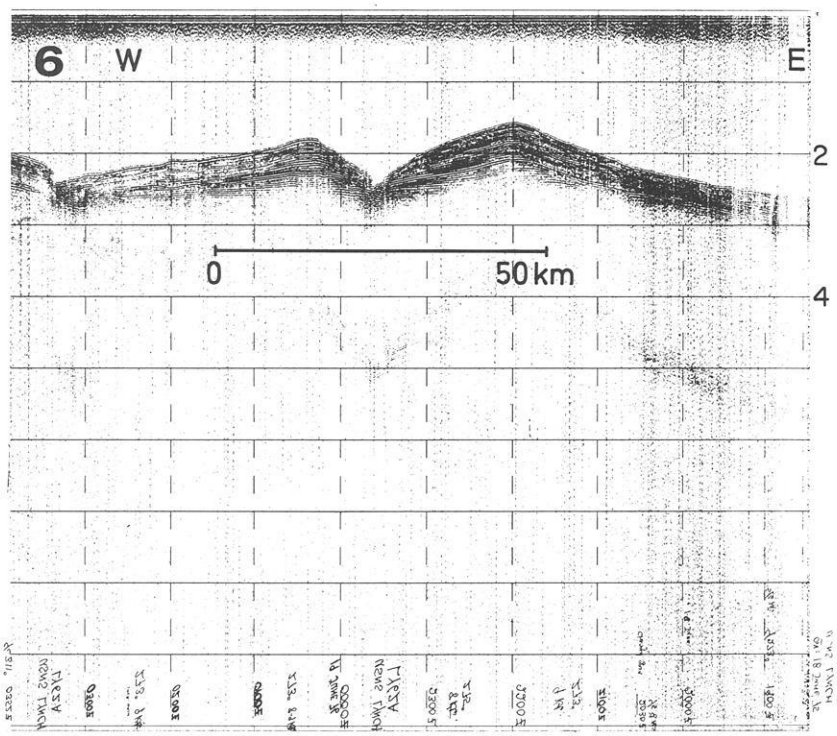

Fig. 6. Seismic reflection line across Mýrdalsjökull and Reynisdjúp Canyons. One second of travel time equals about 1 km. Profile length 140 km. See Fig. 2 for index

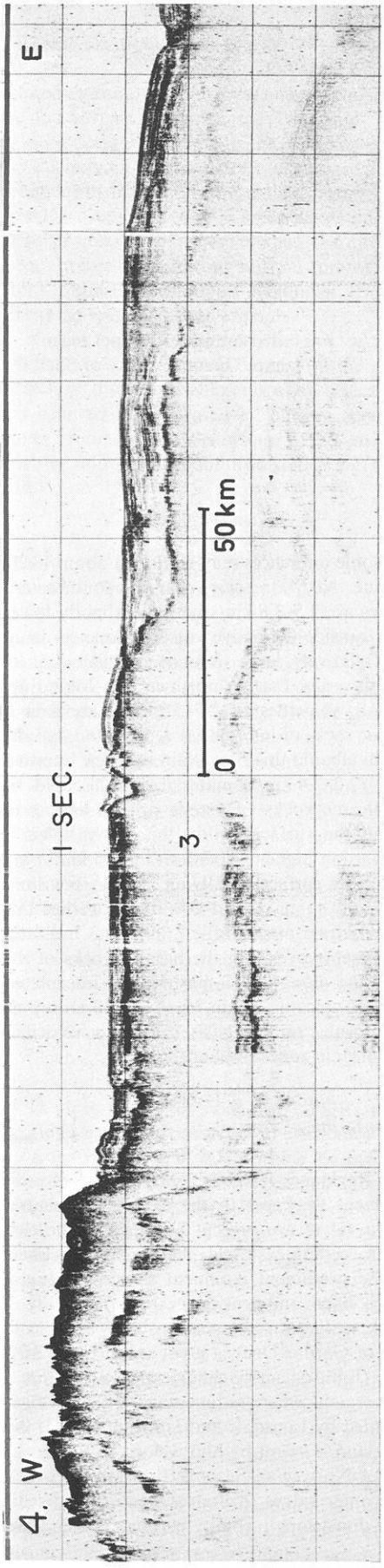

The levees (Katla Ridges) of Mýrdalsjökull Canyon, except within 40 km of the shelf, are higher on the western side (Figs. 4–6). Since a bottom current flowing down the canyon should tilt upward from left to right (looking downstream in the northern hemisphere) and thus deposit sediment preferentially on its western levee, the differential bank heights can be explained as an effect of the rotation of the Earth (Coriolis force). This effect is well documented in the Northwest Atlantic Mid-Ocean Canyon (Heezen et al. 1969). As can be seen in Fig. 6 along the base of the canyon, active erosion or at least non-deposition has formed a small western scarp whereas to the east the canyon floor/wall is more gentle. This is presumably caused by the core of the turbidity current being held against the western bank by the Coriolis force. Neither canyon appears to have buried axes at depth suggesting they are of Plio-Pleistocene origin. Some westward migration of Reynisdjúp Canyon is apparent in Fig. 6; this is presumably a response to the upbuilding of the western levee of Mýrdalsjökull Canyon as well as the Coriolis force. Mýrdalsjökull Canyon apparently has not migrated although deeper sedimentary layers of the eastern levee show some evidence of western migration (Fig. 5). Mýrdalsjökull Canyon is eventually forced to flow eastward along the axis of maximum depth where it is assumed to join the Maury Channel system and eventually debouch in the Biscay Abyssal Plain (Fig. 4).

Reykjanes Ridge

Dietrich (1959) and Ulrich (1960) first defined the morphology of the Reykjanes Ridge. Talwani et al. (1971) extended the knowledge base and related the morphology to other geophysical parameters. In the area of this study the crustal zone is bounded by steep scarps giving a horst-like profile (Fig. 7). As noted by Johnson et al. (1976), this morphologic shape is characteristic of the Mid-Ocean Ridge near hot spots such as Galapagos and Bouvet. North of 63°25′ the horst type topography gives way to *en echelon* linear ridges and occasional volcanic cones (Jakobsson and Johnson, in preparation).

The ridge flanks have generally subdued relief with redistribution by bottom currents the dominant dynamic force (Egloff and Johnson, 1979). This tends to mask prominent crustal scarps (Fig. 7) which occur on both sides of the ridge axis. The more distant scarps, about 135 km equidistant from the axis, are located on magnetic anomaly 6 (21 Ma) (Herron and Talwani, 1972) (Fig. 2). The faults bounding the central horst are coincident with anomaly 2 (3 Ma). Prominent scarps, too, are present on the western insular margin of Iceland (Fig. 3, Profiles 2 and 3). These scarps appear to be regional rather than local and occur in sediment covered, shoaling, rough basement forming the Iceland Plateau (Fig. 2). In Profile 3 (Fig. 3) the fault block is an excellent example of antithetic faulting.

Sediment Cover

Shelf and Slope

The seismic reflection data on the shelf and slope of Iceland is limited primarily to data obtained with single channel equipment

Fig. 7. Seismic reflection line across the crest of the Reykjanes Ridge and UFOR province. Line courtesy of J. Egloff. One second of travel time equals about 1 km. Profile length 248 km. See Fig. 2 for index

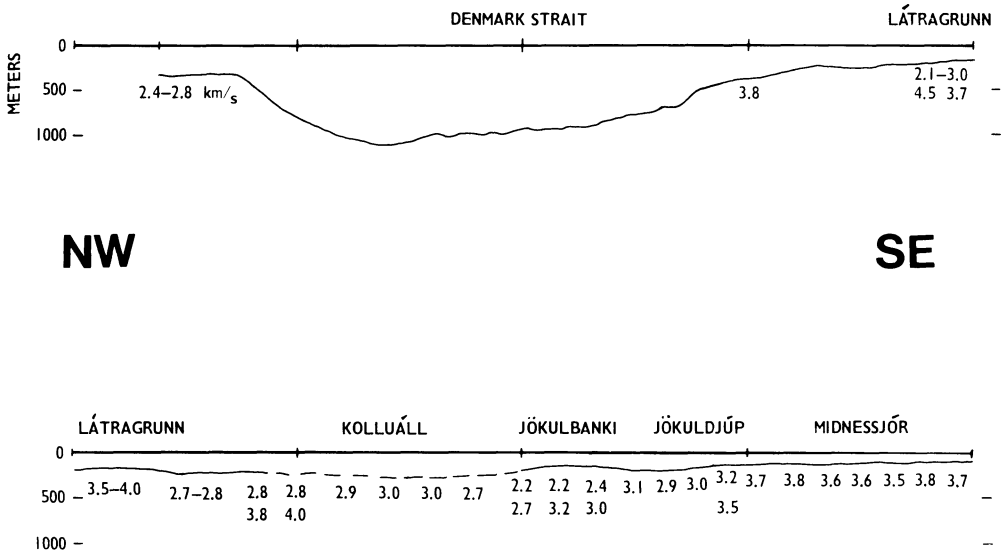

Fig. 8. Subbottom seismic velocities along line S (Fig. 1) based on multi-channel seismic survey. Data courtesy of Shell Oil Co

which has only limited penetration. It is possible, however, to determine that at least west of 25° W the shelf consists of seaward dipping truncated strata overlain by approximately 100–200 m of horizontal layers (Fig. 3, Profiles 2 and 3). The erosion of the deeper layers is most probably caused by scraping by the Pleistocene insular ice sheet and subsequent wave erosion as sea levels rose with retreat of the glaciers. A similar geologic sequence is present on the Jan Mayen Ridge although in that case, the overlying horizontal layers consist of 100–300 m of Pleistocene to middle Late Oligocene sediment (Johnson, 1975).

Total-intensity magnetic anomalies reported by Kristjánsson (1976) reflect a change in the structure of the southern Iceland shelf at 20° W, which was also noted by Pálmason (1974). The western part has subdued magnetic relief indicating basement (basalt) depth of at least 400 m. On the eastern part of the shelf there occur pronounced edge anomalies, apparently due to a basement step of at least 1 km mean thickness and of mean width 3–4 km (Fig. 2).

Supporting evidence of the nature of the southern Iceland shelf comes from a 1565 m-deep hole, drilled in 1964 in Heimaey (Pálmason et al., 1965; Tómasson, 1967). The uppermost 180 m are volcanics forming the base of the Westman Islands. This is followed by about 600 m of mostly sediments, containing foraminifera shells, and thus deposited in a marine environment (Einarsson, 1978). The lowest 500 m or so in the hole are basalt lavas, considered to be of Tertiary age.

The available data as summarized by Pálmason (1974) indicate that the shelf is built chiefly of basalts and that sediments from land have been deposited mainly in front of the shelf margin. Volcanic activity and glacial action has then later modified the edge of the shelf (Egloff and Johnson, 1979). The shallow, more or less constant depth shelf would have been the combination of the above with shore erosion and isostatic readjustments. Figure 5 shows that the base of the insular slope of southern Iceland contains in excess of one kilometer of sediments. The stratification probably represents pulses of glacial erosion. The transparent layers reflect periods when pelagic or hemipelagic sedimentation dominated.

A single multi-channel seismic reflection line across the western shelf (S in Fig. 1) gives information on subbottom velocities at shallow depth (Fig. 8). By comparison with seismic velocities on land (Pálmason, 1971) some inferences may be drawn about likely rock types along the line. At Midnessjór, near the southeastern end of the line, velocities are 3.5–3.8 km/s which is slightly lower than for surface basalts outside the active volcanic zone on land, and might point to a relatively large amount of hyaloclastites or sediments in the basalt series. Farther northwest, in Jökuldjúp, Jökulbanki and Kolluáll, velocities of 2.7–3.2 km/s are found. This is typical of volcanic rocks of interglacial age on land, basalts and hyaloclastites. At Jökulbanki this is overlain by a few hundred meters of low velocity (2.2–2.4 km/s) material, which could be either sediments or volcanic rocks of recent origin, similar to the rock types found at the surface within the active volcanic zone on land. At Látragrunn higher velocities (3.5–4.5 km/s) are again found, typical of older surface basalts on land. A few hundred meters of low velocity material (2.1–3.0 km/s) overlies this near the shelf edge on Látragrunn. Profile 1 in Fig. 3 indicates that this material is sediments overlying the basaltic rocks of the shelf. The seismic velocities along line S may well be interpreted to indicate rocks of recent volcanic origin on the shelf southwest of the Snaefellsnes peninsula, on the basis of similar velocities in rocks of the active volcanic zones on land.

Reykjanes Ridge and Basin Floor

The crestal zone of the Reykjanes Ridge is nearly devoid of sediments. On Fig. 7, sediment thickness to the east of the central horst is variable. Up to 400 m are present adjacent to the east of the central Block. Proceeding eastward, the average thickness is about 200 m until the prominent basement scarp whereupon the thickness increases to 700 m and near the eastern end of Fig. 7 to over 1 km. This thick wedge of sediments probably represents the northern most part of Gardar Drift, a great sedimentary drift in the Eastern Atlantic (Johnson and Schneider, 1969). Figure 2 delineates two separate regions where sedimentary drifts have accumulated. As documented by Lonsdale and Hollister (1976), the insular rise of South Iceland is swept by high velocity (> 20 cm/s) thermohaline currents of Norwegian Sea overflow water, which have constructed large outer ridges (drifts) of hemipelagic sediment, and is crossed by downslope turbidity currents, which have eroded deep valleys.

The pelagic sedimentary cover of the Reykjanes Ridge and adjacent sea floor (Figs. 3 and 7) is not uniformly draped over the basement, but forms an undulating relief which is not directly related to the underlying basement. Ruddiman (1972) noted this on the eastern flanks of the Reykjanes Ridge and ascribed it to reworking of sediments by bottom currents. Talwani et al. (1971) noted the same effect in this region and deduced from sediment distribution patterns that bottom flow is strong enough to inhibit sedimentation in some areas, and preferentially deposit in other areas. From these studies, the authors suggested the existence of a relatively strong bottom current flowing southwestward along the eastern flank of Reykjanes Ridge and northeastward along the western flank.

Figure 3, Profile 1 across the axis of Denmark Strait shows a highly reflective channel flanked on the eastern side by a 60 km stretch of disturbed sediments. The undulations of the sea floor are believed to be caused by bottom currents creating sea-floor dunes (Johnson and Schneider, 1969) and active sculpturing of the sea floor by the southward flowing bottom currents (Shor and Poore, 1978).

Ultra-Flat Opaque Reflectors (UFORs)

As is apparent on Fig. 7, a peculiar seismic reflector, anomalously flat and opaque, hereafter referred to as a UFOR (Ultra-flat opaque reflector) is present. The difference between UFOR and normal basement is rather striking. The areal extent of these reflectors within our study is charted on Fig. 2. The UFORs seem to be arranged in slightly tilted terraces, separated by scarps, valleys, or stretches of normal basement. Within each such terrace, basement dips do not exceed 1.500. The traversed portions of the UFORs lie 2.1–2.5 km below sea level, and are buried by 0.3 to 0.5 km poorly stratified sediment, evidently reworked by strong bottom currents. These values assume an average velocity of 2.0 km/s in the sedimentary column. Water depth varies from 1,200 to 1,600 m, and crustal age is 3 to 4 Ma (Vogt and Johnson, 1973). Possible explanations for the UFORs include: 1 The reflector represents a highly consolidated sediment layer or a sill intruded more or less horizontally into a preexisting sediment layer; however, this is considered unlikely (Fridleifsson, 1977). 2. The reflector is volcanic ash, either directly deposited (pelagically draped) or redeposited, in nearly horizontal sheets, by by turbidity flow.

There is no mirror image of UFORs on the western side of the ridge axis, and therefore they cannot have been formed at the axis. Windows through which basement can be seen have been reported (J. Egloff, 1979, personal communication and therefore the volcanic ash hypothesis suggested by Vogt and Johnson (1973) may be valid. Therefore, until the reflector is drilled, the best estimate of its nature is that of extrusive basalt, but with an atypically low initial viscosity, or extruded at a higher than average rate and total quantity, such that the effects of rapid cooling and lithification in the submarine environment were overcome.

A much more detailed discussion of the various hypotheses of UFOR origin is contained in Vogt and Johnson (1973). They note that low inherent viscosity as well as rapid, voluminous discharge are characteristic of plateau basalts extruded on Iceland in middle to late Neogene times and, 60 to 55 Ma ago in the Faeroes, west and east Greenland, and Baffin Island. Similar flood basalts have occurred at various places during geological time, presumably all as the surface manifestation of mantle convection plumes or hot spots. There is every reason to expect similar flood basalts adjacent to oceanic hot spots such as Iceland. Other UFOR occurrences are in the North and central Atlantic and are found on anomalous crust created during proposed (on independent grounds) peaks in hot spot activity-around 80-60 and 140-110 Ma ago. This makes sense if the UFORs are submarine flood basalts (Vogt, 1972).

Conclusions

Dynamic geologic processes have been active in the area of this study. Sediment redistribution by bottom currents is the rule, with dune and drift structures being formed in the regions of maximum activity. Submarine canyons with well developed levees attest to the vigorous erosion of the insular platform.

Fault scarps parallel to the Reykjanes Ridge spreading center are conspicuous, as are areas of anomalous flat basement. The latter, found on the eastern flank of the Reykjanes Ridge, may represent extrusive basaltic layers.

References

Davies, T.A., Laughton, A.S. Sedimentary processes in the North Atlantic. Init. Rep. Deep Sea Drill. Proj. Washington, D.C.. U.S. Gov. Print. Office **12**, 905–934, 1972

Dietrich, G.. Zur Topographie und Morphologie des Meeresbodens im nordlichen Nord Atlantischen Ozean. Dtsch. Hydrogr Z., Ergänzungsheft Reihe B: 26–34, 1959

Egloff, J., Johnson, G.L. Erosional and depositional structures of the Southwest Iceland insular margin. Thirteen Geophysical Profiles, AAPG Memoir **29**, In: *Continental margins,* vr. 2a J.S. Watkins, L. Montadert, P.W. Dickson, eds.. pp. 43–63. Tulsa, Oklahoma 1979

Einarsson, Th. Jardfraedi (Geology). Mál og menning (Reykjavík), 3rd eds., 240 pp. 1978

Fridleiffson, I.B. Distribution of large basaltic intrusions in the Icelandic crust and the nature of the layer 2 – layer 3 boundary. Bull. Geol. Soc. Am. **88**, 1689–1693, 1977

Heezen, B.C., Johnson, G.L., Hollister, C.D. The Northwest Atlantic Mid-Ocean Canyon. Can. J. Earth Sci. **6**, 1441–1453, 1969

Heezen, B.C., Tharp, M., Ewing, M. The Floors of the Oceans, 1, The North Atlantic. 122 pp, Geol. Soc. Am. Spec. Pap. **65**, 1959

Herron, E.M., Talwani, M.. Magnetic anomalies on the Reykjanes Ridge. Nature **238**, 390–392, 1972

Johnson, G.L. The Jan Mayen Ridge. In. Canada's Continental Margins and Offshore Petroleum Exploration, C.J., Yorath, E.R., Parker, D.J. Glass, eds. Can. Soc. Petrol. Geol. Mem. **4**, 225–234, 1975

Johnson, G.L., Schneider, E.D. Depositional ridges in the North Atlantic. Earth Planet. Sci. Lett. **6**, 416–422, 1969

Johnson, G.L., Tanner, B. Geophysical observations on the Iceland-Faeroe Ridge. Jökull. **21**, 45–52, 1971

Johnson, G.L., Vogt, P.R., Hey, R., Campsie, J., Lowrie, A. Morphology and structure of the Galapagos Rise. Mar. Geol. **21**, 81–120, 1976

Kristjánsson, L. (ed.): Geodynamics of Iceland and the North Atlantic Area, 323 pp. Dordrecht, Boston. D. Reichel Publishing Company 1974

Kristjánsson, L.: A marine magnetic survey off southern Iceland. Mar. Geophys. Res. **2**, 315–326, 1976

Lonsdale, P., Hollister, C.D.: Cut-off of an abyssal meander on the Icelandic insular rise. Trans. Am. Geophys. Union **57**, 269, 1976

Pálmason, G. Crustal structure of Iceland from explosion seismology. Rit **40**, Soc. Sci. Isl. 187 pp. 1971

Pálmason, G. Insular margins of Iceland. In: The geology of continental margins, C.A. Burk, C.L. Drake, eds. pp. 375–379. Berlin, Heidelberg, New York: Springer 1974

Pálmason, G., Jónsson, J., Tómasson, J., Jónsson, I. Deep drilling in the Westman Islands (In Icelandic). Raforkumálastjóri, Reykjavík, 43 pp. (mimeographed), 1965

Pálmason, G., Saemundsson, K. Iceland in relation to the Mid-Atlantic Ridge. Ann. Rev. Earth Planet. Sci. **2**, 25–50, 1974

Ruddiman, W.F. Sediment redistribution on the Reykjanes Ridge: Seismic evidence. Geol. Soc. Am. Bull. **83**, 2039–2062, 1972

Ruddiman, W.F., Bowles, F.A. Molnia, B.: Maury channel and fan. 24th I.G.C., Sec. **8**, 100–107, 1972

Shor, A.N., Poore, R.Z.: Bottom currents entering the NE Atlantic from the Norwegian Sea. Initiation and development of modern day circulation (DSSP Leg 49). Trans. Am. Geophys. Union **59**, 296, 1978

Talwani, M., Windisch, C.C., Langseth, M.G.: Reykjanes Ridge crest: A detailed geophysical study. J. Geophys. Res. **76**, 473–517, 1971

Tómasson, J. On the origin of sedimentary water beneath Westman Islands. Jökull **17**, 300–311, 1967

Ulrich, J. Zur Topographie des Reykjanes-Rückens. Kiel. Meeresforsch. pp. 155–173, 1960

Vogt, P.R.: Evidence for global synchronism in mantle plume convection, and possible significance for geology. Nature **240**, 338–342, 1972

Vogt, P.R., Johnson, G.L. A longitudinal seismic reflection profile of the Reykjanes Ridge, Part II. Implications for mantle hot spot hypothesis. Earth Planet. Sci. Lett. **18**, 49–58, 1973

Received March 19, 1979; Accepted June 18, 1979

J. Geophys 47, 31–42, 1980

Journal of Geophysics

Stratigraphy and Paleomagnetism of the Esja, Eyrarfjall and Akrafjall Mountains, SW-Iceland

L. Kristjansson[1], I.B. Fridleifsson[2], and N.D. Watkins[3]†

[1] Science Institute, University of Iceland, Dunhaga 3, 107 Reykjavik, Iceland
[2] National Energy Authority, Grensasvegur 9, 108 Reykjavik, Iceland
[3] Graduate School of Oceanography, University of Rhode Island, USA

Abstract. Detailed geological and magnetic mapping in an area of Pliocene and Plio-Pleistocene volcanic rocks in Southwestern Iceland has enabled us to correlate a 2,100-m-thick lava succession with similar dated sequences in Iceland and with the ocean-floor geomagnetic polarity time scale. This correlation, supported by additional K-Ar dating, implies (1) that the succession is between 4.2 and 1.8 Ma in age, (2) that at least 13 glaciations occurred in Western and Southwestern Iceland between 3.1 and 1.8 Ma ago, and (3) that at least two geomagnetic events are present in the Lower Matuyama epoch.

Paleomagnetic results from 353 igneous units, mostly basalt lavas, are tabulated. Analysis of directions from 258 of these shows them to possess some serial correlation; their mean is very close to a central axial dipole field value, but explanations are proposed for observed systematic departures from this field in other Icelandic paleomagnetic survey results.

Key words: Paleomagnetism – Basalt lavas – Stratigraphy – Glaciations – Geomagnetic time scale – Iceland.

1. Introduction

The area around Hvalfjördur, (Fig. 1) is mostly built up of basalt lavas, and belongs to the uppermost part of the 'plateau basalt' succession of Western Iceland. Regional stratigraphic mapping in the area was initiated by Einarsson (1957) who successfully employed field measurements of remanence polarity in lavas to distinguish and correlate age groups. Further stratigraphic work in the Hvalfjördur area, as well as in the rest of Iceland, has continued to depend heavily on magnetic polarity mapping, and laboratory studies (Sigurgeirsson, 1957; Wilson et al., 1972) have confirmed Einarsson's polarity results in the area.

A few early K-Ar dates from the south shore of the fjord have been reviewed by Pálmason and Sæmundsson (1974); their reliability is low due to the high atmospheric argon content. Piper (1971) first suggested how Einarsson's local polarity groups might be correlated with the geomagnetic polarity time scale then available from dated formations (Cox, 1969). His interpretation included Einarsson's reversed groups R2 and R3 being equivalent to the lower Matuyama epoch. Fridleifsson (1973) and Fridleifsson

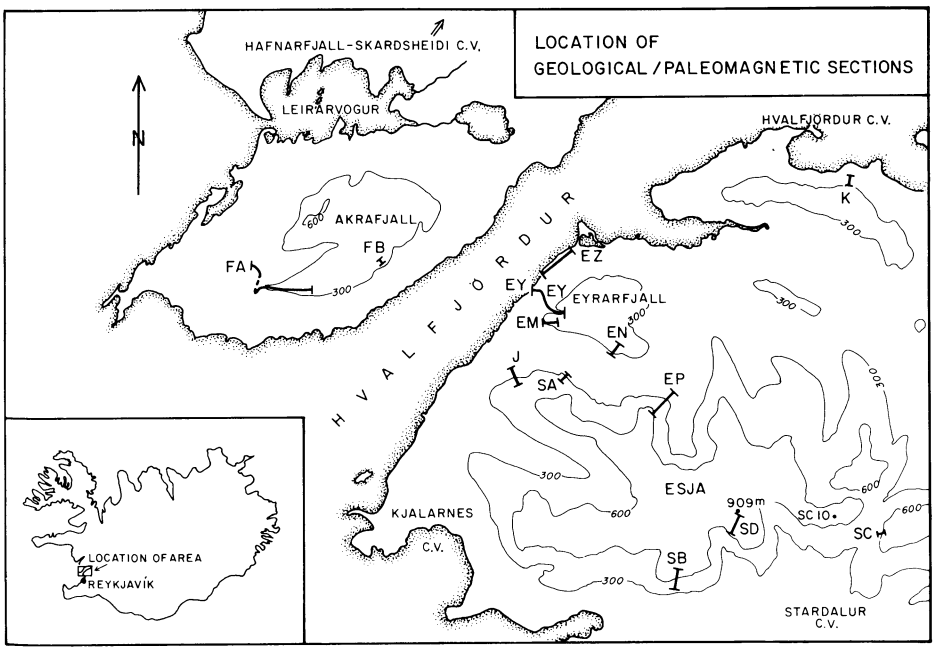

Fig. 1. Location of stratigraphic/paleomagnetic sections in Esja, Eyrarfjall, and Akrafjall. Sections *J*, *K* of Wilson et al. (1972) are also included

0340-062X/80/0047/0031/$02.40

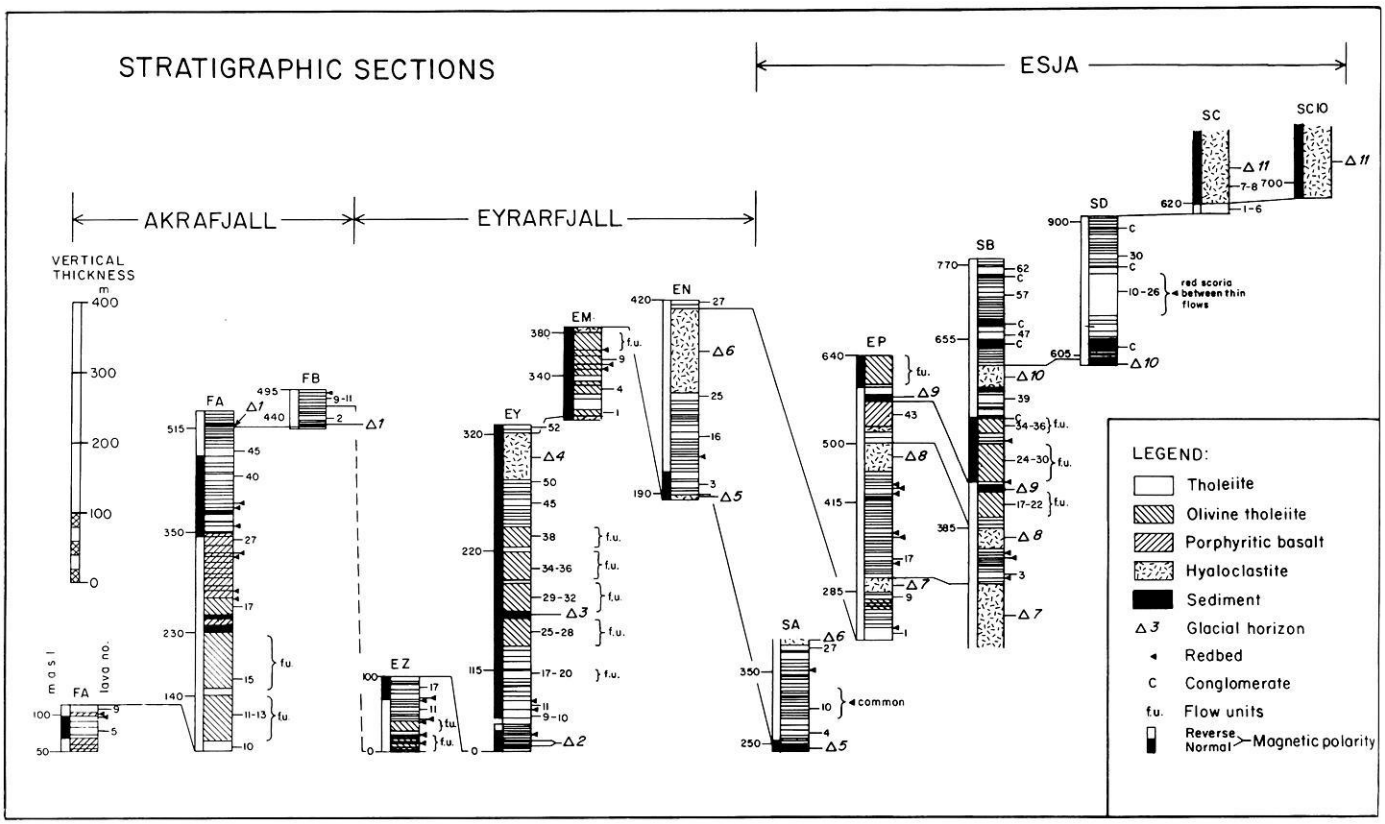

Fig. 2. Stratigraphy of each sampled section, showing lava types and polarities, formations of glacial origin, sediments, and stratigraphic ties between sections. Occasional numbers to the left of the columns are barometric altitudes

and Kristjansson (1972) subsequently assumed the thin group N3 in the Esja area to belong to the Olduvai event and N2, occurring at the top of the Esja volcanics, to belong to the Gilsá event.

In the course of detailed geological mapping of the Esja area (Fridleifsson, 1973) it appeared that a third event of normal magnetization might be present in continuously exposed cliff sections in the area. Sampling for laboratory measurements in Esja was therefore initiated by us in 1973 (Sect. SA, SB, SC), to help clarify the much disputed problem of the time intervals covered respectively by the Gilsá, Olduvai and Reunion events. AF treatment of samples showed, however, that the normal polarity remanence of the lowest event (lavas SB 1–5) was of secondary origin.

After these results were obtained it was decided to extend sampling to obtain a complete profile down to the oldest lavas exposed on the south shore of Hvalfjördur, interpreted as reaching into the middle Gauss epoch. Sections SD, EP, EM, EY, and EZ were therefore cored in 1974–1976, as well as section EN to replace badly altered lavas of section SA. Sections FA and FB on the northern side of the fjord were added in 1977.

2. Geology

2.1. Geological Setting

The research area (Fig. 1) lies 10–40 km west of the active Reykjanes-Langjökull volcanic zone. The rocks dip 5–8° southeastwards. Geological mapping suggests continuous volcanic activity within this segment of the zone since about 7 Ma to the present (Fridleifsson, 1973; Franzson, 1978; McDougall et al., 1977). The rate of volcanism was, however, not uniform as four central volcanoes were active in the vicinity of our cross section during the growth of the strata described here, and these are characterised by a very high extrusion rate. Our area lies 15–20 km S and SW of the Hafnarfjall-Skardsheidi and Hvalfjördur central volcanoes, and about 1–10 km north of the Kjalarnes and Stardalur central volcanoes (Fig. 1).

The area is bisected by a major fjord, Hvalfjördur, and the correlation across it is by no means certain. The geological mapping north of the fjord (Sect. FA, FB) was originally conducted by Franzson (1978) but our work south of the fjord is based on mapping of Eyrarfjall by students at the University of Iceland under the supervision of Dr. K. Saemundsson (Jonasson et al., 1973; Sects. EZ, EY, EM, EN) and on mapping of Esja by Fridleifsson (1973; Sects. SA, EP, SB, SC, SD).

All the sections were, however, selected and described specially as a part of the present study (Fig. 2). They are mostly in steep slopes with nearly complete outcrops. Farther east along the fjord, considerable mapping and sampling work has been carried out by Einarsson (1957), Piper (1971), Wilson et al. (1972) and by students; the latter work is not yet completed (K. Saemundsson, 1979, personal communication) and will not be discussed here.

2.2 Pliocene Strata

The profile starts in the mountain of Akrafjall, where Franzson (1978) interpreted the short normal polarity event of lavas FA 4–7 as belonging to the Nunivak event, and this view is maintained

here. Franzson found the Cochiti event missing both in Akrafjall and in the Hafnarfjall-Skardsheidi region farther north. McDougall et al. (1977) suggested that these two events were recorded as one in their Borgarfjördur profile.

The profile up to FA 51 is a typical Tertiary lava sequence with basaltic lavas (tholeiites, olivine tholeiites, and plagioclase-phyric tholeiites) separated by thin red partings. Two thick olivine tholeiite compound lavas occur. There are several thin sedimentary layers and one thick fluviatile conglomerate horizon (7–34 m, FA 15–16); it thickens eastwards and may represent a river bed.

Section FA begins in the sequence belonging to the last volcanic phase of the Hafnarfjall-Skardsheidi central volcano (Heidarhorn phase of Franzson, 1978). Section FA ends in, and FB is within, lavas that correspond to the onset of the Hvalfjördur central volcano (Heidarhorn tholeiite series of Franzson, 1978).

2.3 Plio-Pleistocene Strata

After the onset of glaciations, the character of the volcanic pile changed markedly. Instead of the relatively uniform lava sequence in the Pliocene part of the lava pile, the glaciations left their marks in the lava sequences in the form of widespread coarse conglomerate horizons (tillites) and more spectacularly by thick hyaloclasitite sequences which form by volcanic eruptions under ice sheets. After a glaciation, hyaloclastite ridges (with a pillow lava core enveloped by pillow breccias and tuffaceous hyaloclastites) with steep slopes are the dominant features of the topography. In subsequent volcanic eruptions, lava flows bank up against the hyaloclastites or flow down their slopes depending on the eruptive site. The lava may fill the valleys between the hyaloclastites and eventually bury them. Due to the rugged topography after a glaciation, valleys, a short distance apart, may be physically isolated from one another. Thus, an absence of volcanism in one valley may allow the development of aprons of sediment spreading out over the lava plains at the feet of the easily eroded hyaloclastite mountains, while simultaneous active volcanism in an adjacent valley may give rise to a pile of lavas with no sedimentary intercalations (Fridleifsson, 1973). One has therefore to be even more careful than in Pliocene strata in connecting profiles far apart. For this reason it was deemed necessary to let the paleomagnetic profiles overlap considerably with one another.

Glacial Horizon 1 The first major conglomerate horizon (5–22 m) is found between lavas FA 51–52 and FB 0–1. In western Akrafjall the lowest part of the horizon is a grey, ill sorted conglomerate with boulders up to 1.5 m i. d. (Franzson, 1978). It is found both in Akrafjall and Skardsheidi and occurs one to three lava flows above the lower boundary of what are interpreted as Mammoth event lavas (Franzson, 1978). This horizon has also been found in upper Borgarfjördur where glacial striations are found on the underlying basalt flow (Saemundsson and Noll, 1974). This is thought to be the lowest tillite horizon in western Iceland and has been dated at about 3.1 Ma (McDougall et al., 1977). A similar age was found for the lowermost tillite in NE Iceland (McDougall and Wensink, 1966), but there is evidence for even earlier cool-climate deposits in other parts of the country (McDougall et al., 1976; Johannesson, 1975; Albertsson, 1976).

Glacial Horizon 2. Coarse conglomerate, fluviatile sediment and siltstone, 10 m thick, occur between lavas EY 1–3. Striations are seen on the boulders (Jonasson et al., 1973). In the lava sequence between glacial horizons 2 and 3 there are two sediment horizons (2 m each) both of which have small pebbles of basalt and rhyolite (above EY 14 and EY 20).

Glacial Horizon 3. Coarse conglomerate with pebbles and boulders up to 30 cm set in a grey matrix, 5 m thick with 5 m of finer grained sediment above, lying between lavas EY 28–29.

Glacial Horizon 4. Fluviatile sediment with a conglomerate horizon (15–20 m) overlain by a hyaloclastite sequence (tuffaceous hyaloclastite, pillow breccia and pillow lava) 40–200 m thick, which thickens towards the Kjalarnes central volcano. It lies between lavas EY 50–51. The underlying tholeiite lavas are thought to represent the first volcanic phase of the Kjalarnes central volcano (Esja unit 3, Fridleifsson 1973).

Glacial Horizon 5. Tuffaceous hyaloclastite, pillow breccia and pillow lava, 10–200 m thick, between lavas EM 11–EN 1. It thickens towards the Kjalarnes central volcano. (Esja unit 7).

Glacial Horizon 6. Tuffaceous hyaloclastite, pillow lava and pillow breccia, 25–200 m thick, with a thin sedimentary base, lying between EN 25–26, right above SA 27, right under EP 1. (Esja unit 10).

Glacial Horizon 7. Tuffaceous hyaloclastite, pillow breccia and pillow lava, 20–300 m thick, underlain by conglomerate in SE-Esja, and occuring between EP 10–11, right under SB 1. (Esja unit 12, considered uppermost hyaloclastite belonging to the Kjalarnes central volcano).

Glacial Horizon 8. Tuffaceous hyaloclastite, pillow breccia and pillow lava, 10–200 m thick, succeeded by a 10 m grey, ill sorted conglomerate in N-Esja. (Esja unit 15). It occurs between EP 40–41 and SB 12–14.

Glacial Horizon 9. Tuffaceous hyaloclastite, pillow breccia and pillow lava in E-Esja, brown and grey, ill sorted conglomerates with pebbles up to 20 cm in W-Esja. Thickness ranges from 5–300 m. (Esja unit 18; forms the base of the Stardalur central volcano).

Glacial Horizon 10. Grey ill sorted conglomerate blanket with boulders commonly 20–30 cm and sometimes over 100 cm, about 20 m in W-Esja and over 100 m in E-Esja where it interfingers with up to 240 m-thick hyaloclastite sequence of basalt and basaltic andesite compositions with a minor rhyolite. This unit was formed after the collapse of the Stardalur caldera. (Esja unit 23). It lies between lavas SB 40–41, and right under SD 1. This major glacial horizon was noted by Pjeturss (1910), and Rutten (1958) referred to it as the morainic horizon at the base of the 'Graue Stufe', and drew the Tertiary-Pleistocene boundary at the base of the conglomerates.

The conglomerate horizon between lavas SB 36–37 could possibly represent a separate glaciation. Above Glacial horizon 10 there are similarly three major sediment/conglomerate horizons in profile SB, all of which are characterized by coarse conglomerate (with pebbles up to 20 cm and more rarely 50 cm) at the base, overlain by gravel and finer sediment. These are between SB 46–47 (15 m), SB 48–49 (10 m), and SB 61–62 (5 m). The thickness varies considerably along strike. In Sect. SD there are also three horizons with the same characteristics between lavas SD 3–4 (15 m), SD 27–28 (1.5 m), and SD 38–39 (3 m). The most likely correlation of the conglomerates between the two sections is

Table 1. K-Ar ages of two rhyolite samples (from I. McDougall)

Lab. no.	Field no.	K (wt.%)	Rad. ^{40}Ar 10^{-12} mol/g	$\frac{100 \cdot \text{Rad. } ^{40}Ar}{\text{Total } ^{40}Ar}$	calc. age Ma ± 2S.D.
73-1483	SC 10A	2.369, 2.362	7.96	11.5	1.89 ± 0.08
73-1484	SC 10B	2.350, 2.372	7.49	20.1	1.78 ± 0.04
			7.76	5.6	1.85 ± 0.18

SB 46–47 ≙ SD 3–4, SB 61 ≙ SD 27–28, which indicates the presence of four conglomerate horizons between what is termed here Glacial horizons 10–11 But as no volcanic hyaloclastites were found associated with the conglomerate horizons in spite of the high volcanicity, the horizons are considered to be of a local nature rather than representing major glaciations. More detailed work on these might alter that view.

Glacial Horizon 11 Basaltic and rhyolitic hyaloclastites at the top of the present profile, with thickness over 100 m. SC 7 and SC 8 are feeder plugs within the basaltic hyaloclastite, but SC 10 is the feeder dyke of the rhyolite hyaloclastite. The rhyolite was erupted on an arched sheet just outside the Stardalur caldera fault during the final volcanic phase of the Stardalur central volcano (Esja units 25 and 26).

2.4. Potassium-Argon Dates, Correlation of Glaciations

Dr. I. McDougall of the Australian National University in 1973 collected samples from sections SA, SB, SC to investigate their suitability for K-Ar dating. No useful basalt samples were found, but Dr. McDougall has obtained, and kindly allowed us to quote, the results from two samples of the rhyolite unit SC 10 (Table 1). Both samples are composed mainly of spherulitic cryptocrystalline feldspathic material rather than glass, with minor dark altered areas.

The decay constants are the same as those used by McDougall et al. (1977). If the recently recommended decay constants for ^{40}K (Steiger and Jäger, 1977) are used, these (and other ages mentioned in the present paper) will increase by 2.67%.

In the profile presented here there are signs of a least 11 and possibly 16 glaciations. The lower part of the sequence overlaps in time with the Husafell area 60 km further NE which is set in the same configuration with respect to the Reykjanes-Langjökull volcanic zone. There, Saemundsson and Noll have mapped 8 glacial horizons in strata dating from the Mammoth event to just above the transition Gauss/Matuyama (Saemundsson and Noll, 1974, McDougall et al., 1977). The first two glacial horizons of Saemundsson and Noll (1974) are represented in the present profiles, but out of their five glacial horizons, 3 to 7, in the uppermost part of the Gauss epoch only three are present here (3 to 5). There may thus be signs of 13 and possibly 18 glaciations in the volcanic strata of western Iceland dating from the Mammoth event (~3.1 Ma) to the uppermost glacial unit in Esja, the rhyolite SC 10. According to the new K-Ar dates just tabulated, this normally magnetized unit is more likely to belong to the Olduvai than to the Gilsá geomagnetic event.

2.5 Rock Alteration

Secondary alteration in the study area has been found (Fridleifsson, 1973; Franzson, 1978) to follow generally the zonal pattern demonstrated by Walker (1960) for the Tertiary basalts of eastern Iceland. The profile FA in Akrafjall starts near the top of the mesolite-scolecite zone; the tops of sections FA and FB are zeolite-free. In Esja and Eyrarfjall the profiles also start in the mesolite-scolecite zone which extends up to about 300 m elevation. Above 700 m zeolites are rare except in Sect. SC, which is just outside the thermal aureole associated with the Stardalur central volcano.

3. Paleomagnetic Sampling and Measurement

A total of 353 units were sampled in 11 sections. All were lava flows except SC 7–11 (intrusions), and SB 13, SA 28–30 (hyaloclastites). In case of multiple pahoehoe 'flow units' or composite flows, only one flow unit was sampled, and some very thin or poorly preserved flows were left out, e.g., in EZ and SA. Flows having an A or B suffix were located after the original mapping and numbering took place. In all sections, numbering begins at the bottom.

Three or more 2.5-cm cores were drilled from each unit and orientated in place by geographic sightings. One specimen of 2.2-cm length was cut from each core for remanence measurements, which were made at the University of Rhode Island using spinner magnetometers, and at the Universities in Munich and Reykjavik using mostly Institut Dr. Förster static fluxgate magnetometers. Remanence intensity and direction was measured both at the total N.R.M. level and after treatment in 100 and 200 Oe peak alternating fields (1 Oe = 10^{-4} T). In the poorly stable flows EN 1–15, 150 Oe treatment was also applied, flows EP 36, SD 42–44 have been affected by lightning, and some samples from these were demagnetized to 300 Oe.

Direction data obtained at Rhode Island were averaged within each unit using the minimum-scatter criterion used by Watkins et al. (1977); in other units, the more internally consistent of the results after 100 or 200 Oe was selected for use in subsequent analysis. The difference between these techniques is generally small here.

Random errors in the orientation and marking of a core may be of the order of 3°, and random errors in magnetic direction measurement on a stable specimen may amount to 2° Table 2 shows the mean field direction obtained from each unit after tectonic tilt correction. It also gives the within-unit 95% confidence angle for the field direction, a virtual geomagnetic pole position and an arithmetic mean remanence intensity in volume units after 100 Oe demagnetization.

When α_{95} exceeds 60° (Vincenz and Bruckshaw, 1960), we consider the computed average field direction to be meaningless and it is not given in Table 2; however, this is often due to anomalous behaviour in one sample, and the polarity of the other two then agrees with that of adjacent units. Units marked with a small a in Table 2 have α_{95}-values exceeding 23.5° (i.e., a vector sum R less than 2.93 if $N=3$), and these have been excluded from computation of mean magnetic properties in the collection.

Table 2

No.	*N*	*D*	*I*	*Lon*	*Lat*	alf	*J*	pol
FA Akrafjall								
FA 01	3	108	−68	83	−52	28	2.2	R[a]
FA 02	3	164	−52	4	−57	7	1.1	R
FA 03	3	161	−45	5	−51	18	0.9	R
FA 04	4	348	+86	333	+72	20	3.3	N
FA 05	3	12	+76	71	+85	10	0.7	N
FA 06	4	340	+68	208	+73	6	1.0	N
FA 07	3	48	+77	44	+70	6	0.7	N
FA 08	3	191	−64	314	−71	3	2.2	R
FA 09	3	204	−70	277	−74	11	1.0	R
FA 10	3	197	−85	170	−74	13	0.7	R
FA 12	3	140	−53	36	−51	5	4.2	R
FA 14	3	190	−65	316	−72	4	1.7	R
FA 15	3	206	−79	212	−79	2	0.8	R
FA 16	3	152	−61	27	−63	5	1.1	R
FA 17	3	102	−34	66	−22	3	0.6	RT
FA 18	3	346	−81	164	−48	6	2.0	R
FA 19	3	148	−78	93	−77	3	7.6	R
FA 20	3	184	−71	323	−81	5	5.4	R
FA 21	3	205	−67	282	−71	8	3.8	R
FA 22	3	172	−75	43	−86	5	8.9	R
FA 23	3	202	−71	276	−76	7	7.4	R
FA 24	3	210	−79	218	−78	4	8.1	R
FA 25	3	164	−57	5	−62	11	0.9	R
FA 26	4	209	−70	268	−73	14	0.7	R
FA 27	3	235	−78	217	−68	6	1.0	R
FA 29	3	108	+78	15	+51	15	1.0	N
FA 30	3	354	+75	213	+87	1	6.3	N
FA 31	3	347	+64	186	+70	10	3.8	N
FA 32	4	359	+78	333	+87	4	2.7	N
FA 33	3	76	+74	38	+57	5	1.1	N
FA 34	3	47	+79	34	+71	5	9.9	N
FA 35	3	101	+71	29	+44	19	3.5	N
FA 36	3	83	+66	48	+45	6	8.2	N
FA 37	3	87	+68	42	+46	7	7.6	N
FA 38	3	85	+71	38	+50	3	3.3	N
FA 39	3	310	+70	251	+64	5	2.9	N
FA 40	3	30	+48	115	+50	2	6.1	N
FA 41	3	346	+76	246	+83	4	5.2	N
FA 42	3	11	+73	110	+82	6	1.9	N
FA 43	3	20	+77	54	+81	4	6.9	N
FA 44	3	6	+66	143	+74	5	1.5	N
FA 45	3	13	−51	147	−7	12	0.5	E
FA 46	3	32	−59	133	−17	6	0.6	RT
FA 47	3	36	−57	129	−15	5	0.6	RT
FA 48	3	26	−50	135	−7	9	0.5	E
FA 49	3	199	−63	300	−68	2	5.8	R
FA 50	3	196	−62	307	−67	5	6.9	R
FA 51	4	179	−83	156	−79	3	5.6	R
FA 52	3	287	−73	202	−44	9	3.1	R
FB Kuludalur								
FB 00	3	20	+16	135	+32	20	2.1	NT
FB 01	3	200	−55	305	−60	3	2.1	R
FB 02	3	128	+60	18	+23	8	1.0	NT
FB 03	3	221	−57	276	−54	4	3.9	R
FB 04	3	234	−69	245	−60	5	3.5	R
FB 05	3	239	−78	214	−66	3	3.8	R
FB 06	3	233	−74	234	−65	5	4.2	R
FB 07	3	220	−69	260	−67	2	4.7	R
FB 08	3	122	−57	58	−47	1	1 7	R
FB 10	3	151	−60	27	−62	7	2.8	R
FB 11	3	149	−60	30	−60	5	3.3	R
FB 12	3	181	−72	334	−82	2	3.4	R
FB 13	3	209	−81	197	−77	4	4.5	R
EZ Hvalfjardareyri								
EZ 03	3	141	−72	66	−70	6	1.5	R
EZ 05	3	186	−76	276	−87	5	2.3	R
EZ 08	3	191	−61	318	−67	14	1.8	R
EZ 12	3	186	−68	322	−77	4	5.4	R
EZ 14	3	190	−74	285	−84	6	1.3	R
EZ 15	3	5	+59	149	+66	3	1.9	N
EZ 16	3	11	+75	89	+85	5	9.2	N
EZ 17	3	354	+69	177	+77	4	2.7	N
EZ 18	3	0	+71	157	+81	4	8.9	N
EZ 19	3	336	+69	217	+74	9	2.9	N
EZ 20	3	356	+67	167	+75	3	6.8	N
EY Fossardalur								
EY 01	4	340	+59	193	+63	26	0.2	N[a]
EY 02	4	67	+79	30	+64	2	2.2	N
EY 03	3	328	+74	248	+75	3	1.5	N
EY 04	3	27	+72	85	+75	5	1.3	N
EY 05	4	50	+69	69	+62	34	0.5	N[a]
EY 06	3	310	+70	250	+64	4	1.2	N
EY 07	5	170	−53	355	−58	4	0.5	R
EY 08	3	177	−47	342	−54	12	1.4	R
EY 08A	4	170	−58	356	−63	3	1.5	R
EY 08B	3	163	−56	7	−61	5	2.7	R
EY 09	3	137	+88	345	+61	12	1.4	N
EY 10	3	169	+84	342	+51	4	4.5	N
EY 11	3	4	+77	47	+88	6	2.2	N
EY 12	3	345	+71	205	+78	3	17.2	N
EY 13	4	16	+71	110	+77	12	3.3	N
EY 14	3	10	+70	128	+78	4	12.2	N
EY 15	3	351	+72	192	+81	2	2.8	N
EY 16	3	307	+66	243	+57	4	1.7	N
EY 17	3	308	+67	245	+59	2	6.5	N
EY 18	3	296	+65	253	+52	3	2.6	N
EY 19	3	303	+65	247	+55	2	3.3	N
EY 20	3	314	+76	267	+70	5	0.6	N
EY 21	4	58	+76	44	+65	8	0.8	N
EY 22	3	8	+71	131	+80	8	0.5	N
EY 23	3	11	+66	132	+73	3	2.5	N
EY 24	3	15	+71	111	+79	5	3.3	N
EY 25	3	13	+72	112	+80	4	7.7	N
EY 26	3	23	+74	78	+79	3	8.1	N
EY 27	3	7	+74	120	+85	6	8.7	N
EY 28	3	18	+76	64	+82	3	2.5	N
EY 29	3	44	+78	41	+72	6	3.3	N
EY 30	3	50	+81	24	+71	2	1.5	N
EY 31	4	26	+81	16	+78	3	2.7	N
EY 32A	3	58	+81	22	+68	4	5.5	N

Table 2 (Continued)

No.	*N*	*D*	*I*	*Lon*	*Lat*	alf	*J*	pol
EY Fossardalur								
EY 32B	3	52	+81	25	+70	7	3.6	N
EY 33	3	209	+82	326	+50	5	3.1	N
EY 34	3	207	+75	322	+37	2	3.0	NT
EY 35	3	201	+77	327	+40	4	2.2	N
EY 36	3	212	+75	320	+38	3	3.7	NT
EY 37	3	52	+81	24	+70	6	2.8	N
EY 38	3	333	+84	319	+74	3	2.9	N
EY 39	3	6	+64	144	+72	1	6.0	N
EY 40	3	343	+79	293	+82	4	6.1	N
EY 41	4	4	+79	354	+85	2	5.7	N
EY 42	4	354	+80	318	+84	5	3.0	N
EY 43	4	25	+77	49	+79	7	2.5	N
EY 44	3	294	+77	281	+63	4	3.1	N
EY 45	3	65	+57	70	+44	8	0.5	N
EY 46	3	103	−41	67	−27	12	2.2	RT
EY 47	3	105	−39	65	−26	13	2.2	RT
EY 48	3	109	−32	59	−24	10	5.2	RT
EY 49	3	94	+ 1	65	− 1	53	0.5	E[a]
EY 50	3	102	−38	67	−24	13	1.2	RT
EY 51	3	346	+71	204	+79	8	6.7	N
EY 52	3	15	+75	85	+82	5	7.8	N
EY 53	3	113	+80	8	+53	9	2.9	N
EM Morastadir								
EM 01	3	27	+72	84	+76	7	7.6	N
EM 02	3	37	+74	64	+72	1	9.3	N
EM 03	3	54	+70	63	+62	13	2.0	N
EM 04	4	19	+61	123	+65	8	4.7	N
EM 05	4	31	+71	85	+72	8	2.9	N
EM 06	3	354	+68	174	+76	3	3.0	N
EM 07	3	353	+83	330	+78	7	1.1	N
EM 08	3	4	+79	2	+86	5	1.6	N
EM 09	3	8	+70	136	+78	5	3.8	N
EM 10	4	8	+72	126	+81	6	8.2	N
EM 11	3	81	−35	85	−13	6	0.7	RT
EN Middalur								
EN 02	3	34	+66	92	+66	3	0.9	N
EN 03	3	21	+68	109	+73	9	1.3	N
EN 04	3	39	+83	9	+73	9	2.4	N
EN 05	3	112	+85	355	+60	6	1.9	N
EN 06	3	136	−57	43	−53	6	0.4	R
EN 08	3	232	+17	286	− 7	7	0.6	E
EN 10	3	86	+ 4	71	+ 3	10	0.5	E
EN 11	3	92	+13	64	+ 5	31	0.4	E[a]
EN 12	3	80	+38	68	+23	7	1.2	NT
EN 13	3	143	−63	43	−61	11	0.9	R
EN 14	3	212	+16	305	−14	45	0.5	RT[a]
EN 15	3	75	−69	108	−40	16	0.3	R
EN 16	3	96	−75	103	−54	13	0.6	R
EN 17	3	178	−75	5	−88	8	1.7	R
EN 18	3	172	−52	352	−58	6	2.9	R
EN 19	3	181	−66	335	−74	7	2.4	R
EN 20	3	181	−76	273	−89	12	5.6	R
EN 21	2	170	−68	5	−76	11	2.1	R
EN 22	3	173	−74	21	−85	8	3.9	R
EN 23	4	177	−72	349	−83	8	1.2	R
EN 24	3	175	−69	353	−78	6	2.2	R
EN 25	3	173	−58	350	−64	21	0.9	R
EN 26	3	80	−72	108	−46	18	0.7	R
EN 27	3	97	−71	96	−51	9	1.9	R
SA Kerlingargil								
SA 01	3	46	+69	74	+63	9	2.6	N
SA 02	3	229	−47	274	−42	20	2.5	R
SA 05	3	181	−72	332	−82	32	1.2	R[a]
SA 06	3	227	−10	286	−22	41	0.4	RT[a]
SA 07	3	232	−36	275	−34	29	0.6	RT[a]
SA 08	3	217	−65	271	−64	23	0.4	R
SA 09	3	232	−45	271	−40	30	0.3	RT[a]
SA 10	3	267	+20	255	+ 8	27	0.3	E[a]
SA 12	3	63	+47	80	+37	8	1.1	NT
SA 13	3	89	+36	60	+19	5	1.5	NT
SA 14	3	266	−61	230	−39	28	0.3	RT[a]
SA 15	3	211	−46	295	−48	50	0.7	R[a]
SA 16	3	198	−40	314	−47	36	0.5	R[a]
SA 20	3	110	−75	97	−60	3	0.9	R
SA 21	3	28	−87	152	−58	20	1.4	R
SA 22	3	140	−82	123	−73	24	4.0	R[a]
SA 23	3	180	−71	338	−82	12	3.5	R
SA 24	3	180	−75	343	−87	11	2.2	R
SA 25	3	220	−62	272	−59	25	1.6	R[a]
SA 26	3	157	−63	22	−67	23	2.3	R
SA 27	3	192	−76	250	−85	9	5.0	R
SA 28	3	177	−51	344	−57	5	14.0	R
SA 30	4	249	−86	179	−66	5	5.2	R
EP Thornyjartindur								
EP 01	3	171	−61	355	−67	5	6.4	R
EP 02	3	162	−55	7	−59	6	2.7	R
EP 03	3	158	−59	16	−63	5	3.8	R
EP 04	3	161	−56	10	−60	2	2.0	R
EP 05	3	164	−53	4	−58	10	1.7	R
EP 06	3	146	−74	68	−74	3	3.3	R
EP 07	3	120	−74	88	−63	4	3.0	R
EP 09	3	175	−78	126	−86	13	5.9	R
EP 10	3	180	−76	341	−89	5	3.8	R
EP 11	3	196	−68	298	−74	8	8.8	R
EP 12	3	190	−78	205	−85	9	4.8	R
EP 13	3	199	−74	266	−80	4	7.1	R
EP 14	3	171	−81	139	−82	9	5.2	R
EP 15	3	249	−71	231	−56	8	5.0	R
EP 16	3	238	−67	246	−57	3	9.6	R
EP 17	3	242	−73	230	−61	5	7.8	R
EP 18	3	218	−73	248	−71	8	6.3	R
EP 19	3	240	−70	239	−59	5	7.6	R
EP 20	3	236	−74	231	−64	2	6.3	R
EP 21	3	239	−72	235	−61	7	6.0	R
EP 22	3	218	−77	230	−74	10	6.0	R
EP 23	3	225	−75	234	−70	5	5.4	R
EP 24	3	193	−82	176	−79	2	7.8	R
EP 25	3	138	−88	152	−67	5	7.9	R

Table 2 (Continued)

No.	*N*	*D*	*I*	*Lon*	*Lat*	alf	*J*	pol
EP Thornyjartindur								
EP 26	3	158	−84	140	−75	5	7.5	R
EP 27	3	157	−82	132	−77	1	6.7	R
EP 28	3	177	−78	139	−87	6	4.2	R
EP 29	4	186	−76	270	−87	5	7.6	R
EP 30	3	206	−70	276	−73	6	5.6	R
EP 31	3	177	−74	357	−85	6	6.4	R
EP 32	3	160	−69	29	−74	10	3.7	R
EP 33	3	181	−75	326	−88	7	7.9	R
EP 34	3	172	−74	22	−84	10	7.1	R
EP 35	4	154	−56	20	−58	5	3.7	R
EP 36	3	166	−66	9	−72	8	(2.3)	R
EP 37	3	168	−75	42	−84	10	1.3	R
EP 38	3	169	−69	9	−77	12	1.0	R
EP 39	3	161	−76	70	−82	5	3.7	R
EP 40	3	198	−76	243	−82	10	4.8	R
EP 41	3	132	−86	139	−69	1	11.0	R
EP 42	3	194	−62	311	−67	8	7.3	R
EP 43	3	219	−75	240	−72	5	3.8	R
EP 43 A	3	187	−63	325	−69	13	4.8	R
EP 44	3	274	−63	222	−37	13	2.5	RT
EP 45	3	349	+68	188	+76	4	1.5	N
SB Kistufell								
SB 01	3	144	−57	34	−55	3	0.8	R
SB 02	3	163	−53	5	−57	4	2.1	R
SB 03	3	153	−53	19	−55	6	3.0	R
SB 04	3	159	−59	16	−63	5	0.9	R
SB 05	3	216	−77	231	−75	12	1.6	R
SB 06	3	153	−55	21	−56	12	1.4	R
SB 07	3	159	−57	13	−61	9	2.2	R
SB 08	3	155	−56	18	−58	5	1.8	R
SB 09	3	126	−52	51	−44	19	0.5	R
SB 10	3	148	−54	26	−54	14	2.7	R
SB 11	3	165	−58	5	−63	9	0.3	R
SB 12	3	167	−72	26	−81	2	3.4	R
SB 13	4	162	−71	26	−76	11	1.3	R
SB 14	6	147	−74	64	−74	12	0.5	R
SB 15	3	194	−68	302	−75	12	1.8	R
SB 16	3	190	−78	204	−85	5	3.5	R
SB 17	3	243	−76	222	−63	5	4.2	R
SB 18	3	214	−77	230	−76	5	5.1	R
SB 19	3	224	−79	215	−73	2	4.2	R
SB 20	3	234	−81	203	−69	5	3.9	R
SB 21	3	223	−76	229	−72	8	1.9	R
SB 22	3	228	−76	229	−69	2	4.9	R
SB 23	3	276	−71	212	−45	5	1.2	R
SB 24	3	18	+68	116	+73	8	0.7	N
SB 25	3	359	+75	161	+87	12	0.3	N
SB 26	3	20	+70	106	+75	2	0.7	N
SB 27	3	8	+67	139	+74	7	1.2	N
SB 28	3	6	+72	130	+82	7	1.0	N
SB 29	3	50	+72	60	+65	30	0.3	N[a]
SB 30	3	332	+61	208	+63	29	0.9	N[a]
SB 31	3	357	+61	165	+68	21	1.4	N
SB 32	3	49	+68	72	+62	2	5.9	N
SB 33	3	57	+71	59	+61	5	5.8	N
SB 34	3	64	+73	50	+60	2	3.0	N
SB 35	3	70	+73	46	+57	11	1.2	N
SB 38	3	163	−44	3	−50	7	4.3	R
SB 39	3	172	−49	351	−55	4	3.9	R
SB 40	3	152	−57	24	−58	12	3.2	R
SB 41	3	186	−65	326	−73	4	3.4	R
SB 42	3	208	−67	279	−69	9	4.2	R
SB 43	3	209	−73	260	−75	2	4.9	R
SB 44	3	166	−75	50	−83	4	7.9	R
SB 45	3	157	−71	41	−75	7	6.7	R
SB 46	3	172	−70	3	−79	3	5.0	R
SB 47	3	204	−71	274	−75	8	3.0	R
SB 48	3	185	−66	326	−73	14	7.6	R
SB 49	3	146	−65	42	−65	18	1.4	R
SB 50	3	208	−55	294	−57	6	1.9	R
SB 51	3	182	−71	330	−82	4	4.1	R
SB 52	3	151	−62	30	−63	4	6.3	R
SB 54	3	156	−61	22	−64	5	3.8	R
SB 55	3	211	−81	199	−76	14	2.6	R
SB 56	3	204	−69	282	−73	9	6.1	R
SB 57	3	142	−79	103	−74	3	3.3	R
SB 58	3	155	−74	58	−77	13	3.3	R
SB 60	3	197	−72	282	−79	7	3.3	R
SB 61	3	182	−69	332	−79	6	1.4	R
SD Grafardalur-Hatindur								
SD 01	3	189	−76	250	−86	7	4.3	R
SD 03	3	196	−79	207	−82	2	1.5	R
SD 04	3	237	−73	235	−63	2	1.4	R
SD 05	3	228	−74	236	−68	5	5.7	R
SD 06	3	214	−73	252	−73	4	7.9	R
SD 07	3	223	−82	198	−73	4	4.3	R
SD 08	3	233	−82	198	−70	12	4.6	R
SD 09	3	282	−83	184	−59	2	1.7	R
SD 10	3	163	−79	112	−82	7	3.1	R
SD 11	3	178	−75	2	−88	5	2.2	R
SD 12	3	155	−73	52	−77	3	2.0	R
SD 13	3	70	−76	121	−48	4	2.4	R
SD 14	3	78	−74	112	−47	5	3.3	R
SD 15	3	102	−77	105	−58	6	2.5	R
SD 16	3	111	−73	92	−58	7	2.3	R
SD 17	3	182	−85	160	−75	6	2.8	R
SD 18	3	276	−83	188	−59	3	3.8	R
SD 19	3	176	−82	153	−79	6	2.5	R
SD 20	3	279	−80	195	−56	6	8.7	R
SD 21	3	28	−87	153	−59	4	5.7	R
SD 22	3	187	−71	313	−81	4	4.1	R
SD 23	3	178	−74	354	−86	5	4.2	R
SD 24	3	181	−84	159	−76	2	10.0	R
SD 25	3	193	−65	310	−71	5	5.4	R
SD 26	3	183	−68	330	−76	5	4.1	R
SD 27	3	201	−63	298	−67	8	11.0	R
SD 28	3	179	−77	135	−89	12	3.0	R
SD 29	3	175	−76	39	−87	5	5.2	R
SD 30	3	184	−74	311	−86	8	4.5	R
SD 31	3	171	−79	118	−85	5	2.2	R
SD 32	3	137	−73	74	−69	35	2.2	R[a]
SD 34	3	197	−81	189	−80	18	2.6	R

Table 2 (Continued)

No.	*N*	*D*	*I*	*Lon*	*Lat*	alf	*J*	pol
SD Grafardalur-Hatindur								
SD 37	3	307	−88	165	−62	6	8.3	R
SD 38	3	35	−85	149	−56	8	2.5	R
SD 39	4	134	−85	139	−70	5	2.6	R
SD 40	3	82	−73	108	−47	16	3.1	R
SD 41	3	177	−74	5	−86	12	3.1	R
SD 42	4	191	−75	267	−85	6	(3.8)	R
SD 43	3	194	−77	226	−84	3	(3.4)	R
SD 44	4	202	−76	239	−81	6	(3.5)	R
SC Svinaskard								
SC 01	2	271	−71	216	−47	(9)	3.3	R
SC 02	3	274	−73	211	−49	11	1.3	R
SC 03	3	96	−85	133	−63	27	3.0	R[a]
SC 04	3	166	−71	22	−78	10	0.4	R
SC 05	3	138	−16	26	−27	27	0.3	RT[a]
SC 07	4	177	+78	340	+42	6	2.8	N
SC 08	5	91	+84	4	+62	5	4.7	N
SC 09	7	25	+78	39	+80	20	1.4	N
SC 10	4	128	+61	18	+24	18	1.4	NT
SC 11	4	62	+84	9	+68	4	5.3	N
Mean direction not significant (alf > 60)								
FA 28	3	Poor stability					0.1	(?)
EZ 01	3	Scattered-near dyke					2.5	(?)
EN 01	5	Scattered-near dyke					0.8	(?)
EN 07	5	Poor stability					0.5	(R?)
EN 09	5	Poor stability					1.2	(?)
SA 03	3	Two N, one unstable					2.7	(N?)
SA 11	3	Scattered					0.6	(?)
SA 17	3	Scattered R/RT					1.1	(RT?)
SB 36	3	Scattered N/NT					1.8	(N?)
SB 37	3	Two R, one NT					1.5	(R?)
SB 53	3	Two R, one E					4.4	(R?)
SB 59	3	Two R, one NT					3.8	(R?)
SD 02	3	Two R, one N					3.0	(R?)
SD 36	3	Two R, one N					3.3	(R?)

List of all units sampled for magnetic measurements
N = Number of samples per flow
D, *I* = Declination and inclination of best mean field after tectonic tilt correction
Lon, *Lat* = Coordinates of virtual geomagnetic pole
alf = α_{95} of mean field
J = Mean remanence intensity after 100 Oe, in amperes/m
pol = Magnetic polarity of unit
[a] If alf > 23.5°, *T* if |Lat| < 40°, *E* if |Lat| < 10°

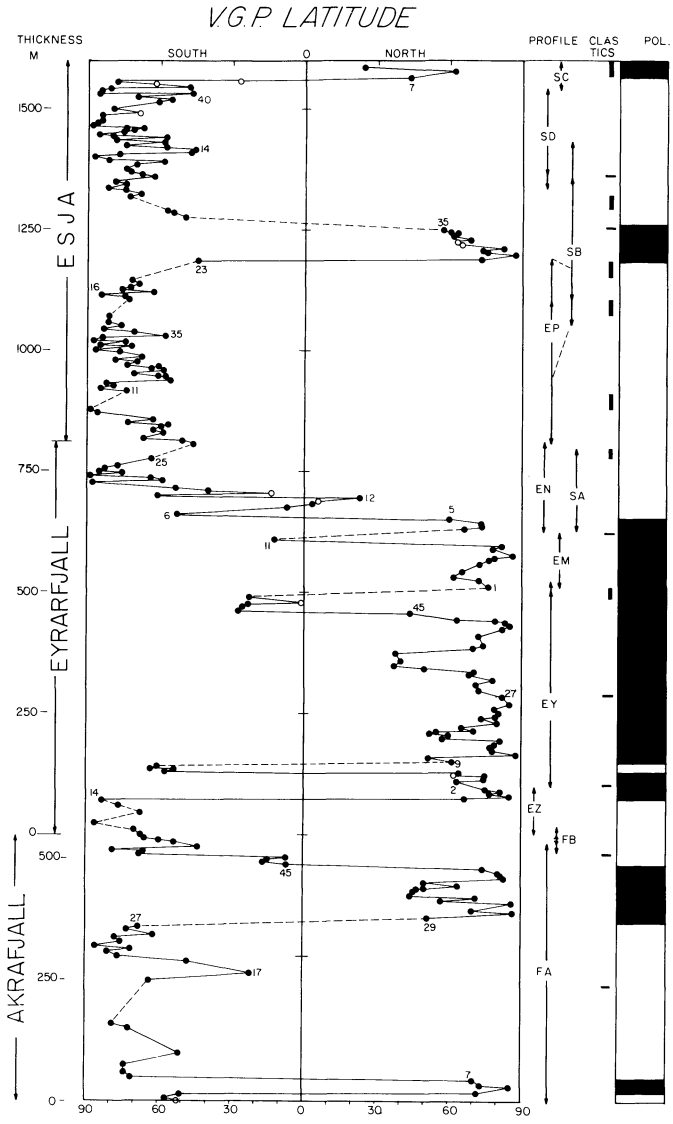

Fig. 3. Plot of virtual geomagnetic pole latitude versus stratigraphic thickness for a composite profile through area of Fig. 1. Some lavas numbered to aid comparison with Fig. 2 and Table 2. *Open circles* are lavas where field direction has α_{95} exceeding 23.5°. *Broken lines* indicate minor gaps, uncertain correlations, or hyaloclastites (see text). *Double arrows in right hand column* show amount of partial overlap between sections. Simplified polarity structure on far right; *black* is normal magnetization

From geological correlations, 77 sampled units are considered to overlap in time with sampled units in other sections of the composite profile, although they are very unlikely to be identically the same as any of those. The overlaps are as follows: FB 0–2 overlap with the top flows of FA; FB 8–13 overlap with EZ; EY 51–53 overlap with the bottom flows of EM; SA 1–30 overlap with EN; EP 41–45 overlap with SB above SB 13; SB 1–13 and 47–61 overlap with EP and SD, respectively; SD 1–3 overlap with SB below SB 47; SC 9 and 11. Omitting these and all units with $\alpha_{95} > 60°$, we are left with 268 in our main composite profile shown in Fig. 3, where computed geomagnetic pole latitudes are plotted against stratigraphic height. In this figure, each major hyaloclastite sequence has been reduced to one tenth of its maximum recorded thickness, to allow for the fact that it would have taken on very different dimensions in a subaerial environment.

4. Magnetic Stratigraphy and Correlation; Discussion

For lack of dated material in the present sections, their interpretation must be limited for the time being to a straightforward correla-

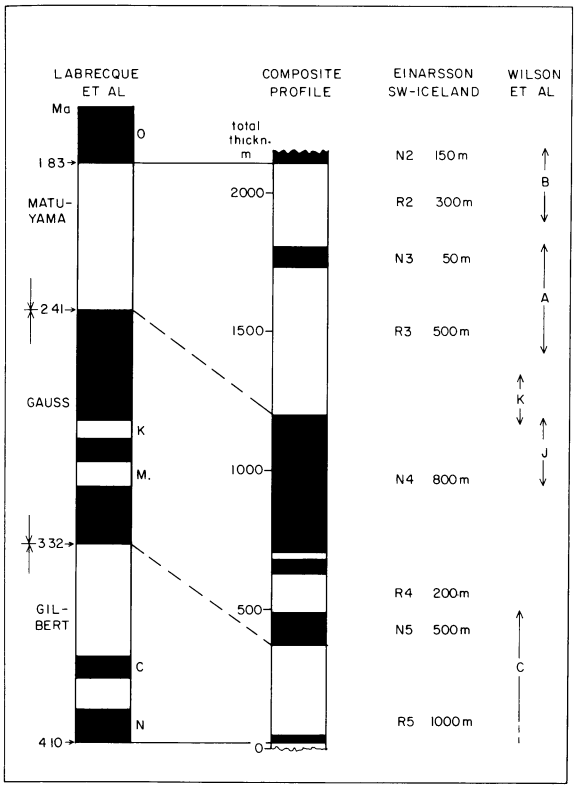

Fig. 4. Polarity column from Fig. 3, showing proposed correlations with the ocean-anomaly geomagnetic time scale of Labrecque et al. (1977) and with the stratigraphic thickness of Einarsson's (1957) polarity groups. Approximate position of some sections sampled by Wilson et al. (1972) shown on the right

tion with one recently proposed global magnetic time scale (Fig. 4) and remarks of mostly local interest.

The Gilbert-Gauss Boundary is represented at most by one flow here (FA 28, unstable), but by several flows in section C of Wilson et al. (1972). The Gauss-Mammoth boundary here includes four transitional flows (FA 45–48) but at most one flow in C or in Borgarfjördur (NT2, not sampled). In general, it appears unlikely that transitional directions will be of use in stratigraphic correlation of lavas in Iceland.

Mammoth and Kaena Events (Einarsson's R 4). The Mammoth event, beginning at FA 45, is here much thicker than the Kaena, which may be due to inclusion of a series of rapidly erupted flows from the Hvalfjördur volcano. Flows younger than Mammoth are not found in Akrafjall (Franzson, 1978). The Kaena comprises only four flows, plus possibly two obscured by soil cover. In section NT of McDougall et al. (1977) a series of 8 thin flows at the presumed upper boundary of the Kaena event have yielded normal poles near 25° N, 100° E; but corresponding transitional directions have not been found south of Hvalfjördur. A suggestion by Kristjansson et al. (1975) that a 'rebound' occurred in this transition, has later turned out to be inapplicable because lavas NT 31–36 are, in fact, repeated by a fault as NT 37–43.

Upper Gauss Epoch, 'Fossá event' The Upper Gauss, termed *N* 4 by Einarsson, is represented by most of our EY and EM sections. It includes five flows of similar, shallow reverse magnetic directions (EY 46–50), noted by Jonasson et al. (1973) and called by them the Fossá event. However, in the absence of any high-latitude poles in this group of flows, we hesitate to designate it to a separate polarity event. The same argument applies to the low-latitude reverse flow EM 11 and to flow FB 2. The paleomagnetic Sect. J of Wilson et al. (1972) similarly belongs to the Upper Gauss epoch, but in their Fig. 1 they have erroneously designated a reversely magnetized sill (J 22) as a separate polarity interval.

Gauss-Matuyama Boundary. In the lower parts of sections EN and SA (EN 2–14; SA 2–16) which are stratigraphically equivalent, we see a similar pattern of rapid polarity fluctuations and transitional directions (Table 2). Although these flows are magnetically the least stable of the present collection, we believe that these fluctuations are real and indicate details of a complex Gauss-Matuyama transition. Such complexities have also been found in sedimentary rocks (Gurariy, 1977). Other details of the Gauss-Matuyama transition may be recorded by Sigurgeirsson (1957), by Wilson et al. (1972) in Sect. K as 12 mostly thin flows with pole positions near the equator at 80° E, and in flows NT 93–97 of McDougall et al. (1977).

Reunion (or Olduvai) Event. At SB 24 there begins a series of 13 normally magnetized flows, belonging to the thin N 3 series of Einarsson (1957). At its lower boundary, Sigurgeirsson (1957) observed a remarkable series of transitional flows, at various localities in the area, later investigated in more detail by Shaw (1975). Only one transitional flow occurs at this reversal in our Sect. SB and EP.

The dating at 1.8 Ma of a normally magnetized series stratigraphically higher than this event, present in our view convincing evidence that at least two separate events occurred in the Lower Matuyama epoch. Therefore, if the Olduvai was the major event in the Matuyama (Labrecque et al., 1977) the N 3 must be identified for the time being with the Reunion event. We do not, however, consider the problem of Matuyama events to be settled, and further sites for the dating of these are being looked for in Iceland.

Brunhes Age Flows. The younges volcanic rocks in the Esja area are the so-called Reykjavik grey or 'dolerite' lavas. These have not been radiometrically dated or mapped in detail by us, but they are generally believed to be of late Brunhes age. Laboratory results by us from samples of 33 'flow units' at 11 sites around Reykjavik confirm the conclusion of Wilson et al. (1972) based on data from one site, that the magnetic directions in these lava flows are quite tightly grouped and hence that most of them may have been emplaced within a short period compared to the time scales of secular variation. Our results, using 4 samples per flow unit, yield a mean field having $D=8.3°$, $I=70.6°$ ($\theta_{63}=10°$, with $N=33$).

5. Mean Paleomagnetic Field and Secular Variation

5.1 Rates of Eruption

In the interpretation of Fig. 4, the present composite profile contains some 300 lavas covering 2.4 Ma in time. Due to uncertainty in translating thicknesses of hyaloclastite sequences into equivalent lava thickness, it is difficult to compare the mean rate of build-up

in this pile to data from other studies in Iceland. However, the rate is relatively high, due to the nearness of central volcanoes, and according to Fig. 4, it may increase by a factor of three or more between the bottom (Gilbert) part and the top (Matuyama) part of the profile.

5.2 Serial Correlation

On close inspection of Table 2, a grouping of paleomagnetic directions is commonly seen in 3 to 7 successive lavas. Examples include FA 45–48, EY 16–19, EP 1–5, SB 32–35 and SD 13–16; possibly a third of all lava flows in the Table may belong to such groups. It is mostly likely that these groupings are due to tight grouping of the respective eruptions in time, rather than to chance or to secular variation peculiarities. The observed extent of the serial correlation obviously depends much on circumstances such as the completeness of exposures and the mappers' criteria for distinguishing separate lava flows. However, it is instructive to test whether a serial correlation of this sort might affect statistical properties of the overall data set.

Watson and Beran (1967) suggested a testing method analogous to the autocorrelation function of scalar time series. A simplified statement of this test for a unipolar Fisher's (1953) distribution of N unit vectors X_t is that the mean product

$$S(u)=\sum_{t=1}^{N-u} X_t X_{t+u}/(N-u)$$

at lag $u \neq 0$ should be significantly larger than the value of $(1-1/K)^2$ in case of serial correlation between the vectors. $1-1/K$ is also the value of cos θ_{63} or R/N, if N is large and $K>5$. We have applied this test to three comparable populations of paleomagnetic vectors from long stratigraphic sequences of Icelandic flows; the results are presented in Table 3.

The data from W-Iceland are those of Watkins et al. (1977), with later minor corrections, while those from the north are from a study by Saemundsson et al. (1980). Each includes only non-overlapping units having α_{95} less than 23.5°, with reverse field vectors inverted before computation. It is seen that definite serial correlation exists in all these collections at lags of one and two flows, and it is relatively strongest in Esja.

The above results support the view (Kristjansson, 1968) that it is inadvisable to draw conclusions regarding the geomagnetic or tectonic causes of differences between populations of Icelandic lava flows if N is less than 50 or 100. However, averaging lava directions in smaller groups, e.g., with $N=20$, may help to elucidate some aspects of geomagnetic field behaviour (Watkins et al., 1977; Saemundsson et al., 1980).

5.3 Mean Fields and Systematic Errors

Even in collections of hundreds of magnetically stable flows spanning several geomagnetic reversals, such as the three profiles just referred to, it is not certain that we have obtained a precise and meaningful average geomagnetic field for each area and time interval. Besides the observation that R/N values vary considerably between the three entries above, several systematic sources of errors in the data may not average to zero and it is necessary to estimate their sizes. Among these we shall mention three.

Magnetic anomalies of crustal origin are common over Iceland (Haines et al., 1970), some extending tens of kilometers and amounting to more than 1° in direction at 3 km altitude, especially near the volcanic zones. In the past, such regional anomalies may have caused the geomagnetic field at ground level to deviate systematically by 2° or more from the core-generated field during large parts of geomagnetic epochs.

Tectonic tilt corrections are often uncertain in work on Icelandic lava sequences, especially in gentle stream or hill sections and where the surfaces of lava flows are uneven. Tilts commonly decrease with altitude in the sections sampled, but only an average tilt value is used for correction. This error source may well reach 2° in means of say 50 lava flow directions.

Systematic errors of orientation and measurement include map errors (especially in work in narrow valleys), errors in the measurement of drill core inclination due to loose fitting of the orienting tool, unconscious 'handedness' in marking cores and aligning them for remanence measurement, and so on. The latter types of error will be minimized by coring equally often towards all directions, but in practice the choice of coring direction will be much restricted by the landscape. Thus, in two cases of large paleomagnetic collections in Iceland we have found, from field work notebooks, that about 80% of the cores of each were drilled towards one half of the horizon, mostly at low positive inclinations. Errors from these sources may amount to 2–3°

The above estimates indicate that it should not be surprising to find mean paleomagnetic field directions from different parts of the country deviating from one another by up to 6° of arc, even in large collections of roughly contemporaneous strata.

As an example, it was noted by Watkins et al. (1977) that mean field directions from lavas of similar age in Borgarfjördur and in Eastern Iceland have inclinations that are, respectively, a few degrees lower and a few degrees higher than a central axial dipole field value. On the other hand the mean field from the present collection of 258 lavas all having an internal α_{95} value of 23.5° or less, is $D=3.4°$, $I=76.8°$, which is within one degree of the expected dipole field values $D=0°$, $I=76.5°$ ($\theta_{63}=18.8°$, $\alpha_{95}=2.1°$). We thus see that allowing for the presence of systematic errors in mean paleomagnetic field directions may explain minor observed differences between them, so that recourse to physically improbable tectonic or geomagnetic scenarios, as discussed by Watkins et al. (1977), is avoided.

Further statistical analysis of the present collection of paleomagnetic data is being published elsewhere (Saemundsson et al., 1980) along with results from Northern Iceland lava flows.

Table 3. Qualitative test for serial correlation in three populations of Icelandic paleomagnetic vectors

Area	N	$S(u)$					$(R/N)^2$
		$u=0$	1	2	3	4–9 (av.)	
W-Iceland	325	1.0	0.887	0.877	0.874	0.868	0.867
N-Iceland	292	1.0	0.846	0.809	0.794	0.794	0.789
Esja etc.	258	1.0	0.944	0.918	0.905	0.898	0.896

6. Conclusions

Recent detailed geological studies in the area of the Esja, Eyrarfjall, and Akrafjall mountains by the authors and others have confirmed the local magnetic polarity stratigraphy of Einarsson (1957) and its correlation with geomagnetic time scale by Piper (1971). Some new detail has been added, such as the demonstration of two separate magnetic events in Gauss epoch lavas in Eyrarfjall, and it now appears that the two normal Lower Matuyama series in Esja may belong to the Reunion and Olduvai events rather than to the Olduvai and Gilsá.

As remarked by Piper (1973), there is fairly good correspondence between the magnetic polarity of outcropping basalt sequences in the Hvalfjördur area and the polarity of low-altitude aeromagnetic anomalies (Sigurgeirsson, 1970) in the area. The anomaly trend is also similar to the general geological strike direction, although the linearity of these magnetic anomalies is not as persistent as it is over mid-ocean ridges near Iceland. For instance, a prominent positive anomaly correlated with the Gauss age rocks of Eyrarfjall may peter out towards southwest (Kristjansson, 1978).

Hyaloclastites and conglomerate horizons of glacial origin are common in the area and are first observed in strata of Lower Mammoth age. Their presence complicates stratigraphic considerations, but also enables correlations to be made with dated sequences of lavas elsewhere. By correlating with other dated sequences in western Iceland (Saemundsson and Noll, 1974; McDougall et al., 1977) we conclude that at least 13 glaciations occurred in Western and Southwestern Iceland between 3.1 and 1.8 Ma ago.

A mean paleomagnetic direction, computed from 258 lava flows with good internal consistency in non-overlapping parts of 11 sections in the lava pile, is very close to the local value of the central axial dipole field. Possible sources of systematic direction errors in large paleomagnetic collections of Icelandic lava flows are discussed, and it is concluded that minor differences between means of these need not be significant. Due to serial correlation between adjacent lavas and to unpredictable features of the paleomagnetic field, it is also increasingly evident that differences in statistical properties of the field are not eliminated between groups of 20–30 or even of 200–300 flows, when all valid data including low-latitude poles are included. This conclusion reduces the confidence with which tectonic and geomagnetic inferences can be drawn from paleomagnetic data in other regions.

Acknowledgements. We wish to thank Dr. Hjalti Franzson, Gudmundur I. Haraldsson, Arny Sveinbjörnsdottir, and Johann Helgason for help in geological mapping. Dr. Brooks B. Ellwood, Olafur Flovenz, Bjarni Kristinsson, and Örn Gunnarsson assisted with the field work; Dr. Ellwood also wrote computer programs used at U.R.I. Tomas Johannesson carried out magnetic measurements on FA and FB samples, and Linda Steere and other technicians at U.R.I. measured EY, EZ, SA, SB, SC.

Dr. Ian McDougall of the Research School of Earth Sciences, Australian National University, collected and dated samples from unit SC 10, and has kindly allowed us to quote his results. This work was supported by N.S.F. grant no. GA 37178 to N.D.W. L.K. thanks the Alexander von Humboldt Stiftung for a fellowship to carry out magnetic measurements at the Institut für Allgemeine und Angewandte Geophysik, Ludwig-Maximilian Universität, Munich, and Professor Dr. G. Angenheister and staff of that Institute are acknowledged for help and encouragement. The Alexander von Humboldt Stiftung is also thanked for a donation of equipment for paleomagnetic research, to the University of Iceland.

References

Albertsson, K.: K-Ar ages of Plio-Pleistocene glaciations in Iceland with special reference to the Tjörnes sequence 268 pp. University of Cambridge: Ph. D. Thesis 1976

Cox, A.: Geomagnetic reversals. Science **163**, 237–245, 1969

Einarsson, T Magneto-geological mapping in Iceland with the use of a compass. Philos. Mag. [Suppl.] **6**, 232–239, 1957

Fisher, R.A.. Dispersion on a sphere. Proc. R. Soc. London Ser. A:**217**, 295–305, 1953

Franzson, H. The structure and petrochemistry of the Hafnarfjall-Skardsheidi central volcano and the surrounding basalt succession, W-Iceland, 264 pp. University of Edinburgh Ph. D. Thesis 1978

Fridleifsson, I.B. Petrology and structure of the Esja Quaternary volcanic region, southwest Iceland, 208 pp. Oxford University D. Phil. Thesis 1973

Fridleifsson, I.B., Kristjansson, L.. The Stardalur magnetic anomaly, SW-Iceland, Jökull (J. Glaciol. Soc. Icel.) **22**, 69–78, 1972

Gurariy, G.Z.. Some geomagnetic field inversions in the late Cenozoic from investigations in Western Turkmenia (in Russian). Izv. Earth Phys. **13**, 581–586, 1977

Haines, G.V., Hannaford, W., Serson, P.H. Magnetic anomaly maps of the Nordic countries and the Greenland and Norwegian Seas. Publ. Dom. Obs. Ottawa **39**, 123–149, 1970

Johannesson, H. Structure and petrochemistry of the Reykjadalur central volcano and the surrounding areas, midwest Iceland, 273 pp. Durham University: Ph. D. Thesis 1975

Jonasson, B., Hallsdottir, M., Fridriksdóttir, S., Zophoniasson, S., Skaftadóttir, T The geology of Eyrarfjall (unpublished report in Icelandic), 45 pp., University of Iceland, 1973

Kristjansson, L. The paleomagnetism and geology of northwestern Iceland. Earth Planet. Sci. Lett. **4**, 448–450, 1968

Kristjansson, L. Magnetic trends around the Reykjanes peninsula, SW-Iceland. Report, Science Institute, University of Iceland, 11 pp. 1978

Kristjansson, L., Watkins, N., McDougall, I., Saemundsson, K.: A detailed study of the polarity transition marking the upper boundary of the Kaena event (abstract), IAGA Bull. No. **36**, 172, 1975

Labrecque, J.L., Kent, D.V., Cande, S.C.. Revised magnetic polarity time scale for Late Cretaceous and Cenozoic time. Geology **5**, 330–335, 1977

McDougall, I., Watkins, N.D., Kristjansson, L.. Geochronology and paleomagnetism of a Miocene-Pliocene lava sequence at Bessastadaa, Eastern Iceland. Am. J Sci. **276**, 1078–1095, 1976

McDougall, I., Saemundsson, K., Johannesson, H., Watkins, N.D., Kristjansson, L. Extension of the geomagnetic polarity time scale to 6.5 m.y. K-Ar dating, geological and paleomagnetic study of a 3,500-m lava succession in western Iceland. Bull. Geol. Soc. Am. **88**, 1–15, 1977

McDougall, I., Wensink, H.: Palaeomagnetism and geochronology of the Plio-Pleistocene lavas in Iceland. Earth Planet. Sci. Lett. **1**, 232–236, 1966

Pálmason, G., Saemundsson, K.. Iceland in relation to the Mid-Atlantic ridge. Annu. Rev. Earth Planet. Sci. **2**, 25–50, 1974

Piper, J.: Ground magnetic studies of crustal growth in Iceland. Earth Planet. Sci. Lett. **12**, 199–207, 1971

Piper, J.: Interpretation of some magnetic anomalies over Iceland. Tectonophysics **16**, 163–187, 1973

Pjeturss, H.: Island (Iceland). Handbuch der regionalen Geologie, 22 pp. Heidelberg 1910

Rutten, M.G.: Geological reconnaissance of the Esja-Hvalfjördur-Armannsfell area, SW-Iceland. Verh. Ned. Geol.-Mijnb. Genootsch. 221–298, 1958

Saemundsson, K., Kristjansson, L., McDougall, I., Watkins, N.D.: K-Ar dating, geological and paleomagnetic study of a 5 km-lava succession in northern Iceland. J. Geophys. Res. **85**, in press, 1980

Saemundsson, K., Noll, H.: K/Ar ages of rocks from Husafell, Western Iceland, and the development of the Husafell central volcano. Jökull (J. Glaciol. Soc. Icel.) **24**, 40–59, 1974

Shaw, J.: Strong geomagnetic fields during a single Icelandic polarity transition. Geophys. J. R. Astron. Soc. **40**, 345–350, 1975

Sigurgeirsson, T: Direction of magnetisation in Icelandic basalts. Philos. Mag. [Suppl.] **6**, 240–247, 1957

Sigurgeirsson, T Aeromagnetic survey of SW-Iceland. Sci. Icel. **2**, 13–20, 1970

Steiger, R.H., Jäger, E. Subcommission on geochronology· convention on the use of decay constants in geo- and cosmochronology. Earth Planet. Sci. Lett. **36**, 359–362, 1977

Vincenz, S., Bruckshaw, J.M.: Note on the probability distribution of a small number of vectors. Proc. Cambridge Philos. Soc. **56**, 21–26, 1960

Walker, G.P.L.: Zeolite zones and dike distribution in relation to the structure of the basalts of eastern Iceland. J. Geol. **68**, 515–528, 1960

Watkins, N.D., McDougall, I., Kristjansson, L.: Upper Miocene and Pliocene geomagnetic secular variation in the Borgarfjördur area of Western Iceland. Geophys. J. R. Astron. Soc. **49**, 609–632, 1977

Watson, G.S., Beran, R.J.: Testing a sequence of unit vectors for serial correlation. J. Geophys. Res. **72**, 5655–5659, 1967

Wilson, R.L., Watkins, N.D., Einarsson, T., Sigurgeirsson, T., Haggerty, S.E., Smith, P.J., Dagley, P., McCormack, A. Paleomagnetism of ten lava sequences from southwestern Iceland. Geophys. J. R. Astron. Soc. **29**, 459–471, 1972

Received April 3, 1979; Revised Version July 9, 1979

J. Geophys. 47, 43–56, 1980

Journal of Geophysics

Magnetic Anomalies (ΔZ) in NE-Iceland and Their Interpretation Based on Rock-Magnetic Investigations

H. Becker
Institut für Allgemeine und Angewandte Geophysik, Theresienstr. 41, D-8000 München 2, Federal Republic of Germany

Abstract. A magnetic survey (ΔZ) was carried out on long profiles with 50 m spacing in northern and eastern Iceland combined with sampling for rock-magnetic investigations in 1967, 1970, and 1973 by the Institut für Allgemeine und Angewandte Geophysik, Universität München. Some of the profiles cross the neovolcanic zone from the western to the eastern Tertiary flood-basalts. Local and regional geomagnetic anomalies were separated by two-dimensional wavelength filtering and upward field continuation. Anomalies with shorter wavelengths (< 5 km) could be interpreted by geological features such as dikes, groups of dikes, lavas, lava-piles, decreased magnetization at silicic centres caused by intensive hydrothermal activity, and terrain effects. The regional geomagnetic anomalies can be correlated along the strike of the neovolcanic zone. They strongly resemble rift anomalies and are interpreted with dike-swarms with mainly the same magnetic polarization over long distances. A magnetic survey in the Reydarfjördur-Thingmuli area crossing several well known dike-swarms could not prove this interpretation. The rock-magnetic investigation of more than 1,000 samples from the main geological formations show differences in the magnetic properties of lavas and dikes mainly in a higher magnetization and lower Curie temperature of the dikes. But investigations of later remagnetization at the dike contacts, as well as the primary magnetic properties of fresh dikes and of hydrothermally altered ones did not support the interpretation of the regional anomalies by dike-swarms.

Key words: Northern Iceland – Magnetic survey (ΔZ)-Magnetic properties of lavas and dikes – Interpretation of regional magnetic anomalies.

1. Introduction

Iceland should be considered a major anomaly of the Mid-Atlantic Ridge: the axial rift zone crosses Iceland in a complex way divided by fracture zones (Ward, 1971). Even in northern Iceland where at first sight the main structures appear clear and symmetric, one can demonstrate this complexity (Saemundsson, 1974). There are reasons to suggest that Iceland is not a suitable land laboratory for the study of geodynamic processes of mid-oceanic ridges. However, the most significant structures of Iceland are controlled by spreading and can in some way be described by its terminology. The complex structure of Iceland is also revealed by the geomagnetic anomalies which are a major feature in the concept of sea-floor spreading and plate tectonics. This is well illustrated by

Table 1. Magnetic surveys (ΔZ) 1967, 1970, and 1973 with 50 m point spacing

Year	Name of profile	Length in km		Measured by	Reference
1967	B 67 Haupt	150	245	G. + W. Schönharting	Schönharting (1969)
	E 67 Nord	95			
1970	A 70 Süd	70	325	H. Becker P. Mohr	Becker and Mohr (1971) Angenheister et al. (1972)
	C 70 Hlidarfjall	70			
	D 70 Krafla	100			
	F 70 Reykjaheidi	20			
	G 70 Gardur	65			
1973	L 73 Ljosavatnsskard	18	364	H. Becker C. Schweitzer H. Soffel	Angenheister et al. (1977) Becker (1978)
	P 73 Peistareykjabunga	80			
	F 73 Reykjaheidi	45			
	G 73 Gardur	25			
	S 73 Süd	30			
	Tj 73 Tjörnes-NS	40			
	Jo 73 Jökulsa-NS	42			
	RN 73 Reydarfjördur-N	40			
	RS 73 Reydarfjördur-S	44			

0340-062X/80/0047/0043/$02.80

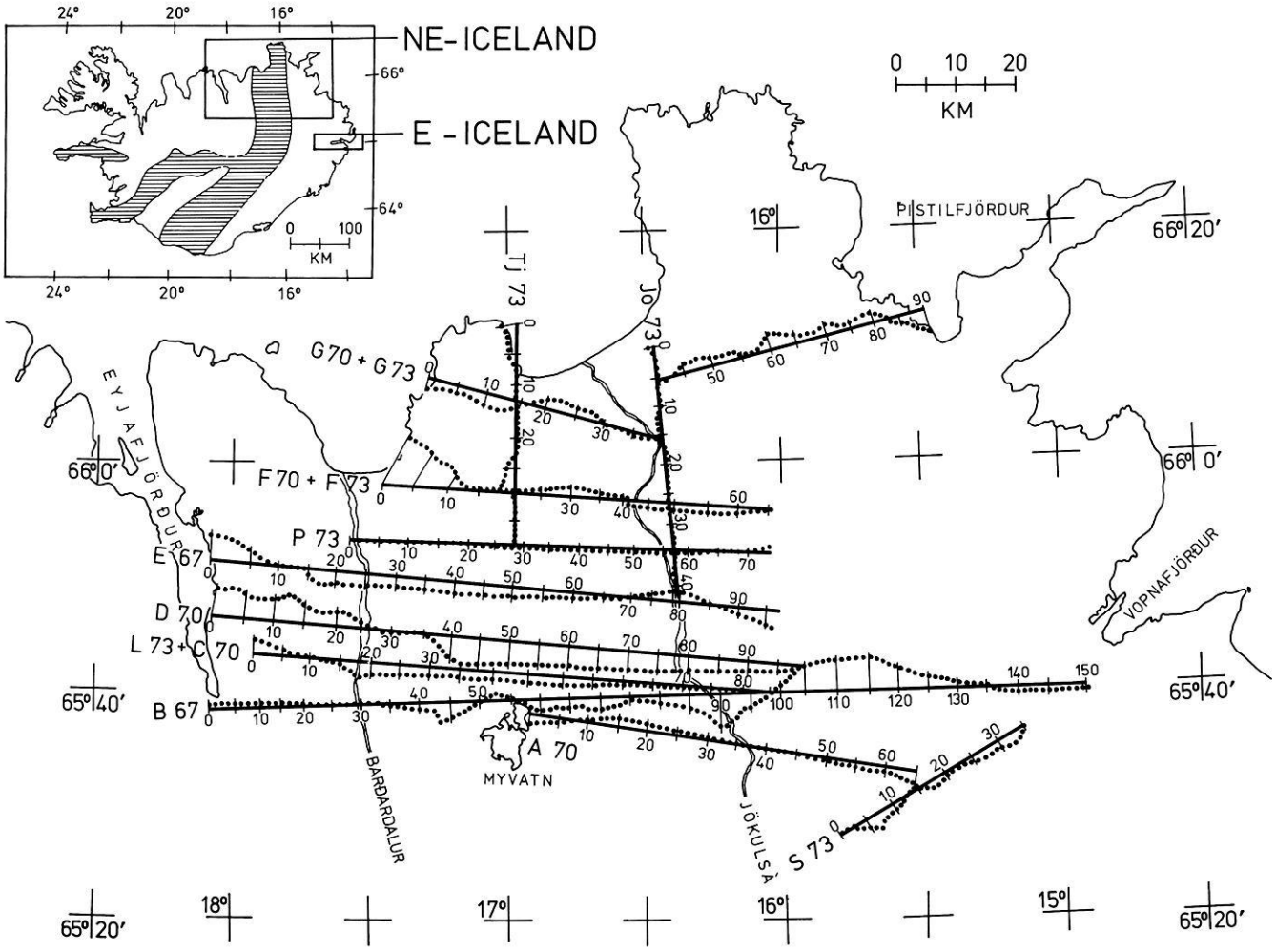

Fig. 1. Location map of the profiles (ΔZ) in NE-Iceland. The measured profiles are *dotted*; the lines with the 10 km marks are the projection for further presentation. The zone of postglacial volcanism is shaded. For location map of E-Iceland (Reydarfjördur) see Fig. 8

the aeromagnetic survey of Serson et al. (1968) with its symmetrical and linear anomalies over Reykjanes Ridge and its completely different characteristics over Iceland. Although the main geomagnetic anomalies follow roughly the branches of the neovolcanic zone, a detailed analysis of the two-dimensionality and spectrum of the anomalies (Rutten 1975) shows that there are no ridge-type anomalies over Iceland. This paper describes a ground magnetic survey in northern and eastern Iceland combined with rock-magnetic investigations in the same areas. This should assist the interpretation, especially when combined with thorough studies of geological and tectonic features (e.g., Walker, 1959; Saemundsson, 1974).

2. Magnetic Survey (ΔZ) in Northern and Eastern Iceland

In 1967, 1970, and 1973 field magnetic measurements were carried out on long profiles (total about 1,000 km) with 50 m point-distance by the Institut für Allgemeine und Angewandte Geophysik, Universität München (Table 1 and Fig. 1; see also Becker, 1978). In northern Iceland these profiles run from Eyjafjördur to Vopnafjördur crossing the neovolcanic zone; both profiles in the Reydarfjördur region in eastern Iceland are situated in Tertiary basalts. For all measurements torsion balances (Askania Gfz) were used; the data for all profiles were processed in the same way using the following programmes on a TR 440 computer:

(a) graduation, levelling, local, and regional correction;
(b) wavelength filtering (two-dimensional) (Fig. 3);
(c) field continuation upward (filtering in the frequency band; two-dimensional) (Fig. 4);
(d) graphical display;
(e) model computation (two-dimensional).

The reference field of ΔZ was calculated by averaging the values of the western and eastern half of the 150 km long profile B 67, which revealed an EW-gradient of 2 nT/km in agreement with the regional field derived from aeromagnetic (Serson et al., 1968; Sigurgeirsson, 1970). The N-S gradient of the aeromagnetic regional field was also considered; again there was good agreement with the gradient calculated by averaging ΔZ even for the distant profiles in eastern Iceland (for details and absolute value of regional field refer to Becker, 1978).

Figure 2 shows the geomagnetic data (ΔZ) from northern Iceland. The main characteristics are a wide range in amplitude (up to 17000 nT) and wavelength which make the aforementioned

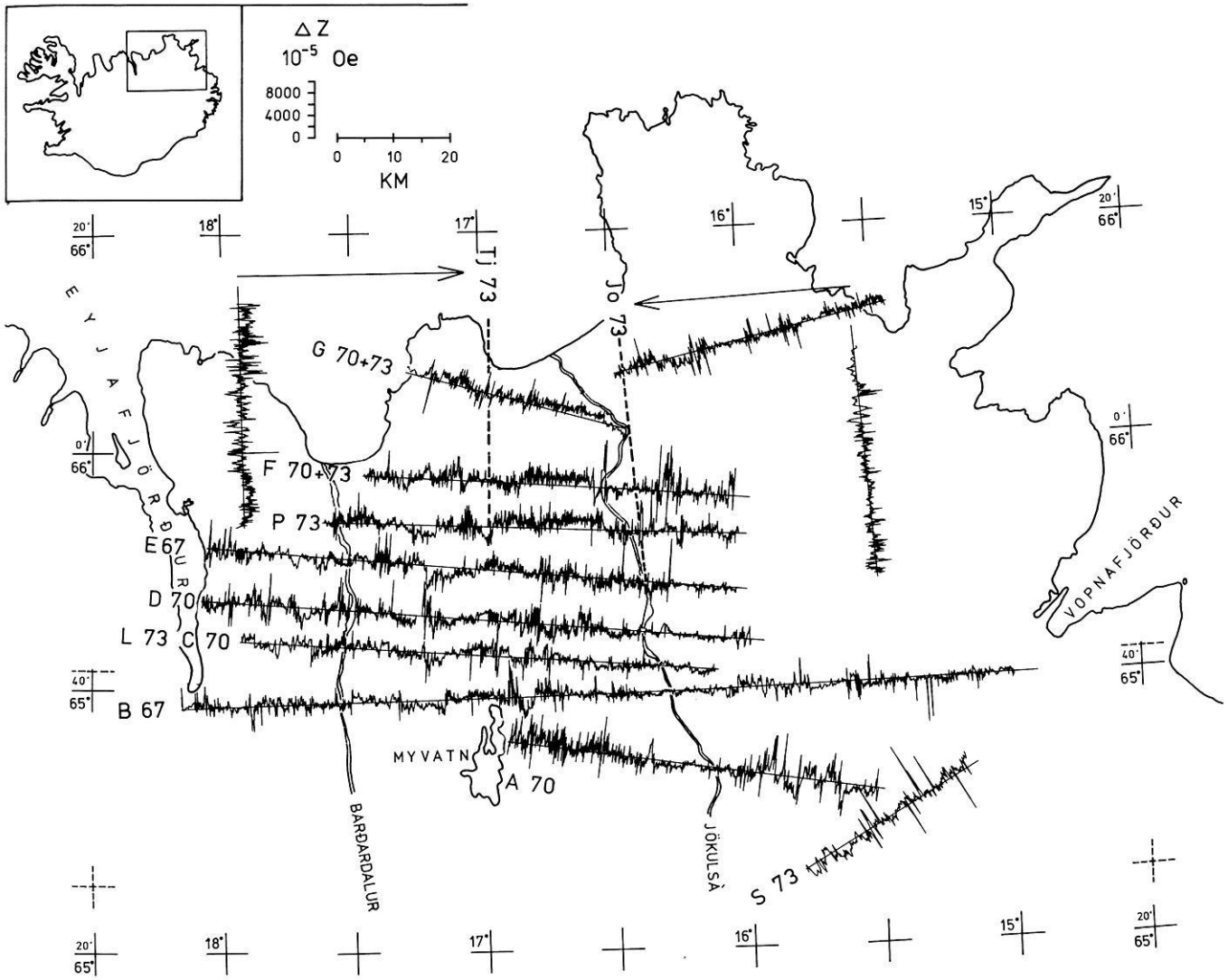

Fig. 2. Profiles of the magnetic survey (ΔZ) in NE-Iceland. The NS-scale from 65° 20′ to 65° 45′ has been omitted for clearer reproduction of the data; the two NS profiles are drawn separately

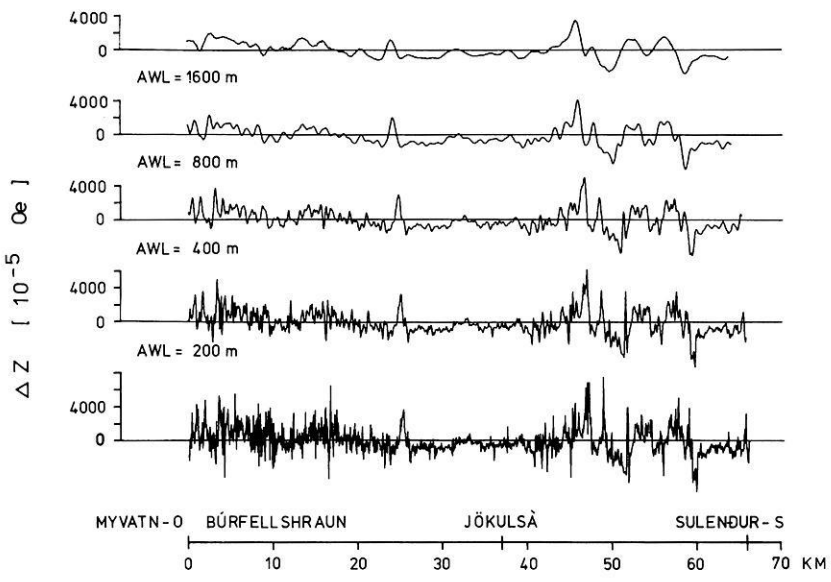

Fig. 3. Effect of wavelength filtering (low-pass). Part of the profile A 70 was filtered with increasing AWL = cut-off wavelength (point distance = 50 m). (For details see Becker, 1978)

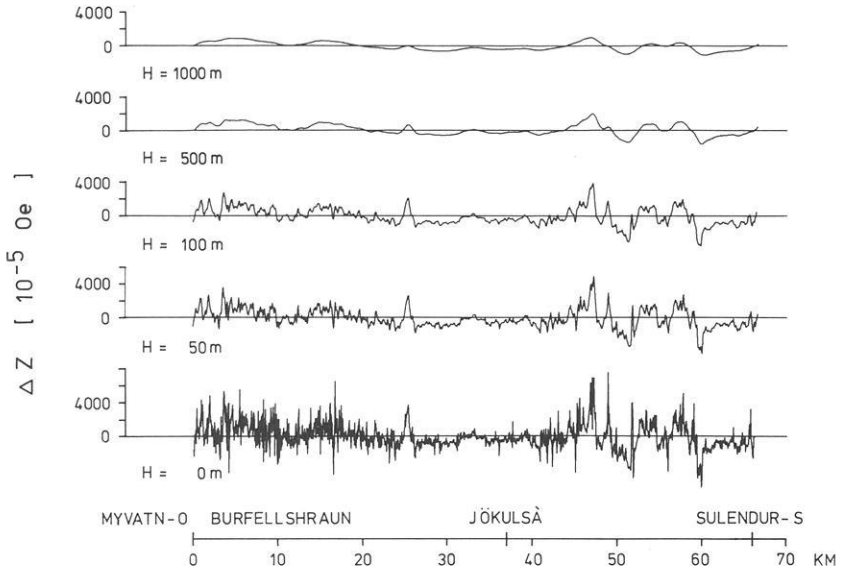

Fig. 4. Effect of the upward field continuation. The same part of profile A 70 was continued to increasing heights. $H=O$ stands for the ground data. Same scale for amplitude

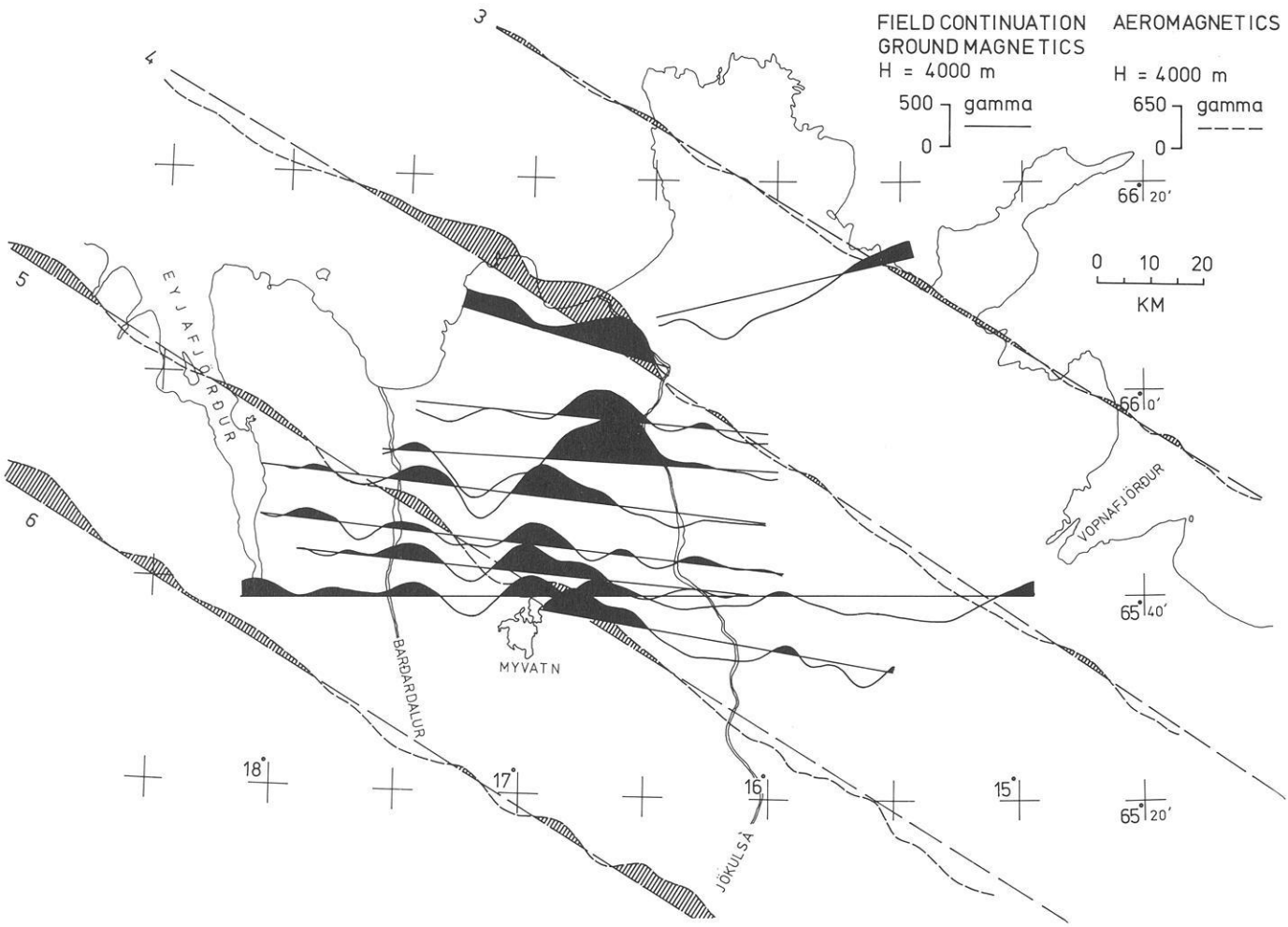

Fig. 5. Upward continuation to 4,000 m altitude and comparison of the anomalies calculated from ground-magnetics (ΔZ) with four aeromagnetic (T) profiles of Serson et al. (1968) (*hatched*)

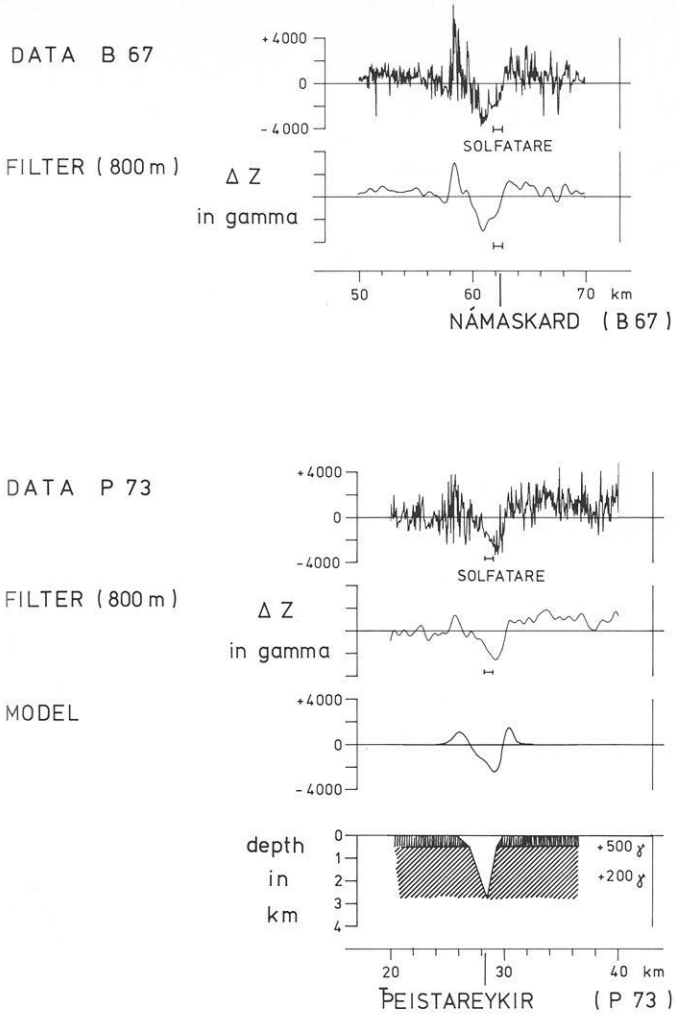

Fig. 6. Negative anomalies (ΔZ) in the central positive anomaly over high-temperature areas Námaskard (Profile B 67) and Peistareykir (Profile P 73) in the central neovolcanic zone. The anomalies were interpreted by decreased magnetization (see model) which may be caused by intensive hydrothermal alteration. (ΔZ in gamma $=10^{-5}$ Oe; magnetization in $\gamma = 10^{-5}$ Gauss)

filtering procedures necessary for clear separation of local and regional anomalies. The various filtering effects are shown in Figs. 3 and 4. The upward continuation not only shows the filtering effect, but also renders possible a comparison with the aeromagnetic survey (e.g., for 1,000 m altitude Sigurgeirsson, 1970; 4,000 m altitude Serson et al., 1968; see Fig. 5).

There was no problem regarding the interpretation of anomalies of less than 5 km wavelength by means of observed near-surface geological features. The anomalies are mainly caused by the following (examples are given by Becker, 1978):

horizontal or slightly dipping plates which represent lavas or groups of lavas;
vertical dikes or dike swarms;
large intrusions (gabbro);
regions of low magnetization (silicic centres);
terrain effects.

The regional anomalies are revealed by upward continuation; a comparison with the aeromagnetic profiles which cross NE-Iceland (Serson et al., 1968), shows satisfactory correlation in the central positive anomaly. It is flanked by a negative anomaly (in the west) and by a positive one at the border of the neovolcanic zone (Fig. 5). The correlation ends at the western border of the neovolcanic zone near Bardardalur. East of the central positive anomaly there is a very broad negative anomaly which is interrupted by positive anomalies over postglacial fissure eruptions (dike-swarms of Kraeduborgir, Rauduborgir, Sveinagjá, Sveinar, Fjallagjá and other fissure eruptions east of Jökulsá á Fjöllum). Other interesting features are negative anomalies of more than 1 km width which were measured in the very centre of the zone of postglacial volcanism and of the central positive anomaly.

These negative anomalies were found over the high-temperature areas of Námaskard and Peistareykir (Fig. 6) and can be explained by the destruction of magnetization by hydrothermal alteration.

The regional anomalies of more than 5 km wavelength, cannot be explained by geological surface features apart from the central positive anomaly which correlates roughly with the zone of postglacial volcanism; other regional anomalies show to some extent the opposite polarity to that of the magnetic stratigraphy of lavas in northern Iceland described by Piper (1973).

The sources for these regional anomalies must be large and highly magnetized bodies whose surface should not be below 500 m as indicated by the steep gradients. They are interpreted by dike-swarms and described in terms of sea-floor spreading along the ideas of Bödvarsson and Walker (1964) and Schönharting (1969) (Fig. 7). This dike-swarm model requires at least the following assumptions:

(a) mainly one polarity of magnetization;
(b) higher magnetization of dikes;
(c) high Curie temperatures of dikes for Curie depths of more than 2–4 km;
(d) considerable percentage of dikes or substantial remagnetization at contacts.

In order to test this hypothesis, a magnetic survey crossing several exposed dike-swarms was carried out in eastern Iceland (Figs. 8 and 9); in addition rock-magnetic investigations should prove the difference between the magnetic properties of lavas and dikes and the effect of remagnetization and hydrothermal alteration.

The southern profile (ΔZ) RS 73 in the Reydarfjördur region stretches from the eastern border of the Thingmuli dike-swarm to the southern part of the Bardsnes dike-swarm passing through the Breiddalur dike-swarm following the shore of Reydarfjördur and then crossing the Reydarfjördur central volcano (Figs. 8 and 9).

K-Ar age determinations give roughly 1 Ma for the formation of such a dike-swarm which results in the distribution of polarity of the magnetization of the dikes as given in Table 2. A more recent palaeomagnetic investigation of the Reydarfjördur dike-swarm revealed a majority of reversed dikes, though without distinct polarity grouping (Piper et al., 1977). The magnetic profiles (ΔZ) in this area show a similar pattern with high-amplitude but short wavelength anomalies produced by single dikes or dike-groups (Fig. 9). Only the Breiddalur dike-swarm causes a broad negative anomaly with 3.5 km wavelength, which still is short in comparison with the ridge-type anomalies observed in the neovolcanic zone. The low amplitude of the anomalies over the centre of the Reydarfjördur dike-swarm illustrates the high hydrothermal alteration in the central volcanoes.

Most of the regional anomalies in the Reydarfjördur show the opposite sign of polarity to the lava-piles (Fig. 10); these anom-

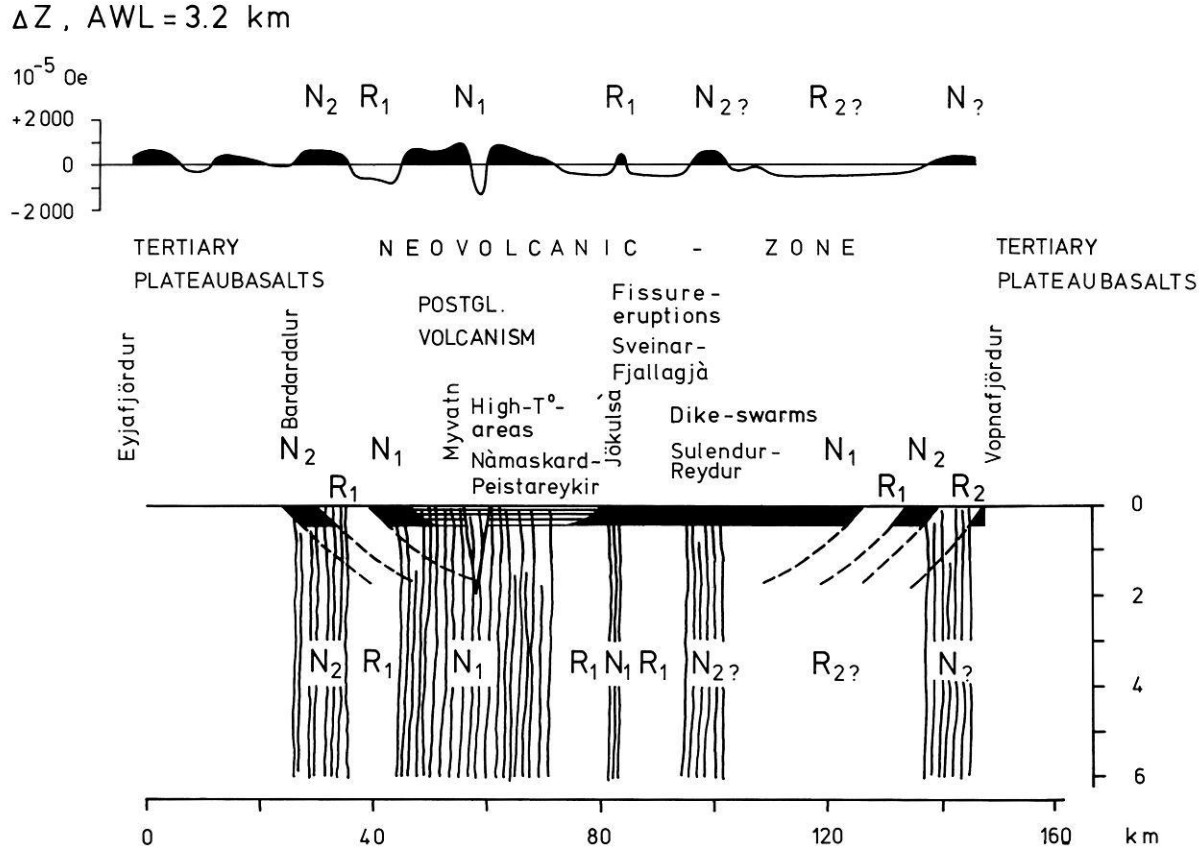

Fig. 7. Interpretation of the regional geomagnetic anomalies by dike-swarms. The regional anomalies ΔZ filtered with cut-off wavelength AWL = 3.2 km are shown schematically. The model gives the main structures of interpretation. The polarity of the magnetization of the lavas refer to Piper (1973); the existence and polarity of the dike-swarms are hypothetical. (N = normal polarity; R = reverse polarity)

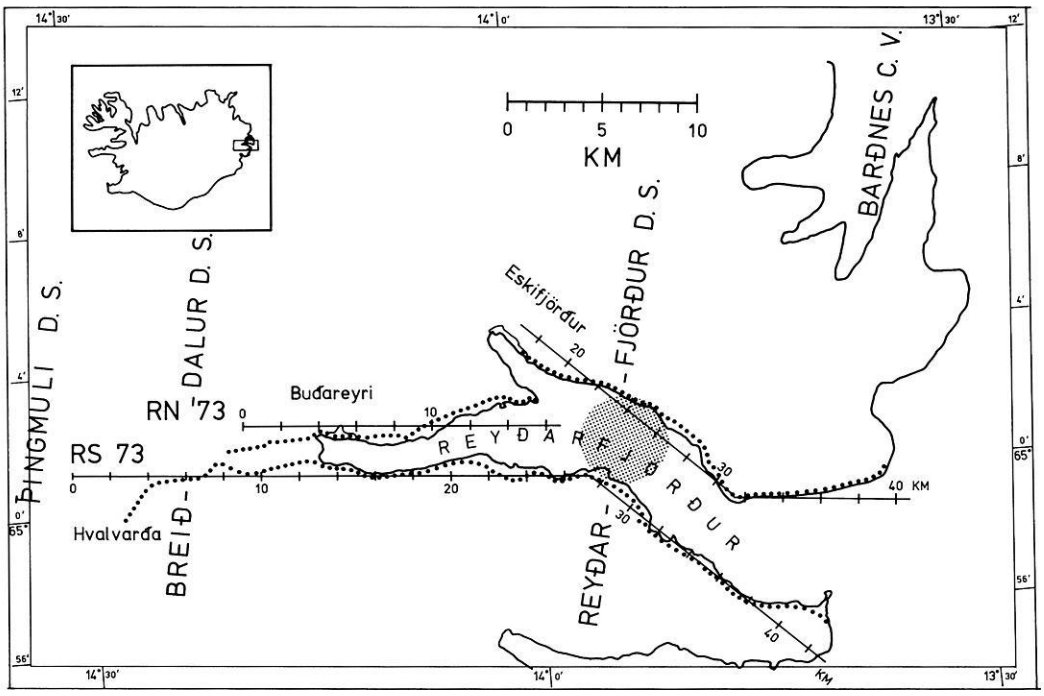

Fig. 8. Location map of the profiles (ΔZ) in the Reydarfjördur-Thingmuli area in E-Iceland with dike-swarms (D.S.) and approximate location of Reydarfjördur central volcano *(shaded)* after Walker (1959, 1963)

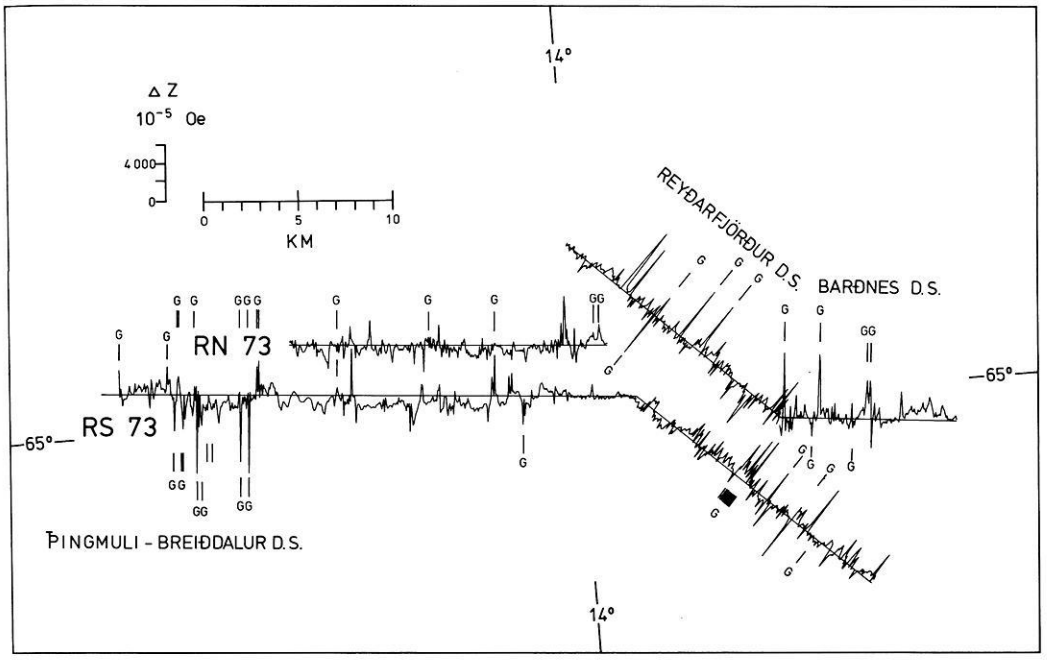

Fig. 9. Magnetic survey (ΔZ) in the Reydarfjördur-Thingmuli area. 'G' specifies dikes which are observed in the field

Table 2. Age and polarity of magnetization of the dike-swarms in the Thingmuli-Reydarfjördur region according to K-Ar determinations by Gale et al. (1966), Moorbath et al. (1968) and McDougall et al. (1976) and epoches of geomagnetic time scale from Heirtzler et al. (1968)

Central volcano	Thingmuli	Breiddalur	Reydarfjördur	Bardsnes
Age Ma	9.5	8.9 (10.5)	11.5	12.5
Epoch of geomagnetic time scale	9	8 (10)	12	13
Main geomagnetic polarity	N	R (R)	R	N

The age in brackets of the Breiddalur central volcano is based on the hypothesis of a continuous development of central volcanoes related to the axial rift-zone
N = Normal polarity, R = Reverse polarity

Table 3. Mean values (arithmetic) of natural remanent magnetization J_{nrm}, susceptibility K, and Q-ratio

	n Sites	n Samples	J_{nrm} 10^{-5} G	K 10^{-5} G/Oe	Q
Postglacial lavas	35	610	1520	78	45
Postglacial dikes	8	121	2250	120	40
Pleistocene lavas	30	177	545	114	13
Tertiary lavas	55	500	340	180	3.2
Tertiary dikes	37	460	500	310	3.2
Tertiary dikes + contacts			620	360	4
Gabbro	1	8	1850	1080	3.4
Hyaloclastite	4	11	4		
After Kristjansson (1970)					
Miocene dikes	10	126	420	140	6
Pliocene dikes	10	20	750		
Gabbro	10	21	650	500	2.6
After Piper (1973)					
Dike-swarms in E- and W-Iceland		500	500	320	3.1

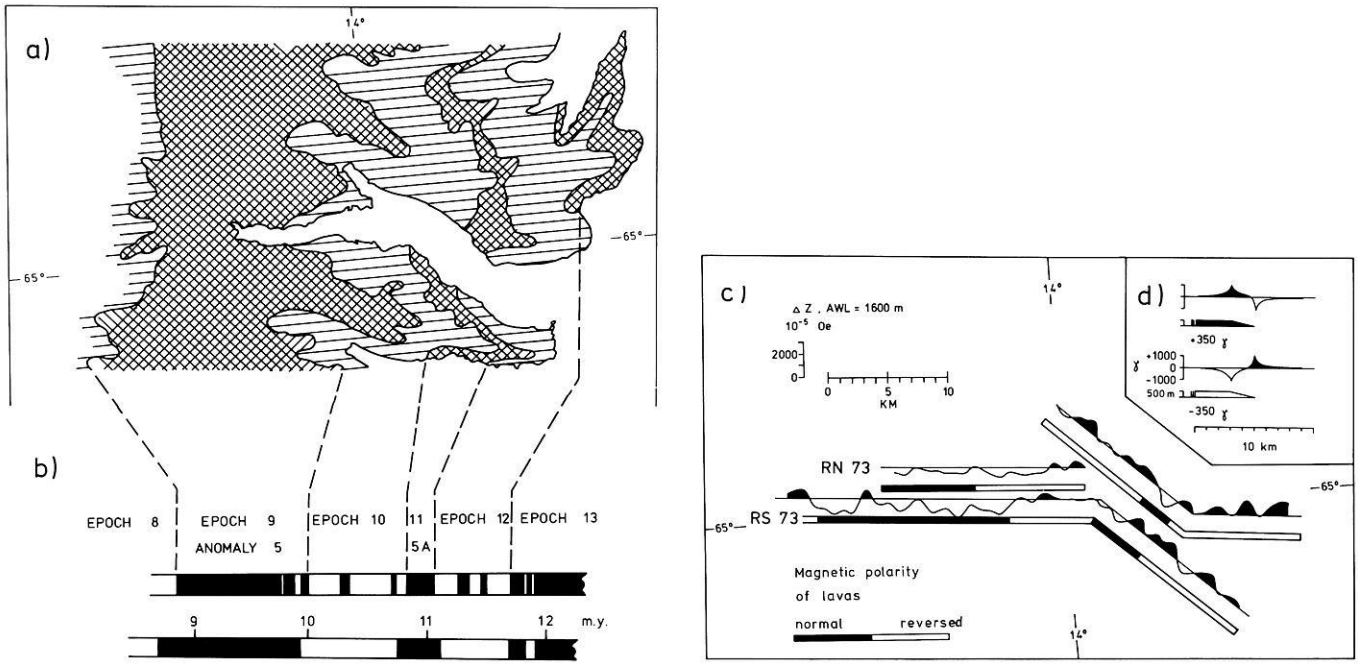

Fig. 10a–d. Comparison of the polarity of the floodbasalts magnetization at Reydarfjördur with the low-pass filtered profiles (ΔZ) and calculation of the terrain effect. **a** Polarity zones of the flood basalts after Piper (1973) (checked = normally magnetized; hatched = reversely magnetized). **b** Measured polarity of the floodbasalts after Dagley et al. (1967) and Piper (1973) and geomagnetic time scale after Heirtzler et al. (1968). **c** Long wavelength anomalies (ΔZ) and polarity of the magnetization of the flood basalts. **d** Calculated terrain effect of a 500 m oblique step having normal and reverse magnetization of 350 γ ($=10^{-5}$ Gauss)

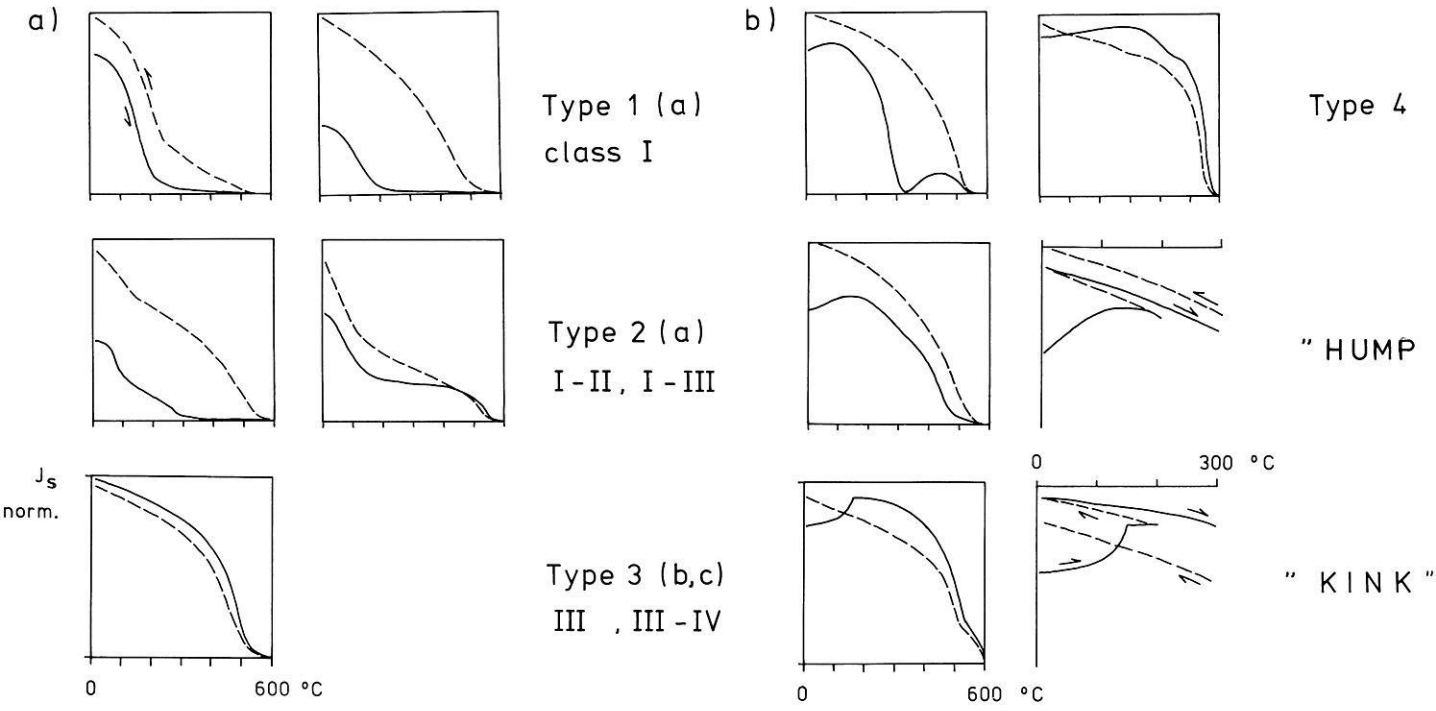

Fig. 11a. Type of J_sT-curve (saturation magnetization versus temperature) and class of deuteric oxidation (HTO). Measurement in air at 240 KA/m (3,000 Oe) with 40 min heating-cooling cycle; a, b, c = cooling curve above, below heating curve, reversible. *Type 1:* homogeneous titanomagnetite (HTO class I); *Type 2:* titanomagnetite with rare dissolution lamellae of ilmenite (left side: 'internal dissolution'; HTO class I/II); right side: partial oxidation by air, HTO class I–III); *Type 3:* internally dissolved titanomagnetite (HTO) class III–V) or highly oxidized titanomagnetite (e.g., reheating). **b** Type of J_sT-curve after low-temperature oxidation and hydrothermal alteration; *Type 4:* maghemitization of homogeneous titanomagnetite (*left side*); maghemitization and hydrothermal alteration of titanomagnetite (*right side*); *'Hump'* hydrothermal alteration of titanomagnetite at temperatures under 200° C; *'Kink'* (right side gives details of the heating and cooling curve)

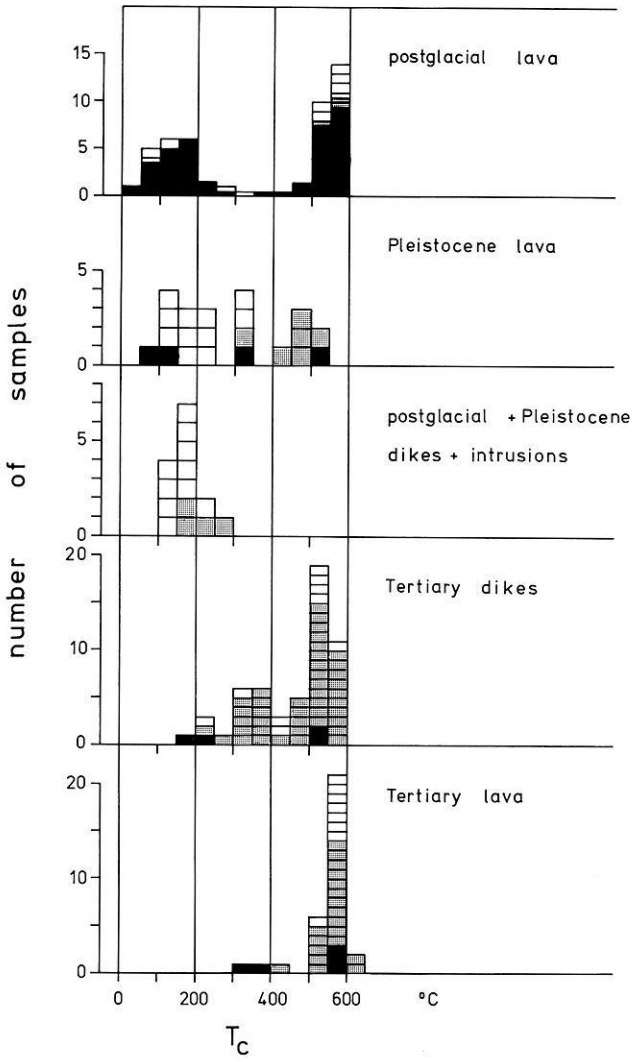

Fig. 12. Normalized histogram of the Curie temperature T_c of lavas and dikes in chronological sequence: *White:* one Curie-point (J_sT-type 1; $0° < T_c < 300°$ C; J_sT-type 3; $500 < T_c < 600°$ C); *black:* two or more Curie-points (J_sT-type 2; $0° < T_{c1} < 200°$ C; $500 < T_{c2} < 600°$ C); *shaded:* low temperature oxidation or hydrothermal alteration (J_sT-type hump or kink)

alies are obviously caused by the terrain effect of the steep slopes of the fjord as modelled in Fig. 10c.

3. Rock-Magnetic Investigation: Primary Magnetic Properties, Remagnetization and Hydrothermal Alteration of Lavas and Dikes

More than 1,000 rock samples from 170 sites (mostly tholeiitic basalts) were drilled covering the main geological formations (for sample list and localities refer to Becker, 1978). The investigation concentrated on properties which are important for the interpretation of the geomagnetic anomalies, such as natural remanence J_{nrm}, susceptibility K and Curie temperature T_c.

Verifying the dike-swarm model, one has to prove the differences of these parameters between dike and lava. As far as possible the samples were taken at various sections of the dikes, lavas, and their contacts in order to study the variation of the magnetic parameters in a single structure and the effect of remagnetization.

Table 4. Internal dissolution of titanomagnetite. Changes in the grade of deuteric oxidation (HTO class) with increasing width of dikes

Number of dikes	Width in m	HTO class				
		I	I/II	II	II/III	III
1	0.15	*				
1	0.5	*				
2	1.0	**				
1	1.5	*				
2	2.0	*	*			
1	2.5		*			
4	3.0	*———	***—	*		
2	4.0	*			*	
3	5.0	*———	———	**	*	
2	6.0	*	*			
1	7.0			*		
1	9.0					*
1	12.0			*		
1	15.0					*
1	20.0		*———	———	———	
1	150.0					*

The comparison of the bulk magnetic properties gives some systematic differences between lavas and dikes of various geological ages which in this case represent also different stages of hydrothermal alteration (Table 3). Most of the Tertiary samples are hydrothermally altered on a regional scale, whereas the Pleistocene and postglacial ones are not altered but locally. The magnetization of dikes is clearly higher than that of lavas, especially if one takes into account the remagnetized contact zones.

About 300 polished sections (at least one for every site) were examined and classified into stages of high temperature oxidation (Wilson and Haggerty, 1966) and hydrothermal alteration (Ade-Hall et al., 1971). In addition thermomagnetic measurements were taken. The type of the thermomagnetic curve (J_sT-curve) corresponds to the stage of deuteric oxidation and hydrothermal alteration (Fig. 11; see also Ade Hall et al., 1971). Again there are distinct differences between lavas and dikes from the same formations mainly in the higher Curie temperature range and higher grade of deuteric oxidation and hydrothermal alteration of the lavas (Fig. 12). This is important for the interpretation of geomagnetic anomalies as the Curie temperature determines the maximum depth (Curie depth) of a body for modelling.

Assuming an average temperature gradient of 85° C/km (Pálmason, 1973) in an active rift zone, the carrier of remanence must be magnetite for a Curie depth of about 5 km. Models with dike swarms require the tacit assumption of a high Curie temperature of dikes. The question is now at what dike width primary magnetite develops due to internal decomposition (Petersen, 1976). As most of the Icelandic dikes have been altered in some way, the J_sT-curve does not give the primary composition of titanomagnetites. A better indicator of their primary state is the grade of deuteric oxidation which is normally identifiable by microscope examination even after hydrothermal alteration.

By plotting dike width against grade of deuteric oxidation, one obtains class III for a 10 m dike which suggests the existence of internally decomposed magnetite (Table 4). Walker (1959) describes dike-swarms in the Reydarfjördur area and finds the aver-

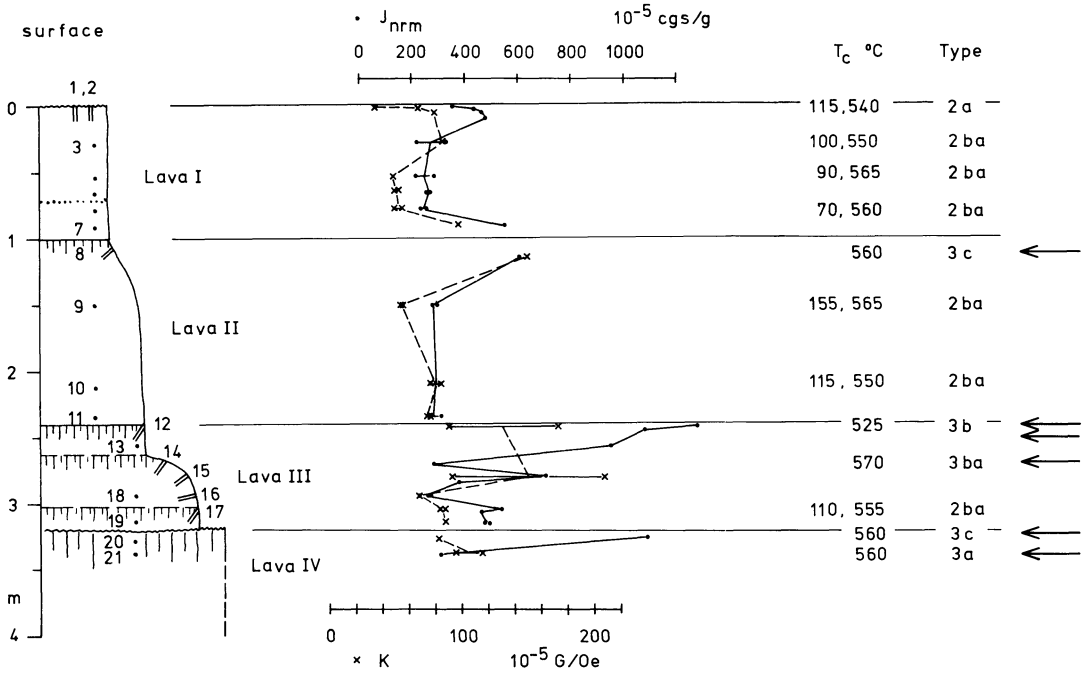

Fig. 13. Remagnetization at lava contacts. The upper four flow-units of the Peistareykjabunga are shown. The uppermost lava (still original surface) is not remagnetized but partially oxidized by atmospheric oxygen. All the other contacts are remagnetized as seen in increased J_{nrm}, T_c, and type of J_sT-curve (*arrows*). J_{nrm} = specific natural remanence (10^{-5} cgs/g); K = susceptibility (10^{-5} Gauss/Oe); T_c = Curie temperature (° C); Type = type of the J_sT-curve (see also Fig. 11a)

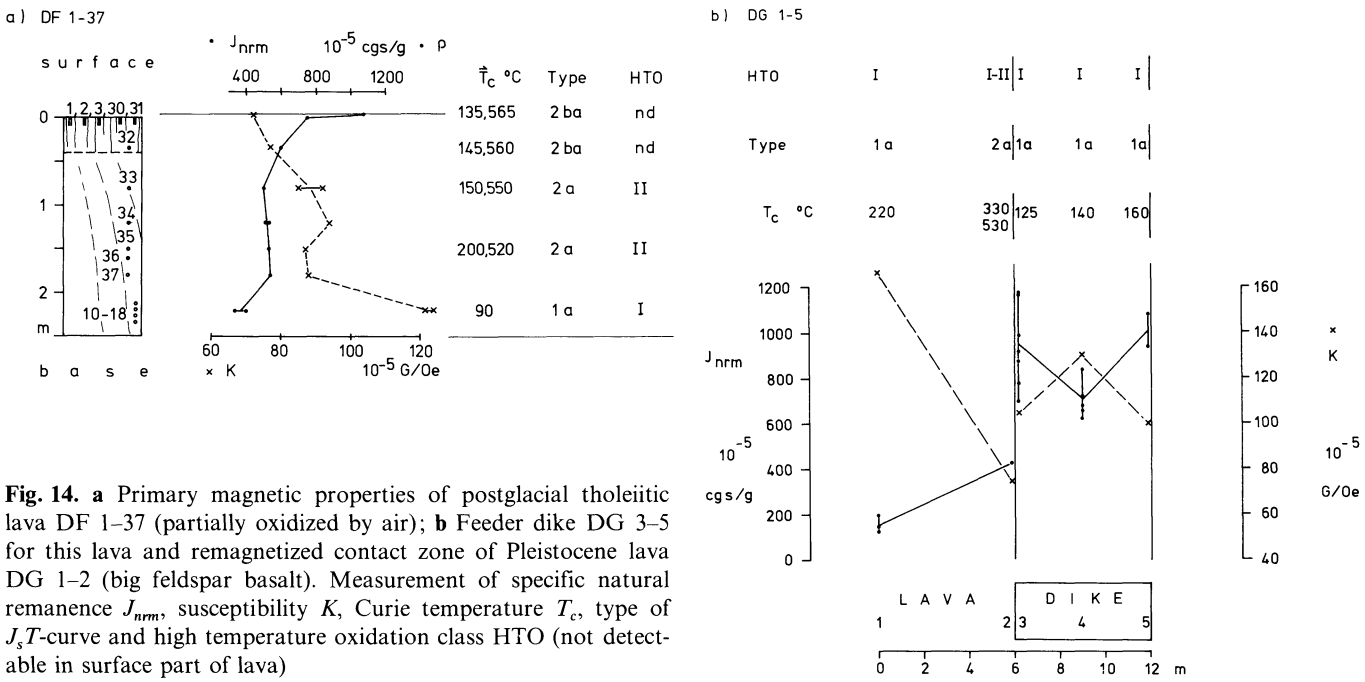

Fig. 14. a Primary magnetic properties of postglacial tholeiitic lava DF 1–37 (partially oxidized by air); **b** Feeder dike DG 3–5 for this lava and remagnetized contact zone of Pleistocene lava DG 1–2 (big feldspar basalt). Measurement of specific natural remanence J_{nrm}, susceptibility K, Curie temperature T_c, type of J_sT-curve and high temperature oxidation class HTO (not detectable in surface part of lava)

age width to be roughly 3.5 m which means that the primary Fe-Ti-oxides are homogeneous or only partly decomposed titanomagnetite. The low primary Curie temperature of dikes therefore restricts the Curie depth – a fact which does not support the interpretation of the regional anomalies by dike-swarms.

On the other hand, remagnetization of the dike contact zones would support a dike-swarm model for the interpretation of the regional geomagnetic anomalies. One can show that remagnetization fundamentally changes the initial magnetic properties (Figs. 13–16; Table 5) by increasing the intensity of the magnetization and the Curie temperature. On the basis of the model calculations one would expect a highly remagnetized contact zone of about 20% of the width of a lava or dike which actually should be more when taking into account multiple activity of feeder dikes and convection of heated groundwater (Jaeger, 1957; Mundry, 1968; for more details see Becker, 1978): The observed remagnetization of lava and dike contacts was also found to be in the range of 20% (Table 5), which again is rather unsatisfactory con-

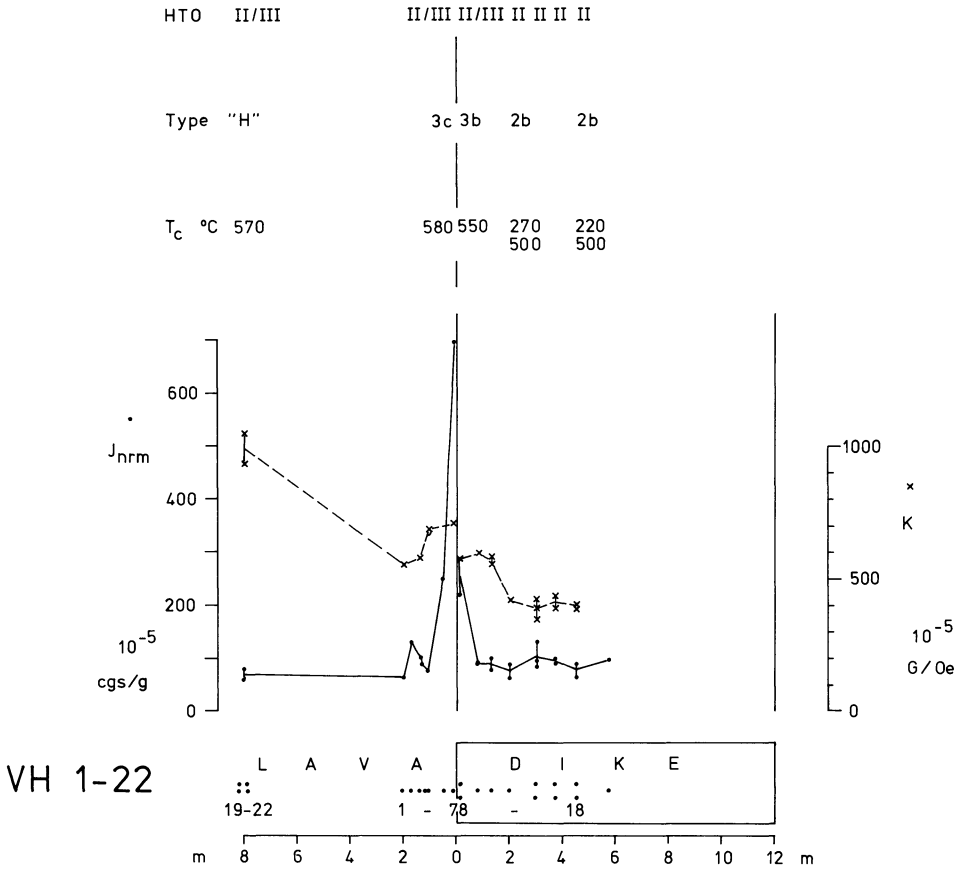

Fig. 15. Remagnetization at the contact of a 12 m Tertiary dike near Vikurvatn (site number *VH 1–22*) at 600 m altitude (stage D of hydrothermal alteration = mesolite/scolecite zone after Ade-Hall et al., 1971, see Figs. 13 and 14 for legend

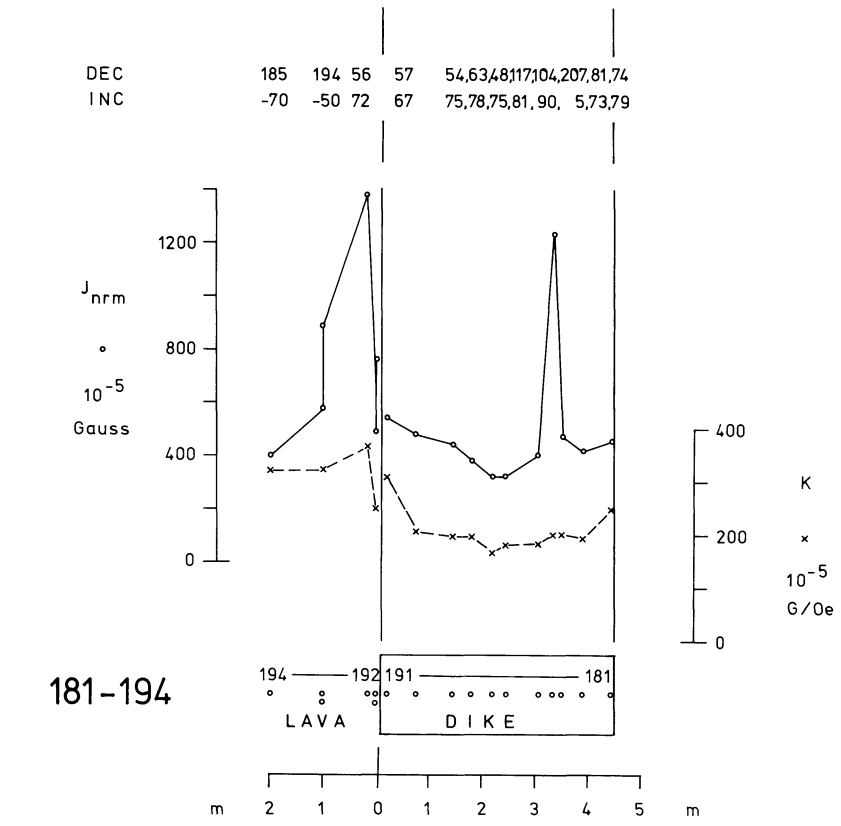

Fig. 16. Remagnetization at a dike contact (see Fig. 14 for legend). A 4.5-m-thick normally magnetized dike has remagnetized a reversely magnetized lava; dike and lava are hydrothermally altered (stage F = laumontite zone after Ade-Hall et al., 1971).
Dike. deuteric oxidation class II, J_sT-curve type: hump, $T_c = 470$, (550)° C.
Lava. deuteric oxidation class II/III; J_sT-curve type: kink, $T_c = 565$° C.

Table 5. Remagnetization (J_{re}) of the natural remanent magnetization (J_{nrmo} = undisturbed remanence) at contacts of dikes

1 Site number	2 Width of dike in m	3 Remagnetized contact zone with $J_{re}=2\times J_{nrmo}$ in m	4 in %	5 J_{re} total in m	6 J_{nrmo} in 10^{-5}G	7 J_{re} in 10^{-5}G
RF45–79	1.0	0.2–0.7	50	(1.8)	40	3000
Ba1–18	3.0?	0.6	20	0.8	210	2500
(263–280)	3.0?	0.6?		1.5	300	20
(181–194) (Fig. 16)	4.5	0.5?			600?	1350
RF32–44	5.0	0.8	16	1.0	150	1000
DG1–5 (Fig. 14)	6.0				150	1300
RN21–35	7.0	1.2	17	1.5	40	1000
VH1–21 (Fig. 15)	12.0	1.0	8	2.0	80	2000
RF1–31	7 (1)	1.5	21	1.6	25	1000
RF94–128	9(1)	–	1	–	80	
Mean.			20%			

1 Site number referring to sample list (Becker, 1978); see also Figs. 13–16
2: Width of dike in m
3: Width of remagnetized contact zone with $J_{re}=2\times J_{nrmo}$
4: Same in % of dike width
5: Total width of remagnetized zone with observable increase of magnetization
6: Intensity of natural remanence not remagnetized; J_{nrmo} in 10^{-5} Gauss
7: Maximum intensity of remanence due to remagnetization J_{re} in 10^{-5} Gauss

sidering the large bodies which must have been magnetized in the same polarity in order to cause the regional anomalies described.

Regarding the differences of primary magnetic properties between dike and lava, only the natural remanence gives evidence for the dike-swarm model. In thin tholeiitic dikes and lavas one expects homogeneous titanomagnetite with Curie temperature below 200° C (Petersen, 1976) which was also observed (Figs. 12 and 14b). Very often lavas are partially oxidized during effusion by the influence of air (Fig. 12; top lava in Fig. 13; Fig. 14). Only in thick lavas or thick dikes an internal decomposition takes places which results in the development of magnetite as a high Curie temperature phase (Petersen, 1976). For dikes a minimum width of about 10 m was observed for high primary Curie temperature (Table 4). This is rather rare; dikes are normally about 3 m in width (Walker, 1959; Piper et al., 1977).

Reheating of the basalt by further intrusion or effusion causes the titanomagnetite to oxidize into magnetite (Figs. 13–16). It was found that the remagnetized contact zone with a considerable increase of natural remanence and Curie temperature is only about 20% of the width of the dike or thickness of lava (Table 5). In view of the observed intensity of dike-swarms with less than 10% strain (Walker, 1959, 1974), this percentage is not sufficient to remagnetize the required large bodies of one polarity and high Curie temperature.

Apart from these processes at high temperature the magnetic minerals are altered at relatively low temperature. One should distinguish between normal weathering at temperatures less than 50° C, which produce maghemite, and hydrothermal alteration which is caused by active solutions at temperatures of 50°–300° C. Therefore one should consider that for model calculations the original magnetic properties are not correct – especially not for older rocks or rocks at depth. A good indicator for all of the above mentioned processes at high and low temperature is the type of the J,T-curve which shows the alteration of the thermomagnetic properties and in the case of hydrothermal alteration the characteristic hump and kink type (Fig. 17; see also Ade-Hall et al., 1971).

In eastern Iceland the hydrothermal alteration can be studied at 1.5 km depth of burial at maximum temperatures of 200° C using the zeolitization as an indicator for the paleo-temperature (Walker, 1960; Ade-Hall et al., 1971). The magnetic properties of the basalts are strongly affected by hydrothermal alteration (Table 3; Figs. 12 and 17). The intensity of natural remanence decreases while the Curie temperature and susceptibility increase (for a quantitative graph of the decrease of magnetization versus stage of hydrothermal alteration see Watkins and Walker, 1977). It seems that the Curie temperatures of dikes are less affected than those of lavas at the same stage of regional metamorphism (Fig. 12). This could be explained by the greater water content of the porous lava. But the trend in the hydrothermal alteration due to burial leads to the suggestion, that at a depth of about 2 km the magnetic properties of lavas and dikes will be equalized. The simple dike-swarm model therefore should be modified to one in which gabbros are connected at depth with the dike-swarms.

4. Conclusions

The regional geomagnetic anomalies of more than 5 km wavelength and strong resemblance to ocean-ridge anomalies, can only be interpreted by highly magnetized bodies several kilometres thick. Lava piles can therefore be excluded because of their change of polarity every 100 m on average (e.g., Dagley et al., 1967; Watkins and Walker, 1977). The magnetic survey which crossed several dike-swarms in the Reydarfjördur-Thingmuli region, as well as rock magnetic investigations of dikes and the remagnetization of their contacts do not support the interpretation of the elongated anomalies by dike-swarms either. Nevertheless, at least some of

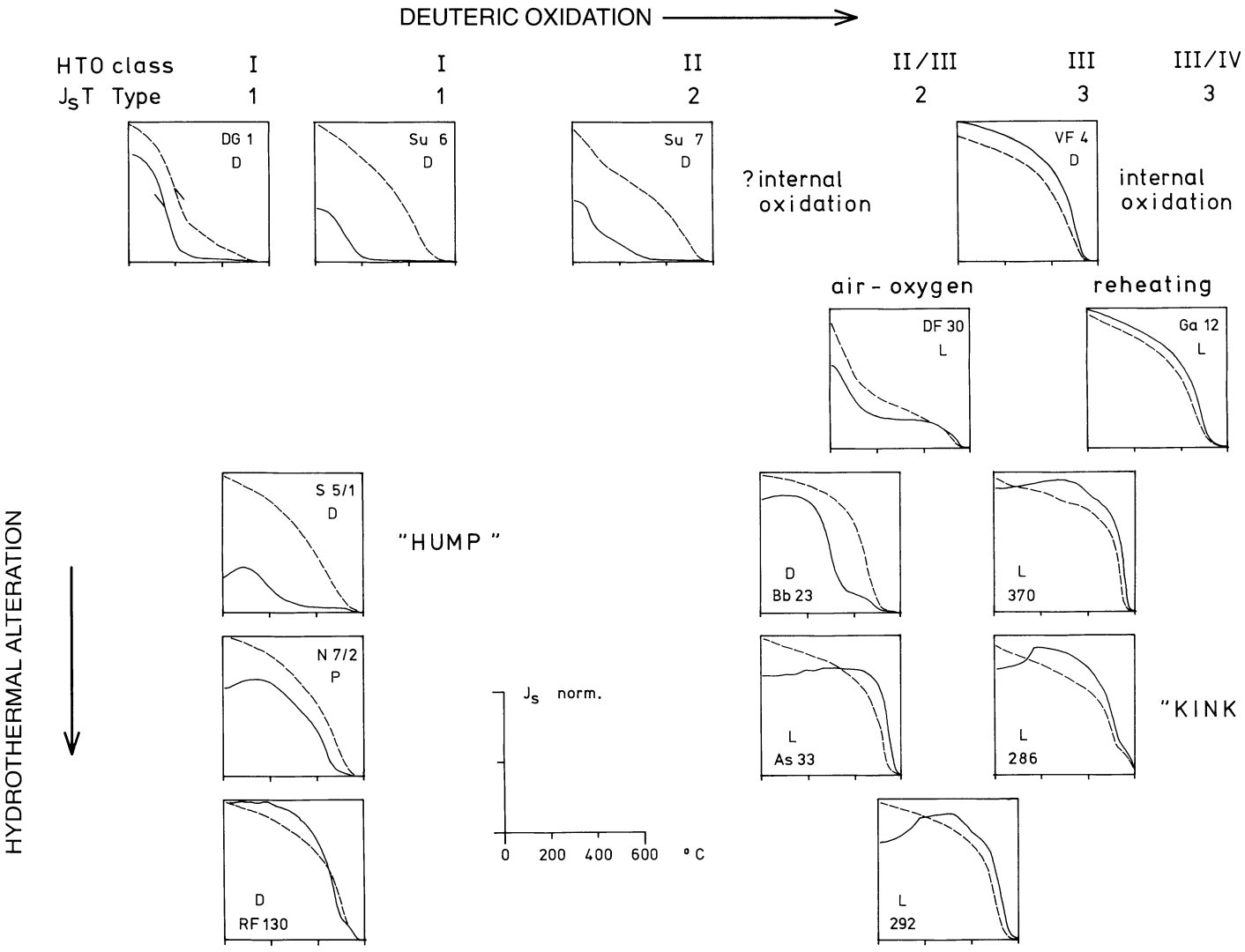

Fig. 17. Alteration of the primary magnetic properties of titanomagnetite by deuteric oxidation, influence of athmospheric oxygen, reheating and hydrothermal alteration indicated by the type of the J_sT-curve (numbers refer to sample list of Becker (1978); L=lava, D=dike or intrusion, P=pillow)

the regional anomalies may be caused by dike-swarms such as the Breiddalur dike-swarm. Another possible explanation for the regional geomagnetic anomalies observed is given by gabbros at depth which should be studied more closely.

5. *Acknowledgements.* Many thanks are due to Professor Dr. H. Soffel, Dr. C. Schweitzer, Dr. U. Kramm, and Dipl. Min. T Sachtleben for their help during the 1973 campaign in Iceland as well to Dr. G. Pálmasson, Dr. K. Saemundsson, Professor T Sigurgeirsson and Dr. L. Kristjansson. The evaluation of the field data and the rock-magnetic investigations were made at the Institut für Allgemeine und Angewandte Geophysik, Universität München under the supervision of Professor Dr. H. Soffel who also read this article. I have benefited greatly from discussions with Professor Dr G. Angenheister, Dr. N. Petersen, Dr. J. Pohl, Dr. A. Schult, Dr. G. Schönharting, Dr. C. Schweitzer, and Dr. L. Kristjansson. Most of the microscope work was done at Mineralogisch-Petrographisches Institut, Universität zu Köln under the supervision of Dr. U. Kramm. The financial support of Deutsche Forschungsgemeinschaft is gratefully acknowledged.

References

Ade-Hall, J.M., Palmer, H.C., Hubbard, T.R. The magnetic and opaque petrological response of basalts to regional hydrothermal alteration. Geophys. J. R. Astron. Soc. **24**, 137–174, 1971

Angenheister, G., Becker, H., Mohr, H.P.: Bodenvermessung des erdmagnetischen Feldes (ΔZ) in Nord-Island längs Profilen. In: Das Unternehmen Erdmantel, W. Kertz et al. eds.; pp. 113–118. Wiesbaden 1972

Angenheister, G., Petersen, N., Schönharting, G. Zur Interpretation der Anomalien des Erdmagnetfeldes in Island. Fortschr. Mineral. **54**, 54–92, 1977

Becker, H. Vermessung des erdmagnetischen Feldes (ΔZ) längs Profilen in Nordost- und Ost-Island und der Versuch der Interpretation unter Berücksichtigung gesteinsmagnetischer Untersuchungen. Diss. Universität München, 1–269, 1978

Becker, H., Mohr, H.P. Vermessung des erdmagnetischen Feldes längs einiger Profile in Nord-Island, deren Auswertung und Interpretation. Dipl. Arbeit. Universität München 1971

Bödvarsson, G., Walker, G.P.L. Crustal drift in Iceland. Geophys. J.R. Astron. Soc. **8**, 285–300, 1964

Dagley, P., Wilson, R.L., Ade-Hall, J.M., Walker, G.P.L., Haggerty, S.E., Sigurgeirsson, T., Watkins, N.D., Smith, P.J., Edwards, J., Grasty, P.L. Geomagnetic polarity zones for Icelandic lavas. Nature **216**, 25–29, 1967

Gale, N.H., Moorbath, S., Simons, J., Walker, G.P.L.· K-Ar ages of acid intrusive rocks from Iceland. Earth Planet. Sci. Lett. **1**, 284–288, 1966

Heirtzler, J.R., Dickson, G.O., Harron, E.M., LePichon, X.. Marine magnetic anomalies, geomagnetic reversals and motions of the ocean floor and continents. J. Geophys. Res. **73**, 2119–2136, 1968

Jaeger, J.C.. The temperature in the neighbourhood of a cooling intrusive sheet. Am. J. Sci. **255**, 306–318, 1957

Kristjansson, L.. Palaeomagnetism and magnetic surveys in Iceland. Earth Planet. Sci. Lett. **8**, 101–108, 1970

McDougall, I.M., Watkins, N.D., Walker, G.P.L., Kristjansson, L. Potassium-Argon and paleomagnetic analysis of Icelandic lava flows: Limits on the age of anomaly 5. J. Geophys. Res. **81**, 1505–1512, 1976

Moorbath, S., Sigurdsson, H., Goodwin, R. K-Ar ages of the oldest exposed rocks in Iceland. Earth Planet. Sci. Lett. **4**, 197–205, 1968

Mundry, E. Über die Abkühlung magmatischer Körper. Geol. Jahrb. **85**, 775–776, 1968

Pálmason, G.. Kinematics and heat flow in a volcanic rift zone, with application to Iceland. Geophys. J.R. Astron. Soc. **33**, 451–481, 1973

Petersen, N.. Notes on the variation of magnetization within basalt lava flows and dikes. Pure Appl. Geophys. **114**, 177–193, 1976

Piper, J.D.A.: Interpretation of some magnetic anomalies over Iceland. Tectonophysics **16**, 163–187, 1973

Piper, J.D.A., Fowler, M.G., Gipson, I.L.. Dyke magnetization and upper crustal structure in the Reydarfjördur area of Eastern Iceland. Tectonophysics **40**, 227–244, 1977

Rutten, K.. Two-dimensionality of magnetic anomalies over Iceland and Reykjanes Ridge. Marine Geophys. Res. **2**, 243–263, 1975

Saemundsson, K. Evolution of the axial rifting zone in Northern Iceland and the Tjörnes Fracture Zone. Bull. Geol. Soc. Am. **85**, 495–504, 1974

Schönharting, G.. Vermessung des erdmagnetischen Feldes längs einiger Profile in Nord-Island, deren Auswertung und Interpretation. Diss. Universität München, 1–121, 1969

Serson, P.H., Hannaford, W., Haines, G.V.. Magnetic anomalies over Iceland. Science **162**, 355–357, 1968

Sigurgeirsson, T.: Aeromagnetic survey of SW-Iceland. Science in Iceland **2**, 13, 1970

Walker, G.P.L.. Geology of the Reydarfjördur area, E-Iceland. Q. J. Geol. Soc. London **114**, 367–393, 1959

Walker, G.P.L.: Zeolithe zones and dike distribution in relation to the structure of the basalts of Eastern Iceland. J. Geol. **68**, 515–528, 1960

Walker, G.P.L.: The Breiddalur central volcano, E-Iceland. Q. J. Geol. Soc. London **119**, 29–63, 1963

Walker, G.P.L.: The structure of eastern Iceland. In. Geodynamics of Iceland and the North Atlantic area. L. Kristjansson, ed.; pp. 177–188. Dordrecht: Reidel 1974

Ward, P.L. New interpretation of the geology of Iceland. Bull. Geol. Soc. Am. **280**, 2991–3312, 1971

Watkins, N.D., Walker, G.P.L.: Magnetostratigraphy of eastern Iceland. Am. J. Sci. **277**, 513–584, 1977

Wilson, R.L., Haggerty, S.E.. Reversals of the earth's magnetic field. Endeavour **25**, 104–109, 1966

Received August 1, 1979; Revised Version November 12, 1979

J. Geophys. 47, 57–60, 1980

Journal of Geophysics

Palaeointensity Measurements on Postglacial Lavas From Iceland

Ch. Schweitzer[1] and H.C. Soffel[2]

[1] Gewerkschaften Brigitta-Elwerath, Riethorst 12, 3000 Hannover 51, Federal Republic of Germany
[2] Institut für Allgemeine und Angewandte Geophysik, Theresienstraße 41, D-8000 München 2, Federal Republic of Germany

Abstract. Palaeointensities were determined mainly with the Thellier method (in some cases additionally with the Wilson and the Van Zijl method) on 17 postglacial lava flows from Iceland with ages between 196 and 10,500 years B.P. The mean pole position of all lava flows, at 257. 3° E, 89.1° N, agrees well with the actual pole of rotation. Within the limits of error, the palaeointensities confirm also for Iceland the general trend observed for Europe and Japan of a decreasing palaeofield intensity since the maximum at about 2,000–3,000 years B.P. The field minimum at about 6,000 years B.P. could not be tested as no flows of about that age span have been available. Another maximum at about 9,000 years B.P. and earlier minimum at about 11,000 years B.P. fit also in the palaeointensity secular variation curve determined by Bucha (1967) for Czechoslovakia.

Key words: Iceland – Postglacial lavas – Palaeomagnetism – Palaeointensities – Secular variation.

1. Introduction

The palaeointensity of the geomagnetic field can be determined from lavas, baked rocks and soils by comparing the properties of natural remanence acquired in the unknown palaeofield with an artifical remanence obtained by heating and cooling in a field of known intensity. Various methods have been developed (Thellier and Thellier, 1959; Wilson, 1961; Van Zijl et al., 1962), which have been tested both theoretically and experimentally by various authors in recent years (Coe and Grommé, 1973; Schweitzer, 1975; Dunlop and Waddington, 1975; Kono and Ueno, 1977). Details and advantages of the different methods cannot be discussed here.

This paper reports on palaeointensity measurements made on postglacial lavas from Iceland with the view of contributing to the knowledge of the secular variation in Iceland in the last 10,000 years.

2. Sampling

Sampling was carried out in 1973 in connection with a ground magnetic survey in NE Iceland by Becker (1978). Figure 1 shows the 17 sites at which a minimum of B oriented cores were drilled. Accurate descriptions of the sampling sites are given by Schweitzer (1975). About one half of the samples were oriented by means of a sun compass, otherwise a magnetic compass was used (see Table 1). Whenever possible, samples were taken from various points across a profile from the top to the bottom of the lava flows. However, systematic studies of the variation of palaeointensity across a lava flow have not been made. The ages of the lavas flows (see Table 1) are either known directly as an historical event (H) or have been determined by means of C 14 method on baked peat (C) or by tephrochronology (T) (Brynjolfsson, 1957; Thorarinsson, 1967; Thorarinsson et al., 1973).

3. Palaeomagnetic Measurements

Test specimens from all 17 sites were subjected to AF and thermal demagnetization (1,200 Oe, 550° C). In all cases only a minor component of a secondary viscous remanence was found, which could be erased with AF fields of about 100 Oe or by thermal cleaning at 100° C. Table 1 shows the analysis of the directions of stable remanence. The corresponding pole positions are plotted in Fig. 2 together with the ages. The mean pole position at 257.3° E, 89.1° N ($N=17$, $R=16.58$, $k=37{,}9$, $\alpha_{95}=5.8°$) is in good agreement with the actual pole of rotation. The dashed line shows the migration of the virtual geomagnetic pole determined by Brynjolfsson (1957) from lavas of the last thousand years indicating a very rapid secular variation. Our data are too sparse for the evaluation of a similar curve for earlier periods.

4. Rock Magnetic Investigations

All past experiments on palaeointensity determination have shown that the nature and properties of the ferrimagnetic carriers of remanence strongly influence the applicability of the various methods to a given set of samples. A vital requirement is that the ore fraction is essentially free from hydrothermal or low temperature oxidation which tends to alter the primary fresh titano-

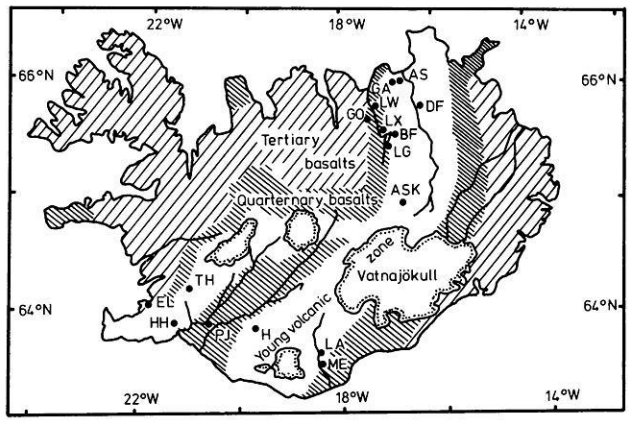

Fig. 1. Sketch map of Iceland showing the sampling sites

0340-062X/80/0047/0057/$01.00

Table 1. Palaeomagnetic data of postglacial lavas from Iceland

1	2	3	4	5	6	7	8	9	10	11	
Locality	Age	Method	Orientation	N	H(Oe)	D	I	α_{95}	k	°N	°E
AS I	10,500	T	mc	31	100	349.4	72.5	1.45	302	80.4	232.5
AS II	10,500	T	mc	16	100	7.9	70.2	2.76	161	77.6	174.5
BF	2,000	T	mc	11	100	31.3	77.4	3.25	169	77.3	91.1
DF	6,000	T	mc	11	100	42.0	76.6	2.06	419	72.6	92.4
EL	4,630	C	mc	12	100	332.9	72.5	2.48	266	75.5	278.1
GA I	10,500	T	mc	7	100	33.9	77.5	5.15	106	76.4	90.7
GA II	10,500	T	mc	6	100	353.7	68.8	4.40	169	75.8	212.6
GO	8,000	T	mc	16	100	339.0	71.0	1.37	653	75.6	252.3
HH I	1,500–2,000	T	mc	15	100	0.9	78.2	1.82	396	86.7	27.3
HH II	1,000	T	sc	13	100	14.4	74.1	3.74	108	82.4	133.4
LA	196	H	sc	12	100	311.1	73.5	2.70	219	66.9	300.2
LG	3,800	T	sc	8	100	334.4	72.6	3.71	183	75.8	266.4
LW	2,000	T	sc	16	100	346.5	79.8	2.39	214	83.3	334.5
LX	2,000	T	sc	16	100	356.7	78.7	2.78	159	87.1	352.3
ME	2,000	T	sc/mc	15	100	348.0	76.8	6.50	32	84.6	307.4
PJ	8,100	C	sc/mc	9	100	20.5	75.2	2.36	391	80.6	112.0
TH	9,100	C	sc	12	100	30.2	84.8	3.19	138	72.4	38.4
Mean pole position				17				5.80	38	89.1	257.3

1 Locality, 2: Age in years, 3: Age determination method (T: tephrochronology, C: C 14 method, H: historic event); 4: Orientation method (*mc*: magnetic compass, *sc*: sun compass). 5: Number of specimens, 6: *AF* demagnetizing field, 7· Declination, 8: Inclination, 9: Radius of cone of 95% confidence, 10: Precision parameter, 11 Pole position

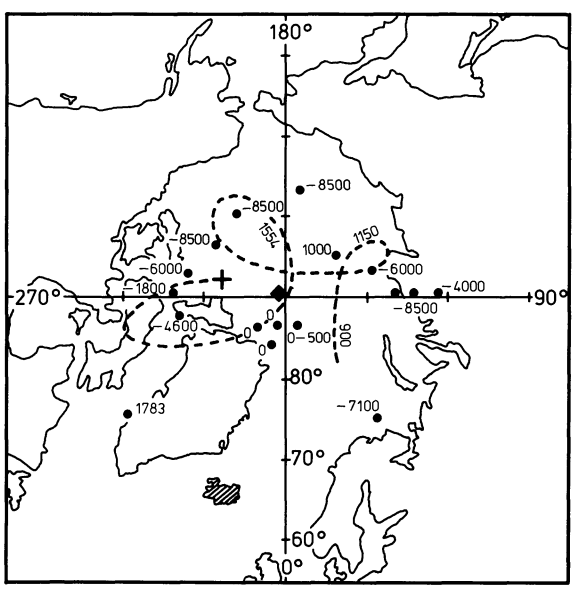

Fig. 2. Virtual geomagnetic pole positions (VGP) of postglacial lavas from Iceland with ages of extrusion. *Square*. mean pole position. *Cross*. geomagnetic pole of the reference field for 1965. *Dashed curve*. migration of the VGP during the last 1,000 years in Iceland after Brynjolfsson (1957)

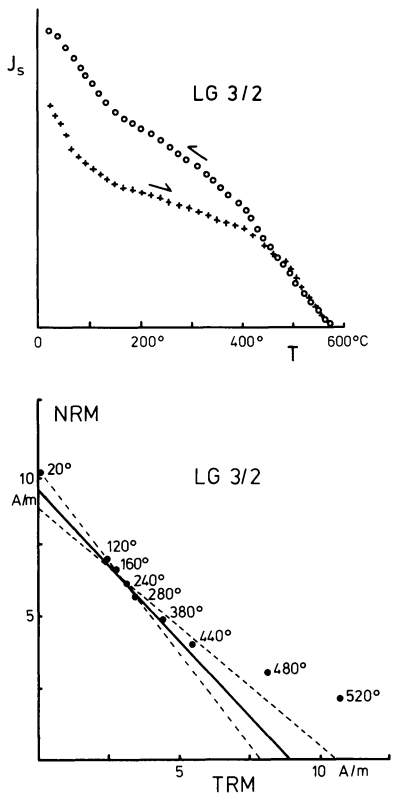

Fig. 3a and b. Older Laxá-lava (age: 3,800 years). **a** J_s/T-curve showing two Curie-temperatures (100° and 560° C). **b** Palaeointensity determination with the Thellier method. For explanation see text

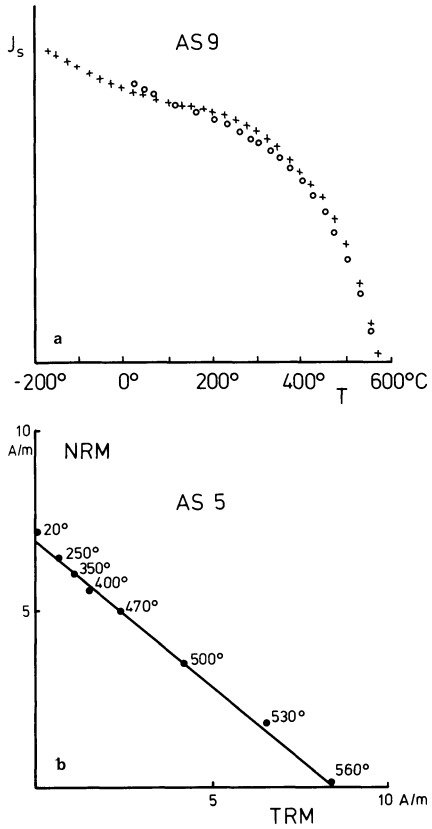

Fig. 4a and b. Lava from Asbyrgi (age: 10,500 years). **a** J_s/T-curve showing a single Curie temperature at 560° C. *Crosses*. heating curve; *circles* cooling curve. **b** Palaeointensity determination with the Thellier method. For explanation see text

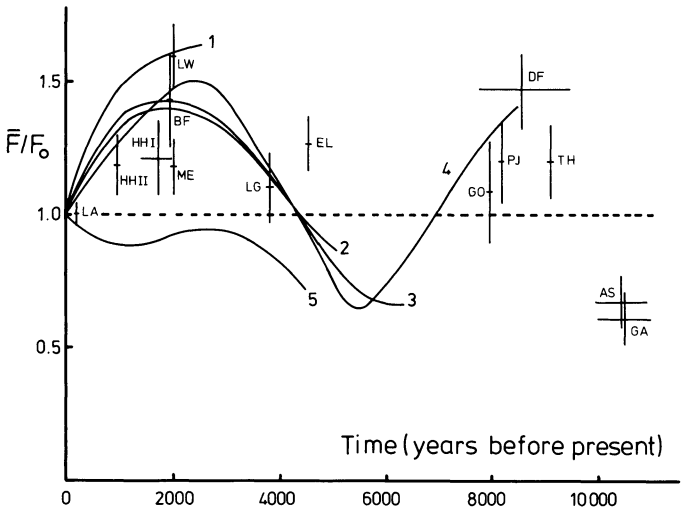

Fig. 5. Normalized secular variation of palaeointensity during the last 10,000 years for France (1), USSR (‘), Japan (3), Czechoslovakia (4) and India (5). For references see text. Normalized palaeointensities of postglacial lavas from Iceland. *Vertical* and *horizontal bars* indicate inaccuracies with respect to intensity and age

magnetites into cation deficient titanomaghemites with other physical parameters.

Ore microscopic studies showed that all lavas possess a primary titanomagnetite phase coexisting with hemoilmenite, both in the form of unexsolved skeletal crystals. They can in general be attributed to classes II and III of high temperature oxidation according to Ade-Hall et al. (1968). Only slight indications of low temperature oxidation could be detected microscopically. In a few cases the ore grains were too small to allow a detailed optical investigation.

Most thermomagnetic (J_s/T) curves are more or less irreversible after heating to temperatures higher than about 400° C and show two Curie temperatures (Fig. 3a). Only the lavas of the shield volcano Theistareikjabunga (As, GA: $T_c = 560°$ C) and from Burfellsrhaun (BF: $T_c = 550°$ C) show a single Curie temperature and more or less reversible J_s/T-curves (Fig. 4a).

5. Palaeointensity Measurements and Results

Details of the equipment used and of the various methods are given by Schweitzer (1975) where it was shown that for those rocks with two Curie temperatures reliable palaeointensity data could be obtained with the Thellier method. An example is shown in Fig. 3b. The decay of partial natural remanence during thermal demagnetization in a zero magnetic field is plotted versus the increase of an artificial partial thermoremanent magnetization in a field of known intensity. The slope, $m = -F/H$ of the best fitting line in a temperature interval with no viscous remanence, represents the ratio between the intensities of the palaeofield F and the laboratory field H. The dashed lines represent the greatest and smallest slope of best fitting lines on the 95% confidence level based on a Student test. This means that the true slope corresponding to the true palaeointensity should be between the dashed lines with 95% probability. The error of the measured palaeointensity is defined accordingly (see Table 2).

Lavas with only one Curie temperature around 550° C and more or less reversible J_s/T-curves produced similar palaeointensity values for different methods (Schweitzer, 1975). An example of a palaeointensity determination with the Thellier method on a lava from Asbyrgi is shown in Fig. 4b.

In Table 2 all palaeoinsity data are listed. Information is also given on the ages and some rock magnetic properties. For details see legend of Table 2.

A plot of the palaeointensities versus age is shown in Fig. 5 together with other intensity variations obtained for France (1), USSR (2), Japan (3), Czechoslovakia (4), and India (5) compliled by Bucha (1967), Kinoshita (1970), Kitazawa (1970). The data from Iceland are in general agreement with the results obtained for Europe and Japan for the last 4,000 years. For the presumed intensity minimum between 4,000 and 8,000 years B.P. no additional data could be provided. Icelandic rocks with ages between 8,000 and 10,000 years seem to confirm the maximum obtained by Bucha (1967) for Czechoslovakia. The older lavas (AS, GA) indicate another intensity minimum following the maximum at about 9,000 years B.P.

Acknowledgement. The measurements were made in the Institute für Allgemeine und Angewandte Geophysik, University of München. We thank its director, Professor Dr. G. Angenheister, as well as Dr. N. Petersen, Dr. A. Schult, and Dr J. Pohl for their help and encouragement. Thanks are also due to various colleagues from Iceland (Dr. G. Pálmasson, Dr. K. Saemundsson, Dr. T Sigurgeirsson, and Dr. L. Kristjansson) for their advice with regard to sampling localities. The financial support of the Deutsche Forschungsgemeinschaft is gratefully acknowledged.

Table 2. Palaeointensity data of postglacial lavas from Iceland

Number	Age	T_c(°C)	T_c(°C)	ΔJ_s	Class	Method	H(Oe)	ΔT, ΔH	F(Oe)	ΔF(Oe)	$\bar{F}$(Oe)	$\bar{F}/F_o$
AS 4	10,500		560	− 5		MWI	0.42	100– 560° C	0.36		0.33	0.65
AS 5						MTH	0.42	100– 530° C	0.35			
AS 6		−100	550	− 3	III/IV	MVZ	0.50	200–1,200 Oe	0.32			
AS 9		− 20	550	0	III/IV	MVZ	0.50	100–1,200 Oe	0.34			
BF 8	2,000		550	+ 1	III	MTH	0.50	20– 440° C	0.74	0.09	0.72	1.41
BF 5						MTH	0.50	50– 440° C	0.70	0.08		
DF 35	8,000–	200	520	+12	II	MTH	0.50	20– 380° C	0.81	0.18	0.76	1.49
DF 37	10,000					MTH	0.50	20– 390° C	0.70	0.14		
EL 1	4,630	170	510	+12	II	MTH	0.50	20– 440° C	0.72		0.66	1.29
EL 3						MTH	0.50	20– 345° C	0.60	0.08		
GA 8	10,500		555	− 6	III/IV	MTH	0.50	20– 520° C	0.31	0.06	0.32	0.63
GA 21			560	− 9		MTH	0.50	20– 550° C	0.33			
GO 2	8,000	200	490	+25	–	MTH	0.50	20– 340° C	0.54	0.15	0.56	1.10
GO 15						MTH	0.50	50– 390° C	0.58	0.19		
HH 2	1,500–	200	540		III	MTH	0.50	20– 390° C	0.63	0.12	0.63	1.24
HH 7	2,000					MTH	0.50	20– 440° C	0.62	0.14		
HH 20	1,000	180	515	+15	II/III	MTH	0.50	50– 440° C	0.61	0.09	0.61	1.20
LA 4	196	170	510	+25	II	MTH	0.50	50– 440° C	0.49	0.02	0.49	0.96
LG 3	3,800	100	560	+35	–	MTH	0.50	50– 440° C	0.54	0.09	0.52	1.02
LG 6						MTH	0.50	50– 440° C	0.49	0.10		
LW 7	2,000	200	560	− 1	II	MTH	0.50	20– 440° C	0.81	0.20	0.82	1.61
LX 7						MTH	0.50	20– 440° C	0.83	0.13		
ME 2	2,000		300	+ 8	I/II	MTH	0.50	20– 380° C	0.61	0.06	0.61	1.20
PJ1	8,100	200	410	+ 9	II/III	MTH	0.50	20– 440°C	0.75	0.20	0.69	1.35
PJ 3						MTH	0.50	20– 390° C	0.62	0.12		
TH 1	9,100	200	560	+33	III	MTH	0.50	20– 440° C	0.56	0.10	0.56	1.10

1: Locality; 2: Age in years; 3: Lower Curie temperature; 4: Upper Curie temperature; 5: Relative change of saturation magnetization at 20° C before and after heating to 600° C in percent; 6: Class of high temperature oxidation after Ade-Hall et al. (1968); 7: Palaeointensity method (*MWI*: Wilson; *MTH*: Thellier; *MVZ*: Van Zijl); 8: Field intensity for the generation of artificial partial thermoremanent magnetization; 9: Best temperature or *AF*-field interval respectively for palaeointensity determination; 10: Palaeointensity, 11. Standard deviation, 12: Mean palaeointensity; 13: Mean normalized palaeointensity with respect to the present field intensity in Iceland

References

Ade-Hall, J.M., Khan, M.A., Dagley, P., Wilson, R.L.: A detailed opaque petrological and magnetic investigation of a single Tertiary lava flow from Skye, Scotland. Geophys. J. R. Astron. Soc. **16**, 375–399, 1968

Becker, H.. Vermessung des erdmagnetischen Feldes (△Z) längs Profilen in Nordost- und Ost-Island und der Versuch der Interpretation unter Berücksichtigung gesteinsmagnetischer Untersuchungen. Univ. München: Dissertation Fak. Geowiss. 1978

Brynjolfsson, A.. Studies of remanent magnetism and viscous magnetism in the basalts of Iceland. Adv. Phys. **6**, 247–254, 1957

Bucha, V. Archaeomagnetic and palaeomagnetic study of the magnetic field of the earth in the past 600,000 years. Nature **213**, 1005–1007, 1967

Coe, R.S., Grommé, C.S.. A comparison of three methods of determining geomagnetic palaeointensities. J. Geomagn. Geoelectr. **25**, 415–435, 1973

Dunlop, D.J., Waddington, E.D. The field dependence of thermoremanent magnetization of igneous rocks. Earth Planet. Sci. Lett. **25**, 11–25, 1975

Kinoshita, H.: Lists of archaeomagnetic and palaeomagnetic results. J. Geomag. Geoelectr. **22**, 507–550, 1970

Kitazawa, K.. Intensity of the geomagnetic field in Japan for the past 10,000 years. J. Geophys. Res. **75**, 7403–7411, 1970

Kono, M., Ueno, N.· Palaeointensity determination by a modified Thellier method. Phys. Earth Planet. Inter. **13**, 305–314, 1977

Schweitzer, Ch.: Vergleich mehrerer Methoden zur Bestimmung der Intensität des Erdmagnetfeldes an rezenten Laven und ihre Anwendung auf mesozoische und paläozoische magmatische Gesteine. Diss. Univ. München. Fak. Geowiss. 1975

Thellier, E., Thellier, O. Sur l'intensité du champ magnétique terrestre dans le passé historique et géologique. Ann. Géophys. **15**, 285–376, 1959

Thorarinsson, S.· Hekla and Katla: Iceland and mid-ocean ridges. Report of a symposium. Reykjavik 1967

Thorarinsson, S., Steinthorsson, S., Einarsson, Th., Kristmannsdottir, H., Oskarsson, N.: The eruption on Heimaey, Island. Nature **241**, 372–375, 1973

Wilson, R.L.· Palaeomagnetism in Northern Ireland. Part I: The thermal demagnetization of natural magnetic moments in rocks. Geophys. J. R. Astron. Soc. **5**, 45–58, 1961

Zijl, I.S.V Van, Graham, K.W., Halls, A.L.: The palaeomagnetism of the Stormberg lavas: II. The behaviour of the magnetic field during a reversal. Geophys. J. R. Astron. Soc. **7**, 169–182, 1962

Received May 3, 1979; Revised Version June 29, 1979

J. Geophs. 47, 61–66, 1980

Journal of Geophysics

On the Evolution of the Reykjanes Ridge South of 60° N Between 40 and 12 Million Years Before Present

D. Voppel and R. Rudloff

Deutsches Hydrographisches Institut, Postfach 220, D-2000 Hamburg 4, Federal Republic of Germany

Abstract. A geophysical reconnaissance survey of the western flank of the Reykjanes Ridge between 56° and 60° N resulted in locating a system of fracture zones in the area of crustal ages between 40 and 12 Ma. This system corresponds to a similar one discovered by Vogt and Avery on the eastern flank of the ridge. Rotating anomaly 13 from the east to the west using a pole of rotation of 68.4° N, 133,8° E and an opening angle of 7.78°, a satisfactory coincidence of anomalies 13 of both surveys could be attained. Accordingly the formation of this system during the seafloor spreading process seems to be proved.

Key words: Magnetic anomalies – Gravity anomalies – Seafloor spreading – Plate tectonics – Reykjanes ridge.

Introduction

Several authors, e.g., Heirtzler et al. (1968), Godby et al. (1968), Talwani et al. (1971), Herron and Talwani (1972), Fleischer et al. (1973), Meyer et al. (1972), Bott (1974), Fleischer et al. (1974),

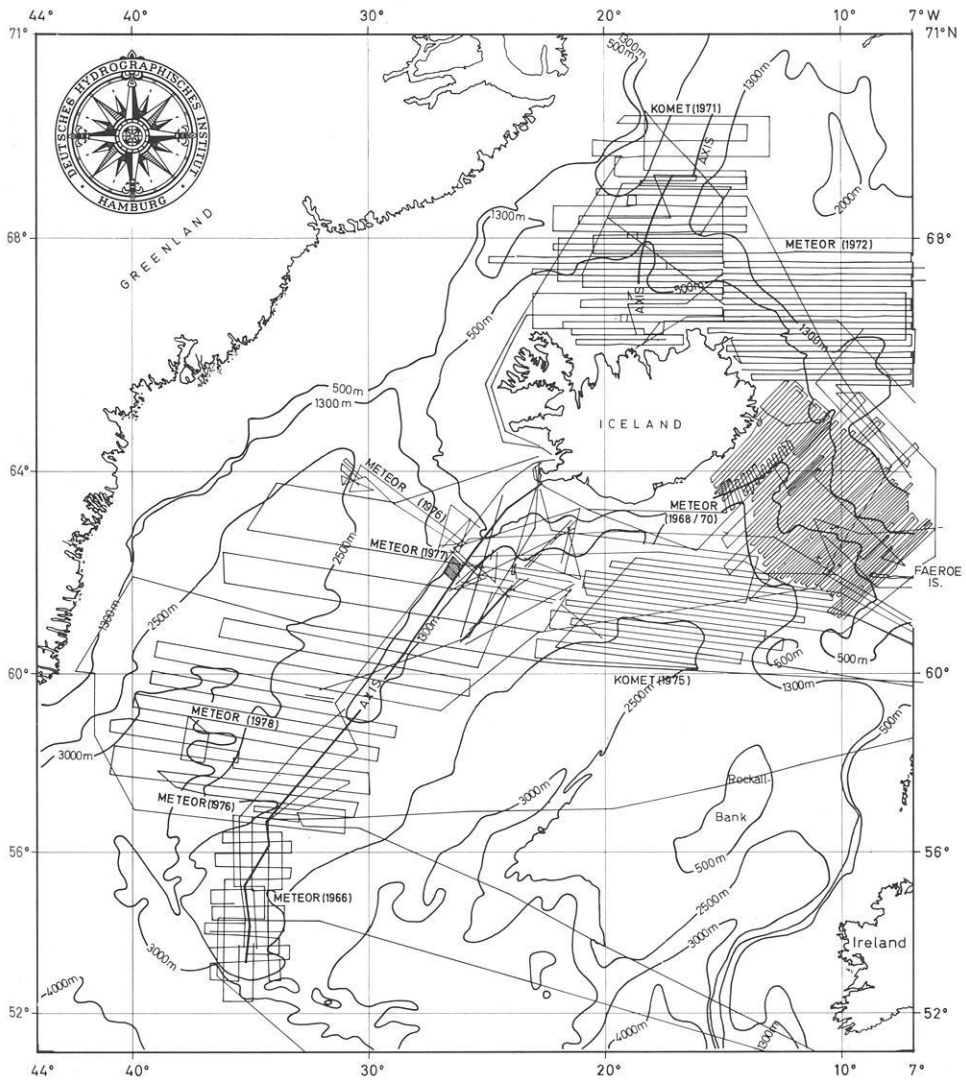

Fig. 1. Location of surveyed areas and tracks of magnetic and gravity measurements of Deutsches Hydrographisches Institut with general bathymetry

0340-062X/80/0047/0061/$01.20

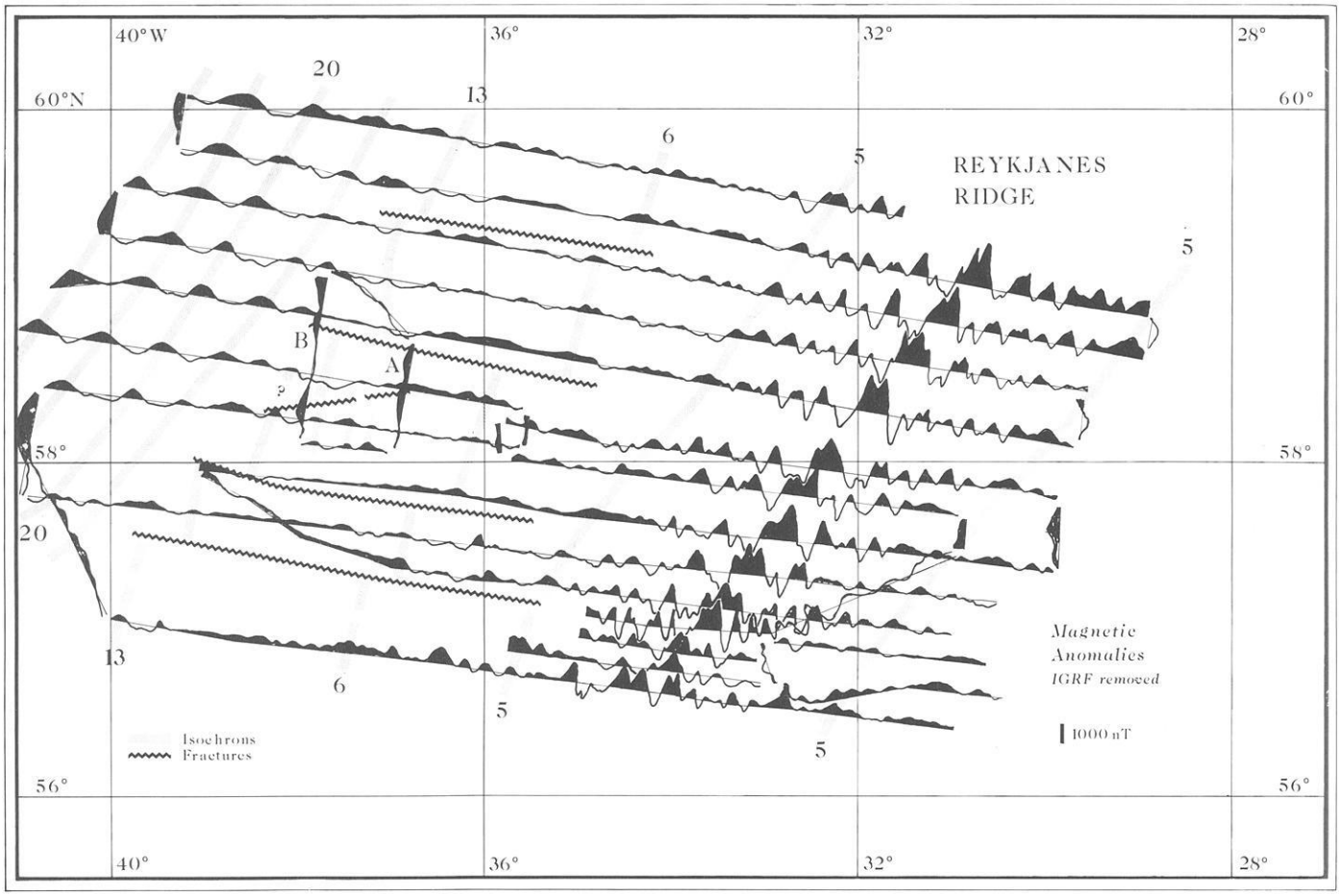

Fig. 2. Plots of profiles of magnetic anomalies. Positive anomalies black. Lineations of anomalies Nos. 5, 6, 13, 18, 20, 21, and 22 indicated. A and B are tracks where reflection seismic data are existing, too

Vogt and Avery (1974), Talwani and Eldholm (1977), contributed to the reconstruction of the main features of the evolution of the North Atlantic Ocean in the area of the Reykjanes Ridge and the Norwegian Sea. The first opening occurred about 60 Ma ago according to the time scale of Heirtzler et al. (1968) which is used in this paper. A revised time scale indicates 56 Ma (LaBrecque et al., 1977). The first positive anomaly developed was anomaly 24. Recently Srivastava (1978) assumed that opening had already started with anomaly 32 at a very slow spreading rate. Greenland was then a plate moving independently from the North American plate from which it was separated by the active ridge in the Labrador Sea (Ran Ridge). When the activity at the Ran Ridge ceased at about 40 Ma (Srivastava, 1978) the Greenland plate became fixed to the North American plate. The development of the Reykjanes Ridge was then characterized by more or less continuous and steady sea-floor spreading. In the Norwegian Sea the sea-floor spreading process terminated at the now extinct ridge axis at anomaly 7 time (28 Ma). The axis jumped to the west and separated the Jan Mayen Ridge from Greenland. A second jump to the Greenland shelf before anomaly 5 time (Talwani and Eldholm, 1977) initiated the development of the now active Iceland-Jan Mayen or Kolbeinsey Ridge (but see Vogt et al., 1979, this volume).

There are some remarkable differences between the Reykjanes Ridge and the southern part of the Mid-Atlantic Ridge. The depth of the ridge crest extends from the sea level near Iceland to 1,500 m at the southern tip north of the Charlie-Gibbs Fracture Zone; whereas south of 57° N a rift valley exists like at the more southern parts of the Mid-Atlantic Ridge, a rift valley is missing at the northern part of the Reykjanes Ridge; but here the lineations of the magnetic anomalies are more clearly developed on both sides of the axis than to the south (Fleischer, 1974).

Some features of the Reykjanes Ridge are not yet completely understood in detail, e.g., the splitting of the ridge centre on the north-south striking part of the ridge near 56° N (Fleischer et al., 1973), the initial opening stage (Srivastava, 1978), the jump of the axis at anomaly 23 time (Featherstone et al., 1977; Voppel et al., 1979), the change of magnetic pattern with approach to Iceland (Serson et al., 1968; Meyer et al., 1972) and a system of fracture zones at the eastern flank south of 60° N between anomalies 13 and 5 (38 and 10 Ma) discovered by Vogt and Avery (1974) magnetically and by Ruddiman (1972) using reflexion seismics.

The last mentioned problem will be taken up in this paper by evaluating the magnetic, gravimetric, bathymetric and reflexion seismic measurements of METEOR cruise No. 48 (May 5 – June 18, 1978). Some tracks of METEOR cruise No. 43, 1976, which was conducted by the late Dr. U. Fleischer, are included in the evaluation. METEOR cruises Nos. 43 and 48 are part of a program of Deutsches Hydrographisches Institut, 'Geophysical investigation of the North Atlantic Ocean around Iceland'. Figure 1 shows the survey areas.

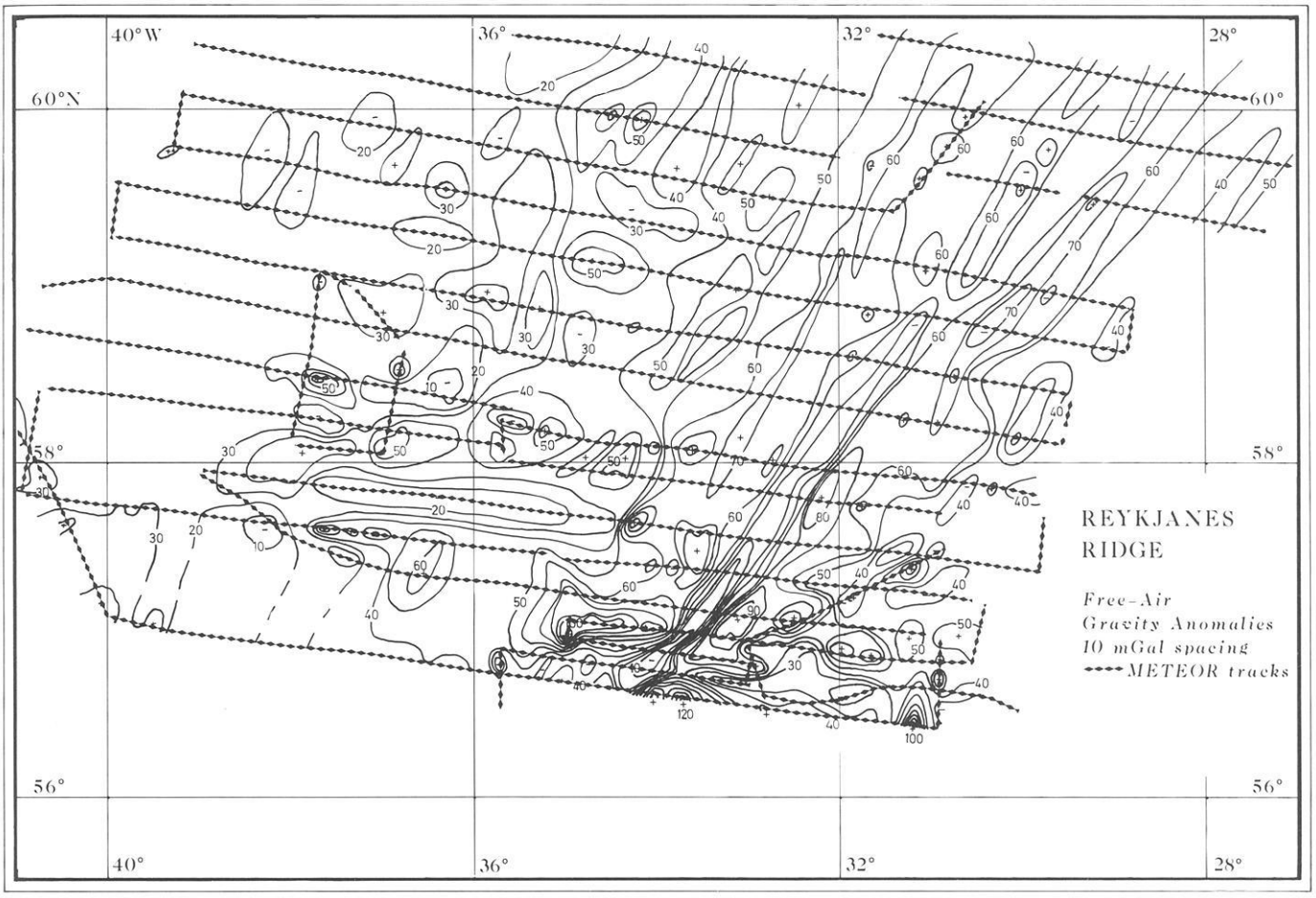

Fig. 3. Free-air gravity anomalies

Measurements

The main objective of METEOR cruise No. 48 was to gain a reconnaissance survey of the western flank of the Reykjanes Ridge area between 60° N and 57° N. This area lies west of a region investigated by Vogt and Avery (1974), south of a region surveyed by USS BARTLETT 1975 and METEOR 1977. To the south there are some lines of METEOR No. 43 (1976) and No. 4 (1966).

The survey lines run E 10° S or W 10° N according to the spreading direction since 40 Ma. These lines are separated 17 naut. miles on the average.

A preliminary rough evaluation of the magnetic lineations during the cruise gave evidence for offsets of anomalies 13 and 6. Accordingly two additional lines A and B (Fig. 2) running perpendicular to the main tracks were measured. The single channel reflection seismic measurements, carried out with a 1.2 l airgun, were expected here to indicate possible fracture zones at the offsets of the magnetic correlation lines. Positioning was performed by an integrated system of satellite and LORAN C navigation.

Magnetics

A proton gradiometer (Geometrics G801G) was used for recording the total intensity of the magnetic field. In principle the gradiometer consists of two proton magnetometers the sensors of which are towed on one cable behind the ship, the 'master' sensor at a distance of about 380 m, and the 'slave' sensor at 230 m.

The magnetic measurements are affected by time variations, especially in the vicinity of the auroral zone. The effect caused by the sun's particle radiation can be characterized by the equivalent planetary amplitude Ap derived from the three-hourly planetary index Kp. For the time of the survey (May 10–May 22, 1978) Ap was 12 on the average. That means the three-hourly range was 26 nT for moderate latitudes. The strongest disturbances occurred on 11 and 21 May with maximum Kp indices of 6 and Ap of 30 and 26, respectively. Compared with the mean Ap of 25 for the entire month of May 1978 the average disturbance during the time of measurements was about a half. Single severe events like ssc's (storm sudden commencements) could be ruled out by comparing the gradiometer (difference 'master' minus 'slave') with the magnetometer ('master' sensor) recordings, since time variations do not influence the gradiometer.

In order to obtain the local magnetic anomalies the IGRF (International Geomagnetic Reference Field) 1965 (Fabiano and Peddie, 1969) updated with the secular variation of the Leirvogur (Reykjavik) and St. Johns (Newfoundland) observatories has been subtracted from the measured values. The anomalies are plotted along the track lines in Fig. 2.

Gravity

Askania gravimeters Gss 3 No. 1 (Prototype) and No. 55 mounted to a platform controlled by an electric gyro (Anschütz), were used for gravity measurements. The instrumental drift has been

computed by comparing the gravity ties in Hamburg and Reykjavik. The difference was less than 1 mGal for the average of both gravimeters. No sudden displacements were detected during the cruise. Since this type of gravimeter is free of cross coupling effects only the Eötvös effect must be corrected for. The free-air gravity anomalies with respect to the normal field represented by the International Potsdam Gravity System are presented in Fig. 3.

Bathymetry

The bathymetric measurements of the Elac 30 kHz narrow beam precision depth recorder have been corrected using the Matthews' tables. A bathymetric map is not published here. Only two profiles A and B whose locations are indicated in Fig. 2, have been plotted in Fig. 4, together with the basement depth and free-air gravity anomalies. A preliminary comparison of a bathymetric map containing only soundings of METEOR cruise No. 48, and parts of the GEBCO Plotting Sheet No. 14 is shown in a publication of Deutsches Hydrographisches Institut (Anonymous, 1979). It reveals considerable differences which are mostly due to poorer navigation aids available in previous cruises as compared to the satellite and Loran C navigation used during the new METEOR cruise.

Results and Discussion

The results of the observations are presented in Fig. 2 (profiles of the magnetic anomalies), Fig. 3 (contours of the free-air gravity anomalies), and Fig. 4 (profiles A and B with bottom and basement topography as well as free-air gravity anomalies).

The magnetic anomalies (Fig. 2) reflect the pattern expected from the knowledge of the Reykjanes Ridge as a whole (Herron and Talwani, 1972; Godby et al., 1968): typically well developed lineations of, e.g., anomalies 20, 5, and the axial anomaly. Anomalies between 5 and about 18 are poorly developed, and their lineations reveal many offsets, the identification of which is at some places difficult and only tentative since the space between profiles is for some cases too large. But anomalies 13 and partly 6 could be identified with sufficient reliability, taking into account their average distances to anomalies 5 and 20 and their parallelity with adjoining anomalies.

The pattern of the gravity anomalies (Fig. 3) is regular only for the northern crest provinces and comparable with the results of Talwani et al. (1971) who investigated the northern part of the ridge crest. The irregular pattern with large anomalies at the southern part of the ridge crest in our survey area is connected with the bend of the ridge and the so-called bight fracture zone (Vogt and Avery, 1974) which is not discussed here. As compared with the $1° \times 1°$ average free-air gravity anomalies published by Cochran and Talwani (1978), the local anomalies over the flank provinces observed with METEOR do not show the parallelity to the strike of the ridge as a whole. Some east-west striking minima and chains of minima or maxima partly correlated with the bottom topography reflect the fracture zones expected from the magnetic anomalies. This can be recognized by comparing the magnetic and gravity maps in Figs. 2 and 3.

The system of fracture zones and the offsets of anomaly 13 (38 Ma) is now considered in detail. The following three observations led to the assumption that the crust aged between 40 and 12 Ma is highly fractured:

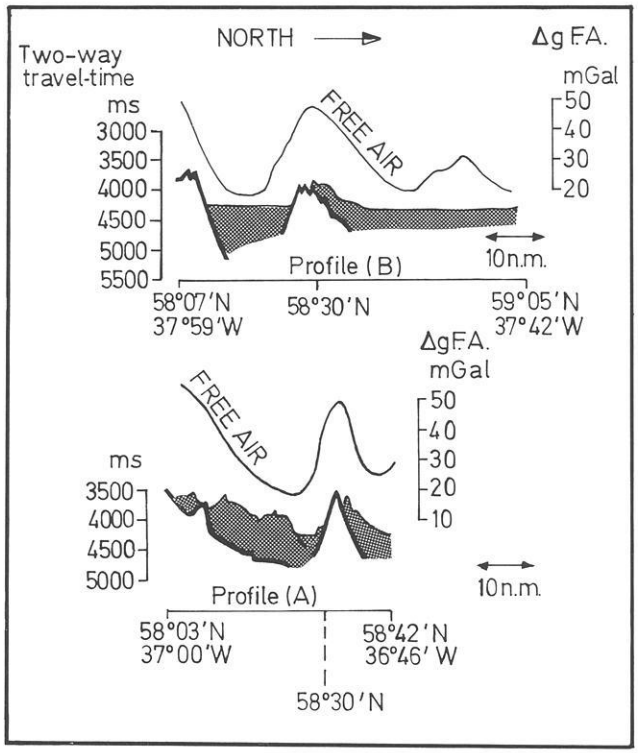

Fig. 4. Profiles of bottom and basement topography and free-air gravity anomaly for tracks A and B from Fig. 2

1. Three short magnetic anomaly strips at 58° 10′ N and between 37° and 38° W (Fig. 2) indicate a strike angle of N 5° E. This strike for 30 Ma old crust deviates considerably from the N 45° E and N 38° E strikes of anomalies generated at 50 Ma (anomaly 20) and since 10 Ma, respectively.

2. The distance between anomaly 13 and anomaly 5 (10 Ma) in the direction of spreading (N 95° E) varies from 204 to 233 km. Similar evidence is found for anomaly 6 (20 Ma) as far as it could be identified.

3. The basement on each profile A and B (Fig. 4) running perpendicular to the spreading direction, shows deep valleys possibly striking about east-west and are interpreted as fracture zones. The free-air gravity anomalies reveal minima over the topographic valleys. They are larger than expected from the water depth alone.

These observations are supported by a visual comparison with the crust of same age east of the Reykjanes Ridge where from seismic measurements a system of fracture zones has been located by Ruddiman (1972). Vogt and Avery (1974) found the magnetic pattern to be irregular with many offsets of anomalies 13 and younger. The strike of these anomalies is nearly N 10° E. The prominent fracture zones (F.Z.) are denoted by Vogt and Avery (1974) by names from the King Arthur legends. These names are inscribed in Fig. 5. It is therefore very probable that this system of F.Z. has been formed within the process of seafloor spreading. It seems justified to assume the strike of anomaly 13 to be nearly N 5° E west of the ridge. Consequently anomaly 13 generally has this strike. This is partly supported by anomalies measured on adjoining tracks, and should be considered tentative.

Each F.Z. at the eastern side must have its counterpart at the western side. In order to examine the relations between anomalies 13 east and west of the ridge axis four steps are taken:

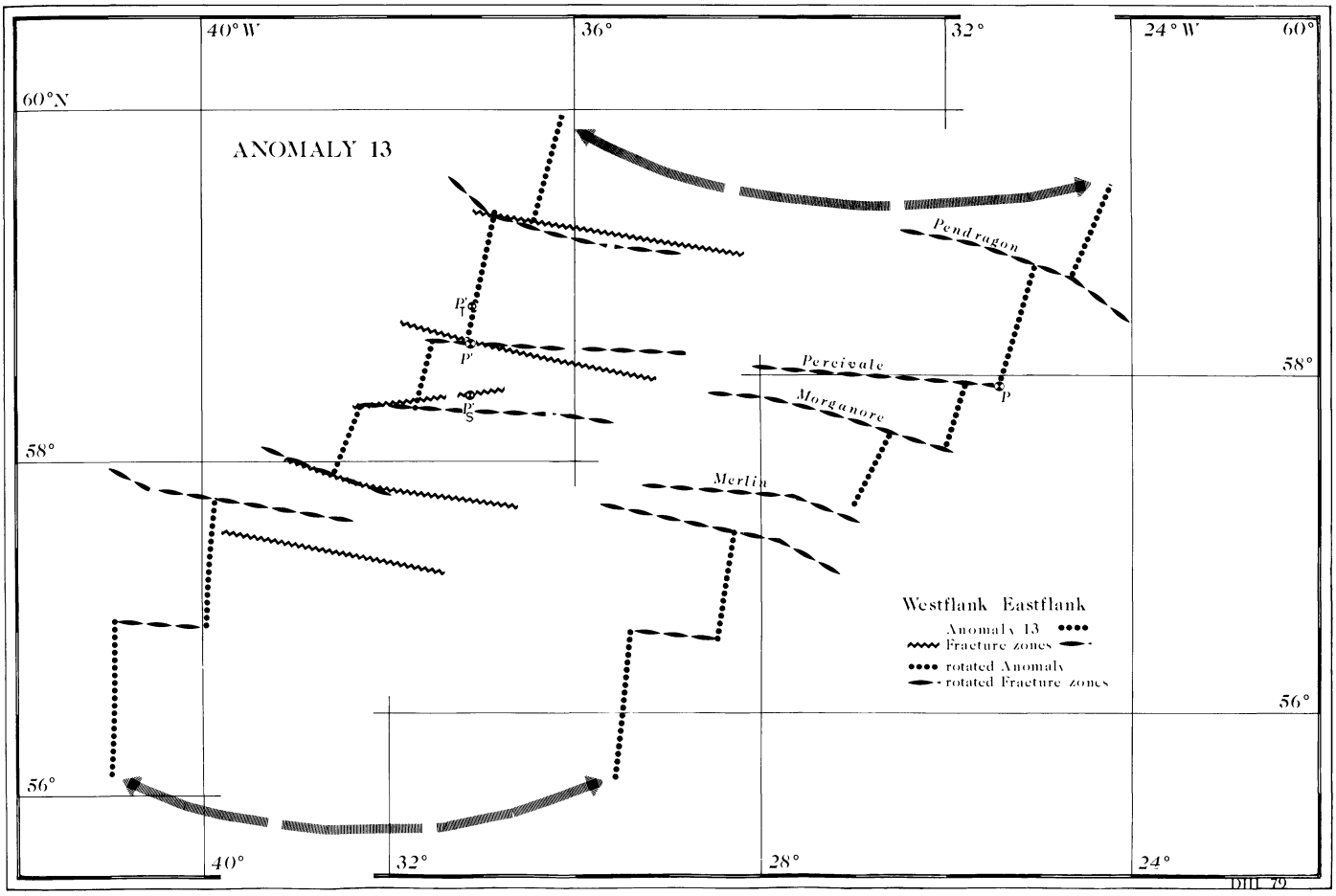

Fig. 5. Lineations of anomalies 13 and fracture zones at the flanks of the Reykjanes Ridge. *Right* At the eastern flank after Vogt and Avery (1974). *Left* At the western flank after METEOR No. 48 data and Vogt and Avery's results rotated from the eastern to the western flank using a pole of rotation at 68.4° N, 133.8° E, with total opening angle of 7.78° Note the different coordinates for the eastern and western flank. For explanation of P, P', P'_T and P'_S see text

(a) Selection of a pair of points at the eastern and western flank where the anomalies 13 can visually be associated.
(b) Rotating the point at the eastern flank to the west applying the formulae for plate rotation on a spherical earth with the pole of rotation at 68.0° N, 129,9° E (Talwani and Eldholm, 1977) with a total opening angle of 7.78° and with the pole at 63.1° N, 142.1° E (Sclater et al., 1977) with an opening angle of 7.24°
(c) Calculation of a refined pole of rotation using the positions observed at both sides.
(d) Rotation of all offsets of anomaly 13 from the eastern to the western side.

For the first step the position of anomaly 13 at the northern edge of the fracture zone named 'Percivale' was selected since the associated position at the western side is strongly supported by the observed magnetic anomaly pattern and the fracture zone found by gravity and seismic measurements on profiles A and B (Fig. 4). In Fig. 5 these positions are denoted by the letters P at the eastern side and P' at the western side.

Secondly the positions P has been rotated to the west using Talwani's and Sclater's poles of rotation and opening angles. The resulting positions are denoted with P'_T and P'_S, respectively. P'_T lies 24 km north of position P' observed, P'_S lies 32 km south (to the east) of P'

Thirdly a new pole of rotation was calculated using the corresponding positions P and P' observed at the eastern and western flanks of the ridge. For this the opening angle of 7.78° of Talwani was taken as a basis because P'_T and P' both lie on anomaly 13. This yielded a pole position of 68.4° N, 133.8° C.

Finally, after this adjustment at one position on anomaly 13 the entire isochron of this anomaly between 56° and 60° N on the east flank of the ridge has been rotated to the west applying the new pole of rotation. The result is shown in Fig. 5.

Deviations between the rotated and observed anomaly lines and fracture zones could be due to different interpretations of anomalies. Generally the anomalies between 13 and 5 have only small amplitudes which reduces the certainty of identification. It is to be noted that the course of the fracture zones rotated from the east to the west are calculated only for the fractures between the offsets of anomalies 13. The inner and outer parts are estimated in order to facilitate their identification. This is indicated by interrupting the markings in Fig. 5.

The coincidence, however, between the anomalies rotated from the eastern to the western side and the anomalies observed or at least tentatively assumed from METEOR measurements is very good in general. The refined position of the pole of rotation (valid for the total opening of anomaly 13) seems to be supported.

The development of these fracture zones during the process of seafloor spreading has been proved by pointing out a mutual fitting system of fracture zones east and west of the Reykjanes Ridge axis. Whether this system extends to the north of 60° N or not, has yet to be determined. Voppel et al. (1979) mentioned that anomaly 13 on the east side of the ridge north of 60° N is missing on four profiles. But an offset could not be detected without doubt. So this phenomenon is assumed to be limited to the area between 56° N and 60° N immediately north of the bend of the ridge axis and the triple junction. Vogt and Avery (1974) argued that this system is a consequence of the ceasing of seafloor spreading in the Labrador Sea at about 40 Ma which was accompanied by a change of the spreading direction in the Reykjanes Ridge area. Why the anomaly strike reoriented to N 38° E at about 12 Ma has not yet been explained.

Conclusions

The result of geophysical measurements carried out with the German research vessel METEOR in 1978 is presented by maps showing magnetic anomaly profiles and free-air contours of gravity as well as by two profiles showing bottom and basement depths. The survey area covered a region on the western flank of the Reykjanes Ridge between 56° N and 60° N where the crust is highly fractured between ages of 40 and 12 Ma.

The fracture zones have been formed by the process of seafloor spreading. This interpretation is based on the comparison with a similar system located at the eastern flank by other authors. A satisfactory fit of both systems could be obtained by rotating the isochron of anomaly 13 from the eastern to the western side around a new pole of rotation located at 68.4° N, 133.8° E with an opening angle of 7.78°.

Future measurements on narrower-spaced magnetic, gravity and bathymetric tracks as well as reflection seismic profiles perpendicular to them could improve the positioning of fracture zones and lead to corrections of isochrons on both sides of the ridge axis. A better understanding of the geophysical process which induced the formation of these fracture zones and the changes of orientation of the ridge axis may then be derived.

Acknowledgment. We wish to thank Dr. S.P. Srivastava for valuable comments on this paper.

References

Anonymous: Forschungsschiff 'Meteor' der Deutschen Forschungsgemeinschaft und des Deutschen Hydrographischen Instituts. Fahrt Nr. **48**, 3.5.–13.6.1978 Geophysik Nordatlantik. Bericht über vorläufige Ergebnisse. Report on preliminary results. Hamburg: Deutsches Hydrographisches Institut 30 S., 1979

Bott, M.H.P.: Deep structure, evolution and origin of the Icelandic Transverse Ridge. In: Geodynamics of Iceland and the North Atlantic Area, L., Kristjansson ed.: NATO Advanced Study Institutes Series C: Math. Phys. Sci. 33–47, 1974

Cochran, J.R., Talwani, M.: Gravity anomalies, regional elevation, and the deep structure of the North Atlantic. J. Geophys. Res. **83**, 4907–4924, 1978

Fabiano, E.B., Peddie, N.W.: Grid values of total magnetic intensity IGRF-1965. ESSA techn. Rep. C and GS No. **38**, 1, 1969

Featherstone, P.S., Bott, M.H.P., Peacock, J.H.: Structure of the continental margin of southeastern Greenland. Geophys. J. R. Astron. Soc. **48**, 15–27, 1977

Fleischer, U.: The Reykjanes Ridge – A summery of geophysical data. In: Geodynamics of Iceland and the North Atlantic Area, L., Kristjansson ed.: NATO Advanced Study Institutes Series C: Math. Phys. Sci. 17–31, 1974

Fleischer, U., Holzkamm, F., Vollbrecht, K., Voppel, D.: Die Struktur des Island-Färöer-Rückens aus geophysikalischen Messungen. Dtsch. Hydrogr. Z. **27**, 97–113, 1974

Fleischer, U., Korschunow, A., Schulz, G., Vogt, P.R.: Eine gravimetrische und erdmagnetische Vermessung des südlichen Reykjanes-Rückens mit F.S. 'Meteor', 22.4.–9.6.1966. Endgültige Auswertung der Forschungsfahrt Nr. 4. Meteor Forschungsergeb. Reihe C: **13**, 64–84, 1973

Godby, A.E., Hood, P.J., Bower, M.E.: Aeromagnetic profiles across the Reykjanes Ridge southwest of Iceland. J. Geophys. Res. **73**, 7637–7649, 1968

Heirtzler, J.R., Dickson, G.O., Herron, E.M., Pitmann III, W.C., Le Pichon, X.: Marine magnetic anomalies, geomagnetic field reversals, and motions of the ocean floor continents. J. Geophys. Res. **73**, 2119–2136, 1968

Herron, E.M., Talwani, M.: Magnetic anomalies on the Reykjanes Ridge. Nature **238**, 389–392, 1972

LaBrecque, J.L., Kent, D.V., Cande, S.C.: Revised magnetic polarity time scale for Late Cretaceous and Cenozoic time. Geology **5**, 330–335, 1977

Meyer, O., Voppel, D., Fleischer, U., Closs, H., Gerke, K.: Results of bathymetric, magnetic, and gravimetric measurements between Iceland and 70° N. Dtsch. Hydrogr. Z. **25**, 193–201, 1972

Ruddiman, W.F.: Sediment redistribution on the Reykjanes Ridge: Seismic evidence. Bull Geol. Soc. Am. **83**, 2039–2062, 1972

Sclater, J.G., Hellinger, S., Tapscott, C.: The palaeobathymetry of the Atlantic Ocean from the Jurassic to the present. J. Geol. **85**, 509–552, 1977

Serson, P.H., Hannaford, W., Haines, G.V.: Magnetic anomalies over Iceland. Science **162**, 355–357, 1968

Srivastava, S.P.: Evolution of the Labrador Sea and its bearing on the early evolution of the North Atlantic. Geophys. J. R. Astron. Soc. **52**, 313–357, 1978

Talwani, M., Eldholm, O.: Evolution of the Norwegian-Greenland Sea. Bull Geol. Soc. Am. **88**, 969–999, 1977

Talwani, M., Windisch, C.C., Langseth, M.G.: Reykjanes Ridge Crest, a detailed geophysical study. J. Geophys. Res. **76**, 473–571, 1971

Vogt, P.R., Avery, O.E.: Detailed Magnetic Surveys in the Northeast Atlantic and Labrador Sea. J. Geophys. Res. **79**, 363–389, 1974

Vogt, P.R., Johnson, G.L., Kristjansson, L.: Morphology and magnetic anomalies north of Iceland. J. Geophys. **47**, 67–80, 1980

Voppel, D., Srivastava, S.P., Fleischer, U.: Detailed magnetic measurements south of the Iceland – Faroe Ridge. Dtsch. Hydrogr. Z. **32**, 154–172, 1979

Received April 5, 1979, Revised Version July 5, 1979

J. Geophys. 47, 67–80, 1980

Journal of Geophysics

Morphology and Magnetic Anomalies North of Iceland

P.R. Vogt[1], G.L. Johnson[2], and L. Kristjansson[3]

[1] Code 8110, Naval Research Laboratory, Washington, D.C. 20375, USA
[2] Code 461, Office of Naval Research, Arlington, Virginia 22217, USA
[3] Science Institute, University of Iceland, Dunhaga 3, Reykjavik, Iceland

Abstract. Detailed low-level aeromagnetic data between Iceland and 70° N are combined with published bathymetric, seismic reflection, and other data to yield a new tectonic synthesis of this region of anomalously shallow sea floor. On Kolbeinsey Ridge short transform faults have repeatedly formed and disappeared over the last 7–8 Ma. Spreading from Kolbeinsey Ridge began about anomaly 6C time (24 Ma); total opening rates increased from 1.5 cm/a to 2 cm/a about 12–13 Ma ago. The Intermediate-Iceland-Plateau extinct axis thus does not exist, and oceanic crust must underlie much of the Greenland margin, perhaps up to the coast itself. This in turn implies locally over 100 km prograding, much of which probably occurred during Plio-Pleistocene glacial periods. The Iceland shelf has been prograded locally 25 km or more. The plate acceleration a 12–13 Ma ago correlates with time-transgressive basement ridges or escarpments previously found on Reykjanes Ridge and here identified north of Iceland as well. The features are proposed to reflect an abrupt mid-Miocene increase in discharge from the Iceland plume. Other time-transgressive basement structures are found on younger Kolbeinsey Ridge crust. Lower Tertiary anomalies 13 to at least 22 are identified in the Denmark Straits, ruling out the hypothesis that the Iceland platform resulted from a westward jump of the spreading center at anomaly 7 time. The magnetic smooth zones being formed where the Kolbeinsey and Reykjanes Ridges enter Iceland have a multiple origin: degassing at depths less than 500 m, coupled with crustal reheating as a result of burial by sediment may be the most important processes.

Key words: Rock magnetism – Magnetic smooth zones – Magnetic anomalies – Sea-floor spreading – Plate tectonics – Iceland – Iceland platform – Iceland plateau – Fracture zones – Hot spots – Aeromagnetics.

Introduction

The region between the Greenland-Iceland-Faeroe aseismic ridge and the Jan Mayen fracture zone exhibits unusual complexities such as jumps in the spreading axis (Johnson and Heezen, 1967; Vogt et al., 1970a; Talwani and Eldholm, 1977) and depth anomalies ranging from near zero in the Norway Basin to over 2 km on the Kolbeinsey Ridge (Vogt and Johnson, 1975; Cochran and Talwani, 1978). These complexities have been attributed to the Iceland hot spot, whose effects extend from the Charlie Gibbs Fracture Zone (52.5° N) northward at least to Mohns Ridge 1,000 km northeast of Iceland (Vogt, 1974). Whether the Iceland hot spot consists of a narrow plume under Iceland, feeding mantle materials north and south under the Mid-Oceanic Ridge (Vogt, 1974; 1976; Vogt and Johnson, 1975), or whether it is a broad hot spot in the upper mantle (Talwani and Eldholm, 1977; Cochran and Talwani, 1978), it is clear that the phenomenon is of regional dimensions and involves a variety of geophysical and geochemical parameters.

In this paper we examine the morphology and magnetic anomalies of the southern Iceland Plateau, a region of relatively shallow sea-floor extending from the Jan Mayen Ridge in the east to Greenland in the west, and from the coast of Iceland north to about 70° N (Fig. 1). The present spreading axis, Kolbeinsey Ridge, lies in part within the area of interest. (The entire 'Iceland Plateau' is defined as the relatively shallow area bounded by the shelf edges of Greenland and northern Iceland, by the Jan Mayen Ridge in the east, and the Jan Mayen F.Z. in the north).

Central to the present paper is an aeromagnetic survey program between the U.S. Naval Oceanographic Office and Iceland. The western part of the survey was published by Johnson et al. (1975). The Project MAGNET survey (Fig. 2) consisted of three parts, each flown at 500 ft (160 m) elevation at line spacings of 3 nautical miles (5.5 km) except on the southeastern Iceland Plateau (east of 15° W and south of 68.5° N) where the tracks were spaced 11 km apart. Navigational accuracy is ± 2 km or better. Analysis of these data is still in progress and the interpretations presented here should be considered preliminary.

Considered together with the new magnetic data are east-west bathymetric profiles across Kolbeinsey Ridge (Meyer et al., 1972; Figs. 7 and 8), a new bathymetric contour chart (Perry et al., 1977; Fig. 1), a sediment isopach chart (Grønlie and Talwani, 1978; Fig. 6) and some deep structural features dicovered under the Greenland margin by Hinz and Schlüter (1978).

Spreading on Kolbeinsey Ridge Since Anomaly-Five Time

Anomalies 5 and younger are well-developed on both flanks of the Kolbeinsey Ridge itself, north of the 1,000 m isobath bounding the Iceland platform (Fig. 2). However, numerous minor fracture zones and bends have formed at varying times subsequent to anomaly-5 time. The magnetic data show that fractures of small

0340-062X/80/0047/0067/$02.80

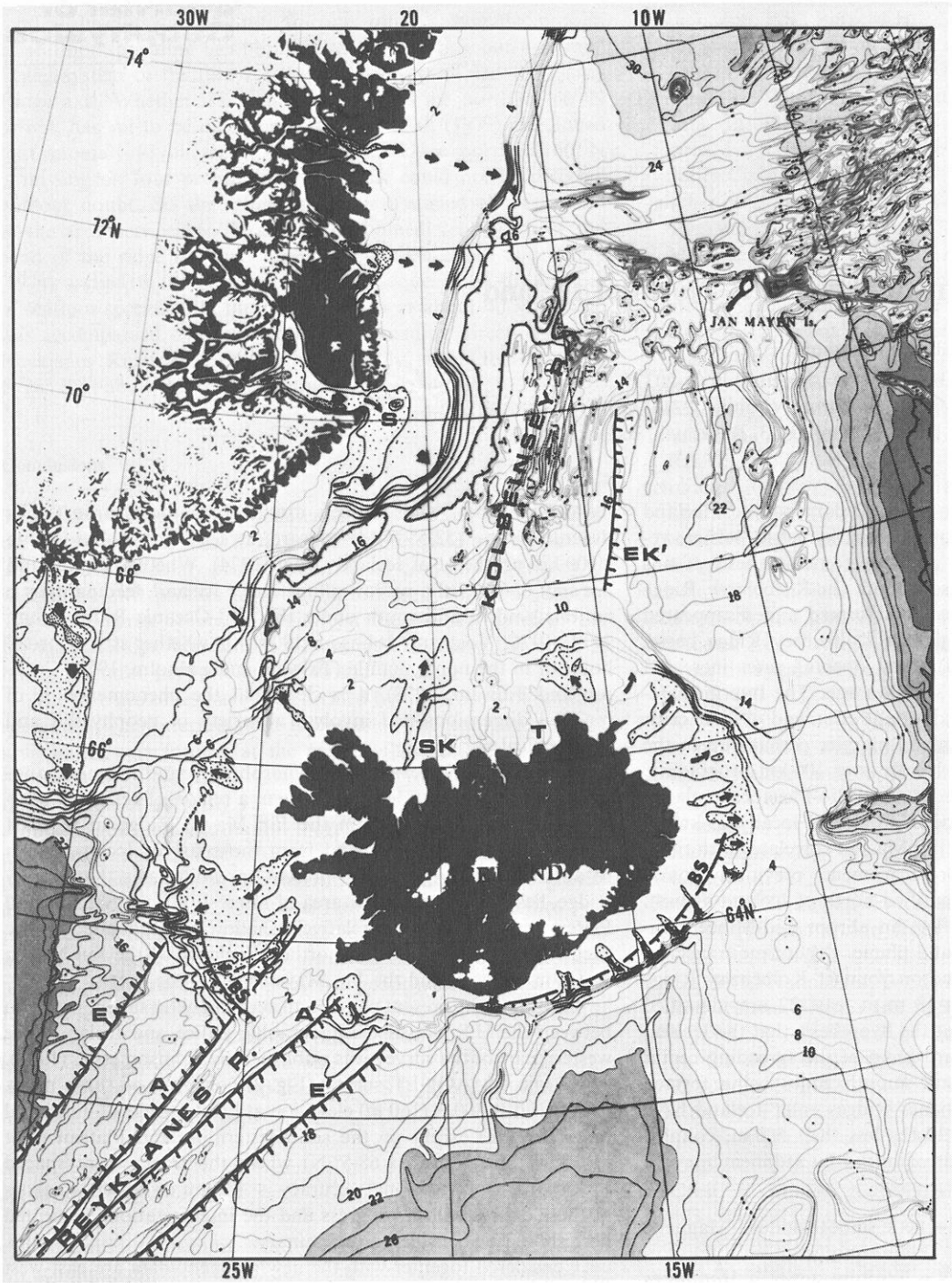

Fig. 1. Bathymetric chart (hundreds of meters) of Iceland area (adapted from Perry et al., 1977). *Stippled areas* show glacially incised troughs and associated shelf-edge deltas (Vogt and Perry, 1978). *Arrows* indicate direction of ice stream movement. Diachronous basement ridges/escarpments (*A, A', E, E'*) from Vogt (1971, 1974) and this paper (*EK'*). *M* is terminal moraine (Olafsdóttir, 1975). '*B.S.*' denotes basement step (southeast Iceland; Kristjansson, 1976a) or paleo-shelf edge (southwest Iceland, Egloff and Johnson, 1979). *SK*=Skagi; *T*=Tjörnes; *S*=Scoresby Sund; Kangerdlugssuaq

offset tend to be ephemeral features: They may form and disappear within a few million years or less. Whether the fractures formed by assymetrical spreading or by small jumps of the spreading axis is a question that awaits detailed analysis of these data (work in preparation) and will not be addressed here. The characteristic spacing between fractures is 30 to 50 km.

Most of the fractures formed subsequent to anomaly 4A time (7.7 Ma) and lie north of 68° N. Why did fractures begin to develop at that time, in an area where few or no such features had existed for the preceding 15 Ma? (In the next section (Figs. 3, 4) we argue that the Kolbeinsey axis actually dates from anomaly 6C time, or 24 Ma). Vogt and Johnson (1975) suggested that trans-

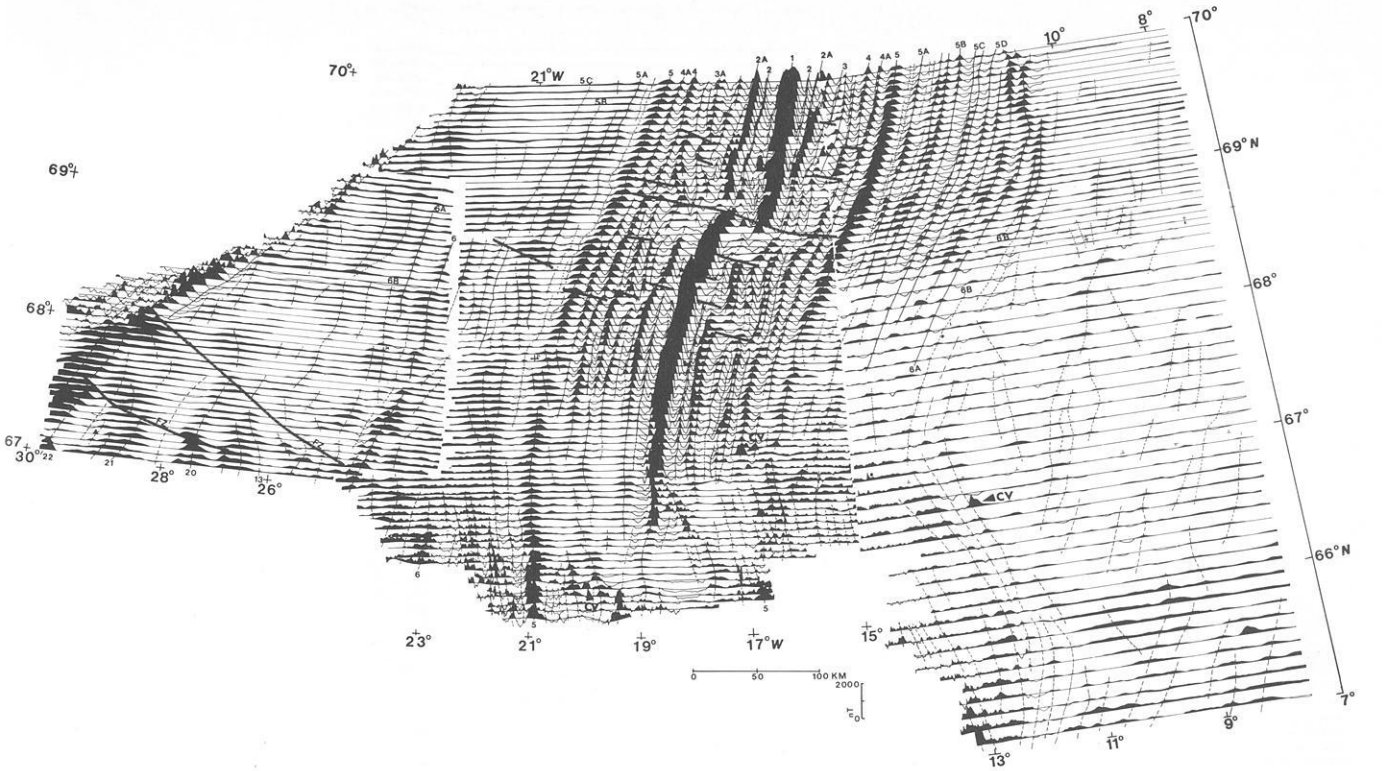

Fig. 2. Residual magnetic anomalies *(total field)* plotted along flight tracks. Anomaly identifications in small numbers; stippled bands, fracture zones (*F.Z.*); *thin solid lines,* convincing anomaly correlations; *dashed,* less certain

form faults disappeared along the Reykjanes Ridge around 20–30 Ma ago on account of increased asthenosphere flow from the Iceland plume. If their arguments are valid, the formation of fracture zones along Kolbeinsey Ridge north of 68° N after anomaly 4A time would mean a weakening of northward flow. Such an inference is independently suggested by morphologic features of Kolbeinsey Ridge, to be discussed in a later section.

The fracture zone of largest offset (30 km) is the Spar F.Z. at 69° N (Johnson et al., 1972; Meyer et al., 1972, Talwani and Eldholm, 1977). The offset terminations of the central anomaly appear to 'overshoot' the trace of relative plate motion, i.e., the theoretical transform trend ($\sim 105°$ *T*). Such *en echelon* spreading might account for the relatively smooth, confused magnetic signature in the vicinity of the Spar F.Z. (Fig. 2). Although the fracture zone came into existence by an eastward shift of the axis about 3 Ma ago (Meyer et al., 1972), anomaly bends or small offsets continue outward to Anomaly-5 (Fig. 2). Thus, a major transform fault may develop at a site 'preconditioned' in some way be the existence of earlier structural complexities.

South of the Spar F.Z., in the area 68.2° to 68.5° N, there exists a pattern of small offsets displaced progressively further northward with decreasing age (Fig. 2). The overall pattern of the fractures is that of an open *V* pointing northward. We think this might be a 'pseudo-transform' fault of the type proposed by Hey and Vogt (1977) on the basis of magnetic data in the area of the Galapagos hot spot.

In areas of unambiguous anomaly identification we measured separations between the same lineations on opposite flanks, in a 105° *T* direction of assumed plate separation. Figure 5 shows these distances plotted against time on the La Brecque et al. (1977) scale. A straight line (2 cm/a, or 1 cm/a half-rate) fits the data

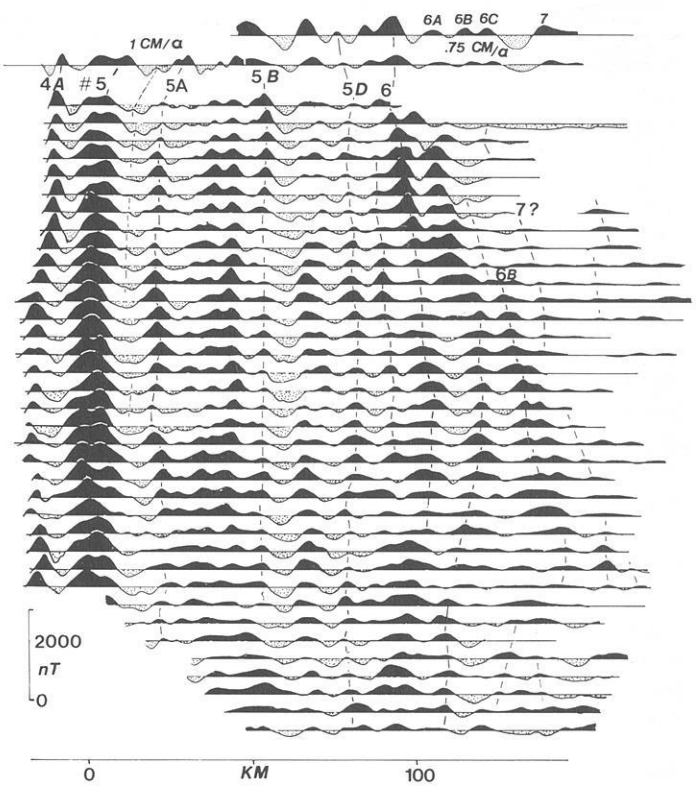

Fig. 3. Residual profiles east of Kolbeinsey Ridge, stacked on anomalies 4A and 5 at left. Models computed at 1 cm/a (after 5B) and 0.75 cm/a (5B to 7). Layer thickness: 0.5 km; magnetization, ± 0.0037 emu/cm^3 *(lower)* and ± 0.0075 emu/cm^3 *(top)*. Transition width: 2 km

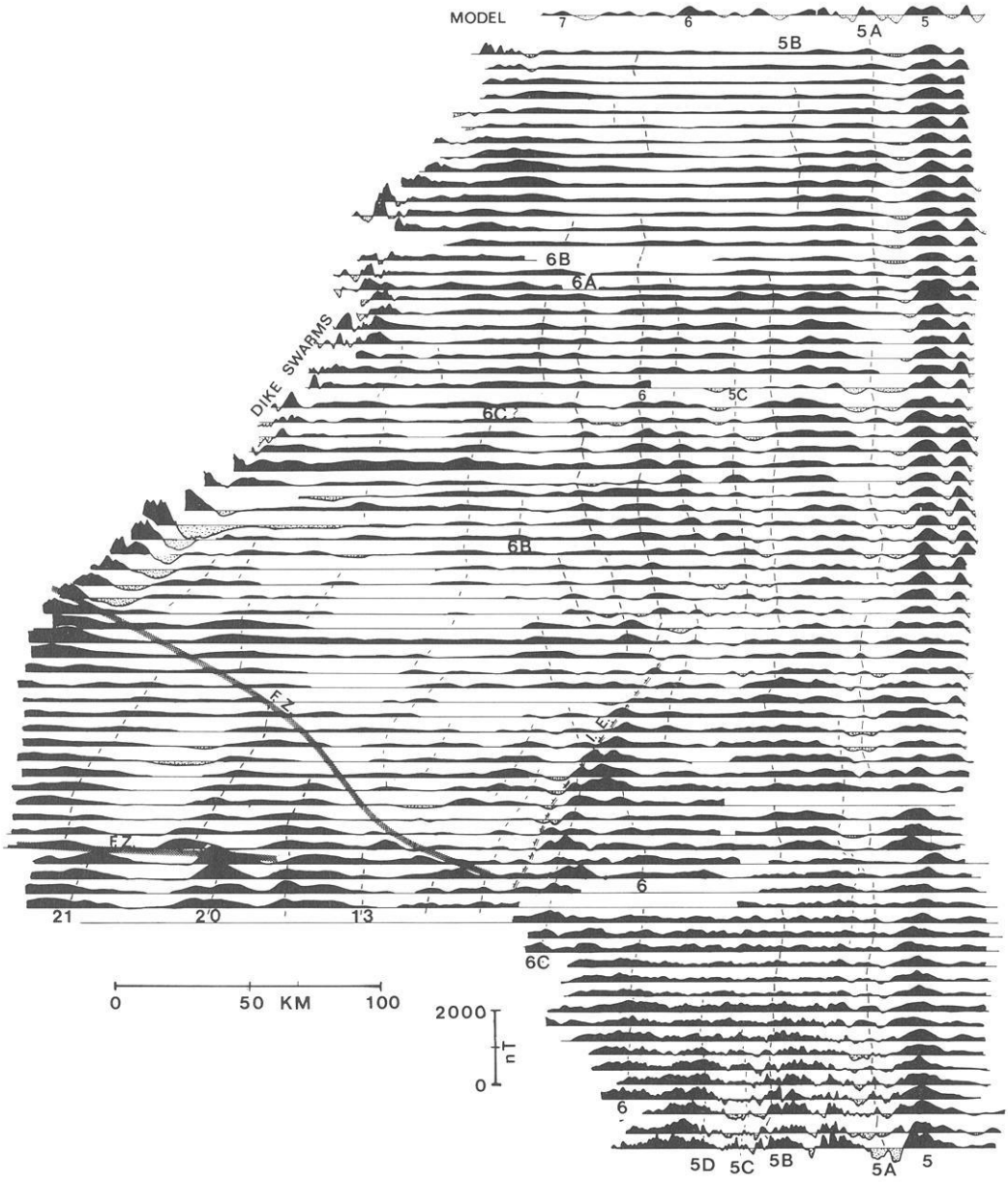

Fig. 4. Residual profiles and selected anomaly identifications west of Kolbeinsey Ridge, stacked on anomalies 4A and 5 (at right). North-northeast trending magnetic lineations labeled '*I.E.*' (Iceland Escarpment; see Hinz and Schlüter 1978) are probably of structural origin. High-frequency anomalies in the south and along Greenland margin (Larsen, 1978) probably reflect aggregations of dikes and perhaps (near Iceland) narrow fissure eruptions. Model profile is reverse of Fig. 3 model. '*F.Z.*' denotes fracture zones inferred from magnetic data only

out to anomaly 5A or 5B. (We discuss pre-anomaly 5 spreading in the next section.) There is a suggestion of slightly faster spreading from 3.2 to 5.2 Ma and slightly slower spreading 1.7 to 3.2 Ma (Fig. 5).

Effective spreading half-rates have been locally much more variable on account of small axis jumps and possibly asymmetric spreading. The 'average' rate since anomaly 5 time is only 0.65 cm/a on the east flank just north of the Spar F.Z., and 1.35 cm/a on the west flank. These values include the effects of axis jumps. At 70° N there has also been more crust added on the Greenland flank of Kolbeinsey Ridge. (Johnson et al., 1972, had suggested a higher *eastward* rate between 69° and 71° N. This conclusion was subsequently challenged on statistical grounds by Pálmason, 1973). Between 67.5° and 69° N it is the eastern flank that has acquired more crust. Between 67.5° N and Iceland the central anomaly lies roughly midway between the two anomaly 5's, although the latter anomaly is locally hard to identify on the east flank (Fig. 2). South of 67.3° N the central anomaly becomes progressively more subdued; the plate boundary is complex in this 'Tjörnes Fracture Zone' region, apparently composed of three *en echelon* rift zones which have developed in geologically recent time (McMaster et al., 1977).

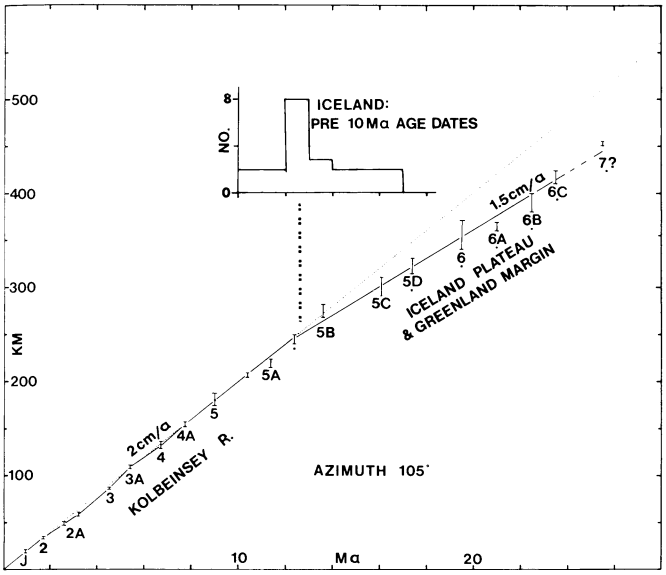

Fig. 5. Distances between corresponding lineations west and east of present spreading axis, plotted against age on the La Brecque et al. (1977) time scale. *Bars* show range of values. Anomalies with dots below them are based only on east-flank measurements, multiplied by two to give estimated total opening rate. *Dotted line* (2 cm/a fits data out to about 12–14 Ma age. Histogram of pre-10 Ma radiometric ages on Iceland (from Pálmason and Saemundsson, 1974) suggests first formation of present day Iceland somehow relates to plate acceleration (from 1.5 to 2.0 cm/a total opening rate) about 12–14 Ma ago. This assumes that coastal erosion has not exceeded a few tens of kilometers except in fjords

Sea-Floor Spreading From the Kolbeinsey Ridge Axis Prior to Anomaly-5: Intermediate Iceland Plateau Axis Does Not Exist

As first postulated by Johnson and Heezen (1967) and later elaborated by other authors (e.g. Vogt et al., 1970a; Talwani and Eldholm, 1977; Grønlie et al., 1979), sea-floor spreading between Iceland and the Jan Mayen F.Z. has not been restricted to a single axis – as it has for example along the Reykjanes and Mohns ridges. A prominent extinct axis (Aegir Ridge) lies in the Norway Basin. The plate boundary jumped westward from Aegir Ridge to the Greenland margin, splitting off a complex segment of continental crust which includes the Jan Mayen Ridge (Gairaud et al., 1978). According to Talwani and Eldholm (1977) the jump occurred at anomaly 7 time, at 25.5 Ma on the La Brecque et al. (1977) time scale.

Vogt et al. (1970a) first noticed that Kolbeinsey Ridge lies closer to the Greenland shelf break than to the postulated Jan Mayen Ridge 'microcontinent'. They postulated an additional region of spreading on the Iceland Plateau. The idea of such an Iceland Plateau Extinct Axis was pursued by Johnson et al. (1972) who tentatively identified a prominent negative anomaly, 50 km east-southeast of anomaly-5, as the axis of symmetry. Talwani and Eldholm (1977) and Grønlie et al. (1979) identified a positive anomaly about 85 km south-southeast of anomaly-5 as the axis of symmetry, which they proposed is anomaly 5D. The Intermediate Iceland Plateau Axis was proposed to have been active from 22.7 Ma to 17.3 Ma (anomaly 5D), whereas spreading on Kolbeinsey Ridge began just prior to anomaly-5. Talwani and Eldholm attribute the unaccounted for gaps in their model (25.5 to 22.7 and 17.3 to 10 Ma) to 'phenomena such as stretching of the crust prior to opening of each shifted center of spreading.' (The dates given here are those given by Grønlie et al., 1979, and are based on the reversal chronology of La Brecque et al., 1977).

According to our interpretation of the detailed Project MAGNET data (Figs. 2–4) all these previous speculations about an extinct intermediate spreading axis on the Iceland Plateau (from Vogt et al., 1970a to Grønlie et al., 1979) are wrong. We find that the Kolbeinsey Ridge lineation pattern simply continues eastward past anomaly-5. Anomalies 5A through 5D, 6, 6A, 6B, and 6C can be readily identified, at least from 68° N to 69.5° N (Fig. 3). This accounts for the gaps in the Talwani-Eldholm model, but is still consistent with a westward jump after anomaly-7 time as they have postulated. The non-existence of a spreading axis also explains the absence of a bathymetric or gravity signature over the supposed extinct axis (Grønlie et al., 1979). The main difference between the early and late (post-anomaly 5A-5B) spreading on Kolbeinsey Ridge is the relatively slower early half-rate (0.75 cm/a). The supposed symmetry axis of Talwani and Eldholm (1977) is actually anomaly 5E. Anomaly 'R' of Grønlie et al. (1979) is actually 5A. Anomaly 6B-6C is associated with an east-dipping basement and bathymetric escarpment (Fig. 6, see also Belousov and Udintsev 1977). We suggest this is the line of initial spreading from Kolbeinsey Ridge. Earlier spreading axes, if any, must lie between the 6D-6C step and the Jan Mayen Ridge.

Anomaly amplitudes are very low east of 6B-6C and a further eastward continuation of the sequence (e.g. to Anomaly-7) is conjectural (Figs. 2 and 3). However, what lineations there are tend to parallel those to the west and may represent some of the spreading between anomaly-20 and-7 time required to account for the fan-shaped lineation pattern in the Norway Basin (Talwani and Eldholm, 1977). In other words, a hypothetical extinct center east of the 6B-6C escarpment may have been active at the same time as Aegir Ridge after Anomaly-20 time. In order to explain the fan-shaped anomaly pattern in the Norway Basin, a complementary spreading axis on the eastern Iceland Plateau would also have had to produce a fan-shaped anomaly pattern, but with a northward convergence. No such pattern is apparent in the data (Fig. 2).

Many authors have overlooked the fact that even young, shallow oceanic crust may be associated with a magnetic smooth zone. Note that the southern Kolbeinsey Ridge has been generating such a smooth zone (Fig. 2). We analyze this problem in a later section. Whatever process or processes are responsible, they may also have operated east of anomaly 6C, and the lack of pronounced anomalies in that region (Fig. 2) is a very weak argument for the existence of continental crust. (Seismic reflection and refraction data are more convincing; Talwani and Eldholm, 1977).

The existence of anomalies 5A to 6C east of Kolbeinsey Ridge (Figs. 2 and 3) requires a similar set of lineations to the west. Indeed, we believe these anomalies do exist between Kolbeinsey Ridge and Greenland (Fig. 4). The anomalies are however reduced in amplitude relative to their eastern counterparts. This relative reduction begins on lineations as young as 4A and 5. We attribute the suppressed amplitudes of these lineations to (1) deep subsidence, caused by 1 to perhaps over 3 km terrestrial sediment (Grønlie and Talwani, 1978; Hinz and Schlüter, 1978) derived from Greenland and (2) erasure of primary magnetization caused by crustal heating made possible by relatively high heat flow and thick insulating sediments (Vogt et al., 1970b). The amplitudes

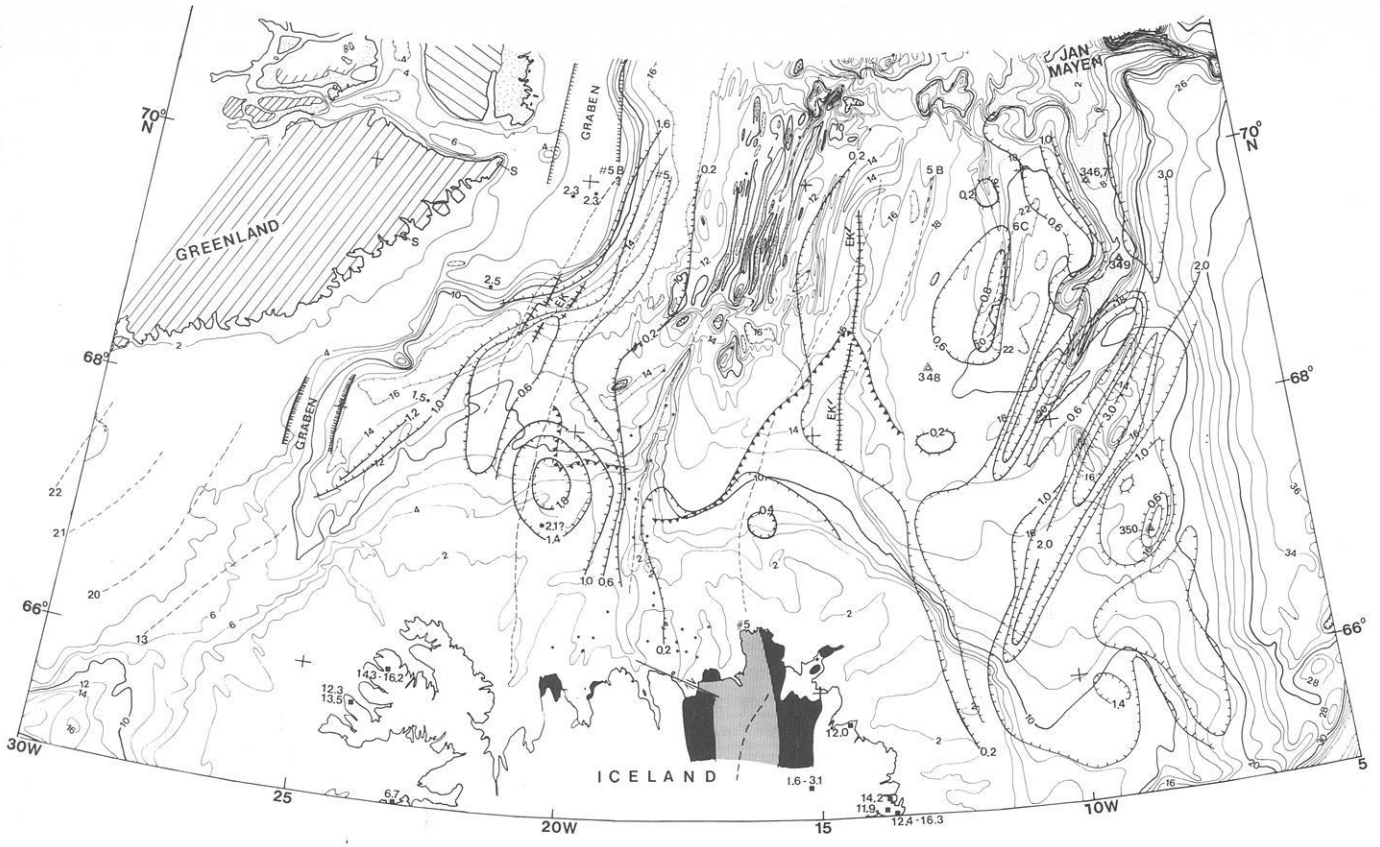

Fig. 6. Base chart: bathymetry in meters (Perry et al., 1977) with areas shallower than 1,000 m stippled on Kolbeinsey and Jan Mayen ridges. Small stars indicate earthquake epicenters. *Heavy contours* show sediment thickness in seconds of two way reflection time (Grønlie and Talwani, 1978). Spot values of sediment thickness based on sonobuoy stations (Grønlie and Talwani, 1978). *Double triangles,* DSDP drill sites on Leg 38 (Talwani et al., 1976). *Thin dashed lines,* principal magnetic lineations (from Fig. 2). Two grabens and homocline (*EK'*) under Greenland margin from Hinz and Schlüter (1978). *EK'*, time-transgressive bathymetric and basement lineament on Iceland Plateau (see also Fig. 7). *Heavy toothed line,* line of greatest southward decrease in anomaly amplitude. *Iceland* (after Pálmason, 1974): *Vertical ruling:* younger than 0.7 Ma; *solid:* 0.7 to 3 Ma; *squares,* older radiometric age determinations. *Greenland* (Anonymous, 1970): NE-SW hatched area, Tertiary igneous province with local Cretaceous to Lower Tertiary sediment outcrops (*S*); NW-SE hatching, Jurassic platform sediments; stippled, Pre-Cambrian

are most attenuated – even completely erased – under the thick sediments seaward of the mouth of Scoresby Sund. The conspicuous arcuate salient of the Greenland margin (Fig. 1) in this area is best explained as a deltaic sediment accumulation dating largely from the Plio-Pleistocene glacial ages (Vogt and Perry, 1978). We believe it is incorrect – particularly along glaciated shelves seaward of fjords or straths – to use the 500-fm bathymetric contour at the base of the continental slope to estimate the line of initial rifting, as Talwani and Eldholm (1977) have done. Instead, the ocean-continent crustal boundary must lie well landward of the shelf-break, perhaps even close to the Greenland coast between 69° and 70° N. In fact, our magnetic anomaly identifications *east* of Kolbeinsey Ridge *require* oceanic crust to continue under the Scoresby Sund salient. Neither the sonobuoy stations (Fig. 6; Grønlie and Talwani, 1978) nor the multi-channel profiles (Hinz and Schlüter, 1978) preclude such an interpretation. Furthermore, Hinz and Schlüter independently concluded that the thick sediment accumulations in the Scoresby Sund area post-date the (25 Ma?) separation of Jan Mayen Ridge from Greenland. This is in keeping with the proposal of Vogt and Perry (1978) that the arcuate shelf outbuilding occurred primarily during the Plio-Pleistocene glacial ages.

Oceanic Crust Older Than Anomaly 6C

We consider now the possibility of ocean crust predating anomaly 6C. In the Jan Mayen Ridge area the anomalies east of 6C are generally low in amplitude and tend to be lineated in a NE to NNE direction. Since similar low-amplitude areas of oceanic crust are found where Kolbeinsey Ridge enters Iceland and along the Greenland margin, we cannot adduce magnetic data as necessarily indicating continental crust in the Jan Mayen Ridge area. We suppose most of the area between anomaly 6C and 7.5° W (Fig. 2) is underlain by oceanic crust of anomaly 13 to 7 age. Continental fragments (Talwani and Eldholm, 1977) cannot be excluded, however.

What about anomaly-7 or older ocean crust along the Greenland margin? There is little or no room for such older crust in the Scoresby Sund area. Southwestwards towards the Denmark Straits there is progressively more room. The graben structure discovered by Hinz and Schlüter (1978) under the Greenland margin about 68° N may contain oceanic crust of anomaly 7 to 22 age even though the graben is associated with a magnetic smooth zone (Figs. 2 and 6).

Further south, we believe to have identified the sequence 13 to 22 in the Denmark Straits area (Figs. 4 and 6). These early to mid-Tertiary lineations appear to end at a major fracture zone, perhaps equivalent to the right lateral offset of the Faeroes block from the Faeroes-Shetland Escarpment (Talwani and Eldholm, 1977). Alternatively, this fracture formed when the spreading axis jumped westward from Aegir Ridge. Our identification of anomalies 13 to 22 in the Greenland-Iceland gap is contrary to the conclusions of Talwani and Eldholm (1977) who postulate spreading from an extinct Iceland-Faeroe Ridge axis until anomaly 13 time. Our interpretation does not conflict with Voppel et al. (1979), who suggest abandonment of an Iceland-Faeroe Ridge center at anomaly 22 time. However, we cannot rule out the existence of anomaly 22 to 24 age crust under the wide Greenland shelf between 66° and 68° N. In fact, Larsen (1978) suggests that crustal extension during anomaly 24 time occurred solely by dike injection along the present Greenland coast from 63.5° N to 70° N. If this is true, we do not need to look for this lineation at sea.

The existence of anomaly 13 to 22 age crust – and possibly older – in the Denmark Straits means that the northwestern and southeastern edges of the Iceland Platform do not necessarily mark jumps in the spreading axis as postulated by Talwani and Eldholm (1977). We prefer to interpret these basement steps as reflecting abrupt increases in mantle-plume discharge and basalt magmatism (Vogt, 1974). The first such increase occurred ca. 25 Ma ago and the second – marked by Iceland's oldest rocks – about 13–17 Ma ago. The 25 Ma increase may also be marked by the initiation of volcanism at what is now the eastern and western extremities of the Iceland insular basement margin. The age of the second increase correlates with the oldest rocks of eastern and western Iceland, but this may also be a fortuitious effect of coastal erosion removing older rocks (e.g., Nilsen, 1978), and furthermore may be meaningless if the rocks at depth below eastern and western Iceland are more than 1 or 2 Ma older than the oldest surface exposures. The existence of old anomalies west of Iceland may remove the need to postulate oceanic crust under the Faeroe Islands. Finally, the identification of anomalies 20–22 and perhaps older in areas of present Greenland shelf implies the existence of oceanic crust at depth. This important conclusion should be testable by seismic refraction methods. Again, the area in question lies seaward of the Kangerdlugsuaq fjord system and probably experienced rapid outbuilding as a result of ice streams delivering continental detritus in great quantity to the edge of the continental shelf (Vogt and Perry, 1978).

Diachronous ('V-shaped') Structures North of Iceland: Implications for the Iceland Mantle Plume Hypothesis

Using the seismic reflection profiles published by Talwani et al. (1971), Vogt (1971) discovered 'V-shaped' (diachronous or time-transgressive) basement ridges and escarpments on the Reykjanes Ridge southwest of Iceland (Fig. 1). From the angle between these structures and the crustal isochrons – , i.e., magnetic lineations – Vogt calculated a southwestward propagation rate of the order of 10 to 20 cm/a. He proposed further that the V-shaped basement structures are generated at the spreading axis by wave-like magmatic irregularities traveling southwest in a conduit of low viscosity below the Reykjanes Ridge (Vogt, 1974; 1976; Vogt and Johnson, 1975). The source of this flow and of the irregularities entrained in it was proposed to be a plume of upwelling mantle (Morgan, 1972) located under south-eastern to central Iceland. The two most prominent V-shaped features on the Reykjanes Ridge are the A-A′ and E-E′ escarpments, proposed to reflect abrupt increases in discharge from the Iceland plume (Fig. 1). These escarpments dip towards older crust; upon approaching Iceland they increase in steepness and relief, tending toward asymmetrical ridges in cross-section. Extrapolation suggested the 'A' and 'E' events would have first influenced Iceland itself around 6–7 Ma and 13–17 Ma respectively. Watkins and Walker (1977) discovered a short-lived 7.3 Ma to 6.4 Ma pulse of increased lava production in eastern Iceland. They suggested this might be a manifestation of the 'A' event on Iceland. However, the increase in lava production may well be a local phenomenon or an artifact of miscorrelation; recent work by Harrison et al. (1979) does not confirm the 7 Ma ago event. Both Watkins and Walker (1977) and Vogt (1974) pointed out that the 17-13 Ma age corresponds to the oldest rocks on Iceland (Fig. 3) and may therefore represent the plume 'event' leading to construction of present-day Iceland. This correlation may be a fortuitous result of coastal erosion, as mentioned previously.

If the mantle-plume interpretation of Reykjanes Ridge basement structures (Vogt. 1971; 1974) has any merit, features similar to the AA′ and EE′ escarpments should exist on the Kolbeinsey Ridge north of Iceland. The 'V'-s should point northward, moreover, in the direction plume materials would be expected to travel under the Kolbeinsey Ridge, i.e., away from Iceland.

Comparing our magnetic isochrons (Fig. 2) with the bathymetric profiles of Meyer et al. (1972), we see both isochronous and 'V'-shaped trends north of Iceland (Fig. 7). The 'V'-shaped structures 'point' northward as predicted by the mantle plume hypothesis (Vogt, 1971, 1974). If interpreted as a measure of northward flow from the Iceland plume, the diachronous bathymetric trends younger than anomaly-5 would imply mantle flow of the order 1 to 5 cm/a, distinctly less than the southwestward flow under the Reykjanes Ridge (Vogt, 1971, 1974). The slower northward flow might reflect (1) competition with a separate Jan Mayen plume, (2) damming at fracture zones such as the Tjörnes or Spar (Vogt and Johnson, 1975), (3) northward motion of the plates over the Iceland plume (Minster et al., 1974) or (4) the northward decrease in spreading rate, hence pipe cross-section (Vogt, 1976). On the other hand, the tectonic complexities of the present plate boundary in the Tjörnes fracture zone area (McMaster et al., 1977) and the repeated formation and disappearance of transform faults on the Kolbeinsey Ridge (Fig. 2) by mechanisms not yet understood could have produced some of the trends in Fig. 7. Although we are not wholly convinced that the diachronous structures north of Iceland do reflect northward flow, the plume model (Morgan, 1972; Vogt, 1971) does explain their existence, at least qualitatively.

Furthermore, the 'E' escarpments, which previously were not thought to exist on Kolbeinsey Ridge (Vogt, 1974), do show up clearly on the east flank (EK′ in Fig. 7). The EK′ structure cuts lineations between 5A and 5B between 68° N and 69° N and on the bathymetric chart (Figs. 1 and 6) can be followed southward as a broad, low ridge which merges with Iceland's northeastern insular margin. The crest of the EK′ ridge has an age of 12.8 Ma at 69° N. Between 68° N and 69° N the implied propagation rate, along the crustal isochrons, is about 10 cm/a, of the same order as on the Reykjanes Ridge (Vogt, 1971, 1974). Crust of corresponding age west of Kolbeinsey Ridge is buried by 600 to 2,000 m sediment (Fig. 6); thus, no western equivalent to EK′ would be expected on bathymetric profiles. However, the reflection profiles of Hinz and Schlüter (1978) reveal a west-dipping basement escarpment ('homocline') 25 to 45 km WNW of anomaly 5 at 69.4° N and 40–50 km WNW at 68.8° N. We propose that this homocline is in fact EK, the western equivalent to the EK′ structure on

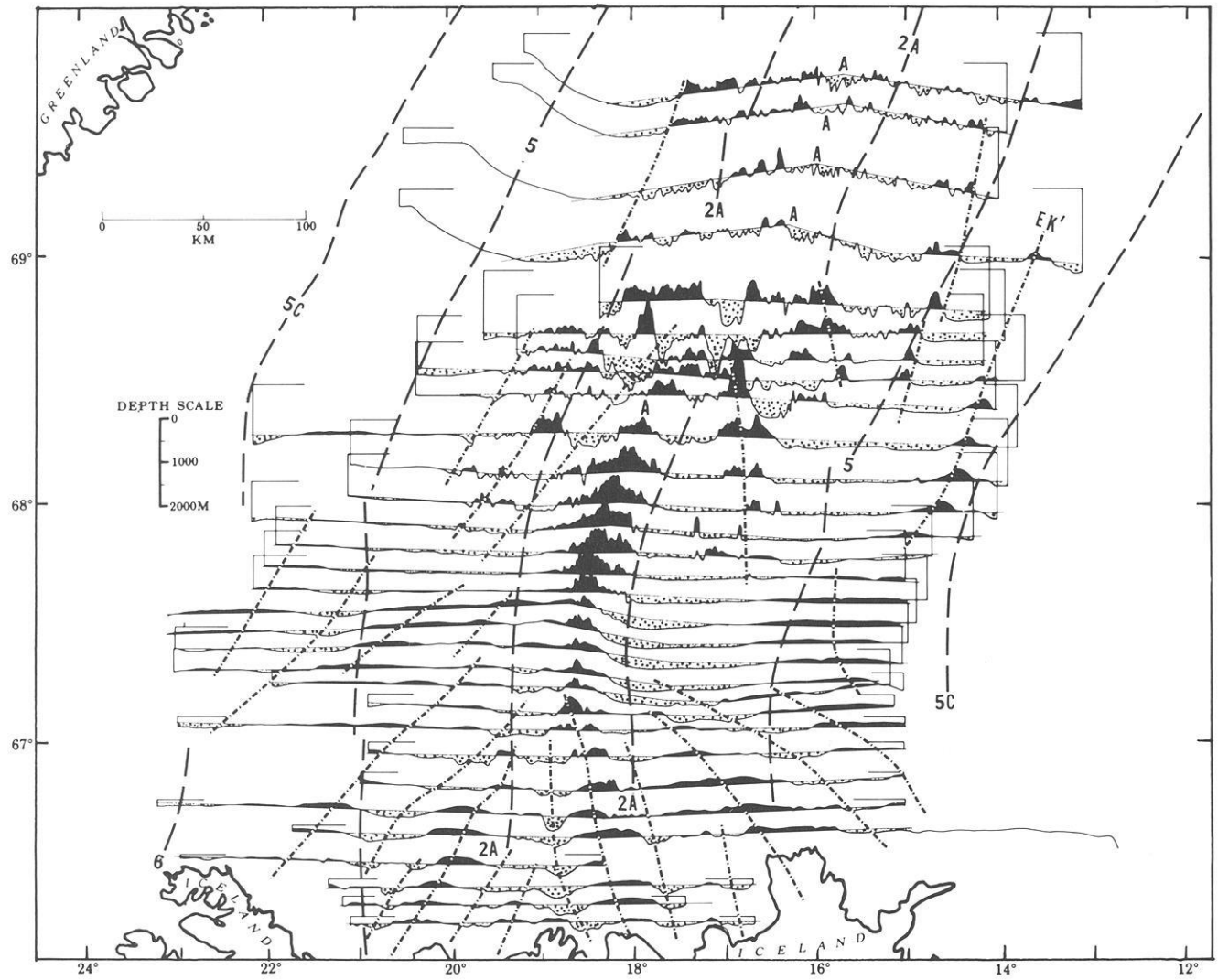

Fig. 7. Bathymetric profiles of Meyer et al. (1972) showing lineation trends which are mainly diachronous with respect to crustal isochrons (*dashed*, anomalies 2A, 5, and 5C). Topography shown black above a smooth curve drawn through each profile

the Iceland Plateau and the E-E′ escarpments on the Reykjanes Ridge.

We concluded earlier (Fig. 5) that spreading half-rates increased rather abruptly from 0.75 to 1.0 cm/a about 12.5 Ma ago (limits: 11 to 14 Ma). Although it has long been known that average spreading rates were lower during the interval anomaly 6 to 5 than subsequently (e.g., Vogt and Avery, 1974; Talwani and Eldholm, 1977), the time of the acceleration is here for the first time shown to be 12.5 ± 1 Ma ago, which is within dating uncertainties identical to the age range of the 'E-EK' event on the Kolbeinsey and Reykjanes ridges. Although this implied correlation of a 'plume'-generated feature with acceleration in plate motion does not prove plumes contribute to driving the plates, such an inference certainly becomes more attractive, particularly since the earliest appearance of the E-EK basement escarpments along the Kolbeinsey and Reykjanes Ridges nearest to Iceland actually occurred around 13–17 Ma ago, slightly prior to the plate acceleration. In other words, we suppose that an increase in plume discharge took a few million years to affect a volume of lithosphere/asthenosphere large enough to alter the parameters of plate motion.

Finally, we call attention to the correlation of the 'E' event in the Iceland area with the Gardner Pinnacles episode of increased basalt discharge by the Hawaii plume. Both events are part of an apparently global middle Miocene magmatic episode (Vogt, 1978).

Dike Swarms and Central Volcanoes

The magnetic field at 500 ft (166 m) altitude near the coasts of Greenland and Iceland is rich in short wavelength anomalies (1 to 5 km), typically 100 to several hundred *nT* in amplitude (Fig. 2). The short wavelength areas reflect shallow magnetic sources, according to a statistical treatment by Kristjansson (1976c) of ship-borne measurements west of Iceland, but we have not completed depth to source processing of the present results.

On the Greenland margin, the observed magnetic anomalies probably reflect dikes or swarms of dikes as suggested by Vogt (1970) and Larsen (1977); this may aid offshore mapping of the East Greenland early Tertiary igneous province (see Noe-Nygaard, 1976; Deer, 1976). In low-level surveys over Iceland and the shelf,

the major sources of magnetic anomalies so far recognized include thick series of lava flows of alternating polarity (see Piper, 1973), central volcanoes (see Kristjansson, 1976b and c) and arcuate structural anomalies associated with the edges of the Iceland platform (Figs. 1 and 2). None of the numerous elongated dike swarms in Iceland has to date been observed to coincide with elongated magnetic anomalies where data are available. This observation makes it doubtful whether the short-wavelength linear anomalies north of Iceland (Fig. 2) represent dike swarms.

Recent developments at the Krafla active central volcano in NE-Iceland (Björnsson et al., 1977; 1979) are of considerable interest in understanding the processes of spreading and anomaly generation. It appears that over intervals of hundreds of thousands of years, rifting on any 100-km ridge segment is accompanied by repeated subhorizontal injection of magma into a fissure system from shallow magma chambers below a central volcano. Material in the volcano, situated at the center of that fissure system, is periodically replenished from below until the volcano is disconnected from its mantle source and transported out of the active zone, even as new centers appear nearby. Similar processes, perhaps on a different scale, may well characterize the mid-oceanic ridge system in general; changes in the relative width and amplitude of small linear magnetic anomalies over the ocean floor (Figs. 2 and 3) would then reflect changes in the activity of individual intrusive centers or groups of these.

In this context it is noteworthy that magnetic anomalies over central volcanoes in SW- and W-Iceland (Sigurgeirsson, 1970; 1979) as well as on the shelf (Kristjansson, 1976c) are generally equidimensional and coincident with caldera structures and hypabyssal intrusions. Central-volcano anomalies are numerous on the shelf east and west of Iceland (Kristjansson et al., 1977) but rare or non-existent south of Iceland. They are also uncommon north of Iceland; only a few such features could be identified in our data ('cv' in Fig. 2). The areal density and degree of development of such volcanoes on any part of the ridge is likely to be strongly related to distance from the center of the mantle plume, through variables such as magma production and chemistry, melt percentage, heat flow, crustal and lithosphere thickness, or other effects. It does not appear that the trace of the Iceland mantle plume, as inferred by Kristjansson (1976b), passes anywhere through the region covered by the present survey.

Erosion and Sedimentation

Iceland represents a large area of anomalous ocean crust up to 16 Ma in age, exposed to erosion by water, and in the last 3 Ma also to ice. During glacial periods lowered eustatic sea level and grounded ice sheets probably exposed the entire Iceland platform above present 200–300 m depth to erosion. Although a mean denudation of 400 m has been estimated for Iceland itself (Einarson, 1963) the erosion was highly selective, concentrated wherever ice streams drained the insular ice shield. Much more spectacular ice streams carved out the east Greenland fjord topography, carrying large quantities of coarse sediment to the depocenters along shelf edges (Sommerhoff, 1973; Vogt and Perry, 1978).

In this section we consider the connection between the magnetic anomaly data (Fig. 2) and present morphology in terms of erosion and deposition.

Much of the present Iceland platform near the coast consists of an outcropping or thinly sedimented basaltic erosion surface (Johnson and Pálmason, 1980). Sediment was evidently carried across this region by the ice, but how far did the ice extend?

West of Iceland, a 20–30 m high, 100 km long moraine ('M' in Fig. 1) lies at present depths of 200–250 m (Olafsdóttir, 1975), near the shelf break. The moraine may represent the maximum advance of the Weichselian (Wisconsin) ice-sheet in this area and suggests the Iceland ice cap extended outward to a calving ice shelf located near the shelf edge. In Greenland (Weidick, 1976) as in most other areas, the Weichsel ice did not advance as far

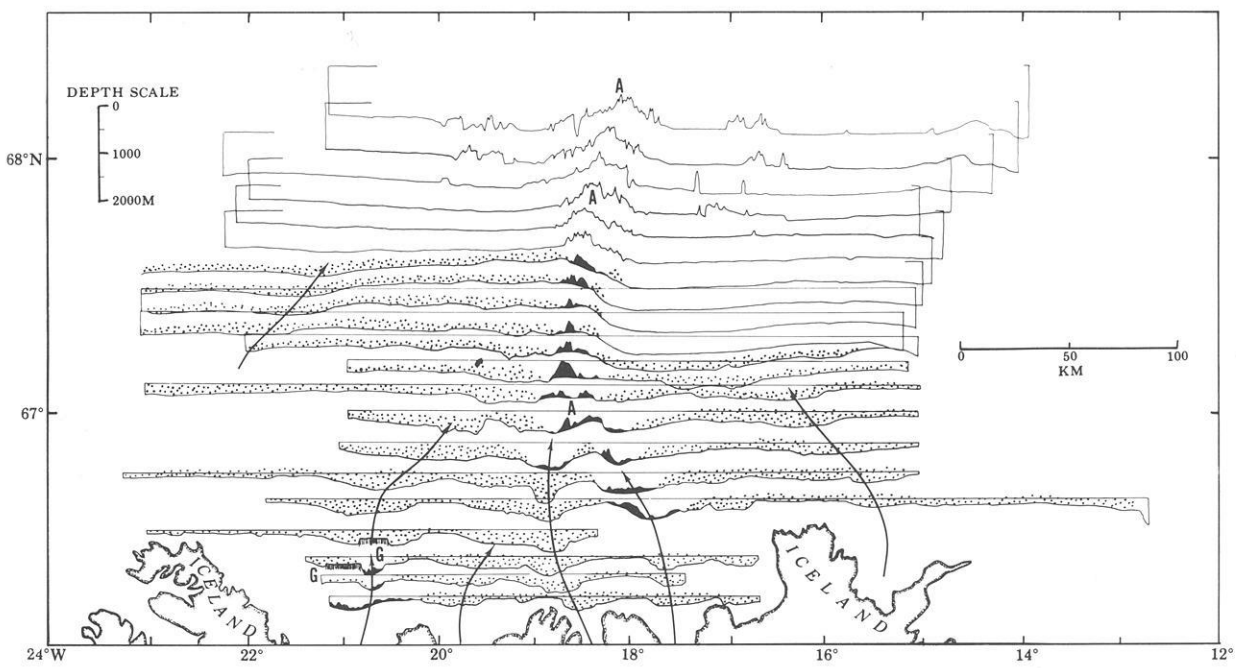

Fig. 8. Bathymetric profiles of Meyer et al. (1972) showing suggested outcropping basement *(black)*, submerged wave-eroded volcanic edifices (*G*), and suggested maximum extent of grounded Pleistocene ice streams *(stippled pattern over sea-floor)*. *Arrows* show direction of ice stream flow and submarine sediment transport along valley floors. (*A*) denotes axis of Kolbeinsey Ridge

as during earlier glaciations. Thus, the moraine reported by Olafsdóttir (1975) represents a minimum position for the seaward limit of grounded ice.

The Iceland platform is indented by numerous shallow U-shaped valleys, many of which appear to be submarine extensions of fjords and other embayments of the Iceland coastline (Perry et al., 1977; Fig. 1). It is most reasonable to explain these submarine valleys as the work of glacial erosion by grounded ice streams flowing radially outward from an ice dome culminating in central Iceland. The bathymetric chart shows recognizable arcuate salients of the shelf edge located at the mouths of the submarine valleys (Fig. 1). These salients most likely represent ice-front deltas composed of debris transported to the shelf edge by grounded ice streams. In most cases the 400 m isobath is deflected seaward where the 200 m isobath shows an embayment. This suggests the ice streams were grounded to depths between 200 and 400 m.

On the southwest and northeast Iceland shelf, even the 400 m isobath is indented landward, suggesting ice streams possibly were grounded below 400 m there. However, both areas are near the active spreading axis, and tectonic effects cannot be discounted. The bathymetry alone suggests extra shelf-building of the order 1 to 10 km seaward of the valleys (Vogt and Perry, 1978). These are minimum values for total shelf progradation, since sediment was also deposited along platform margins between the glacial valleys. Kristjansson (1976b) has used magnetic anomaly source depths to identify a buried basement step under the outer shelf off southeastern Iceland. The present shelf break has prograded by amounts ranging from 5 km (at 19° W) to 15 km (at 14° W) seaward from the step. The shelf itself is narrow, and prominent submarine canyons incise the insular slope (Johnson and Pálmason, 1980). The prograded sediment wedge is estimated to be about 2 km thick (Kristjansson, 1976b). Single-channel reflection profiles show at least 1 km sediment (Johnson and Pálmason, 1980). Based on seismic reflection profiles, Egloff and Johnson (1979) conclude that the shelf edge has prograded 10 to 35 km off southwest Iceland.

In the area north of Iceland examined in the present study, seismic reflection data (Grønlie and Talwani, 1978) show sediment thicknesses of at least 0.5 km on the insular slope north of Tjörnes peninsula, over 1 km east of northern Iceland, and an extensive lens at least 1.8 km thick lies west of the southern Kolbeinsey Ridge, north of the Skagi peninsula (Fig. 6). Clearly, greater sedimentation in the west explains why the 400 to 1,000 m isobaths extend farther northwards *west* of the present accretion axis, which has acted as an effective barrier to eastwest sediment transport. Based on these data (Fig. 6), we roughly estimate that the shelf break north of Iceland has prograded of the order of 50 km in the area north of Skagi, 10 km north of Tjörnes, and 0 to 30 km east of northern Iceland. Although we have not completed processing the magnetic data for depth to basement, the pattern of short-wavelength magnetic anomalies qualitatively confirms the conclusions from seismic profiling. Shallow magnetic sources extend outwards towards the shelf edge north of eastern and western Iceland (Fig. 2). Thus the northward projections of the Iceland platform in these two areas are basement arches, not the results of sedimentation. However, depressions in magnetic basement occur between the present spreading axis and the outer arches, and these depressions are occupied by sediments, at least near the shelf break. Possibly thick sediments continue southward towards the Iceland coast, but are seismically too reflective to be charted by single-channel techniques. The existence of low-density sediments is also suggested by *relatively* negative free-air gravity anomalies (Pálmason, 1974). Whereas the platform off the Skagi and Tjörnes peninsulas and the Kolbeinsey Ridge north of 66.5° exhibit anomalies of about +50 to +60 mgal, the region of possible sediment accumulation is typically +35 to +45 mgal. A more local free-air negative dips to below 0 mgal near the coast due south of the Kolbeinsey Ridge. This WNW trending anomaly parallels the Husavik faults and may be a deep, sediment-filled trough associated with the Tjörnes F.Z. (Saemundsson, 1974; Johnson, 1974).

Off the Greenland margin, locally extensive shelf prograding is directly implied by our magnetic anomaly identifications (Figs. 2–4 and 6). At 66°–67° N (Denmark Straits), the present shelf break at ~400 m lies well over 100 km southeast of anomalies 20–21 (Figs. 1, 2 and 6). We envision most of the prograding to have occurred in the last 3 Ma as a result of several coalescing ice streams emanating from the Kangerdlugssuaq Fjord complex. Another such 'ice-delta' forms a conspicuous arcuate salient seaward of Scoresby Sund. Prograding of as much of 100 km is suggested by the morphology and indeed required by our magnetic anomaly interpretations (Figs. 2–4). Sonobuoy stations (Grønlie and Talwani, 1978) and multi-channel profiling (Hinz and Schlüter, 1978) suggest sediment thicknesses of the order 2 to 4 km under these deltas. The data published by those authors are not inconsistent with our thesis that oceanic crust forms the basement in these two areas.

As noted by Vogt and Perry (1978), relatively rapid shelf prograding around Iceland (locally 20 km or more) and Greenland (locally 100 km or more) has been facilitated by (a) the young age and large positive depth anomalies, i.e., shallow crust, and (b) the efficient transport of coarse sediment to the shelf edges by ice streams.

Magnetic Smooth Zones Near Iceland

Magnetic smooth zones (or quiet zones) are oceanic areas characterized by magnetic anomalies of relatively low amplitude, generally less than ±50 to 100 nT (e.g. Vogt et al., 1970b; Poehls et al., 1973). Various processes could account for smooth zones, for example, high spreading rate compared to reversal frequency – resulting in broad strips of ocean crust magnetized with constant magnetic polarity. A magnetic smooth zone would then be generated provided that the lateral contrasts in induced and viscous magnetization are small. An accretion axis orthogonal to the equator also generates a magnetic smooth zone, for example the equatorial Mid-Atlantic and East-Pacific ridges. Inspection of Fig. 2 shows that a magnetic smooth zone is being generated where the Kolbeinsey Ridge approaches and crosses the Iceland platform (see also Figs. 4, 9, and 10; Meyer et al., 1972, Vogt and Johnson, 1973, 1974). The data published by Talwani et al. (1971) and Serson et al. (1968) reveal a similar effect where the Reykjanes Ridge enters Iceland (Fig. 10). Magnetic smooth zones are also found in the Jan Mayen Ridge area east of 6C and along the Greenland margin west of anomaly-5 and north of the Greenland-Iceland Ridge (Figs. 2 and 4). The processes responsible for these older smooth zones may resemble those at work at the Reykjanes Ridge-Iceland and Kolbeinsey Ridge-Iceland junctions.

What are those processes? Constant polarity and equatorial polarity can be immediately ruled out, but a number of possibilities remain to be examined. Relevant parameters and model profiles are shown in Figs. 9 and 10.

1. A large fraction of the magnetized layer has been removed by glacial, wave, or/and fluvial erosion. This process may have been significant on the shelf near Iceland, but would require the paleo-coastline to have lain 100 to 200 km north of northern Ice-

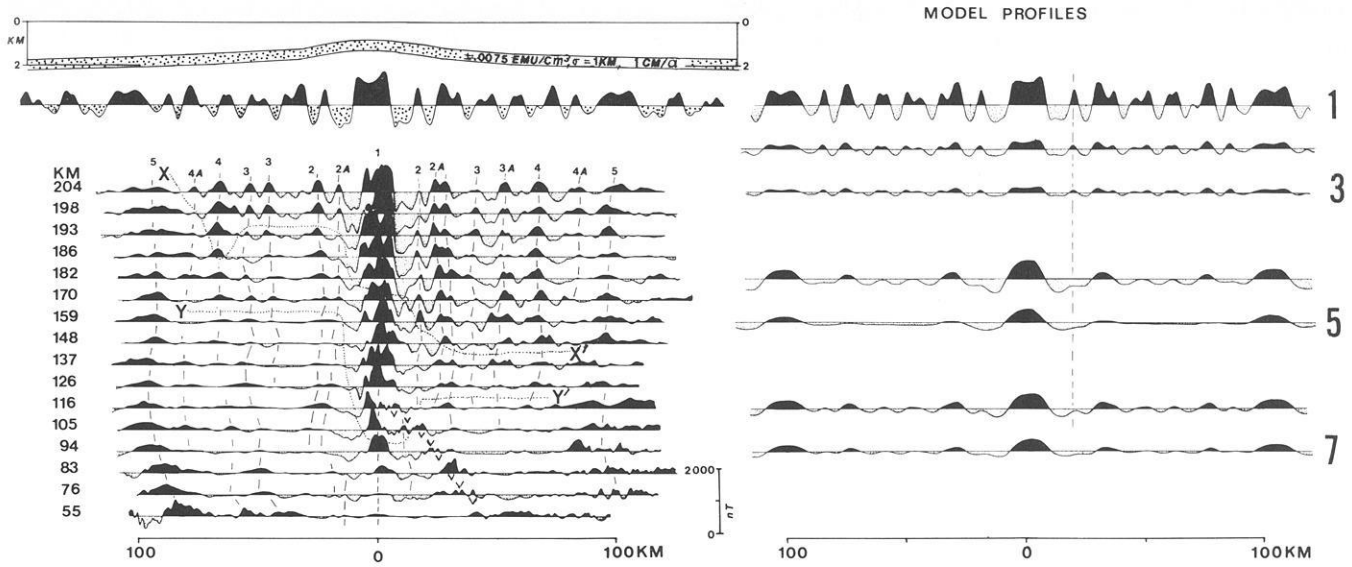

Fig. 9. *Left:* Profiles showing decrease of anomaly amplitude from Kolbeinsey Ridge southward to Iceland. Profiles indexed by distance (km) north of 66° N (Fig. 2). Dotted line XX' indicates amplitude reduction. South of YY' anomalies become smoother, more irregular, and still lower in amplitude. *Right:* Model profiles simulating three possible processes to explain amplitude decrease; magnetized layer is 0.5 km thick in all cases. Top profile (1) was starting point (depth D to top of layer: 1.24 km; magnetization M: ± 0.0075 emu/cm^3; transition width ($\sigma = 1$ km; Blakely, 1976). Profile 2 same, but $M = \pm 0.0025$ cgs; profile 3, same, but $M = \pm 0.0015$ cgs. Profiles 4 and 5 show effect of increasing σ to 3 km and 4 km (other parameters as in 1); profiles 6 and 7 show effect of increasing source depth to 3.84 and 4.84 km (other parameters as in 1)

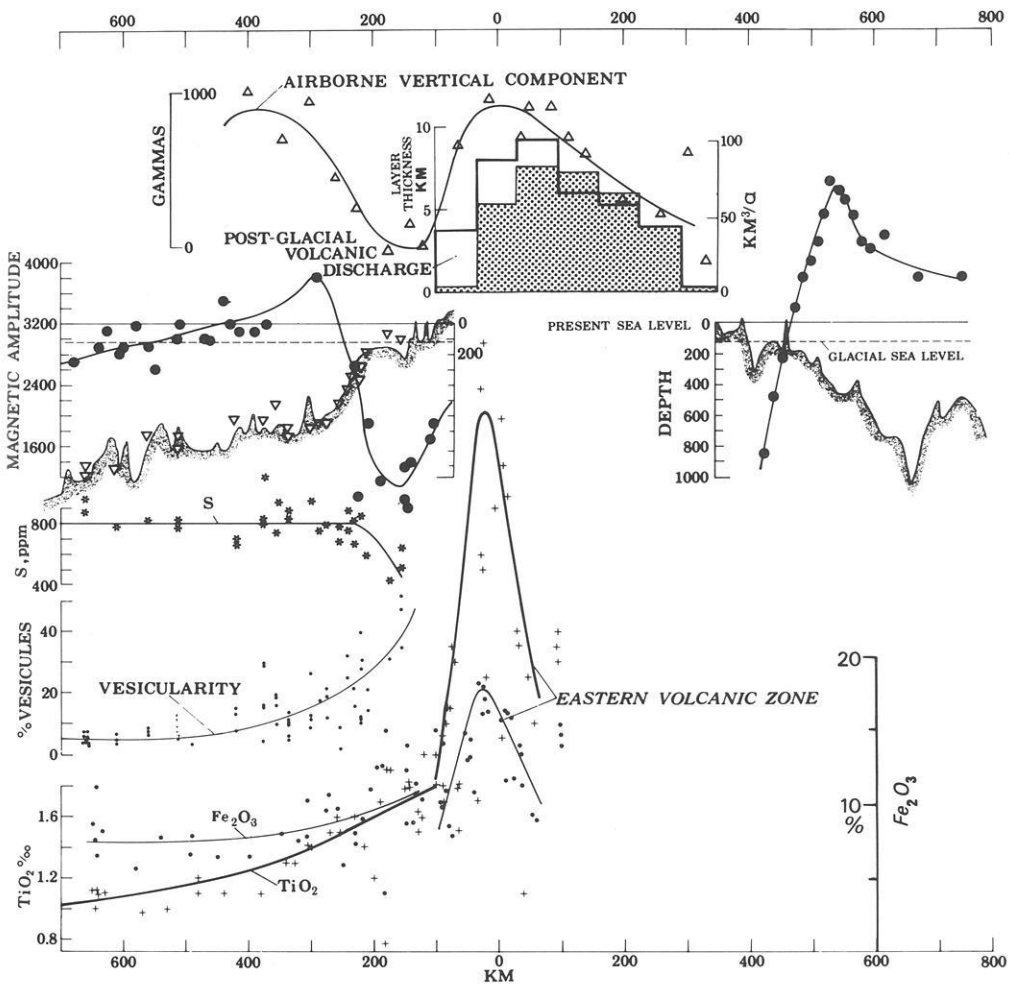

Fig. 10. Profiles of magnetic anomaly amplitude, volcanic discharge, water depth, sulfur concentrations, vesicularity, and Fe-Ti concentration along plate boundary from Reykjanes Ridge *(left)* through Iceland *(center)* to Kolbeinsey Ridge *(right)*. From Vogt and Johnson (1974), based on data from Talwani et al. (1971), Jakobsson (1972), Meyer et al. (1972), Serson et al. (1968), Schilling (1973), Moore and Schilling (1973), and Brooks and Jakobsson (1974)

land and subsided to depths of 1,500 to over 2,000 m. Furthermore, recent work suggests the magnetic layer is at least 1,000 m thick (Huestis and Parker, 1977); drilling in the FAMOUS area (Joint Oceanographic Institutions Deep Earth Sample, 1975) indicates only minor hydrothermal alteration and little effect on remanence at 582 m depth. In Iceland, Kristjansson and Watkins (1977) have suggested that some of the primary remanence in basalt lava flows will survive burial to 3 km (i.e., 200° C); the magnetic mineral in these flows will certainly survive 4 km burial (Pálmason et al., 1979).

2. The magnetization was acquired at shallow confining pressures, leading to degassing, high vesicularity, higher oxidation state, and therefore, perhaps reduced magnetization (Vogt and Johnson, 1974). As a related process the higher vesicularity would facilitate brecciation and subsequent low-temperature alteration, causing a loss of magnetization (Pálmason et al., 1979). In support of this process we note that the decline of magnetic amplitudes along the *present* spreading axis begins at about 400–600 m depth, where vesicularity begins its sharp increase and sulfur content (a measure of gas retention) its decrease (Moore and Schilling, 1973; Fig. 10). The line of magnetic amplitude change (Figs. 6 and 9) would then be a fossil ~500 m isobath. Difficulties for this explanation are that the magnetic anomalies are not simply attentuated but also *smoothed* as Iceland is approached. This might be explained in terms of Blakely's (1976) two-layer model. The upper, pillow layer is less magnetized, leaving the lower layer with its more diffuse polarity boundaries (transition widths) to dominate the signal. A more serious problem is the strongly asymmetrical attenuation (Fig. 2; profiles km 126 to 193 in Fig. 9): How could the east and west flank basement be formed at two different depths?

3. Subsidence of the crust after it was formed would cause both attenuation and smoothing. However, the depths required, 3 to 5 km according to model profiles in lower right of Fig. 2, are unreasonably great. Reflection profiling suggests basement depths of 0 to 2 km (Fig. 6; Grønlie and Talwani, 1978). Gravity data hint at additional sediment in the Tjörnes F.Z. area, hidden by acoustically opaque materials on the platform (Saemundsson, 1974). More serious objections to the subsidence hypothesis is the large amount of it, greatly exceeding sinking of normal ocean crust of comparable age. Finally, subsidence does not account for the decline in central anomaly amplitude (Fig. 10) because the axis is not buried by sediments.

4. Since the extrusion zone is substantially wider on Iceland than along the normal mid-oceanic ridge, it would be reasonable to expect the magnetic transition width to increase as Iceland is approached. Increasing transition width from 2 to 3.5 km does result in a strongly attenuated, smoothed signature (model profiles in Fig. 9). However, it is hard to understand how dikes injected east of the axis are less spread than those on the west flank, as would be required to explain the unequal amplitudes. Furthermore, anomalies between XX′ and YY′ (Fig. 9) are simply attenuated, not smoothed.

5. Thick sediments rapidly deposited on very young crust (high heat flow) would insulate the magnetic layer and cause temperatures to rise, tending to destroy the magnetization. This mechanism is attractive because thick sediments occur predominately on the *west* flank of southern Kolbeinsey Ridge and correlate with the amplitude asymmetry (Fig. 9). Similarly the relatively low amplitudes of anomalies 4A to 6C on the Greenland margin (Figs. 2–4) correlate with thick sediment cover (Fig. 6). However, the mechanism fails to explain why even the axial anomaly declines dramatically toward Iceland. Furthermore, unless substantial thicknesses of sediments can be demonstrated on the Iceland shelf by seismic methods, low amplitudes in that region cannot be attributed to sedimentation.

6. The connection between the Iceland rift zones and Kolbeinsey Ridge may have consisted of complex, time-varying en echelon rift zones (McMaster et al., 1977). For example, the Quaternary volcanic zone crosses previous lineations on a northwest strike (Fig. 9). Such complexities would smooth and attenuate the lineations. However, such a process could not account for the simple amplitude reduction observed between YY′ and XX′ (Fig. 9).

At present, none of the six mechanisms by themselves explain all the observations. Nor can any of them be wholly discounted. We therefore infer that several processes are responsible: Near Iceland (south of YY′ in Fig. 9), 1, 2, 4, and 6 are likely to be most important. Farther north, 2 may be most important at the axis, and 5 for crust more than 1 Ma old.

Conclusions

In this paper we have presented new data which, if we have correctly interpreted them, call for some major revisions regarding the origin of the Iceland Plateau and the position of the continent-ocean crustal boundary.

Our most important conclusions was the 'disproof' of an extinct spreading axis on the Iceland Plateau. The magnetic anomalies previously attributed to the extinct axis actually form the *east* flank of Kolbeinsey Ridge. An important consequence is that the *west* flank anomalies, strongly attenuated in amplitude, and for this reason not previously recognized, occur over the Greenland margin. Even parts of the shelf up to 100 km inland from the shelf break must be underlain by Miocene oceanic crust. We are forced to conclude that the present continental slope (e.g., the 500 fm contour) is a poor guide to the oceanic-continental crustal transition. Our interpretation may explain many of the overlaps that occur when continents are reconstructed. However, conditions have been especially favorable to shelf prograding in the Greenland-Iceland area. Grounded ice streams deposited large sediment volumes at the shelf edge, which could prograde rapidly in the relatively shallow ocean in the Iceland area. Our interpretations may be tested by seismic reflection and refraction. Limited available data (Hinz and Schlüter, 1978; Grønlie and Talwani, 1978) are not inconsistent with oceanic crust underlying at least the outer Greenland shelves. Deep drilling is the only sure test, of course, but drilling in search for hydro-carbons certainly has minimal promise.

The Iceland Plateau has the best 'recording' of anomalies 5A to 6C that we have seen in the Atlantic. This record allowed us to pinpoint the late Tertiary plate acceleration 12–14 Ma ago. All that could be concluded previously was a relatively lower rate between anomaly 6 and 5 time compared to post-anomaly 5 (9.5 Ma). We find the 12–14 Ma time especially interesting because it correlates with the development of the 'E' escarpments around Iceland, perhaps a magmatic 'pulse' of global proportions (Vogt, 1978). The case for a causal connection between hot spot activity and plate dynamics is thus strengthened. Although we cannot disprove the alternative hypothesis, that the plate acceleration at 12–14 Ma caused the 'E' escarpments, we prefer to see both plate acceleration and the escarpments as manifestations of increased plume flow.

A magnetic smooth zone is being formed where the Reykjanes and Kolbeinsey ridges enter the Iceland platform. We could ex-

clude some mechanisms postulated to produce smooth zones, but a lengthy list remains. At this time we prefer (a) degassing at low confining pressures at extrusion depths of 400–600 m and less, followed by (b) sediment loading of the young hot crust, causing reheating and loss of magnetization. Both these mechanisms can be tested – the first by measuring magnetic properties on a large dredge sample collection from the present axis, and the second by deep drilling through the 500–2,000 m thick sediment cover to determine the magnetic properties of the underlying crust.

Acknowledgments. We are particularly indebted to R.H. Higgs, R.N. Lorentzen, and the technical staff of Project MAGNET who carried out and reduced the high-quality magnetic survey described in this paper The senior author was partially supported by the Office of Naval Research. We thank R. Blakely for his magnetic model program. S. Jakobsson first pointed out the 'V-shaped' topographic grain of northern Iceland and its insular shelf. Discussion with H. Fleming, R. Feden, L.C. Kovacs, and J. Brozena were helfful. D. O'Neill and J. Peery assisted with the manuscript.

References

Anonymous: Tectonic/geological Map of Greenland, compiled by A. Escher, The Geological Survey of Greenland, Copenhagen, Denmark, 1970

Belousov, V V., Udintsev, G.B. (eds.): Islandiya i sredinno-okeanicheskii khrebet. Stroenie dna okeana. Iceland and Mid-Oceanic Ridge. Structure of the Ocean Floor (in Russian). 204 pp. Moscow· Nauka 1977

Björnsson, A.G., Johnsen, G., Sigurdsson, S., Thorbergsson, G., Tryggvason, E. Rifting of the plate boundary in North Iceland 1975–1978. J. Geophys. Res. **84**, 3029–3038, 1979

Björnsson, A., Saemundsson, K., Einarsson, P., Tryggvason, E., Grönvold, K. Current rifting episode in North Iceland. Nature **266**, 318–323, 1977

Blakely, R.J. An age-dependent, two-layer model for marine magnetic anomalies. In The Geophysics of the Pacific Ocean Basin and Its Margin. Geophys. Monogr. 19, pp. 227–234. Washington, D.C. Am. Geophys. Union 1976

Brooks, C.H., Jakobsson, S.P. Petrochemistry of the volcanic rocks of the North Atlantic Ridge system. In. Geodynamics of Iceland and the North Atlantic area, L. Kristjansson, ed. pp. 139–154. NATO Advanced Study Institute Series. Reidel. Dordrecht 1974

Cochran, J.R., Talwani, M. Gravity anomalies, regional elevation, and the deep structure of the North Atlantic. J. Geophys. Res. **83**, 4907–4924, 1978

Deer, W.A. Tertiary igneous rocks between Scoresby Sund and Kap Gustav Holm, East Greenland. In Geology of Greenland, A. Escher, W.S. Watt, eds. pp. 405–429. Copenhagen: Geol. Survey of Greenland 1976

Egloff, J., Johnson, G.L. Erosional and depositional structures of the southwest Iceland insular margin Thirteen geophysical profiles. In Geological and Geophysical Investigations of Continental Margins, J.S. Watkins, L. Montadert, P W Dickerson, eds: Am. Assoc. Petrol. Geol., Tulsa, Oklahoma, pp. 43–64, 1979

Einarsson, T On submarine geology around Iceland. Natturu fraedingurinn **32**, 155–175, 1963

Gairaud, H., Jacquart, G., Aubertin, F., Beuzart, P. The Jan Mayen Ridge: Synthesis of geological knowledge and new data. Oceanologica Acta **1**, 335–358, 1978

Grønlie, G., Chapmann, M., Talwani, M. Jan Mayen Ridge and Iceland Plateau· Origin and evolution. Nor Polarinst. Skr 1979 (in press)

Grønlie, G., Talwani, M. Geophysical Atlas: Norwegian-Greenland Sea. Vema Res. Ser. Vol. 4, Lamont-Doherty Geol. Obs., 26 pp., 1978

Harrison, C.G.A., McDougall, I., Watkins, N.D. A geomagnetic field reversal time scale back to 13.0 m. y. before present. Earth Planet. Sci. Lett. **42**, 143–152, 1979

Hey, R., Vogt, P. Spreading center jumps and sub-axial asthenosphere flow near the Galapagos hot spot. In. Subduction Zones, Mid Ocean Ridges, Oceanic Trenches, and Geodynamics, S. Uyeda, ed. pp. 41–52. Amsterdam Elsevier 1977

Hinz, K., Schlüter, H.-U. Der Nordatlantik Ergebnisse geophysikalischer Untersuchungen der Bundesanstalt für Geowissenschaften und Rohstoffe an nordatlantischen Kontinentalrändern. Erdöl, Erdgas Z. **94**, 271–280, 1978

Huestis, S.P., Parker, R.L. Bounding the thickness of the oceanic magnetized layer J. Geophys. Res. **82**, 5293–5303, 1977

Jakobsson, S.P. Chemistry and distribution pattern of Recent basaltic rocks in Iceland. Lithos **5**, 365–386, 1972

Johnson, G.L. Morphology of the mid-ocean ridge between Iceland and the Arctic Basin. In Geodynamics of Iceland and the North Atlantic Area L. Kristjansson, ed. pp. 49–62. Dordrecht. Reidel, 1974

Johnson, G.L. The Jan Mayen Ridge. In Canada's Continental Margins and Offshore Petroleum Exploration, C.J. Yorath, E.R. Parker, D.J. Glass, eds. Can. Soc. Petrol. Geol., Mem. **4**, 225–234, 1975

Johnson, G.L., Heezen, B.C. Morphology and evolution of the Norwegian-Greenland Sea. Deep-Sea Res. **13**, 755–771, 1967

Johnson, G.L., McMillan, N.J., Egloff, J. The continental margin of East Greenland. In Canada's Continental Margins and Offshore Petroleum Exploration, C.J. Yorath, E.R. Parker, D.J. Glass, eds. Can. Soc. Petrol. Geol., Mem. **4**, 205–224, 1975

Johnson, G.L., Pálmason, G. Observations of the morphology and structure of the sea floor south and west of Iceland, J. Geophys. **47**, 23–50, 1980

Johnson, G.L., Southall, J.R., Young, O.W., Vogt, P.R. The origin and structure of the Iceland Plateau and Kolbeinsey Ridge. J. Geophys. Res. **77**, 5688–5696, 1972

Joint Oceanographic Institutions Deep Earth Sample: Sources of magnetic anomalies on the Mid-Atlantic Ridge. Nature **225**, 389–390, 1975

Kristjansson, L. On the thickness of the magnetic crustal layer in southwestern Iceland. Earth Planet. Sci. Lett. **16**, 237–244, 1972

Kristjansson, L. A marine magnetic survey off southern Iceland. Mar Geophys. Res. **2**, 315–326, 1976a

Kristjansson, L. Central volcanoes on the western Icelandic shelf. Mar Geophys. Res. **2**, 285–289, 1976b

Kristjansson, L. Marine magnetic surveys off the west coast of Iceland. Soc. Sci. Isl. Greinar **5**, 23–44, 1976c

Kristjansson, L., Thors, K., Karlsson, H.R. Confirmation of central volcanoes off the Icelandic coast. Nature **268**, 325–326, 1977

Kristjansson, L., Watkins, N.D. Magnetic studies of basalt fragments recovered by deep drilling in Iceland, and the 'magnetic layer' concept. Earth Planet. Sci. Lett. **34**, 365–374, 1977

La Brecque, J.L., Kent, D.V., Cande, S.C.: Revised magnetic polarity time scale for Late Cretaceous and Cenozoic time. Geology **5**, 330–335, 1977

Larsen, H.C.: Offshore continuation of East Greenland dyke swarm and North Atlantic ocean formation. Nature **274**, 220–223, 1978

McMaster, R.L., Schilling, J.-G., Pinet, P.R.: Plate boundary within Tjörness Fracture Zone on northern Iceland's insular margin. Nature **269**, 663–668, 1977

Meyer, O., Voppel., D., Fleischer, U., Closs, H., Gerke, K.: Results of bathymetric, magnetic and gravimetric measurements between Iceland and 70° N. Dtsch. Hydrogr. Z. **25**, 193–206, 1972

Minster, J.B., Jordan, T.H., Molnar, P., Haines, E.: Numerical modeling of instantaneous plate tectonics. Geophys. J. R. Astron. Soc. **36**, 541–576, 1974

Moore, J.G., Schilling, J.G.: Vesicules, water and sulfur in Reykjanes Ridge basalts. Contrib. Mineral. Petrol. **41**, 105–118, 1973

Morgan, W.J.: Deep mantle convection plumes and plate motions. Am. Assoc. Petrol. Geol. Bull. **56**, 203–213, 1972

Nilsen, T.H.: Lower Tertiary laterite on the Iceland-Faeroe Ridge and the Thulean land bridge. Nature **274**, 786–788, 1978

Noe-Nygaard, A.: Tertiary igneous rocks between Shannon and Scoresby Sund, East Greenland. In: Geology of Greenland, A. Escher, W.S. Watt, eds.: Geological Survey of Greenland, Copenhagen, pp. 387–402, 1976

Olafsdóttir, T.: A moraine ridge on the Iceland shelf, west of Breidafjördur. Natturufraedingurinn **45**, 31–36, 1975

Pálmason, G.: Comments on 'Origin and Structure of Iceland of Iceland Plateau and Kolbeinsey Ridge,' by G.L. Johnson, J.R. Southall, P.W. Young, P.R. Vogt, J. Geophys. Res. **78**, 7019, 1973

Pálmason, G., Saemundsson, K.: Iceland in relation to the Mid-Atlantic Ridge, Annu. Rev. Earth Planet. Sci. **2**, 25–50, 1974

Pálmason, G.: Insular Margins of Iceland. In: Geology of Continental Margins, C.A. Burke, C.L. Drake, eds.: pp. 375–379. Berlin, Heidelberg, New York: Springer 1974

Pálmason, G., Arnorsson, S., Fridleifsson, I.B., Kristmannsdottir, H., Saemundsson, K., Stefansson, V., Steingrimsson, B., Tomasson, J., Kristjansson, L.: The Iceland Crust: Evidence from Drillhole Data on Structure and Processes. In: Deep Drilling Results in the Atlantic Ocean: Ocean Crust, M. Talwani, C.G.A. Harrison, D.E. Hayes, eds.: Maurice Ewing Series, Vol. **2**, pp. 43–65. Am. Geophys. Union 1979

Perry, R.K., Fleming, H.S., Cherkis, N.Z., Feden, R.H., Massingill, J.V.: Bathymetry of the Norwegian – Greenland and Western Barents Sea, U.S. Naval Research Laboratory, Washington, DC 1977

Piper, J.D.A.: Interpretation of some magnetic anomalies over Iceland. Tectonophysics **16**, 163–187, 1973

Poehls, K.A., Luyendyk, B.P., Heirtzler, J.R.: Magnetic smooth zones in the world's ocans. J. Geophys. Res. **78**, 6985–6997, 1973

Saemundsson, K.: Evolution of the axial rifting zone in northern Iceland and the Tjörnes Fracture Zone. Geol. Soc. Am. Bull. **85**, 495–504, 1974

Schilling, J.-G.: Iceland mantle plume, geochemical evidence along Reykjanes Ridge. Nature **242**, 565–578, 1973

Serson, P.H., Hannaford, W., Haines, G.V.: Magnetic anomalies over Iceland. Science **162**, 355–357, 1978

Sigurgeirsson, T.: Aeromagnetic maps of SW-Iceland and of middle Western Iceland in scale 1:250,000. University of Iceland, 1970 and 1979

Sommerhoff, G.: Formenschatz und morphologische Gliederung des südostgrönländischen Schelfgebietes und Kontinentalabhanges. Meteor Forschungsergeb. Reihe C:**15**, 1–54, 1973

Talwani, M., Eldholm, O.: Evolution of the Norwegian-Greenland Sea. Geol. Soc. Am. Bull. **88**, 969–999, 1977

Talwani, M., Udintsev, G., Shirshov, P.P.: Tectonic Synthesis. In: Initial Reports of the Deep Sea Drilling Project, XXXVIII. pp. 1213–1242. Washington, D.C.: U.S. Government Printing Office 1976

Talwani, M., Windisch, C.C., Langseth, Jr., M.: Reykjanes Ridge crest: A detailed geophysical study. J. Geophys. Res. **76**, 473–517, 1971

Vogt, P.R.: Magnetized basement outcrops on the southeast Greenland continental shelf. Nature **226**, 743–744, 1970

Vogt, P.R.: Asthenosphere motion recorded by the ocean floor south of Iceland. Earth Planet. Sci. Lett. **13**, 153–160, 1971

Vogt, P.R.: The Iceland Phenomenon: Imprints of a hot spot on the ocean crust, and implicatins for flow below the plates. In: Geodynamics of Iceland and the North Atlantic Area, L. Kristjansson, ed.: NATO Adv. Study Inst. Ser. pp. 49–62. Dordrecht: Reidel 1974

Vogt, P.R.: Plumes, sub-axial pipe flow, and topography along the mid-oceanic ridge. Earth Planet. Sci. Lett. **29**, 309–325, 1976

Vogt, P.R.: Global magmatic episodes: New evidence and implications for the steady-state mid-oceanic ridge. Geology **7**, 93–98, 1979

Vogt, P.R., Avery, O.: Detailed magnetic surveys in the northeast Atlantic and Labrador Sea. J. Geophys. Res. **79**, 363–389, 1974

Vogt, P.R., Johnson, G.L.: Magnetic telechemistry of oceanic crust? Nature **245**, 373–375, 1973

Vogt, P.R., Johnson, G.L.: Magnetic telechemistry is elegant but nature is complex-A reply. Nature **251**, 498–499, 1974

Vogt, P.R., Johnson, G.L.: Transform faults and longitudinal flow below the mid-oceanic ridge. J. Geophys. Res. **80**, 1399–1428, 1975

Vogt, P.R., Anderson, C.N., Bracey, D.R., Schneider, E.D.: North Atlantic magnetic smooth zones. J. Geophys. Res. **75**, 2955–2968, 1970b

Vogt, P.R., Ostenso, N.A., Johnson, G.L.: Magnetic and bathymetric data bearing on sea-floor spreading north of Iceland. J. Geophys. Res. **75**, 903–920, 1970a

Vogt, P.R., Perry, R.: Post-rifting accretion of continental margins in the Norwegian-Greenland and Labrador Seas: Morphologic evidence. Eos Trans. Am. Geophys. Union **59**, 1204, 1978

Voppel, D., Srivastava, S.P., Fleischer, U.: Detailed magnetic measurements south of the Iceland-Faeroe Ridge. Dtsch. Hydrogr. Z., in press, 1979

Watkins, N.D., Walker, G.P.L.: Magnetostratigraphy of eastern Iceland. Am. J. Sci. **277**, 5131–5184, 1977

Weidick, A.: Glaciation and the Quaternary of Greenland. In: Geology of Greenland, A. Escher, W.S. Watt, eds.: pp. 431–458. Copenhagen: Geol. Surv. Greenland, 1976

Received April 17, 1979; Revised Version October 8, 1979

J. Geophys. 47, 81–85, 1980

Journal of Geophysics

Morphology of the Reykjanes Ridge Crest Near 62° N

W.R. Jacoby
Institut für Meteorologie und Geophysik der Universität, Feldbergstr. 47, D-6000 Frankfurt 1, Federal Republic of Germany

Abstract. During the RRISP 1977 experiment FS METEOR conducted a detailed bathymetric survery of a $45 \times 50\ km^2$ quadrangle of the Reykjanes Ridge crest near 62° N with a narrow-beam echosounder. On the basis of the profiles and a contour chart we recognize a central zone of oblique en echelon volcanic ridges filling a < 30-km-wide rift valley nearly to the brim. Thus, at least in the survey area, Reykjanes Ridge does not differ from other slow spreading ridges in having no median rift at all, but only in the valley fill. The orientation of the volcanic fissures tends to be normal to the spreading direction, while the main rift faults rather follow the general ridge morphology. At 61°55′ N the sea floor features are disrupted and depressed and the physiographic character changes from north to south; this suggests a fracture zone though not a clear-cut transform fault. The preferred model is one in which the axial tensile stress leading to fissuring and volcanism is normal to the direction of plate separation (N 095°); the stress field off the axis leading to normal faulting and rift valley formation, on the other hand, is governed by the thermal boundary conditions and is thus rotated into that of the average ridge orientation.

Key words: Bathymetry – Median valley – Mid-Atlantic Ridge – Oceanic volcanism – Rifting – Transform fault.

Introduction

A detailed narrow-beam echosounder survey of the crestal region of Reykjanes Ridge near 62° N was conducted by FS METEOR with the aim to see whether features as volcanic ridges and a median valley could be resolved. Reykjanes Ridge is unusual: oblique spreading and slow spreading but with no apparent rift valley; instead, its known crestal morphology north of 61° N is rather that of a block, about 45 to 55 km wide and standing nearly 1 km above the neighbouring sea floor near Iceland (Dietrich, 1959; Ulrich 1966; Talwani et al., 1971, Vogt, 1974). The block structure is superimposed on the regional subsidence with age (e.g. Sclater and Francheteau, 1970). Between 61° N and 58° N the block gradually disappears and gives way to a well defined rift valley (Laughton et al., 1979). Between Iceland and about 57° N Reykjanes Ridge is remarkably straight, striking N 036°, i.e., about 30° oblique to the direction normal to spreading (N 005°) whose rate is about 2 cm/a (e.g. Vogt and Avery, 1974). A summary of these and other geophysical data on Reykjanes Ridge is given by Fleischer (1974).

Some of the questions we ask are: What is the style of rifting in the crestal block of Reykjanes Ridge? Is there any indication of a rift valley or major normal faults? Can we distinguish volcanic features and faults? The oblique spreading may provide a chance to separate effects of volcanism and faulting or of plate kinematics and cooling.

Data

As part of the Reykjanes Ridge Iceland Seismic Project (RRISP 1977), FS METEOR during cruise No. 45 collected 660 km of echosounder track in 4.5 km spaced profiles perpendicular to the morphological axis of Reykjanes Ridge within a $45 \times 50\ km^2$ quadrangle centered at 62° N. 26°30′ W (Fig. 1). The survey area is just north of the region studied by Shih et al. (1978) with a deep-tow instrument package. The ELAC echosounder has a half-power beam width of 2.8° and uses signal frequencies of 15 and 30 kHz. Navigation was by the integrated INDAS IV system (PRAKLA-SEISMOS 1972) using LORAN (chains SL7W-SL7X) and updated automatically by satellite fixes. The relative position accuracy during the survey is estimated to be only a few hundred meters at most.

In Fig. 1 the original echosounder recordings are reproduced for the first four crest crossings. The direction of Profiles 1 and 3 has been reversed to permit easier visual comparison of topographic features. For reference to age of the seafloor, a generalized magnetic anomaly profile (after Talwani et al., 1971) has been superimposed on the top bathymetric record. Figure 2 shows the locations of the ship's tracks discussed, it is also a composite of simplified bathymetric profiles, corrected for ship speed to give true distance. Simplification was done by picking only the prominent high and low points and conspicuous changes in slope (I owe the readings to captain H. Feldmann who did them aboard the ship during the cruise). A comparison of Figs. 1 and 2 demonstrates the amount of simplification, features of 0.5 km extent or less are generally neglected.

A few attempts to contour the depths shown in Fig. 2 by several expedition members lead to rather similar results. Figure 3 presents as an example the contour chart of the area combining the various efforts; it is preliminary. The correlation of small features from profile to profile is, of course, ambiguous if not impossible in some cases. It is also influenced by the plausible though unproven hypothesis that the topographic features are elongated grossly parallel to the ridge axis. Some confidence in the results can be gained from the fact that several independent contouring attempts yielded similar maps. Our interpretation is also supported by observations further southwest on Reykjanes

0340-062X/80/0047/0081/$01.00

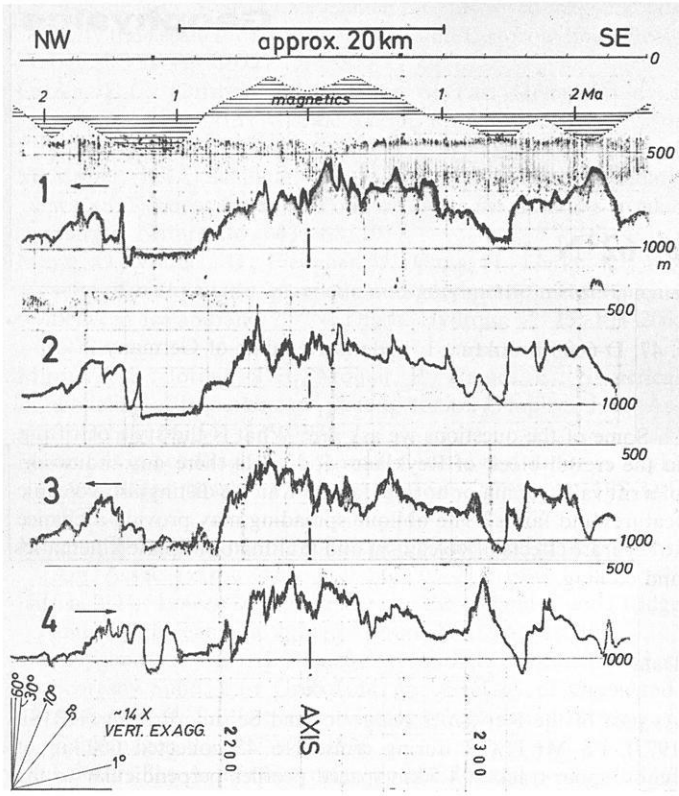

Fig. 1. ELAC narrow-beam echosounder recordings during the four northeasternmost ridge crossings. *Profiles 2 and 4* as recorded, *1 and 3* reversed for better visual correlation of features (*arrows* indicate ship's heading). *Uncorrected depths; horizontal scale:* time along ship's track (*thin vertical lines* in 10 min intervals); approximate length scale (in km) on top; vertically exaggerated slopes in left lower corner. Generalized magnetic anomaly (arbitrary scale, Profile 2 of Talwani et al., 1971) and approximate crustal age in Ma shown on top bathymetric profile

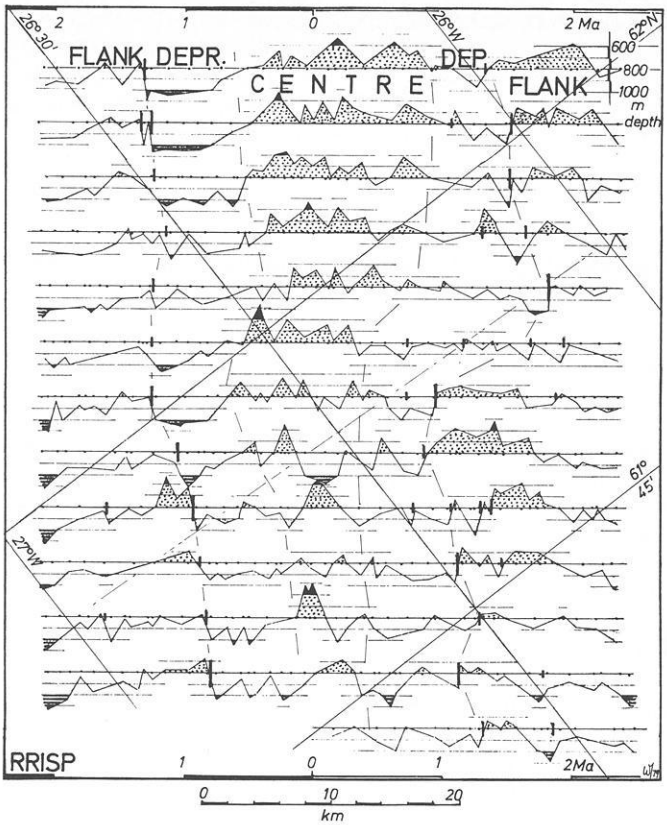

Fig. 2. Simplified echosounder profiles across Reykjanes Ridge crest. Vertical exaggeration about 9; vertical scale in upper right corner. Ship's tracks along 800 m depth lines. *Bold ticks* indicate steep slopes suggestive of normal faults (lengths qualitatively symbolize throw). Morphological provinces 'Center', 'Depression', 'Flank' separated by *thin dashed lines*. Approximate location of proposed minor fracture zone near 61°55′ N shown by *thin dash-dotted line*. Approximate crustal ages indicated at top and bottom frame

Ridge crest by Shih et al. (1978), Laughton et al. (1979), and Laughton and Searle (1979) who used side-scanning sonar. Since it 'sees' parts of the morphology in continuity, the elongated ridges and scarps are unquestionably recognized. Their results and ours are very similar, indeed.

Discussion and Interpretation of Data

With the uncertainties in mind, we shall now discuss some of the features of Figs. 1–3. We can tentatively distinguish three morphological provinces crudely symmetrical about the ridge axis. (1) A central province, about 15 km wide (in the NE), with many narrow oblique en echelon ridges often many hundreds of meters high, is bounded by (2) a series of depressions on either side; their outer borders are about 27 km apart in the NE and about 20 km in the SW where, however, the depressions are poorly defined. (3) A series of outer rises follows; generally they have steep inward facing scarps toward Province 2 (Figs. 1 and 2). The drop in topography at the margins of the survey area marks the sides of the crestal block. The three morphological provinces are tentatively marked on Fig. 2; their boundaries are indicated by thin dashed lines.

I interpret these features to represent a rift valley of normal width between the inward facing fault scarps; the valley floor is, however, abnormal in that it rises in the central region above the elevation of the rift shoulders. The en echelon ridges in this central region are interpreted to be of volcanic origin. Volcanism thus appears to be much more vigorous than in more normal median valleys. It is not clear whether this records temporal variations of volcanicity during the past 2 Ma or whether it represents a quasi-steady state process of crustal generation. The median valley is about half as wide as the so-called crestal block or horst of Reykjanes Ridge and splits it about symmetrically. The crestal block does thus not simply replace the crestal rift of more normal ridges.

The rift valley is perhaps the most conspicuous feature of the northeastern part of the survey area, but it could have been overlooked with less data density and resolution, particularly in the southwest. Very steep slopes mark the sides of the rift on all profiles and sometimes they are near vertical; they have been indicated by vertical ticks at the profiles of Fig 2 (throw and steepness are symbolized by length of the ticks). At places the faults appear to be repeated at short distance on a profile, suggesting staircase or en echelon structures. Small local grabens of a few hundred meters to a kilometer width and with elevated shoul-

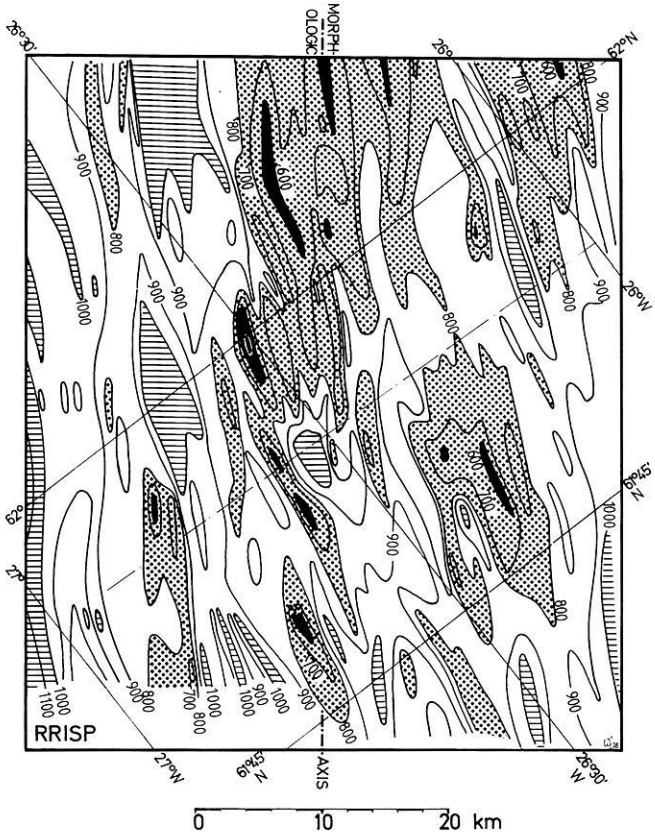

Fig. 3. Tentative depth contours of Reykjanes Ridge crestal region, on the basis of the profiles of Fig. 2. Depths in meter

ders appear to accompany some of the faults at their foot (e.g., at NW side of Profile 1, Fig. 1). This reminds us of similar features in Iceland, such as at Thingvellir.

The central region is mostly characterized by very rough, short-wavelength topography with amplitudes of tens of meters and more. Wavelengths are often less than 100 m perpendicular to the ridge (Fig. 1). This supports the interpretation that the region is of young active volcanic nature. The widths of the topographic features shown in the simplified profiles (Fig. 2) vary from a few hundred meters to several kilometers; note, however, that short wavelengths have been suppressed by the simplification. Figure 4 presents normalized frequency distributions of distances between neighbouring topographic maxima and minima ('half-wavelengths') irrespective of amplitude along all profiles in 0.2 mile or 0.36 km intervals. The left diagram covers the whole area, the others are for each morphological province separately; for depressions and flanks three diagrams are superimposed (NW, SE side, and both sides together). The dominant half-wavelength is less than 0.7 km; values between 1 and 1.5 km are half as frequent. The histograms do not differ very much from province to province, but a trend to more frequent short half-wavelengths and to very long ones can be recognized. This suggests break-up of volcanic forms by progressive fracturing and burrial of low ridges by sediments.

The en echelon ridges in the central zone typically trend between N010° and N030° and are often sub-parallel to the direction normal to spreading (N005°) but oblique to the general ridge morphology (N036°). In contrast, the scarps which are interpreted to be flanking the rift valley mostly trend N020° to N040°, sub-parallel to the ridge at large. There is distinct asymmetry in the ridge morphology. The depressions and the outer rises are more clearly developed on the NW flank than on the SE one. In the NW the inward facing escarpment of the outer rise can be followed through the whole survey area, but in the SE it is split up and irregular. There is generally a trend of topography rising toward SE; this is related to two prominent culminations on the SE side, one near 62° N, 25°55′ W, the other near 61°50′ N, 26°20′ W, with approximate dimensions of 8×20 km^2. On the NW side there is a smaller (3×10 km^2) topographic culmination near 61°55′ N, 26°48′ W. In size and shape these features are reminiscent of the volcanic centres of Iceland.

There are marked changes along the ridge axis, too. Mean water depth increases toward SW from <800 m to >800 m. NE of about 61°55′ N, 26°30′ W the central province is composed of a fairly regular series of volcanic ridges; to the SW its topography is more irregular with one dominant central high ridge. The change is rather abrupt and is marked by a hole about 1,100 m deep; near latitude 61°55′ N there is, in fact, a rather clear dividing line along which the topography is generally depressed indicated in Figs. 2 and 3. The presumed rift valley seems to narrow at this line abruptly (Fig. 2) and the morphological character changes. I interpret the dividing line to represent a poorly developed fracture zone along which some features seem to be offset by up to 15 km right-laterally, while other features as the central volcanic zone change more gradually. This is not unexpected for small fracture zones or transform faults (Courtillot et al., 1974; Macdonald, 1977; Macdonald and Luyendyk, 1977).

Support for the transform may come from the magnetic anomaly map of Heirtzler et al. (1966) which at its NE border contains our survey area. The anomalies are somewhat disturbed along 61°55′ N to the west from the axis out to anomaly 5, i.e., to about 10 Ma age. Other similar disturbances on Heirtzler's map seem to come and go on a somewhat shorter time scale and quite irregularly. The map does not resolve details as 10 km transforms (and corresponding normal spreading segments, some 20 km

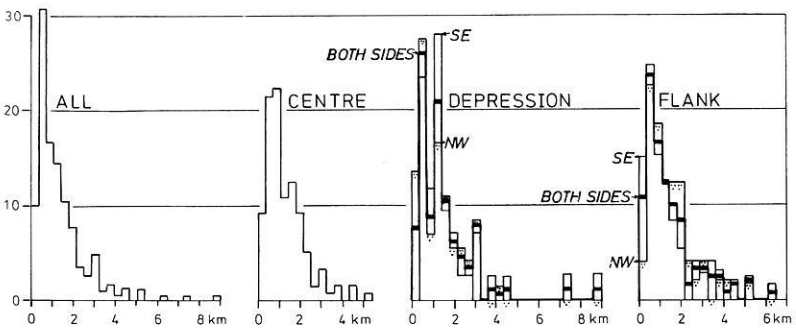

Fig. 4. Frequency distributions of horizontal distances between neighbouring topographic maxima and minima of all profiles of Fig. 2, for whole region and for the three morphological provinces (Fig. 2), separately; for 'Depression' and 'Flank' histograms for either side and both sides combined, superimposed with different symbols. The histograms are normalized to same area. 'Half-wavelengths' in 0.2 mile or 0.36 km intervals

long), but there is an indication of similar disturbances of the straight-axis oblique spreading (Shih et al., 1978).

For a discussion of the tectonics of the area it would be interesting to relate seismicity to morphology by plotting the epicenters of earthquakes on Figs. 2 or 3. Unfortunately the published data are not sufficiently accurate for a meaningful comparison with features of a few kilometers extent. A study with an array of ocean bottom seismometers would be most useful.

Model of Reykjanes Ridge

The most important results are summarized as follows. (1) As other slow-spreading ridges, Reykjanes Ridge, at least near 62° N, has a median rift of normal width. (2) The rift valley is about half as wide as the crestal block or horst of Reykjanes Ridge at 62° N. (3) The valley is largely filled with a great quantity of volcanics, the floor thus rising near the center above the rift shoulders. (4) As on the Reykjanes Peninsula of Iceland, the volcanic ridges in the rift valley and the feeder dykes are arranged en echelon and have the tendency of striking normal to the spreading direction or at least at directions intermediate between the spreading normal and the morphological Reykjanes Ridge axis. (5) In contrast, the normal faults bounding the rift valley have the tendency (or at least a stronger tendency) of striking subparallel to the ridge axis. (6) A small fracture zone has been recognized near 61°55′N. (7) As in Iceland volcanic centers may occur on Reykjanes Ridge.

We can take advantage of the oblique spreading and try to separate the sources of stress causing the fissuring and the normal faulting and rifting. An intuitive model is suggested by Fig. 5. If the stress field in the volcanic zone is tensile normal to plate separation, we should expect here a relatively broad region of very thin lithosphere above a magma chamber or a series of magma chambers. In this zone the stress field would essentially be in reaction to plate kinematics; principally this agrees with Tapponnier and Francheteau's (1978) necking model. The least principal stress would be actually directed outward in the direction of plate divergence. As we go outward we get to a region where cooling becomes the dominant process with rapid thickening of the lithosphere. Since cooling is governed by the boundary conditions, i.e., the geometry of the 0° C isotherm at the sea floor and the axial inflow of hot magma, it is plausible that the principal stresses are rotated from the spreading direction into that of the broad ridge morphology. Still near the culmination of topography, the minimum principal stress is directed normal to the ridge axis, but it need not be negative, i.e., truly tensile; over the depth range of faulting the maximum principal stress is vertical. As a result normal faults form, striking parallel to the ridge axis. Normal faulting with the axial side down is furthered by the volcanics loaded onto that side (Pálmason, 1973; 1980; Cann, 1974). Farther from the axis, down-hill compression in the lithosphere will build up with the topographic gradient, but that is outside the scope of this paper.

Figure 5 addresses itself also to the question why Reykjanes Ridge changes along its axis. In a gross sense this will be related to the balance of tectonic (with sources outside), gravitational, and viscous forces acting on the lithosphere and asthenosphere of the ridge (Sleep, 1969; Lachenbruch, 1973; 1976; Collette et al., 1980). Higher asthenospheric temperatures and melt contents or smaller viscosity would allow the asthenosphere to rise with less restriction than large viscosity would. The change in viscosity and temperature along Reykjanes Ridge may be related to the closeness to Iceland and to horizontal flow (e.g., Vogt, 1974). Vigorous volcanism corresponds to high temperatures and melt contents; at the same time it leads to fast loading of the crust and to subsidence of the rift valley floor (Pálmason, 1973; 1980; Cann, 1974). Detailed studies of slow spreading ridges with less vigorous volcanism and hence a more pronounced rift valley (mainly in the FAMOUS area of the Mid-Atlantic Ridge at 37° N: Ballard and van Andel, 1977; Ramberg and van Andel, 1977; Ramberg et al., 1977; Luyendyk and Macdonald, 1977) support the present model.

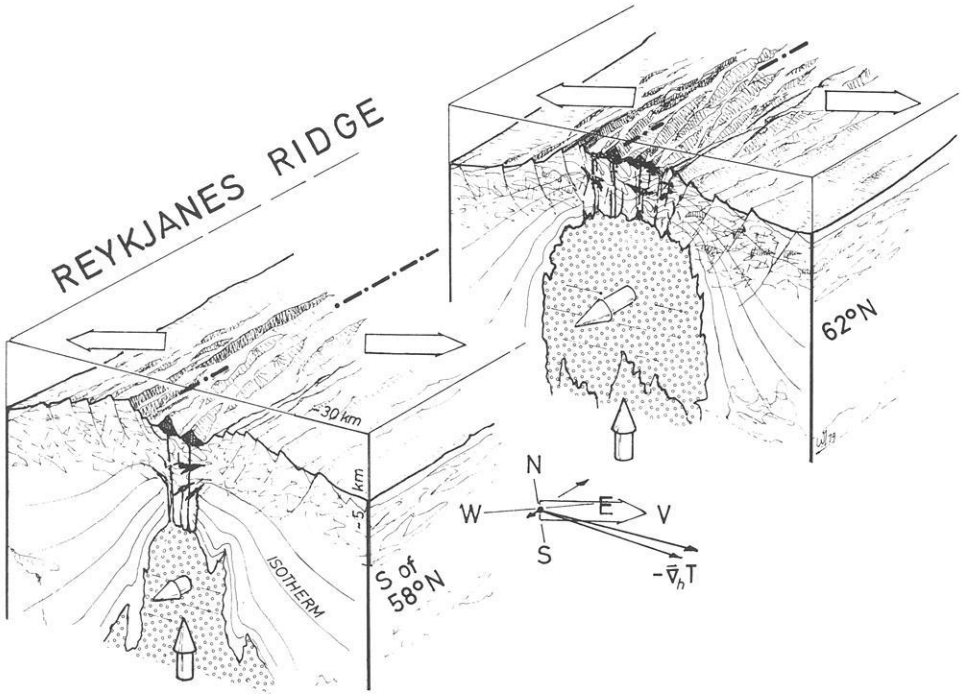

Fig. 5. Cartoon of Reykjanes Ridge model (approximate length scale at 'front corner'): solidified lithosphere, fissures, volcanic ridges, normal faults, isotherms, magma chamber or volume of crystal mush, flow (*round arrows*) partly upward, partly southwestward away from Iceland, oblique spreading direction (N095°, *flat arrows*); horizontal temperature gradient, $\nabla_h T$: shown in wind rose, nearly perpendicular to ridge axis. Righthand block depicts situation near 62° N; lefthand block further south (e.g. south of 58° N). For discussion see text

The crestal horst of Reykjanes Ridge has sometimes been looked upon as replacing the crestal rift usually found on slow-spreading ridges. From our data this appears to be wrong. The existence of a normally wide rift on top of the wider horst block suggests that they are two fundamentally different things, not only different in shape and mutually exclusive. As pointed out by Vogt (1971, 1974) the block is in plan view V-shaped and diachronous or time-transgressive. It is thus believed not to be steady-state (although it might be, if conditions change along the ridge), but rather to record time-varying discharge from the Iceland plume. We shall not discuss Vogt's hypothesis which we cannot prove or disprove, but we note the difficulty of interpreting features as the ones presented if we do not know their history.

Conclusions

The narrow-beam echosounder has proven very useful in studying the morphology and tectonics of the Reykjanes Ridge. It must be noted, however, that we have used only a small part of the information available from the echosounder records. More of the information should be used in the future and a more detailed and thorough interpretation is postponed till then. The combination with other data will also be helpful.

The 4.5 km spacing of the profiles has turned out to be not sufficient to achieve an unambiguous mapping of the topography of the ridge. Future work has to take this into account. In spite of the shortcomings, however, the present preliminary interpretation seems safe enough to present it to the critical reader.

Acknowledgements. The echosounder survey was carried out upon a suggestion by B. Loncarevic during the July 1977 RRISP experiment with W Weigel as the responsible chief scientist on FS METEOR. Captain H. Feldmann prepared the basis for the simplified topographic profiles. D. Voppel supplied the echosounder records kept at Deutsches Hydrographisches Institut. Officiers, crew, scientific, and technical staff aboard FS METEOR cooperated to make the survey a success. W Mahler and H. Roschker helped with the figures. The two anonymous referees made useful comments. Deutsche Forschungsgemeinschaft funded this work. All this is gratefully acknowledged.

References

Ballard, R.D., Andel, T.H. van: Morphology and tectonics of the inner rift valley at lat 36°50′ N on the Mid-Atlantic Ridge. Geol. Soc. Am. Bull. **88**, 507–530, 1977

Cann, J.R.: A model for oceanic crustal structure developed. Geophys. J. R. Astron. Soc. **39**, 169–187, 1974

Collette, B.J., Verhoef, J., Mulder, A.F.J. de: Gravity and a model of the median valley. J. Geophys. **47**, 91–98, 1980

Courtillot, V., Tapponnier, P., Varet, J. Surface features associated with transform faults: a comparison between observed examples and an experimental model. Tectonophysics **24**, 317–329, 1974

Dietrich, G.: Zur Topographie und Morphologie des Meeresbodens im nördlichen Nord-Atlantischen Ozean. Dtsch. Hydrogr. Z., Ergänzungsheft, Reihe B: **3**, 26–34, 1959

Fleischer, U.: The Rekjanes Ridge – a summery of geophysical data. In: Geodynamics of Iceland and the North Atlantic area, L. Kristjansson, ed. pp 17–33, Dordrecht Reidel 1974

Heirtzler, J.R., LePichon, X., Baron, J.G.. Magnetic anomalies over Reykjanes Ridge. Deep Sea Res. **13**, 427–443, 1966

Lachenbruch, A.H.: Dynamics of a passive spreading center J. Geophys. Res. **81**, 1883–1902, 1976

Lachenbruch, A.H.. A simple mechanical model for oceanic spreading centers. J. Geophys. Res. **78**, 3395–3417, 1973

Laughton, A.S., Searle, R.C. Tectonic processes at slow spreading ridges. Second Maurice Ewing Symposium. Washington, D.C. Trans. Am. Gephys. Union 1979

Laughton, A.S., Searle, R.C., Roberts, D.G.: The Reykjanes Ridge crest and the transition between its rifted and non-rifted regions. Tectonophysics **55**, 173–178, 1979

Luyendyk, B.P., Macdonald, K.C.: Physiography and structure of the inner floor of the FAMOUS rift valley· observations with a deep-towed instrument package. Geol. Soc. Am. Bull. **88**, 648–663, 1977

Macdonald, K.C.: Near bottom magnetic anomalies, asymmetric spreading, oblique spreading, and tectonics of the Mid-Atlantic Ridge near lat 37° N. Geol. Soc. Am. Bull. **88**, 541–555, 1977

Macdonald, K.C., Luyendyk, B.P. Deep-tow studies of the structure of the Mid-Atlantic Ridge crest near lat 37° N. Geol. Soc. Am. Bull. **88**, 621–636, 1977

Pálmason, G.: A continuum model of crustal generation in Iceland; kinematic aspects. J. Geophys. **47**, 7–18, 1980

Pálmason, G.. Kinematics and heat flow in a volcanic rift zone, with application to Iceland. Geophys. J. R. Astron. Soc. **33**, 451–481, 1973

PRAKLA-SEISMOS: INDAS, our integrated navigation and data acquisition system with automatic steering for RV Valdivia. PRAKLA-SEISMOS Report 4/72, 4–6, 1972

Ramberg, I.B., Andel, T.H. van. Morphology and tectonic evolution of the rift valley at lat 36°30′ N, Mid-Atlantic Ridge. Geol. Soc. Am. Bull. **88**, 577–586, 1977

Ramberg, I.B., Gray, D.F., Raynolds, R.G.H.: Tectonic evolution of the FAMOUS area of the Mid-Atlantic Ridge, lat 35°50′ to 37°20′ N. Geol. Soc. Am. Bull. **88**, 609–620, 1977

Sclater, J.G., Francheteau, J.: The implications of terrestrial heat flow observations on current tectonic and geochemical models of the crust and upper mantle of the earth. Geophys. J. R. Astron. Soc. **20**, 509–542, 1970

Shih, J.S.F., Atwater, T., McNutt, M.: A near-bottom geophysical traverse of the Reykjanes Ridge. Earth Planet. Sci. Lett. **39**, 75–83, 1978

Sleep, N.H.. Sensitivity of heat flow and gravity to the mechanism of sea floor spreading. J. Geophys. Res. **74**, 542–549, 1969

Talwani, M., Windisch, C.C., Langseth, M.G. Jr.: Reykjanes Ridge crest: a detailed geophysical study. J. Geophys. Res. **76**, 473–517, 1971

Tapponier, P., Francheteau, J.. Necking of the lithosphere and the mechanics of slowly accreting plate boundaries. J. Geophys. Res. **83**, 3955–3970, 1978

Ulrich, J.. Zur Topographie des Reykjanes Rückens. Kiel. Meeresforsch. pp. 155–173, 1966

Vogt, P.R.. Asthenosphere motion recorded by the ocean floor south of Iceland. Earth Planet. Sci. Lett. **13**, 153–160, 1971

Vogt, P.R.. The Iceland phenomenon. imprints of a hot spot on the ocean crust, and implications for flow below the plates. In: Geodynamics of Iceland and the North Atlantic Area, L. Kristjansson, ed.. pp 105–126. Dordrecht: Reidel 1974

Vogt, P.R., Avery, O.E.: Detailed magnetic surveys in the Northeast Atlantic and Labrador Sea. J. Geophys. Res. **79**, 363–398, 1974

Received June 1, 1979; Revised Version August 3, 1979

J. Geophys. 47, 86–90, 1980

Journal of Geophysics

New Heat Flow Observations on the Reykjanes Ridge

K. Bram

Niedersächsisches Landesamt für Bodenforschung, Stilleweg 2, D-3000 Hannover 51, Federal Republic of Germany

Abstract. During METEOR cruise 45 in August 1977 14 heat flow measurements were obtained along a profile east of the Reykjanes ridge and perpendicular to the ridge axis covering a distance range from 30 to 240 km. Closely spaced measurements were grouped together. The mean heat flow of all groups amounts to 109 ± 20 mW m^{-2}. The values do not reveal a distinct increase with decreasing distance from the ridge axis as may be expected from the theoretical heat flow distribution based upon a cooling plate model. Including earlier measurements a high and very uniform heat flow in the distance range from 170 to 340 km was observed with a mean value of about 100 mW m^{-2}. In order to explain this high heat flow a temperature of 930° C is required at the lower boundary of the lithosphere at a depth of 50 km, assuming a purely conductive heat transport. Compared with the results obtained from previous measurements west of the Reykjanes ridge, the data reveal an asymmetric thermal behaviour of the ridge area. The average heat flow east of the ridge amounts to 93 mW m^{-2} being nearly twice the heat flow of the region west of the ridge.

Key words: Geothermics – Heat flow – Reykjanes Ridge.

Introduction

The mid-Atlantic ridge and Iceland which forms part, and represents a remarkable anomaly of, this ridge are regarded to be the result of geodynamic processes in the interior of the earth. To get a better understanding of those processes, knowledge not only of the structure of the earth's crust is necessary but also of the terrestrial heat flow which reflects the thermal behaviour of the earth's interior.

A compilation of all heat flow values obtained until 1970 in the region of the Reykjanes ridge was given by Talwani et al. (1971). The mean heat flow of the stations, most of which lie west of the ridge, amounts to 53 mW m^{-2} which is still below the average heat flow of the Atlantic ocean. This result does not correlate with the theoretically expected heat flow distribution at an active sea-floor spreading center without additional assumptions about convective heat transport (e.g., Elder, 1965; Palmason, 1967; Williams et al., 1974). Later measurements in the same region are reported by Langseth and Zielinski (1974), yielding a somewhat higher value of 67 mW m^{-2}.

Within the scope of geophysical investigations of the deeper crustal structure of oceanic ridges, geothermal investigations were carried out during leg 2 of the RV METEOR cruise 45 in August 1977. The aim was to increase the number of heat flow data in the region of the Reykjanes ridge and to study the thermal state of the lithosphere.

Geothermal Stations

The Reykjanes ridge extends with a nearly constant strike of N 35° E from lattitude 56° N to the Reykjanes peninsula of Iceland. Geothermal investigations were performed along an observation line perpendicular to the ridge axis at the eastern part of the ridge (Fig. 1). This profile was selected according to known ocean bottom topography and sedimentary cover obtained from a high resolution sparker profile during leg 1 (Fig. 2). Topography and the approximate thickness of the sediments are shown in Fig. 3 together with the total intensity of the earth's magnetic field recorded along the profile.

The topography in the area of stations 316 through 318, situated outside the range covered by the sparker profile, was obtained from an ELAC narrow-beam echosounder. The positions of the stations were determined by satellite and Loran C navigation with an accuracy better than 1,000 m. The station next to the ridge axis lies just at the beginning of the eastern flank whereas the easternmost stations are situated on the flat und obviously undisturbed deep sea bottom. The age of the ocean bottom covered by the geothermal profile ranges from about 2.5 Ma to about 25 Ma. The magnetic anomaly 5 corresponding to an age of 9 Ma is clearly indicated at a distance of 90 km from the ridge axis (Fig. 3).

The Measurements

The measurements were carried out with a modified deep sea probe (Haenel, 1972). Five outriggers equally spaced and fixed on a piston core barrel measure the temperature of the sediment and the thermal conductivity in situ with the needle probe method (Von Herzen and Maxwell, 1959). A pressure vessel contains the electronic recording equipment. The length of the core barrels used was 3.5 and 5.0 m respectively.

According to the length of the core barrels the maximum depth penetration up to the base of the pressure vessel was 4 and 5.5 m, respectively. In addition to the in situ measurements the thermal conductivity of the sediments recovered in the core barrels was also measured by the needle probe method. Measurements were made every 0.2 m down the core sample. In general, the cores were about 1.5 m shorter in length than the depth of penetration. In order to correlate the conductivity values of the core with the positions of the measured temperature, a loss of the upper 1.5 m of sediments was assumed. The reason is probably that the piston may not have started to suck before the core barrel has penetrated to this depth.

The temperature of the sediments and their thermal conductivities are presented in Fig. 4. The temperatures are related to the bottom water temperature measured at the different stations. A

0340-062X/80/0047/0086/S01.00

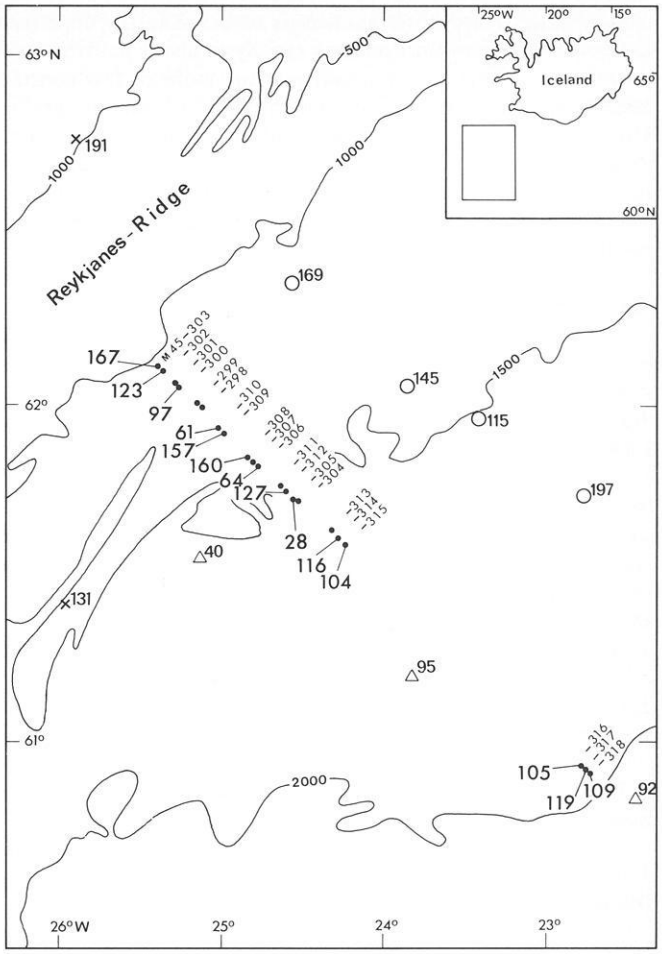

Fig. 1. Survey area and position of the geothermal stations. (*dots*). Stations of previous surveys are indicated by crosses (Talwani et al., 1971); *circles* (Scheljagin et al., 1973), and triangles (Langseth and Zielinski, 1974). Heat flow values are given in mW m^{-2} and depth contours in m

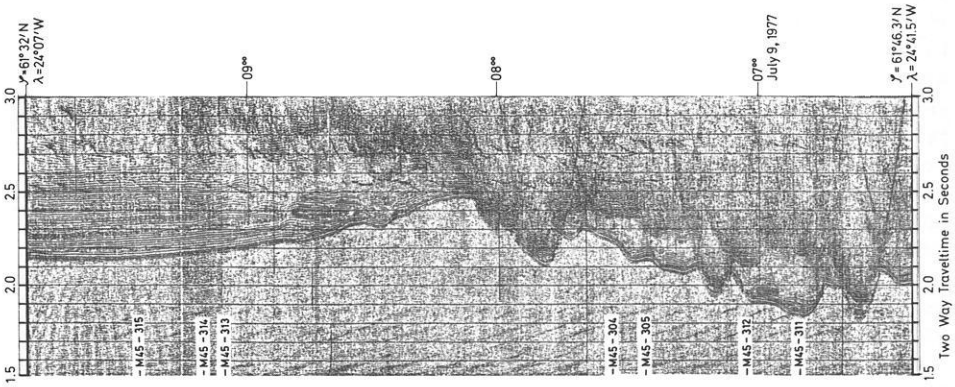

Fig. 2. Section of the sparker profile IV (by courtesy of the Institute of Geophysics, University of Kiel)

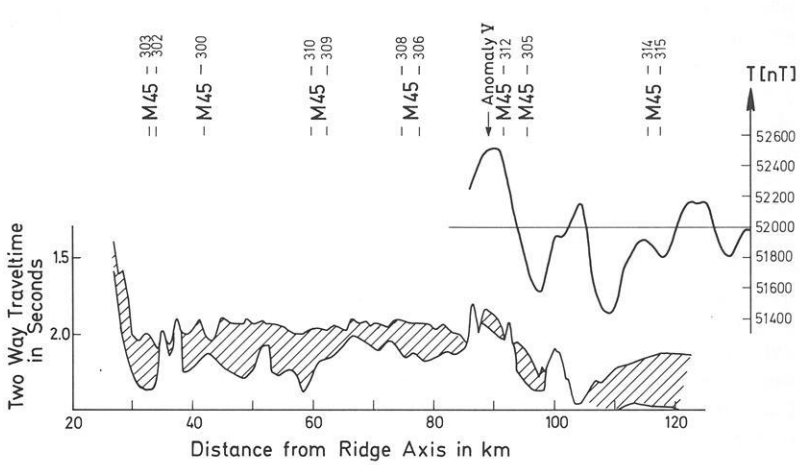

Fig. 3. Topography and sedimentary cover along the geothermal profile as obtained from the sparker profile IV and total intensity of the earth magnetic field recorded along the profile (by courtesy of Deutsches Hydrographisches Institut, Hamburg)

large positive temperature gradient is observed in the uppermost sediments. The gradient decreases rapidly to about half the value above a depth of 2 to 2.5 m and remains more or less constant below that depth at the stations 300 through 315. For the stations 316 through 318 the temperature gradient becomes nearly linear below a depth of about 3.5 m. Both the conductivity values measured in situ and from the core samples scatter considerably, but neither a significant difference nor an obvious depth dependence can be seen. Therefore it is very likely that the temperature distribution in the uppermost sediments is caused by variable bottom water temperatures.

It was shown, e.g., by Worthington and Volkmann (1965), Jones et al. (1970), Vogt and Johnson (1973) that the Norwegian Sea water crossing the Iceland-Faeroe ridge flows southwestward along the eastern flank of the Reykjanes ridge at a depth greater than 1,500 m. The temperature disturbances up to a depth of only 2.5 m, observed at the stations 300 through 312, may be explained, therefore, by a short-period emerging of cold water above the 1,500 m level. The mean bottom water temperature measured in the depth interval of 1,380 to 1,560 was 3.6° C. Extrapolating the linear segment of the temperature curve up to the sediment-water boundary, an average temperature variation of $\pm 0.3°$ C results. Based upon this value and assuming a temperature diffusivity of 0.003 $cm^2\ s^{-1}$, the minimum temperature was probably reached during May or June. A similar result was obtained by Sclater and Crowe (1979), (John G. Sclater, personal communication) from the interpretation of geothermal measurements, carried out in July 1977 along the magnetic anomaly 13 east of the Reykjanes ridge.

Discussion of Heat Flow Data

The heat flow values were calculated by multiplying the mean of the temperature differences between each pair of thermistors from the nearly linear segment of the temperature curve and the mean thermal conductivity. In the error range given for each gradient an error of 0.01° C is taken into account for the temperature measurements. In general, the instrumental error does not exceed 10% of the actual value. No corrections of the temperature gradient were applied with respect to the influence of topography and sedimentation. The estimated sedimentation rate is about 0.05 cm/a which would reduce the heat flow at least by 5% (Kappelmeyer and Haenel, 1974). In Table 1 the computed heat flow values are listed together with the station positions, bottom water temperature, conductivity, temperature gradient, and the deviation from vertical of the probe in the sediments. An estimation of the local environment according to the classification given by Sclater et al. (1976) is shown in the last column of Table 1.

The heat flow values vary between 27.9 and 167.2 mW m^{-2} This large scatter is not very surprising in the vicinity of active sea floor spreading centers. Today it is generally accepted that the variation of heat flow in those regions is due to hydrothermal circulation within a porous basement and/or through fissures and faults as was shown by investigations of, e.g., Pálmason (1967), Lister (1972), Williams et al. (1974). There is a high probability that the extremely low heat flow of 27.9 mW m^{-2} at station 305 is strongly affected by thin sedimentary cover and nearby outcropping basement. Obviously, a similar situation cannot account for the relatively low values at stations 306 and 310. It is likely that the small gradients result from downward migrating water into the sediments, but a reliable answer to this question is difficult to obtain in the absence of a temperature log down to at least

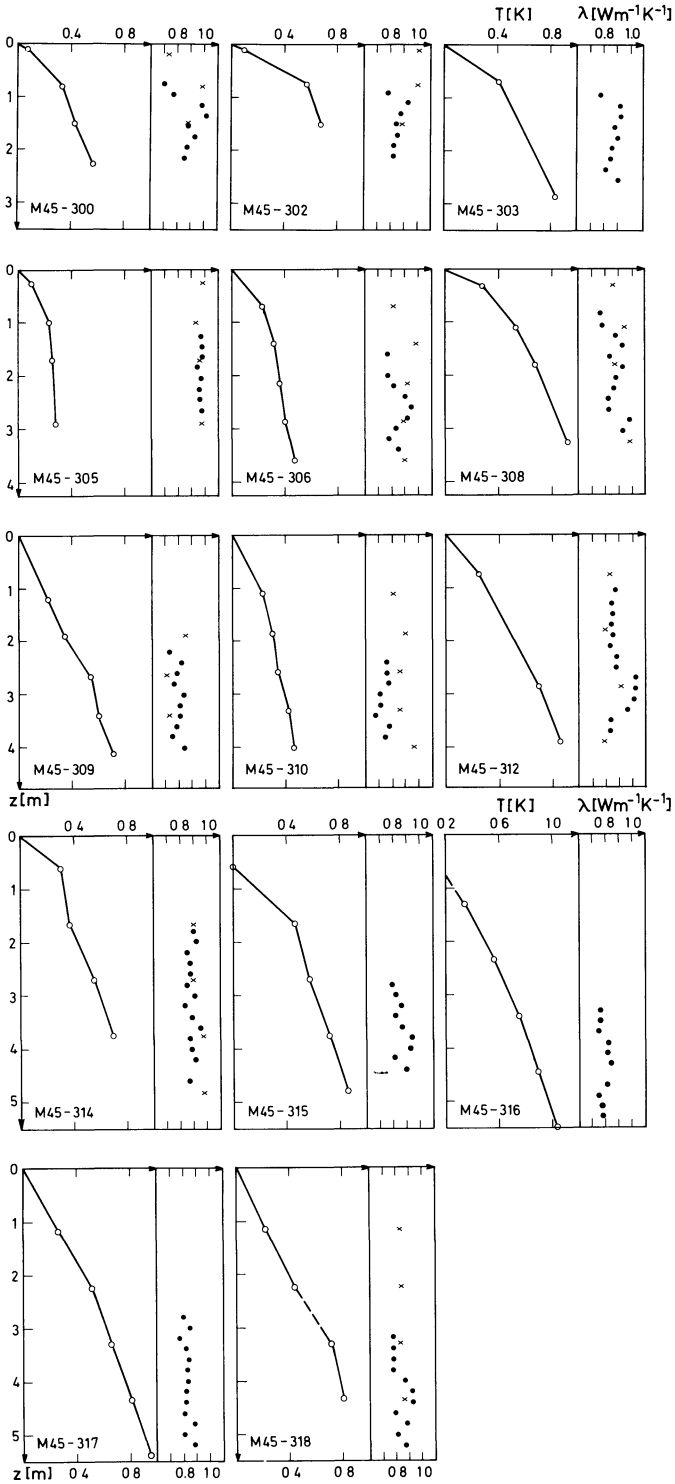

Fig. 4. Sediment temperatures and thermal conductivities obtained from in situ measurements (*crosses*) and from core samples (*dots*)

several tenths of meter, showing a clear deviation from linearity. It is worth noting that the values at stations 314 through 318 are very uniform (110 ± 7 mW m^{-2}). Two heat flow values, reported from Langseth and Zielinski (1974) for the same distance range and close to the profile (s. Fig. 1), support this result. This may be explained by the rapidly increasing thickness of the sediments beyond the distance of 105 km (Fig. 3). Lister (1972) and

Table 1. Heat flow data from Reykjanes Ridge

Station No.	Latitude (N)	Longitude (W)	Depth (m)	Bottom Water (Temperature °C)	Mean Cond. ($Wm^{-1}K^{-1}$)	Mean Temp. Grad. (Km^{-1})	Mean Heat Flow ($mW\,m^{-2}$)	Incl.	Station evaluation
M45-300	62° 3.5′	25° 15.2′	1,418	3.63	0.88±0.12	0.11±0.03	96.8±37.4	4°	C
302	62° 6.2′	25° 21.0′	1,544	3.63	0.88±0.08	0.14±0.04	123.2±47.0	3°	C
303	62° 7.1′	25° 23.1′	1,392	3.63	0.88±0.07	0.19±0.05	167.2±21	5°	C
305	61° 43.2′	24° 32.5′	1,557	(3.0)	0.93±0.06	0.03±0.01	27.9±12.8	6°	C
306	61° 49.4′	24° 46.5′	1,438	3.43	0.87±0.07	0.07±0.01	63.6±18.4	7°	B
308	61° 51.0′	24° 49.2′	1,468	3.43	0.89±0.07	0.18±0.01	160.2±24.9	5°	B
309	61° 55.2′	24° 59.0′	1,498	3.50	0.78±0.06	0.20±0.06	157.1±41.7	4°	B
310	61° 56.2′	25° 0.9′	1,495	3.50	0.81±0.06	0.05±0.03	60.7±40.2	4°	B
312	61° 45.0′	24° 36.1′	1,379	3.65	0.91±0.09	0.14±0.03	127.4±40.0	3°	C
314	61° 36.2′	24° 16.8′	1,660	(2.7)	0.90±0.04	0.13±0.05	116-4±49.4	3°	B
315	61° 35.3′	24° 13.8′	1,615	(2.7)	0.86±0.05	0.12±0.02	103.8±12.4	4°	A
316	60° 55.6′	22° 46.4′	1,934	2.30	0.79±0.03	0.13±0.01	105.3± 7.5	3°	A
317	60° 55.2′	22° 45.5′	1,943	2.28	0.83±0.03	0.14±0.01	118.6± 4.6	5°	A
318	60° 54.3′	22° 43.4′	1,949	2.33	0.84±0.04	0.13±0.08	104.2±67	3°	A

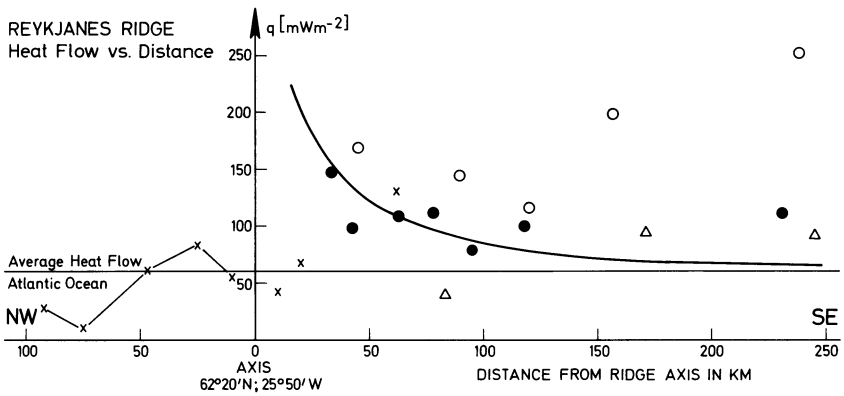

Fig. 5. Heat flow distribution versus distance. *Heavy dots* represent mean values of a group of stations, for the other symbols refer to Fig. 1. The heat flow calculated for a cooling plate model described in the text is indicated by the *solid curve*

Sclater et al. (1974) suggested that a thick and impermeable sedimentary cover seals the basement decreasing the influence of hydrothermal circulation.

A more representative heat flow for a small area is given if the values of closely spaced stations are averaged. Up to three stations, only 1.5 to 3 km apart (s. Fig. 1), are grouped together and their mean heat flow value is plotted versus distance of the ridge axis in Fig. 5 (heavy dots). Within the variation of 77 to 145 $mW\,m^{-2}$ the values are in agreement with previously published results (Talwani et al., 1971, Langseth and Zielinski, 1974) in the same region. Considerably higher heat flow values from stations closer to Iceland (s. Fig. 1) are reported by Scheljagin et al. (1973). A mean heat flow of about 83 $mW\,m^{-2}$ is given by Sclater and Crowe (1979), (John G. Sclater, personal communication) along magnetic anomaly 13.

Parker and Oldenburg (1973) presented a thermal model of ocean ridges which overcame the problem of infinite heat flow at the ridge crest as inherent in the cooling plate model proposed by McKenzie (1967). Yet the predicted heat flow does not differ markedly from that of McKenzie's model except very near the ridge crest. Therefore, and with regard to the scatter of the presented heat flow values, these data are compared with a calculated heat flow distribution from the simple cooling plate model.

The thickness of the lithosphere increases as the square root of crustal age (e.g., Parker and Oldenburg, 1973; Parsons and Sclater, 1977). Using the expression given by Parker and Oldenburg (1973) a value of 47 km results for the thickness of the lithosphere at a distance of 240 km (about 25 Ma) from the ridge crest. From a half-width of 60 km of the geothermal anomaly of the Mid-Atlantic Ridge (Lee and Uyeda, 1965), McKenzie (1967) deduced a lithosphere thickness of about 60 km. Therefore, the value of 50 km may be taken as an approximate thickness of the lithosphere in the observed range of distances. The average heat flow of the Atlantic ocean amounts to about 60 $mW\,m^{-2}$ (Von Herzen and Lee, 1969). Based upon this value and on assuming a thermal conductivity of 4.19 $W\,m^{-1}\,K^{-1}$ a temperature of 715° C results for the depth of 50 km. The boundary condition both at the lower side and the side where new material is accreted was taken to be of a constant temperature of 715° C. The spreading rate was taken to be 1 cm/a (Vine, 1966; Fleischer, 1974). The computed heat flow distribution as a function of distance from the ridge axis is shown by the solid curve in Fig. 5. The tendency of the few data to increase with decreasing distance from the ridge axis, as suggested by the theoretical heat flow curve, should be considered very carefully. The uniform values beyond the distance of 170 km, except those reported by Scheljagin et al. (1973), are approximately 30% above the computed heat flow. As discussed above, it is not likely that the observed gradients are too low (because of the relatively low depth of penetration) and, therefore, smaller heat flow values can be excluded. If the transport of heat is governed by pure conductivity only, a high heat flow had to be explained by a less thick lithosphere and/or high temperature at the lower boundary of the lithosphere, neglecting any radioactive heat sources within the lithosphere.

More reliable temperatures at the lower boundary of the lithosphere are obtained if the observations of heat flow are made at distances several times greater than the halfwidth of the geothermal anomaly (McKenzie, 1967), since it is in this region that the heat flow depends strongly on the lower boundary condition. The length of 240 km of the profile hardly satisfies this condition. But taking into account two previously reported values of 92 and 95 mW m^{-2} (Langseth and Zielinski, 1974) the profile is extended to a length of 340 km, thus permitting a reasonable estimate of the temperature at the lower plate boundary. If the average heat flow is increased by 30% to 78 mW m^{-2} and the thermal conductivity is that given above, a temperature of 930° C is required at a depth of 50 km. This temperature is somewhat lower than the temperature of 1,000° to 1,100° C deduced from a low-resistivity layer in a depth range of 12 to 22 km beneath Iceland (Beblo and Björnsson, 1978). According to the results of geochemical investigations along the Reykjanes ridge, Schilling (1973) proposed a hot mantle plume mixing model in the Iceland-Reykjanes ridge region. In the model temperatures vary between 1,200° C and 1,300° C at a depth range of 50 to 60 km, above which partial melting rapidly increases. Therefore, the value of 930° C may be regarded as the minimum temperature at a depth of 50 km in the region east of the Reykjanes ridge.

Mid-oceanic ridges show in several ways a more or less symmetric structure. A comparison of the heat flow values of the regions east and west to the ridge indicates an asymmetric thermal behaviour (Fig. 5). An average heat flow of 93 mW m^{-2} results for the region east of the ridge being nearly twice the heat flow of the western region. The values given by Scheljagin et al. (1973) are not included.

Vogt (1971) suggested a southwestward asthenosphere flow away from the hot spot Iceland. This suggestion received some support from the hot mantle plume mixing model, proposed by Schilling (1973). Although such a flow would plausibly explain high temperatures in the upper mantle south of Iceland, the available heat flow observations cannot resolve any details or even uniquely determine the sources.

Acknowledgement. This work was supported by Deutsche Forschungsgemeinschaft. Many thanks are due to Captain Feldmann and his crew aboard RV METEOR. I am very grateful to F. Böker who did his best to keep the deep sea probes in operation. I am indebted to Dr. H. Rodemann for stimulating discussions and also to Dr. R. Haenel for critical reading of manuscript.

References

Beblo, M., Björnsson, A.: Magnetotelluric investigations of the lower crust and upper mantle beneath Iceland. J. Geophys. **45**, 1–16, 1978

Elder, J.W. Physical processes in geothermal areas. In: Terrestrial heat flow, W.H.K. Lee, ed. Washington D.C. Geophys. Monogr. Am. Geophys. Union **8**, 211–237, 1965

Fleischer, U. The Reykjanes Ridge – a summary of geophysical data. – In: Geodynamics of Iceland and the North Atlantic Area, L. Kristjansson, ed. 17–31, Dordrecht. D. Reidel 1974

Hänel, R. Heat flow measurements in the Ionian Sea with a new heat flow probe. Meteor Forschungsergeb. Reihe C: **11**, 105–108, 1972

Herzen, R.P. Von, Maxwell, E.A. The measurement of thermal conductivity of deep sea sediments by a needle-probe method. J. Geophys. Res. **64**, 1557–1565, 1959

Herzen, R.P. Von, Lee, W.H.K.: Heat flow in oceanic regions. In: The Earth's Crust and Upper Mantle, P.J. Hart, ed. Washington D.C. Geophys. Monogr. Am Geophys. Union **13**, 88–95, 1969

Jones, E.J.W., Ewing, M., Ewing, J.I., Eittreim, S.L.: Influences of Norwegian Sea overflow water on sedimentation in the northern North Atlantic and Labrador Sea. J. Geophys. Res. **75**, 1655–1680, 1970

Kappelmeyer, O., Hänel, R.: Geothermics with special reference to application. Geoexploration Monographs, Ser. 1, No. 4, p. 238. Berlin: Gebr. Borntträger 1974

Langseth, M.G., Zielinski, G.W Marine heat flow measurements in the Norwegian-Greenland sea and in the vicinity of Iceland. In: Geodynamics of Iceland and the North Atlantic Area, L. Kristjansson, ed.. pp. 277–295. Dordrecht: D. Reidel 1974

Lee, W.H.K., Uyeda, S. Review of heat flow data. In. Terrestrial heat flow. W.J.K. Lee, ed. Washington D.C. Geophys. Monogr Am. Geophys. Union **8**, 87–190, 1965

Lister, C.R.B. On the thermal balance of a mid-ocean ridge. Geophys. J.Roy. Astron. Soc. **26**, 515–535, 1972

McKenzie, D.P. Some remarks on heat flow and gravity anomalies. J. Geophys. Res. **72**, 6261–6273, 1967

Pálmason, G.: On heat flow in Iceland in relation to the mid-Atlantic ridge. In Iceland and Mid-Ocean-Ridges, S. Björnsson, ed. Soc. Sci. Isl. **38**, 111–127, 1967

Parker, R.L., Oldenburg, D.W Thermal model of ocean ridges. Nature Phys. Sci. **242**, 137–139, 1973

Parsons, B., Sclater, J.G. An analyses of the variation of ocean floor bathymetry and heat flow with age. J. Geophys. Res. **82**, 803–827, 1977

Sclater, J.G., Crowe, J., Anderson, R.N. On the reliability of oceanic heat flow measurements. J. Geophys. Res. **81**, 2997–3006, 1976

Sclater, J.G., Crowe, J.: A heat flow survey at anomaly 13 on the Reykjanes Ridge: a critical test of the relation between heat flow and age. J. Geophys. Res. **84**, 1593–1602, 1979

Sclater, J.G., Herzen, R.P. Von, Williams, D.L., Anderson, R.N., Klitgord, K. The Galapagos spreading center, heat flow low on the north flank. Geophys. J. Roy. Astron. Soc. **38**, 609–626, 1974

Scheljagin, W.A., Buatschidse, J.M., Buatschidse, G.J., Schoar, M.P.. In. Catalogue of data (3). Moscow: Soviet Geophysical Committee of the Akademy of Sciences of the USSR, 1973

Schilling, J.G. Iceland mantle plume: geochemical study of Reykjanes ridge. Nature **242**, 565–571, 1973

Talwani, M., Windisch, C.C., Langseth, M.G. Reykjanes Ridge crest: a detailed geophysical study. J. Geophys. Res. **76**, 473–517, 1971

Vine, F.J.: Spreading of the ocean floor: new evidence. Science **154**, 1405–1515, 1966

Vogt, P.R. Asthenosphere motion recorded by the ocean floor south of Iceland. Earth Planet. Sci. Lett. **13**, 153–160, 1971

Vogt, P.R., Johnson, G.L. A longitudinal seismic reflection profile of the Reykjanes Ridge: Part I-Evidence for west-flowing bottom water. Earth Planet Sci. Lett. **18**, 45–48, 1973

Williams, D.L., Herzen, R.P. Von, Sclater, J.G., Anderson, R.N. The Galapagos spreading center: lithospheric cooling and hydrothermal circulation. Geophys. J. Roy. Astron. Soc. **38**, 587–608, 1974

Worthington, L.V., Volkmann, G.H. The volume transport of the Norwegian Sea overflow water in the North Atlantic. Deep-Sea Res. **12**, 667–676, 1965

Received February 21, 1979; Revised Version July 4, 1979

J. Geophys. 47, 91–98, 1980

Journal of Geophysics

Gravity and a Model of the Median Valley

B.J. Collette, J. Verhoef, and A.F.J. de Mulder
Vening Meinesz Laboratorium, University of Utrecht, Budapestlaan 4, NL-3584 CD Utrecht, The Netherlands

Abstract. The average median valley of the Mid-Atlantic Ridge between 12° and 18° N is described as a smooth depression flanked on both sides by a high. This applies both to the bathymetry and to the gravity anomalies. This picture of the median valley and its walls was obtained by stacking profiles across the valley in 50- to 70-km-wide bands. The reduced median valley can then be interpreted as the result of the parting of the lithosphere and the response of the asthenosphere as a viscous layer to repeated unloading. Fluid dynamic equations show that the response is in general broader than the original load disturbance. We describe this as a viscous lag of the shorter wavelength components. A steady-state solution was reached by numerical methods, showing a depression accompanied by a high on both sides. For the asthenosphere under the Mid-Atlantic Ridge at these latitudes a value followed for the kinematic viscosity of 1.5×10^{19} stokes. The model can be extended to other parts of the mid-ocean ridge system by adapting the time-dependent constants (viscosity and spreading rate). If the viscosity is a factor 5 lower, no median valley results. Rising to isostatic equilibrium of a light body under the floor of the median valley then accounts for the existence of a median ridge like found at Reykjanes Ridge and at the East Pacific Rise. The coefficient of viscosity under the East Pacific Rise would be about 0.4×10^{18} stokes. The concept of a viscous lag of the short-wavelength components replaces Sleep's (1969) original notion of a 'loss of head'. The secondary valleys and ridges found in the median valley and on the flanks of the Mid-Atlantic Ridge crest cannot be explained by the model. They represent essentially a non-continuum process, in which presumably an episodic jumping of the inner valley plays an important role. Additional faulting occurs at the hinge line between the floor and the walls of the median valley.

Key words: Gravity – Median valley – Asthenosphere – Rheology – Mid-Atlantic Ridge.

Introduction

In a few consecutive surveys in the years 1975 to 1978 the Mid-Atlantic Ridge crest was surveyed between latitudes 12° and 18° N (Fig. 1). In total 55 E-W and 5 NE-SW sections were made. For the reconstruction of the 15°20′ N or Fifteen-Twenty fracture zone additional use was made of older data (Collette et al., 1974a and b; Peter et al., 1973). The measurements consisted of continuous seismic profiling, total magnetic field and gravity measurements. The tracks were controled by satellite navigation.

The present paper deals with the gravity field over the median valley and its walls. From our data it follows that the median valley is below its isostatic equilibrium position and that the walls are upheaved. This information is used for developing a model of the median valley based on fluid dynamics. The asthenosphere is treated as a viscous Newtonian fluid which reacts on the parting of the overlying lithosphere. The negative load created by this parting gives rise to a steady-state wave pattern in the underlying viscous layer. This wave accounts for the primary topography of the ridge crest. By lowering the coefficient of viscosity of the asthenosphere the mechanism can be made to yield a mid-ocean ridge crest without a median

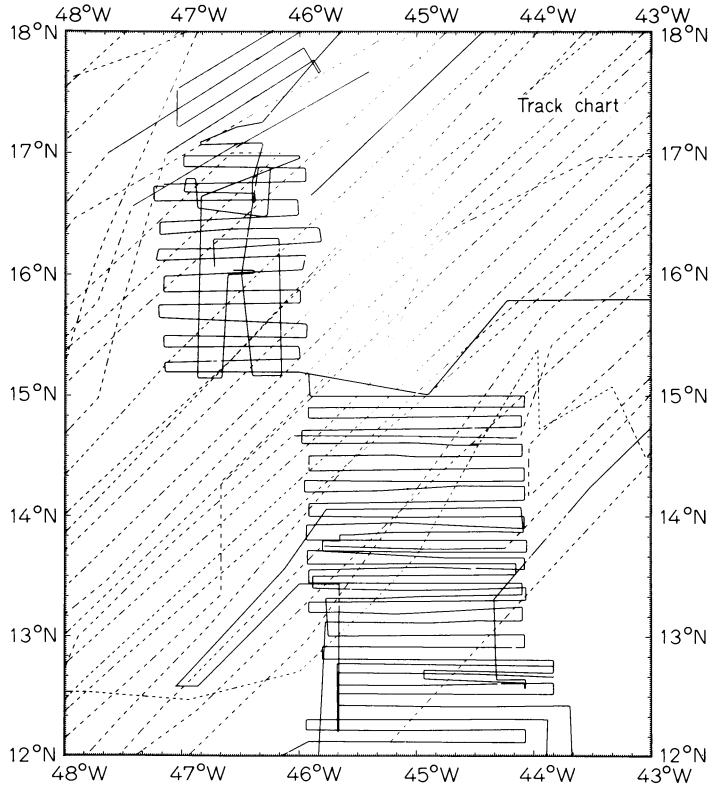

Fig. 1. Track chart. *Solid lines* are tracks of MV Aegeon Express, MV Tyro, MV Mercurius, MV Ares, and MV Marathon. *Dashes* are other tracks of the KROONVLAG-project

0340-062X/80/0047/0091/$01.60

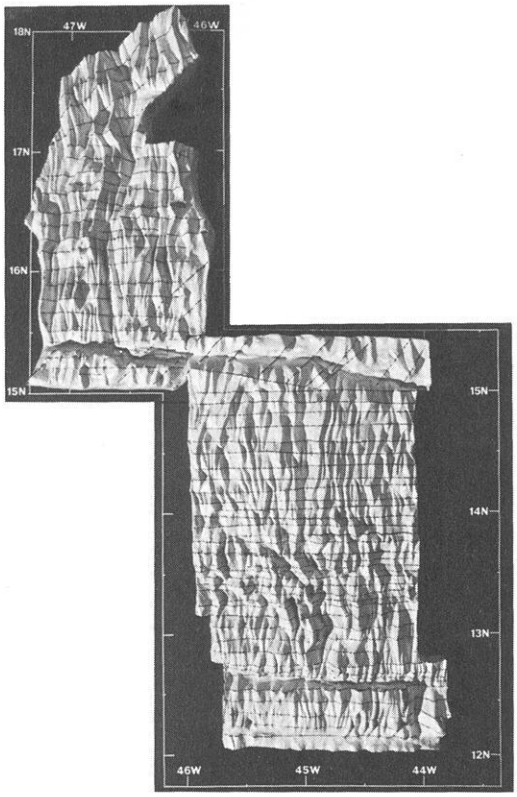

Fig. 2. Plasticine model of the Ridge Crest. Due to the light falling in from the SW, the 12°10′ fz shows less clearly

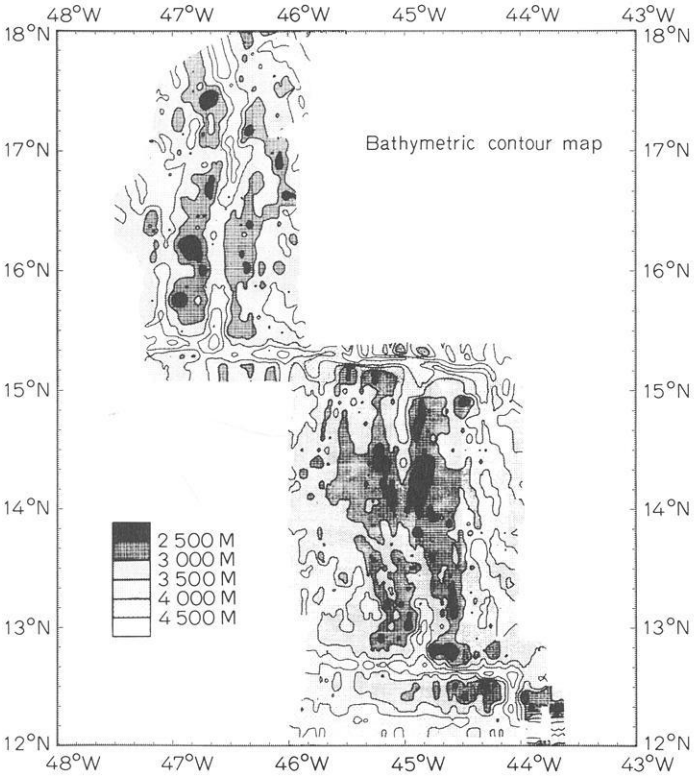

Fig. 3. Bathymetric contour map. Filter setting for the northern section $6dB/10.5$ nm, for the southern part $6dB/7.5$ nm. N–S anisotropy factor for both areas 1.5. The eastern part of the Fifteen-Twenty fz has been contoured by hand

valley, like on Reykjanes Ridge and the East Pacific Rise. A lower viscosity can be related to a higher molten fraction in the asthenosphere. The relation between a different thermal regime and the absence of a median valley was also proposed by Cochran (1979).

The secondary topography, viz. the ridges and valleys parallel to the spreading axis, cannot be accounted for by the proposed mechanism. This is essentially a non-continuum process in which we recognize two aspects: an episodic jumping of the inner valley (Collette et al., 1979) and relaxation faulting of the accreting lithosphere at the hinge line of the floor of the median valley to the walls, as described by Laughton and Searle (in press). The flexure in the lithosphere as such is caused by the steady-state wave pattern in the asthenosphere described in this paper. Our data do not contribute to the discussion whether horst and graben formation occurs at the flanks of the mid-ocean ridges, i.e., outside the median valley, as proposed by Luyendyk and Macdonald (1977).

The outcome of our study is compared with several other papers approaching the problem of the median valley and its walls from a mechanical point of view. Sleep (1969) originally introduced the effect of viscous forces in the asthenosphere using the term 'loss of head'. Sleep and Rosendahl (1979) published a study of numerical fluid dynamic models for mid-ocean ridge axes. Without explicitly saying so, these authors also arrive at the conclusion that the walls of the median valley, the lithospheric lid, are elevated above their equilibrium position by the fluid dynamic response of the asthenosphere. Lachenbruch (1976) speaks of an upward traction of the rising mantle on the adjoining lithosphere. Such an effect may be present under specific geometric conditions in addition to the vertical forces exerted on the lithosphere by the flowing asthenosphere, the steady-state wave described in this paper. Tapponnier and Francheteau (1978) relate the gravity anomalies to the effect of 'necking' of the spreading lithosphere which nevertheless would retain sufficient strength to react as an elastic plate. From the present data, we cannot exclude that this process also plays a role in the formation of the median valley.

The Topography

The topography is presented in the form of a plasticine model (Fig. 2) and a contour map (Fig. 3). The contour map is a hybrid composition of three detail maps. The northern and the southern part were produced by a computer program designed by Slootweg (1978). This method implies the use of a filter accounting for the finite spacing of the track lines. To allow for the obvious overall N–S linearity of the area, an anisotropy factor of 1.5 was introduced, thus giving more weight to this direction. The eastern part of the Fifteen-Twenty Fracture Zone was contoured by hand on the basis of older data (Collette et al., 1974a; Peter et al., 1973). Both the plasticine model and the contour map show that important deviations of the N–S linearity occur, i.e., apart from the three major fracture zones that can be recognized. The plasticine model brings out the lineations in more detail and shows alining over distances of several tens of kilometres. This alining also becomes evident from comparing adjoining sections. For showing these lineations by computer a more sophisticated program is needed which would be able to recognize slopes from the correlation between individual sections. For the time being, we still have to work with the plasticine model as an artist's impression.

The Fifteen-Twenty Fracture Zone (fz) with an offset of 165 km divides the area into two parts. To the south we further find the 12°40′ N fz and the 12°10′ N fz with offsets of 80 km and 45 km, respectively. The pattern is clearly orthogonal with local deviations of the general N–S direction of about 10 degrees. The Fifteen-Twenty fz measures 93° ± 2° with respect to the direction of the median valley, the 12°40′ N fz and the 12°10′ N fz both measure 90.0° ± 0.5°. From this we conclude that the present spreading direction is 90°. At the boundaries of the surveyed area indications can be found for the earlier sea-floor spreading direction with an azimuth of 105°. This especially applies to the non-active sections of the Fifteen-Twenty fz to the east and of the 12°40′ N fz to the west.

In addition to the large offset orthogonal fracture zones, several twists can be seen in the median valley. The most obvious ones occur at 17°40′ N, 16°40′ N, and 13°45′ N. A minor feature is found at 12°55′ N. The magnetics (W. Twigt, internal report) indicate that also at 14°45′N the N–S linearity is disturbed, though here the median valley seems not affected. The effective offset of the median valley by the 'twists' is never more than about 20 km. In a previous paper (Collette et al., 1979) we suggested that the twists are oblique transform faults or zones. We also might call them leaky transforms or narrow zones of oblique spreading. All these descriptive terms are applicable. Until recently this type of transform was not recognized as such (cf. Searle and Laughton, 1977; Rea, 1978). Searle and Laughton relate the anomalous character of these short-offset fracture zones to the circumstance that the adjoining ends of the spreading axes are physically so near that no cold zone can develop in between. We support this interpretation. The asthenospheric conduit in terms of temperature and magma supply, is evidently not interrupted by offsets which are of the same order of magnitude as that of the width of the median valley. However, the strength of the growing lithosphere is large enough to imprint its preferred faulting direction on the topography, thus influencing the course of the asthenospheric conduit. The preferred faulting direction is perpendicular to the maximum tension or the spreading direction. Oblique transforms are probably not stable. The offset would disappear by a small jumping of the spreading axis. We have the impression that such jumps indeed occur, forming one of the mechanisms that are responsible for the origin of the second-order topography. We come back to this later.

The resolution of our data is not large enough to define the exact character of the oblique fracture zones. En echelon spreading centers seem to occur at several places, of the same type as described by Ramberg et al. (1977) for the FAMOUS area, e.g. in Fracture Zone C which too has only a minor offset. Small E-W faults of the type found in FAMOUS area Fracture Zones A and B would escape our attention. In this context we refer to the clay experiments of Courtillot et al. (1974), which help to understand the type of yielding in oblique transform zones.

The question arises how oblique transform zones originate. One might think of them as the product of a primary instability of the median valley as such, caused by a haphazard jumping of sections of the spreading center, the inner valley(s). We prefer, however, the interpretation that they are caused by changes in the sea floor spreading direction. The offset of a fracture zone can be reduced considerably by a change in spreading direction to the effect that the two spreading centers (the points of intersection of the median valley segments with the fracture zone) come so close that they merge. The cold zone in between is no longer wide enough for an orthogonal fracture zone to subsist

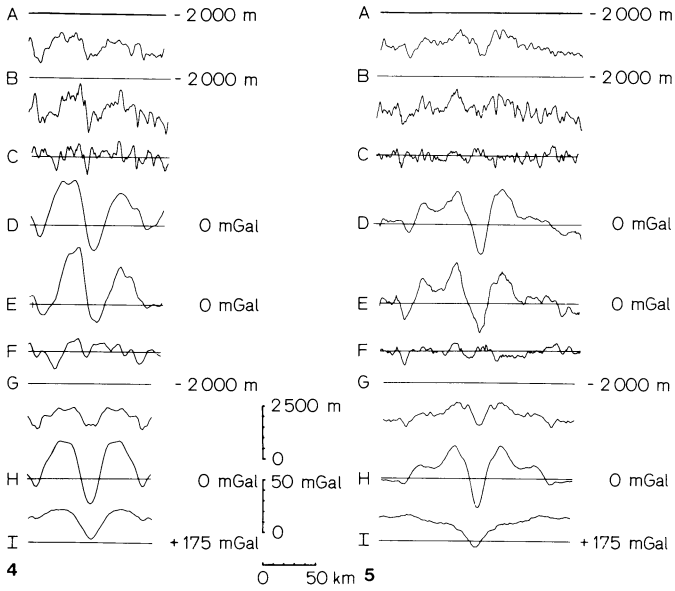

Fig. 4. *A* Stacked bathymetry for the profiles between 15°40′ and 16°25′ N. *B* Individual bathymetric profile at 16°10′ N. *C* Residual for the same profile. *D* Stacked free-air anomalies for the profiles of (*A*). *E* Free-air anomalies for the profile of (*B*). *F* Residual free-air anomalies for the same profile. *G* The stacked bathymetry symmetrized. *H* The free-air anomalies symmetrized. *I* Bouguer anomalies of the symmetrized profile

Fig. 5. *A* Stacked bathymetry for the profiles between 14°10′ and 14°40′ N. *B* Individual bathymetric profile at 14°30′ N. *C* Residual for the same profile. *D* Stacked free-air anomalies for the profiles of (*A*). *E* Free-air anomalies for the profile of (*B*). *F* Residual free-air anomalies for the same profile. *G* The stacked bathymetry symmetrized. *H* The free air anomalies symmetrized. *I* Bouguer anomalies of the symmetrized profile

and it passes into an oblique transform zone. This may explicitly be true for the oblique transform zones at 17°40′ N, at 14°45′ N (where we have only magnetic indications of a disturbance) and at 13°45′ N. An earlier reconstruction of the area (Collette et al., 1974b) postulated the existence of fracture zones at or near these latitudes. Also, the adjustment of the median valley to a new spreading direction may involve the origin of new transforms with small offsets (cf. Menard and Atwater, 1968, Fig. 5). We suppose that these new transforms are of the oblique type. In the course of time the median valley segments could straighten again by annihilation of the offsets of the oblique transforms effected by a jumping of one or both of the spreading centers involved. This jumping would not be haphazard but on the average be directed towards the warmer mid-line, thus reducing the twist in the asthenospheric conduit.

We needed this digression on oblique transform zones to account for our selection of median valley segments to be used for developing a standard model of the median valley. This standard model must define which part of the topography is 'primary', i.e., essential for the phenomenon of the median valley as such, and which part is 'secondary', varying from one place to

the other. We chose for this two areas well away from the orthogonal fracture zones and from the oblique transform zones. The first area is between 15°40′ and 16°25′ N, comprising 6 profiles, the second between 14°10′ and 14°40′ N with 5 profiles. We stacked the topography along a N–S direction and obtained the curves of Figs. 4A and 5A. The stacking procedure appears to reduce the median valley to an about 20-km-wide depression with a high to both sides. This generalized form of the median valley can also be read from the filtered contour map (Fig. 3). In the residuals we can no longer recognize a central valley (Figs. 5B and C and 6b and c). Actually, the spreading center could be any of the 'secondary' valleys. The problem of the origin of the ridge crest topography therefore falls apart into two questions:

(a) to account for the smooth curve of Figs. 4A and 5A, the reduced median valley, as a steady-state phenomenon with respect to the central axis;

(b) to explain the pseudo-linear ridges and valleys which form the secondary topography of the rift flanks and of the ocean floor in general, and which are superimposed on this smooth curve.

The Gravity Field

Figure 6 shows the contoured free air anomalies. We did not incorporate the few existing data over the eastern part of the Fifteen-Twenty Fracture Zone. Since the gravity field is much smoother than the topography, the effect of filtering (same procedure as for the topography but with isotropic filtering) is far less. The contours are reasonably parallel in the two areas chosen for the model. Figures 4D and 5D give the stacked anomaly curves for these areas, using the same profiles as for the topography. Figures 4E and 5E give two individual gravity profiles, Figs. 4F and 5F the residuals for these sections, i.e., the anomalies after subtraction of the stacked curves.

The stacked curves of Figs. 4 and 5 still show the effect of some large valleys that are found to the west and east of the median valley, in Fig. 4 at a distance of 55 km and in Fig. 5 at 70 km. We consider these valleys as incidental features occurring in these special sections of the ridge and not specific for the history of sea-floor spreading in the area as a whole. However, since such hazards still may influence our starting point, we cannot attach too much value to the way the positive anomalies fall back to zero on the flanks. In addition, we have to bear in mind that the zero level needs further definition. Cochran and Talwani (1977) demonstrated that in general a regional positive free-air anomaly of the order of 30 mGal exists over mid-ocean ridges. In view of the circumstance that the mean anomaly is +14 mGal in the nothern part and +6 mGal in the southern part, the area as a whole must be regarded as negative (cf. Cochran and Talwani, 1978). We will not dwell on this aspect here.

In Figs. 4G and H and 5G and H we symmetrized the stacked topography and the stacked free-air anomalies by averaging both sides. Next we computed the Bouguer anomalies for these profiles with densities ranging from 2.5 to 2.9 g cm^{-3}. The smoothest curves were obtained with densities 2.5 and 2.6 g cm^{-3}. Figures 4I and 5I give the results with 2.5 g cm^{-3}. The curves differ since the southern survey covers a broader area. Figure 5I therefore shows more of the regional effect of the isostatic compensation of the ridge. Talwani et al. (1965; cf. Talwani, 1970, Fig. 16) showed that the isostatic compensation is situated in the upper mantle, i.e., in the asthenosphere. Since the asthenosphere

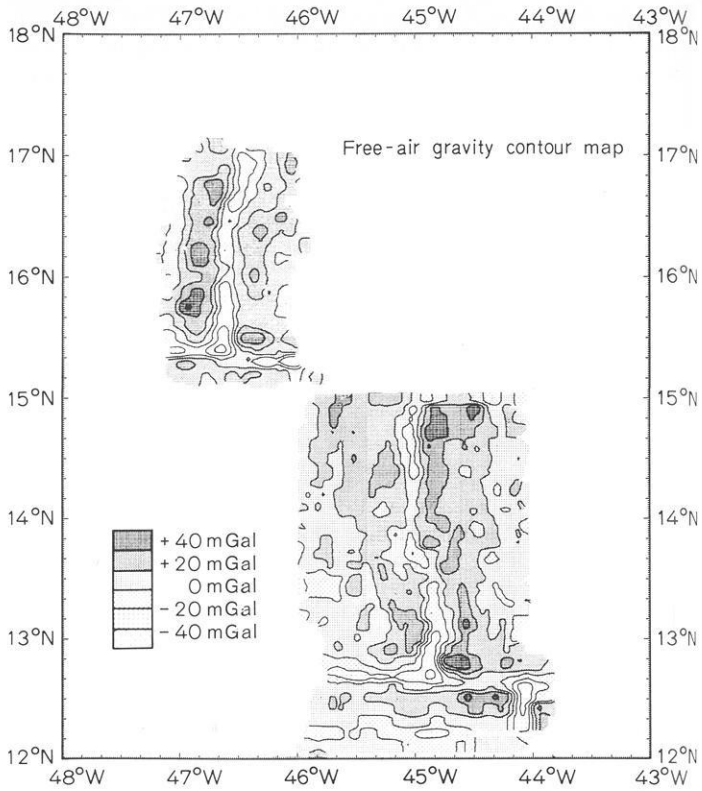

Fig. 6. Free air anomaly contour map. Filter setting is the same as for Fig. 3. No anisotropy factor applied

cannot statically bear the involved stress, this configuration does not represent a real equilibrium and can only be explained in terms of sea-floor spreading. The asthenosphere is less dense under the ridge than farther away which may be attributed to a larger molten fraction.

Since in this study we are only interested in the short wavelength components of the gravity field, we have to subtract the 'regional' from the Bouguer anomaly curves. This regional is ill-defined. Nevertheless, we can isolate a negative anomaly under the median valley which can only be caused by a shallow body. The anomaly can be modelled by a two-dimensional body of rectangular cross-section immediately beneath the surface, with a density contrast of $-0.15\,g\,cm^{-3}$ and which is 12 km wide and 14 km deep, on both sides accompanied by a body with a density contrast of $+0.15$ g cm^{-3}, with its top at 7 km and its bottom at 9 km depth beneath sea-level and between 12 and 24 km from the axis. As always with gravity anomalies, other solutions are possible but they all have in common that the walls of the median valley are not compensated locally. The geometry of the light body causing the central negative anomaly is corroborated by seismic results obtained in the Famous area (Fowler, 1976).

Model of the Median Valley

From Figs. 4G and I and 5G and I we derived a total vertical load curve by adding the anomalous subsurface masses to the masses of the averaged bathymetric stacks. The resulting curve is given as Fig. 7a. This curve is taken to represent the load on an otherwise free surface of a viscous fluid layer of thickness h. This

load can be considered to consist of a negative part, due to the separation of the lithosphere which creates a gap, and the positive and more regional response of the asthenosphere to this. The configuration is much like the idea of regional isostatic compensation with an elastic lithosphere. However, now it is not a static elastic problem, but a dynamic viscous one.

The hydrodynamic equations for dealing with this can be found in Burgers and Collette (1958). They arrived at the following expression for the decay of a two-dimensional sinusoidal wave of small amplitude z_0 and wavelength $2\pi/a$ at the surface of a viscous fluid

$$z = z_0 \exp(-kt)\cos(ax) \tag{1}$$

in which k is a decay constant, equalling

$$k = \frac{g}{2va} \tag{2a}$$

for an infinite halfspace (g being the acceleration of gravity and v the coefficient of viscosity) and

$$k = \frac{g}{2va} \cdot \frac{\cosh(ah)\cdot\sinh(ah) - ah}{\cosh^2(ah) + (ah)^2} \tag{2b}$$

for a layer with thickness h.

If we next express the surface load disturbance $p(x,0) = \rho g z(x,0)$ (ρ being the density) as a Fourier series with

$$z(x,0) = C_o + \sum_{n=1}^{N} C_n \cdot \cos\frac{n\pi x}{L}, \tag{3a}$$

the deformation of the surface as a function of t becomes

$$z(x,t) = C_o + \sum_{n=1}^{N} C_n \cdot \exp\left(-\frac{k' t}{n}\right) \cdot \cos\frac{n\pi x}{L}. \tag{3b}$$

In these expressions $2L$ is the interval at which the surface load disturbance repeats itself. This interval was chosen at 2,000 km in our computations. The decay constant k' becomes

$$k' = \frac{gL}{2\pi v} \tag{4a}$$

for an infinite halfspace, and

$$k' = \frac{gL}{2\pi v} \cdot \frac{\cosh(n\pi h/L)\cdot\sinh(n\pi h/L) - n\pi h/L}{\cosh^2(n\pi h/L) + (n\pi h/L)^2} \tag{4b}$$

for a layer with thickness h.

From here we proceeded as follows. Different forms for the surface load $p(x,0)$ were taken, ranging from a narrow gap via a rectangular form to a smooth identation for which we took a Gauss function. Then the form of the surface after a time dt was computed with Eq. (3b). In principle this form consists of a broad positive bulge superimposed on the initial disturbance. Next a new load of the same initial form was added and the resulting form of the surface after a time $2\,dt$ was computed, and so on. The results best resembling Fig. 7a were obtained with the Gauss function

$$z(x,0) = z_o \cdot \exp\left(-\frac{x^2}{a_o^2}\right). \tag{5a}$$

The halfwidth of this function is

$$d = (-\ln 0.5)^{\frac{1}{2}} a_o = 0.83\, a_o. \tag{5b}$$

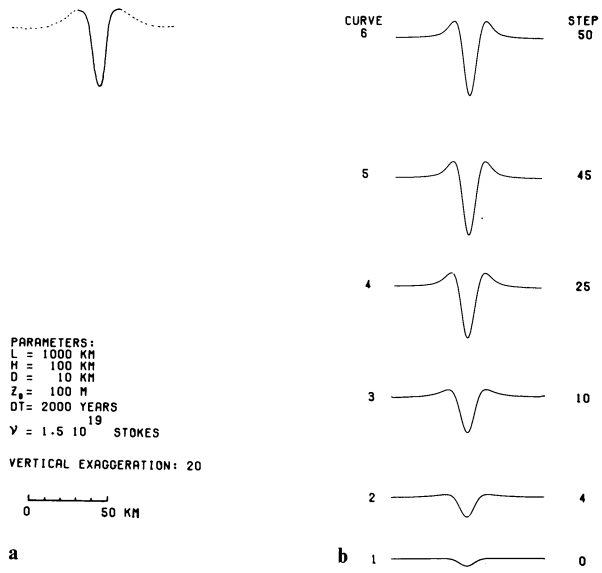

Fig. 7. a Load curve derived from Figs. 4 and 5. **b** Steady-state solution *(Curve 6)* for a periodically renewed negative load *(Curve 1)*. *Curves 2 to 5* give intermediate stages

The solution could be made steady state in a fairly rapid way by choosing the right value of v (see Fig. 7b). The convergence of the method can be proved for an infinite halfspace. For a layer with finite thickness h the convergence cannot be proven rigorously, but follows indirectly since the effect of h is only important for a finite number of terms, the long wavelength components. This implies that for reasonable values of h the method remains valid.

The amplitude of the resulting curve, the steady state solution, depends on v and on the ratio z_o/dt. This ratio forms together with a_o a measure for the bulk of the flow involved. The value of h appeared not to be critical. The largest effects of varying h occur in the outward flank of the positive bulge, a part of the experimental curve which is ill-defined as mentioned before. For h a value of 100 km was taken.

Discussion of the Model

At this point the spreading velocity enters the discussion. For this we have to quantify the renewal of the initial indentation. If the lithosphere is moved apart over a distance of $2dx$, we have to consider three aspects:

1. the creation of a gap along the central axis,
2. the viscous drag of the lithosphere on the asthenosphere while moving, and
3. the accretion of the lithosphere over a much broader area.

This accretion equals the difference between two cooling curves for the oceanographic lithosphere, which are mutually shifted over a distance dx. This difference consists only of very long wavelengths.

The short-wavelength gravity data describe only the first two aspects, the parting of the lithosphere along the central axis and the drag of the lithosphere on the asthenosphere. If we take the thickness of the lithosphere at the ridge crest at 10 km, the first effect is $10^6 \times b\,\mathrm{cm}^2/\mathrm{a}$, if b is the spreading velocity (halfrate).

The flow needed to balance the drag of the lithosphere on the asthenosphere is half the thickness of the asthenosphere h times the spreading rate. Again putting h at 100 km, this flow equals $5 \times 10^6 \times b\ \mathrm{cm}^2/\mathrm{a}$.

We now make the following assumptions:

(a) a non-viscous process which might be called 'necking' after Tapponnier and Francheteau (1978) transforms the gap at the ridge crest into a shallow indentation;

(b) the horizontal drag exerted by the lithosphere on the asthenosphere creates also a depression near the axis (a very crude description, but sufficient for the present purpose); and

(c) the sum of both effects can be described by a Gauss function with halfwidth $d = 0.83\, a_o$.

With these assumptions the relation between the spreading velocity b and the bulk of the flow expressed in z_o/dt and a_o becomes

$$6\ \ 10^6\ \ b\,\mathrm{cm}^2/\mathrm{a} = \frac{z_o}{dt} \int_0^\infty \exp\left(-\frac{x^2}{a_o^2}\right) dx\,\mathrm{cm}^2/\mathrm{a}. \qquad (7)$$

The value of the integral of (7) is 10.6×10^{10} if we take d at 10 km. This gives

$$\frac{z_o}{dt} = 5.66 \times 10^{-5} \times b.$$

This value was used to estimate v. b was taken at 1 cm/a, z_o at 0.1 km and dt at 2,000 a. Different values of v were tried. With $v = 1.5 \times 10^{19}$ stokes the steady state curve has an amplitude of 975 m. This is considered a fair approach of the experimental curve of the median valley. The steady state solution was reached in 50 steps (change in peak-to-peak amplitude of the last step well within 0.5 %).

Reykjanes Ridge and East Pacific Rise

The model can be extended to explain the different physiography of other parts of the mid-ocean ridge system like Reykjanes Ridge and the East Pacific Rise by adjusting the time dependant parameters, viscosity v and spreading rate b. If the effective viscosity is diminished by a factor 5, no appreciable median valley results. This might apply to the configuration of Reykjanes Ridge where the median valley gradually disappears going north to change into a positive topographic feature (Talwani et al., 1971; Laughton et al., 1979). The positive topography can be explained by a rise to isostatic equilibrium of the light material which, according to Figs. 4 and 5, is found in a narrow zone under the median valley, or more correctly, the spreading axis. If the spreading rate is increased by a factor 5, we again obtain the configuration of Fig. 7b. This means that in order to explain the positive topography of the East Pacific Rise we have to lower the effective viscosity again by the appropriate factor. The viscosity there would then be about 0.4×10^{18} stokes.

The correlation of a low viscosity with a larger molten fraction of the asthenosphere is readily made in both cases. The observations on profuse volcanism (R.D. Ballard, personal communication) on the East Pacific Rise are direct evidence for this as well as the abundant volcanism on Iceland. A larger molten fraction does not mean that the temperature would necessarily be higher. Instead the heat content (or the Helmholtz free energy) would be higher under the East Pacific Rise and under Reykjanes Ridge than under the Mid-Atlantic Ridge.

Origin of the Secondary Topography

The gravity data thus yield a clue to the mechanism that is responsible for the presence or absence of the median valley. For the explanation of the secondary ridges and valleys that are found at the ridge crest, the residuals of Figs. 4C and 5C, we turn our attention to the plasticine model of Fig. 2. It appears that the secondary topography *in* the median valley (which is defined by the curve of Fig. 7a) and *on* the flanks is essentially the same, i.e., on this scale and with this resolution. It therefore seems reasonable to conclude that the secondary topography originates in the median valley as originally proposed by Needham and Francheteau (1974). This could be effectuated by an episodic jumping of the actual spreading axis, the inner valley. Considering the en echelon character of the inner valley at places, which as such cannot be a steady state configuration, a jumping of the inner valley seems plausible. The mean mutual distance between the secondary valleys (about 6 km) against a spreading rate of 1 cm/a then tells us that such a jumping takes place every $6 \cdot 10^5$ a on the average (Collette et al., 1979).

The secondary topography is furthermore affected by the faulting which takes place at the hinge line of the median valley floor and the walls. Laughton and Searle (in press; see also Searle and Laughton, 1977) describe this faulting for four different sections of the Mid-Atlantic Ridge. The faults have a typical spacing of 2 to 2.5 km, equivalent to initiation of a new fault about every 2×10^5 a. According to their data, reduction of the effective vertical throw of the faults is realized by a rotation of the blocks between the consecutive faults once they have been transported over the crest of the wall of the median valley. This is contrary to the interpretation of Luyendyk and Macdonald (1977) who suppose that the reduction is realized by another faulting process with faults facing outward from the spreading axis. This would result in a horst/graben formation at the flanks. The resolution of our data is not such that they can contribute to the discussion. All we can say is that in our concept there is no actual need for additional horst/graben formation on the flanks.

General Discussion

Sleep and Rosendahl (1979) recently presented a study of numerical fluid dynamic models of mid-ocean ridge axes. These authors take also the temperature dependance of the coefficient of viscosity into account (see also Sleep, 1975). Furthermore they introduce the effect of a magma chamber, a small one for slow spreading ridges and a large one for fast spreading ridges. The introduction of this effect makes it possible to model also such details as asymmetric spreading. However, we doubt whether this is realistic in view of the occurrence of non-continuum processes. This puts restrictions to the applicability of any steady state model including ours. Apart from that, their result is very similar to ours. The outcome of our computations then proves that the origin of the median valley with its elevated walls is not dependant on the existence of a 'conduit' or a magma chamber, but follows directly from the rheology of the asthenosphere as a horizontal viscous layer. The original, rather loosely defined concept of a 'loss of head' by Sleep (1969; see also Sleep and Biehler, 1970) may now be written more precisely as a 'viscous lag' of the short wavelength components of a (continuously renewing) disturbance.

In the approach by Lachenbruch (1973, 1976) the concept of a conduit plays an overall important role. Lachenbruch arrived

at an upward traction of the upwelling viscous mantle on the solid(ifying) walls of the conduit, the lithosphere. If the conduit walls are steep, a bottleneck effect may indeed become important. Further computations are necessary to estimate the effect of different shapes of the upper surface of the viscous layer on the response function to a load disturbance.

An entirely different mechanical approach to the problem of the median valley and its walls is given by Tapponnier and Francheteau (1978), to which paper we referred earlier when discussing the mechanism by which the hypothetical 'gap' in the lithosphere is transformed into a smoother load disturbance at the boundary between lithosphere and asthenosphere. We supposed that this was realized by a non-viscous thinning of the lithosphere, called 'necking' by Tapponnier and Francheteau. However, the authors go further and describe the effect of the thinning of the lithosphere as a negative loading on an elastic plate which reacts with a regional upwarping according to the theory developed by Vening Meinesz (Heiskanen and Vening Meinesz, 1958). Essentially, the authors thus treat the problem as pseudo-static, in contrast to a fluid dynamic approach. The following comment can be made. Since both the static elastic solution and the fluid dynamic approach lead to a same result, it is not possible to distinguish between them in an empirical way. Also on theoretical grounds, it is difficult to make an exclusive choice. The accreting lithosphere, however weak, will have some elasticity and the assumptions of Tapponnier and Francheteau with regard to Young's modulus and to the thickness of the viscoelastic lithosphere, are not excessive. For the time being, we therefore cannot decide how the two processes interrelate and whether elastic upwarping indeed contributes in a material way to the phenomenon of a depressed median valley accompanied by elevated walls.

Finally, we mention a study by Cochran (1979) who made an analysis of the gravity field over the mid-ocean ridge crest on a worldwide basis. This author describes the relation between gravity and bathymetry in the form of a filter obtained by cross-spectral techniques. The interpretation of the filter is entirely static in terms of the response of a thin elastic plate overlying a weak fluid. The best fitting elastic thickness to explain gravity and bathymetry then is 7 to 13 km for the Mid-Atlantic Ridge and 2 to 6 km for the East Pacific Rise and for Reykjanes Ridge. Cochran relates this difference to different temperature structures under these ridges. Essentially, Cochran's approach is thus the same as the one by Tapponnier and Francheteau and the same comment can be made. With regard to the filter method as such, we want to point out that the interpretation may disguise certain features like the presence of low density bodies under the spreading axis. The extreme low surface density of $2.3\,g\,cm^{-3}$, which followed from the interpretation of the East Pacific Rise filter, may result from this.

Conclusions

The outcome of the study of the gravity field over the Mid-Atlantic Ridge crest between 12° and 18° N can be summarized as follows.

1. The median valley is characterized by a negative free-air anomaly. This anomaly finds its source partly in the topography and, for another part, in a light body under the floor of the median valley. The walls of the median valley are accompanied by positive anomalies which can be explained partly by the direct topographic effect and, for a smaller part, by the upheaved position of the walls. In terms of gravity, the median valley can thus be described as a depressed zone, accompanied on both sides by elevated zones.

2. Alternatively, one can describe this configuration as a negative anomaly superimposed on a broader positive anomaly. The broad positive anomaly then can be considered as the response of the asthenosphere (upwarping) to a continuously renewing negative load. This renewed loading is the effect from the parting of the lithosphere in the oceanfloor spreading process.

3. The upwarping can be reproduced in a steady-state model by using the fluid dynamic equations for a viscous layer. The regional upwarping results from the circumstance that the decay time of a sinusoidal wave is inversely proportional to its wavelength. Hence short wavelength components of a disturbance have a longer decay-time than long wavelengths. This leads to a systematic viscous lag of the short wavelengths components.

4. The coefficient of viscosity v of the asthenosphere under the Mid-Atlantic Ridge is 1.5×10^{19} stokes with an assumed thickness of the asthenosphere of 100 km.

5. The model can be extrapolated to Reykjanes Ridge and the East Pacific Rise by lowering the viscosity. If the viscosity is reduced by a factor 5, the depression or median valley disappears. The light body under the floor of the median valley will also try to reach its equilibrium position, which gives positive topography or a median ridge. If the spreading rate becomes larger, this effect is undone. The foregoing means that the effective viscosity of the asthenosphere under Reykjanes Ridge must be about 5 times lower and under the East Pacific Rise about 40 times lower than under the Mid-Atlantic Ridge.

6. The secondary topography, i.e., the ridges and valleys parallel to the median valley on the ridge flanks and, in general, in the ocean floor, can best be explained as resulting from an episodic jumping of the inner valley. The data suggest that such a jumping takes place about every 6×10^5 a. In addition, the young lithosphere is faulted along the hinge line between floor and wall of the median valley when transported uphill (every 2 km or 2×10^5 a, as concluded by Searle and Laughton, 1977).

7. The results are in agreement with model studies by Sleep and Rosendahl (1979). Our concept of a 'viscous lag' of the short wavelength components of a disturbance replaces Sleep's original notion (1969) of a 'loss of head'. A bottleneck effect may be present and add to the upwarping (Lachenbruch, 1976). Also elastic upwarping of the lithosphere in response to a local thinning in and near the median valley, or 'necking' as described by Tapponnier and Francheteau (1978), may form part of the mechanism.

Acknowledgments. The investigations in 1975 and 1977 were carried out on board of MV Aegeon Express and MV Tyro. These ships were chartered on the account of the Netherlands Commission for Sea Research of the Royal Netherlands Academy of Arts and Sciences as part of the project VAARPLAN 1974–1978. Additional measurements were made on board of MV Ares and MV Mercurius of the Royal Netherlands Steamship Company as part of the KROONVLAG-project. This project was sponsored by the Netherlands organization for the advancement of pure science (ZWO). We thank the Royal Netherlands Steamship Company for its continued assistance to our research. Special thanks goes to the crews of the ships for their cooperation. A.P. Slootweg and P.J. de Vrijer built the cross-coupling computer that was used in 1975, before the original GSS2 Graf

Askania gravity meter was renovated by Bodenseewerk Geosystem GmbH and converted into a KSS5 system. From the students who assisted with the measurements we mention P.J. de Vrijer, C.G. Langereis, and J.W.G. Peeters who processed the gravity data.

References

Burgers, J.M., Collette, B.J.. On the problem of the post-glacial uplift of Fennoscandia. Proc. K. Ned. Akad. Wet. Ser. B: **61**, 221–241, 1958

Cochran, J.R.: An analysis of isostasy in the world's oceans: Part 2. Mid-Ocean Ridge crests. J. Geophys. Res. **84**, 4713–4729, 1979

Cochran, J.R., Talwani, M.. Free-air gravity anomalies in the world's oceans and their relationship to residual elevation. Geophys. J. R. Astron. Soc. **50**, 495–552, 1977

Cochran, J.R., Talwani, M.: Gravity anomalies, regional elevation, and the deep structure of the North Atlantic. J. Geophys. Res. **83**, 4907–4924, 1978

Collette, B.J., Rutten, K., Schouten, H., Slootweg, A.P.: Continuous seismic and magnetic profiles over the Mid-Atlantic Ridge between 12° and 18° N. Mar. Geophys. Res. **2**, 133–141, 1974a

Collette, B.J., Schouten, H., Rutten, K., Slootweg, A.P.: Structure of the Mid-Atlantic Ridge province between 12° and 18° N. Mar. Geophys. Res. **2**, 143–179, 1974b

Collette, B.J., Slootweg, A.P., Twigt, W Mid-Atlantic Ridge crest topography between 12° and 15° N. Earth Planet. Sci. Lett. **42**, 103–108, 1979

Courtillot, V., Tapponnier, P., Varet, J.: Surface features associated with transform faults: a comparison between observed examples and an experimental model. Tectonophysics **24**, 317–329, 1974

Fowler, C.M.R.: Crustal structure of the Mid-Atlantic ridge crest at 37° N. Geophys. J. R. Astron. Soc. **47**, 459–491, 1976

Heiskanen, W.A., Vening Meinesz, F.A. The earth and its gravity field., New York: McGraw-Hill 1958

Lachenbruch, A.H.: A simple mechanical model for oceanic spreading centers. J. Geophys. Res. **78**, 3395–3417, 1973

Lachenbruch, A.H.. Dynamics of a passive spreading center. J. Geophys. Res. **81**, 1883–1902, 1976

Laughton, A.S., Searle, R.C.. Tectonic Processes on Slow Spreading Ridges. 2nd Maurice Ewing Symposium, Am. Geophys. Union in press, 1979

Laughton, A.S., Searle, R.C., Roberts, D.G.. The Reykjanes Ridge crest and the transition between its rifted and non-rifted regions. Tectonophysics **55**, 173–179, 1979

Luyendyk, B.P., Macdonald, K.C.: Physiography and structure of the inner floor of the FAMOUS rift valley: Observations with a deep-towed instrument package. Bull. Geol. Soc. Am. **88**, 648–663, 1977

Menard, H.W., Atwater, T.: Changes in direction of sea-floor spreading. Nature **219**, 463–467, 1968

Needham, H.D., Francheteau, J.: Some characteristics of the rift valley in the Atlantic Ocean near 36°48′ North. Earth Planet. Sci. Lett. **22**, 29–43, 1974

Peter, G., Merrill, G., Bush, S.: Caribbean Atlantic Geotraverse. NOAA-IDOE 1971, Report No. 1, Project Introduction. Bathymetry, 1973

Ramberg, I.B., Gray, D.F., Raynolds, R.G.: Tectonic evolution of the FAMOUS area of the Mid-Atlantic Ridge, lat 35° 50′ to 37° 20′ N. Bull. Geol. Soc. Am. **88**, 609–620, 1977

Rea, D.K. Spreading-center offsets that are not transform faults. Eos. **59**, 370, 1978

Searle, R.C., Laughton, A.S.: Sonar studies of the Mid-Atlantic Ridge and Kurchatov Fracture Zone. J. Geophys. Res. **82**, 5313–5328, 1977

Sleep, N.H.: Sensitivity of heat flow and gravity to the mechanism of sea-floor spreading. J. Geophys. Res. **74**, 542–549, 1969

Sleep, N.H.: Formation of oceanic crust: some thermal constraints. J. Geophys. Res. **80**, 4037–4042, 1975

Sleep, N.H., Biehler, S.: Topography and tectonics at the intersections of fracture zones with central rifts. J. Geophys. Res. **75**, 2748–2752, 1970

Sleep, N.H., Rosendahl, B.R.: Topography and tectonics of mid-oceanic ridge axes. J. Geophys. Res. **84**, in press, 1979

Slootweg, A.P.: Computer contouring with a digital filter. Mar. Geophys. Res. **3**, 401–405, 1978

Talwani, M.: Gravity. In: The sea, vol. **4** Part 1, A.E. Maxwell, ed.: pp. 251–297. New York: Wiley-Interscience 1970

Talwani, M., Le Pichon, X., Ewing, M.. Crustal structure of mid-ocean ridges. 2. Computed model from gravity and seismic refraction data. J. Geophys. Res. **70**, 341–352, 1965

Talwani, M., Windish, C.C., Langseth, M.G., Jr.: Reykjanes ridge crest: A detailed geophysical study. J. Geophys. Res. **76**, 473–517, 1971

Tapponnier, P., Francheteau, J.. Necking of the lithosphere and the mechanics of slowly accreting plate boundaries. J. Geophys. Res. **83**, 3955–3970, 4497, 1978

Received May 16, 1979; Revised Version July 19, 1979

J. Geophys. 47, 99–109, 1980

Journal of Geophysics

Deformation, Stress, Seismicity

Statistical Analysis of Damaging Earthquakes and Volcanic Eruptions in Iceland From 1550–1978

G. Gudmundsson[1] and K. Saemundsson[2]

[1] Central Bank of Iceland, Reykjavík

[2] Orkustofnun, National Energy Authority, Reykjavík

Abstract. Records of all known eruptions and damaging earthquakes in Iceland since 1550 were produced containing 82 and 44 events, respectively. Neither record exhibits a significant trend. Analysis of the second order properties of the records reveals no indication of clustering or periodicity in either record. There is a significant relationship between the two kinds of events. Some of this may be due to triggering effects, but there is also a more long term relationship with eruptions leading the earthquakes. This relationship was examined further by classification of the events geographically and by types of the eruptions. The relationship seems to embody the whole area rather than local effects.

Key words: Iceland – Earthquake statistics – Volcanism – Seismicity – Poisson process.

Introduction

The idea that volcanic activity in Iceland is episodic or even periodic has been discussed from time to time. This was first suggested by Thoroddsen (1925). In recent years the idea has come up again, especially in view of the active period from 1961 onwards compared to the two or so decades before. Thorarinsson (1966) pointed out that this might apply to the entire Mid-Atlantic Ridge. Later expressions of this view include Björnsson et al. (1977) who suggest that rifting episodes occur in northern Iceland at 100–150 years intervals, Saemundsson (1978) who observed a simultaneity in the occurrence of eruptions and major earthquakes for the last few centuries and Tómasson (personal communication), who suggests that 25 years of volcanic quiescence alternate with 25 years of volcanic and tectonic unrest.

Earthquake sequences where one earthquake triggers off another in a neighbouring area or even a series within a short span of time is characteristic of the South Iceland seismic zone (Björnsson and Einarsson, 1974). A triggering effect between a volcanic eruption and an earthquake was suggested at the outset of the Krafla rifting episode in 1975/1976 (Björnsson et al., 1977). This has also been mentioned in case of the Laki eruption of 1783 followed by the large South Iceland earthquake sequence of 1784 which in turn was followed by rifting of the Hengill swarm still farther west in 1789.

There has been a great deal of research into the history of eruptions and earthquakes. We shall provide a resumé of this in the next section and a record of 82 eruptions and 44 major earthquakes since 1550.

An analysis has been presented so far only for eruptions of the central volcanoes Hekla and Katla in southern Iceland from 1100 up to the present time (Thorlaksson, 1967). The distribution of the intervals between eruptions differed from a purely random process in such a way that very short and very long intervals were less likely. There have also been studies of earthquakes in single seismic zones, e.g., in New Zealand by Vere-Jones (1970). These studies cover shorter time intervals than our records, but include much smaller earthquakes. There is highly significant clustering of the earthquakes within each zone, connected with fore- and aftershocks of the larger earthquakes.

The main purpose of the present work is to examine statistically possible relationships between eruptions and earthquakes in Iceland and regularity in the pattern of events. It is not difficult to find at least a qualitative explanation of a variety of hypothetical relationships within each record or between them. Apart from the triggered earthquake sequences we are, however, not aware that strong evidence exists for any such regularities except for what may be divined from the records themselves. It is then a useful precaution to start by testing the hypothesis that there is no relationship at all before using the data for a quantitative examination of such relationships as we think may exist. Failure to reject the hypothesis does not necessarily imply that the original idea was wrong. But it shows at least that the data contain little useful information about the relationship except that it cannot be very strong.

Records of Eruptions and Damaging Earthquakes

Written sources mention natural hazards from the earliest settlement of Iceland, but the records are very occasional up to the 16th century. From about 1550 the records seem to be sufficiently complete for our purpose. Eruptions and earthquakes occurring in this period are briefly mentioned in numerous annals and chronicles (Sigurdsson, 1868; Ann. Isl. 1400–1800, publ. 1922–1961). Letters and reports describing such events become more numerous in the 18th century. Magazines and newspapers bring such reports since the middle of the 19th century. Thorarinsson (1967, 1973, 1974, 1975) has evaluated the existing sources with respect to their reliability. Our listing of 82 eruptions (Table 1) is based mainly on his work. We have added a few more eruptions that are not quite definite (1661, 1896), or have been detected since (1697, 1706, 1720, 1739, 1768, 1854). The last six are from Steinthorsson (1978) who recorded representative tephra layers in an ice core from Vatnajökull. A few eruptions have been left out

0340-062X/80/0047/0099/$02.20

because they seem unlikely in view of later research. Thus an eruption in Vatnajökull in 1897 is refuted because the sources mention only a water flood but not definitely an eruption, also a representative tephra layer is not recorded in the ice core (Steinthorsson, 1978), although easterly winds were prevailing at the time of the presumed eruption. We have also refuted a 1823 eruption of Leirhafnarskörd (allotted with a question mark in Thorarinsson, 1974) on the basis of a recent description (Eliasson, 1977). Further we have moved the starting year of the Askja eruptive period of the nineteen-twenties back to 1919 (Steinthorsson, 1978). Regarding other eruptions lasting more than a year only the starting year is included in the table.

Table 1. List of volcanic eruptions since 1550

Date/year		Location	North Iceland	Vatna-jökull	South Iceland	Reykja-nes	Rift type	Central type
Spring	1554	SE of Hekla			×		×	
August 11,	1580	Katla			×			×
	1583	Eldeyjar				×	×	
January 3,	1597	Hekla			×			×
November 7,	1598	Grimsvötn		×				×
October 31,	1603	Vatnajökull		×				
October 21,	1612	Katla			×			×
July 29,	1619	Grimsvötn		×				×
September 2,	1625	Katla			×			×
	1629	Grimsvötn		×				×
May 8,	1636	Hekla			×			×
February	1638	Grimsvötn		×				×
Spring	1655	Kverkfjöll	×					×
	1659	Grimsvötn		×				×
November 3,	1660	Katla			×			×
December	1661	Grindavik				×	×	
April 10,	1681	Grimsvötn		×				×
November	1684	NW-Vatnajökull		×				
December	1684	Grimsvötn		×				×
February 13,	1693	Hekla			×			×
	1697	Vatnajökull?		×				
Winter	1702	Vatnajökull		×				
Autumn	1706	Grimsvötn		×				×
	1706	Vatnajökull		×				
Winter	1711	Kverkfjöll	×					×
October 6,	1716	Grimsvötn		×				×
August	1717	Kverkfjöll	×					×
	1720	Vatnajökull		×				
May 11,	1721	Katla			×			×
May 17,	1724	Krafla	×				×	
February	1725	Grimsvötn		×				×
April 2,	1725	S of Hekla			×		×	
	1726	NW-Vatnajökull		×				
August 8,	1727	Öræfajökull		×				×
	1729	Kverkfjöll	×					×
	1739	Vatnajökull		×				
July 10,	1746	Krafla	×				×	
Autumn	1753	SW-Vatnajökull		×				
October 17,	1755	Katla			×			×
April 5,	1766	Hekla			×			×
July	1766	Grimsvötn		×				×
	1768	Vatnajökull		×				
February	1774	NW-Vatnajökull		×			×	
May 1,	1783	Eldeyjar				×	×	
June 8,	1783	Laki/Grimsvötn		×			×	
Summer	1794	W-Vatnajökull		×				
	1797	N-Vatnajökull		×				
	1807	N-Vatnajökull		×				
December 19,	1821	Eyjafjallajökull			×			×

Table 1 (Continued)

Date/year		Location	North Iceland	Vatna-jökull	South Iceland	Reykja-nes	Rift type	Central type
February	1823	SW-Vatnajökull		×				
	1823	Katla			×			×
March 13,	1830	Eldeyjar				×	×	
	1838	Grimsvötn		×				×
September 2,	1845	Hekla			×			×
	1854	Grimsvötn		×				×
May 8,	1860	Katla			×			×
June 30,	1862	Tröllahraun		×			×	
December	1867	Mánáreyjar	×				×	
August 29,	1867	Grimsvötn		×				×
January 8,	1873	Grimsvötn		×				×
December	1874	Askja/Sveinagjá	×				×	
February 27,	1878	NE-Hekla			×		×	
May 30,	1879	Eldeyjar				×	×	
January 15,	1883	Grimsvötn		×				×
August	1887	SW-Vatnajökull		×				
March	1892	Grimsvötn		×				×
September	1896	Vestmannaeyjar			×			×
May 28,	1903	SW-Vatnajökull		×				×
June 18,	1910	W-Vatnajökull		×				
April 25,	1913	NE-Hekla			×		×	
October 12,	1918	Katla			×			×
	1919	Askja	×				×	
September	1922	Grimsvötn		×				×
June	1926	Eldeyjar				×	×	
	1933	NW-Vatnajökull		×			×	
March 30,	1934	Grimsvötn		×				×
March 29,	1947	Hekla			×			×
October 26,	1961	Askja	×				×	
November 14,	1963	Vestmannaeyjar			×			×
May 5,	1970	N+S-Hekla			×		×	
January 23,	1973	Vestmannaeyjar			×			×
December 20,	1975	Krafla	×				×	

Tryggvason et al. (1959) have evaluated the earthquake records and presented a list of all earthquakes or earthquake sequences that were strong enough to cause the collapse of houses. We have used this list in our analysis with two minor corrections only: A reference to an earthquake in South Iceland in 1828 stands actually for an earthquake in the year after (Björnsson, S., personal communication). An earthquake in 1876 is misspelled in Tryggvason et al. (1959). It should read 1879 (see Thoroddsen, 1925). We have added also an earthquake in North Iceland in 1624 with reference to Larusson (1951). The analyzed earthquake record is thus by necessity selective because for most of this period no earthquakes were mentioned except such that caused damage. In the twentieth century information about earthquake magnitude became available (Tryggvason 1973), at the same time as constructions became more rigid. For this period we have chosen to include most earthquakes reported by Tryggvason (1973) as magnitude 6 or larger. From earthquakes that have occurred in the seismic zone north of Iceland we have omitted the smallest one of magnitude 6; it would certainly not have been included in the annals. The high proportion of earthquakes on the eastern Reykjanes Peninsula during the 20th century raises doubts about the completeness of the records for this area also. Incompleteness could be due to the fact that the interior of the Reykjanes Peninsula is unpopulated. But also chronicles relating to this area are rather meagre.

From triggered earthquake sequences we have chosen to include in our analysis only the first shock if the earthquakes are clustered within a short spell of time (weeks or months). The two most dramatic examples of such sequences are the 1784 and 1896 earthquakes of the South Iceland seismic zone with earthquakes of magnitude 6–8 propagating generally from east to west across it.

No information is available about earthquake magnitudes for the period 1550–1700. But for earthquakes after 1700 Tryggvason (1973) has given an estimate for all 'major destructive earthquakes' which he found to be of magnitude 6–$6^1/_2$ and larger. From a comparison with Tryggvason (1973) we expect that the magnitudes of earthquakes dealt with here are on the order of $5^1/_2$–6 up to $7^1/_2$–8. A graphical representation of all events included in our analysis is given in Fig. 1.

Table 2. List of damaging earthquakes since 1550

Date/year		North Iceland seismic zone	South Iceland seismic zone	Borgarfjördur seismic zone
May 30,	1581		×	
	1584	×		
Spring	1597		×	
	1614		×	
Autumn	1618	×		
November	1624		×	
	1624	×		
February 21,	1630		×	
Early	1633		×	
March 16,	1657		×	
	1663		× (R)[a]	
Summer	1671		×	
January 28,	1706		×	
August	1724		× (R)	
April 1,	1725		×	
Summer	1726		×	
September 7,	1732		×	
March 21,	1734		×	
	1749		×	
	1752		×	
September 11,	1755	×		
	1757		×	
September 9,	1766		×	
August 14,	1784		×	
June 10,	1789		× (R)	
February	1829		×	
June 11,	1838	×		
December 30,	1867	×		
April 17,	1872	×		
Late May	1879		× (R)	
January 25,	1885	×		
April 19,	1889		× (R)	
August 26,	1896		×	
January 22,	1910	×		
May 6,	1912		×	
August 23,	1921	×		
July 23,	1929		× (R)	
June 10,	1933		× (R)	
June 2,	1934	×		
October 9,	1935		× (R)	
March 28,	1963	×		
December 5,	1968		× (R)	
June 12,	1974			×
January 13,	1976	×		

[a] (R) = Reykjanes Peninsula

Regional Distribution of Eruptions and Earthquakes

Figure 2 shows the neovolcanic zones of Iceland and the zones of seismic hazard. The activity is far from evenly distributed with time. Since 1550 no volcanic activity has been recorded in the Snaefellsnes volcanic zone nor within the Langjökull and Hofsjökull volcanic complexes. Even the Reykjanes Peninsula has been quiescent apart from its submarine continuation, the Eldeyjar area, and one doubtful eruption (1661) on land. A rifting episode occurred on the Hengill swarm farther east (1789) which is likely to have been associated with magmatic movement similar to the present rifting episode of Krafla (Björnsson et al., 1977). Most of the volcanic activity has been confined to the eastern volcanic zone in this period of time.

We have divided the volcanic eruptions into four groups with regard to location. Two groups are obvious from tectonic implications. i.e., the Reykjanes and South Iceland volcanic zones. The latter includes stratovolcanoes that erupt alkalic to transitional rocks and rift structures are poorly developed (Saemundsson, 1978). The division between a Vatnajökull zone and a North Iceland zone is somewhat arbitrary being based primarily on a possible transverse structure connecting the volcanoes under the ice sheets of Central Iceland.

Among the eruptions we make a distinction in Table 1 between eruptions associated with rifting of the crust similar in nature to the recently described Krafla rifting episode (Björnsson et al., 1977) and eruptions of central volcanoes accompanied by no or minor rifting. Many of the latter appear to be triggered by processes within magma chambers beneath the volcanoes themselves rather than release of tensional stress accumulated as a result of spreading. For consistency we have grouped all eruptions occurring on the fissure swarms that pass through the volcanoes with the rift type, but all eruptions that were confined to the actual central volcano were classified as central type. Thus the eruptions of Hekla proper are classified as central type. This may be inappropriate in view of the pronounced rift that opens up along the volcanic axis of this volcano during eruptions. Indeed Thoroddsen (1925) and Tryggvason et al. (1959) have pointed out that damaging earthquakes have more than once occurred in the Ölfus district of South Iceland following shortly upon a Hekla eruption. For the period considered here this has happened twice. In this context we must also mention that two rifting episodes that were not accompanied by a volcanic eruption appear in Table 2 among the earthquakes (1618, 1789). In a separate examination we have, however, also added them to the rift type eruptions.

The seismic zones are clearly defined as transverse shear zones in the case of North and South Iceland. We have grouped earthquakes occurring in the eastern part of Reykjanes with the South Iceland earthquakes, although in the case of Reykjanes we are obviously dealing with an oblique rift zone and not a zone dominated by shear. The Borgarfjördur seismic zone bridges the gap between Langjökull and the Snaefellsnes volcanic zone. Only one earthquake (1974) from this zone is included here (Einarsson et al., 1977). The last earthquakes before that were reported in 1928 (Vedrattan, 1928). One of them was moderately strong but probably did not reach magnitude 6, so we have left it out. Apparently earthquakes in this zone are rare and they do not reach the same magnitude as in the other two areas.

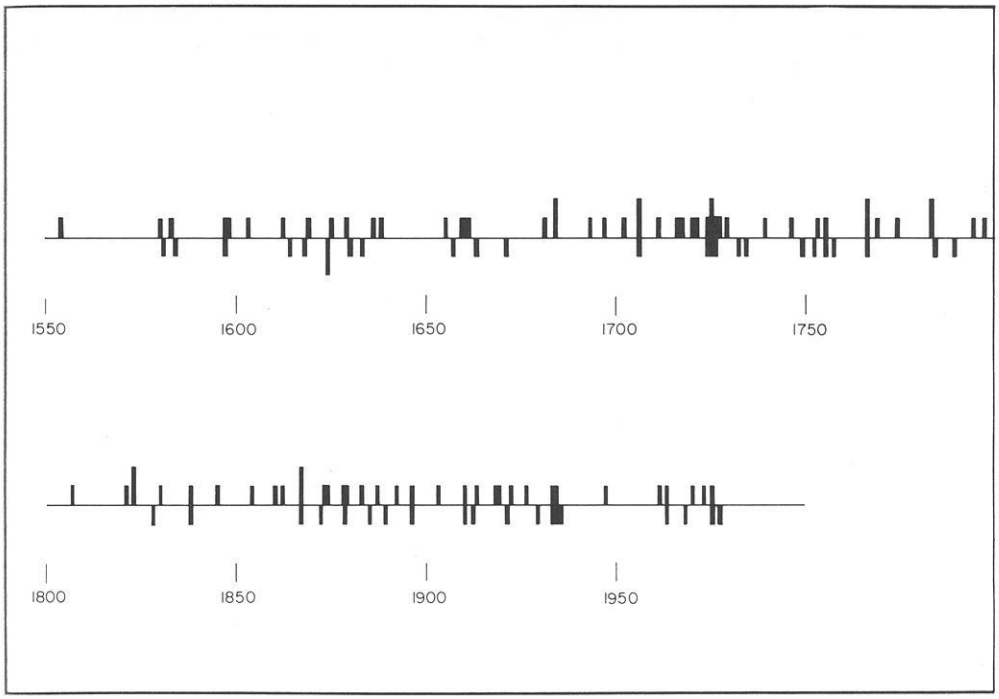

Fig. 1. Graphical representation of the records of eruptions and earthquakes

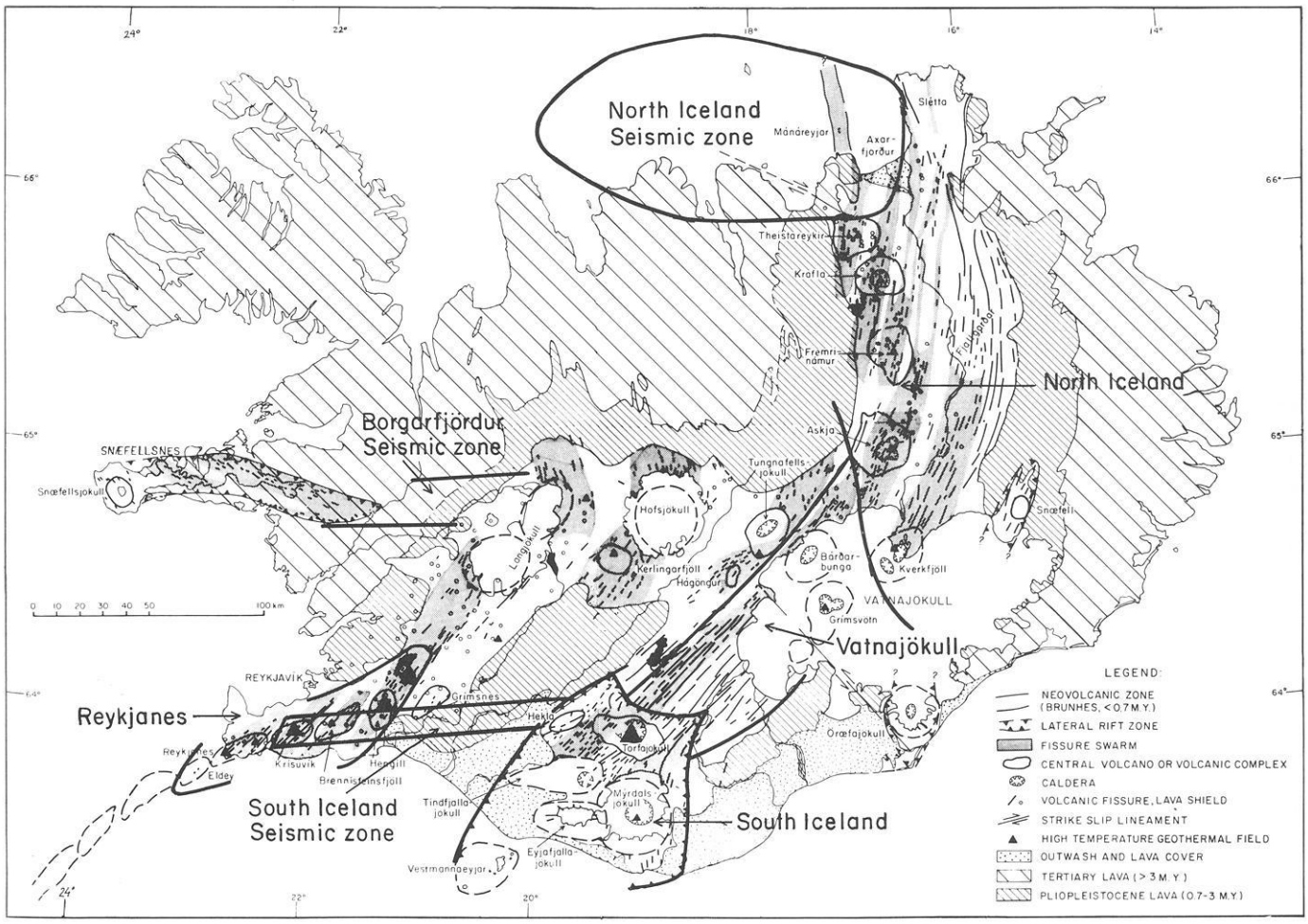

Fig. 2. Divisions of the neovolcanic zones of Iceland forming the basis for discussion in text. Seismic zones form connections between offset segments of the axial rift zones. The map is from Saemundsson (1978)

Analysis of the Total Records

Our records can be regarded as observations of stochastic point processes. There is a large mathematical literature on this subject, but less experience with the analysis of actual data than in the related field of time series analysis. We have analysed our data partly by a slightly modified version of a procedure described by Ripley (1976, 1977) and partly by turning them into time series.

A basic model in studies of this kind is the Poisson process with constant intensity (expected number of events/length of the record). In a Poisson process with intensity λ, the probability of an event in the interval from t to $t+\Delta t$ approaches $\lambda\Delta t$ when $\Delta t \to 0$, independent of the position of other events. A Poisson process is thus totally devoid of memory between events or any resemblance to periodicity.

An important characteristic of the Poisson process is that the duration of the intervals between events is exponentially distributed with the average value of λ^{-1}. According to this distribution the shortest intervals are always most likely, but the probability of obtaining relatively large intervals, say >3 standard deviations above the mean value which is 0.0014 for the normal distribution is about 0.018 for the exponential distribution. Even in small samples we can therefore expect the appearance of some intervals much longer than the mean or median value.

For many events only the year when they took place is known and we shall also only use this part of the information about all events. Much of the analysis will consist of comparing these data with hypothetical records of the number of events from a Poisson process in each year. We shall retain the name Poisson process for such records.

Considering the uncertainties in the recording of the events it would hardly be surprising to find that the intensity of events was not equal throughout the time interval. This applies in particular to the earthquakes. The possibilities of large earthquakes being unrecorded are probably greater in the earlier years, but systematic misjudging of the size of earthquakes might equally produce a negative as a positive trend.

A simple method for testing the hypothesis that an observed process is free of trend is described by Cox and Lewis (1966, p. 47). When the observations come from a Poisson process with a constant intensity the value of the test statistic is distributed as a normal random variable with zero mean and unit variance. The hypothesis is thus rejected with 95% confidence if the result lies outside ± 1.96. Our results were 1.1 for both the eruptions and for the earthquakes. Although these results provide no ground for assuming that the records are realizations from trend-free processes they suggest that eventual trends can be ignored, as the data are too few to distinguish them from such processes.

This test is only useful for detecting a monotonous change in the intensity. Deviations from the Poisson process resulting from various departures from the assumption of independent events would not be detected at all. A fairly general method of investigating interconnection between events is to count the number of events that take place in the same year as another event, one year after another event, 2 years etc. Let us call the number of events taking place less than or equal to n years after another event on the record $\phi(n)$. Observations of $\phi(n)$ contain all information in the records about the second order properties of the process, which is equivalent to the variances and correlation coefficient of two random variables.

Comparison of the two records is carried out by counting the number of eruptions preceding an earthquake by $\leq n$ years which we call $\theta(n)$. The number of earthquakes preceding an eruption by $\leq n$ years is then $\theta(-n)$. The expected value of $\theta(n)$ is only equal to $\theta(-n)$ if the two events are independent or related without any time lag.

It is easy to calculate the expected value of $\phi(n)$ or $\theta(n)$ when a given number of eruptions or earthquakes are distributed purely at random on 429 years. In an actual experiment we cannot expect to obtain exactly the theoretical values, but large discrepancies between observed and expected values would indicate that the events are not independent. How large the discrepancy needs to be for rejecting with confidence the hypothesis of a Poisson process depends upon the distribution of $\phi(n)$ or $\theta(n)$ which is rather complicated. But for low values of n the variance is approximately equal to the expected value.

The number of observations on our records is very small for the analysis of stochastic processes. Methods of analysis which use less of the information of the records than estimation of $\phi(n)$ and $\theta(n)$ are therefore not likely to produce worthwhile results. But because of the small number of observations we can, at moderate costs, investigate the relevant statistical properties of $\phi(n)$ and $\theta(n)$ empirically by simulation on a computer.

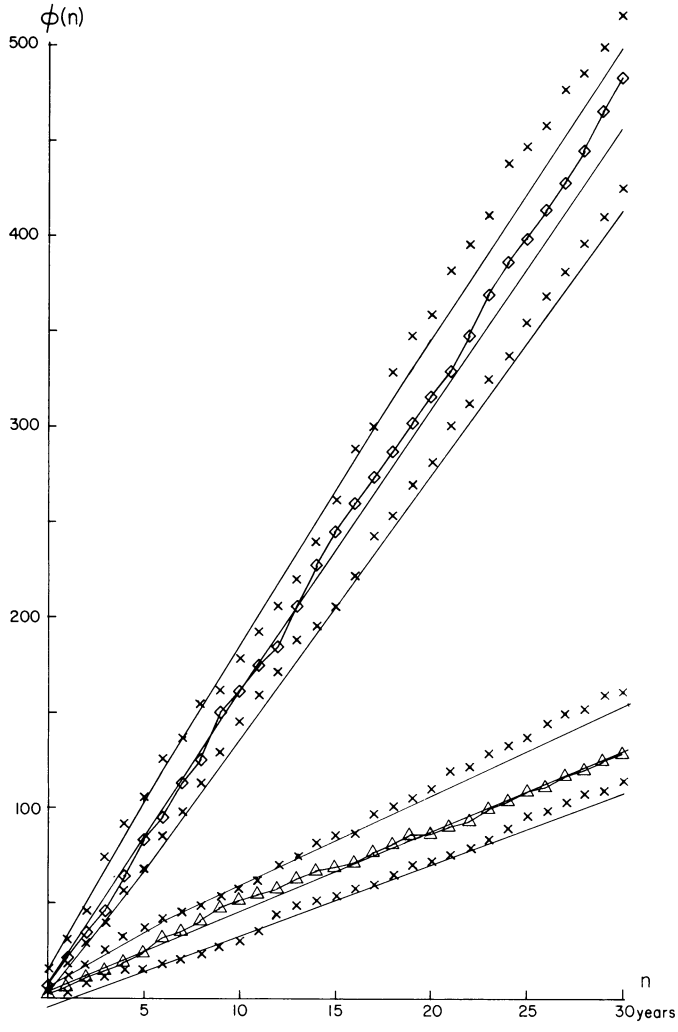

Fig. 3. Estimates of $\phi(n)$ from the records of all eruptions and all earthquakes. Also the extreme values of 20 simulations of Poisson processes corresponding to each record. Symbols are explained on Fig. 4

We estimated $\phi(n)$ and $\theta(n)$ for 20 pairs of independent Poisson processes with 82 and 44 events respectively, distributed at random on 429 years. The results are presented in Figs. 3 and 4. Figure 5 gives the result of the estimations of $\theta(n)$a nd $\theta(-n)$ from the 5 first simulations. We do not distinguish between the estimates of $\theta(n)$ and $\theta(-n)$ in the simulated values as their distribution is identical for independent processes. The largest and smallest values of $\phi(n)$ and $\theta(n)$ obtained in the simulations at each value of n are shown in Figs. 3–5. Lines two square roots above and below the expected values of ϕ and θ are shown on Figs. 3–8. We notice that the relative positions of these lines and the extreme values are very similar for all functions. (The extreme values of $\theta(n)$ were obtained from 40 estimates whereas the extreme values of $\phi(n)$ were only based on 20. It is therefore to be expected that the extreme values of θ lie relatively farther away from the expected value than those of ϕ although there is of course no certainty of observing this in a single experiment).

Turning now to our records we see that the estimates of $\phi(n)$ from the total records of eruptions and earthquakes presented in Fig. 3 do not differ much from the expected values for Poisson processes. Many of the simulated records produce larger deviations from the theoretical values. Interconnections of periodic or almost periodic kind may not produce very large differences from the expected values of ϕ (n) for Poisson processes if they only account for a small proportion of the total variation. The power spectrum contains the same information as $\phi(n)$, but is better suited for

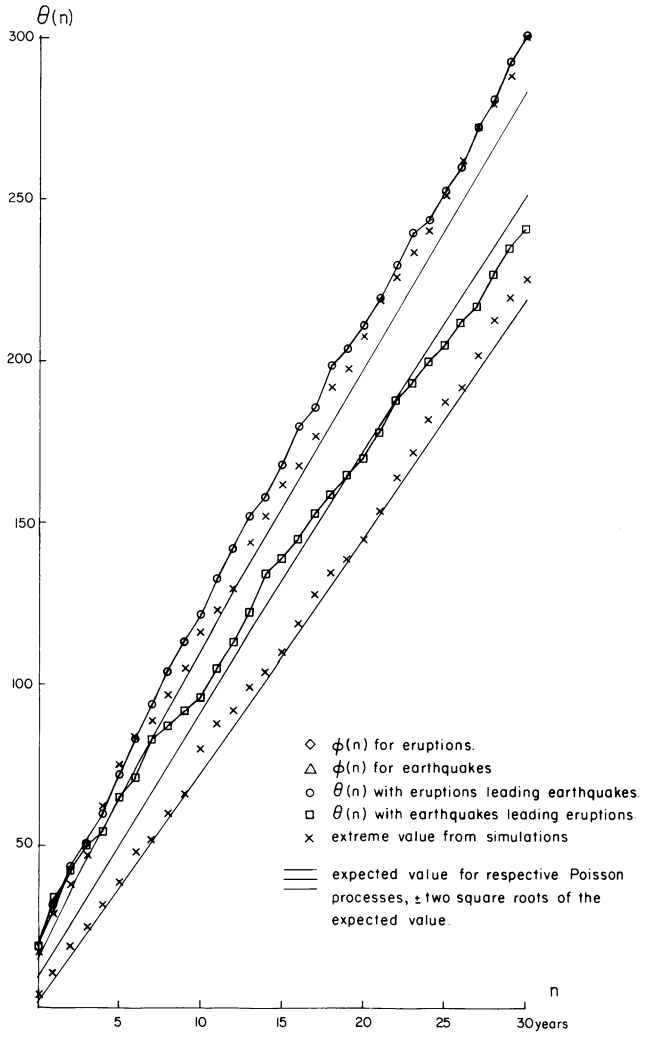

Fig. 4. Estimates of $\theta(n)$ from the records of all eruptions and all earthquakes. Also the extreme values of $\theta(n)$ from 20 pairs of independent Poisson processes

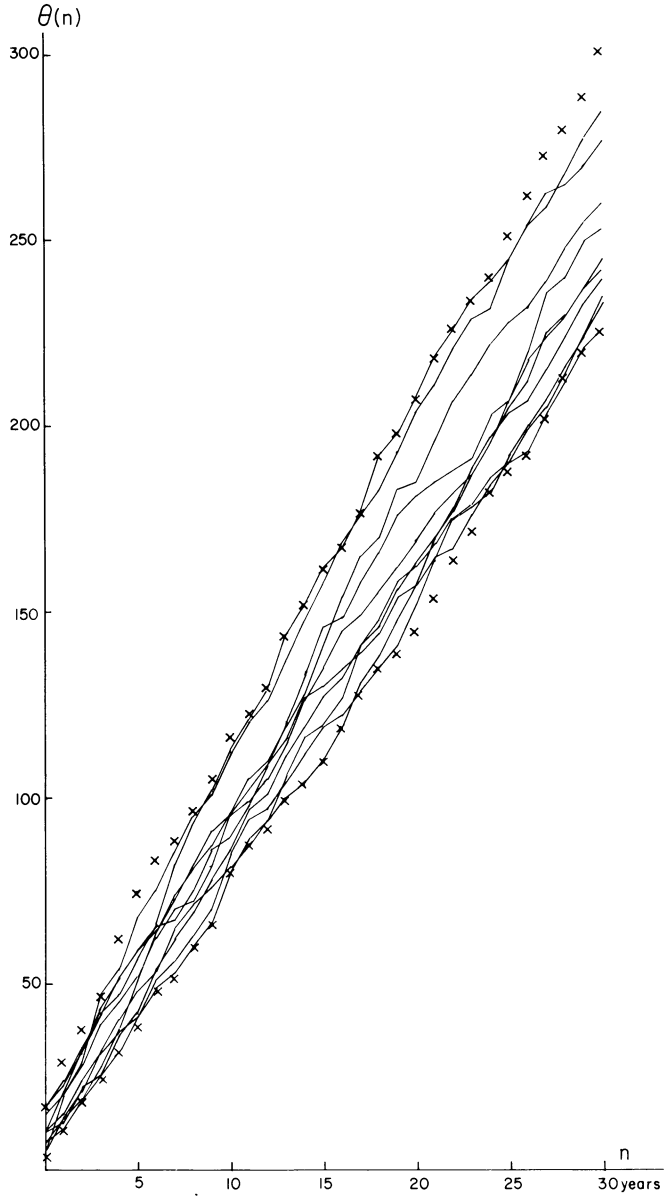

Fig. 5. Estimates of $\theta(n)$ from pairs of simulated independent Poisson processes. Also the extreme values of 20 simulations. Symbols are explained on Fig. 4

detecting periodicities. The statistical properties are not fully known here and the estimation of the power spectrum is a less straight-forward matter than the calculation of $\phi(n)$. We shall not enter the details here beyond mentioning that spectral analysis was carried out and produced no indication whatsoever of periodic effects.

The main result of the analysis described above is that neither record differs significantly from a Poisson process. This is different from results concerning single central volcanoes or seismic zones. But if the occurrence of eruptions in each volcano is independent of other volcanoes, the records are too short for detecting the small regularities associated with the events from one central volcano when it is included in the record of all eruptions. As only the largest earthquakes are included, clustering effects due to aftershocks (or triggered earthquake sequences) will not appear in these records. The clusters due to triggered earthquake sequences are eliminated from the record by regarding them as single events.

These conclusions differ from the common view that volcanic and seismic activity is periodic or episodic. One explanation of this may be that perfectly normal features of a purely random process have been misinterpreted as evidence for episodic characteristics. Thus although the average interval between eruptions is 5.2 years, neither the occurrence of 9 eruptions within a spell of 20 years nor of a period of that length without a single eruption is in any way remarkable in a record of this length.

Tomasson's suggestion (op. cit) of a periodicity with a 50 years cycle is based on slightly different data. On our records the evidence for this hypothesis, starting from the year 1579, would be that there are 54 eruptions in years ending on 10–34 and 60–84, and 27 in the remaining years. By moving the intervals 2 years forwards the corresponding numbers for earthquakes are 32 and 12. Even granted that these numbers were obtained by data-mining, the difference is high, 3 standard deviations from the mean in a binomial distribution with equal probabilities. It would be expected that a periodic effect with 1 cycle/50 years entails large correlations at short lags and at about 50 years lag, low correlations at 25 lags and a peak in the power spectrum at this frequency. The correlations would produce a maximum at $\phi(12)$ and a minimum at $\phi(37)$. In fact none of our estimates of these effects approaches any respectable level of significance. It thus appears that the mechanism controlling this phenomenon keeps account of the calender, but not of the past history of the events themselves. Considering the difficulties in producing a physical explanation of this kind of periodic effects, lacking the normal associated second order properties, little weight can be attached to the possibility of a 50-years period. But the records are not final, new evidence may appear, or, against the odds, a meaningful explanation of all the present results. There is, therefore, no reason to forget altogether about the curious numbers obtained by counting events in 25-years intervals.

Figure 4 shows the results of the calculation of $\theta(n)$ from the records of all eruptions and all earthquakes. The value of $\theta(o)$, which is the number of eruptions and earthquakes taking place during the same year, is large, and the values of $\theta(n)$ when eruptions are leading earthquakes is consistently larger than the simulated values for independent random processes. The difference between the observed value of $\theta(n)$ and the expected value increases with n. The values of θ where earthquakes lead eruptions are not different from what can be expected from random processes.

The relationship between two processes can also be studied by means of the cross-spectrum. A separate measure of the strength of the relationship, the coherence, is then obtained for each frequency band and an estimate of the phase difference or time lag. With a bandwidth of 0.045 cycle/year the average coherence in this frequency range is 0.28 and the phase difference lies between 16° and 37° The coherences are not high, but they are larger than in any of the simulation examples. The relationship seems to be mainly confined to frequencies below 0.1 cycle/year which is in accordance with the observation that the covariances seem to be positive up to long time-lags. As a result of the low coherences, estimates of the phase difference are very inaccurate, but the average time lag seems to be of the order of 3 years. Notice that this does not imply that it is most likely to observe an earthquake 3 years after an eruption. The relationship could rather be described so that following an eruption the probability of an earthquake is a little higher than normal for a fairly long time.

As the eruptions are leading the earthquakes we might be observing a causal relationship. A different explanation would be that both events are influenced by a common factor affecting the volcanic activity before the seismic activity.

The most obvious causal explanation of a relationship between those two kinds of activities is the triggering of latent events. This would produce an abnormally large number of short intervals, compensated by a reduction of longer intervals. But our records show no sign of such reduction. Triggering effect is therefore not a satisfactory single explanation of the results.

For many of the events more accurate timing is known than the year when they happened. Our analysis does not make use of this information. In principle there are no difficulties in designing methods of analysis which also take into account the known dates, e.g., by a modification of the method of Charnock (1977). But this would entail a substantial increase in the program writing and computing. Obviously it would make no difference to the geophysical interpretation if the number of eruptions leading an earthquake by 6 years was increased somewhat and the numbers corresponding to 5 and 7 years decreased accordingly. But considering the large number of earthquakes and eruptions in the same year, and 13 earthquakes leading an eruption by one year, a relationship where earthquakes trigger off eruptions must be considered a possibility, alongside the relationship where eruptions lead the earthquakes. But our analysis provides rather inaccurate information about this; an eruption in January and an earthquake in December the same year would be regarded as simultaneous whereas an earthquake in December and an eruption in January the following year appear as events with an interval of one year. In order to investigate this further we looked for all intervals shorter than one year between the two kinds of events. We found 11 cases where eruptions lead an earthquake by an interval of less than a year and 12 cases with the earthquakes leading. The expected value, taking into account the number of dated events, is about 5.

Another possible explanation of a causal relationship would be that the volcanic activity contributes directly to the strain that is subsequently released in the earthquakes. An eruption would then, presumably, be more likely to precede an earthquake in a neighbouring seismic zone than a more distant one. We could expect such effects to be most pronounced in South Iceland where both activities are confined within the same area.

We estimated separately the functions $\phi(n)$ for the 24 eruptions and 30 earthquakes in the Southern area. The results are given in Figs. 6 and 7. There is in fact no indication of a relationship between the two activities in these results. The distribution of the earthquakes is similar to the Poisson process, but $\phi(n)$ is rather low for the eruptions. This could be due to the fact that a large proportion of the eruptions is confined to the two central volcanoes where Thorlaksson's (1967) investigations showed that

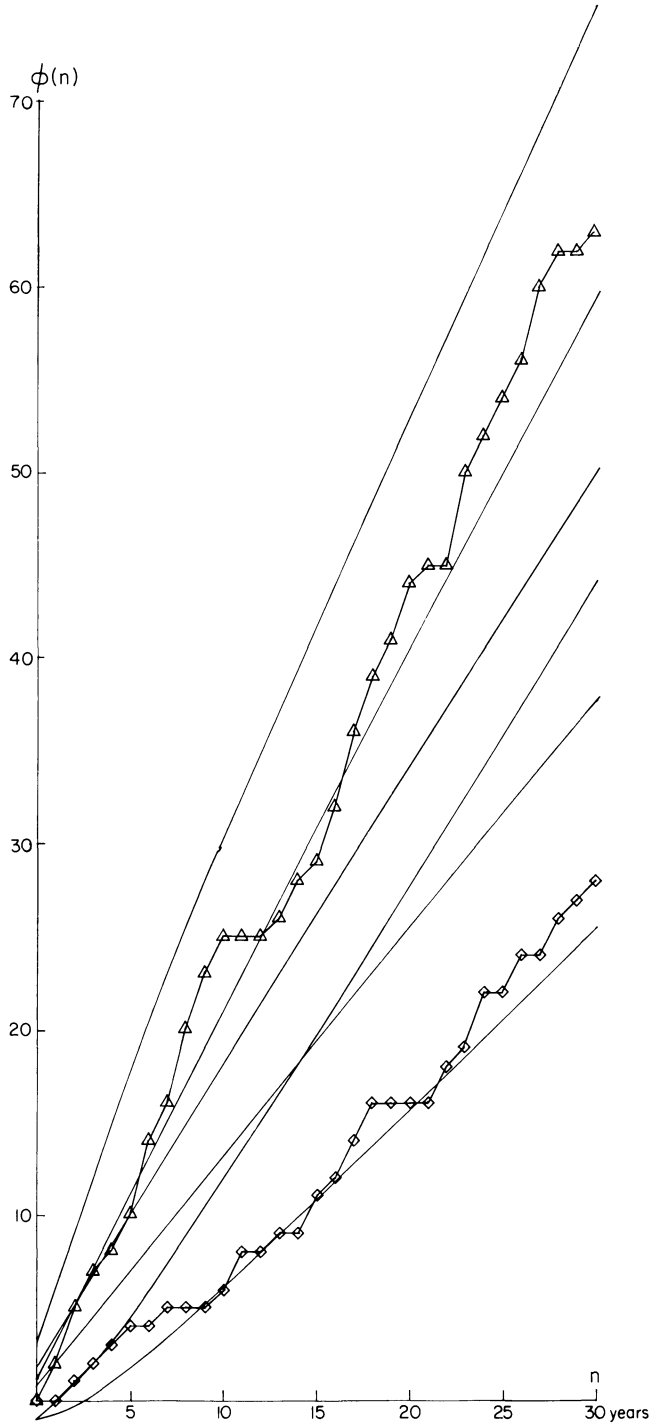

Fig. 6. Estimates of $\phi(n)$ from eruptions and earthquakes in South Iceland. Symbols are explained on Fig. 4

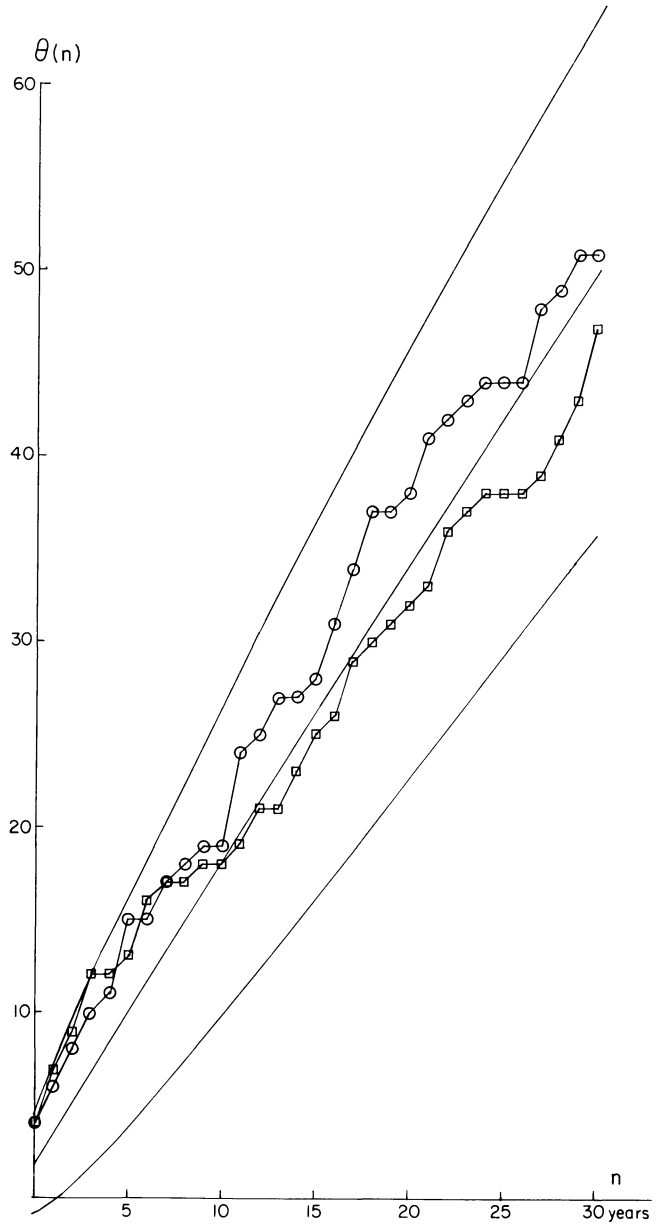

Fig. 7. Estimates of $\theta(n)$ from eruptions and earthquakes in South Iceland. Symbols are explained on Fig. 4

short intervals were less frequent than would be expected in a Poisson process.

The ratio between the released energies in the largest and smallest earthquakes on our records is about 10^3 The ratio between the largest and smallest masses of erupted material may be about 10^2 Little is, however, known about the size of many eruptions, especially those taking place under glaciers. Analysis of the dates of the events alone is therefore an inadequate method of investigating possible causal relationships between these activities.

Having failed to establish any causal link between eruptions and large earthquakes the possibility remains that the timing of both kinds of events is affected by a common factor. Plate movement is the obvious choice. Constructive plate boundaries consist of rift zones offset by transform faults. Plate accretion and volcan-

ism are confined to the rift zones and large earthquakes to the transverse fault zones. The present activity at Krafla has clearly demonstrated a connection between volcanism and rift movements (Björnsson et al., 1977). The difference in the respective structures of rift- and fault zones, with frequent small earthquakes on rift zones as compared to the concentration around a few large earthquakes along the transverse fault zone, indicate larger friction in the fault zones than the rift zones. The average time-lag between movements on the two types of plate boundaries would therefore be with the rift movement leading. But the kind of relationship envisaged here does not exclude the possibility that an earthquake, related to an eruption through plate movement, could occasionally precede it. The large number of occurrences of both events within one year could therefore all be the consequence of the connection with plate movements without any separate triggering effect.

It might be expected that eruptions associated with rifting of the crust would be more closely associated with earthquakes on the transverse fault zones than the eruptions of central volcanoes. We have therefore compared the two kinds of eruptions separately with all earthquakes, including the rifting episodes in 1618 and 1789 with the rift-type eruptions. The estimates of $\theta(n)$ are given in Fig. 8.

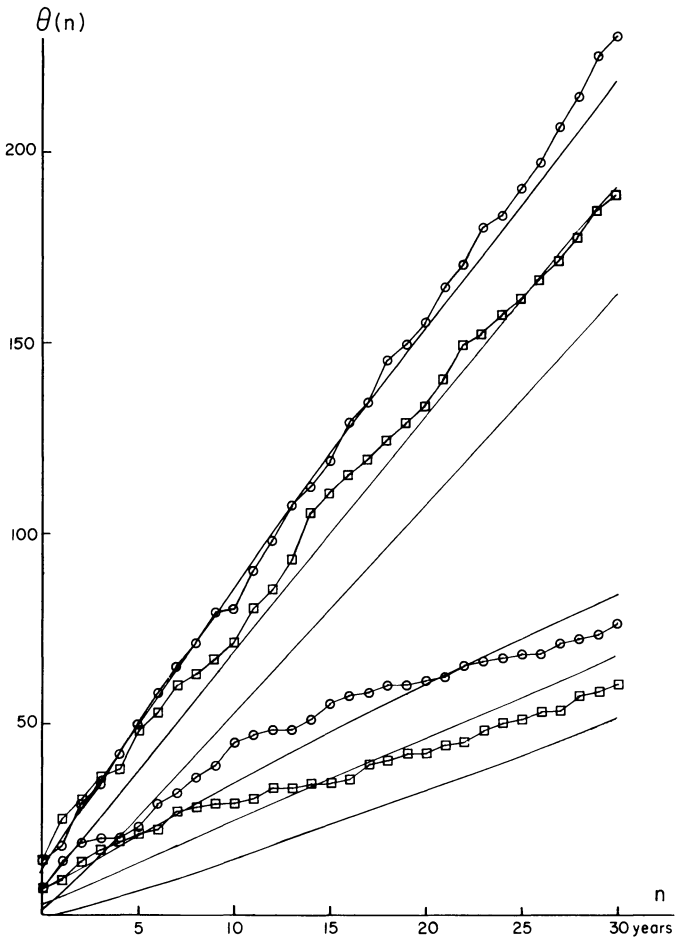

Fig. 8. Estimates of $\theta(n)$ from the record of all earthquakes and records of rift type- and central eruptions respectively. The larger values belong to the central eruptions. Symbols are explained on Fig. 4

For the rift type eruptions $\theta(n)$ is highly significant at the lower values of n, but returns to normal values for independent Poisson processes at $n > 20$. The values of $\theta(n)$ calculated from the central type eruptions lie consistently about two square roots above the expected value. This behaviour, which is also present in $\theta(n)$ from the record of all eruptions, implies that correlations remain positive up to very large values of n. It is more difficult to find a plausible explanation for this than for zero or even negative correlations after positive correlations at short lags as with the rift type eruptions. (Negative correlations could originate from repose periods following strain release). It should be kept in mind that persistent non-zero correlation at long lags can easily arise from systematic time-dependent errors in the records. These results provide no occasion for rejecting the idea that the relationship between eruptions and earthquakes, apart from possible triggering effects, is confined to the rift type eruptions. But they do not provide strong support for it either.

Conclusions

Rather against our expectation the analysis of second order properties revealed no indication of clustering or other regularities within the records of eruptions or earthquakes, respectively. This should not be regarded as evidence for the total absence of such phenomena. Regarding the earthquakes we are in fact fairly sure that the result is merely a consequence of leaving out all but the largest events and the treatment of triggered sequences. But it shows that the data provide an inadequate basis for any quantative conclusion about relationships within respective records. In prediction the only relevant information on each record about its own future is the intensity of events. Thus the best prediction of the number of events during the next n years is the product of n and the intensity. And the best prediction of the interval until the next eruption takes place is the inverse value of the intensity. Knowledge of the dates of past events is irrelevant. (This does not of course apply to individual central volcanoes or seismic zones.)

A rather weak, but apparently significant, relationship exists between eruptions and earthquakes with the eruptions leading. Triggering may be present too, but it is not the main factor in the relationship which embodies the whole area rather than local effects. We prefer to explain this by plate movement affecting both kinds of events rather than any causal link from eruptions to large earthquakes. This relationship is too weak to contribute much to the prediction of earthquakes.

Acknowledgement. This work was supported by the Icelandic Science Foundation. We thank Professor Sveinbjörn Björnsson for constructive criticism of the manuscript.

References

Annales Islandici 1400–1800 Reykjavík. Hid islenska Bokmenntafelag (Icelandic Literary Society) 1922–1961, (in Icelandic)

Björnsson, S., and Einarsson, P.: Seismicity of Iceland. In: Geodynamics of Iceland and the North Atlantic Area, L. Kristjánsson, ed. pp. 225–239. Dordrecht Reidel: 1974

Björnsson, A., Saemundsson, K., Einarsson, P., Tryggvason, E., Grönvold, K.. Current rifting episode in North Iceland. Nature **266**, 318–323, 1977

Charnock, D.M.: Spectral analysis of intervals between events in stationary bivartiate point processes. J. R. Statist. Soc., Ser. B: **39**, 230–237, 1977

Cox, D.R., Lewis, P.A.W.: The statistical analysis of series of events. London, Methuen 1966

Einarsson, P., Klein, F.W., Björnsson, S.. The Borgarfjördur earthquakes of 1974 in West Iceland. Bull. Seismol. Soc. Am. **67**, 187–208, 1977

Eliasson, S.· Sprengigigur i Leirhafnarskördum a Slettu. (Explosion crater at Leirhafnarskörd on Sletta Peninsula) (in Icelandic). Tyli **7**, 33–36, 1977

Larusson, M.M.. Landskjalftinn 1584. (Earthquake of 1584) (in Icelandic). Natturufraedingurinn **21**, 81–83, 1951

Ripley, B.D.: The second-order analysis of stationary point processes. J. Appl. Prob. **53**, 255–266, 1976

Ripley, B.D.. Modelling spatial patterns. J. R. Statist. Soc., Ser. B: **39**, 172–212, 1977

Saemundsson, K.: Fissure swarms and Central volcanoes of the neovolcanic zones of Iceland. In: Crustal evolution in Northwestern Britain and adjacent regions. D.R. Bowes and B.E. Leake, eds. Geol. J. Spec. Issue **10**, 415–432. Liverpool: Seal House Press 1978

Sigurdsson, J. (ed.): Biskupaannalar Jons Egilssonar (Jon Egilsson's bishops annals) (in Icelandic). In: Safn til sögu Islands **1**, pp. 15–136. Reykjavík: 1868

Steinthorsson, S.: Tephra layers in a drill core from the Vatnajökull ice cap. Jökull **27**, 2–27, 1978

Thorarinsson, S.: Surtsey, the new Island in the North Atlantic. Reykjavík: Almenna Bokafelagid 1966

Thorarinsson, S.: Eruptions of Hekla in historical times, Reykjavík: Soc. Sci. Isl. 1967

Thorarinsson, S.: Vötnin strid (Swift flowing rivers) (in Icelandic). Reykjavík: Menningarsjodur 1973

Thorarinsson, S.: Sambud lands og lyds i ellefu aldir. (Land and people through eleven centuries) (in Icelandic). In: Saga Islands 1, S. Lindal, ed.. pp. 29–97. Reykjavík: Hid islenska Bokmenntafelag, Sögufelagid 1974

Thorarinsson, S.. Katla og annall Kötlugosa (Katla and a record of Katla eruptions) (in Icelandic). Arbok Ferdafél. Islands pp. 125–149, 1975

Thorlaksson, J.E.. A probability model of volcanoes and the probability of eruptions of Hekla and Katla. Bull. Volcanol. **31**, 97–106, 1967

Thoroddsen, Th.: Die Geschichte der isländischen Vulkane, Copenhagen. D. Kgl. Danske Vidensk. Selsk. Skrifter, Naturvidensk. og mathem. Afd. **8**, Række, IX 1925

Tryggvason, E.: Seismicity, earthquake swarms and plate boundaries in the Iceland region. Bull. Seismol. Soc. Am. **63**, 1327–1348, 1973

Tryggvason, E., Thoroddsen, S., Thorarinsson, S.: Report of Earthquake risk in Iceland. Timarit Verkfraedingafelags Isl. **43**, 81–97, 1959

Vedrattan (Monthly review of the Icelandic Meterological Office), 1928, 44, 1928

Vere-Jones, D.: Stochastic models for earthquake occurrence. J. R. Statist. Soc., Ser. B: **32**, 1–62, 1970

Received March 29, 1979; Revised Version July 23, 1979

J. Geiophys. 47, 110–119 (1980

Journal of Geophysics

Geodetic Measurements and Horizontal Crustal Movements in the Rift Zone of NE-Iceland

D. Möller and B. Ritter

Institut für Vermessungskunde, Technische Universität Braunschweig, Pockelsstraße 4, D-3300 Braunschweig, Federal Republic of Germany

Abstract. Based on the special geodetic network set up by Niemczyk and Emschermann in 1938 in order to determine horizontal movements of the earth's crust in the fissure area of the neo-volcanic zone of NE-Iceland, a number of repeated measurements were carried out from 1965 to 1977. In this article, modern geodetic measuring techniques and the (constantly improving) positional accuracy achieved are described; this is followed by an evaluation showing significant crustal movements in the riftzone. In the period of 1965 to 1971, movements in the total area of approximately 110 km from east to west were restricted to compressions, whereas afterwards, and in particular since 1975, expansions of up to 2 m/km have occurred in the central rift area. At present, this expansion is largely compensated by compression in the peripheral areas of up to 0.05 m/km, so that between 1971 and 1977 a total east-west expansion of the neovolcanic zone of only about 0.4 m has resulted over a distance of about 90 km.

Key words: Icelandic rift zone – Recent crustal movements – Geodetic measurements.

1. Introduction

Niemczyk (1943) was the first to recognize the possibility of determining relative horizontal movements of the earth's crust in Iceland by repeated measurements of geodetic planimetric networks, and in 1938 he paved the way for putting this idea into practice by setting up, and measuring, a special geodetic network crossing the neo-volcanic zone of NE-Iceland.

The Institut für Vermessungskunde, Technische Universität Braunschweig, under the direction of Gerke since 1964 and Möller since 1975, has taken up this work again, continued it, and extended it to further areas, including SW-Iceland (Gerke et al., 1978).

This paper is concerned with the work and the results achieved in the main network in NE-Iceland (in the period of 1965 to 1977), in the Gjastikki deformation figure (1975–1977), and in the Kelduhverfi profile (1977–1978); see Fig. 1.

2. The Measuring Techniques

2. 1. The Measuring Techniques Used in the Main Network NE-Iceland

2. 1. 1. Observation Period of 1964/1965. The special network set up in 1938 (Niemczyk, 1943) was reconstructed in 1964/1965 with considerable improvements in its configuration (Gerke, 1967; Heumann, 1972). In the process, it was possible, for the first time, to abandon the principle of pure triangulation with one base extension line only to determine the scale. This was achieved with the use of the new microwave distance-measuring equipment (Tellurometer MRA 3) for the measurement of 30 distances well distributed over the whole network resulting in a decisive improvement in accuracy and reliability of scale (Fig. 2).

In general, the directions were eccentrically observed in complete sets by means of Wild T3 precise theodolites and directed to flagsignals. For the first time, zenith distances were necessary to achieve the geometrical reduction of the electromagnetically measured slope distances. The trigonometrical vertical control survey network was connected at 13 bench marks to the precise levelling line from Akureyri to Jökulsá á Fjöllum which was also measured in 1965 (Spickernagel, 1966).

The accuracies achieved for the observation period of 1964/1965 – and for all subsequent measurements – are given

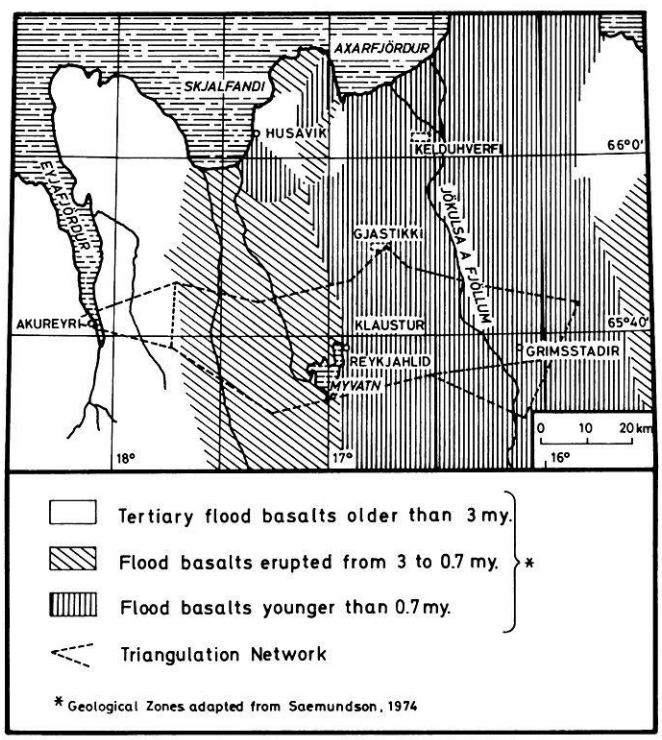

Fig. 1. Location of study areas in NE-Iceland

0340-062X/80/0047/0110/$02.00

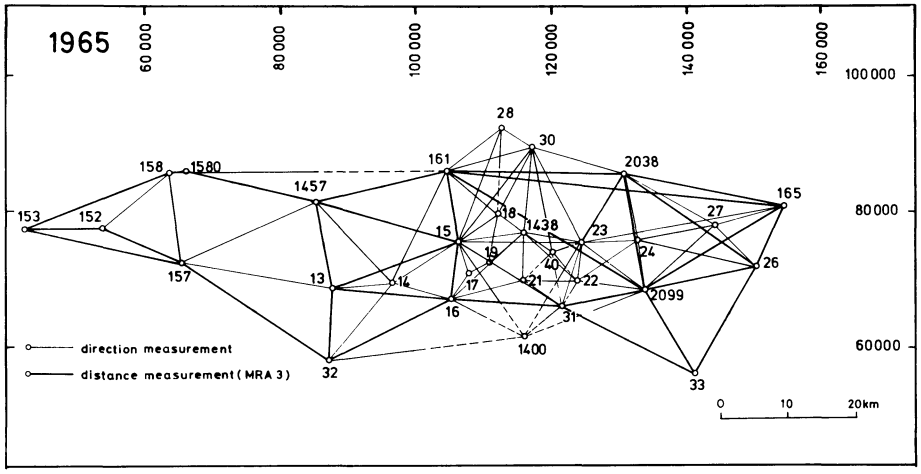

Fig. 2. Geodetic measurements in the triangulation network 1964/1965

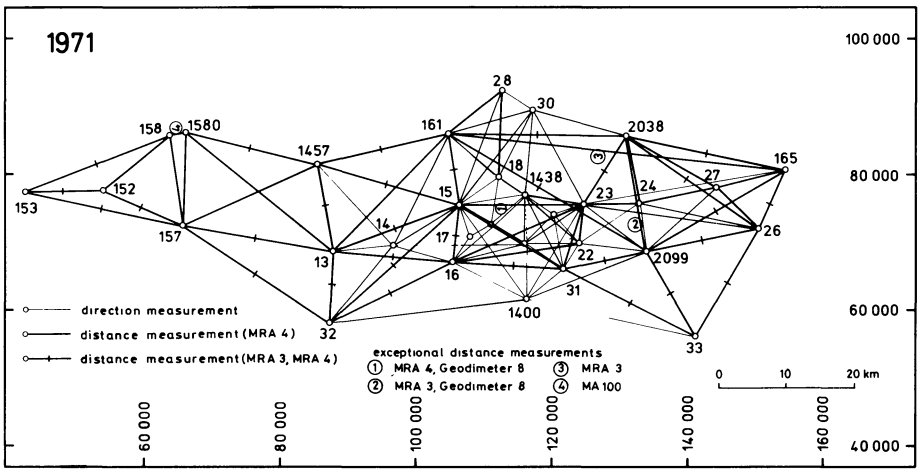

Fig. 3. Geodetic measurements in the triangulation network 1971

in Tables 1 and 2. Figure 6 indicates the size and orientation of the standard ellipses. The positive influence of the electronically measured distances can also be seen in the error ellipses: these are not only markedly smaller in comparison to the 1938 results, but also more convenient in their forms, since in the Niemczyk network the large axes of the appreciably flattened ellipses ran mainly in an E-W direction and were thus expecially unsuitable for determining the crustal movements in this direction.

2. 1. 2. Observation Period 1971. The principal features of the 1971 measurements were the extension of microwave distance-measuring in the whole network, using two different types of instruments (Tellurometer MRA 3 and MRA 4), and at the same time, an increase of direction measurements with the aid of a refined measuring technique (complete sets of directions in individual sectors) using a Wild T3. A trigonometrical vertical control survey network was also observed again in order to meet the accuracy requirements for distance reduction.

All measurements were made at eccentric stations; the target points used for the directions and zenith distances were triangulation signals with cylinders. Two longer distances were measured with Geodimeter 8. In 1971 for the first time an adjustment was possible for a pure trilateration network over 21 points by the method of variation of coordinates (Fig. 3). The planimetric accuracy of the points could again be improved.

2. 1. 3. Observation Period 1975. A further increase in accuracy and reliability in the central part of the network was aimed at in 1975 (Fig. 4), since according to the previous analyses detection of crustal movements was more likely in this part than in the hitherto 'quiet' peripheral areas of the network.

For this reason

- centric observations were carried out only at the marked stations in the network, with Kern-centering for all instruments;
- the horizontal angles were observed with Wild T3 and Kern DKM 2A, using fixed light signals from opposite stations;
- an increased number of distances in the network was measured electronically;
- most distances were measured with microwave *and* light-wave instruments (MRA 4 and Geodimeter 8) in order to increase the level of distance-measuring accuracy and to make the network scale as reliable as possible.

The great advantage of microwave over light-wave measurement is that measurements can be made even when visual contact is only theoretically possible (e.g. when there is fog or culminating points are obscured by cloud). However, it must not be forgotten that the influence of absolute humidity on the microwave phase velocity is about 100 times greater than that on light wave velocity.

For this reason, the determination of scale by methods using light is, as a rule, more precise. If both measurements are carried out simultaneously or almost simultaneously, the differences in

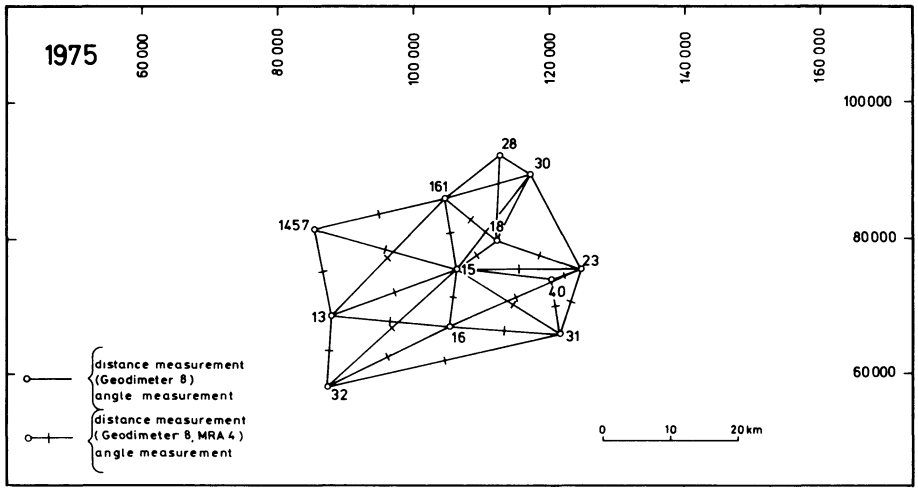

Fig. 4. Geodetic measurements in the central triangulation network 1975

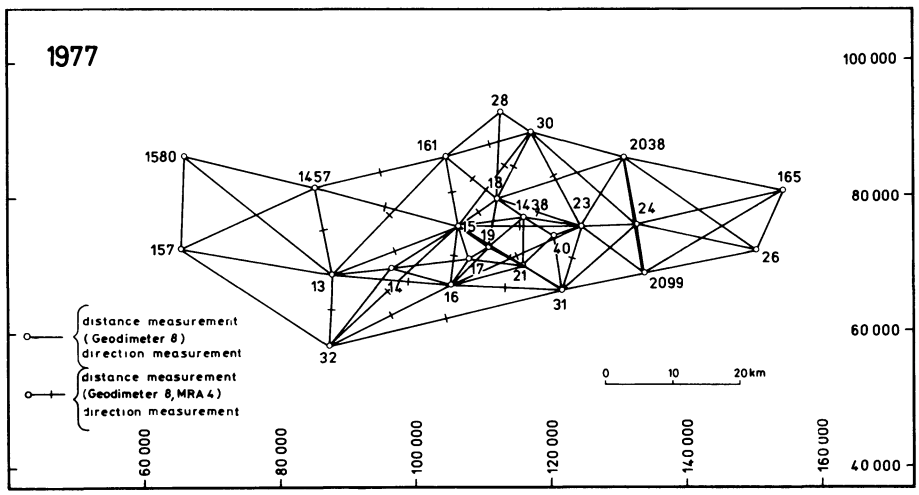

Fig. 5. Geodetic measurements in the triangulation network 1977

Table 1. Extent and accuracy of geodetic measurements in the triangulation network, NE-Iceland 1964/65–1977

Observation period	Direction measurements	Distance measurements	
		Microwave	Lightwave
	Number of stations	Number of measured distances	Number of measured distances
	Standard deviation of adjusted directions	Standard deviation s	Standard deviation s
1964/1965	31 $\pm 1.8''$	30 (MRA 3) $\pm(3\text{ cm}+4\cdot10^{-6}\cdot\text{d})$[a]	– –
1971	31 $\pm 1.4''$	34 (MRA 3) $\pm(3\text{ cm}+4\cdot10^{-6}\cdot\text{d})$ 50 (MRA 4) $\pm(1\text{ cm}+3\cdot10^{-6}\cdot\text{d})$	2 (Geod. 8) $\pm(1\text{ cm}+2\cdot10^{-6}\cdot\text{d})$
1975	12 $\pm 1.0''$	24 (MRA 4) $\pm(1\text{ cm}+3\cdot10^{-6}\cdot\text{d})$	37 (Geod. 8) $\pm(1\text{ cm}+2\cdot10^{-6}\cdot\text{d})$
1977	24 $\pm 1.5''$	41 (MRA 4) $\pm(1\text{ cm}+3\ 10^{-6}\cdot\text{d})$	131 (Geod. 8) $\pm(0.5\text{ cm}+1\cdot10^{-6}\cdot\text{d})$

[a] d = Distance

Table 2. Accuracy of adjusted point positions, NE-Iceland 1964/65–1977

Observation period	Triangulation net	Trilateration net	Combined triangulation and trilateration net
	Number of stations	Number of stations	Number of stations
	Average internal error of position	Average internal error of position	Average internal error of position
1964/1965	31	–	31
	±0.17 m	–	±0.08 m
1971	21	21	31
	±0.11 m	±0.06 m	±0.05 m
1975	12	12	12
	±0.06 m	±0.02 m	±0.02 m
1977	24	24	24
	±0.12 m	±0.02 m	±0.02 m

distance between the light-wave and microwave measurements indicate possible systematic distance errors which are caused by inadequate observation of the meteorological data (resulting from measurements at the endpoints only, Kuntz and Möller, 1971). The calculated average scale difference of 3.5 ppm in Iceland is plausible, but must on no account be neglected when different instruments are used. For all comparisons in the main network, the microwave scale (with shorter reduced distances than in the case of light-wave measurements) was retained.

2. 1. 4. Observation Period 1977. After the beginning of the rift-phase (Björnsson et al., 1977) which started with a fissure eruption near Leirhnjukur a few kilometers west of Point 18 in December 1975, the program for 1977 was drawn up:
- repetition of the 1975 measurements,
- densification of the central part of the network by means of five points which had last been measured in 1971,
- extension of the main network to the east by three points which had also last been measured in 1971.

To confirm the difference in scale between microwave and light-wave distances, almost simultaneous measurements were made with both instruments in 1977 (Fig. 5), to the same extent as in 1975 (Fig. 4). The time consuming method of individual angle measurements was dropped in favour of direction measurements aimed at rotating halogen lamps at the particular stations in use. Using Kern-centering these lamps were clipped onto tripodheads, so that all stations served simultaneously as measuring stations and target points. This construction made also possible simultaneous reciprocal zenith distance measurements which contributed to a perceptible increase in accuracy of the height measurements. The height connection to Spickernagel's (1977) precision levelling was carried out via 4 bench marks (Fig. 8). However, the most important part of the survey in the network was definitely the distance measurements carried out with 2 Geodimeter 8″ Not only was it possible to increase the accuracy of these measurements perceptibly again (Table 1), but also to include four additional points at the periphery of the network, although this had not originally been planned; the error of position for the network which now covered twice the original area was kept down to ±0.02 m; this corresponds to an accuracy of ±0.01 m for the central part of the network (Table 2).

The mean microwave/light-wave scale difference arrived at in the 1977 measurements was 4.6 ppm – a good confirmation of the 1975 value. Under Icelandic working conditions, the limit of accuracy, at present, attainable has probably been achieved.

This high accuracy is indispensable to permit reliable conclusions on variations in any case, particularly if the current rifting episode ends and only small deformations are expected, and to significantly contribute to crustal deformation models.

2. 2. The Measuring Techniques Used in Selected Minor Deformation Figures

2. 2. 1. Gjastikki – Observation Periods of 1975 and 1977. With an area of ~3 km × 1 km the regional Gjastikki network covers a pronounced fissure area which was selected for initial special measurements as early as 1938 (Niemczyk, 1943). The deformation figure consists of a virtually rectilinear profile 3 km in length, with three main and seven supplementary points. In 1967, two quadrilaterals were formed from the profile by setting up three additional main points (Gerke, 1974). The connection with the main network is achieved by distance and direction measurements via Point 28 (Fig. 9).

For the determination of the figure and connection with the main network, 37 distances were measured from August 6 to 9, 1975, using the precise electronic distance-measuring instrument Kern ME 3000 (Mekometer) in the range of 70 m $\leqq d \leqq$ 3,300 m with a standard deviation of $s = \pm(0.1\text{ cm} + 2 \cdot 10^{-6} \cdot d)$. Almost simultaneously all distances were measured with the Tellurometer MA 100 [$s = \pm(0.25\text{ cm} + 2 \cdot 10^{-6} \cdot d)$]. The directions and zenith distances in the quadrilaterals, the connection with Point 28 and the alignments in the profile from the terminal points 300 and 200 were established by means of the Kern DKM 2A theodolite. All measurements were made using Kern-centering. The standard deviation of the direction observations can be estimated to be ±1.0″ For 1975, this means an average internal error of position for the special network of ±0.005 m (without taking into account the accuracy of position of the main network).

During the measurements from August 8 to 11, 1977, a Hewlett Packard 3 800 B was used as third measuring instrument particularly suitable for distances of >2,500 m ($s = \pm 0.5\text{ cm} + 3 \cdot 10^{-6} \cdot d$). The number of distances measured with ME 3 000 and MA 100 corresponded to the 1975 value. Alignments were also carried out from Point 100 to the east and west. It was principally on account of this last procedure that the average internal error of

position could be reduced to ± 0.003 m providing adequate measurement accuracy.

2. 2. 2. Kelduhverfi Deformation Profile, Observation Periods of 1977 and 1978. After considerable fissure-expansions in the period of 1975–1977, a deformation profile, approximately perpendicular to the main fissures and consisting of only four points, was set up in the Kelduhverfi area about 25 km north of Gjástikki (Fig. 1) on August 11/12, 1977, and was observed by means of the measuring techniques that had proved their value in Gjástikki. In a local system, average internal errors of position of ± 0.002 m were achieved for the adjusted coordinates. In June 1978, the profile was measured again by Icelandic scientists. The results of these measurements (not yet published) were kindly made available by A. Björnsson and G. Thorbergsson for comparison. The average internal error of position computed on the basis of these measurements is ± 0.011 m.

3. Results of the Deformation Analyses for the Individual Periods

3. 1. Fundamentals

The deformation analyses carried out here are based on the test procedure given by Pelzer (1971; 1974). The area investigated is covered by a number of points; possible changes in position of these points are assumed to be valid for the area surrounding the points as well. After repeated measurements and the separate adjustment by the method of variation of coordinates in both observation periods, the first question to be asked is whether it is actually possible to prove statistically the occurrence of deformations for the period between the observations. The parameters in this global test are:

$$s = \sqrt{\frac{f_0 \; s_0^2 + f_1 \; s_1^2}{f_0 + f_1}}$$

estimated value for the theoretical standard error σ of both measurements in the geodetic network, the unit of weight being constant (measurement i: standard error s_i, number of degrees of freedom f_i)

$$\Theta = \sqrt{\frac{d' P d}{h}}$$

a further estimate for the theoretical standard error, computed on the basis of the difference in coordinates d between the two networks, the matrix of weights P as a generalized inverse of the singular cofactor matrix Q, and the number h of linearly independent components of the vector d

$F_{1-\alpha, h, f}$ = confidence limit of the F-distribution with h degrees of freedom in the numerator and $f = f_0 + f_1$ degrees of freedom in the denominator for a previously determined significance level α.

The global test is prepared by computing the vectors of the coordinate unknowns x_0 and x_1 of the two networks and the relevant singular cofactor matrices Q_0 and Q_1, the vector of differences $d = x_1 - x_0$ and the corresponding cofactor matrix $Q = Q_0 + Q_1$.

The null hypothesis H_0, i.e., that no deformations have occurred, is valid as long as the difference between the two estimates s and Θ is random. The following probability relation exists:

$$P\left\{\frac{\Theta^2}{s^2} > F_{1-\alpha, h, f} \,\middle|\, H_0\right\} = \alpha.$$

If the quotient θ^2/s^2 in an experiment is greater than the relevant confidence limit, then H_0 can be rejected at the selected significance level (usually $\alpha = 5\%$). In this case, the attempt is made to localize the deformations indicated by the global test. An important indicator of the points which are deformed in comparison with neighbouring points is the proportion of the individual points in θ^2 In addition to delimiting stable zones this analysis makes it possible to localize disturbed zones.

Deformation vectors which were calculated by using the method of deformation analysis as described here are not invariant either in their direction or their size, but are highly dependent on the number of points and their distribution in the area under investigation – i.e., it is not possible to calculate absolute shift vectors. The vector of differences d calculated here is characterized by the sum of the individual elements resulting to zero in the axes of coordinates. Nevertheless, this procedure certainly is suitable for initial interpretations, if the vectors are clearly visible on a diagram and the accuracy of the point determinations (e.g., by means of standard ellipses) is clear from initial and repeated measurements.

Beside this deformation analysis there is the possibility to proceed from different hypotheses, e.g., that definite points or areas are unchanged in their position, see Fig. 7b. Without the chance to carry out absolute positioning with an accuracy comparable to relative methods, a suitable model for the movement of the earth's crust in the rift zone of Iceland could only be developed in cooperation with geophysicists and geologists.

3. 2. Main Network

3. 2. 1. Changes in Position From 1965 to 1971. The analysis of the main NE-Iceland network for this period (31 points) reveals a disturbed zone running roughly from north to south (Fig. 6a). This zone is situated between two extensive blocks, each of which, when considered individually, exhibits no deformations in a deformation analysis where $\alpha = 5\%$.

The east block covers an area of 35 km × 30 km and contains 13 points. The maximum changes of two peripheral points with shift vectors of approximately 10 cm are not significant. The west block contains 10 points and measures approximately 60 km × 20 km. Although in an isolated analysis of this block, shift vectors of approximately 10 cm are not significant. The west block contains 10 points and measures approximately part, these 'changes' also prove to be compatible with the null hypothesis. Eight points are situated in the disturbed zone between the two blocks. Significant changes in position beyond the disturbed zone result in significant contractions of up to 50 cm at the southern periphery of the network – an unexpected result for many geophysicists. A marked shifting towards the north is located inside the disturbed zone. The possibility cannot altogether be excluded that a portion of this northward drift may be caused by inevitable distortions in the middle of the narrow network. When Figs. 6 and 7 are examined, it should be noted that all scales have been kept unchanged to permit straightforward comparisons. In the interest of clarity, the ellipse axes were enlarged 2.5 times in comparison to the vectors.

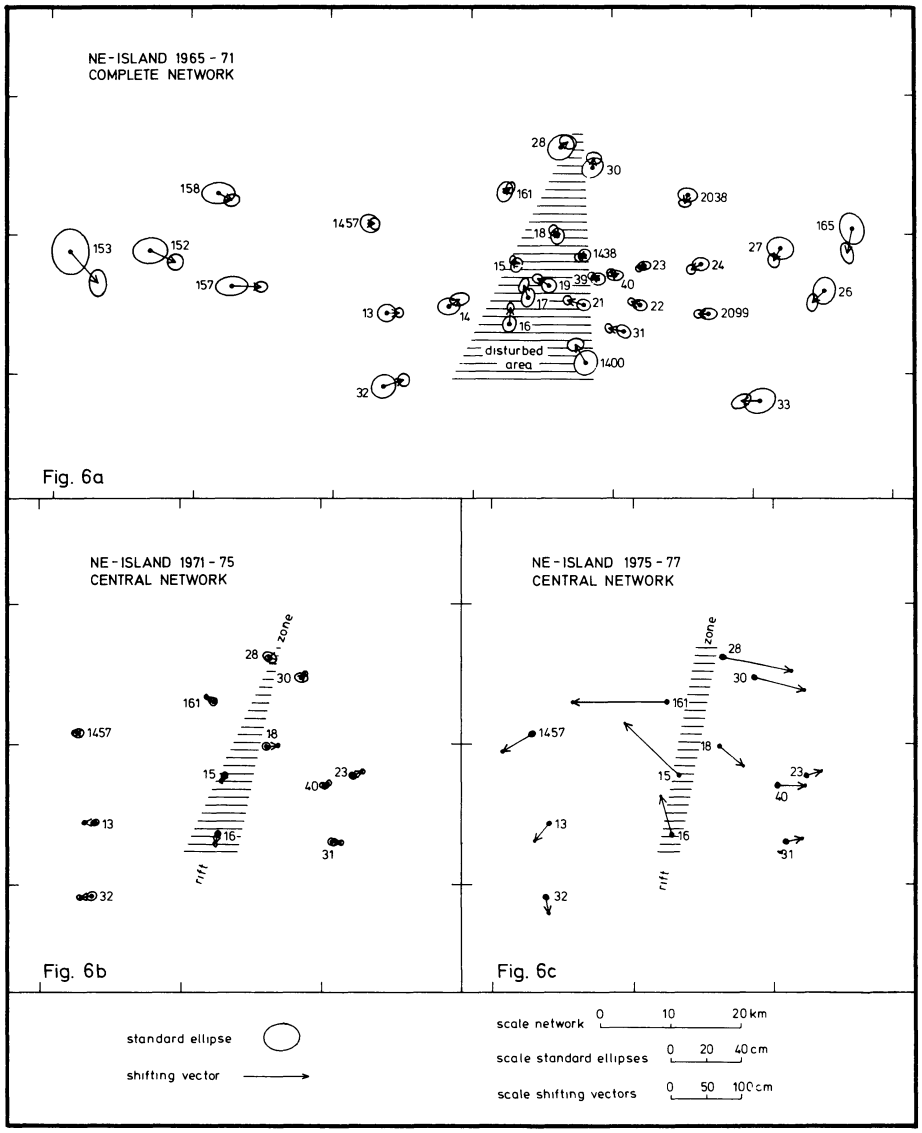

Fig. 6. Models of deformation in the study area 1965–1977

3. 2. 2. Changes in Position From 1971 to 1975. A deformation analysis was carried out for the central part of the network on either side of the zone which had exhibited disturbances from 1965 to 1971, using a total of 12 points; it showed changes for the period of 1971–1975 at a singificance level of $\alpha = 1\%$ (Fig. 6b). A division of the network into two peripheral zones and one disturbed zone showed deformations in the eastern (five points) and western (five points) peripheral zones with $\alpha = 5\%$. However, if the significance level was reduced to 1%, acceptance of the null hypothesis was possible. The analysis of the total network produced a quotient $\bar{F} = \theta^2/s^2$ of 9.1 with a relevant limit $\bar{F}(\alpha = 5\%)$ of 1.6. In the peripheral zones, the corresponding values were $\bar{F} = 2.7$ and $\bar{F} = 2.1$. On the basis of these results, the following model was developed for this period: the location of the central disturbed zone in the period of 1965–1971 is confirmed, but with the directions of movement reversed. Two points in the middle of the disturbed zone (15 and 16) have a definite motion component towards south. In the far more stable east and west blocks, extensions of 0.3 m at the southern periphery of the network and of 0.1 m at the northern periphery can now be detected – in contrast to the compression phase in the period of 1965–1971. This drift is significant and although the last measurements were made 4 months before the first eruption, it may be interpreted as an indication of the beginning rift phase.

3. 2. 3. Changes in Position From 1971–1975–1977. In the period of 1975–1977 the main activity in the area under investigation shifted to the north (Fig. 6c), where an east-west expansion of approximately 2.5 m show between Points 161 and 28. The expansions in the southern part of the network are distinctly smaller; on the other hand, the location of the points in relation to the rift zone could also be significant. A strong northward movement (15, 16) can now be seen in the expansion zone. Surprisingly, considerable compressions can be demonstrated in the transitional zones bordering the rift zone. The strongest compression on the basis of the main network is approximately 1 m/20 km (161–1457), i.e., 50 mm/km. The compressions towards the west decrease rapidly to the limits of accuracy (2–3 mm/km); in the east the compressions do not completely disappear at the edge of the research area, possibly 5–10 mm/km beyond the periphery. (Fig. 7a). This

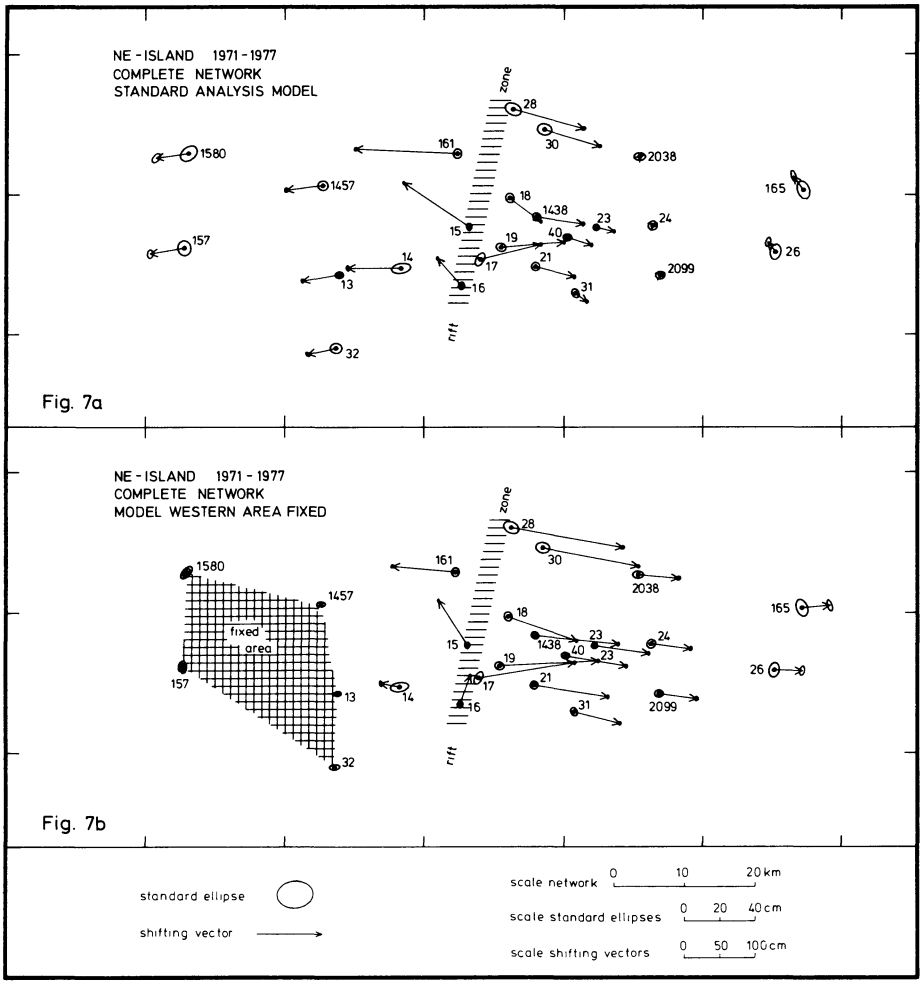

Fig. 7. Two different models of deformation in the study area 1971–1977

asymmetry can also be interpreted geologically, since radiometric dating (Saemundsson, 1974) shows that the present rift phase is taking place in the western section of the neo-volcanic zone.

A further deformation analysis for the period of 1971–1977 is carried out assuming that part of the network in the extreme west is stable (Fig. 7b). Unlike all previous analyses, the observations of both periods of measurement are here adjusted together: this method postulates unchanged positions for the five points 1 457 – 13 – 32 – 157' – 1 580 and the possibility of change for all other points. The following results can be given: five points in the rift zone itself or in its immediate vicinity (15, 16, 17, 18, 19)[a] cannot be fitted into the general deformation model which runs at an azimuth of approximately 100°E. The direction of the expansion is perpendicular to the main direction of the fissure system. While the four points 15, 16, 17, 19 have northward components, Point 18 has a southward component. At the eastern periphery, the 1971–1977 expansion is about 0.4 m (Fig. 7b), but the direction of these peripheral vectors is less certain because of the large distance from the block assumed to be stable.

3. 2. 4. Height Changes During the Period of 1971–1977. The height changes of the triangulation points in the main network were also calculated for the period of 1971 to 1977 (Fig. 8). This was a byproduct of the trigonometrical height measurements that were necessary in each case for the reduction of the electronically measured distances. These height changes can be summarized as follows:

- pronounced subsidence occurs only in the rift zone (Points 100 and 16),
- the uplifts in the compression zones are not homogenous but rather irregular,
- the large uplifts near the eastern height connection are surprising (Points 2099 and 24),
- the unusual 'changes' at the eastern and western periphery of the network (+0.5 m) cannot be interpreted as significant on account of the rather large standard errors in both measurements in these areas.

3. 3. Deformation Figures

3. 3. 1. Gjástikki Deformation Figure – Changes in Position From 1975–1977. The Gjástikki deformation figure was investigated from 1965 onwards for changes in position in the periods of 1965–1967, 1967–1971, and 1971–1975. Apart from an expansion of the profile of 0.04 m in the period of 1965–1967 and some local movements of individual points, no regional deformations could be discovered. For the period 1975–1977, exceptionally large expansion of approximately 2.8 m between the main points 300 and

[a] 15 Hlidarfjall, 16 Hverfjall, 17 Námafjall, 18 Krafla, 19 Sandfell

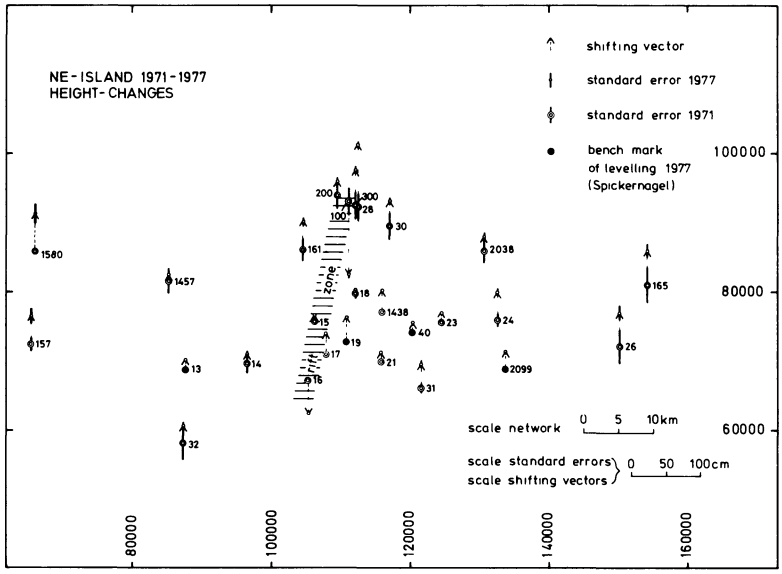

Fig. 8. Height changes in the study area 1971–1977

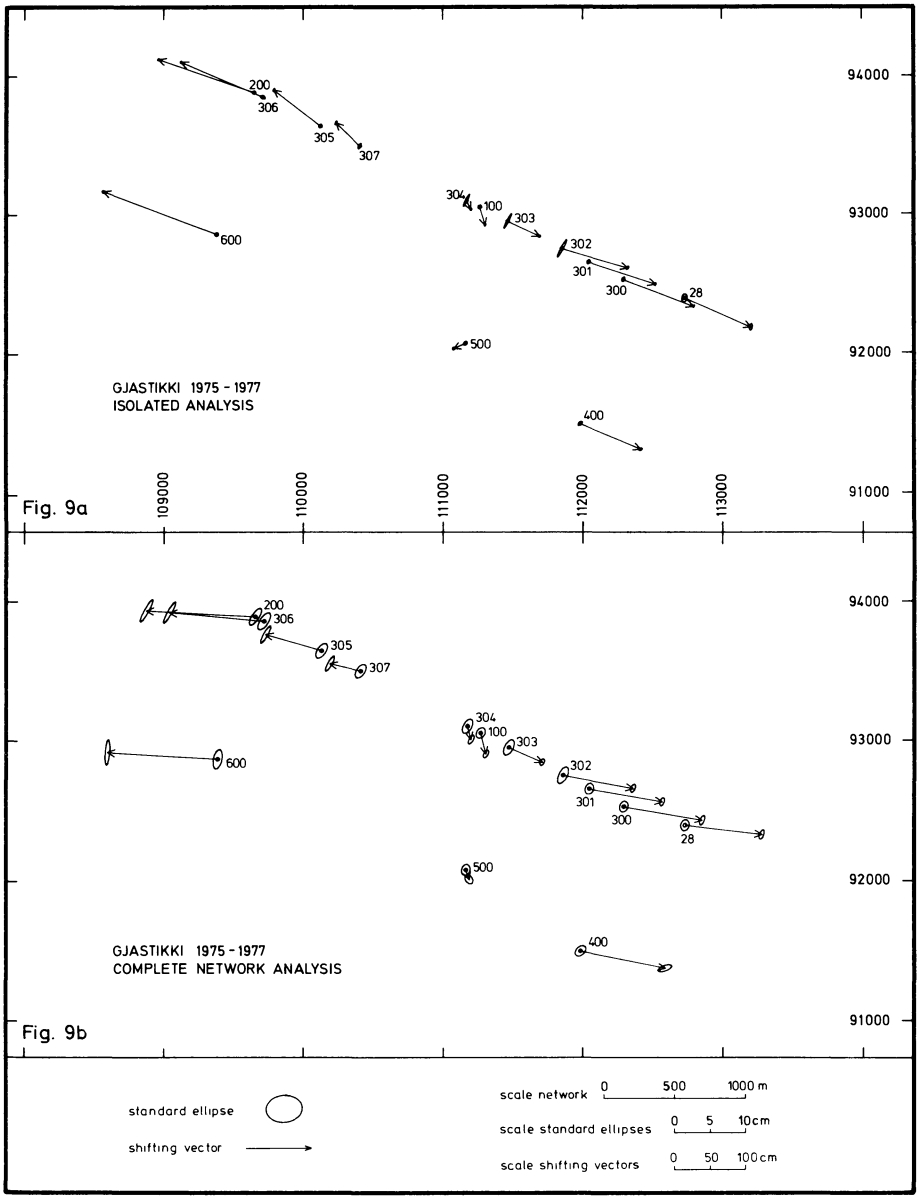

Fig. 9. Two different models of deformation in Gjástikki 1975–1977

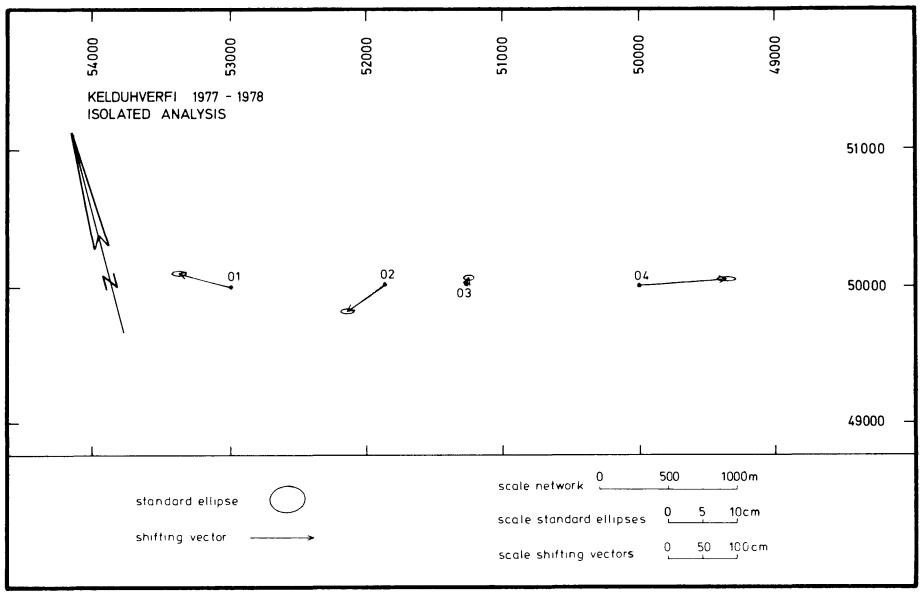

Fig. 10. Model of deformation in Kelduhverfi 1977–1978

600, i.e., along a distance of 3 km (Fig. 9a), can be demonstrated. These deformations are not uniform. For some sections of the profile, the mean rate of expansion remains below 500 mm/km (304–100, 302–301, 301–300). For the section from 300 to 28 there is, in fact, a small compression. On the other hand, average expansion rates of over 2,000 mm/km (200–306, 100–303) can also be demonstrated. A southward drift of the points in the centre is clearly recognizable.

In a second deformation analysis, the data for the main network were evaluated, this time in conjunction with the Gjástikki deformation figure (Fig. 9b). In addition to the increased error ellipses of the overall analysis, the azimuth of the main direction of the deformation vectors has changed from 110°E to 95°E. This direction of movement, derived from an analysis of a large 25 points network, is perpendicular to the mean direction of the main fissures and consistent with the conception derived from the main network analyses. In Figs. 9 and 10 the enlargement of the ellipse axes to the shifting vectors is in the ratio of 10:1.

3. 3. 2. Kelduhverfi Deformation Profile – Changes in Position From 1977–1978. The deformation analysis of the Kelduhverfi profile which is, at present, not connected to the main network, shows that the present rift-phase had not yet come to a halt in August 1977 (Fig. 10). The expansion of ~2.0 m over the approximately 3-km-long profile during a period of only 10 months is in the same order of magnitude as the expansion in the Gjástikki region in the previous 2 years.

4. Conclusions

The results of the deformation analyses in the neo-volcanic zone of NE-Iceland which were conducted on the basis of extensive geodetic measurements carried out at intervals of a few years from 1964/1965 onwards can briefly be summarized as follows:

- in the period 1965–1971 compression occurred, for the first time, it was possible to fix the approximate limits of the disturbed zone; the centre of the movement was the south of the study area,
- from 1971–1975 evidence was found of the first significant expansions between points situated on either side of the previously located and confirmed disturbed zone,
- from 1975 to 1977 unusual expansions of up to 1,000 mm/km · a were resolved; the expansion zone can be clearly delineated in the Gjástikki area, a clear definition of the zone is not possible in the south of the study area owing to the greater distances between points here. The direction of the expansion is perpendicular to the rift axis. In areas bordering the rift zone, considerable compression (25 mm/km a) was found which decreases rapidly to the west but only gradually to the east. The maximum expansion detected in the fissure swarm was 2.8 m; the peripheries of the network expanded by only 0.4 m between 1971 and 1977,
- the movements of points inside and at the peripheries of the rift zone exhibit considerable components in the direction of the fissure, but are not continuous or uniform,
- the crustal movements which had increased after 1975 continued beyond 1977.

Acknowledgements. The authors wish to thank the National Research Council of Iceland for giving permission to perform the geodetic measurements in the study areas in Iceland, and their Icelandic colleagues for many fruitful discussions. For permission to use as yet unpublished triangulation data (1978) and height values (1977) they are grateful to Dr. Axel Björnsson, National Energy Authority, Reykjavik, and Professor Dr. H. Spickernagel, Institut für Markscheide- und Bergschadenkunde, Montanuniversität Leoben. They are much obliged to the following institutions for lending valuable geodetic instruments: Deutsches Geodätisches Forschungsinstitut, München (Geodimeter 8), Geodätisches Institut, Technische Universität München (DKM2A), Geodätisches Institut, Universität Karlsruhe (DKM2A), Fachhochschule Hamburg (DKM2A), and Institut für Höhere Geodäsie, Technische Universität Berlin (MRA 4, DKM 2). The authors would also like to thank all those who helped in carrying out field work, often under difficult circumstances. To Professor Dr. K. Gerke, on whose initiative the German geodetic research programme in Iceland was resumed in 1964, we are very much indebted for his untiring efforts directed at

successful and properly coordinated research work. The authors are very grateful to Deutsche Forschungsgemeinschaft which has consistently sponsored the investigations.

References

Björnsson, A., Saemundsson, K., Einarsson, P., Tryggvason, E., Grönvold, K.: Current rifting episode in north Iceland. Nature **266**, 318–323, 1977

Gerke, K.: Ein Beitrag zur Bestimmung rezenter Erdkrustenbewegungen. In: Festschrift zum 70. Geburtstag von Professor Dr.-Ing. Walter Großmann, pp. 66–78, Stuttgart: Wittwer 1967

Gerke, K.: Crustal movements in the Myvatn- and in the Thingvallavatn-area, both horizontal and vertical. In: Geodynamics of Iceland and the North Atlantic Area, L., Kristjansson ed.: pp. 263–275. Dordrecht: Reidel 1974

Gerke, K., Möller, D., Ritter, B.: Geodätische Lagemessungen zur Bestimmung horizontaler Krustenbewegungen in Nordost-Island. In: Festschrift für Walter Höpcke zum 70. Geburtstag, pp. 23–33. Hannover: Lehrstühle für Geodäsie, Photogrammetrie und Kartographie an der TU Hannover 1978

Heumann, F.W. Untersuchungen im geodätischen Sondernetz in Nordost-Island zu Messungen von 1938 und 1965. Dissertation Technische Universität Braunschweig, 1972

Kuntz, E., Möller, D.: Gleichzeitige elektronische Entfernungsmessungen mit Licht- und Mikrowellen. Allg. Vermessungsnachrichten **78**, 254–266, 1971

Niemczyk, O. Spalten auf Island. Stuttgart: Wittwer 1943

Pelzer, H.: Zur Analyse von Deformationsmessungen. Deutsche Geodätische Kommission Reihe C, München **164**, 1971

Pelzer, H. Neuere Ergebnisse der statistischen Analyse von Deformationsmessungen. XIV Intern. Kongreß der Vermessungsingenieure, Inv. Paper Nr 608.3, Washington, 1974

Saemundsson, K. Evolution of the axial rifting zone in northern Iceland and the Tjörnes fracture zone. Bull. Geol. Soc. Am. **85**, 495–504, 1974

Spickernagel, H.: Höhenmessungen in Nord-Island. Mitt. Markscheidewesen **73**, 139–152, 1966

Received May 21, 1979, Revised Version August 1, 1979

J. Geophys. 47, 120–124, 1980

Journal of Geophysics

Results of Height Measurements in Northern Iceland 1965/1977

H. Spickernagel
Institut für Markscheide- und Bergschadenkunde, Montan-Universität Leoben, Franz-Josef-Straße 18, A-8700 Leoben, Austria

Abstract. Results of repeated height measurements in NE Iceland are reported. In 1965 a 142 km levelling line was set up from Akureyri towards east to Jökulsá á Fjöllum. It crosses the entire young volcanic zone of Northern Iceland in WE direction. The observed changes in height should answer the question of the width of the zone of vertical movements related to the volcanic and rifting activity. The results show this width to be 35 km W-E. It is, however, possible that the zone is wider, because the levelling line was too short in the east.

Key words: Iceland rift zone – Changes of height – Precise levelling.

1. Introduction

Niemczyk (1943) and Emschermann made the first geodetic measurements in Northern Iceland in 1938. When in 1965 the measurements could be repeated, and simultaneously expanded, the Institut für Markscheide- und Bergschadenkunde, Montan-Universität, Leoben, Austria, carried out the height measurements. The program for 1965 included also a new 142-km-long-levelling line extending from the port of Akureyri along Eyjafjördur across Vadlaheidi, Másvatn, Mývatn, and Námaskard toward the east to Jökulsá á Fjöllum. The line consisted of more than 150 bench marks. In 1977 the line was remeasured by precision levellings.

2. Conditions and Methods of Measurements

The height measurements involved considerable problems partly from climatic, partly from morphological factors (H. Spickernagel, 1966). The measurements were performed with automatic levelling instruments (Ni 2, Ni 002, KONI 007) equipped with optical micrometers and invar rods with 0.5-cm intervals. The coast stations were stabilized by heavy 7-kg-levelling supports. With the exception of the Ni 002 which was first used in 1977, the same instruments and measuring equipment were employed in all field seasons. The rods had been checked by the Austrian Federal Office of Measures and Weights. The correction for the rod pair between 1965 and 1977 was only ± 0.005 mm/m, a negligible value.

Reading the rods, we followed the recommended change of reading and levelling the instruments when using levels with automatic setting of the sight line. For each instrument the readings were done in the sequence R F F R or F R R F (R=Rear rod reading, F=Forward rod reading). In difficult conditions the sequence of measurements was occasionally disregarded. To counteract this possible source of error, all height measurements were carried out with two instruments resulting in eight values measured per station. The simultaneous use of two instruments represents a safeguard against possible mistakes in reading or writing. Both instruments were positioned symmetrically between the two rods with an accuracy of about ± 0.1 m. The distance between rod positions was, depending on surface conditions, kept at 40 to 60 m. This resulted in sight line distances of 20 to 30 m. However, when crossing ridges or cliffs this had to be reduced to 3 or 6 m occasionally.

3. Evaluation of the Results

The height measurements were evaluated as follows: first, the height differences measured by the two instruments in both directions were compared. Then the mean error per kilometer was calculated in conventional manner, in spite of the disadvantage for instruments with automatic levelling of the sight line. Invariably there are remaining errors which become manifest as systematic errors.

The mean kilometer-errors calculated for the above observational procedure amounted to ± 0.78 mm/km and for the KONI 007 to ± 0.79 mm/km. The height differences and the mean kilometer errors calculated for 14 levelling sections of about 10-km length and for each instrument show no expectional values (Table 1).

The observed height differences between all bench marks are given in the Annex. The mean values of the two-way measurements of the sum of the height differences along the line Akureyri to Jökulsá á Fjöllum amount to

Ni 2/Ni 002 = +364.499 m
KONI 007 = +364.489 m.

The differences over the total distance of 142 km is only 10 mm. Height measurements conducted in 1965 had also shown good agreement of the height differences obtained by both instruments (only 5 mm difference). The mean kilometer-errors in 1965, 0.8 mm/km and 0.7 mm/km, also agree well with those in 1977. Differences between forward and backward levelling of 10 mm (1977) and 5 mm (1965) correspond to 0.84 mm $\sqrt{R}$ and 0.4 mm $\sqrt{R}$ where R is the simple levelling distance in km. The differences are therefore very satisfactory in view of the demands on this kind of precise levelling.

The results of the height measurements in 1977 are compared with those of 1965. Apart of the influence of the current tectonic activity the following points are important:

0340-062X/80/0047/0120/$01.00

Table 1. Subsections of levelling line: height differences and mean kilometer-errors

Sub sections	Pt.-Pt.	Length	Height differences Ni 2/Ni 002	KONI 007	Mean	Mean kilometer errors Ni 2/Ni 002	KONI 007
		(km)	(m)	(m)	(m)	(mm/km)	(mm/km)
I	Adalstr. Nr. 5–5	9.6	+149.934	+149.932	+149.933	0.63	0.73
II	5–22	10.1	+383.646	+383.644	+383.645	0.43	0.46
III	22–N2097	9.3	−397.952	−397.951	−397.952	0.96	0.84
IV	N2097–61	12.9	− 3.089	− 3.088	− 3.088	0.42	0.42
V	61–73	11.3	− 9.888	− 9.888	− 9.888	0.60	0.50
VI	73–311	9.4	− 84.222	− 84.218	− 84.220	0.91	1.12
VII	311–95	10.0	+136.178	+136.178	+136.178	1.12	1.37
VIII	95–105	10.3	+151.220	+151.218	−151.219	1.09	1.13
IX	105–114	10.2	− 51.206	− 51.208	− 51.207	0.61	0.51
X	114–124	10.6	+ 0.865	+ 0.866	+ 0.866	0.73	0.92
XI	124–304	11.7	+ 80.330	+ 80.329	+ 80.329	0.37	0.32
XII	304–136	9.4	+ 36.856	+ 36.849	+ 36.852	0.18	0.53
XIII	136–143	10.2	− 38.254	− 38.250	− 38.252	1.08	0.86
XIV	143–151	11.7	+ 10.120	+ 10.118	+ 10.119	0.93	0.39

$n = 14$

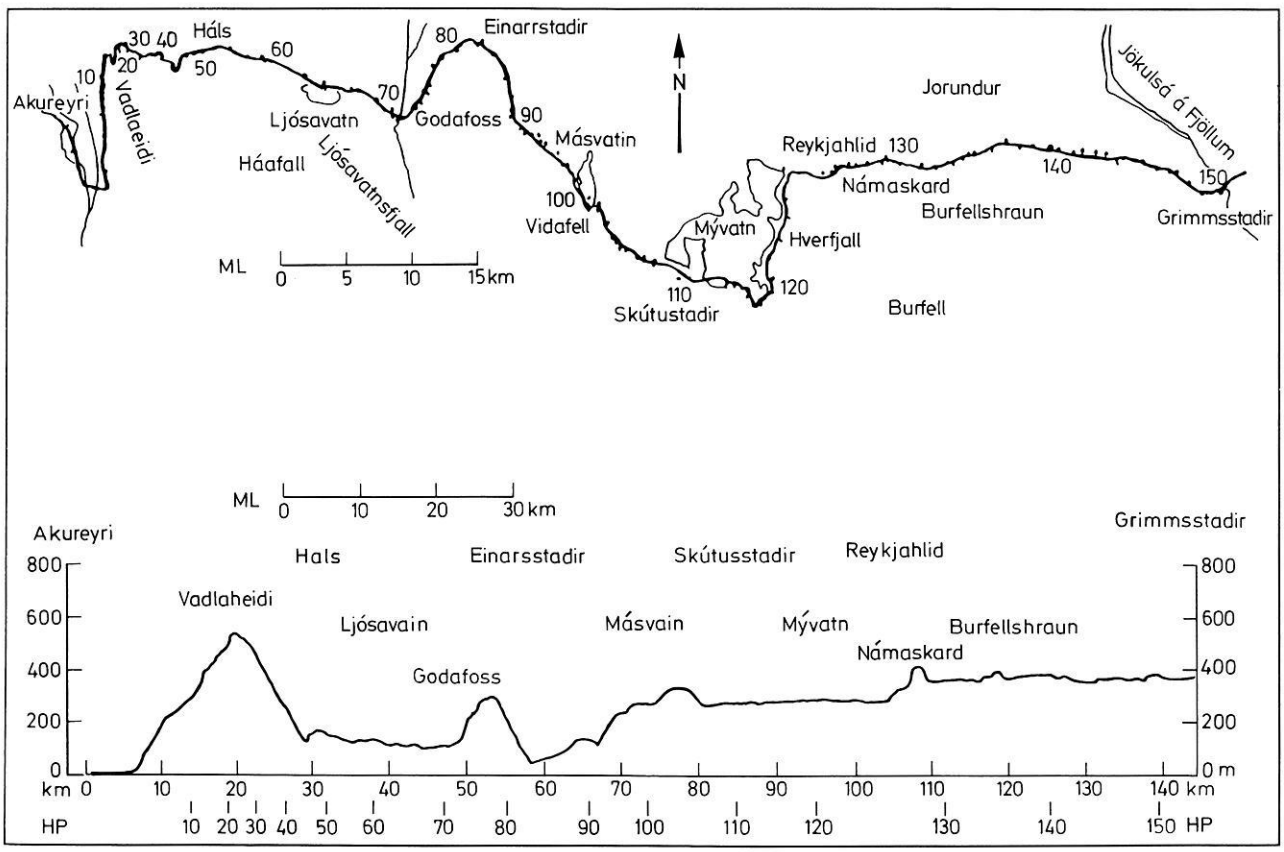

Fig. 1. The levelling line Akureyri-Jökulsá á Fjöllum; location and height profile

- The height change between Akureyri and the bench mark 142 km to the east in the bridge over Jökulsá á Fjöllum is 103 mm.
- Far to the west of the young volcanic zone, the Vadlaheidi area has been uplifted by as much as 65 mm, depending on the interpretation. This cannot be explained by measurement errors.

The levelling line Akureyri – Jökulsá á Fjöllum had been planned in 1965 with the intention to cross the young volcanic zone, and to make certain that the end points could be assumed con-

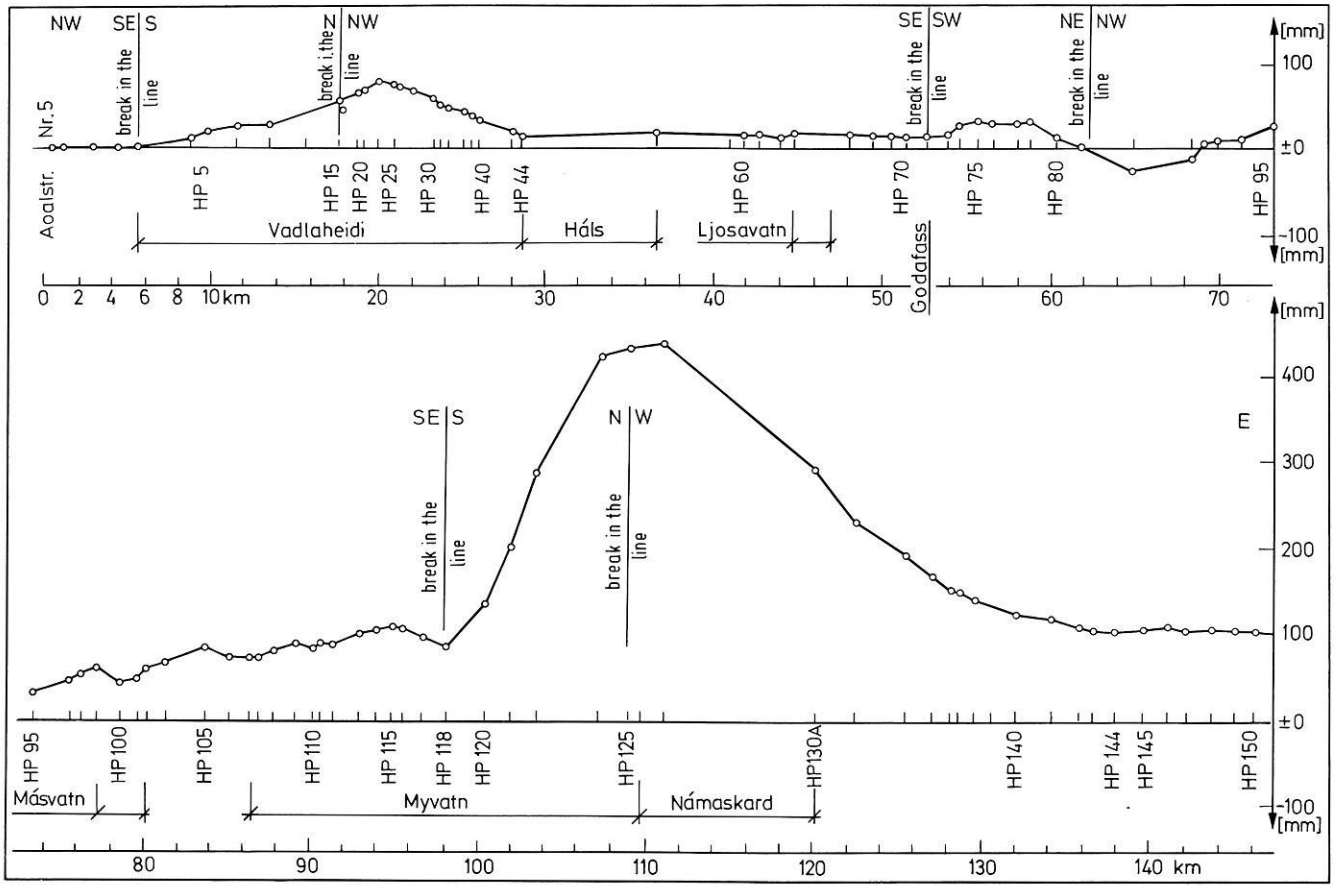

Fig. 2. Levelling line Akureyri-Jökulsá á Fjöllum; uplifts and subsidences between 1965 and 1977

stant; the stations were not to be affected by the recent events in the young volcanic zone. Even in 1965 it had been doubted that the bench marks in the large concrete bridge across Jökulsá á Fjöllum were realy stable. The large canyon through which the river flows represents a major tectonic structure. At the time, however, we were not able to continue our measurements further east because of the early advent of winter.

We then thought that the fix point at Akureyri was sufficiently west of the young volcanic zone to be considered constant. This assumption may require correction: the Vadlaheidi area is not stable in height. Measurements in 1977 revealed uplift of up to 60 mm compared with those of 1965. Only at Bench Mark 2 in a great bolder east of Eyjafjördur and at bench marks on the west side of Eyjafjördur no changes of altitude were observed. This is, of course, true only with respect to the reference station, i.e., bench mark at Adalstraeti No. 5 and must be kept in mind in the geotectonic discussion of northwest Iceland.

The height change between the endpoints of the levelling line by 103 mm is remarkable. Therefore the possibility of systematic errors, has to be investigated. First of all it has to be stated, that the measurements of 1965 and 1977 have been performed under comparable conditions by using the same methods and the same equipment (with the exception of the Ni 002 which has been used only in 1977). Even one of the two observers had been the same. Thus, the systematic errors were probably comparable.

If the heights were referred to the bench marks in the bridge over Jökulsá á Fjöllum a subsidence of 103 mm at the western end of the line would be the result. It is possible that the Akureyri district has changed its vertical position since 1965; but such changes should not be as large as 103 mm. The Akureyri district is assumed to be much more stable than the district of Jökulsá á Fjöllum; therefore the height measurements have been referred to the bench marks in Akureyri.

The levelling profile passes the Mývatn – Námaskard region (Fig. 1), which was affected by the rifting activity centered at Krafla to the north. Figure 2 shows the influence of the volcanic and rifting activity. It is best seen in the stations from HP 87 to HP 142. The maximum amount of 420 mm uplift may not be the final maximum. Movements still took place in September 1977 after our measurements (E. Tryggvason, personal communication). It must also be mentioned, that 6 bench marks had been destroyed between 1965 and 1977 between HP 127 and HP 130a.

The current vertical movements raise the question, whether the uplift of 103 mm in the east may be explained by motion during the progress of measurements. A provisional evaluation was carried out in order to eliminate such possible errors. However, from observations made by the Nordic Volcanological Institute of the University of Iceland, it can be seen that during the time of our height measurements no noticeable vertical movements occurred near the levelling line (E. Tryggvason, personal communication).

Further, the elevation changes deduced from geometrical height measurements were compared with the gravity changes observed by A. Schleusener and W. Torge. Torge and Drewes (1977) confirm that in the Vadlaheidi district gravity decreases

between 1965 and 1975, and between 1975 and 1977. The corresponding elevation factor is about 0.15 mgal/m. In addition, we have noted new cracks of 1 to 3 cm width in the area around Peturskirkja in 1977. In spite of the considerable scatter of gravity values in general the gravity measurements concur with the geometric height measurements.

After all these checks, we can offer no other explanation for the 103 mm uplift at the east end of the profile than that it is real.

4. Conclusions

The evaluation of the height measurements performed in 1965 and 1977 between Akureyri and Jökulsá á Fjöllum has had the following results:

1. Uplift has occurred in the Vadlaheidi district, far to the west of the young volcanic zone of Northern Iceland. This is interpreted to be of tectonic nature.
2. The volcanic and rifting episode since 1975 (until August 1977) has influenced the profile Akureyri – Jökulsá á Fjöllum. This influence was particularly pronounced in the profile section between bench mark HP 100 and HP 140. The length of the section is 54 km, projected onto the east-west direction, 35 km.
3. Because of the loss of six bench marks in the Námaskard district the maximum uplift until the end of August 1977 could probably not be observed, for the same reason, subsidence in the central zone (e.g., Torge and Kanngieser, 1979) has not been seen. The location of the maximum uplift may not have been determined. Maximum uplifts amount to more than 420 mm. The direct distance to the Krafla volcano is about 7 km.
4. East of HP 143 an almost constant uplift of 103 mm has taken place with respect to Akureyri. This extends across about 10 km to Jökulsá á Fjöllum. A comparison with gravity observations appears to confirm the uplift.

Acknowledgements. The author is thankful to the Nordic Volcanological Institute of the University of Iceland, and especeally to Dr. Eysteinn Tryggvason as well as to Professor W Torge, Institut für Theoretische Geodäsie, Technische Universität Hannover, for relevant information. The author is very grateful to Fonds zur Förderung der wissenschaftlichen Forschung in Österreich.

Annex

Akureyri to Jökulsá á Fjöllum: mean of the height differences 1977

Pt.	Ni 2/ Ni 002 m	KONI 007 m	Pt.	Ni 2/ Ni 002 m	KONI 007 m	Pt.	Ni 2/ Ni 002 m	KONI 007 m	Pt.	Ni 2/ Ni 002 m	KONI 007 m
Adalstr. Nr. 5	− 3.954	− 3.954	HP 61	− 25.127	− 25.127	HP 100	− 7.302	− 7.301	HP 139	+ 3.117	+ 3.116
Adalstr. Nr. 21	+ 0.435	+ 0.432	HP 62	+ 6.288	+ 6.288	HP 101	− 0.349	− 0.348	FM 320	+ 5.183	+ 5.183
HP 1	+ 0.916	+ 0.916	HP 63	− 0.165	− 0.166	HP 102	+39.858	+39.858	HP 140	−19.051	−19.053
HP 2	+ 90.402	+ 90.403	HP 64	+ 4.637	+ 4.638	HP 103	+14.950	+14.948	FM 107	− 0.502	− 0.503
HP 4	+ 62.136	+ 62.135	HP 66	−21.910	−21.910	HP 104	− 0.995	− 0.995	HP 141	− 0.310	− 0.307
HP 5	+ 68.080	+ 68.080	HP 67	+ 0.920	+ 0.920	HP 105	−38.257	−38.255	HP 142	− 8.634	− 8.634
HP 6	+ 6.377	+ 6.377	HP 68	+ 8.053	+ 8.053	HP 107	−33.856	−33.856	HP 143	− 1.730	− 1.728
HP 7	+ 15.764	+ 15.763	HP 69	+ 3.103	+ 3.104	FM 2	+ 1.368	+ 1.368	HP 144	+ 5.008	+ 5.006
HP 8	+ 10.815	+ 10.815	HP 70	− 3.728	− 3.726	HP 108	+ 5.681	+ 5.681	HP 145	+11.131	+11.129
HP 9	+ 50.580	+ 50.579	HP 71	− 0.018	− 0.018	HP 109	+10.770	+10.769	HP 146	−11.446	−11.449
HP 11	+ 31.868	+ 31.869	HP 72	+17.759	+17.759	FM 6415	+ 8.913	+ 8.913	HP 147	+ 5.853	+ 5.854
HP 13	+100.311	+100.312	HP 73A	+ 0.262	+ 0.262	HP 110	− 1.704	− 1 704	HP 148	+11.403	+11.403
HP 15	+ 1.890	+ 1.890	HP 73	+52.396	+52.396	HP 111	− 4.741	− 4.741	HP 149	+ 5.819	+ 5.818
HP 16	+ 39.232	+ 39.232	HP 74	+63.982	+63.984	HP 112	+ 7.721	+ 7.720	HP 150	−15.917	−15.918

Pt.	Ni 2/ Ni 002	KONI 007	Pt.	Ni 2/ Ni 002	KONI 007	Pt.	Ni 2/ Ni 002	KONI 007	Pt.	Ni 2/ Ni 002	KONI 007
	m	m		m	m		m	m		m	m
HP 19			HP 75			HP 113			HP 151		
	+ 20.566	+ 20.567		+ 8.130	+ 8.130		− 7.103	− 7.102			
HP 20			HP 76			HP 114					
	+ 38.162	+ 38.162		+26.142	+26.142		− 0.243	− 0.242			
HP 22			HP 77			HP 115					
	− 3.705	− 3.705		+24.679	+24.679		+ 0.922	+ 0.922			
HP 23			HP 78			HP 116					
	− 12.558	− 12.558		− 7.144	− 7.144		− 1.570	− 1.571			
HP 24			HP 79			HP 117					
	− 7.604	− 7.604		−90.380	−90.379		+ 0.678	+ 0.679			
HP 25			HP 80			HP 118					
	− 6.654	− 6.654		−83.842	−83.841		+ 2.100	+ 2.100			
HP 26			HP 81			HP 120					
	+ 1.477	+ 1.477		−26.092	−26.092		+ 8.384	+ 8.384			
HP 27			HP 82			HP 121					
	− 20.483	− 20.483		−32.222	−32.223		− 6.167	− 6.165			
HP 28			HP 84			HP 122					
	− 22.299	− 22.298		+40.686	+40.685		− 3.240	− 3.241			
HP 29			HP 86			HP 124					
	− 10.103	− 10.103		+30.601	+30.600		+ 4.754	+ 4.754			
HP 30			HP 87			HP 125					
	− 28.004	− 28.003		+ 9.561	+ 9.561		− 6.580	− 6.579			
HP 31			HP 88			Kongsp.					
	− 22.934	− 22.934		− 3.079	− 3.079		+15.686	+15.686			
HP 32			HP 89			FM 5604					
	− 21.987	− 21.987		+ 0.544	+ 0.544		+26.445	+26.446			
HP 33			HP 89A			HP 127					
	− 55.713	− 55.714		−10.483	−10.484		− 0.016	− 0.017			
HP 36			HP 91			FM 6412					
	− 24.113	− 24.113		−21.635	−21.634		+37.799	+37.795			
HP 37			HP 92			FM 115					
	− 16.240	− 16.239		+40.348	+40.348		+ 7.074	+ 7.072			
HP 38			HP 93			HP 130A					
	− 32.276	− 32.275		+ 9.839	+ 9.839		− 0.556	− 0.561			
HP 40			HP 94			HP 133					
	− 58.697	− 58.697		+19.924	+19.924		+18.093	+18.092			
HP 42			HP 95			HP 135					
	− 40.995	− 40.995		+65.542	+65.543		+14.487	+14.488			
HP 44			HP 97			HP 136					
	− 21.010	− 21.008		+23.748	+23.748		−24.140	−24.138			
HP 312			HP 98			HP 137					
	− 8.632	− 8.632		+ 7.508	+ 7.508		+ 2.794	+ 2.797			
HP 59			M 6			HP 138					
	+ 11.657	+ 11.656		+ 0.071	+0.071		− 0.002	− 0.002			
HP 60			HP 99			FM 109					
	− 0.170	− 0.170		+ 8.189	+ 8.187		+ 3.290	+ 3.292			
HP 61			HP 100			HP 139					

References

Niemczyk, O. Spalten auf Island. Stuttgart. Wittwer 1943

Spickernagel, H. Höhenmessungen in Nord-Island. Mitt. Markscheidewesen **73**, 139–152, 1966

Torge, W., Drewes, H.: Gravity variations with time in Northern Iceland 1965–1975. J. Geophys. **43**, 771–790, 1977

Torge, W., Kanngieser, E.: Gravity and height variations during the present rifting episode in Northern Iceland. J. Geophys. 125–131, 1980

Received March 29, 1979; Revised Version June 19, 1979

J. Geophys. 47, 125–131, 1980

Journal of Geophysics

Gravity and Height Variations During the Present Rifting Episode in Northern Iceland

W. Torge and E. Kanngieser
Institut für Theoretische Geodäsie, Universität Hannover, Nienburger Str. 6, D-3000 Hannover 1, Federal Republic of Germany

Abstract. In 1975, a rifting episode started in the neovolcanic zone of northern Iceland, consisting of a succession of slow inflation periods and rapid subsidence events, which is still going on. The center of activity is situated below the Krafla caldera, and the rifting process is affecting the 80-km-long fissure swarm associated with this central volcano. Gravity and height variations associated with this process have been investigated by re-observing profiles earlier established in the Námafjall and in the Gjástikki area, situated nearly 10 km south and north of Krafla respectively, as well as by the re-observation of a number of gravity stations in the northern part of the fissure zone, in 1976, 1977, and 1978. By repeated observations with 2 or 3 LaCoste-Romberg gravity meters, the accuracy obtained in each gravity survey is of the order of $\pm 10 \times 10^{-8}$ ms^{-2}. In the profiles crossing the fissure zones, a rate of gravity increase of more than 100×10^{-8} ms^{-2}/a has been found in the central part, while gravity at the flanks decreases at the same order. These variations are correlated with subsidence and elevation rates of the order of 0.5 m/a.

Key words: Icelandic rift zone – Recent gravity and height variations – Precise gravity measurements.

1. Introduction

Repeated gravity measurements in areas of earthquake and volcanic activity are an information source about the mass displacements occurring especially in the vertical direction. Among other regions, northern Iceland is an outstanding area of investigation into this problem, especially since 1975, when a rifting episode started there. Continuing former gravity surveys in this region, the Institut für Theoretische Geodäsie, Universität Hannover, carried out gravity and height measurements along three profiles in the area of current activity, in the years 1976–1978. After a short description of the present rifting episode, the gravity and height measurements are presented and the resulting variations discussed.

The neovolcanic zone in Iceland represents a supramarine part of the axial rift zone of the Mid-Atlantic Ridge and thus the plate boundary between the American and the Eurasian tectonic plates (for a detailed description, see e.g., Pálmason and Saemundsson, 1974). In northern Iceland, this zone has a north-south direction and a width of 50 to 80 km. In the east and west it is bordered by Pleistocene basalts followed by Tertiary plateau basalt, which form the larger part of Iceland. Volcanic and earthquake activity of the neovolcanic zone is restricted to a few north-south striking fissure swarms of several kilometers width; one of them is the Krafla-swarm, which passes through the caldera of the Krafla volcano (Fig. 1, Björnsson et al., 1977). Since the extensive volcanic and tectonic events in the Krafla-Námafjall area between 1724 und 1729, this fissure swarm has been inactive until 1975. On December 20, 1975, a basaltic eruption occurred at Leirhnjúkur in the Krafla caldera, associated with an intense earthquake swarm and significant ground movements. This opened the current period of activity, which forms a rifting episode within the kinematic processes at a constructive plate boundary (Björnsson, 1976). The activity center is below the Krafla caldera, where the ground undergoes slow uplift movements (maximum ~7 mm/d in the center) over some months, interrupted by short subsidence (maximum ~2 m) pulses of a few days duration. The latter are accompanied by earthquake and thermal activity, fissure formation and vertical ground movements along the Krafla

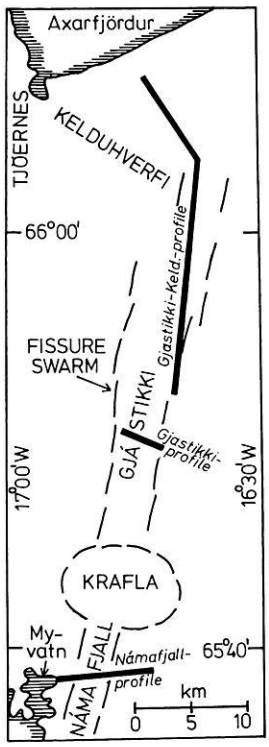

Fig. 1. Location of gravity profiles observed in northern Iceland between 1965 and 1978

0340-062X/80/0047/0125/$01.40

fissure zone at different locations during the single pulses. This rifting process is very carefully monitored by the Icelandic scientists, employing a broad spectrum of different observation methods, which include levelling, tilt and gravity measurements (Björnsson, 1976; Björnsson et al., 1977; 1978).

In the region in question, high precision gravity measurements have been carried out since more than 10 years by the Institut für Theoretische Geodäsie, Technische Universität Hannover. They form the basis for the comparison with the more recent observations.

2. Gravity Measurements in the Rift Zone

Gravity measurements in the neovolcanic zone of northern Iceland started in 1938, when Schleusener (1943) established 40 gravity stations, in order to investigate the regional gravity field and by later repetition measurements, its variation with time. Re-observations had been taken up in 1964 and were continued in 1965, 1967, 1970, 1971, and 1975, now employing LaCoste-Romberg (LCR) gravity meters. As the result we now have

- a monumented high-precision ($\pm 10 \times 10^{-8}$ ms^{-2})[1] *gravity profile* crossing the neovolcanic zone in *west-east-direction* ($\phi \sim 65°40'$) and covering about 50 km of the adjoining Pleistocene and Tertiary basalt zones (profile length ~150 km, average station spacing 1 km). This profile has been observed in 1965, 1970/1971, and 1975. The comparison of the results revealed for this epoch a gravity increase in the neovolcanic zone relative to the basalt zones, reaching $+7.8 \times 10^{-8}$ ms^{-2}/a. The maximum gradient of variation occurred in the Myvatn-Námafjall part of the profile, which is part of the Krafla fissure swarm (see Fig. 1); Schleusener and Torge (1971), Torge and Drewes (1977a);
- a *regional gravity control* of about 1000 stations ($\pm 20...30 \times 10^{-8}$ ms^{-2}) covering the neovolcanic zone and the adjoining older basalt zones between 65°30–66°10′ N and 18°10′–15° W, observed between 1964 and 1970; Schleusener et al. (1976);
- *gravity profiles* ($\pm 20 \quad 30 \times 10^{-8}$ ms^{-2}) across *local geological structures,* including the monumented profile crossing the *Gjástikki* fissure zone (observed 1965), about 10 km north of the Krafla caldera, Schleusener (1974).

In order to investigate the gravity influence of mass displacements connected with the present rifting process, repeated gravity and, partly, also height measurements have been carried out at different locations of the Krafla fissure swarm, in 1976, 1977, and 1978.

The surveys were concentrated on three *profiles,* see Fig. 1

- the Námafjall-profile (length ~8 km), part of the west-east profile situated nearly 10 km south of the Krafla caldera,
- the Gjástikki profile (length ~3 km),
- the Gjástikki-Kelduhverfi profile (length ~30 km).

The Námafjall- and the Gjástikki-profiles cross the Krafla fissure zone, while the Gjástikki-Kelduhverfi profile follows this zone. Details are given in Table 1 From the adjustments of the different epochs *r.m.s. errors of one observed gravity difference* have been derived and are given in Table 2. Linear drift factors, obtained from the adjustments, do not exceed 1 2×10^{-8} ms^{-2}/h and are hardly significant.

The *gravity datum* in the single epochs is given by the gravity value at the base station Akureyri 60932 (western edge of the west-east profile) to which the gravity profiles have been connected via intermediate base stations. This value ($g = 982{,}348.39 \times 10^{-5}$ ms^{-2}, Potsdam gravity system with $g = 981{,}277.30 \times 10^{-5}$ ms^{-2} Hannover 21629 A) has been kept fixed since 1965, as the frequent control to the station Hannover (via Reykjavik) did not reveal a significant gravity change there. The results of the gravity measurements between Hannover and Iceland, in 1976, 1977, and 1978, are given in Annex 1 Linear *calibration factors* for the instruments have been derived in the scale of the International Gravity Standardization Net 1971 (IGSN71) by a gravity survey along a special calibration line established 1975 in Norway, at the Iceland gravity range. The calibration factor for LCR G 298 has been determined from the gravity difference Hannover-Akureyri, measured 1975 simultaneously with LCR 79, 85, 87, and 298 (Torge and Drewes, 1977a). Due to the installation of a new long lever with welded pivot in LCR G 79 (November 1976) the calibration changed. The value for 1978 was derived from the D14 measurements carried out simultaneously. The calibration factors are given in Table 3.

Tidal reductions have been calculated using the Cartwright-Tayler-Edden development and regional tidal parameters for the main waves, which were determined 1975 at the temporary gravimetric earth tide station Laugaskoli, near the west-east profile (Torge and Wenzel, 1976).

From the adjustments, *r.m.s. errors* of the final *gravity values* at the single epochs, referring to the base station Akureyri, are

Table 1. Statistics of gravity observations

Epoch	Observation period	Number of stations	LCR gravity meters	Observations per station
Námafjall-profile				
1975	23.7.–28.7.	9	G79, G85 G87, D14	4
1976	6.8.– 7.8.	14	G79, G85	2
1977	8.8.–16.8.	18	G298, D14	4
1978	24.7.–28.7.	19	G79, D14	6
Gjástikki-profile				
1976	10.8.	10	D14	1
1977	9.8.–15.8.	16	G298, D14	2···3
1978	30.7.– 1.8.	14	G79, D14	4
Gjástikki-Kelduhverfi-profile				
1976	4.8.–6.8.	12	D14	1
1978	26.7.–2.8.	12	G79, D14	2

Table 2. R.m.s. errors of single observed gravity differences

Observed gravity difference: r.m.s. error (10^{-8} ms^{-2})				
Epoch	G79	G85	G298	D14
1976	±14	±14	–	±31
1977	–	–	±16	±13
1978	±15	–	–	±12

[1] 1×10^{-8} ms^{-2} = 1 μgal, 1×10^{-5} ms^{-2} = 1 mgal

Table 3. Calibration factors of gravimeters used

G 79 (1976)	1.00055 ± 0.00007
G 79 (1978)	1.00069 ± 0.00005
G 85	0.99988 ± 0.00010
G298	1.00098 ± 0.00002
D 14	1.00031 ± 0.00009

Table 4. R.m.s. errors of final gravity values in single epochs

Adjusted gravity: r.m.s. error (10^{-8} ms^{-2})			
Profile	1976	1977	1978
Námafjall	$\pm 3 \cdots 16$	$\pm 6 \cdots 10$	$\pm 8 \cdots 12$
Gjástikki	± 20	$\pm 10 \cdots 16$	$\pm 8 \cdots 15$
Gjást.-Keld.	± 20	–	$\pm 9 \cdots 17$

obtained (Table 4). We may conclude that in each profile a relative accuracy, with respect to the other profile stations, of $\pm 10 \times 10^{-8}$ ms^{-2} has been achieved.

As in the previous epochs, the *heights* of the gravity stations in the *Námafjall-profile* have been determined by geometric levelling in 1976···1978, simultaneously with the gravity measurements. A Zeiss Ni2 automatic level has been used, and the readings were controlled by double turning points (1976) or by forth and back levelling. From the misclosures obtained in 1977 and 1978, the r.m.s. error of the heights, referring to the height datum of the corresponding epoch, is estimated to be ± 0.01 to 0.02 m.

The *height datum* is

1976: profile station no. 110, about 20 km west of the starting point of the Námafjall profil, connected to it by geometric levelling. The height of this station, which according to the 1976 survey is not affected by the present activity, is given in the height system introduced by Spickernagel (1966),

- 1977: the heights of the bench marks of the precise levelling 1976 along the profile Akureyri-Grimsstadir, carried out by Prof. Spickernagel, Leoben, Austria, and kindly made available to us before final publication,
- 1978: the height of the bench mark HP 302 in the eastern part of the profile which according to the 1978 gravity survey should not have significantly changed between 1977 and 1978.

Height determination in the *Gjástikki profile* has been carried out in 1978, by geometric levelling and (at one steep slope) by trigonometric levelling, simultaneously with the gravity measurements. The relative accuracy within the profile is estimated to be ± 0.01 to 0.02 m.

The height datum was derived from the 1977 height of station no. 82544, situated at the northwestern end of the profile. The station heights 1977 have been determined by the Institut für Vermessungskunde, Technische Universität Braunschweig (Professor Möller), between August 8 and 11, 1977, and kindly put at our disposal before publication.

The results of the gravity and height measurements are given in Annexes 2–4.

3. Comparison of the Gravity and Height Observations 1976–1978

The gravity and height variations with time observed along the *Námafjall profile* are given in Fig. 2 (Δg and ΔH). Reference epoch for all observations is 1965, when gravity and height measurements started.

The straight lines connecting the observed point differences have been drawn for clarity only and have no physical meaning (this is valid also for Figs. 3–5). The changes at the additional

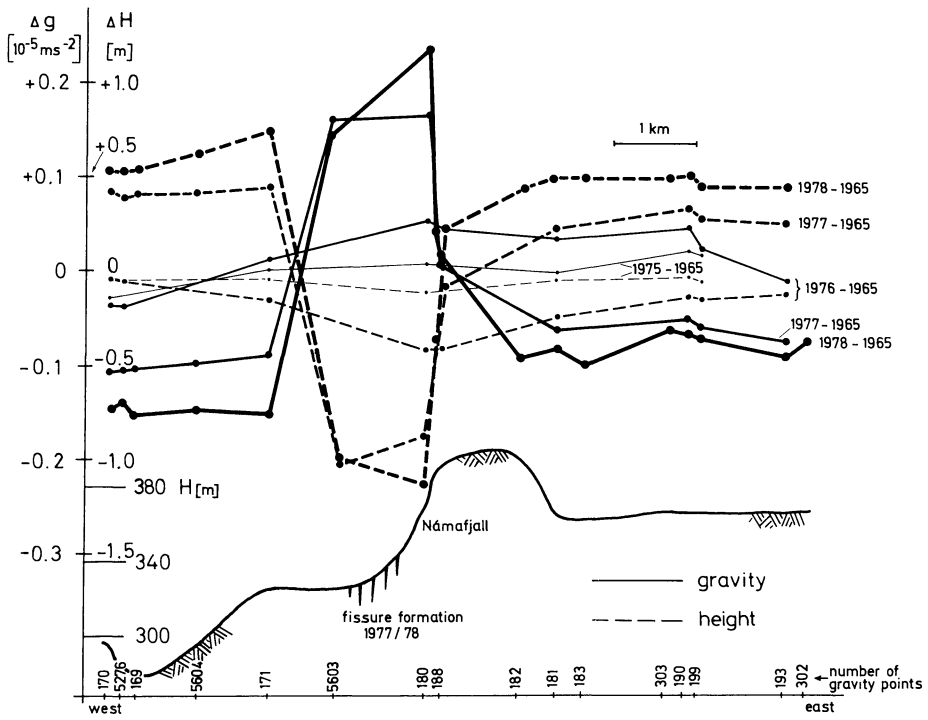

Fig. 2. *Námafjall gravity profile,* northern Iceland: *Gravity and height variations between 1975 and 1978,* referred to epoch 1965. Additional intermediate values interpolated from previous epoch, assuming linear behaviour of variations. Height datum 1978 fitted to gravity datum in western part of profile

stations, established in the periods following the reference epoch, have been fitted to the previous variation curves by adding them the to corresponding straight lines (this is valid also for Fig. 3).

The *comparison 1975–1965* indicates a small gravity increase ($+20$ to 30×10^{-8} ms^{-2}) west of Námafjall, correlated with a few centimeters ground subsidence. The rifting process which started in December 1975 affected the profile stations more strongly. For *1976–1975* we find that gravity decreased slightly at the western (lake Myvatn) and the eastern border of the profile ($\sim-10\times10^{-8}$ ms^{-2}). It increased at the western edge of Námafjall (maximum $+40$ to 50×10^{-8} ms^{-2}) in connection with a subsidence of -0.3 m. For *1977–1976* the continuing activity in the Krafla area led to a considerable gravity decrease in the western part of the profile (-70 to 100×10^{-8} ms^{-2}), correlated with a rise of $+0.3$ to 0.5 m. The same is true for the eastern part of the profile (-30 to 100×10^{-8} ms^{-2}, $+0.3$ to 0.4 m). Since 1977 fissure formation and thermal activity occurred at the western edge of Námafjall, giving a maximum gravity increase of $+110$ to 130×10^{-8} ms^{-2} and a corresponding subsidence of 0.5 to 0.8 m. Between *1978 and 1977* these tendencies continued, although with smaller magnitude. Gravity decrease in the western part of the profile amounted to 30 to 60×10^{-8} ms^{-2}, and in the eastern part to 10 to 50×10^{-8} ms^{-2}, the corresponding uplifts were 0.1 to 0.3 m and 0.2 to 0.3 m, respectively. The gravity increase west of Námafjall reduced to 70×10^{-8} ms^{-2}, and the subsidence to 0.3 m. H. Spickernagel (1980) could not detect these local height variations, as his stations were destroyed in this region.

In the comparison 1978–1977, the height datum 1978 has been changed no longer assuming that station no. HP 302 did not vary between 1977 and 1978. For station no. 5276, at the western edge of the profile, the gravity change of -35×10^{-8} ms^{-2} has been converted into a height change of $+0.18$ m with the gravity/height factor -0.2×10^{-5} ms^{-2}/m. By this transformation, an average conversion factor of -0.2×10^{-5} ms^{-2}/m has been obtained for the profile. This Bouguer-type relation (density 2.6 g/cm^3) has been found also from the comparison 1977–1976.

Figure 3 gives the gravity variations along the *Gjástikki profile*, referred to the first observation epoch 1965. The gravity decrease at the flanks is even more pronounced than in the Námafjall profile with a similar magnitude in different comparisons (NW: 60 to 100×10^{-8} ms^{-2}/a, SE: 100 to 170×10^{-8} ms^{-2}/a). A small zone of the central part, with new fissures and thermal activity since 1977/1978, shows a gravity increase of 50 to 110×10^{-8} ms^{-2}/a. Transforming these values into height varia-

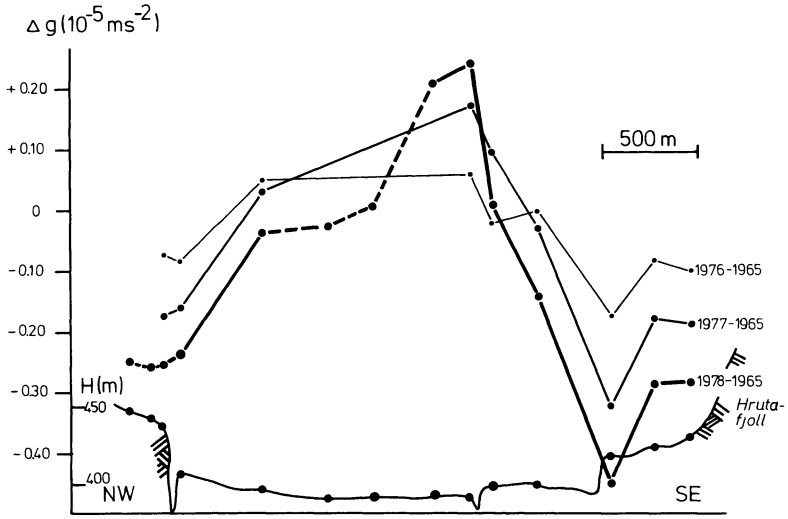

Fig. 3. *Gjástikki gravity profile,* northern Iceland: *Gravity variations between 1965 and 1978,* referred to epoch 1965. Additional intermediate values interpolated from previous epoch, assuming linear behavious of variations

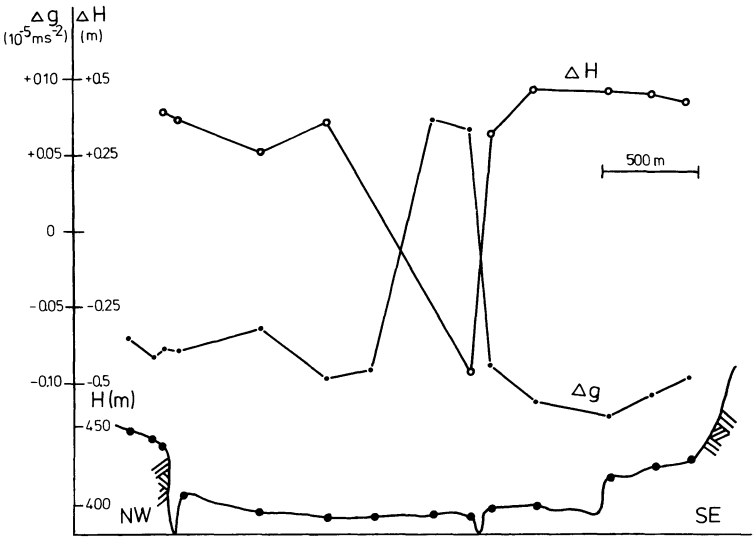

Fig. 4. *Gjástikki gravity profile,* northern Iceland. *Gravity and height variations 1978–1977.* Height datum 1978 fitted to gravity datum in northwestern profile part. Heights 1977 from Geodetic Institute, Technische Universität Braunschweig

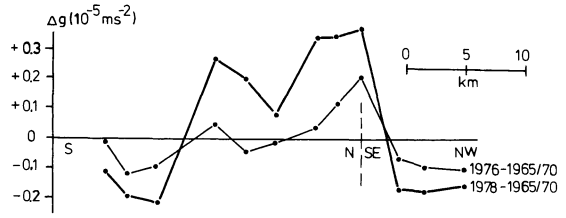

Fig. 5. *Gjástikki-Kelduhverfi gravity profile,* northern Iceland: *Gravity variations between 1965/1970* and 1978, referred to epoch 1965/1970

tions with the factor of -0.2×10^{-5} ms^{-2}/m, we obtain for 1978–1977 a maximum subsidence relative to the flanks of 0.80 m (NW) and 0.97 m (SE), respectively. This is in good agreement with the height variation directly observed (Fig. 4) of −0.83 m and −0.93 m, respectively.

The height datum 1978 has been corrected, since according to the gravity variations all profile stations had changed, between 1977 and 1978. For station no. 544 (NW edge of the profile) the gravity variation of -77×10^{-8} ms^{-2} was transformed into a height change of +0.39 m

The gravity variations along the *Gjástikki-Kelduhverfi profile* are given in Fig. 5. They refer to the inactive epoch 1965/1970, when the regional gravity stations in north Iceland had been established. There is a significant gravity variation of different sign along the profile, of magnitudes $\pm 200 \times 10^{-8}$ ms^{-2}/a and more with three areas of gravity decrease and two of gravity increase (corresponding to uplift and subsidence). Dimensions are 5 to 10 km.

4. Conclusions

From gravity and height measurements in the Krafla fissure swarm, carried out during the current rifting episode, and from the comparison with previous observations we conclude that

- a slight gravity increase south of the Krafla caldera occurred before the beginning of the present episode, possibly a precursor of the later activity;
- activated areas south and north of Krafla are characterized by gravity decrease and uplift at the flanks, and by gravity increase and subsidence in narrow central zones;
- the magnitude of the observed variations in gravity and height reaches the order of $\pm 100 \times 10^{-8}$ ms^{-2}/a and ±0.5 m/a, respectively;
- the gravity/height relationship corresponds approximately to a Bouguer-type factor, although with some scattering;
- with a stable gravity datum an uncontrolled height datum can be corrected,
- activated areas along the fissure swarm show gravity variations of $\pm 200 \times 10^{-8}$ ms^{-2}/a and more;
- individual regions of the fissure swarm have generally changed height and gravity without change in sense during the whole observation period from 1975 to 1978 revealing some kind of continuity;
- according to the 1978 survey, the period of activity is still in progress.

These results, and hopefully also future observations, will contribute to the understanding of the mass movements in time and space which are related to the present rifting episode.

Acknowledgements. The authors thank the National Research Council of Iceland for the permission to carry out the gravity surveys in northern Iceland. For fruitful discussions they are grateful to Dr Axel Björnsson and Dr. Gudmundur Pálmason, National Energy Authority, and to Dr. Eysteinn Tryggvason, Nordic Volcanological Institute, Reykjavik. They are much obliged to Professor Dr. S. Heitz, Geodätisches Institut, Technische Universität Berlin, for lending the LCR-Gravity meter no. 85, and to Professor Dr. D. Möller, Institut für Vermessungskunde, Technische Universität Braunschweig, and Professor Dr. H. Spickernagel, Institut für Markscheide- und Bergschadenkunde, Montanuniversität Leoben, for making available the height values 1977 of the Gjástikki and Námafjall profil. Calculations have been carried out at the CDC 73/76 of the Regional Computing Centre of Lower Saxony. Beside the authors, the following persons participated in the field surveys: W. Adolf (1976, 1978), H. Drewes, H. Lehrke, G. Terwey (1976), A. Weise (1976, 1978). The authors are very grateful to Deutsche Forschungsgemeinschaft for generous financial support.

Annex 1. Gravity connection Hannover – Reykjavik – Akureyri 1976–1978[a]

No.	Instrument	Observer	Station	No.	Date	Time (UT)	Reading	Manufacturer's scale	Tidal correction	Corrected mgal-value
1	G 79	Drewes	Hannover	21629A	31.7.76	5.02	4555.648	4723.165	−0.037	4723.128
2	G 79	Drewes	Reykjavik	21941L	31.7.76	17.47	5519.455	5723.621	−0.058	5723.563
3	G 79	Drewes	Akureyri	60932	31.7.76	20.46	5586.979	5793.701	−0.095	5793.606
4	G 85	Lehrke	Hannover	21629A	31.7.76	5.02	4661.090	4826.626	−0.037	4826.589
5	G 85	Lehrke	Reykjavik	21941L	31.7.76	17.28	5626.248	5827.665	−0.054	5827.611
6	G 85	Lehrke	Akureyri	60932	31.7.76	20.32	5693.856	5897.765	−0.093	5897.672
7	G 79	Drewes	Akureyri	60932	18.8.76	13.35	5586.964	5793.686	−0.042	5793.644
8	G 79	Drewes	Reykjavik	21941L	18.8.76	16.28	5519.478	5723.645	−0.065	5723.590
9	G 85	Lehrke	Akureyri	60932	18.8.76	13.22	5693.915	5897.826	−0.040	5897.786
10	G 85	Lehrke	Reykjavik	21941L	18.8.76	16.14	5626.332	5827.752	−0.062	5827.690
11	G 79	Drewes	Reykjavik	21941L	21.8.76	4.14	5519.522	5723.691	−0.067	5723.624
12	G 79	Drewes	Keflavik	21941K	21.8.76	6.39	5515.731	5719.756	−0.030	5719.726
13	G 79	Drewes	Hannover	21629A	21.8.76	17.22	4555.787	4723.310	−0.086	4723.224
14	G 85	Lehrke	Reykjavik	21941L	21.8.76	4.07	5626.390	5827.812	−0.067	5827.745
15	G 85	Lehrke	Keflavik	21941K	21.8.76	6.28	5622.559	5823.840	−0.033	5823.807
16	G 85	Lehrke	Hannover	21629A	21.8.76	17.22	4661.263	4826.805	−0.086	4826.719

Annex 1 (Continued)

No.	In-strument	Observer	Station	No.	Date	Time (UT)	Reading	Manufacturer's scale	Tidal correction	Corrected mgal-value
17	G298	Kanngieser	Hannover	21629A	6.8.77	5.33	4731.240	5005.818	+0.015	5005.833
18	G298	Kanngieser	Keflavik	21941K	6.8.77	14.34	5672.207	6002.048	−0.051	6001.997
19	G298	Kanngieser	Reykjavik	21941L	6.8.77	20.01	5675.921	6005.978	−0.072	6005.906
20	G298	Kanngieser	Akureyri	60932	6.8.77	22.21	5742.114	6076.034	−0.085	6075.949
21	D 14	Lehrke	Reykjavik	21941L	6.8.77	20.06	25.033	27.887	−0.072	27.815
22	D 14	Lehrke	Akureyri	60932	6.8.77	22.37	87.958	97.985	−0.085	97.900
23	G298	Kanngieser	Keflavik	21941K	20.8.77	5.52	5672.436	6002.290	−0.019	6002.271
24	G298	Kanngieser	Hannover	21629A	20.8.77	15.30	4731.580	5006.178	−0.023	5006.155
25	G 79	Lehrke	Hannover	21629A	22.7.78	5.26	4621.897	4791.935	−0.095	4791.840
26	G 79	Lehrke	Keflavik	21941K	23.7.78	8.05	5582.121	5788.659	−0.084	5788.575
27	G 79	Lehrke	Reykjavik	21941L	23.7.78	10.44	5585.855	5792.535	−0.068	5792.467
28	G 79	Lehrke	Akureyri	60932	23.7.78	13.02	5653.311	5862.541	−0.034	5862.507
29	D 14	Kanngieser	Reykjavik	21941L	23.7.78	10.48	43.372	48.316	−0.067	48.249
30	D 14	Kanngieser	Akureyri	60932	23.7.78	12.47	106.226	118.336	−0.038	118.298
31	G 79	Lehrke	Akureyri	60932	5.8.78	7.57	5653.735	5862.981	−0.073	5862.908
32	G 79	Lehrke	Reykjavik	21941L	5.8.78	11.10	5586.181	5792.873	−0.024	5792.849
33	G 79	Lehrke	Keflavik	21941K	5.8.78	14.05	5582.385	5788.933	+0.010	5788.943
34	G 79	Lehrke	Hannover	21629A	5.8.78	22.33	4622.300	4792.354	−0.045	4792.309
35	D 14	Kanngieser	Akureyri	60932	5.8.78	7.37	106.726	118.893	−0.075	118.818
36	D 14	Kanngieser	Reykjavik	21941L	5.8.78	10.56	43.781	48.772	−0.028	48.744

[a] The results of the gravity measurements in 1975 are given in Torge and Drewes (1977a)

Annex 2. Gravity and height values 1976, 1977, and 1978 along the Námafjall profile[a]

Station no.	ϕ (°)	λ west (°)	g (1976) (10^{-5} ms^{-2})	g (1977) (10^{-5} ms^{-2})	g (1978) (10^{-5} ms^{-2})	H (1976) (m)	H (1977) (m)	H (1978) (m)
			982...	982...	982..			
60932	65.676	18.098	348.390	348.390	348.390			
93	65.720	17.365	353.560	353.565	353.547			
143	65.569	17.045	285.583	285.555	285.551	287.52	287.62	
170	65.679	16.927	292.447	292.373	292.334	295.66	296.06	295.98
5276	65.706	16.923	297.109	297.040	297.005	284.16	284.53	284.49
169	65.701	16.920	298.128	298.060	298.012	279.03	279.41	279.37
5604	65.699	16.904	294.568	294.483	294.434	294.66	295.09	295.10
171	65.698	16.886	289.260	289.158	289.096	321.02	321.54	321.64
5603	65.694	16.869	289.169	289.300	289.286	320.23	319.40	319.24
307[b]	65.694	16.863		287.718	287.640		325.76	325.56
180	65.700	16.846	279.977	280.089	280.157	363.94	363.43	362.98
306	65.704	16.841		274.782	274.729		389.44	389.54
188	65.695	16.840	282.574	282.538	282.504	349.33	349.58	349.69
182	65.709	16.819		274.046	273.993		349.00	394.12
181	65.706	16.812	282.121	282.028	282.005	358.96	359.38	359.45
115	65.706	16.812	282.134		282.013	358.89	359.31	359.38
183	65.708	16.803		281.623	281.586		361.93	361.98
303	65.709	16.781		282.001	281.992		358.60	358.62
190	65.715	16.778	281 723	281.631	281.616	359.00	359.35	359.37
199	65.713	16.776	281.450	281.365	281.356	359.26	359.61	359.62
193	65.717	16.752	282.294	282.229	282.214	358.60	358.90	358.90
302	65.716	16.748		282.078	282.077		359.22	359.22
234	65.640	16.371	276.833	276.801	276.817			
263	65.644	16.118	276.109		276.098			

[a] The gravity and height values before 1976 are given in Torge and Drewes (1977a)

[b] The thermal activity around this station changed strongly between 1977 and 1978, resulting in an extremely anomalous gravity/height coefficient

Annex 3. Gravity and height values along the Gjástikki profile

Station no.	ϕ (°)	λ west (°)	g (1965/70) (10^{-5} ms^{-2})	g (1976) (10^{-5} ms^{-2})	g (1977) (10^{-5} ms^{-2})	g (1978) (10^{-5} ms^{-2})	H (1978) (m)
			982···	982··	982··	982···	
82061	65.830	16.731			281.811	281.716	430.45
82561	65.830	16.731	281.95	281.85	281.764		
82591	65.831	16.735	285.73	285.65	285.548		
82592	65.831	16.735			285.277	285.170	421.98
82558	65.832	16.741	286.64	286.47	286.315	286.194	416.90
82556	65.834	16.750	290.18	290.18	290.148	290.036	401.46
82554	65.834	16.754	290.78	290.76	290.877	290.790	398.59
82553	65.835	16.756	292.89	292.95	293.059	293.126	388.73
82552	65.836	16.760			293.067	293.139	389.11
82550	65.838	16.764			293.319	293.229	392.32
82549	65.839	16.769			293.785	293.689	391.14
82548	65.840	16.780	293.36	293.41	293.389	293.324	394.07
82545	65.842	16.788	290.33	290.25	290.172	290.094	406.59
82544	65.842	16.790	283.82	283.75	283.643	283.566	434.50
82539	65.842	16.791			284.282	284.200	434.47
82538	65.842	16.793			283.540	283.470	438.13

Annex 4. Gravity values along the Gjástikki-Kelduhverfi profile

Station no.	ϕ (°)	λ west (°)	g (1965/70) (10^{-5} ms^{-2})	g (1976) (10^{-5} ms^{-2})	g (1977) (10^{-5} ms^{-2})	g (1978) (10^{-5} ms^{-2})
			982···	982···	982··	982···
82284	65.868	16.700	291.41	291.40	291.363	291.301
82285	65.885	16.674	298.48	298.37		298.289
82286	65.904	16.678	307.44	307.35		307.235
82289	65.948	16.662	335.39	335.44		335.663
82290	65.971	16.660	345.83	345.79		346.027
82291	65.992	16.655	360.33	360.32		360.414
82293	66.022	16.637	382.10	382.14		382.446
82294	66.040	16.627	389.07	389.19		389.407
82295	66.056	16.643	389.20	389.41		389.569
81296	66.074	16.689	397.76	397.70		397.603
81297	66.076	16.716	397.37	397.33		397.202
81298	66.099	16.689	398.90	398.81		398.726
81299	66.123	16.730	404.54	404.44		404.394
81300	66.123	16.730				404.300

References

Björnsson, A. Rifting and volcanism in the Krafla area 1975–1977. Náttúrufraedingirinn **46**, 177–240, 1976 (in Icelandic, with English summary)

Björnsson, A., Johnsen, G., Sigurdsson, S., Thorbergsson, G., Tryggvason, E. Rifting of the plate boundary in North Iceland 1975–1978. Nordic Volcanological Institute 7807, 1–31, 1978

Björnsson, A., Saemundsson, K., Einarsson, P., Tryggvason, E., Grönvold, K. Current rifting episode in north Iceland. Nature **266**, 318–323, 1977

Pálmason, G., Saemundsson, K. Iceland in relation to the Mid-Atlantic Ridge. Annu. Rev. Earth Planet. Sci. **2**, 25–50, 1974

Schleusener, A. Die Gravimetermessungen. In: Spalten auf Island, O. Niemczyk, ed.: pp. 124–175. Stuttgart. Wittwer 1943

Schleusener, A. Gravity measurements in N-Iceland between Eyjafjord and Vopnafjord. Presented at NATO Adv. Study Inst. Geodynamics of Iceland and the North Atlantic Area, Reykjavik 1974

Schleusener, A., Torge, W Investigations of secular gravity variations in Iceland. Z. Geophys. **37**, 679–701, 1971

Schleusener, A., Torge, W., Drewes, H. The gravity field of northeastern Iceland. J. Geophys. **42**, 27–45, 1976

Spickernagel, H. Höhenmessungen in Nord-Island. Mitt. aus dem Markscheidewesen **73**, 139–152, 1966

Spickernagel, H. Results of height measurements in Northern Iceland 1965/1977. J. Geophys. **47**, 120–124, 1980

Torge, W., Drewes, H. Gravity variations with time in northern Iceland 1965–1975. J. Geophys. **43**, 771–790, 1977a

Torge, W., Drewes, H. Gravity changes in connection with the volcanic and earthquake activity in northern Iceland 1975/1976. Jökull **27**, 60–70, 1977b

Torge, W., Wenzel, H.-G. Gravimetric earth tide observations in Iceland. Bull. d'Inf. marées terr. no. **74**, 4312–4318, Bruxelles 1976

Received March 1, 1979; Revised Version May 16, 1979

J. Geophys. 47, 132–140, 1980

Journal of Geophysics

Gravity and Elevation Changes Caused by Magma Movement Beneath the Krafla Caldera, Northeast Iceland

G.V. Johnsen, A. Björnsson, and S. Sigurdsson*
National Energy Authority, Grensásvegi 9, Reykjavík, Iceland

Abstract. Prior to the present activity of the Krafla volcano, which started in 1975, levelling and gravity surveys had been carried out in the area. The network has since been extended, and measurements are carried out about every second month. The measurements reveal a quasi-periodic behaviour of the tectonic activity, characterized by slow inflation of the caldera for several weeks or months at a rate of 6–10 mm/d, interrupted by sudden subsidence events lasting for one or a few days. Elevation changes within the caldera are described by a deflation-inflation swelling with its apex near the center of the caldera. Calculations, using a model of a spherical chamber with varying pressure at 3 km depth, show good agreement with the measured elevation values. Comparison of gravity and levelling data, using a Bouguer type relationship, suggests that inflation and deflation of the floor of the caldera is caused entirely by in- and outflow of magma. Some discrepancies between the levelling and gravity data immediately after subsidence events can be explained by additional mass flow of groundwater.

Key words: Gravity – Elevation changes – Magma flow – Iceland – Current rifting episode.

Introduction

In north Iceland the structure of the neovolcanic zone is characterized by several northsouth oriented fissure swarms running through central volcano complexes. Volcanic and tectonic activity in this region is episodic rather than continuous and each time is confined to one central volcano complex and it's associated fissure swarm (Saemundsson, 1974, 1978; Björnsson et al., 1977). The Krafla fissure swarm, which became active in 1975, extends from Axarfjördur in the north to the mountainous area southeast of Myvatn in the south, some 100 km in length. It's average width is estimated at 5 to 10 km. During the last interglacial period the Krafla central volcano developed a caldera which has been filled to a large extent with eruptive material during the last glacial and postglacial period, see Fig. 1. In postglacial time volcanic activity has remained high in the Krafla fissure swarm. About 35 postglacial eruptive fissures are known along the fissure swarm (Björnsson et al., 1977). A high-temperature geothermal field with temperatures exceeding 340° C at 2 km depth exists within the Krafla caldera. This geothermal field is now being harnessed in a geothermal power plant, see Fig. 2.

During the summer of 1975 it became apparent that the Krafla caldera was in a period of increased seismic activity. Seismic activity kept building up during the summer and fall. On the 20th of December 1975 a major volcano-tectonic event began within the Krafla caldera and part of the associated fissure swarm became active (Sigurdsson, 1976; Björnsson, 1977). A small volcanic eruption took place near the center of the caldera. During the next days and weeks, land subsided some 2.5 m inside the caldera and tectonic movements took place in the northern part of the fissure swarm some 60 km north of the Krafla caldera. Since then the Krafla caldera and the associated fissure swarm have been at

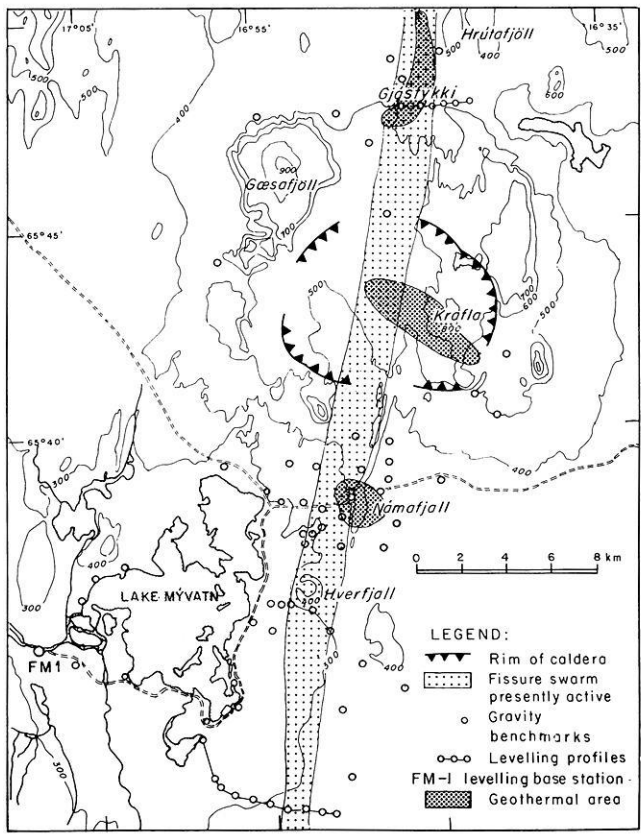

Fig. 1. The Krafla central volcano and it's surroundings in NE-Iceland. The caldera and the center part of the active fissure swarm are shown. *Open circles* show gravity and levelling benchmarks outside the caldera

* *Present address:* Science Institute, University of Iceland, Reykjavík, Iceland

0340-062X/80/0047/0132/$01.80

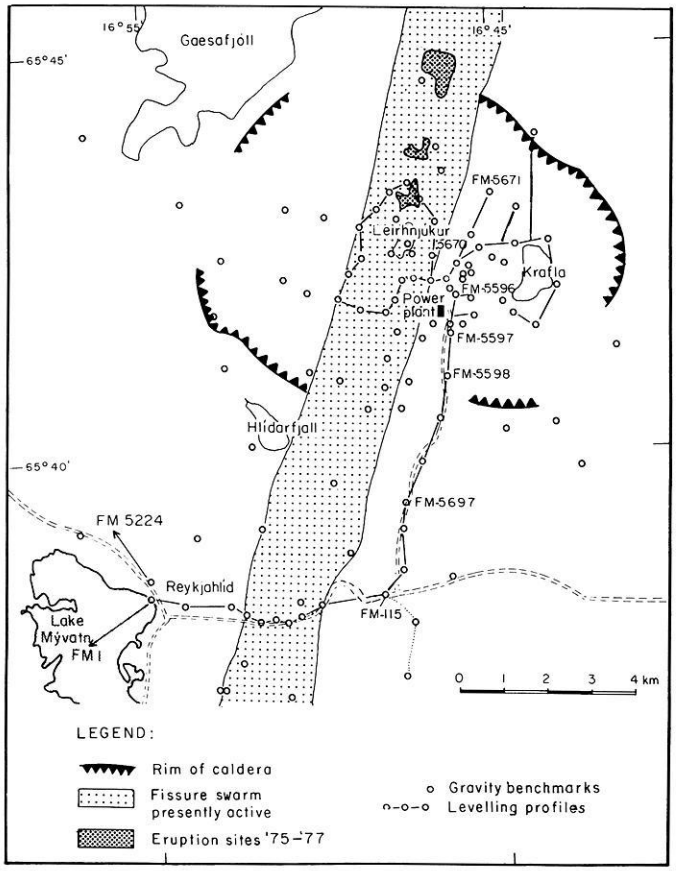

Fig. 2. Gravity and levelling benchmarks inside and around the Krafla caldera. Benchmarks, referred to in the text, are marked with *numbers*. *Arrows* indicate locations of gravity and levelling base stations

unrest. The activity is characterized by slow inflation of the caldera, at a rate of 6–10 mm/d at the center, lasting for several weeks or months, interrupted by sudden subsidence events lasting from one to a few days. The inflation has been interpreted as being caused by inflow of magma from below, at a rate of 5 m^3/s, into a magma chamber at shallow depth. The subsidence of the Krafla caldera is caused by horizontal flow of magma out of the magma chamber along a dike into the fissure swarm towards north or south. This is associated with horizontal and vertical ground movement and seismic activity within a confined part of the fissure swarm outside the caldera (Björnsson et al., 1979; Brandsdóttir and Einarsson, 1979). The existence of a magma chamber beneath the Krafla caldera has further been supported by the observation of a S-wave attenuating zone at a 3 to 7 km depth (Einarsson, 1978).

Great effort has been put into studying the present volcano-tectonic episode in the Krafla fissure swarm. The measurements include regular levelling and gravity surveying of the area, tilt measurements, monitoring movement of fissures, distance measurements, monitoring ground temperature and ground water level. A dense seismic network is in operation in the area. Temperature, pressure, and chemical composition of borehole discharge is monitored and gases emitted from fumaroles are analysed. In this paper, however, only the levelling and gravity data from the Krafla caldera and its surroundings will be presented supplemented with tilt measurements from one site inside the caldera.

The land elevation in and around the Krafla caldera has proved to be a most important parameter for understanding the nature of the present volcano-tectonic activity of the Krafla area. It has been possible to delineate the most active area and determine quantitatively the elevation variations, which is the base for further theoretical work. Elevation and seismic activity inside the caldera have been the most important indicators for surveillance of the volcano for the civil defence.

Geodetic and gravimetric measurements were started by Niemczyk (1943) in 1938 in order to observe tectonic movements in NE-Iceland. A high precision gravity profile across the neovolcanic zone in NE-Iceland, established in 1938 and re-observed in 1965, 1970, and 1975 for the investigation of secular gravity variations, indicates an increase of gravity by 0.05–0.1 $\mu m/s^2$ per year in the neovolcanic zone compared with the older plateau basalts to the west (Spickernagel, 1966; Schleusener and Torge, 1971; Torge and Drewes, 1977a; Torge and Kanngieser, 1979). Further measurements by Torge and Drewes (1977b) in 1975 and 1976 and by Björnsson et al. (1979) from 1975 to 1978 showed major changes in gravity and elevation near the caldera and along the active part of the fissure swarm. Repeated geodetic distance measurements of the Krafla-Mývatn area, indicate that slight contraction took place between 1965 and 1971, but significant expansion took place between 1971 and 1975 (Gerke, 1974, 1977; Gerke et al., 1978; Möller and Ritter, 1979).

The Observational Techniques

Levelling was originally carried out in the Krafla area in 1974 along the road from Myvatn to Krafla. Additionally several benchmarks were measured trigonometrically in the area for mapping purposes. The levelling network has gradually been extended and presently it includes some 70 benchmarks (see Figs. 1 and 2). The levelling has been carried out using a Zeiss Ni2 level and wooden measuring rods, which are periodically compared with Wild Invar rods. The standard error is approximately 1.5 $\sqrt{L}$ mm, where L is the length of the forward and backward measured levelling profile in kilometers. All profiles are measured in this manner except a profile around the hill Leirhnjukur, where one way levelling starts and ends at the same benchmark. Regular levelling of the Krafla area, started in early March 1976. Since then large parts of the network have frequently been levelled, usually at intervals of one to two months and the remainder at longer intervals. The main profiles east of Myvatn have a number of times been connected to benchmark FM-1 southwest of the lake by using the surface of the lake as a reference level in very calm weather. This benchmark serves as a base station for the levelling surveys. The levelling is performed by a team of three men. Under favourable weather conditions levelling of all benchmarks takes about a week.

A water tube tiltmeter is operated in the Krafla power house which is situated about 1,300 m south of the apex of maximum elevation changes (see Fig. 2 for location). The reading accuracy is about 1 μrad in the north-south component and readings are made at least once a day. An excellent correlation has been found between the tilt variations at this site and elevation changes of the caldera. Hence it is possible to monitor daily elevation changes during inflation and deflation by using the tilt variations for interpolation between levelling surveys. Further in this way it is possible to estimate the value of maximum subsidence during each subsidence event (Björnsson et al., 1979).

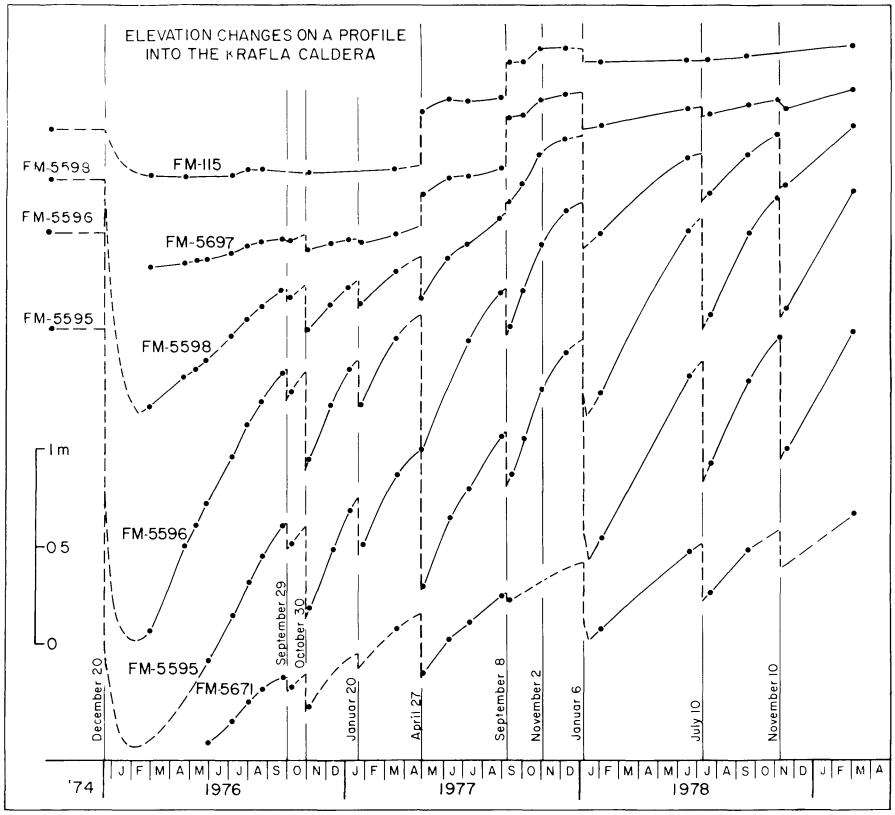

Fig. 3. Measured elevation changes on a 9-km-long profile leading from Námafjall into the Krafla caldera. For location of benchmarks see Fig. 2. *Filled circles* are levelling data and the *connecting lines* interpolations based on daily tilt observations

A gravity survey was first carried out in the Krafla area in August 1975. The purpose was to monitor gravity variations that might accompany the utilization of fluid from drillholes in the Krafla high temperature geothermal field. The network included some 30 benchmarks and was measured with a LaCoste-Romberg gravity meter, G-10. In March and June 1976 this network was remeasured using an old Worden gravity meter, W-68. Since September 1976 gravity surveys have been carried out with a LaCoste-Romberg gravity meter, G-445. Gravimeter readings are corrected for tidal effects using the method of Longman (1959). Correction is made for instrumental drift by using a looping technique. The accuracy of the gravity values is about ± 0.2 $\mu m/s^2$ for the G-gravity meters. Gravity changes are always measured with respect to stations within the Icelandic gravity base station network (Pálmason et al., 1973). Base station FM-5276 at the church of Reykjahlid was used for this purpose. After the subsidence event in April 1977 change was noted at this station in relation to the general network and the base station was transferred to FM-5224 at Husavik airport, some 40 km away from the Krafla caldera. Since June 1976 the gravity network has gradually been extended and presently includes some 150 gravity benchmarks (see Figs. 1 and 2). Most gravity surveys are carried out at the same time as levelling. The whole gravity network may under favourable conditions be covered by one man in about one week's time.

Characteristics of the Elevation and Gravity Changes

A levelling survey carried out in early March 1976 showed that up to 2 m subsidence had occurred within the Krafla caldera, accompanying the volcano-tectonic activity, which started on December 20, 1975. Further levelling surveys, carried out in the summer of 1976, showed that the floor of the Krafla caldera was rising. The rate of inflation had an average value of 6.5 mm/d at benchmark FM-5596 near the power house. In a similar manner a gravity survey, carried out in June 1976, showed considerable increase in gravity near the center of the caldera compared with measurements from 1975. Decrease in gravity was observed from June to September 1976 in correlation with the increasing elevation. In late September 1976 another volcano-tectonic event occurred within the Krafla fissure swarm. After a period of continuous inflation, lasting for eight months, land subsided within and around the Krafla caldera, and tectonic rifting took place in the fissure swarm, in Gjástykki. Since then eight other subsidence events have occurred in the area.

Figure 3 shows the elevation variations at several benchmarks on a 9 km long north-south profile stretching from Námafjall into the Krafla caldera (for location see Fig. 2). Tilt measurements have been used to interpolate between the levelling data. It is evident from Fig. 3 that the maximum elevation variations are taking place at the benchmarks FM-5596 and FM-5595 near the center of the caldera. At benchmark FM-115 near Námafjall, about 8 km south of the center of the caldera, the elevation variations are an order of magnitude smaller. The first subsidence event in December 1975 is accompanied by the greatest subsidence, while the event in November 1977 was too small to be shown on this scale. The subsidence events in April and September 1977 are the only ones associated with activity in the fissure swarm south of the caldera and hence having the greatest effect on eleva-

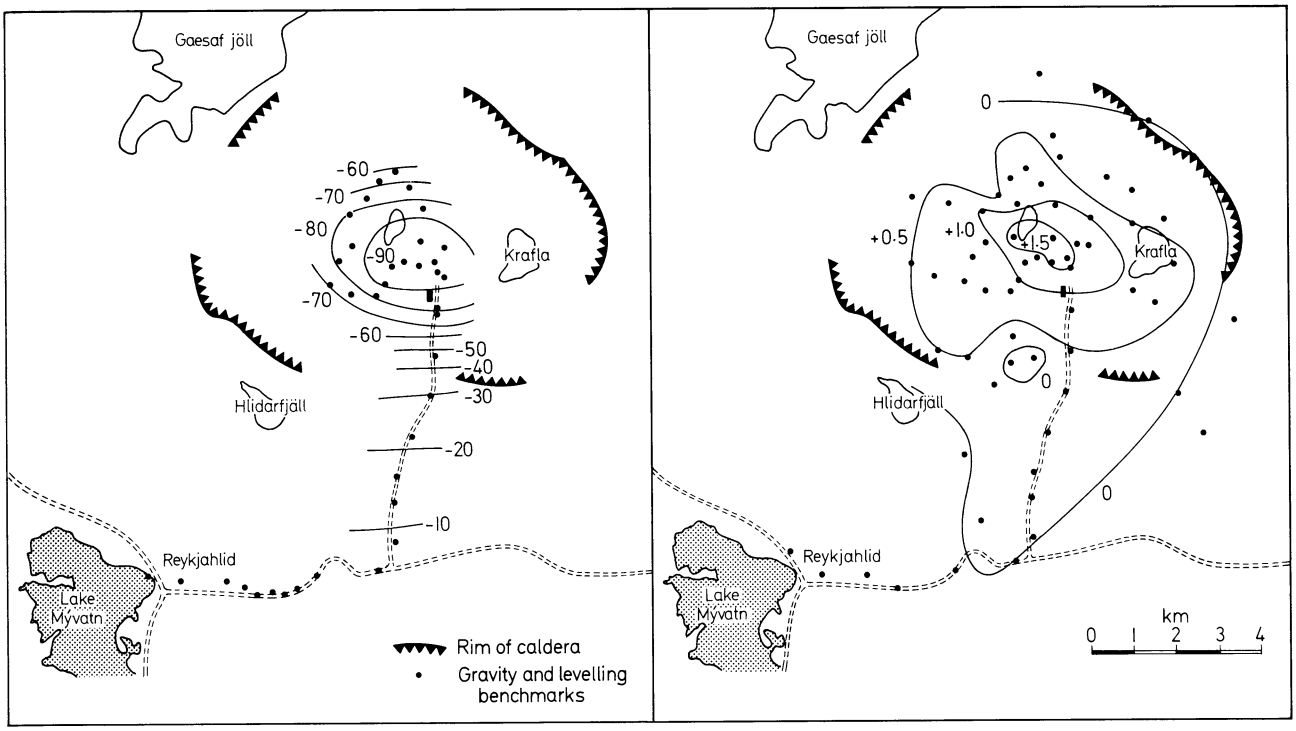

Fig. 4. Measured elevation changes in cm (*left*) and gravity changes in $\mu m/s^2$ (*right*) during the subsidence event in January 1978. *Filled circles* show the benchmarks occupied at the time

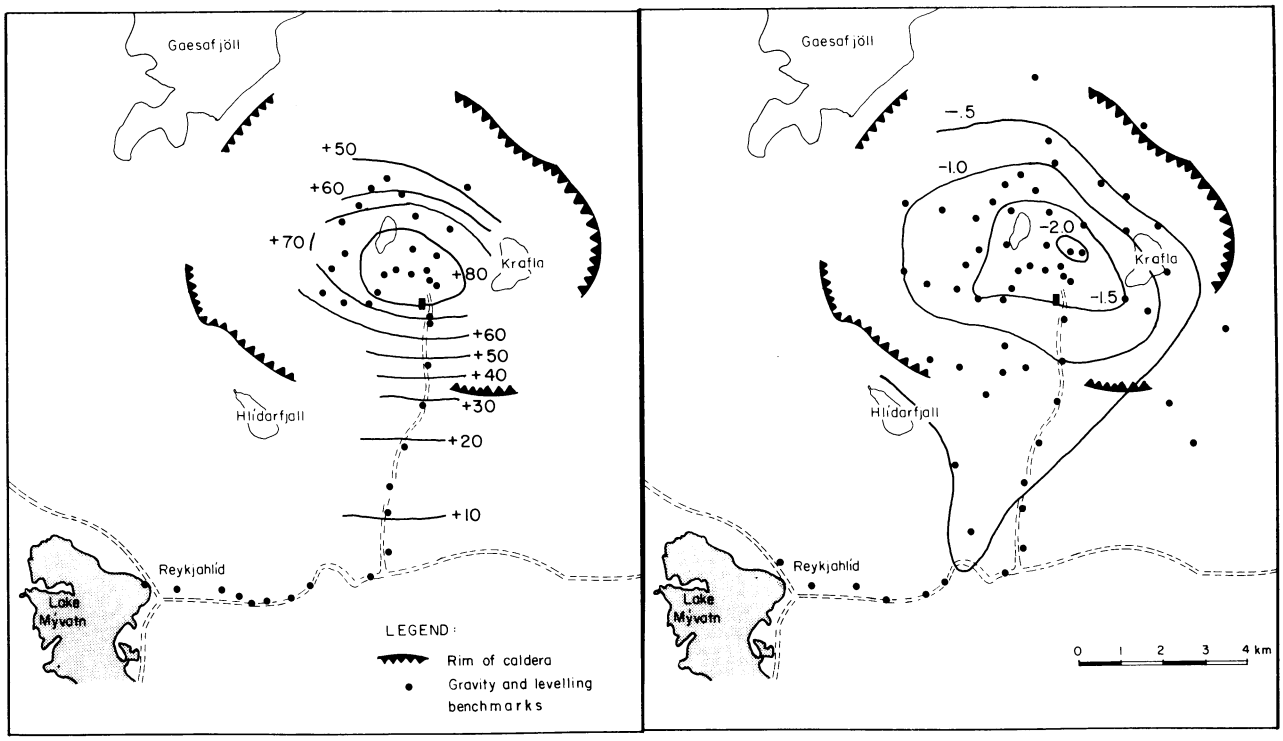

Fig. 5. Measured elevation changes in cm (*left*) and gravity changes in $\mu m/s^2$ (*right*) during the inflation period from January to June 1978. *Filled circles* show the benchmarks occupied at the time

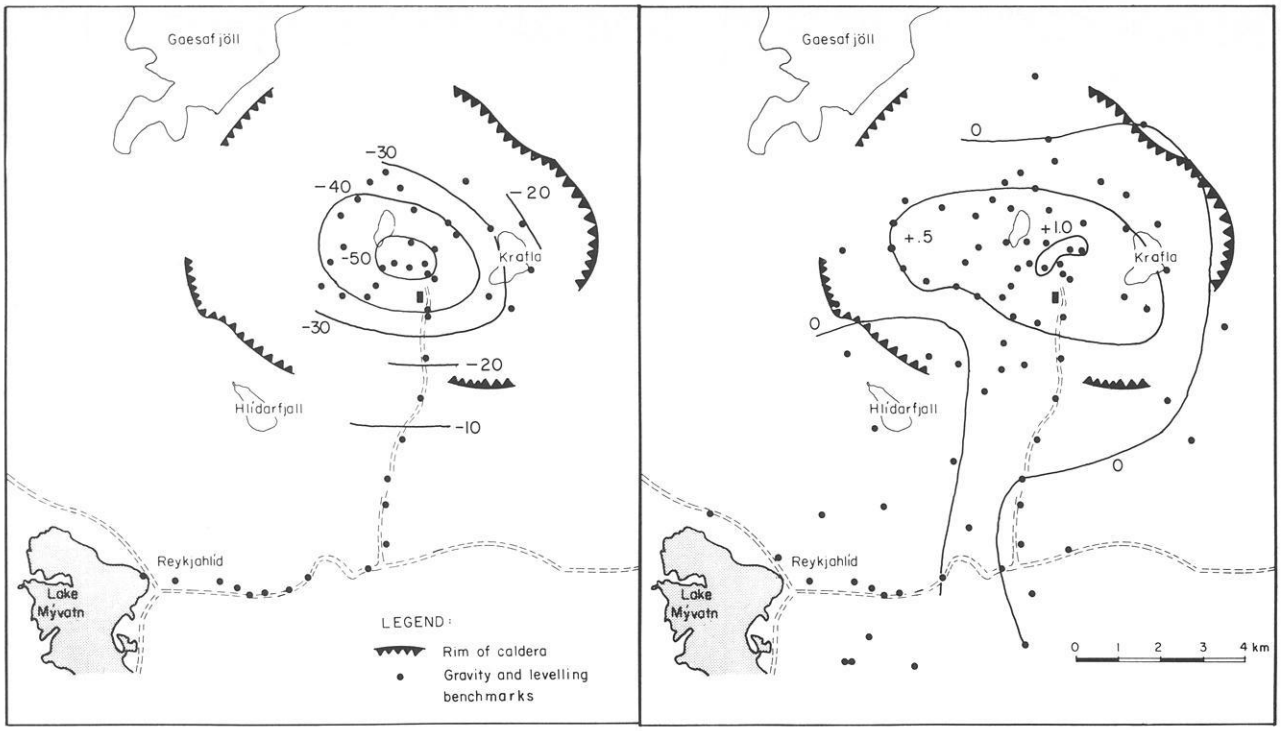

Fig. 6. Measured elevation changes in cm (*left*) and gravity changes in $\mu m/s^2$ (*right*) during the subsidence event in July 1978. *Filled circles* show the benchmarks occupied at the time

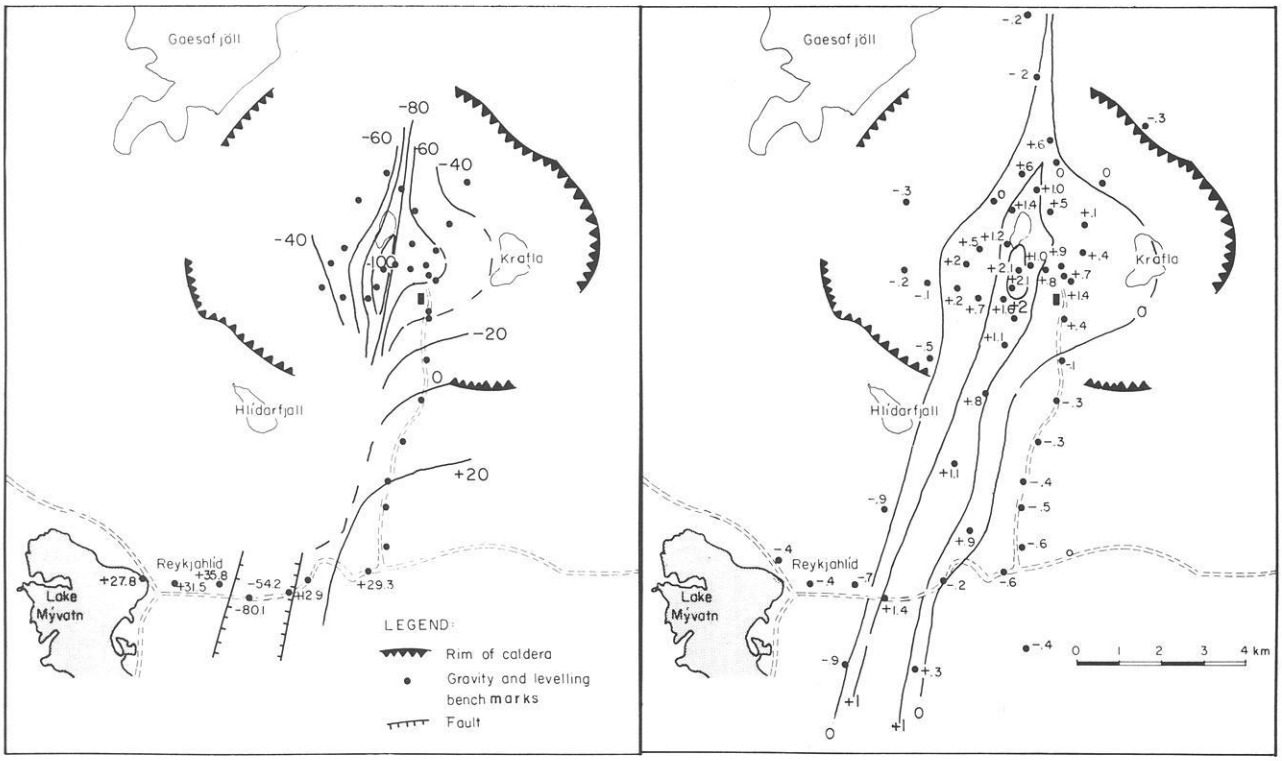

Fig. 7. Measured elevation changes in cm (*left*) and gravity changes in $\mu m/s^2$ (*right*) during the subsidence event in April 1977. *Filled circles* show the benchmarks occupied at the time

tion at the southernmost benchmarks. The inflation periods range from less than one to more than seven months. Elevation variations from other benchmarks in the measuring network give similar results as shown in Fig. 3.

In order to better demonstrate the elevation and gravity changes of the Krafla area we have chosen four sets of survey data covering two subsidence events and one inflation period. Figure 4 illustrates the subsidence event in January 1978, Fig. 5 the following, 6 months long inflation period, and Fig. 6 the subsidence event in July 1978. These figures are typical for the elevation and gravity changes in the Krafla area. A common feature of all three figures is a deflation-inflation bowl, the center of which is a somewhat elongated northwest-southeast oriented plateau, where maximum elevation changes occur. This plateau is situated between the hill Leirhnjukur and the southern slopes of the mountain Krafla. This area coincides with the Krafla high temperature geothermal field. The rate of elevation changes on this plateau during periods of inflation is 6–10 mm/d and the size of the area is approximately 4 km^2 Elevation changes diminish rapidly as one leaves the plateau and has dropped to about 40% of its maximum value at the southern rim of the caldera and to less than 5% at a distance of 10 km from the apex of uplift. Gravity surveys usually cover a greater area than levelling. Maximum gravity changes usually occur in the same area as maximum elevation changes, sometimes distorted, though, in a north-south direction along the fissure swarm.

As indicated in Fig. 3, measured elevation changes during the volcano-tectonic events in April and September of 1977 were somewhat different compared with other events. This is due to the fact that these events activated the southern branch of the fissure swarm within and just south of the caldera and hence influenced the elevation and gravity changes inside the caldera much more than activity further away during other subsidence events. Figure 7 illustrates the elevation and gravity changes during the subsidence event in April 1977. The subsidence bowl inside the caldera can still be seen, but major movement within the fissure swarm just south of the caldera are superimposed on the circular subsidence bowl. From gravity, levelling and distance measurements both south and north of the Krafla caldera it is known, that the activity in the fissure swarm is characterized by subsidence of the central part of the fissure swarm, while the flanks on each side are uplifted. This is accompanied by expansion over the most active part of the fissure swarm, up to 2 m each time resulting in the formation of new fissures and new geothermal areas, while a much larger area outside the fissure zone is contracted (Björnsson et al., 1979; Gerke et al., 1978). This tectonic rifting of the fissure swarm is usually also accompanied by an earthquake swarm (Brandsdóttir and Einarsson, 1979). Elevation changes of this sort were first detected gravimetrically in Gjástykki in January 1977.

Discussion

Elevation Variations – The Mogi Model

Björnsson et al. (1979) have shown that model calculations, using Mogi's (1958) model of a spherical chamber (magma chamber) with varying pressure within a homogeneous elastic half-space shows good agreement between calculated and observed elevation variations from the Krafla area. Thereby the elevation changes, Δh, at the distance x from the apex of a circular bowl is given by

$$\Delta h = h_o \cdot d^3 \cdot (d^2 + x^2)^{-3/2} \quad (1)$$

Table 1. Elevation and volume changes, direction of magma flow during subsidence events

Dates of Subsidence events	Maximum elevation changes at the apex	Estimated total volume change	Main direction of flow
December 20, 1975 to January, 1976	−230 cm +140 cm	$130 \cdot 10^6$ m^3 80 m^3	N (eruption)
September 29 to October 4, 1976	− 17 cm + 18 cm	9 m^3 10 m^3	N
October 30 to November 1, 1976	− 51 cm + 56 cm	29 m^3 32 m^3	N
January 20–21, 1977	− 32 cm + 59 cm	18 m^3 33 m^3	N
April 27–28, 1977	− 81 cm + 95 cm	46 m^3 54 m^3	S (eruption)
September 8–9, 1977	− 24 cm + 48 cm	14 m^3 27 m^3	S (eruption)
November 2, 1977	− 3 cm + 27 cm	2 m^3 15 m^3	?
January 6–25, 1978	−119 cm +108 cm	67 m^3 61 m^3	N
July 10–12, 1978	− 64 cm + 76 cm	36 m^3 43 m^3	N
November 10–15, 1978	− 72 cm	41 m^3	N

where h_o is the elevation variation at the center of the inflation/deflation bowl and d is the depth to the center of the spherical chamber. Best agreement was found for $d = 3$ km. By integrating over the inflation/deflation bowl the volume increase or decrease can be estimated. For the inflation periods a mean value of 5 m^3/s was found for the volume increase. Assuming no compression of the magma or the crustal rock, i.e., that the volume increase of the magma chamber is identical to the volume change at the surface, this corresponds to about $1.25 \cdot 10^4$ kg/s mass flow from below into the magma chamber, if a density of $2.5 \cdot 10^3$ kg/m^3 is used. Similarly mass flow out of the magma chamber during subsidence events can be estimated. Table 1 gives a summary of the elevation variations at the apex of the inflation/deflation bowl. Tilt variations in the power house which is about 1,300 m south of the apex have been used to extrapolate the maximum values at the apex, from the measured values at benchmark FM-5596, which is about 800 m south of the apex. Further, the table gives an estimate of the total volume change during inflation and deflation and the direction of the magma flow into the fissure swarm during subsidence events.

Mass Movement Beneath the Krafla Caldera Inferred From the Gravity Data

During the early stages of the present volcano-tectonic episode in the Krafla area some debate took place on the causes of the observed elevation changes. One model explained the inflation of the caldera by inflow of magma from below into a magma

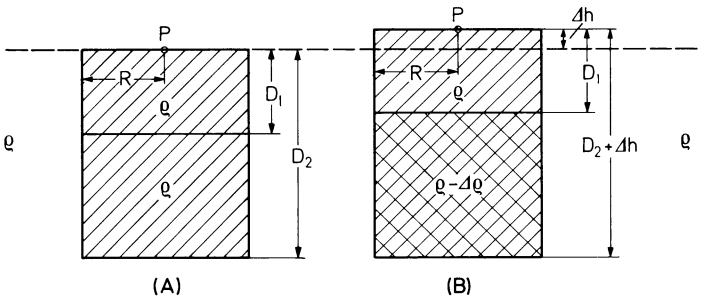

Fig. 8. Model of gravity change due to an expanding vertical cylinder. *A*. before expansion. *B*: after expansion. *P*· point of observation

chamber at shallow depth and the deflation events by flow of magma from the magma chamber into the fissure swarm to the north or south. In another model the inflation and deflation were interpreted as being caused by generation and condensation of steam in the geothermal water system. It is possible to test these models by converting measured elevation changes, Δh, into gravity values, Δg, using some assumption on mass distribution, and plot them along with measured gravity values as a function of time. As the changes in mass distribution accompanying level and gravity changes are not known we have used two simple models:

(1) A free air model described by the equation $\Delta g = -3.086\ \Delta h$, where Δg is measured in $\mu m/s^2$ and Δh in m. A change in gravity of 0.1 $\mu m/s^2$ will thus be obtained by an elevation change of approximately 3 cm.

(2) A Bouguer model described by the equation $\Delta g = -3.086\ \Delta h + 0.0004191\ \rho\ \Delta h$ where the density, ρ, is measured in kg/m^3 Using the value $\rho = 2.5\ 10^3\ kg/m^3$ leads to $\Delta g = -2.038\ \Delta h$. A change in gravity of 0.1 $\mu m/s^2$ will thus be obtained by an elevation change of approximately 5 cm.

If the elevation changes are entirely accompanied by complete mass (magma) compensation inflow or outflow the Bouguer model is clearly the more appropriate one. The relevance of the free-air model may, on the other hand, be judged from the simple case where we assume that the elevation change is caused by a uniform expansion or contraction within a vertical cylinder of radius R, which is situated directly under the point of observation, the depth to the top of the cylinder being D_1 and the depth to the bottom being D_2 before the expansion (contraction) and $D_2 + \Delta h$ after the expansion (contraction) (see Fig. 8). In this case the gravity change Δg due to the change Δh in elevation is approximately given by

$$\Delta g = 3.086\ \Delta h + 0.0004191\ \rho\ \Delta h\ c \tag{2}$$

where

$$c = \frac{(D_1 + D_2)/R}{\sqrt{1 + (D_1/R)^2} + \sqrt{1 + (D_2/R)^2}} \tag{3}$$

This can be seen from the fact that the gravitational attraction at P in Fig. 8 is

$$g_1 = 2\pi G \rho D_2$$

before expansion and

$$g_2 = 2\pi G(\rho(D_2 + \Delta h) - \Delta\rho$$
$$(D_2 + \Delta h - D_1 + \sqrt{R^2 + D_1^2} - \sqrt{R^2 + (D_2 + \Delta h)^2}))$$

after expansion with $\Delta\rho \simeq \Delta h\,\rho/(D_2 - D_1)$. After some arithmetic and neglect of small terms:

$$\Delta g = g_2 - g_1 \simeq 2\pi G \rho \Delta h\ \ c \text{ with}$$

$$c = (\sqrt{1 + (D_2/R)^2} - \sqrt{1 + (D_1/R)^2})/[(D_2 - D_1)/R]$$

which is identical to (3) as can be verified easily.

If $c = 0$ as becomes the case when $D_2/R \to 0$ we get the free air model, whereas if $c = 1$ as becomes the case when $D_2/R \to \infty$ we get a Bouguer model. Typical intermediate cases are, for example:

$R = 2$ km, $D_1 = 0$ km, $D_2 = 2$ km,
i.e., $D_1/R = 0$, $D_2/R = 1$ giving $c = 0.41$

$R = 2$ km, $D_1 = 0$ km, $D_2 = 4$ km,
i.e., $D_1/R = 0$, $D_2/R = 2$ giving $c = 0.62$

$R = 2$ km, $D_1 = 2$ km, $D_2 = 4$ km,
i.e., $D_1/R = 1$, $D_2/R = 2$ giving $c = 0.82$.

It is further clear that if inflation is caused both by magma inflow and rock expansion, and deflation by magma outflow and rock compression and ρ represents both the density of the magma and the rock, then the relationship (2) will still remain valid with a value of c less than 1 If, on the other hand, magma inflow is accompanied by rock compression and magma outflow by rock expanison (2) remains valid with a value of c larger than 1. We refer below to the factor c as the *correction factor*.

Figure 9 shows the result of the free air model and the Bouguer model with $\rho = 2.5\ 10^3\ kg/m^3$ at benchmark FM-5597 (for location see Fig. 1). The comparison indicates that the Bouguer model is the more appropriate if we observe:

(a) the increase in gravity that occurs during deflation

(b) the rate of decrease of gravity during inflation apart from a relatively short period immediately after the deflation event.

In fact, the closest agreement between gravity and elevation changes is in general found by using a value for $\rho \cdot c$ that lies in the range from approximately $3 \cdot 10^3$ km/m^3 to over $4 \cdot 10^3$ km/m^3 The regional value of density of basalts within the neovolcanic zone in NE-Iceland, based on seismic refraction work (Pálmason, 1971) and on rock weighing and Nettleton profiles (Schleusener et al., 1976) is considered to be $2.3 \cdot 10^3$ kg/m^3 On the other hand, Ito and Kennedy (1971) have discussed a relation between the density of molten basaltic magma and pressure, indicating that for molten basalts, density values of around $3.0 \cdot 10^3$ kg/m^3 may be quite realistic. In any case, there is clearly little justification for assuming that the correction factor, c, should take on a value any lower than one. This supports the theory that the inflation and deflation of the Krafla caldera is caused by in- and outflow

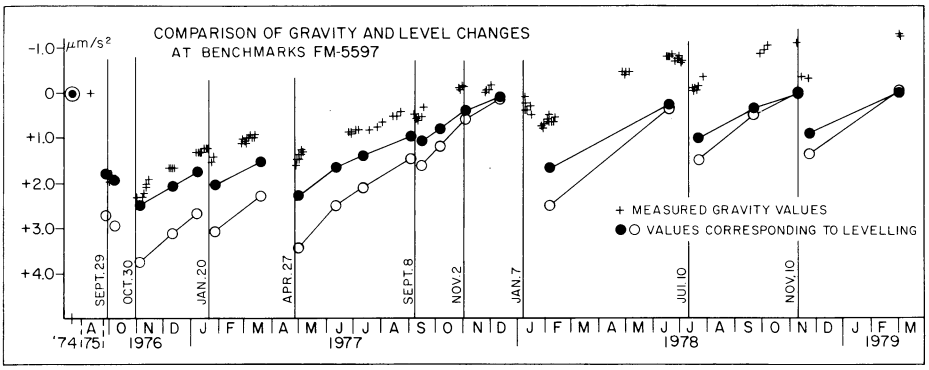

Fig. 9. Comparison of gravity and elevation changes with time at benchmark FM-5597, for location see Fig. 2. *Crosses* are measured gravity values. *Filled circles* are gravity values calculated from measured level values assuming a Bouguer model. *Open circles* are gravity values calculated from level values using a free air model

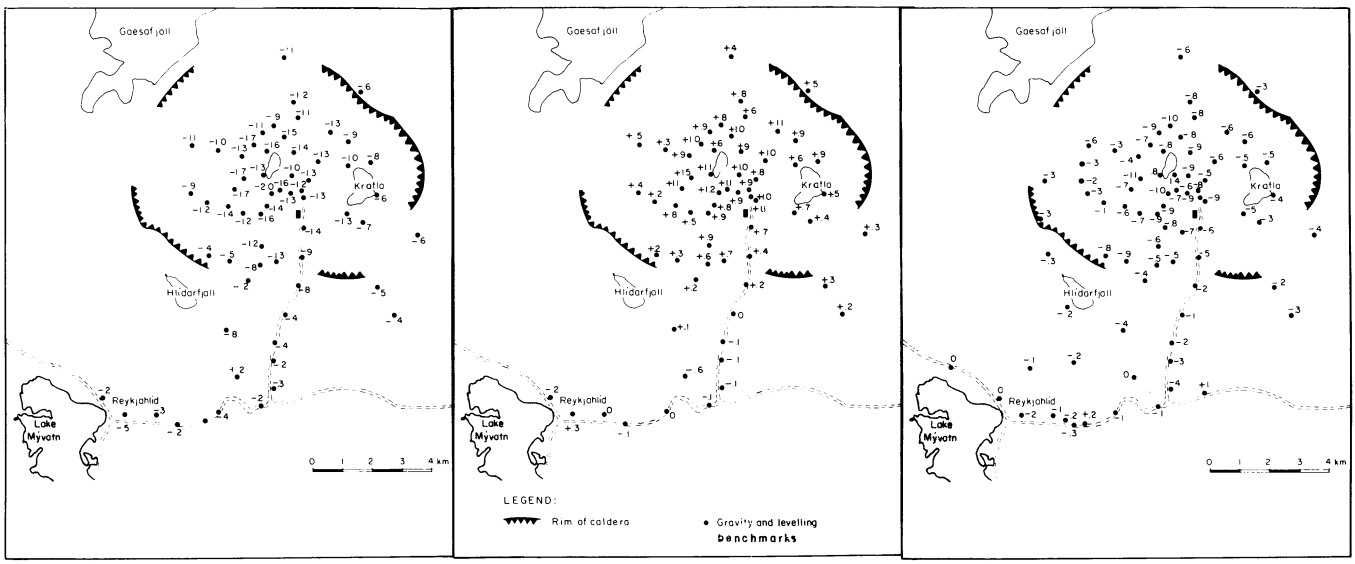

Fig. 10. Reduced gravity values in $\mu m/s^2$, for the time periods shown in Figs. 4–6. Reduced gravity is the difference between measured gravity and gravity calculated from levelling using a free air model

of magma into a chamber. We observe, however, also that immediately after the deflation there usually occurs a rapid decrease in gravity with the gap between observed and calculated gravity persisting during inflation and thus, after each deflation event, increasing with time. The rate of gravity decrease is such that it cannot even be explained by a correction factor of 0. Thus, although some expansion of crustal rocks due to, e.g., steam generation or intrusion of magmatic gases, may take place after deflation this cannot be the sole explanation. Another plausible explanation is a rapid sinking of the groundwater level after each deflation event. Such sinking could be caused by the rifting and opening of new fissures in the area and hence the flow of groundwater from the Krafla central volcano. In order to explain the difference between measured and calculated gravity values in 1979 the accumulated sinking of groundwater level must amount to some 20 m assuming a porosity of 15%. If less were observed some permanent rock expansion would be indicated. Unfortunately there are no groundwater data available to test this.

Gravity observations at other benchmarks are much less detailed than those at benchmark FM-5597. In general we only have one observation in the short period after the deflation event when the rapid decrease in gravity has been observed at benchmark FM-5597 and this observation most often takes place towards the end of that period. Observations at other benchmarks thus do not shed any additional light on the nature of the rapid decrease in gravity. They do however indicate that it is not confined to benchmark FM-5597 in that

(a) estimates of the density of the compensating mass based on the Bouguer model and observations over a deflation event in general give a higher value than those based on observations during an inflation period,

(b) a comparison of two gravity observations, many deflation events apart, that correspond to approximately the same elevation value reveals, in general, a decrease in the gravity value.

Hunt (1976) has outlined a simple method to estimate total mass variation by comparing measured elevation and gravity changes. The procedure used is as follows: First the measured elevation changes are converted into gravity changes using the normal free air gravity reduction ($\Delta g = -3.086 \cdot \Delta h$). Then the free air gravity value is subtracted from the measured value of gravity, obtaining a reduced gravity value, Δg_c. Finally applying Gauss' potential theorem in the form $M = (\Sigma\, \Delta g_c \cdot \Delta S)/2\pi G$ where M is the mass not recovered, ΔS is the area corresponding to the reduced gravity change and G is the gravitational constant, an estimate of total change of mass can be found. This can be applied both to periods of inflation, to determine the rate of inflow into

Table 2. Mass and volume changes and estimated density of mass flow between November 27, 1977 and July 21, 1978

Dates of observations	Changes in total mass from gravity measurements	Changes in total volume from the Mogi model	Estimated density by full mass compensation
November 27, 1977			
	$-2.43 \cdot 10^{11}$ kg	$-56 \cdot 10^{6}$ m^3	$4.3 \cdot 10^{3}$ kg/m^3
February 5, 1978			
	$+1.69 \cdot 10^{11}$ kg	$+56 \cdot 10^{6}$ m^3	$3.0 \cdot 10^{3}$ kg/m^3
June 22, 1978			
	$-1.64 \cdot 10^{11}$ kg	$-30 \cdot 10^{6}$ m^3	$5.5 \cdot 10^{3}$ kg/m^3
July 21, 1978			

the caldera, and also to subsidence events for estimating the related total change in mass. The results, at least theoretically, are not affected by possible mass redistribution due to, e.g., rock expansion or compression.

Figure 10 shows gravity values for the three periods of time shown in Figs. 4–6, i.e., for the two deflation events in January and July 1978 and the inflation period between these events. Levelling and gravity surveys are not always carried out at the same time, but the levelling data can be interpolated to the same date as the gravity data using the daily tilt observations. The Mogi model can subsequently be used to calculate volume change corresponding to the mass changes obtained from the gravity measurements. The results are presented in Table 2.

Estimates of density are based on the assumption that both inflation and deflation are entirely caused by mass inflow and outflow. Keeping in mind an earlier remark about the lack of detail in gravity observations after the deflation events, this is in good agreement with the inference made from the observations at benchmark FM-5597, i.e., that one is justified in assuming that inflation and deflation are accompanied by mass (magma) inflow and outflow provided one can further assume that some additional mass (groundwater) outflow takes place immediately after deflation.

Acknowledgements. We are thankful to G. Thorbergsson for drawing the attention of the authors to the relation (2), and to A. Gunnarsson for carrying out the levelling measurements.

Reference

Björnsson, A. Jardhraeringar vid Kröflu (in Icelandic with English summary). Natturufraedingurinn **46**, 177–240, 1977

Björnsson, A., Johnsen, G.V., Sigurdsson, S., Thorbergsson, G., Tryggvason, E.: Rifting of the plate boundary in North Iceland 1975–1978. J. Geophys. Res. **84**, in press, 1979

Björnsson, A., Saemundsson, K., Einarsson, P., Tryggvason, E., Grönvald, K.: Current rifting episode in North Iceland. Nature **266**, 318–323, 1977

Brandsdóttir, B., Einarsson, P.. Seismic activity associated with the September 1977 deflation of the Krafla central volcano in NE-Iceland. J. Volc. Geotherm. Res. in press; 1979

Einarsson, P.: S-wave shadows in the Krafla caldera in NE-Iceland, evidence for a magma chamber in the crust. Bull. Volcanol. **41**, 1–9, 1978

Gerke, K.: Crustal movements in the Myvatn- and the Thingvallavatn-area, both horizontal and vertical. In: Geodynamics of Iceland and the North Atlantic area, L. Kristjansson, ed. pp. 263–275. Dordrecht, Boston: D. Reidel Publishing Company 1974

Gerke, K.. Über neuere horizontale und vertikale Krustenbewegung in Island. Mitteilungen der Technischen Universität Carolo-Wilhelmina zu Braunschweig XII, Heft III/IV, 1977

Gerke, K., Möller, D., Ritter, B.. Geodätische Lagemessungen zur Bestimmung horizontaler Krustenbewegungen in Nordost-Island. In: Festschrift für W. Höpcke, Wiss. Arb. d. Lehrst. f. Geodäsie, Photogramm. u. Kartogr. an d. T.U. Hannover, Nr. **83**, Hannover 1978

Hunt, T.M.. Recharge of water in Wairakei geothermal Field determined from repeated gravity measurements. N. Z. J. Geol. Geophys. **20**, 307–317, 1976

Ito, K., Kennedy, G.C.: An experimental study of the basalt-garnet granulite-eclogite transition. In: The structure and physical properties of the Earth's crust, Vol. 14, J.G. Heacock, ed. pp. 303–314. Washington, D.C. Geophys Monogr. Am. Geophys. Union 1971

Longman, I.M. Formulas for Computing the tidal accelerations due to the Moon and the Sun. J. Geophys. Res. **64**, 2351–2355, 1959

Möller, D., Ritter, B. Geodetic measurements and horizontal crustal movements in the rift zone of NE-Iceland. J. Geophys. **47**, 110–119, 1980

Mogi, K.: Relations between the eruptions of various volcanoes and the deformation of the ground surfaces around them. Bull. Earthq. Res. Inst. **36**, 99–134, 1958

Niemczyk, O.. Spalten auf Island. Stuttgart: Wittwer, 1943

Pálmason, G.: Crustal structure of Iceland from explosion seismology. Soc. Sci. Islandica, Rit XL, 1971

Pálmason, G., Nilsen, T.H., Thorbergsson, G.. Gravity base station network in Iceland 1968–1970. Jökull **23**, 70–125, 1973

Saemundsson, K.. Evolution of the axial rifting zone in Northern Iceland and the Tjörnes Fracture Zone. Geol. Soc. Am. Bull. **85**, 495–504, 1974

Saemundsson, K.. Fissure swarms and central volcanoes of the neovolcanic zones of Iceland. In. Crustal evolution in Northwest Britain and adjacent regions. Geol. J. Spec. Issue **10**, 415–432, 1978

Schleusener, A., Torge, W.: Investigations of secular gravity variations in Iceland. Z. Geophys. **37**, 679–701, 1971

Schleusener, A., Torge, W., Drewes, H.. The gravity field of Northeastern Iceland. J. Geophys. **42**, 27–45, 1976

Sigurdsson, O.. Náttúruhamfarir i Thingeyjarthingi (In Icelandic with English summary). Tyli **6**, 3–20, 1976

Spickernagel, H.: Höhenmessungen in Nord-Island. Mitt. Markscheidewesen **73**, 139–152, 1966

Torge, W., Drewes, H. Gravity variations with time in Northern Iceland 1965–1975. J. Geophys. **43**, 771–790, 1977a

Torge, W., Drewes, H.: Gravity changes in connection with the volcanic and earthquake activity in Northern Iceland 1975/1976. Jökull **27**, 60–69, 1977b

Torge, W., Kanngieser, E.. Gravity and height variations during the present rifting episode in northern Iceland. J. Geophys. **47**, 125–131, 1980

Received May 19, 1979; Revised Version July 9, 1979

J. Geophys. 47, 141–153, 1980

Journal of Geophysics

Subsidence Events in the Krafla Area, North Iceland, 1975–1979

E. Tryggvason
Nordic Volcanological Institute, University of Iceland, Reykjavik, Iceland

Abstract. In the inflation-deflation sequence of the Krafla magma chamber since its beginning in 1975, 12 deflation or subsidence events have been identified until May, 1979. The tilt and distance measurements relating to these subsidence events are discussed in some detail. All of these subsidence events are associated with horizontal magma flow along the N-S trending fissure zone, which goes through the central part of the Krafla caldera, to form a dike 3 to 5 m wide, 80 km long, and 1.0 to 2.5 km high from the bottom to the top. The total volume of magma, which flowed out of the Krafla magma chamber during these 12 events, is estimated as 481×10^6 m^3, whereof 407×10^6 m^3 are estimated to have flowed northwards, 72×10^6 m^3 southwards and about 2×10^6 m^3 came to the surface as basaltic lava.

Key words: Krafla volcano Iceland – Ground deformation – Magma flow.

Introduction

The volcano-tectonic sequence, which started in 1975 in the Krafla-Mývatn area, North Iceland, is characterized by repeated uplift and subsidence of an area centered near Leirhnjúkur in the central part of the Krafla caldera (Björnsson et al., 1977). The inflation progresses at a relatively constant rate over periods of several months, to be interrupted by rather sudden subsidence events.

The first very noticeable event in this volcano-tectonic sequence was the subsidence, which started on December 20, 1975 (Björnsson et al., 1977; Björnsson, 1976; Sigurdsson, 1976), when the area around Leirhnjúkur subsided more than 2 m over a period of 1 or 2 months.

There are some indications that tectonic unrest had been increasing in the Krafla region for some years before 1975. During a microearthquake survey in Iceland in 1967, the Krafla area was found to be very active, with higher frequency of microearthquakes than any other surveyed region in Iceland (Ward et al., 1969). However, this high frequency of microearthquakes had subsided by a factor of nearly 100 in 1968 (Ward and Björnsson, 1971). Repeated geodetic measurements of high precision indicate a slight horizontal contraction of the Krafla-Mývatn area between 1965 and 1971, but significant horizontal expansion occurred between 1971 and 1975 (Gerke, 1977; Gerke et al., 1978). Seismic activity increased markedly in the Krafla area in the spring of 1975, and the high activity continued until the beginning of the first subsidence event (Björnsson et al., 1977). These observations indicate, that some signs of the coming volcano-tectonic sequence may have been observed several years before it became obvious on December 20, 1975.

Many individuals from several research institutions have participated in the research of the tectonic unrest in the Krafla area. The first three subsidence events were described in some detail by Björnsson et al. (1977), and these and the subsequent events have been discussed by Björnsson et al. (1979). The first event, which started on December 20, 1975, caused considerable ground movements in Kelduhverfi (Tryggvason, 1976) and elsewhere on the Krafla fissure swarm (Björnsson et al., 1977), and small basaltic lava eruptions occurred (Sigurdsson, 1976). Subsequent subsidence events have been associated with volcanic tremors, earthquake swarms and widening of portions of the fissure swarm, and small volcanic eruptions occurred during two of them, on April 27 and September 8, 1977 (Björnsson et al., 1979). The seismic activity associated with the event of September 8 to 9, 1977, has been described in details by Brandsdóttir and Einarsson (1979). The distance and tilt measurements of the Nordic Volcanological Institute and the University Science Institute in 1976 and 1977 were reported by Tryggvason (1978a and b).

Observations

This report is primarily based on tilt and distance observations of the Nordic Volcanological Institute and the University Science Institute.

The *tilt measurements* are of three types. A water tube tiltmeter of two components was installed in the Krafla power house on August 19, 1976, and has been observed daily since then with few exceptions. During times of very rapid subsidence of the Krafla area, additional readings were made. One arm of this tiltmeter is 68.95 m in direction N13 °E and the other arm is 19.50 m long in direction E13 °S.

Two electronic continuously recording tiltmeters (Sindrason and Ólafsson, 1978) were installed in the Krafla-Mývatn area in 1977, one in the Krafla power house, another in Reynihlíd by Mývatn. A third tiltmeter of the same construction was installed about 1 km north of the explosion crater Víti in 1978.

Twelve spirit level tilt stations were constructed in the Krafla-Mývatn area in 1976 and 1977 (Fig. 1). Observations at these stations have been made approximately once each month during summer, but at longer intervals in the winter (Tryggvason, 1978a). Most of these spirit level tilt stations consist of five bolts in solid bedrock, placed on the circumference of a circle of 25-m radius. When observations are made, an optical level is placed in the center of this circle and invar leveling rod is carried from one

0340-062X/80/0047/0141/$02.60

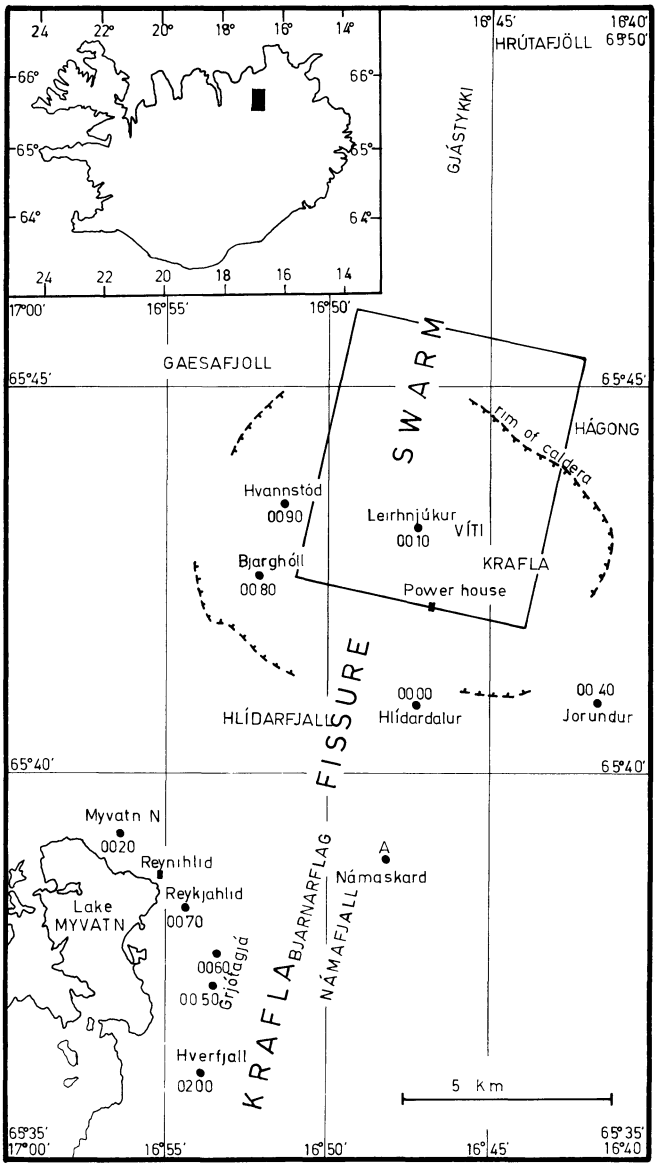

Fig. 1. Location of the spirit level tilt stations in the Krafla-Mývatn area (*filled circles*) and the electronic tiltmeters at the Krafla power house and Reynihlíd. The rim of the Krafla caldera is shown for reference on this and all subsequent maps. A rectangle outlines the area covered by the maps on Figs. 9 and 12

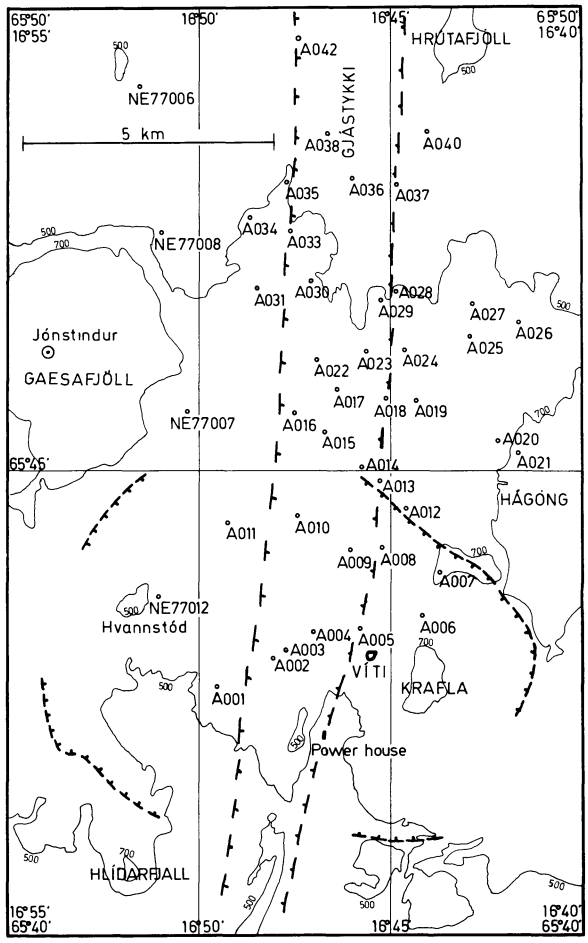

Fig. 2. Location of the stations used in distance measurements with geodimeter in the Krafla-Gjástykki area

bolt to another around the circle. Under favourable conditions the leveling accurancy is approximately 0.1 mm. Minor movements of the bolts together with observational errors make the probable error of tilt roughly 5μ rad.

A program of repeated geodimeter measurements in the Krafla-Mývatn area was initiated in early 1977 (Tryggvason, 1978b). The present stations in the northern part of the area are shown on Fig. 2. This network has been measured several times, both distances between the markers, and also the vertical angles by theodolite. Thus a crude observation of vertical displacements is obtained at the same time as the horizontal displacements.

Other observations, which improve the overall understanding of the subsidence events, are seismic observations by the Science Institute of the University of Iceland, precision leveling and gravity measurements by the National Energy Authority, and a variety of other observations by the large number of scientists working in the Krafla-Mývatn area.

The Model

The geological model, which has been developed during the present sequence of events in the Krafla region, is as follows.

Below the central part of the Krafla area, near Leirhnjúkur, lies a magma chamber. A continuous flow of molten magma enters this chamber from below, and the rate of this flow can be estimated from the rate of uplift during inflation periods. Occasionally, a relatively sudden outflow of magma from this chamber occurs along the fissure swarm, which goes through the Krafla area in direction N10 °E to N15 °E. Minor lava eruptions occurred three times in 1975 and 1977 (Björnsson et al., 1977; Björnsson, 1976; Björnsson et al., 1979; Tryggvason, 1978a; Einarsson, 1978).

The depth of the Krafla magma chamber has been estimated from tilt and level observations using the equations developed by Mogi (1958). The depth estimates, which best agree with the observations are close to 3.0 km to the center of a spherical chamber (Tryggvason, 1978a, Björnsson et al., 1979). The assumption of a spherical magma chamber is certainly not correct, but observations of tilt and variations in ground elevation fit such

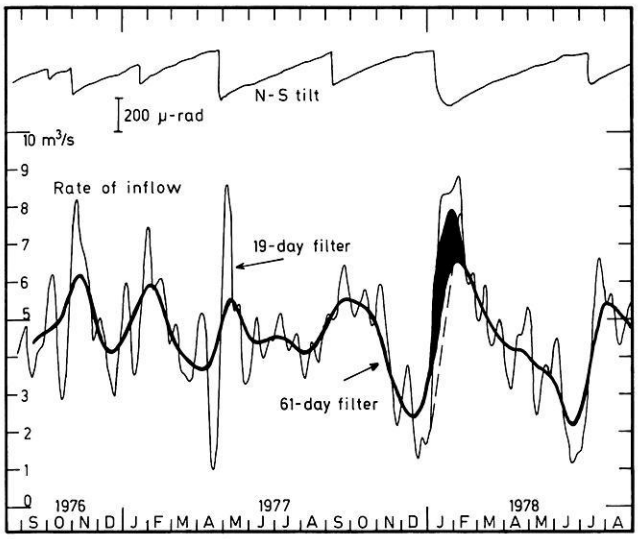

Fig. 3. The north component of tilt measured by the water tube tiltmeter in the Krafla power house (*upper trace*). Uplift to the north is up on the graph. The *lower traces* show the rate of tilt converted into rate of volume increase (*inflow*) of the Krafla magma chamber. This rate is filtered with a low pass filter to clarify the general trend. In January 1978 the inflow rate is uncertain due to prolonged subsidence event

a model rather well. Observations of *S*-wave shadows (Einarsson, 1978) indicate that the top of the magma chamber lies at a depth of approximately 3 km and the bottom at or above 7-km depth.

The observations suggest another magma chamber of great but unknown depth below the Krafla region. This lower chamber is so large, that no limits have as yet been seen for its capacity to supply magma to the shallower chamber.

The magma that flows out of the Krafla magma chamber during subsidence periods is deposited as a dike in the Krafla fissure zone (Björnsson, 1976; Björnsson et al., 1979). The velocity with which the front of the forming dike moves forward, can be obtained from the movement of earthquake epicenters (Brandsdóttir and Einarsson, 1979) and from the time of formation of new fissures or opening of old ones (Björnsson et al., 1979). This velocity is approximately 0.5 m/s in the cases studied.

The portion of the dike that is formed during each subsidence event can be located with seismic epicenters (Brandsdóttir and Einarsson, 1979) and new or reopened ground fissures and new or intensified steam vents (Björnsson et al., 1979). The depth to the dike can be estimated from the width of the zone of new or reopened fissures, and the thickness of the dike from the widening of the fissure zone. However, the widening of the fissure zone as measured on the surface may be greater than the thickness of the new dike due to change in the stress release pattern with depth in the earth's crust. This effect has not been estimated as yet.

In estimating the volume of magma, which flows into and out of the Krafla magma chamber, tilt observations in the Krafla power house are of greatest use. It is assumed that the location of the magma chamber does not change with time. A study of the inflation period between the subsidence events of April 27–28, 1977, and September 8–9, 1977, which is primarily based on tilt observations at 7 stations, including the Krafla power house, gave the following results (Tryggvason, 1978a).

(a) Depth to the center of a spherical magma chamber, which best fitted the observations, was 2.9 km.

(b) The total volume of uplift, assumed to be equal to volume of magma influx, was 59.5×10^6 m^3 during this inflation period.

(c) The calculated uplift of the ground at the point of greatest uplift was 110 cm.

(d) The total north component of tilt at the Krafla power house was 312 μ rad.

Thus one μ rad tilt at the Krafla power house corresponds to 0.19×10^6 m^3 of magma influx. In the light of the inaccuracies in this determination, especially in depth of the magma chamber, the rounded value of 0.2×10^6 m^3 is accepted in this paper as corresponding to one microradian of N-S tilt at the Krafla power house. As the average tilt at the power house is 2.0 to 2.1 μ rad per day during inflation periods, the average influx of magma into the Krafla magma chamber is about 0.4×10^6 m^3/d or about 5 m^3/s. It is assumed that the influx continues during subsidence periods, so the magma outflow is slightly greater than that calculated from tilt during the subsidence periods.

The rate of tilt at the Krafla power house is converted into rate of magma flow in Fig. 3. There seem to be considerable fluctuations in this rate. It is very noticeable that the influx rate appears to be high first after a subsidence event, and low before such an event.

The Subsidence Event of December 1975 to January 1976

The first subsidence event of the present volcano-tectonic sequence in the Krafla area started on December 20, 1975, simultaneously with observed seismic tremor. Repeated leveling of the base of the Krafla power house showed tilt of approximately 750 μ rad down to the north between November 20, 1975, and February 10, 1976. Several measurements between January 18 and February 10, 1976, showed slight northward tilt to continue, but measurement on March 1, 1976, showed that uplift towards north had commenced at the power house. Leveling in early March 1979 along a line from lake Mývatn showed subsidence exceeding 2 m in the Krafla area since 1974 (Björnsson et al., 1977). It may be assumed that this subsidence occurred on December 20, 1975, and the days that followed.

Opening of fissures and faulting was observed in the Krafla fissure swarm, primarily in the Kelduhverfi area 30 to 60 km north of Krafla, but to a lesser extent in other parts of the fissure zone, as far south as lake Mývatn (Tryggvason, 1976; Björnsson, 1976).

The tilt at the Krafla power house and the subsidence indicate that roughly 150×10^6 m^3 of magma was removed from a magma chamber below the Krafla area. If magma entered the chamber from below during this subsidence event at a rate similar to that observed during the following years, the volume of magma entering the fissure swarm during this event may have been as much as 180×10^6 m^3. Most of this magma flowed northwards to be deposited in the northernmost 30 km of the fissure zone, which supposedly terminates at 66° 20′ north. Rifting in the Mývatn area indicates that a minor fraction of the magma flowed southwards.

Subsidence Events of September 29 to October 4, 1976 (Fig. 4)

Observations of the water tube tiltmeter in the Krafla power house show tilt towards north from September 29 to October 4, 1976.

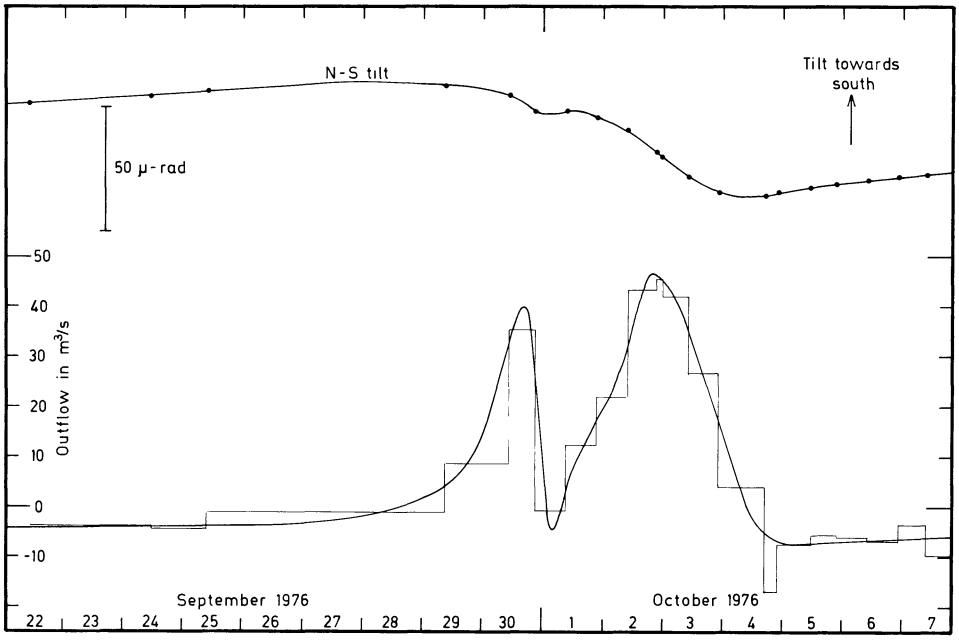

Fig. 4. North component of tilt at the Krafla power house and rate of magma outflow from the Krafla magma chamber during the subsidence events of September 29 to October 4, 1976. *Filled circles* show the actual water tube tiltmeter observations. The average rate of outflow between tilt observations is shown by thin line rectangular curve, while the smooth curve is the authors interpretation

The beginning of this event is poorely recorded as no readings were taken between September 25, 10^h and September 29, 10^h This tilt event seems to be a double event or rather two separate subsidence events (Fig. 4).

Two spirit level tilt stations provide information on these subsidence events, Hlídardalur (0000) and Leirhnjúkur (0010). Observations were made at both stations on September 18, October 2, and October 23, 1976. The good correlation between the tilt at these stations and the N-S component of tilt at the Krafla power house allows us to estimate the tilt during each of these subsidence events.

In estimating the tilt during subsidence events, the observations are reduced to the time of the event. This reduction is based on the average ratio between tilt components at each station and the daily observations of the north component of tilt at the Krafla power house.

The first of these two events, lasting from September 29 (or earlier) to September 30, 21^h appears to have caused a tilt of 11 μ rad towards N80 °E at Hlídardalur and 26 μ rad towards S63 °E at Leirhnjúkur, while the north component of tilt at the Krafla power house was 14 μ rad. The tilt directions indicate that this event was associated with uplift of the Krafla fissure swarm south of Leirhnjúkur but not as far south as Hlídardalur.

The second subsidence event lasted from October 1 to 4, 1976. It caused a tilt of 22 μ rad towards N22 °W at Hlídardalur and 45 μ rad towards west at Leirhnjúkur, while the north component of tilt at the Krafla power house was 40 μ rad. This tilt is roughly in opposite direction to that of normal inflation periods, indicating that subsidence in the Krafla caldera is responsible for the observed tilt, but uplift outside the caldera is not noticeable. This can best be explained by magma flow towards north.

The volume of the magma flowing out of the Krafla magma chamber during the subsidence events of September 29 to October 4, 1976, can best be estimated from tilt observations at the Krafla power house. If the N-S component of tilt at the power house is solely due to volume changes in the magma chamber, the first phase of the subsicence event (September 29–30, 1976) is due to removal of approximately 3×10^6 m^3 of magma. Certain fraction of the observed tilt may have been due to uplift south of the power house and thus less magma is required. The easterly tilt at Hlídardalur requires a minimum of 2×10^6 m^3 to have been injected at 3-km depth. Thus it can be assumed that 2 to 3×10^6 m^3 of magma was injected towards the south from the Krafla magma chamber during this first subsidence event.

Tilt during the second subsidence event is apparently related to subsidence above the magma chamber. If this subsidence was distributed in the same way as uplift during inflation periods, the volume of magma which was emitted from October 1 to 4, 1976, was roughly 8×10^6 m^3

The estimated rate of outflow of magma (Fig. 4), reached about 40 m^3/s during the first event, on October 30, and nearly 50 m^3/s during the second event in the afternoon or night of October 2, 1976.

The Subsidence Event of October 30 to November 1, 1976 (Fig. 5)

The tilt measurements showing this subsidence event are the north and east components at the Krafla power house twice a day and five times in addition on October 31 and November 1, 1976, and measurements at the spirit level tilt stations Hlídardalur and Leirhnjúkur on October 23 and November 1, 1976.

If the last measurement before the subsidence event is extrapolated to November 1, we get the tilt during the event as follows: at the Krafla power house 162 μ rad towards N10 °E, at Hlídardalur 71 μ rad towards N7 °W and at Leirhnjúkur 160 μ rad towards S35 °W The tilt at these stations is nearly in the opposite direction to that observed during inflation periods. This shows that the subsidence is caused by northward flow of magma, as southward flow would have effected the direction of tilt at Hlídardalur. Opening of fissures and earthquake swarm north of the Krafla area support this view (Björnsson et al., 1977). The total volume of outflow as calculated from tilt at the power house is 32×10^6 m^3 and the rate of outflow probably exceeded 800 m^3/s between 4^h and 6^h in the morning of October 31 (Fig. 5).

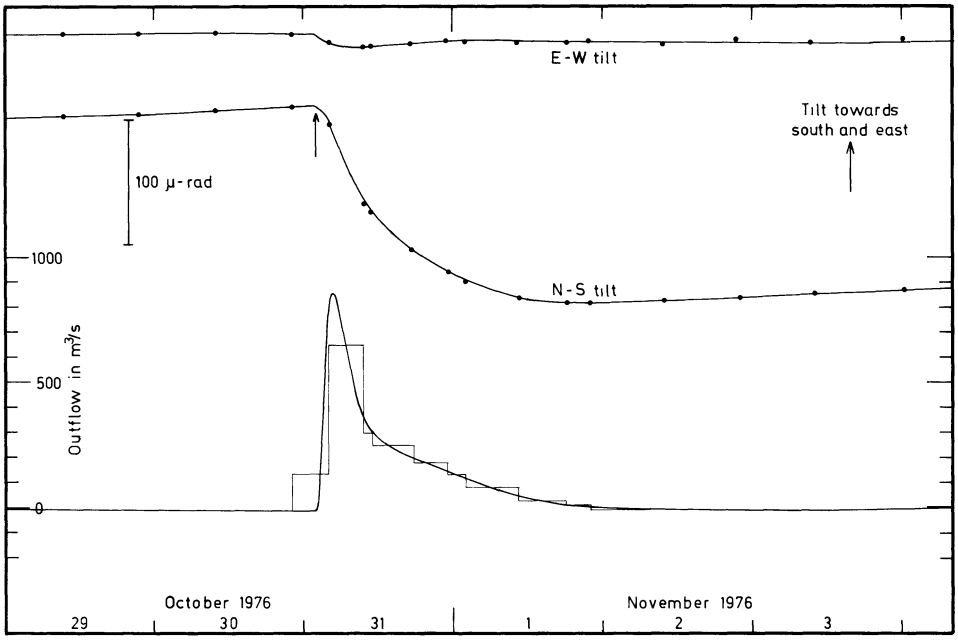

Fig. 5. Tilt in the Krafla power house as observed by the water tube tiltmeter, and the rate of magma flow out of the Krafla magma chamber during the subsidence event of October 31 to November 1, 1976. Notation as in Fig. 4

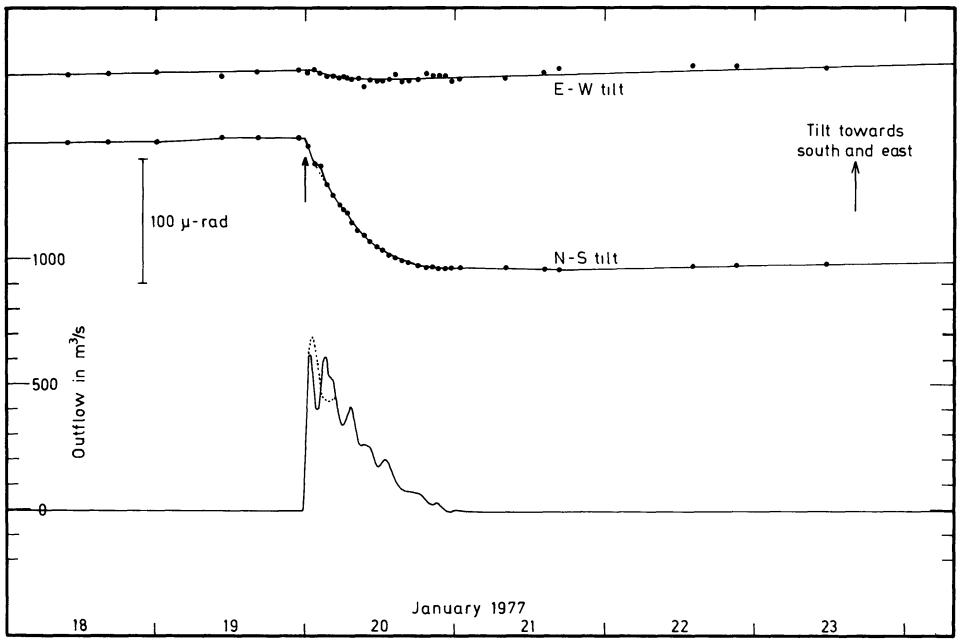

Fig. 6. Tilt in the Krafla power house as observed by the water tube tiltmeter, and the smoothed rate of magma flow out of the Krafla magma chamber during the subsidence event of January 20, 1977. *Dotted portion of curves* is obtained if one suspicious observation is omitted

The beginning of the subsidence event is clearly after the tilt observation on October 30, 22^h22^{min} and before October 31, 2^h15^{min} Seismic tremor was observed on seismometers at Húsavík and Reynihlíd on October 31, 2^h0^{min} or few minutes later. This represents the first sign of the subsidence. The subsidence ended before the tilt observation on November 1, 21^h45^{min}, but after the observation on November 1, 18^h10^{min} Thus the subsidence lasted roughly 42 h, from October 31, 02^h to November 1, 20^h.

The Subsidence Event of January 20, 1977 (Fig. 6)

The only tilt observations showing this event are those of the water tube tiltmeter in the Krafla power house. All spirit level stations in the area were convered by snow. Readings were taken at the power house tiltmeter two to four times a day before the subsidence event and the last observation on January 19, at 23^h00^{min} did not show any sign of the coming event.

Seismometers in Reynihlíd showed continuous tremor, which started about 23^h50^{min} on January 19 and the tiltmeter reading taken at 00^h30^{min} on January 20 showed clearly that subsidence had started in the Krafla area. It is assumed, that the beginning of the continuous seismic tremor coincided with the beginning of the subsidence. Hourly tiltmeter readings show clearly the progress of the subsidence until it almost ceased at 22^h January 20, but minor additional subsidence was observed between 8^h and 16^h on January 21 (Fig. 6).

The frequent tiltmeter observations during this subsidence event show that the rate of subsidence fluctuated considerably.

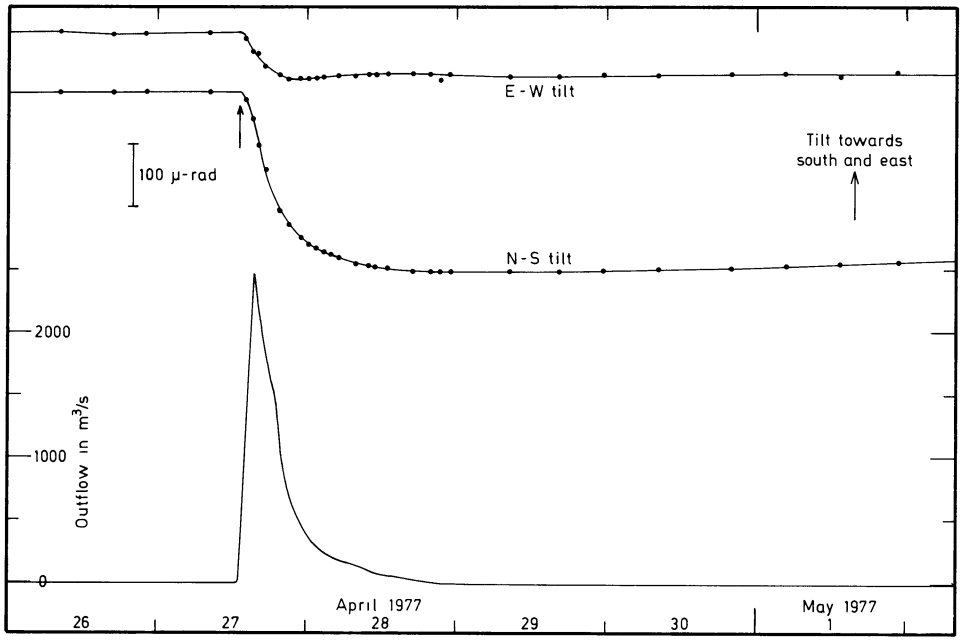

Fig. 7. Tilt in the Krafla power house as observed by the water tube tiltmeter, and the rate of magma flow out of the Krafla magma chamber during the subsidence event of April 27 to 28, 1977. The outflow rate as shown is probably some 10–20% too high (see text)

The maximum rate of subsidence was reached about one hour after the subsidence started. The subsidence rate corresponds to a rate of magma outflow of approximately 700 m^3/s. The east component of tilt was very small compared to the north component, indicating that the center of subsidence was towards N13 °E from the power house.

The total tilt at the power house from the beginning of the subsidence event on January 19 at 23^h50^{min} to its end on January 21 at 16^h was about 105 μ rad, corresponding to 21.0×10^6 m^3 of magma flowing out of the magma chamber, providing the tilt was only due to removal of magma from the same region as is inflated during inflation periods. There are no known indications of magma flowing towards south, so it is assumed that the magma movement during this event was towards north only. Opening of fissures and an earthquake swarm north of the Krafla area also show that magma flowed towards north (Björnsson et al., 1977; Sigurdsson, 1977).

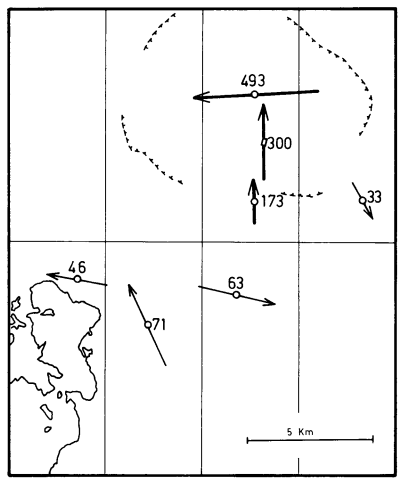

Fig. 8. Tilt vectors related to the subsidence event of April 27 to 28, 1977. Numbers give the estimated tilt in microradians

The Subsidence Event of April 27–28, 1977 (Figs. 7–9)

The tilt and distance observations relating to this subsidence event, are:

(1) Observations of the water tube tiltmeter in the Krafla power house three times a day and additional readings during the event.

(2) Tilt observations at six spirit level tilt stations in the Krafla-Mývatn area on May 16–20, 1977, but previous measurements at these stations had been made in the fall of 1976.

(3) Geodimeter and vertical angle theodolite measurements on 14 lines in the Krafla-Gjástykki area in late February and again in July 1977.

The first sign of the beginning of this subsidence event was continuous seismic tremor on the local seismometers, which commenced at 13^h17^{min} on April 27 (Sigurdsson, 1977). The tiltmeter reading in the Krafla power house at 8^h30^{min} the same morning did not show any sign of the subsidence, but at 14^h10^{min} the subsidence had started and it continued at a rapid rate during the following hours (Fig. 7). The rate of subsidence slowed down towards the evening of April 27, but it did not come to a complete stop until at about 20^h on April 28, some 31 h after the subsidence started. The tilt at the power house during these 31 h was some 290 μ rad towards north. The tilt at the spirit level tilt stations during this subsidence event, is estimated with a low degree of accuracy because of few observations prior to the event (Fig. 8).

Distance measurements with a geodimeter in the Krafla-Gjástykki area on Fabruary 26–March 3, 1977, and again on July 19–21, 1977, (Tryggvason, 1978b), show distance changes on 14 lines, which are believed to have occurred during the subsidence event of April 27–28, 1977. East-west widening of the fissure zone 63 to 93 cm was observed (Fig. 9). The zone that has widened is only about 1 km wide. Outside the zone of east-west extension, contraction of some 2 to 10 cm/km was observed. In the Mývatn area near Reykjahlíd other measurements showed 2.0 m widening of the fissure zone and 1.0 m shortening of a 7.2 km line outside the active fissure zone (Björnsson et al., 1979).

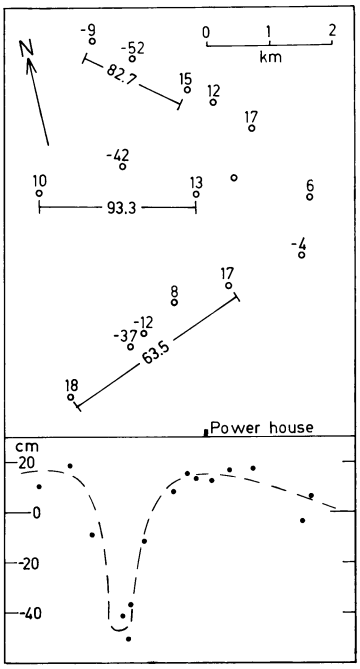

Fig. 9. Lengthening of three lines in the Krafla area and vertical displacements during the subsidence event of April 27 to 28, 1977. The *upper part* is a map (see Fig. 1 for location) showing the three lines across the active fissure zone, giving the calculated lengthening in centimeters, and the numbers by the stations give the vertical displacements in centimeters. On the *lower part* are the vertical displacements projected on a line parallel to the lower edge of the map

Elevation of the geodimeter points in the Gjástykki network were observed with a theodolite. These show about 60 cm subsidence of the active part of the fissure zone, relative to the surrounding area (Fig. 9). Similar vertical movements were observed on a leveling line from Reykjahlíd towards east across Námaskard, where the flanks of the fissure zone were uplifted about 40 cm, while the fissure zone subsided some 80 cm (Björnsson et al., 1979).

All these observations are interpreted as due to magma flow out of the magma chamber beneath the Krafla area into a fissure or fissures. The major part of this magma flowed southwards as indicated by the large tilts and widening of the fissure zone in the Mývatn area. Evidence of some northward flows in the small lava eruption on April 27, at the northern edge of the Krafla caldera (Björnsson et al., 1979; Sigurdsson, 1977).

The volume of magma, which was removed from the magma chamber can be crudely estimated from the 290 μ rad tilt at the Krafla power house. If this tilt is solely due to subsidence above the magma chamber, the volume of the subsidence bowl is about 58×10^6 m^3 However, in this case the majority of the magma moved southward causing uplift of the area south of the Krafla power house, increasing the tilt by an unknown amount. If we assume, that the tilt effect of the uplift is similar at the power house as the tilt near Mývatn (spirit level tilt stations A, 0020 and 0030, Fig. 8), which is 50 to 70 μ rad, the tilt at the power house related to subsidence to the north is estimated as 220 to 240 μ rad, corresponding to the removal of 44 to 48×10^6 m^3 of magma.

The rate of outflow of magma as shown on Fig. 7 is based on the assumption that the tilt is solely due to subsidence north of the power house. This shows a maximum rate of magma flow of some 2500 m^3/s, about 2 h after the beginning of the subsidence event. As a fraction of the tilt is due to uplift to the south of the power house, the actual flow rate is lower. Thus the maximum rate of outflow during this event was probably about 2000 m^3/s.

The Subsidence Event of September 8–9, 1977 (Figs. 10–12)

The tilt and distance observations, which provide information on this subsidence event, are:

1. Readings of the water tube tiltmeter in the Krafla power house once a day, with eight additional readings on September 8–10. Only the north component was observed.
2. Continuous recording of an electronic tiltmeter at the Krafla power house (Sindrason and Ólafsson, 1978). This tiltmeter is oriented parallel to the water tube tiltmeter.
3. Tilt observations at 11 spirit level tilt stations once a month.
4. Distance measurement with a geodimeter and vertical angle measurements with a theodolite on several lines inside the Krafla caldera and in the Mývatn area to the south of the caldera.

The water tube tiltmeter in the Krafla power house showed tilt towards north of 190 μ rad between the readings of September 8, 08^h50^{min} and September 10, 16^h40^{min} The new electronic tiltmeter with the sensor in a concrete cellar a few meters west of the power house, showed the beginning of the subsidence to be on September 8, 15^h40^{min} or possibly some five minutes earlier. The rate of subsidence increased rapidly until 17^h10^{min}, when it reached about 35 μ rad/h, whereafter the subsidence rate decreased even more rapidly to become zero at 18^h00^{min}. Then the tiltmeter indicated uplift to the north of the power house for 20 min, whereafter the subsidence started again and increased rapidly to reach maximum of about 50 μ rad/h at 18^h50^{min} Following this maximum the subsidence rate decreased gradually to zero on September 9, 15^h, whereafter slight inflation commenced. The total tilt according to the electronic tiltmeter was 198 μ rad towards N3 °W (Fig. 10).

Observations of the spirit level tilt stations were made on August 15–17, some 25 days before, and on September 10–12, 1977, immediately after the subsidence event. The tilt vectors at these stations (Fig. 11) clearly indicate subsidence in the western part of the Kraftla caldera and uplift around the active fissure swarm south of the caldera.

Distance measurements with a geodimeter made in July and August before the subsidence event and again in September and October, after the event, show considerable lengthening of lines crossing the Krafla fissure swarm. Within the Krafla caldera the widening is 70–100 cm (Fig. 12) and the zone that widened is roughly 1 km wide. South of the Krafla caldera only two measuring lines crossed the fissure swarm, one from Reykjahlíd to Námafjall, which increased in length by 104.9 cm, and another some 6 km farther south, which increased in length by only 7.4 cm, indicating that this line is at the southern end of the strip, which widened. An east-west line, 7250 m long, wholly outside the active part of the fissure zone from Reykjahlíd to Vindbelgur, was shortened by 25.4 cm, or about 3.5 cm per km. Short lines east of the active fissure zone within the Krafla caldera showed no systematic length changes during the event, but these lines regularily expand and contract as the magma chamber is inflated and deflated, so their length depends on the inflation stage at the time of measurements.

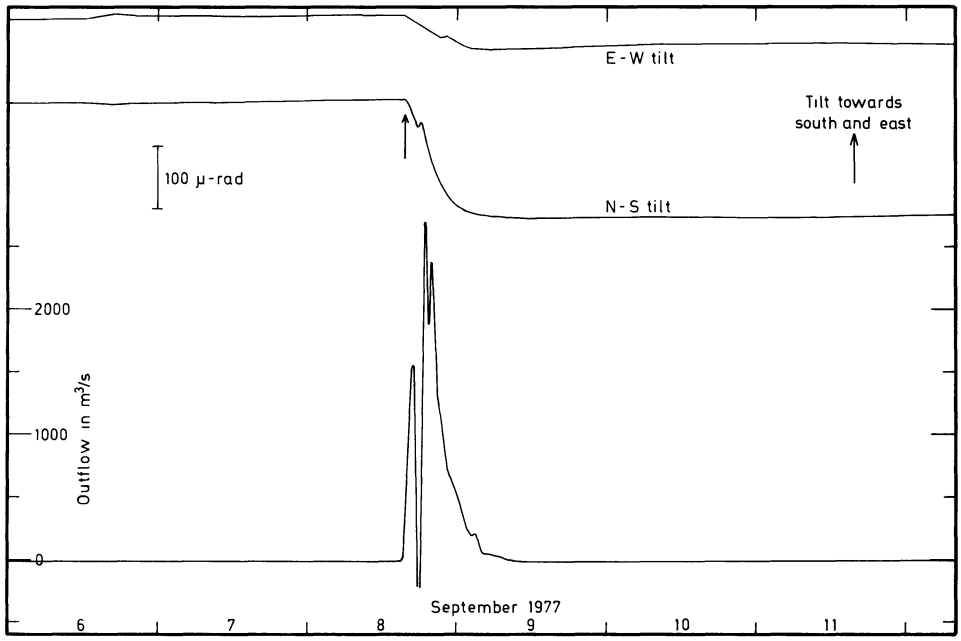

Fig. 10. Tilt in the Krafla power house as measured by the electronic tiltmeter, and the rate of outflow of magma from the Krafla magma chamber during the subsidence event of September 8 to 9, 1977. The outflow rate as shown may be 40–50% too high (see text)

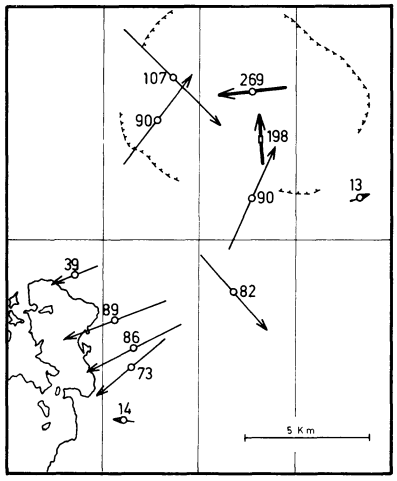

11

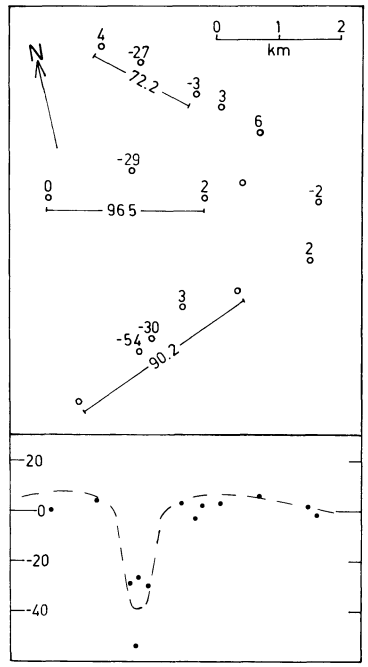

12

Fig. 11. Tilt vectors related to the subsidence event of September 8 to 9, 1977. *Numbers* give the calculated tilt in microradians

Fig. 12. Lengthening of geodimeter lines and vertical displacements of stations during the September 8 to 9, 1977 subsidence event. See Fig. 9 for explanation

The total volume of magma, which flowed out of the magma chamber during the event, can be estimated roughly from the observed tilt. The *N* component of tilt at the Krafla power house was about 194 μ rad. Part of this tilt is due to uplift south of the power house. If this part is equal to the maximum tilt near the south end of the injected zone (about 90 μ rad) the remaining part, about 100 μ rad, is due to subsidence of the Krafla caldera. This means that about 20×10^6 m^3 of magma moved out of the Krafla magma chamber. This number may be in error by some 20% due to the uncertainity of the effect of the uplift south of the power house.

The rate of outflow as calculated from the tilt change at the power house alone, is about 2700 m^3/s at its maximum (Fig. 10). This estimate is certainly too high, due to the effect of land rise to the south of the power house. If the calculated rate of flow is reduced by the same factor as the tilt in the discussion above, the maximum rate of magma outflow was about 1400 m^3/s.

It is obvious from the tilt and distance measurements, that the majority of the magma moved southwards. However, the widening of the fissure zone within the northern part of the Krafla caldera and the eruption of some 2×10^6 m^3 of lava near the northern edge of the caldera (Sigurdsson, 1977), shows that some magma flowed towards north. A rough estimate, based on widening of the fissure swarm, indicates that 80% of the magma flowed southwards, 10% flowed northward into subsurface fissures and 10% came to the surface as lava.

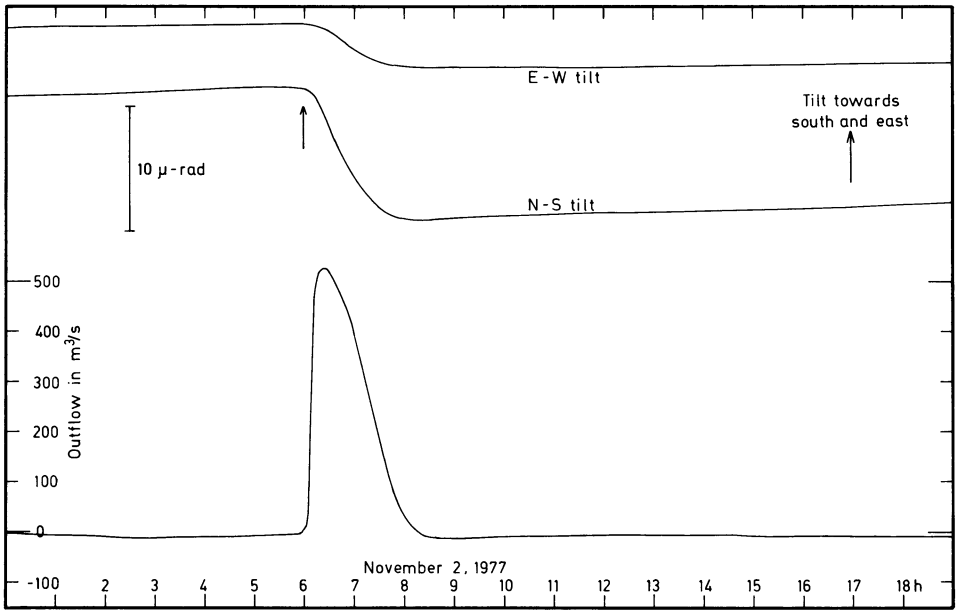

Fig. 13. Tilt in the Krafla power house as measured by the electronic tiltmeter, and the rate of outflow of magma from the Krafla magma chamber during the subsidence event of November 2, 1977

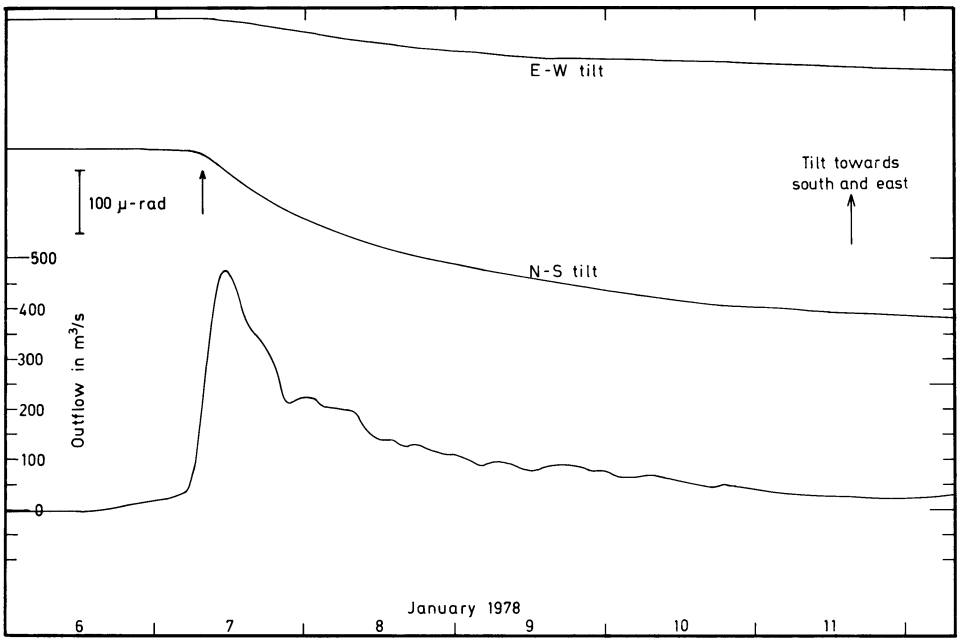

Fig. 14. Tilt in the Krafla power house as measured by the electronic tiltmeter, and the rate of outflow from the Krafla magma chamber during the first days of the January 1978 subsidence event

The Subsidence Event of November 2, 1977 (Fig. 13)

This event was small and the only clear observations of it were the recordings of the electronic tiltmeter at the Krafla power house, and the local seismometers. The subsidence started at about 6^h00^{min}, and the rate of tilt reached a maximum of about 10 μ rad/h at 6^h20^{min}, whereafter it decreased and the subsidence ceased altogether between 8^h00^{min} and 8^h30^{min} The total tilt at the Krafla power house was about 11 μ rad towards N6 °W. This represents a removal of 2×10^6 m^3 of magma from the Krafla magma chamber and the maximum rate of flow was about 500 m^3/s (Fig. 13). The direction of the magma flow is not known with certainty, but the ratio of north and east components of tilt at the Krafla power house is very similar to that of the inflation periods, which indicates flow towards north.

The Subsidence Event of January, 1978 (Figs. 14–16)

The following tilt and distance observations were made:

1. the water tube tiltmeter at the Krafla power house once a day;
2. Continuous recordings of the electronic tiltmeters at the Krafla power house and at Reynihlíd,
3. 11 spirit level tilt stations in the Krafla-Mývatn area before, during, and after the subsidence event;
4. distance with geodimeter in the Krafla-Gjástykki area before and after the event, and
5. tilt at two spirit level tilt stations in Kelduhverfi before and after the event.

The water tube tiltmeter at the Krafla power house showed tilt down to the north to commence before the observation on January

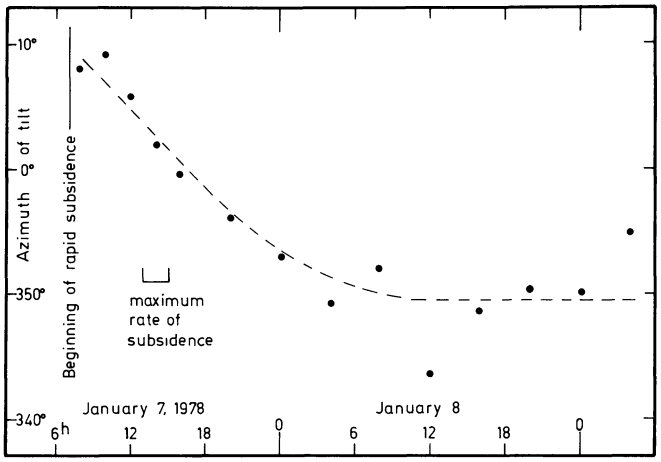

Fig. 15. Direction of tilt at the Krafla power house during the first two days of the January 1978 subsidence event. *Filled circles* give average directions over 2–4 h periods. The *dashed* line is the authors interpretaition of the variation of tilt azimuth with time

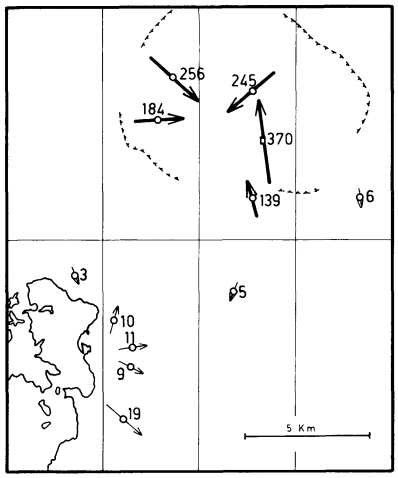

Fig. 16. Tilt vectors related to the subsidence event of January 1978. Numbers give the estimated tilt in microradians

7, 07^h, but after the observation on January 6, 09^h. The tilt continued until January 25, and had then reached 317 μ rad. The east component of the water tube tiltmeter did not operate.

The electronic tiltmeter at the Krafla power house showed slight subsidence to commence on January 6, at 15^h approximately, but this was very slow the first 16 h, when the tilt had reached only 4 μ rad. On January 7, at about 07^h, the subsidence rate started to increase dramatically, and the maximum rate of *N*-tilt of 8.9 μ rad/h was reached between 12^h and 15^h on January 7, or 5–8 h after the rapid increase in tilt rate. The subsidence continued, although its rate fluctuated greatly, unit about January 22, when the observed tilt had reached 370 μ rad towards N7 °W (Fig. 14). Both *N* and *E* components of this tiltmeter showed great fluctuations in rate during this event and for several weeks after, indicating that some processes associated with the event continued for a month or more after the subsidence of the Krafla region ceased on January 22–25, 1978. The direction of tilt during the first hours showed continuous variation from N10 °E at the very beginning of the rapid subsidence to about N12 °W a day later (Fig. 15).

The electronic tiltmeter at Reynihlíd showed great irregularities during this subsidence event, so the tilt cannot be determined with accurancy.

The spirit level tilt stations 0000, 0010, 0080, and 0090 show the event clearly, although observations were not made after the event until mid May, 1978. The other spirit level tilt stations in the Krafla-Mývatn area showed no definite tilt due to this subsidence event, probably because no observations were made after the event until mid May 1978 (Fig. 16).

Distance measurements with the geodimeter on 24 lines in the Krafla-Gjástykki area in October and November 1977, and again in March 1978, show irregular length changes, usually less than 5 cm on each line, although shortenings of 6 to 17 cm were observed on 6 lines near the center of subsidence. These length changes are largely or wholly the result of vertical ground displacements and associated bending of the elastic crust. They do not indicate any widening of the fissure zone, as was observed during the subsidence events of April and September 1977.

Tilt observations at two spirit level tilt stations in Kelduhverfi were made on July 15, 1977, before the subsidence event, and on May 21, 1978, after the event. At the station Hóll (66°02′.8 N, 16°38′.0 W) a tilt of 210 μ rad towards south (azimuth 180.0°) was observed, while at the station Lón (66°06′.0 N, 16°54′.2 W) the observed tilt was about 14 μ rad towards WNW (azimuth 284.2°).

The near zero ground deformation in the Mývatn area together with large scale ground deformation and a major earthquake swarm in Kelduhverfi some 40 km north of Krafla, shows that the magma flowed northward from the Krafla magma chamber. Some of it reached the tilt station Hóll, 39 km north of the center of subsidence.

As no magma was deposited in the southern part of the fissure system north of Krafla, the tilt at the Krafla power house is a rather reliable indicator of the volume of the magma, which left the chamber. However, the subsidence event lasted for approximately 3 weeks, so it may be assumed that a considerable amount of magma flowed into the chamber from below at the same time. Under these assumptions, the total volume of the magma, which flowed out during the subsidence event, is estimated 70 to 75×10^6 m^3 The rate of flow reached a maximum of approximately 500 m^3/s near noon on January 7 (Fig. 14), and decreased irregularly towards the end of January 1978. There were several noticeable increases in the outflux rate, especially on January 14–15 and on January 19, when it reached 60 to 70 m^3/s and on January 30 and February 2, when it reached approximately 40 m^3/s.

The Subsidence Event of July 10–12, 1978 (Figs. 17–21)

The tilt and distance observations showing this event are:

1. daily readings of the water tube tiltmeter in the Krafla power house;

2. continuous recording of electronic tiltmeters in the Krafla power house and in Reynihlíd,

3. observation of 11 spirit level tilt stations in the Krafla-Mývatn area about once each month, and

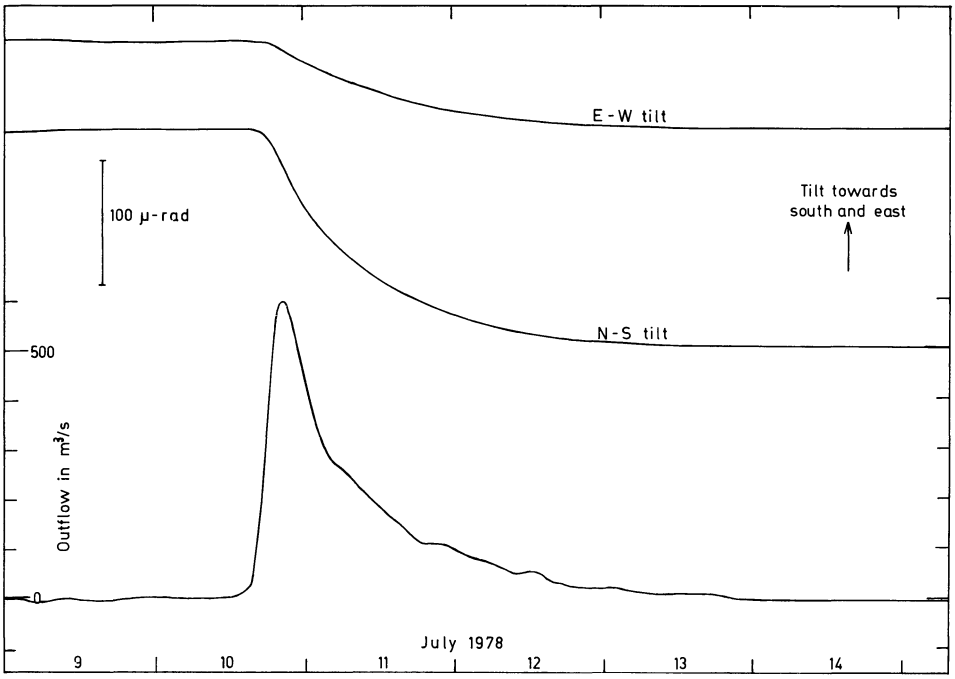

Fig. 17. Tilt in the Krafla power house as measured by the electronic tiltmeter, and the rate of outflow from the Krafla magma chamber during the July 10 to 12, 1978 subsidence event

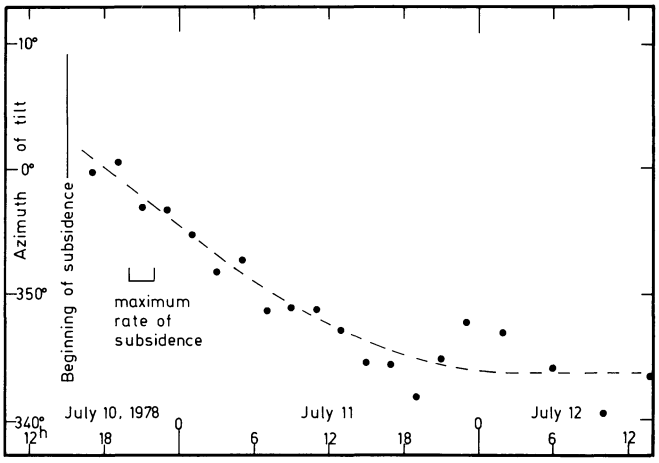

Fig. 18. Direction of tilt at the Krafla power house during the subsidence event of July 10 to 12, 1978. See Fig. 15 for explanation

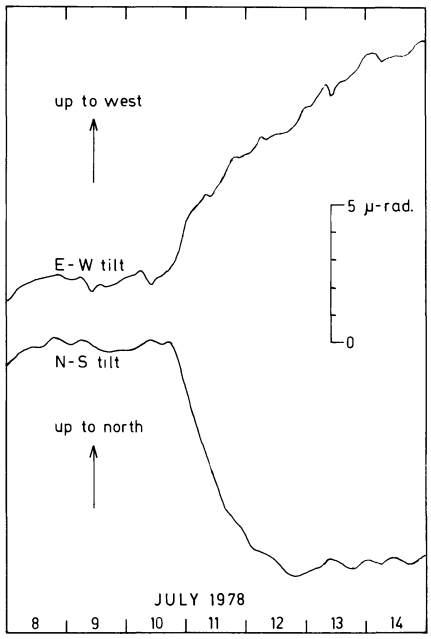

Fig. 19. Redrawn traces of the electronic tiltmeter in Reynihlíd during the July 10 to 12, 1978 subsidence event

4. distance measurements with a geodimeter on about 100 lines in the Krafla-Gjástykki area and similtaneous theodolite observations of elevation differences.

The water tube tiltmeter in the power house shows a total tilt of 177 μ rad towards north between July 10, 9^h and July 13, 13^h40^{min} The east component of the water tube tiltmeter showed no significant tilt.

The continuously recording electronic tiltmeter at the power house showed that the tilt started on July 10 at about 11^h, although it was very slow until about 15^h (Fig. 17). The rate of tilt increased rapidly until it reached its maximum between 20^h and 21^h, about 11.1 μ rad/h. Thereafter the rate of tilt decreased gradually until July 12, 20^h when a new inflation period started. The total tilt according to the electronic tiltmeter, was 188 μ rad towards N8 °W.

The direction of tilt, according to the electronic tiltmeter, was approximately N3 °E at the beginning of the subsidence event, and changed gradually to N17 °W in the afternoon of July 11 (Fig. 18).

The electronic tiltmeter at Reynihlíd (Fig. 19) showed definite tilt to start at about 19^h on July 10, or several hours later than at the Krafla power house. The tilt was about 8 μ rad towards north and a slightly smaller east component. The north component reached a maximum in the evening of July 12, as at the Krafla power house, while the east component showed progressive tilt for several days. This can be interpreted as change in direction of tilt at Reynihlíd from some 20° east of north at the beginning

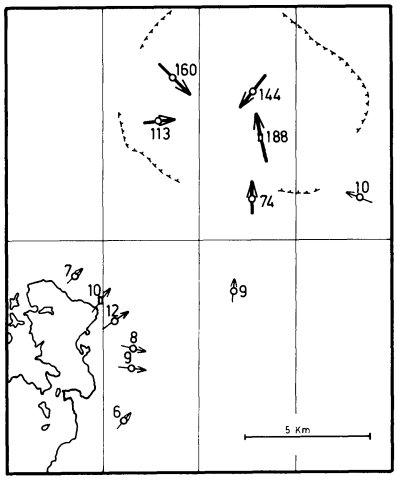

Fig. 20. Tilt vectors related to the subsidence event of July 10 to 12, 1978. Numbers give the calculated tilt in microradians

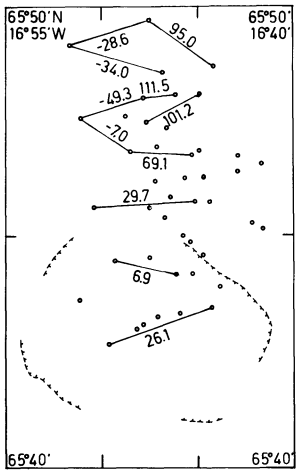

Fig. 21. Length changes of selected geodimeter lines in the Krafla-Gjástykki area between March and August 1978, in centimeters. The changes in the northern part of the area of measurement occurred during the July 10 to 12 subsidence event. See Fig. 2 for location

of the subsidence event towards east and even slightly south of east on July 13.

The spirit level tilt stations were occupied on June 24–29, 1978, before the event and in late July or early August after the event. The tilt at these stations related to the subsidence event are shown on Fig. 20. The tilt in the Mývatn area is so small that observational errors and minor tilt at times other than during the subsidence event may affect the results significantly. However, the very close correlation between observed tilt on the electronic tiltmeter at Reynihlíd and that at nearby spirit level stations (0020 and 0070) supports the opinion that the tilt shown on Fig. 20 is primarily related to this subsidence event.

Distance measurements in the Krafla-Gjástykki area in March 1978, and again in August 1978 (Fig. 21), show no noticeable permenent horizontal deformation within the Krafla caldera, but a widening of the fissure zone of approximately 1 m is observed in the northernmost part of the area of measurements. This widening is accompanied by subsidence of 50–70 cm of the central part of the fissure zone, relative to its flanks, and an east-west shortening of lines immediately outside the fissure swarm. The lengthening of 26 cm across the central part of the Krafla caldera is explained by the different stages of inflation during the two measurements.

The tilt measurements do not indicate any magma flow towards south, while the distance measurements strongly indicate deposition of magma below the southern part of Gjástykki, where the fissure zone was widened by 1 m. The present measurements do not show how far north the magma flow reached.

The total volume of magma, which flowed out of the Krafla magma chamber during the subsidence event, can be estimated from the north component of tilt at the Krafla power house to be about 37×10^6 m^3

The Subsidence Events of November 10–15, 1978, and May 13–18, 1979

These two events were very similar to that of July 10–12, 1978, although slightly larger. A preliminary analysis of the observational data indicates, that 44 to 45×10^6 m^3 of magma flowed out of the Krafla magma chamber during each event. Geodimeter measurements in April 1978 and May 1979 indicated 3.5 m widening of the fissure swarm, 18 km north of Krafla. This widening occurred during three subsidence events, July and November 1978 and May 1979, which all affected the same section of the fissure swarm.

Concluding Remarks

The present interpretation accounts for 12 subsidence events in the Krafla area from December 1975 to May 1979. The number of subsidence events is somewhat questionable. The two events at the end of September and beginning of October 1976 are sometimes considered as only one event (Björnsson et al., 1977). The event on November 2, 1977, is very small and of short duration, so it may be of limited significance in the sequence of events. Still smaller subsidence events may have occurred, without being noticed, espicially before the water tube tiltmeter was installed in the Krafla power house on August 20, 1976.

Of the twelve events, three have been associated with magma flowing primarily towards south and nine with magma flowing mainly or wholly towards north (Table 1). The total amount of magma flowing out of the Krafla magma chamber during these twelve events is estimated as 4.81×10^8 m^3 (0.481 km^3) of which 4.07×10^8 m^3 has been deposited in dikes to the north, and 0.72×10^8 m^3 to the south of the center of the Krafla caldera. About 2.4×10^6 m^3 has erupted.

It is assumed that magma, which flowed into the fissure swarm, formed a dike of width about equal to the widening of the fissure swarm. The subsidence of the central zone of the fissure swarm is supposedly caused by slumping into the void above the dike. Thus the depth to the dike can be estimated from the widening of the fissure swarm and the cross-sectional area of the subsidence. The depth to the dike appears to be 500–1,000 m within the Krafla caldera (Figs. 9 and 12), while a depth of 1,000–1,500 m is indicated in the Mývatn area according to data given by Björnsson et al. (1979). This depth is probably controlled by the cooling affect of groundwater in highly permeable formations. The new and intensified steam fields along the fissure swarm clearly show interaction between magma and the groundwater system.

Table 1. Estimated volume of magma flow in the Krafla subsidence events in 10^6 m^3

Event	Volume of flow towards north	Volume of flow towards south	Volume of lava	Total volume of flow
December 20, 1975	140	10	0.4	150
September 29, 1976		2		2
October 1, 1976	8			8
October 31, 1976	32			32
January 20, 1977	21			21
April 27, 1977	2	44	0.01	46
September 8, 1977	2	16	2	20
November 2, 1977	2			2
January 7, 1978	74			74
July 10, 1978	37			37
November 10, 1978	45			45
May 13, 1979	44			44
Total	407	72	2.4	481

The accumulated widening of the Krafla fissure swarm during the sequence of events which started in 1975 can only be estimated. The only precise distance measurements across the fissure swarm before 1975 were made by German scientists and remeasurements during the summer of 1977 showed lengthening of up to 1.8 m of lines which exceeded 10 km in length (Gerke et al., 1978). If the contraction of the flanks of the fissure swarm and the effect of line direction is added to the line lengthening, a widening of 2 to 3 m of the fissure swarm is estimated. A further widening of about 1 m occurred in the same area in September 1977 to July 1978 (this paper). A widening of 3.2 m in the Mývatn area was measured in two subsidence events (Björnsson et al., 1979; this paper) and some additional widening occurred in December 1975. In Kelduhverfi, 40 km north of Krafla, a widening of 1.5 m was indicated by opening of fissures in December, 1975 (Björnsson, 1976), and similar widening occurred at the same place in January 1978. Thus the widening of the Krafla fissure swarm probably equals or exceeds 3 m throughout its whole length from Mývatn to Axarfjördur. In places it exceeds 4 m.

The contraction of the flanks of the fissure swarm has been measured as 1 m on 20 km line or 5×10^{-5} between 1975 and 1977 (Gerke et al., 1978), 1.25 m on 7.2 km line or 1.7×10^{-4} in April and September, 1977 (Björnsson et al., 1979; this paper) and 0.49 m on 2.7 km line or 1.8×10^{-4} in July, 1978 (this paper). Thus the maximum relative east-west shortening of the flanks of the fissure zone is about 2×10^{-4}

The average cross-sectional area of the new dike is found to be about 6,000 m^2 by dividing the dike volume of 4.8×10^8 m^3 by the total length of the active fissure swarm of about 80 km. An average width of 3 m gives 2 km average height of the dike. With 1 km depth to the top of the dike, its bottom is apparently at only 3 km depth. If the dike narrows downwards, it extends deeper.

Acknowledgements. The observations of the water tube tiltmeter in the Krafla power house have been made by the staff of the National Energy Authority and the tilt observations of the spirit level stations were funded by the Science Institute of the University of Iceland until August 1977. The accomodation for tiltmeters in the Krafla power house is greatly appreciated, and also the assistance and goodwill of Jón Ármann Pétursson, who made it possible to operate a recording tiltmeter in Reynihlíd.

References

Björnsson, A. Jardhræringar vid Kröflu (Rifting and volcanism in the Krafla area 1975–1977) (in Icelandic). Náttúrufrædingurinn **46**, 177–240, 1976

Björnsson, A., Saemundsson, K., Einarsson, P., Tryggvason, E., Grönvold, K.: Current rifting episode in north Iceland. Nature **266**, 318–323, 1977

Björnsson, A., Johnsen, G., Sigurdsson, S., Thorbergsson, G., Tryggvason, E.: Rifting of the plate boundary in north Iceland 1975–1978. J. Geophys. Res. **84**, 3029–3038, 1979

Brandsdóttir, B., Einarsson, P.: Seismic activity associated with the September 1977 deflation of the Krafla central volcano in NE-Iceland. J. Volcanol. Geothermal Res. in press 1979

Einarsson, P.: S-wave shadows in the Krafla caldera in NE-Iceland, evidence for a magma chamber in the curst. Bull. Volcanol. **41**, 1–9, 1978

Gerke, K.. Über neuere horizontale und vertikale Krustenbewegung in Island. Mitteilungen der Technischen Universität Carolo-Wilhelmina zu Braunschweig **XII**, 4 pp., 1977

Gerke, K., Möller D., Ritter, B. Geodätische Lagemessungen zur Bestimmung horizontaler Krustenbewegungen in Nordost-Island. In: *Festschrift für Walter Höpcke,* pp. 23–33. Hannover Technische Universität, 1978

Mogi, K.: Relations between the eruptions of various volcanoes and the deformation of the ground surfaces around them. Bull. Earthq. Res. Inst. **36**, 99–134, 1958

Sigurdsson, O.: Natturuhamfarir i Thingeyjarthingi (Natural catastrophes in Northeast Iceland) (in Icelandic). Tyli **6**, 3–20, 1976

Sigurdsson, O. Natturuhamfarir i Thingeyjarthingi (II) 1976–1978 (Natural catastrophes in Northeast Iceland (II) 1976–1978) (in Iceland). Tyli **7**, 41–56, 1977

Sindrason, S., Ólafsson, H.: A magnetoresistor geotiltmeter for monitoring ground movent. Nordic Volcanological Institute **78 06**, 1–7, 1978

Tryggvason, E. Landslagsbreytingar samfara jardskjalftunum 1975–1976 (Ground movement in North Iceland during the earthquake swarm of 1975–1976) (in Icelandic). Natturufrædingurinn **46**, 124–128, 1976

Tryggvason, E. Tilt observations in the Krafla-Mývatn area 1976–1977. Nordic Volcanological Institute **78 02**, 1–45, 1978a

Tryggvason, E.: Distance measurements in 1977 in the Krafla-Mývatn area and observed ground movements. Nordic Volcanological Institute **78 10,** 1–47, 1978b

Ward, P.L., Björnsson, S. Microearthquake swarms and the geothermal areas of Iceland. J. Geophys. Res. **76**, 3953–3983, 1971

Ward, P.L., Pálmason, G., Drake, C. Microearthquake survey and the Mid-Atlantic Ridge in Iceland. J. Geophys. Res. **74**, 665–684, 1969

Received April 2, 1979; Revised Version July 13, 1979

J. Geophys. 47, 154–159, 1980

Journal of Geophysics

Surface Deformation of the Krafla Fissure Swarm in Two Rifting Events

O. Sigurdsson
National Energy Authority, Grensásvegur 9, 108 Reykjavík, Iceland

Abstract. The Krafla rifting episode in North Iceland has had 11 main tectonic events during the period December 1975 to May 1979. Each event has lasted from a few hours to several weeks. The first and eighth events affected to some extent the same part of the Krafla fissure swarm. These two tectonic events in the fissure swarm were characterized by down-faulting of a central area of the fissure swarm about 5-km-wide E-W and 20-km-long N-S. The resulting graben was boarded on both sides by an intensely faulted and fractured zone. These fracture zones showed spreading of 1.5 m in the first event and 2.66 m in the eighth one along the same reach. Elastic contraction on both sides of the fissure swarm added up to 1.4 m in the eighth event. The graben floor is estimated to have subsided about 1 m in the first event while a further subsidence of 1.1 m was observed in the 8th event. The flanks of the graben rose about 0.5 m during the latter event. The rise diminished away from the fissure swarm.

Key words: Iceland – Rifting events – Fissures – Surface deformation – Geodetic observations.

Introduction

The rifting episode of the Krafla plate boundary in North Iceland (Fig. 1) has been in progress since December 20, 1975 as described by Sigurdsson (1976), Björnsson et al. (1977), Björnsson (1977), and Sigurdsson (1978). During the period 1975–1979 the Krafla caldera floor was rising at a steady rate interrupted by eleven sudden subsidence events. Each subsidence event was accompanied by rifting in confined areas at different places within the 80 km long fissure swarm, which crosses the caldera and strikes N9 °E.

Subsidence and rifting events occurred in December 1975, September 1976, October 1976, January 1977, April 1977, September 1977, November 1977, January 1978, July 1978, November 1978, and May 1979. These events were similar in nature but varied greatly in magnitude. The fifth and the sixth event affected the fissure swarm within the caldera and towards south, but the rest of the events affected the northern part of the fissure swarm with the possible exception of the event of November 1977, which was so small that its direction could hardly be determined. Small volcanic eruptions occurred within the caldera during three of the events, the first, fifth, and sixth one. Small amounts of volcanic material were erupted through a borehole within the fissure swarm during the sixth event.

This paper describes the horizontal and vertical movements of the ground surface in the area of rifting of the fissure swarm during the first and the eighth event. This part of the fissure swarm runs through inhabited area and is much more easily accessible than most other parts of the fissure swarm. Therefore this area was chosen for geodetic measurements.

These rifting events obviously continue a much older process, since almost all recent faulting occurs on older faults. Thus it can be very difficult to determine how much of the faulting movement took place in the events described here. The sandur plaines of the glacial river Jökulsá á Fjöllum cover all older fissures and offer excellent opportunity for studying the fault movements of a single event (Fig. 2).

The Event of December 1975 to February 1976

The first event of the rifting episode started at about 10 h on December 20, 1975. This was by far the greatest of the events that have occurred so far. The subsidence of the Krafla caldera floor exceeded 2 m (Thorbergsson, 1977). The subsequent earthquake swarm migrated northwards through the fissure swarm in about two hours and concentrated in the fissure swarm about 40–50 km north of Krafla caldera where surface faulting occurred (Björnsson et al., 1977) (Fig. 1). Two severely fractured parallel zones striking about N9 °E boarded a down-faulted area about 5 km wide and some 20 km long (Fig. 2).

Changes in Elevation

Very few bench marks were within the subsided area prior to 1975 and it is impossible to scale the subsidence in absolute values. Some statements can be made, however, as to the relative changes in elevation of the down-faulted area. The largest vertical displacement measured at one point was about 3 m. Within the southern part of the new graben a lake formed.

The maximum depth measured in this new lake by local people was 1.5 m in several places. This suggests that the minimum relative vertical displacement between the areas inside and outside the graben must be at least 1.5 m. As there were no signs of fissuring or subsidence at the beach the graben does not seem to reach into the sea.

In 1962 the Public Road Administration measured a line across the graben. The marks were 40-cm-long pegs driven half-way into the ground at 20-m intervals. The line has been destroyed at both ends leaving only 4.7 km intact (Fig. 2). Relevelling of the line in 1976 and 1977 gave the results presented in Fig. 3. The westernmost point is assumed to have a fixed elevation. The

0340-062X/80/0047/0154/$01.20

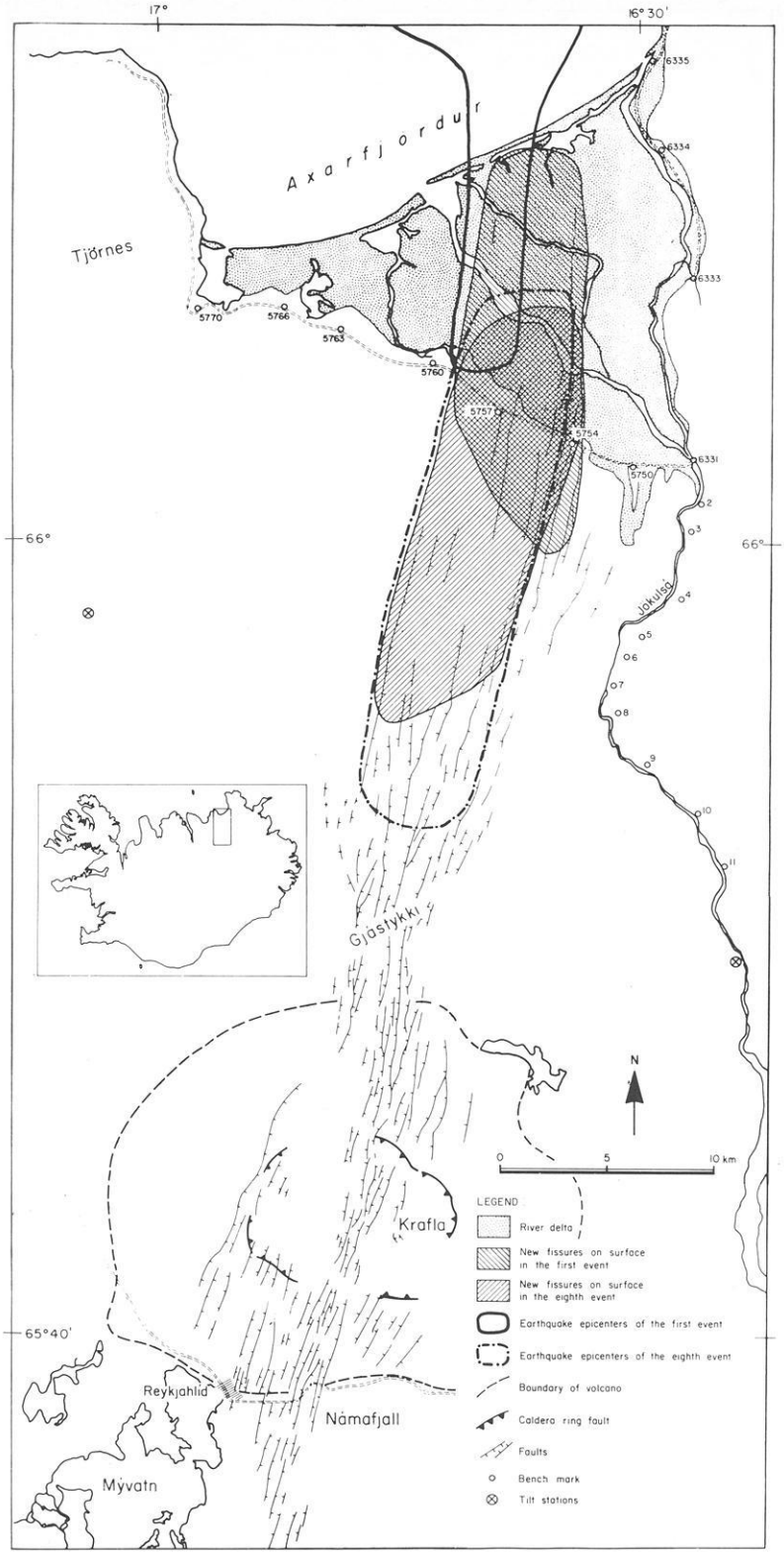

Fig. 1. The Krafla fissure swarm NE Iceland. Earthquake epicenter data from P. Einarsson et al., 1980. Volcano, caldera and faults by K. Sæmundsson.

ground at the levelling line was tilted towards N and E, but on the whole, the graben floor seems to have subsided rather evenly.

The westernmost 0.5 km of the line was steeply tilted towards east but no distinct fault escarpment could be seen at that place.

Several bench marks were established between 1958 and 1963 to the E and SE of the subsided area. Some of these (Fig. 1) were remeasured in 1976 and showed considerable changes in elevation. The bench marks are too far apart to allow drawing of contours for elevation changes, but they give a clue to the general picture. To the east of the graben the ground has been elevated. The rise is greatest close to the main faults but decreases

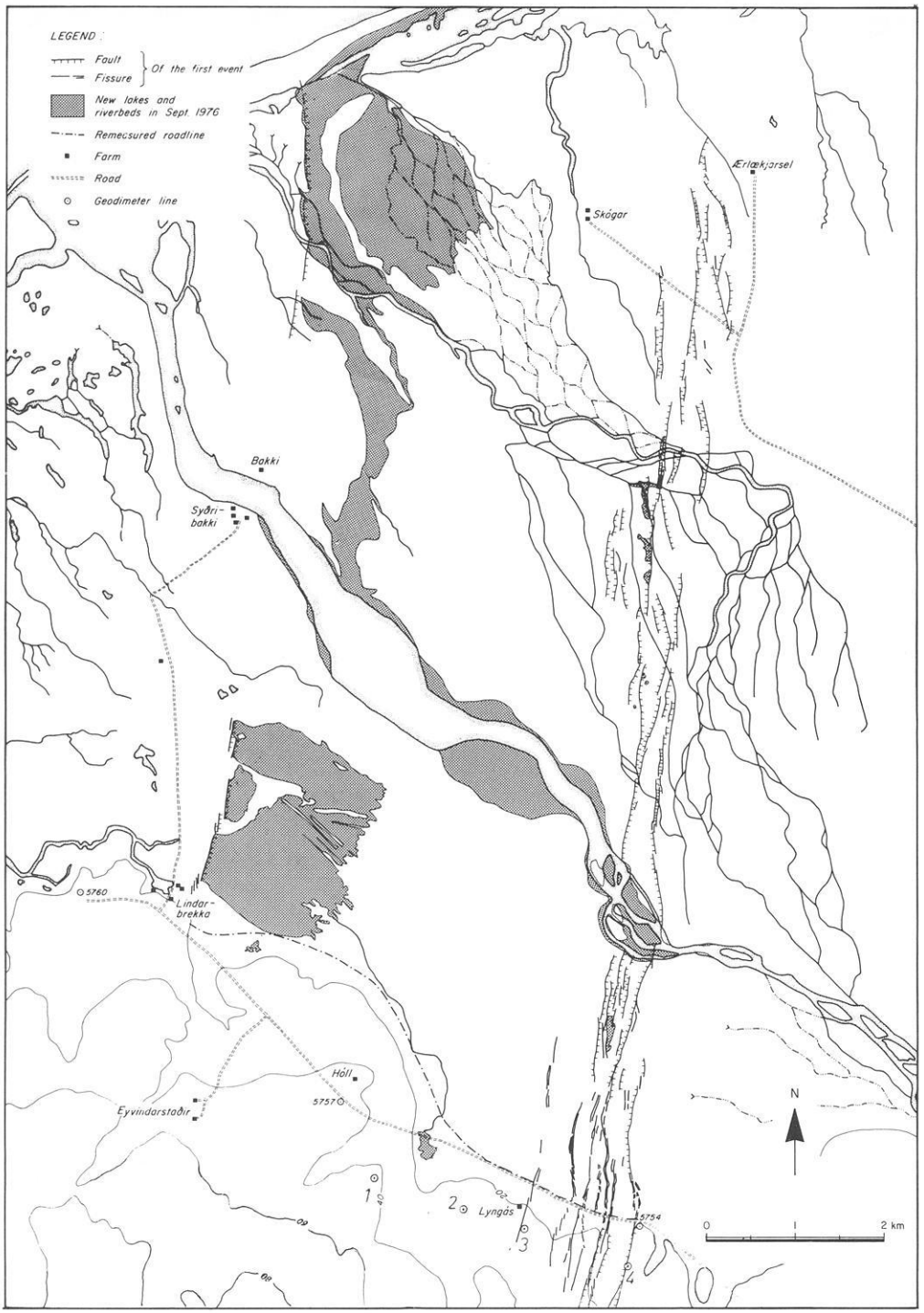

Fig. 2. The fault and fissure system of the first event in the sandur plains of Jökulsá á Fjöllum. Mainly from aerial photographs of September 1976

gradually away from the graben. The greatest relative elevation change measured was about 40 cm.

Apparently a vast area has been affected during this event. Relevelling of a 20-km-long line of bench marks towards SSE from the subsided area showed relative elevation changes of all the bench marks (Fig. 4). Five kilometer farther to the S (Fig. 1) a few precission levelling lines (Tryggvason, 1972) which have remained relatively stable for 5 years showed a tilt of 3 μrad to the SW. A tilt station 25 km to the SW of the graben tilted to the SW (Tryggvason, 1977).

Horizontal Movement

One of the most obvious features of the events was the formation of fissures and widening of old ones. No distances within the area had been measured before the event and accordingly no comparative distance measurements can be made.

On January 17 and 18, 1976 all fissures in the frozen ground by the road across the faulted fissure zones were measured with a ruler. The total spreading across the eastern fissure zone was 127 cm and that of the western zone was 30 cm. This method

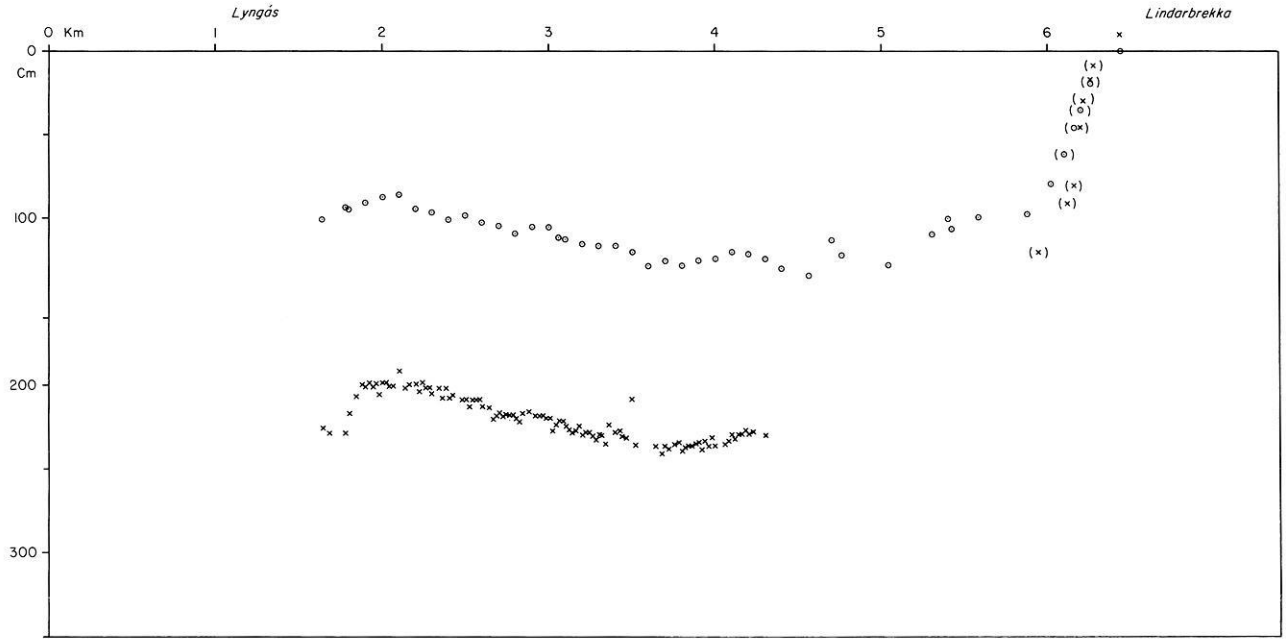

Fig. 3. Change of elevation of a road profile across the graben floor, see Fig. 2. *Legend*:—: 1962; ⊙⊙⊙⊙: 1976 (1977); × × × × × : 1978

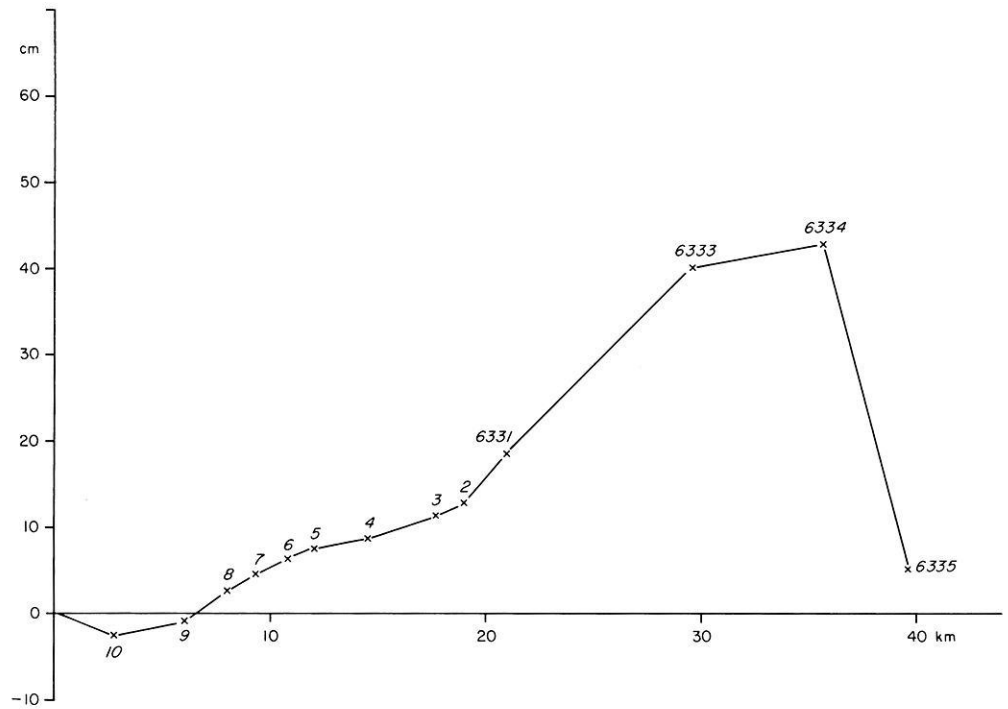

Fig. 4. Change in elevation along the Jökulsá á Fjöllum in the first event, see Fig. 1

has proved surprisingly consistent with geodimeter measurements (Björnsson, 1977). Similar measurements were carried out in March 1976, 15 km to the south and showed only 7 cm spreading. The spreading across the fissure zone was also obvious from stretching and breaking of telephone lines and fences.

Event of January 1978

The eighth event of the Krafla rifting episode started on January 7, 1978. This event took a similar course as the first one and was the second largest in terms of subsidence within the Krafla

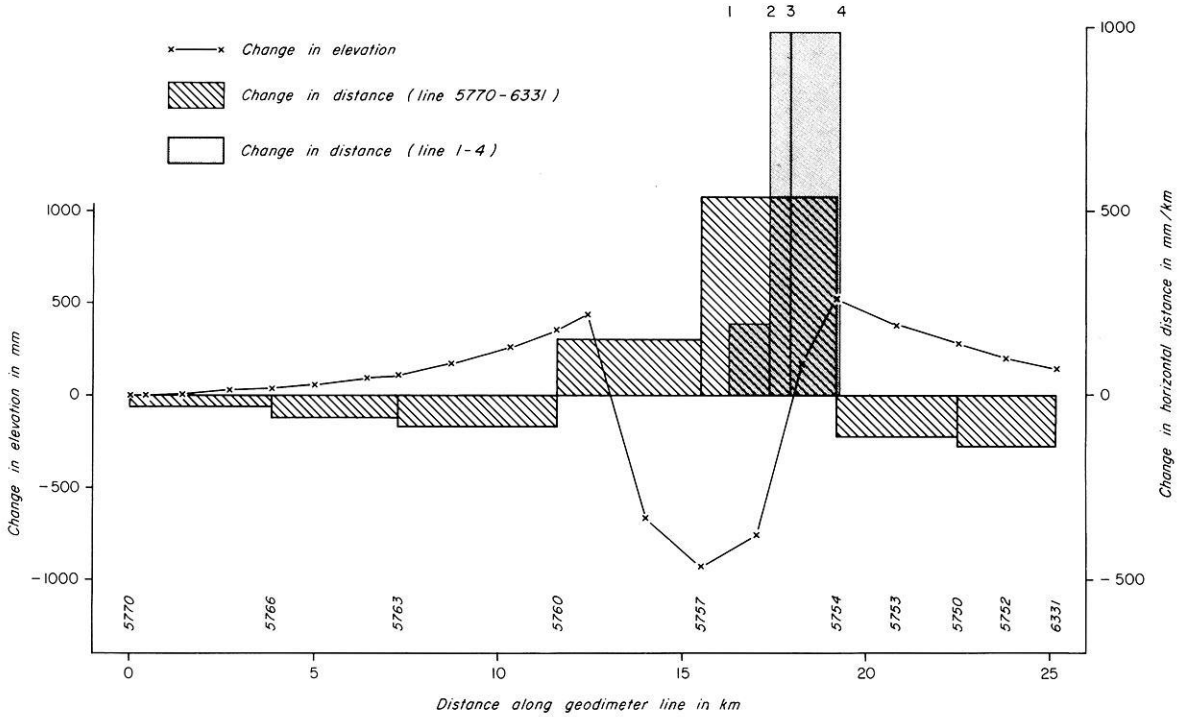

Fig. 5. Change in elevation and horizontal distance in the eighth event, see Fig. 1; for location of numbered stations see Figs. 1 and 2

caldera. The earthquake swarm did not reach as far to the north as the first one (Fig. 1).

South of Axarfjördur much the same features appeared as in the first event. Fissures were reactivated, and a large area subsided while other areas were uplifted. The new lake increased in area and depth, new springs appeared and others increased, while some disappeared.

Changes in Elevation

A new geodetic line of 21 bench marks was established by Gunnar Thorbergsson in May 1976. Repeated measurements on parts of the line during 1976 and 1977 did not show any significant changes in relative elevation of the bench marks. Relevelling of the line in June 1978 gave the results shown in Fig. 5. This reveals an almost symmetrical figure of a graben between elevated flanks. The rise diminishes with distance from the graben as was anticipated after the first event. Similar changes were measured after the fifth and sixth events in the southern part of the fissure swarm (Björnsson et al., 1979).

The road profile of 1962 was also remeasured in June 1978 (Fig. 3). This time the bench mark 5770 (Fig. 1) was defined as zero for comparison. The results are very similar to those in the first event, but the subsidence of the graben floor has increased by about 1.1 m.

Only very limited measurements were carried out outside the vicinity of the fissure swarm, but they suggest that vast areas were affected also this time.

Horizontal Movement

The line of bench marks mentioned above was used for geodimeter measurements. Seven different distances were measured in 1977 by Gunnar Thorbergsson and remeasured in June 1978. An extra geodimeter line (1–2–3–4 on Fig. 5, location see Fig. 2) was established and measured by Professor Dr. Ing. D. Möller, Braunschweig, in 1977 and remeasured by G. Thorbergsson in June 1978. Each of the distances had changed significantly and some greatly. The changes are given in Fig. 5. As the geodimeter line is not perpendicular to the fissure swarm the actual spreading and contraction, respectively, are somewhat greater than measured.

Considerable horizontal extension occurred within the downfaulted area. This extension was obviously inelastic as revealed in the field by extensive surface faulting. The extension was far from being uniform across the section and was generally much greater on the east side of the graben.

No recent surface faulting could be found in the elevated areas on either side of the graben except a few small fissures just east of bench mark 5754 which explains the anomalous contraction on the right hand side of the diagram on Fig. 5. This indicates a very uniform and probably elastic contraction that diminishes away from the fissure swarm.

Discussion

All the tectonic events of the Krafla plate-rifting episode so far seem to be very similar. They only differ in magnitude and the associated rifting and earthquake swarms occur in different places within the fissure swarm. Events 1, 5, 6, and 8 have been better recorded by geodetic measurements than most of the other events, mainly because they occurred at more easily accessible places than the other events.

The diagram of the change in elevation in Fig. 5 is quite analogous to the deformation caused by the intrusion of a vertical dike at some depth below the surface as put forward in the models of Dieterich and Decker (1975).

According to the diagram in Fig. 5 and additional information from Fig. 3, the area of the uplift curve (the right-hand side being extrapolated along an exponential line to zero) above the zero line exceeds the area of depression below the line by some 500 m^2. The length of the fissure system of the eighth event is estimated to be 20 km with maximum elevation changes at the geodimeter line diminishing linearly to both ends. All this adds up to a volume increase of about 5×10^6 m^3 This could be accounted for by the injection of a dike in accordance with the interpretation of Björnsson et al. (1977). Tryggvason (1978) estimated the outflow from the caldera to be 70×10^6 to 75×10^6 m^3 which is quite compatible with the above-mentioned value which is a very conservative estimate. It is also to be considered that some of the material did not reach the area discussed here all the way from the caldera.

Acknowledgements. The author is indepted to Gunnar Thorbergsson who is responsible for most of the geodetic measurements. Professor Dr. Ing. D. Möller, Braunschweig, is thanked for kindly permitting us to use his geodimeter line and measurements. Dr. Páll Einarsson read a preliminary draft of this paper and suggested many improvements.

References

Björnsson, A. Rifting and volcanism in the Krafla area 1975–1977 (In Icelandic with English summary). Náttúrufrædingurinn, Reykjavík **46**, 177–198, 1977

Björnsson, A., Johnsen, G., Sigurdsson, S., Thorbergsson, G., Tryggvason, E.: Rifting of the plate boundary in North Iceland 1975–1978. J. Geophys. Res. **84**, in press, 1979

Björnsson, A., Sæmundsson, K., Einarsson, P., Tryggvason, E., Grönvold, K.: Current rifting episode in North Iceland. Nature **266**, 318–323, 1977

Dieterich, J.H., Decker, R.W.: Finite element modeling of surface deformation associated with volcanism. J. Geophys. Res. **80**, 4094–4102, 1975

Einarsson, P., Brandsdóttir, B.: Seismological evidence for lateral magma intrusion during the July 1978 deflation of the Krafla volcano in Northeast Iceland. J. Geophys. **47**, 160–165, 1980

Sigurdsson, O. Náttúruhamfarir í Þingeyjarþingi veturinn 1975–76 (Volcanic activity in Thingeyjarsýsla county in the winter 1975–1976) (In Icelandic with English summary). Týli, Akureyri **6**, 3–20, 1976

Sigurdsson, O.: Report of the rifting episode in Northeast-Iceland 1976–1978 (In Icelandic with English summary). Týli, Akureyri **7**, 41–56, 1978

Thorbergsson, G.: Hædarmælingar vid Kröflu 1976 (Levelling in Krafla area in 1976) (In Icelandic). OS-ROD-7712 National Energy Authority, Reykjavík 1977

Tryggvason, E. Precision levelling in the Dettifoss area during July and August 1971. National Energy Authority, Reykjavík 1972

Tryggvason, E.: Ground-movement in North Iceland during the earthquake swarm of 1975–1976 (In Icelandic with English summary). Náttúrufrædingurinn, Reykjavík **46**, 124–128, 1977

Tryggvason, E. Subsidence events in the Krafla area. Nordic volcanologic Institute 78 14, University of Iceland, 1978

Received July 23, 1979; Accepted August 6, 1978

J. Geophys. 47, 160–165, 1980

Journal of Geophysics

Seismological Evidence for Lateral Magma Intrusion During the July 1978 Deflation of the Krafla Volcano in NE-Iceland

P. Einarsson and B. Brandsdóttir
Science Institute, University of Iceland, Dunhaga 3, Reykjavík, Iceland

Abstract. The July 1978 deflation of Krafla volcano in the volcanic rift zone of NE-Iceland was in most respects typical of the many deflation events that have occurred at Krafla since December 1975. Separated by periods of slow inflation, the deflation events are characterized both by rapid subsidence and volcanic tremor in the caldera region, as well as extensive rifting in the fault swarm that transects the volcano. Earthquakes increase in the caldera region shortly after deflation starts and propagate along the fault swarm away from the central part of the volcano, sometimes as far as 65 km. The deflation events are interpreted as the result of subsurface magmatic movements, when magma from the Krafla reservoir is injected laterally into the fault swarm to form a dyke. In the July 1978 event, magma was injected a total distance of 30 km into the northern fault swarm. The dyke tip propagated with a velocity of 0.4–0.5 m/s during the first 9 h, but the velocity decreased as the length of the dyke increased. Combined with surface deformation data, these data can be used to estimate the cross-sectional area of the dyke and the driving pressure of the magma. The cross-sectional area is variable along the dyke and is largest in the regions of maximum seismic energy release. The average value is about 1,200 m^2 The pressure difference between the magma reservoir and the dyke tip was of the order of 10–40 bars and did not change much during the injection.

Key words: Deflation – Krafla volcano – Iceland – Rifting – Earthquakes – Lateral magma injection – Dyke.

Introduction

On July 10, 1978 rapid subsidence started in the caldera region of the Krafla central volcano in the volcanic rift zone of NE-Iceland, and during the following 3 days the central part of the caldera subsided about 60 cm. This deflation event was the ninth in a series of such events that has been in progress since December 20, 1975. The tectonic setting and the course of events of this activity have previously been described in some detail in the literature (e.g. Björnsson et al., 1977; 1979; Einarsson, 1978, Brandsdóttir and Einarsson, 1979) and will not be repeated here.

In the time intervals between the deflation events, Krafla volcano inflates at a relatively constant rate. The inflation has been interpreted as the result of constant inflow of about 5 m^3/s of magma into a magma reservoir at depth of about 3 km under the central part of the caldera. This interpretation is supported by levelling, tilt, and gravity measurements (Björnsson et al., 1979; Tryggvason, 1978a), and is further strengthened by the geological association with the central volcano and the existence of a zone of high *S*-wave attenuation near the center of inflation (Einarsson, 1978).

Deflation events are characterized by rapid subsidence of the caldera region, continuous volcanic tremor, extensive rifting and earthquakes along the Krafla fault swarm that crosses the volcano from north to south. Earthquakes begin within or near the caldera and then migrate along the fault swarm away from the caldera, sometimes as far as 65 km. The largest events of the earthquake swarm are confined within a well defined but each time different section of the fault swarm. Rifting, often exceeding 1 m, may occur in the fault swarm, and the area of maximum rifting generally coincides with the area of maximum earthquake activity. Three of the deflation events have been accompanied by a small basaltic eruption in the caldera region. The spatial relationship between the Krafla caldera, the Krafla fault swarm and the epicentral areas of the different earthquake swarms is shown in Fig. 1 together with some of the major tectonic elements of the active zones in NE-Iceland.

The deflation events were interpreted by Björnsson et al. (1977) as the result of lateral migration of magma away from the reservoir under Krafla. This interpretation has since been supported by gravity and crustal deformation data (Björnsson et al., 1979; Tryggvason, 1978a and b), seismological data (Brandsdóttir and Einarsson, 1979), and petrochemical data (Grönvold and Mäkipää, 1978). During the deflation event of September 1977, e.g., the propagation of the magma could be followed by the seismic events (Brandsdóttir and Einarsson, 1979). The hypocenters migrated horizontally from the reservoir area southwards along the Krafla fault swarm to the Námafjall geothermal area, where small amounts of magma were subsequently erupted through a drill hole. The maximum speed of migration occurred early in the event and was 0.5 m/s.

In the present paper another case of lateral migration of seismic activity associated with deflation of the Krafla volcano is documented. In this deflation event of July 1978, magma was injected into the fault swarm to the north of the caldera, a total distance of 30 km.

The Course of Events

After the deflation event of January 1978 the Krafla volcano inflated at the normal rate. Towards the end of June the elevation of the caldera region was approaching the level it had before the January deflation. A new deflation event, possibly associated with an eruption, was anticipated soon thereafter. Monitoring of the area was therefore intensified and several portable seismographs were set up in the caldera region and south of it. The

0340-062X/80/0047/0160/$01.20

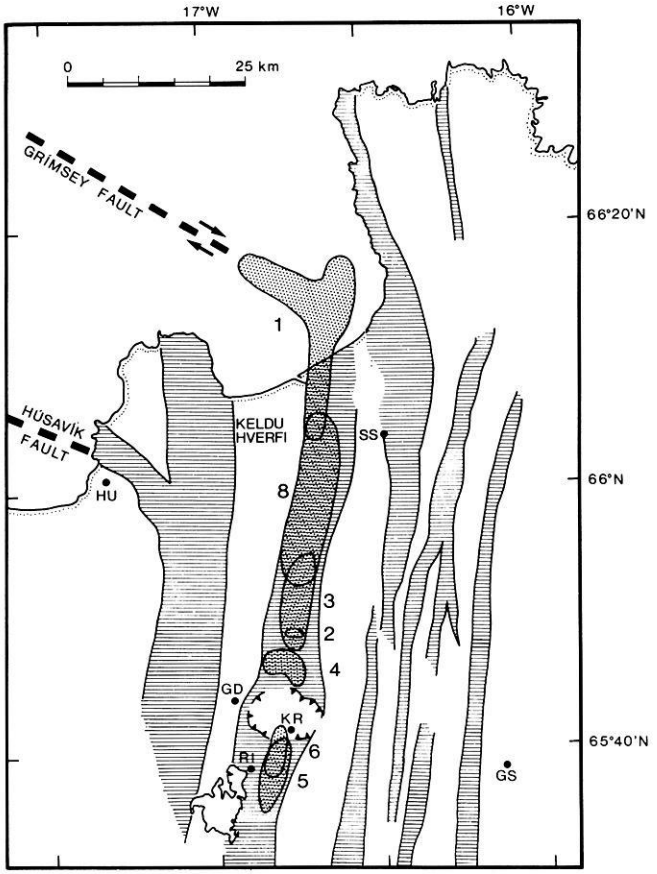

Fig. 1. Index map of the northern part of the volcanic rift zone in NE-Iceland. Dots mark permanent seismograph stations. The hatched areas are fault swarms as mapped by Kristján Saemundsson in Björnsson et al. (1977). The Krafla caldera is located within the Krafla fault swarm. The stippled areas are the areas of maximum earthquake activity during the different deflation events at Krafla. Area No. 1 is the epicentral area of the first earthquake swarm of December 1975–February 1976; No. 2, a small swarm of October 1–2, 1976; No. 3, swarm of October 31–November 1, 1976; No. 4, swarm of January 1977; No. 5, swarm of April 1977; No. 6, swarm of September 1977; a small swarm in November 1977 could not be located and is not shown; No. 8, swarm of January 1978. The Grímsey fault was delineated by seismicity (Einarsson, 1976) and the sense of fault displacement was derived from focal mechanism solutions (Einarsson, 1979)

seismic activity of the area was low, of the order of 1–2 locatable microearthquakes per day.

Slow deflation started on July 10 at about 11 h (all times are UTC), according to the continuously recording tiltmeter near the Krafla power house that is located within the caldera (Tryggvason, 1978c). The rate of tilting increased and when continuous tremor appeared on the seismograph station GD (Fig. 1) shortly before 17 h it was clear that a deflation event had started. Earthquakes were small in the beginning but increased gradually in magnitude and number. They clearly originated in the northern part of the caldera and north of it, which indicated that the magma was injected into the northern fault swarm. The tilt rate and the volcanic tremor reached a maximum at about 20 h and then slowly decreased. The earthquake activity increased markedly after about 22 h, and a magnitude 4.1 earthquake occurred in the fault swarm at 22:44 h (Fig. 2).

A helicopter was made available by the Icelandic Coast Guard, which made it possible to move a seismograph into the epicentral area. A station was set up at Snagi (SN) at 23:20 (Fig. 3). While the seismograph was being set up, earthquakes could be heard every minute and many earthquakes were felt. The magnification of the seismograph had to be set 42 *dB* lower than normal because of the high activity. Nothing else unusual could be observed in the Snagi area. Steam fields that had formed near Snagi in previous deflation events (e.g., Björnsson et al., 1979) were not noticeably changed, and the sheep were grazing quietly in the bright, Icelandic summer night.

The earthquake activity decreased significantly after 2 h in the morning (Fig. 2), but about 6 h it increased again and was very intensive for 12 h. The activity had now moved 10–15 km farther north. The earthquakes were not large but very frequent. Only two earthquakes were felt in the inhabited areas. The earthquake of July 11, 12:28 h (magnitude 3.9) was vaguely felt in the Kelduhverfi district at an epicentral distance of 5–10 km and the earthquake of July 12, 17:59 (magnitude 4.0) was widely felt in the Kelduhverfi district.

It was noticed in the morning of July 11 that a column of steam was rising from the area north of Krafla. The steam emission started between 03:04 and 03:14 according to photographs taken by a time lapse camera (Oddur Sigurdsson, personal communication). Subsequent inspection revealed that the steam came from a steam field located about 1.5 km SE of Snagi. This steam field was probably formed in January 1977, but now the steam emission had increased about an order of magnitude. During the following days the emission decreased slowly.

Several new steam fields have formed in the Snagi area in previous deflation events and most of them are aligned along one prominent normal fault. This fault moved a few tens of centimeters during the July 1978 event and was the easternmost fault that moved in this part of the fault swarm in that event. A total movement of 50–150 cm was estimated from the widening of the fissures in this area. The movement was distributed on numerous parallel fissures, some of which had moved in previous events. The estimate is therefore inaccurate. Much more accurate measurements were obtained with a geodimeter. In the Snagi area the extension across the fault swarm was found to be 95–111 cm (Tryggvason, 1978c). Compression occurred immediately outside the faulted zone, which is a pattern also found in previous rifting events in other parts of the fault swarm (Tryggvason, 1978b and c; Gerke et al., 1978; Björnsson et al., 1979).

Fault movements were also observed in the northern part of the epicentral zone. On a profile across the fault swarm near 65°56′N a total of 80 cm extension was estimated from the widening of the individual fissures. About 50 cm of this movement were estimated to be due to the July rifting. The rest of the movement took place in a previous event, most likely the January 1978 event. No geodimeter measurements are available for this part of the fault swarm.

The deflation stopped and inflation resumed at Krafla on July 13. The total volume removed from the magma reservoir during this deflation event is estimated to be 37×10^6 m^3 (Tryggvason, 1978c).

The Hypocentral Zone

Zypocenters have been calculated for 397 earthquakes from the swarm. Generally the largest earthquakes were selected for analysis

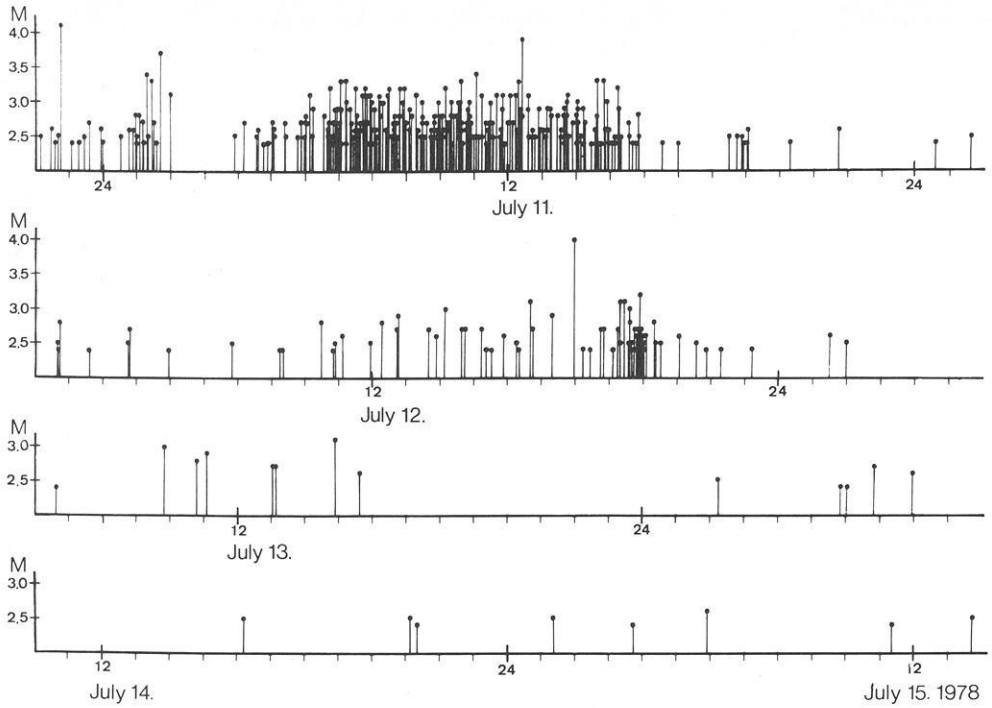

Fig. 2. The time sequence of earthquakes. Magnitude is plotted as a function of time

because they were recorded by the largest number of stations. Sometimes large earthquakes had to be omitted, however, because the first arrivals were obscured by tremor or small earthquakes, especially during periods of high activity. The set of located earthquakes may be regarded as nearly complete above magnitude 2.5. Many smaller earthquakes were located as well.

The computer program HYPOELLIPSE (Lahr and Ward, 1975) was used for the locations. *P*-wave arrival times and, where possible, also *S*-wave arrival times are used. The location procedure has been discribed in some detail by Einarsson (1978) and Brandsdóttir and Einarsson (1979) and will not be repeated here.

The epicenters are plotted on a map in Fig. 3. The epicentral zone is about 4–7 km wide, 25 km long, and extends from the northern rim of the caldera to Kerlingarhóll, which is a flat lava hill built up around the northernmost eruptive fissure in the Krafla fault swarm (Saemundsson, 1977). Nearly all the epicenters are located within the Krafla fault swarm. The zone is divided in two by a gap near the hyaloclastite hill Mófell. A large concentration of activity occurs in the northern end near Kerlingarhóll.

Depths of hypocenters could be determined with fair confidence in the area around Snagi because of the seismic station located there. In the northern part of the epicentral zone the depths are not considered to be reliable because of the relatively large distance to the nearest seismograph station. A transverse cross section of the hypocenters near Snagi is shown in Fig. 4. Hypocenters within 4 km distance from Snagi are projected on a vertical, E-W plane. Most of the hypocenters are at the depth of 1–4 km. An isolated event occurs at 14 km depth.

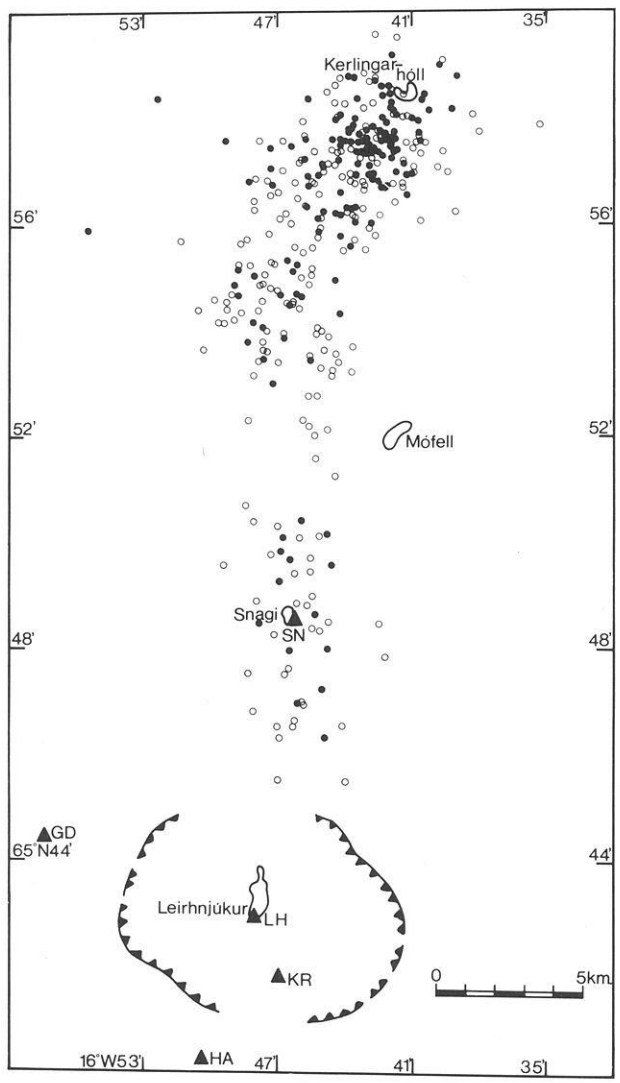

Fig. 3. Epicentral map of the July 1978 earthquake swarm. *Dots* mark epicenters located with horizontal standard error of 1 km and less, *circles* denote epicenters with errors between 1 and 2 km. Seismograph stations are shown with *triangles*. The stations HA, LH, and SN were temporary stations. Several stations outside of this map were also used in the locations

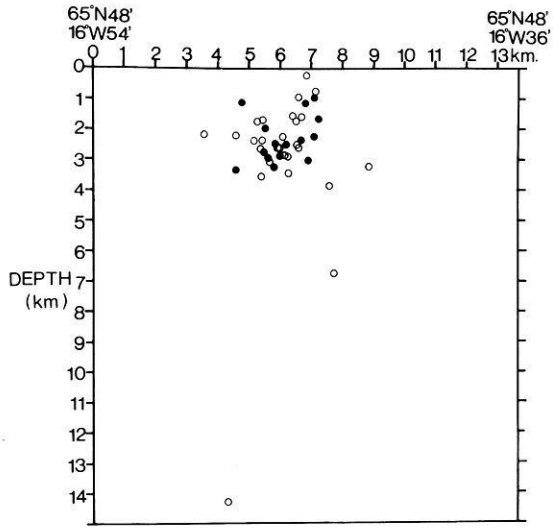

Fig. 4. Depth of hypocenters in the Snagi area. Hypocenters within 4 km horizontal distance from the station SN are projected on a vertical E–W plane. Dots are hypocenters determined with horizontal and vertical standard error of 1 km and less, circles denote hypocenters with errors between 1 and 2 km

The Migration of Seismic Activity

One of the most remarkable characteristics of the Krafla fault swarm earthquakes is the propagation of epicenters away from the caldera region. The July 1978 event provided one of the best examples of this. The latitude of the epicenters is plotted as a function of the time of occurrence in Fig. 5. The continuous tremor started in the caldera region at 17 h, the first earthquakes were there also but were too small to be located accurately. The earthquakes between 22 h on July 10 and 2 h on July 11 were located in the Snagi area. It is interesting to note that the gap in the epicentral zone near Mófell is also a gap in time. One may say that a strain pulse migrated aseismically across the gap and continued propagating with accompanying seismicity on the other side with a velocity similar to that before. If one assumes that the activity started in the center of the caldera, the total distance is 30 km. The speed of propagation during the first 9 hours is 1.6 km/h or 0.4–0.5 m/s. The speed decreases only slightly during the next 8 h, but during the time period 11 h–19 h on July 11 the average speed is only about 0.1 m/s.

The Magnitude-Frequency Distribution

Magnitudes were obtained for 354 earthquakes from the maximum trace amplitude on the short period seismograms of the WWSSN station AKU at a distance of 65–75 km from the epicentral area. The magnitude data were supplied by Thórunn Skaftadóttir at the Icelandic Meteorological Office. The magnitude distribution is shown in Fig. 6. The log N vs. M distribution is reasonably linear. The negative slope of the curve, or the b-value of the swarm, is 1.7 ± 0.2 assuming a linear relationship. These are a maximum likelihood estimate and 95% confidence limits, respectively.

The main deviation from linearity is a dip in the curve near $M = 3.5$. Similar dip, only more pronounced, was found in the

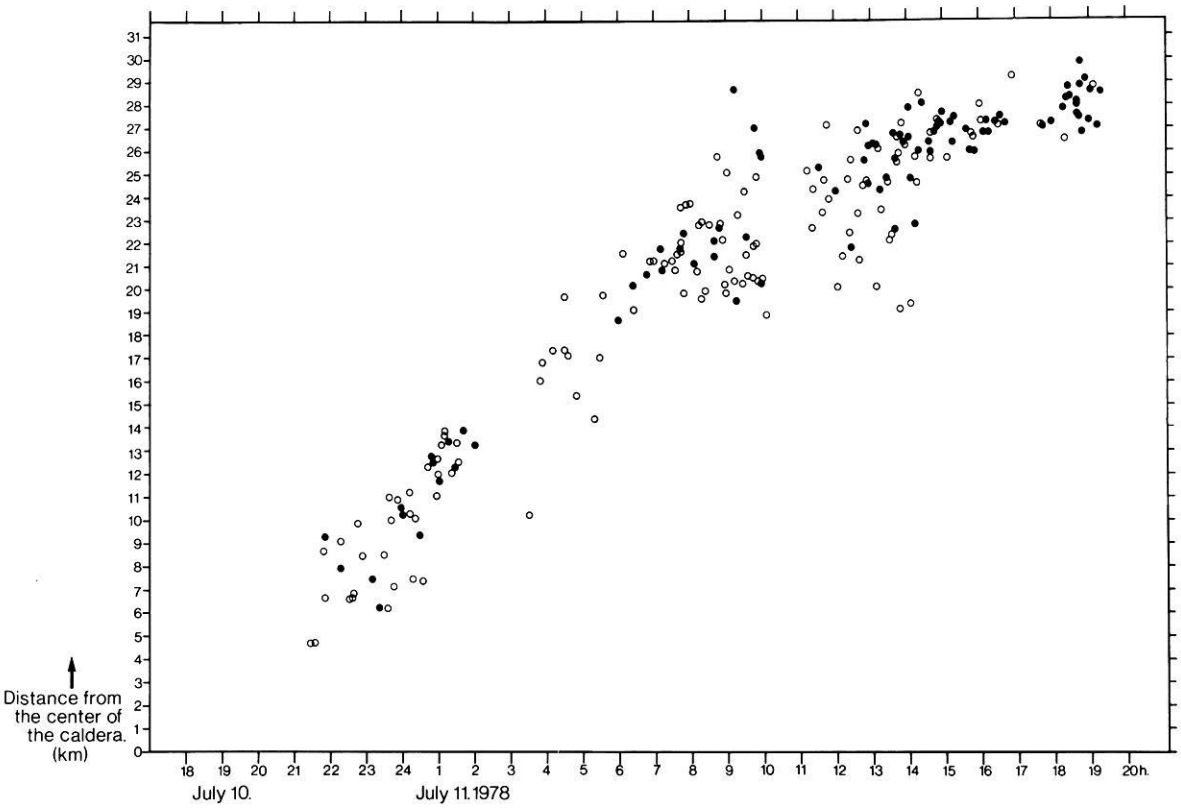

Fig. 5. The migration of seismic activity. The distance of epicenters from the center of the Krafla caldera is plotted as a function of time. *Dots* and *circles* have the same meaning as in Fig. 3. The apparent gap in the activity between 10 h and 11 h on July 11 is caused by a time signal failure. Tremor and deflation start about 17 h

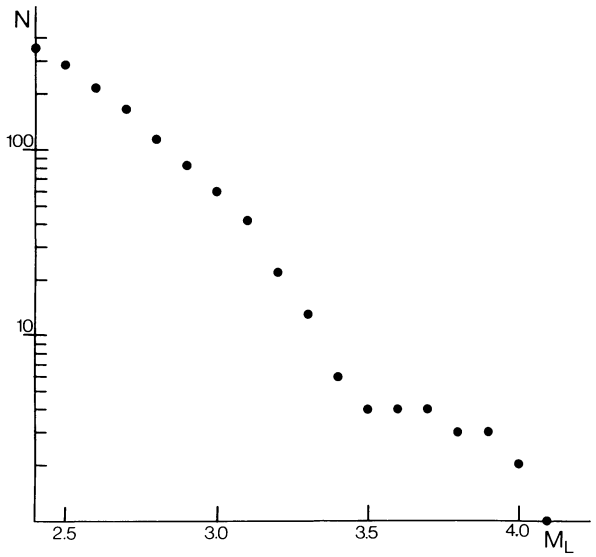

Fig. 6. The frequency-magnitude relationship of the July 1978 earthquakes. The number (N) of earthquakes of magnitude M_L and larger is plotted as a function of M_L

magnitude-frequency curve for the September 1977 earthquakes (Brandsdóttir and Einarsson, 1979), where it was interpreted as the result of mixing two earthquake sequences with different b-values. This interpretation is hardly justified in the present case because of the small number of events larger than magnitude 3.5.

Discussion

It seems reasonable to assume that the front of the earthquake activity that migrates away from the subsiding Krafla area marks the tip of a dyke that is injected into the fault swarm. Thus the length of the dyke can be found as a function of time. Tryggvason (1978c) has given the tilt at the Krafla power house and the rate of outflow of magma as functions of time for the different subsidence events. With these data it is possible to make some further quantitative estimates of the dimensions of the dyke. The total volume is 37×10^6 m^3 and the final length of the dyke is 30 km. The average cross sectional area is thus 1.2×10^3 m^2 If the width and the height of the dyke are uniform, for example, a 0.5 m wide and 2400 m high or a 1.0 m wide and 1200 m high dyke would have the required cross sectional area. There are indications, however, that the dimensions of the dyke are not uniform along its length. The seismic energy release is clearly not uniform, and the rifting measured in the Snagi area decreases towards the south (Tryggvason, 1978c). Areas of maximum earthquake activity and areas of maximum surface faulting usually coincide. These may be areas where the top of the dyke reaches the smallest depths or where the width of the dyke is largest.

It is possible to show that the average cross sectional area changed as the dyke became longer. From Tryggvason's (1978c) record of tilt above the Krafla reservoir the volume of magma escaped from the reservoir can be estimated as a function of time. This volume equals the volume of the dyke. Thus, using the relationship in Fig. 5, the average cross-sectional area can be found for a given length of the dyke. This is shown in Table 1.

The differences between the numbers are significant, even though the volume estimate is associated with large uncertainties.

Table 1. Cross-section of dyke, estimated from its length and the volume of magma discharge from the chamber, both determined independently as functions of time

Length of dyke (km)	Volume of dyke (10^6 m^3)	Average Cross-sectional area (10^3 m^2)
10	12.3	1.23
15	15.6	1.04
20	18.8	0.94
25	22.5	0.90
27	25.2	0.93
30	37.0	1.23

Table 2. Viscosity over pressure drop, estimated from dyke length and rate of magma outflow from chamber

l (km)	w (m^3/s)	$\eta/\Delta p$ (poise/bar)	
		(b=0.5 m)	(b=1 m)
10	460	5.4	22
15	300	5.6	22
27	200	4.6	19

These changes in the average cross-sectional area can be interpreted in a number of ways. If one assumes, for example, that the dyke attains its final cross-sectional area immediately behind the tip of the propagating dyke, one can calculate the cross-sectional area as a function of distance from the reservoir. Without going into detailed calculations one may conclude that the dyke reached the largest cross-sectional area near its northern end and in the area south of Snagi. These are also the areas where the largest earthquakes occurred. It is not possible on the basis of these data to say, whether the increased cross-sectional area and seismicity are the result of larger height or width of the dyke in these areas.

With the knowledge of the dimensions of the dyke, the rate of flow and a few simplifying assumptions it is possible to derive the relationship between the viscosity and the pressure drop in the dyke. Let us assume that the dyke is a rectangular plate of uniform thickness b, length l and height a. This is a simplifying assumption, since we know that the cross-sectional area is not uniform. Let us further assume that the dyke changes its volume by changing its length only. Then only the dimension l is a function of time, and $\frac{dl}{dt} = \frac{W}{ab}$ where W is the rate of flow into the dyke. For a Newtonian fluid of viscosity η flowing through a rectangular box of dimensions $a \times b \times l$ $(a \gg b)$ we have

$$W = \frac{ab^3 \Delta p}{12 \eta l} \quad \text{or} \quad \frac{\eta}{\Delta p} = \frac{ab^3}{12 l W}$$

where Δp is the difference between the pressure in the reservoir and that near the tip of the dyke. We can now tabulate the values of $\eta/\Delta p$ for different lengths of the dyke and different assumptions for the width (Table 2). The values of W are taken from Tryggvason (1978c). The cross-sectional area $a \cdot b$ used in the calculation is 1200 m^2

From Table 2 we see that the change in the pressure difference is relatively small assuming that the viscosity is constant. The

rate of flow is therefore primarily governed by the length of the dyke. If a, b, η and Δp are constant, one can solve the differential equation

$$\frac{dl}{dt} = \frac{b^2 \Delta p}{12 \eta l}$$

and find that l is proportional to $\sqrt{t}$, where t is the time from the beginning of the intrusion. This relationship does not fit particularly well to Fig. 5, which is hardly surprising in the light of our many simplifying assumptions. The fit can be improved by assuming that the lateral intrusion started a few hours after the onset of deflation and volcanic tremor.

With the values in Table 2 the pressure difference Δp can be estimated if the viscosity is known. Grönvold and Mäkipää (1978) estimated the viscosity of the Krafla magma to be 200 poise from the chemical composition of erupted material using the method of Shaw (1972). In the calculation the magma was assumed to contain 1% water. The viscosity decreases with increasing pressure and temperature (Kushiro et al., 1976), and the estimate is more likely to be too high than too low. With a viscosity of 200 poise it takes a pressure difference of 40 bar to drive the magma through a 0.5 m wide fissure, and if the fissure is 1 m wide the pressure difference is only 10 bar.

In the model of the Krafla deflation presented in this paper a dyke is formed when the tip of a fluid-filled crack propagates through a prestressed medium. The primary driving force of this process is the tectonic stress that has been accumulating on the plate boundary since the last major rifting episode. The mode of strain release depends on the availability of magma. If a magma reservoir is located on the plate boundary a dyke starts propagating away from it when the pressure in the reservoir and/or the regional tectonic stress reach a critical level. The data presented here seem to indicate that the pressure drop in the reservoir associated with the deflation is small compared with the pressure difference between the reservoir and the leading edge of the dyke. The pressure in the magma reservoir probably plays the role of a trigger to initiate the propagation of the dyke. The direction of propagation and the orientation of the intrusion is governed by the regional stress field. The tectonic part of the stress field at the diverging plate boundary in Iceland is likely to be characterized by horizontal tensional stress parallel to the direction of relative plate motion. In this stress field the direction of propagation will be horizontal, and the resulting intrusive body is a dyke oriented perpendicularly to the axis of minimum compressive stress or maximum tensional tectonic stress.

Acknowledgements. Many institutions and individuals contributed to the success of this study. The project was partly financed by the National Energy Authority and a special grant from the Icelandic Ministry of Education. The Icelandic Coast Guard provided helicopter support at a critical time. Gestur Gíslason, Hjörtur Tryggvason and Max Wyss helped with the field work. Axel Björnsson, Eysteinn Tryggvason, Oddur Sigurdsson, and W Jacoby read the manuscript critically and contributed to its improvement. The model of the Krafla events presented in this paper has been the subject of extensive discussion in an informal Krafla working group.

References

Björnsson, A., Johnsen, G., Sigurdsson, S., Thorbergsson, G., Tryggvason, E. Rifting of the plate boundary in North Iceland. J. Geophys. Res. **84**, 3029–3038, 1979

Björnsson, A., Saemundsson, K., Einarsson, P., Tryggvason, E., Grönvold, K.: Current rifting episode in North Iceland. Nature **266**, 318–323, 1977

Brandsdóttir, B., Einarsson, P.: Seismic activity associated with the September 1977 deflation of the Krafla central volcano in NE Iceland. J. Volcanol. Geothermal Res. in press, 1979

Einarsson, P.: Relative location of earthquakes within the Tjörnes Fracture Zone. Soc. Sci. Isl. Greinar V, pp. 45–60, 1976

Einarsson, P.. S-wave shadows in the Krafla caldera in NE-Iceland, evidence for a magma chamber in the crust. Bull. Volcanol. **41**, 1–9, 1978

Einarsson, P.. Seismicity and earthquake focal mechanisms along the mid-Atlantic plate boundary between Iceland and the Azores. Tectonophysics **55**, 127–153, 1979

Gerke, K., Möller, D., Ritter, B.: Geodätische Lagemessungen zur Bestimmung horizontaler Krustenbewegungen in Nordost-Island. Wissenschaftliche Arbeiten der Lehrstühle für Geodäsie, Photogrammetrie und Kartographie an der Technischen Universität Hannover, Nr. **83**, 23–33, 1978

Grönvold, K., Mäkipää, H. Chemical composition of Krafla lavas 1975–1977. Nordic Volcanological Institute, Report 78 16, 49 pp., 1978

Kushiro, I., Yoder, H.S., Mysen, B.O.. Viscosities of basalt and andesite melts at high pressure. J. Geophys. Res. **81**, 6351–6356, 1976

Lahr, J.C., Ward, P.L. HYPOELLIPSE: A computer program for determining local hypocentral parameters, magnitude, and first motion pattern. U.S. Geol. Surv. Open-File Report, 1975

Saemundsson, K.: Geological map of Iceland, sheet 7, NE-Iceland. Icelandic Geodetic Survey and Museum of Natural History, 1977

Shaw, H.R. Viscosities of magmatic silicate liquids: An empirical method of prediction. Am. J. Sci. **272**, 870–893, 1972

Tryggvason, E.. Tilt observations in the Krafla-Mývatn area 1976–1977. Nordic Volcanological Institute, Report 78 02 45 pp., 1978a

Tryggvason, E.: Distance measurements in 1977 in the Krafla-Mývatn area and observed ground movements. Nordic Volcanological Institute, Report 78 10, 47 pp., 1978b

Tryggvason, E.. Subsidence events in the Krafla area. Preliminary report based on tilt and distance measurements. Nordic Volcanological Institute, Report 78 14, 65 pp., 1978c

Received April 18, 1979; Revised Version September 28, 1979

J. Geophys. 47, 166–170, 1980

Journal of Geophysics

Measurements of Distance and Tilt Changes in Fissures of Northern Iceland

H. Pelzer[1] and C. Gerstenecker[2]

[1] Geodätisches Institut der Universität Hannover, Nienburger Str. 1, D-3000 Hannover 1, Federal Republic of Germany

[2] Fachgebiet Experimentelle Methoden der Astronomischen und Physikalischen Geodäsie, TH Darmstadt, Petersenstr. 13, D-6100 Darmstadt, Federal Republic of Germany

Abstract. In an active tectonic fissure about 50 km north of Krafla in N-Iceland, relative movements of the fissure walls were recorded for about one month in the summer of 1976, during an inflation period of Krafla. Distance changes of the walls, measured by two-component extensometers, show a widening tendency of about 5 μm per day; this is superimposed by sudden widenings of up to 0.05 mm and temperature effects with diurnal peroid. Tilt measurements of the fissure walls confirm these results, especially the sudden effects and the diurnal ones, and show, moreover, a northward tilting of the whole region perhaps caused by mass transport at depth and/or in response to the inflation of the Krafla magma chamber.

Key words: Extensometer measurement – Tilt measurement – Fissure movements

1. Introduction

In the rift zones of Iceland the tectonic fissures can be considered a visible expression of crustal deformation. The deformation has been studied by geodetic measurements by several authors (Gerke et al., 1978; Möller and Ritter, 1980; Tryggvason, 1980; Spickernagel, 1980; Torge and Kanngiesser, 1980; Johnson et al., 1980). Details of the movements cannot be detected by classical geodetic measurements, because in most cases there is a time interval of one or more years between two measurements, and the distances between control points are large and cross more then one fissure. Therefore, if we are interested in the character of fissure movements, we have to apply continous measuring techniques as they are used in rock mechanics and engineering surveying. We have chosen to use extensometers and tiltmeters.

North Iceland is currently experiencing a rifting episode with the center of activity in the Krafla caldera (Björnsson et al., 1977; 1979). A magma chamber below the caldera seems to be continuously inflated by inflow from depth; occasionally it is deflated suddenly by magma excaping into opening fissures of the Krafla fissure swarm.

Besides monitoring the movements in the immediate vicinity of Krafla (Tryggvason, 1980), it seems desirable to monitor the fissure movements at greater distance. We have chosen a fissure in the Kelduhverfi area some 50 km to the north (Fig. 1). We report here measurements taken during the first documented inflation phase of Krafla, beginning early 1976 and ending on September 29, 1976. The observations ended before the deflation and thus can give only a limited insight into the behaviour of the fissures. New observations have therefore been made in 1978, the analysis of which has, however, not yet been completed.

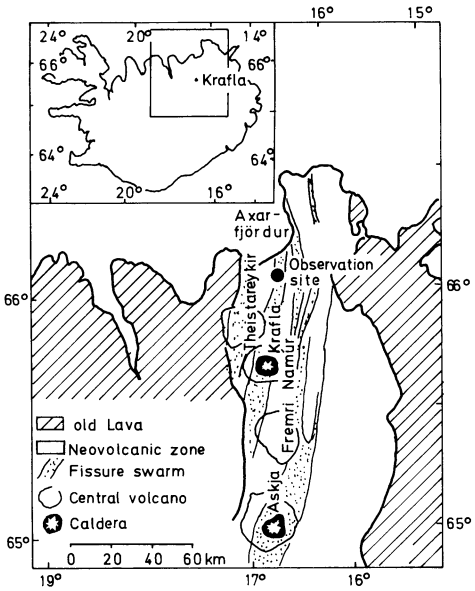

Fig. 1. Location map of fissure investigated

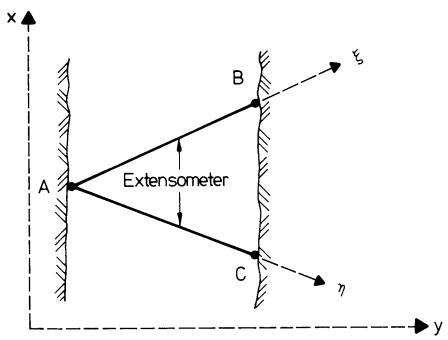

Fig. 2. Two-component extensometer; principle

2. The Two-Component Extensometer Measurements

The first investigations of this kind were carried out by Gerke and Pelzer (1972). In order to record movements along and across

0340-062X/80/0047/0166/$01.00

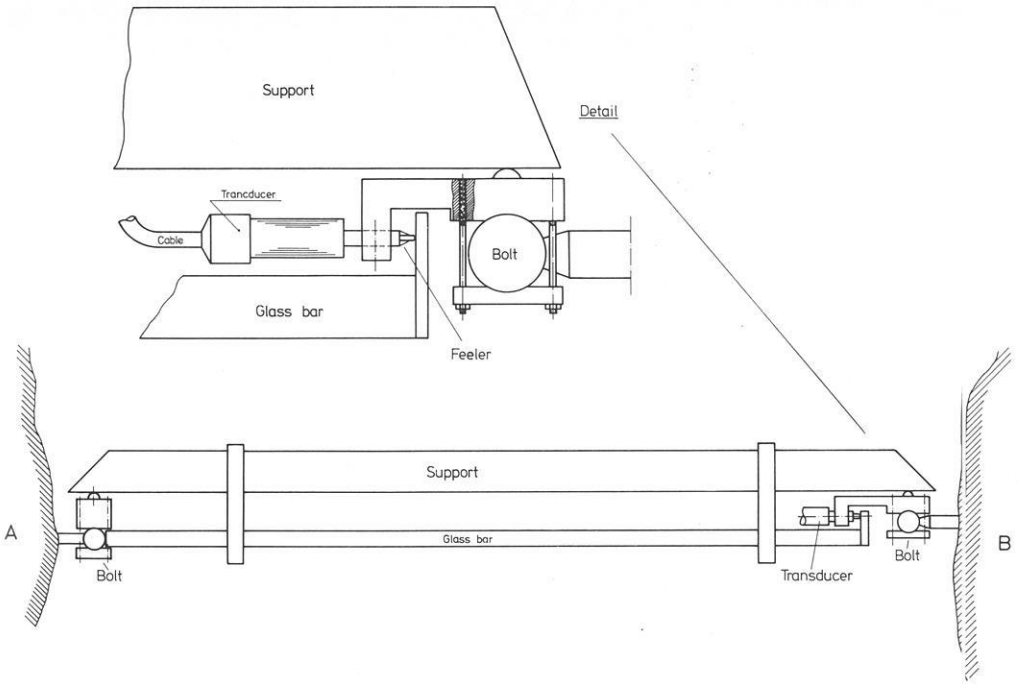

Fig. 3. Details of extensometer

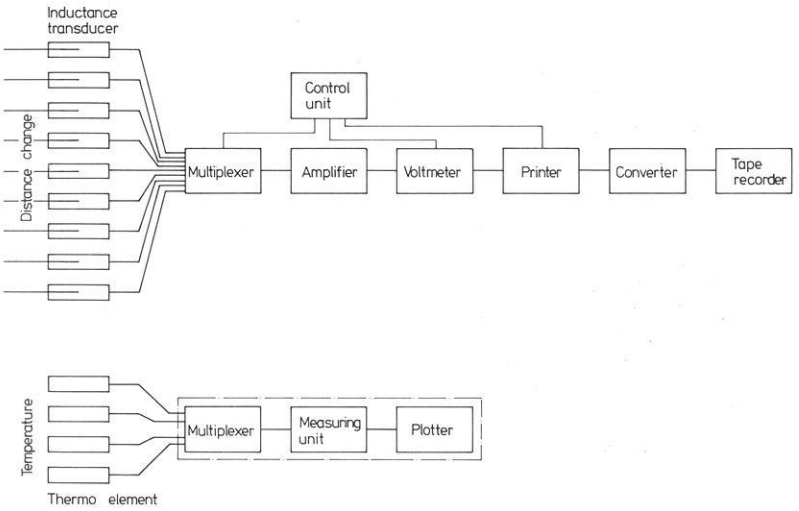

Fig. 4. Measuring and recording device

a fissure a two-component extensometer was developed (Fig. 2) and installed in five fissures in the Gjásticki area. Fissure movements in the ξ- and η-direction could be recorded by mechanical recording devices with a resolution of about 0.2 mm, and transformation of the recorded movements into an arbitrary x,y-coordinate system could be done off-line without difficulties. But, unfortunately, no movements greater than a few tenths of a millimeter occurred within the recording period of about two years (1967–1969). Therefore, in a second attempt, a new higher-resolution two-component extensometer was developed at Geodätisches Institut, Universität Hannover; it is described in detail below.

The basic concept of the extensometer is given in Fig. 2. Changes in distance are measured between a fix point A at one wall of a fissure and fix points B and C at the other wall. Figure 3 shows one component of the measuring device, installed between A and B, for example. The distance between the fixed points, realized by the faces of spherical steel bolts, is bridged by a glass bar which is supported at its BESSEL-points. Because of the small thermal expansion coefficient of the special glass ($10^{-8}K^{-1}$) the length of the bar may be considered invariable. Changes in distance between A and B will result in movements of the feeler of an inductance transducer, where they will be transformed into electric signals.

By a screened cable the transducer is connected via a multiplexer with a central measuring unit (Fig. 4). An automatic control unit allows common recording of the data of eight transducers or four two-component extensometers.

In 1976 the extensometer was installed in Iceland for the first time. In this year new fissuring and opening of existing fissures occurred in the Kelduhverfi area in N-Iceland, related to the volcanic activity near Krafla (Björnsson et al., 1977; 1979). At the time the behaviour of the Krafla caldera and of the fissure swarm was not yet understood in as much detail as it is today. Therefore, one of the active fissures in the area (Fig. 1), i.e., one which

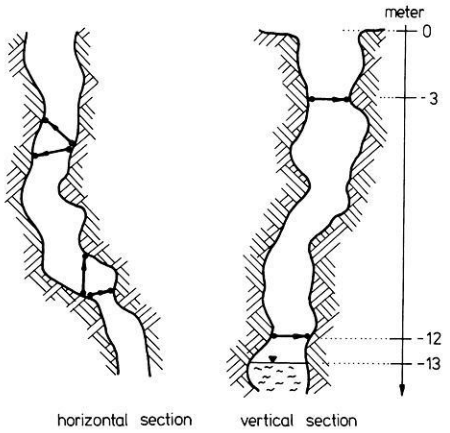

Fig. 5. Installation of two-component extensometers in the fissure

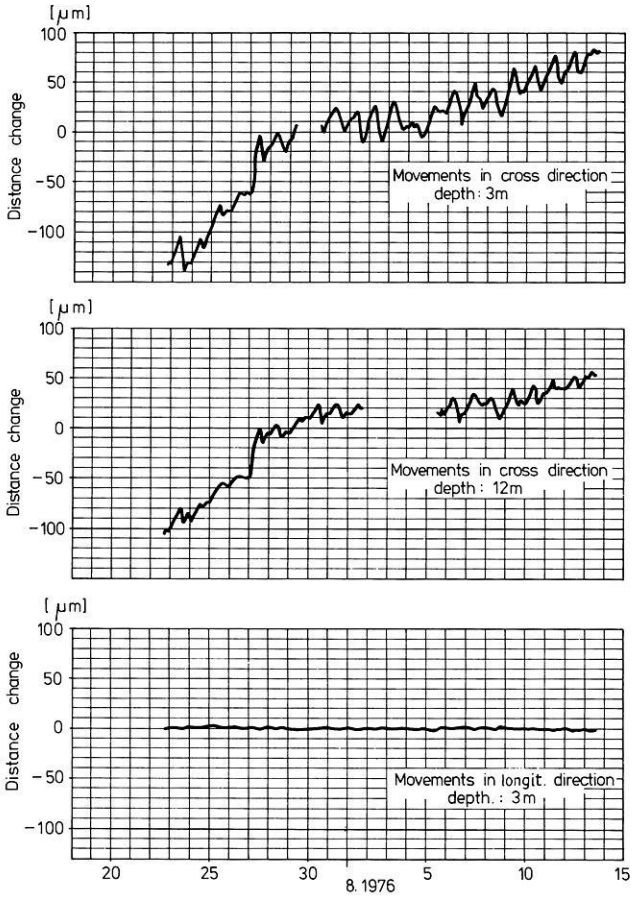

Fig. 6. Movements of a fissure in Kelduhverfi (July 22–August 13, 1976)

had shown extension, was chosen rather arbitrarily and two sets of extensometers were installed in it. Each set consisted of four two-component extensometers arranged as shown in Fig. 5. The extensometers were working for more than three weeks (July 22–August 13); the sampling rate was one per 15 min.

The distances in the ξ,η-directions (Fig. 2) were transformed into an orthogonal x,y-system parallel and perpendicular, respectively, to the fissure direction and plotted as functions of time. Typical plots are shown in Fig. 6, the other plots are very similar in character.

The recording period fell into the first inflation period of Krafla from December 1975/January 1976 to September 29, 1976. The question was wether or not the fissure continued to widen during the inflation period, after it had widened by up to several decimeters, easily detectable, in the beginning.

The result during the period of observation was a widening of the fissure, recorded by the upper and lower extensometers; the amount of widening is of the order of 0.2 mm. In detail we can separate three effects:

(a) a more or less uniform widening tendency of about 5 μm per day,

(b) sudden changes in distance of up 0.05 mm, for example on June 27 and, less significant, on June 23,

(c) periodic distance changes with an amplitude of about 10 μm and a frequency of one cycle per day; they are interpreted as temperature effects (see temperature plot in Fig. 7).

In contrast to this, no significant movements in the longitudinal direction of the fissure were observed (see Fig. 6, bottom).

3. Measurements of Tilt Changes

Tilt measurements were carried out between July 28 and August 15 near the extensometer station No. I. Two Hughes bubble tiltmeters TM 3 (nos. 34 and 35) were used. Each of them measures tilts in two orthogonal directions. The linear range of the instruments is about 49 μrad the resolution is better than $\pm 4.8 \cdot 10^{-3}$ μrad. The construction principles and further details are described by Harrison (1976a). The tiltmeters were installed on both sidewalls of the fissure, about 13 m below the earth's surface (Fig. 8). A special suspension was constructed which permits a strain- and stress-free installation of the instruments. In addition, each tiltmeter was protected against mechanical and meteorological influences by a stainless-steel coverage and a wooden box, which was filled with styrofoam. The orientation of the orthogonal tilt axes is shown in Fig. 8 for both instruments. The signals were recorded by two-channel analog recorders, which were installed in a tent. In addition, temperature and air pressure were measured at different sites (Fig. 8). During the recording period, short interruptions occurred caused by technical failures.

The analog records of the tilt measurements were digitized with a sampling rate of 1 per 5 min. The meteorological data were sampled only once per hour. Gaps in the record were interpolated with smoothing cubic spline functions. The digitized tilt changes are plotted in Fig. 9.

We can see in the beginning a small tilt in the direction of the tiltmeters which conforms to an inclination of the western fissure wall to the west and of the eastern fissure wall to the east. From August 7–11 large, mostly reversible, tilt changes occurred. In this period a strong south storm disturbed the measurements. During the last days of observations, small periodical tilt changes were observed without any obvious drift direction.

The data analysis was performed with the usual statistical methods, such as the computation of regression models, cross-correlation functions, Fourier and power spectra, to find the mean drift terms, correlations with meteorological effects, tilts, and significant frequencies.

The cross-correlation functions between the tiltmeter records and the meterological time series show no significant dependency of the tilts on temperature changes. Only the temperature measured near the tiltmeters rendered correlation coefficients between $+0.5$ and $+0.6$.

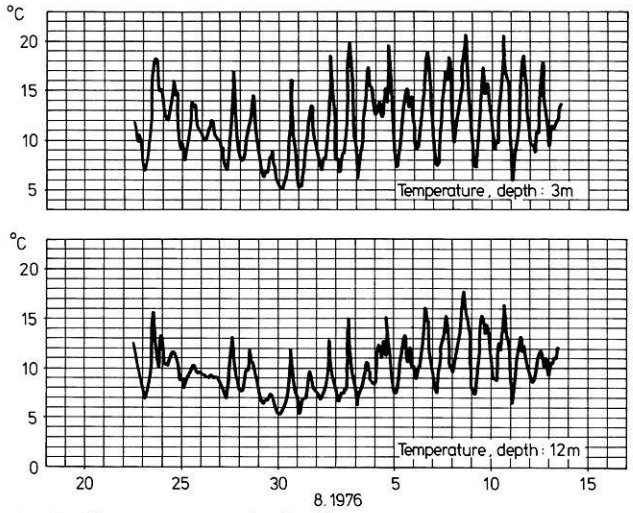

Fig. 7. Air temperature in the fissure

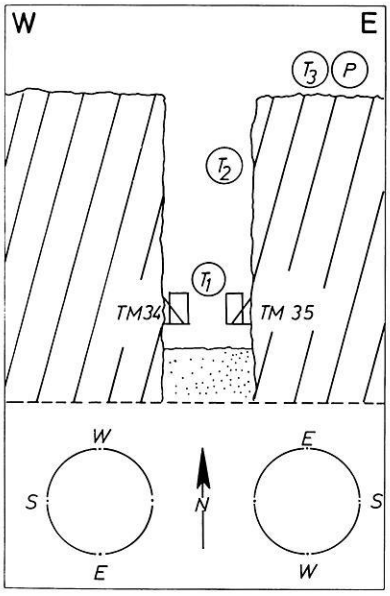

Fig. 8. Installation of tiltmeters *(TM 34, TM 35)* thermometers *(T_1, T_2, T_3)* and barometer *(P)*; on the bottom the geographical orientation of the instrumental tiltaxis are shown

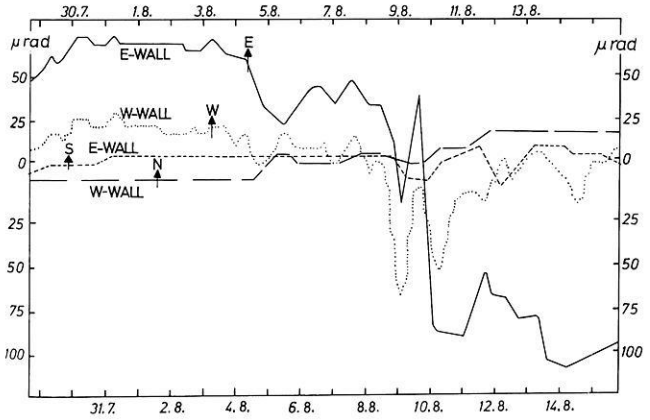

Fig. 9. Plot of the observed tilt changes in μrad; geographical coordinates.

Table 1. Mean tilt rates in μrad/h as obtained by regression analysis

Instrument	Component	Tilt rate (μrad/h)	Tilt to:
TM 35	N-S	−0.591	West
(east wall)	E-W	−0.004	North
TM 34	N-S	−0.106	East
(west wall)	E-W	+0.089	North

The cross-correlation functions between tilts and temperature generally change slowly. The maxima are marked weakly with a lag of nearly one day. The results of the regression analysis of the tilt observations with time are presented in Table 1.

The *mean tilt rates* or drift rates (μrad/h) during the observation period emphasize different inclinations of the fissure walls. The tilting of the eastern wall was about five times greater than the tilting of the western wall. In total, the western fissure wall tilted to east about 148.2 μrad, the eastern wall to west about 30.1 μrad. Parallel to the fissure walls, in the north-south direction, a small inclination of the fissure walls is evident. The tilt of both fissure walls to the north amounts to about 2.4 μrad. The difference between the short-term tilting of the fissure walls away from each other (see above) and the average tilting toward each other is rather striking and has not yet been explained.

The regression coefficients of tilts with temperature and air pressure are only significant for the temperature T_1 measured near the tiltmeters. These temperature changes can explain 29% (TM 3 No. 34) and 41% (TM 3 No. 35) of the observed tilts.

The Fourier- and power spectra of the tilt observations demonstrate daily periods with amplitudes of 7.3 μrad. These oscillations coincide with the daily temperature changes. Furthermore oscillations of 5 and 3 h period are found, which however, have no correlation with the temperature changes.

4. Discussion and Conclusions

The small correlation between temperature and the aperiodic tilt changes demonstrates that the observed tilt is not purely caused by instrumental thermal drift. Only part of the tilts can be explained with such effects. The diurnal tilt and widening periods are correlated well with the daily temperature wave, thus we assume that we have observed some thermally induced motion of the fissure walls.

The interpretation of the aperiodic drift, however, depends on the chosen model and is hampered by the shortness of the measurement period. The simplest assumption is that we have observed the motion of individual disjuncted blocks. Each extensometer and tiltmeter was fixed to such a separate block. The results of the two tiltmeters point to this model, since we have measured tilt rates rather different in magnitude; moreover, the widening of the fissure is accompanied by a mutual tilting of the fissure walls toward each other.

Not in favour of this model is the observation that the direction of the *drift* of the extensometers and tiltmeters is similar. We can deduce then that the motion is caused by one physical phenomen such as the volcanic activity in the Krafla caldera as described by Björnsson et al. (1979).

As shown in Fig. 1 the fissure is located near the northern end of the Krafla fissure swarm. The measurements were carried

out during the inflation phase between January and September 1976 of Krafla, where none or only weak seismic activity in the fissure swarm was observed (Björnsson et al., 1979). In good agreement with Björnsson et al. (1979), in the fissure outside the Krafla caldera the small widening is accompanied by mutual tilting of the fissure walls.

However, it is not possible to give absolute values for the translation (widening) and rotation (tilting) of the fissure walls. Tilt-strain coupling (Harrison, 1976b) acting on the extensometers and tiltmeters prevents an exact separation. Similar to the widening, the tilting of the fissure to the north seems to be correlated with the inflation phase of the Krafla caldera. Direction and magnitude of the tilting coincide with the predictions by the inflation-deflation model of the Mogi-type (Björnsson et al., 1979). However, we cannot yet be sure of observing regional tilting of the Earth's crust. The analysis of extensometer and tilt measurements in the earth-tide range has shown, that aperiodic drift is mostly a local effect, caused by environmental disturbances of the measuring site. The measurements presented therefore have to be understood as a first investigation, to give a qualitative impression of the kind and magnitude of fissure motions. The interpretation of the results can only be definitive, if the observation will be continued for several inflation-deflation phases of the Krafla caldera. Therefore the extensometer measurements were continued in 1978, but results cannot yet be presented here.

Acknowledgement. The authors thank Deutsche Forschungsgemeinschaft for support of the measurements. W Bämpfer and W. Graf constructed and installed the measuring systems.

References

Björnsson, A., Johnson, G.V., Sigurdsson, S., Thorbergsson, G., Tryggvason, E.: Rifting of the plate boundary in North Iceland 1975–1978. J. Geophys. Res. **84**, 3029–3038, 1979

Björnsson, A., Saemundsson, K., Einarsson, P., Tryggvason, E., Grönvald, K.: Current rifting episode in North Iceland. Nature **266**, 318–323, 1977

Gerke, K., Möller, D., Ritter, B.: Geodätische Lagemessungen zur Bestimmung horizontaler Krustenbewegungen in Nordost-Island. In: Festschrift für W. Höpcke, Wiss. Arbeiten d. Lehrst. f. Geodäsie, Photogrammetrie und Kartographie an der TU Hannover, Nr. 83, Hannover 1978

Gerke, K., Pelzer, H.: Island: Triangulation, Deformationsvierecke, Registrierungen. Deutsche Forschungsgemeinschaft, Forschungsbericht Unternehmen Erdmantel, Wiesbaden 1972

Harrison, J.C. Tilt observations in the oorman Mine near Boulder, Colorado. J. Geophys. Res. **81**, 329–336, 1976a

Harrison, J.C.: Gravity and topographic effects in tilt and strain measurements. J. Geophys. Res. **81**, 319–329, 1976b

Johnsen, G.V., Björnsson, A., Sigurdsson, S. Gravity and elevation changes caused by magma movement beneath the Krafla caldera, Northeast Iceland. J. Geophys. **47**, 132–140, 1980

Möller, D., Ritter, B.. Geodetic measurements and horizontal crustal movements in the rift zone of NE-Iceland. J. Geophys. **47**, 110–119, 1980

Sigurdsson, O.· Surface deformation of the Krafla fissure swarm in two Rifting events. J. Geophys. **47**, 154–159, 1980

Spickernagel, H. Results of height measurements in the northern Iceland 1965/1977. J. Geophys. **47**, 120–124, 1980

Torge, W., Kanngieser, E.: Gravity and height variations during the present rifting episode in Northern Iceland. J. Geophys. **47**, 125–131, 1980

Tryggvason, E.. Subsidence events in the Krafla area, North Iceland 1975–1979. J. Geophys. **47**, 141–153, 1980

Received July 6, 1979; Revised Version October 12, 1979

J. Geophys. 47, 171–175, 1980

Journal of Geophysics

Recent Earthquakes in the Hengill-Hellisheidi Area in SW-Iceland

G. Foulger and P. Einarsson

Science Institute, University of Iceland, Dunhaga 3, Reykjavík, Iceland

Abstract. Epicenters of 106 earthquakes ($M_L \leqq 3.7$) have been located in the Hengill-Hellisheidi area during the first four years of operation of a short-period seismograph network in SW-Iceland. This area is part of the active zone of Iceland, and is located near the junction of three branches of this zone, the Reykjanes Peninsula, the Western Volcanic Zone and the South Iceland Seismic Zone, all of which have different tectonic characteristics. The epicenters delineate a NNE trending seismic zone that extends from the Hengill geothermal area about 30 km southwards along the eastern edge of the Hellisheidi highland. An additional, E–W trending seismic lineation is suggested by the distribution of epicenters in the lowland east of Hellisheidi at 63°57.5 N. The earthquake sequences in the Hengill-Hellisheidi area are of different types, ranging from mainshock-aftershock sequences to earthquake swarms. This variability probably reflects the complex tectonic position of the area.

Key words: Iceland – Hengill – Earthquakes – Tectonics.

Introduction

The mid-Atlantic plate boundary in SW-Iceland is expressed by a rather complex pattern of three tectonically active zones. The Reykjanes Peninsula is the direct landward continuation of the submarine Reykjanes Ridge, the Western Volcanic Zone is one of two parallel volcanic zones in the southern part of Iceland, and the South Iceland Seismic Zone is an E–W trending belt of destructive earthquakes that extends across the lowlands in South Iceland. The three active zones join in some kind of a triple point near 64° N and 21° W (Fig. 1). The seismicity near this junction is the subject of the present paper. After the installation of a short-period seismograph network in this part of Iceland in 1974 it was possible to study the seismicity in more detail than before. In the time interval August 1974 to November 1978, 106 locatable seismic events in this area were recorded. The epicentral distribution sheds some new light on the tectonics of the area in spite of the limited number of epicenters. More tectonic elements are expected to emerge when more data become available.

Tectonic Setting

The Reykjanes Peninsula is a zone of volcanism and high seismic activity. It has been interpreted as an obliquely spreading ridge or a transform fault with a component of opening (Tryggvason, 1968; Nakamura, 1970; Klein et al., 1973). The plate boundary as delineated by the seismically active zone has a trend of N70°E (Klein et al., 1973; 1977), and is therefore oblique to the assumed direction of relative plate motion in this region. The surface tectonics is characterized by swarms of normal faults, open and eruptive fissures arranged *en echelon* with respect to the seismic plate boundary. There is a gradual change in the mode of seismic energy release along the peninsula. Near the tip of the peninsula the earthquake sequences are mainly of the swarm type. Mainshock-aftershock sequences become more common towards the east (Tryggvason, 1973; Einarsson, 1979). The seismicity in the eastern part of the peninsula has been very low in the last 10 years. For this reason it has not been possible to trace the seismic plate boundary towards the junction with the Western Volcanic Zone and the South Iceland Seismic Zone.

The seismicity of the Western Volcanic Zone is low to moderate. The structure near the southern end of the zone is dominated by a swarm of fissures and normal faults with a NE strike. This swarm passes through the Hengill central volcano. The structural relationship is therefore somewhat similar to that of the presently active Krafla central volcano and the Krafla fault swarm in the volcanic zone of northern Iceland (Saemundsson, 1974, 1978;

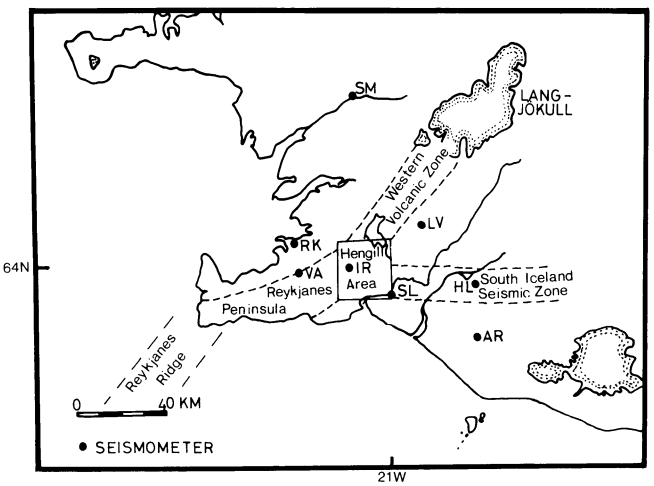

Fig. 1. Map showing the volcanic and seismic zones of southwest Iceland and the relationship of the Hengill area to these zones. The main ice caps are also shown (Jökull in Icelandic). *Rectangle* shows area of Fig. 2. *Black dots* show the main seismic stations

0340-062X/80/0047/0171/$01.00

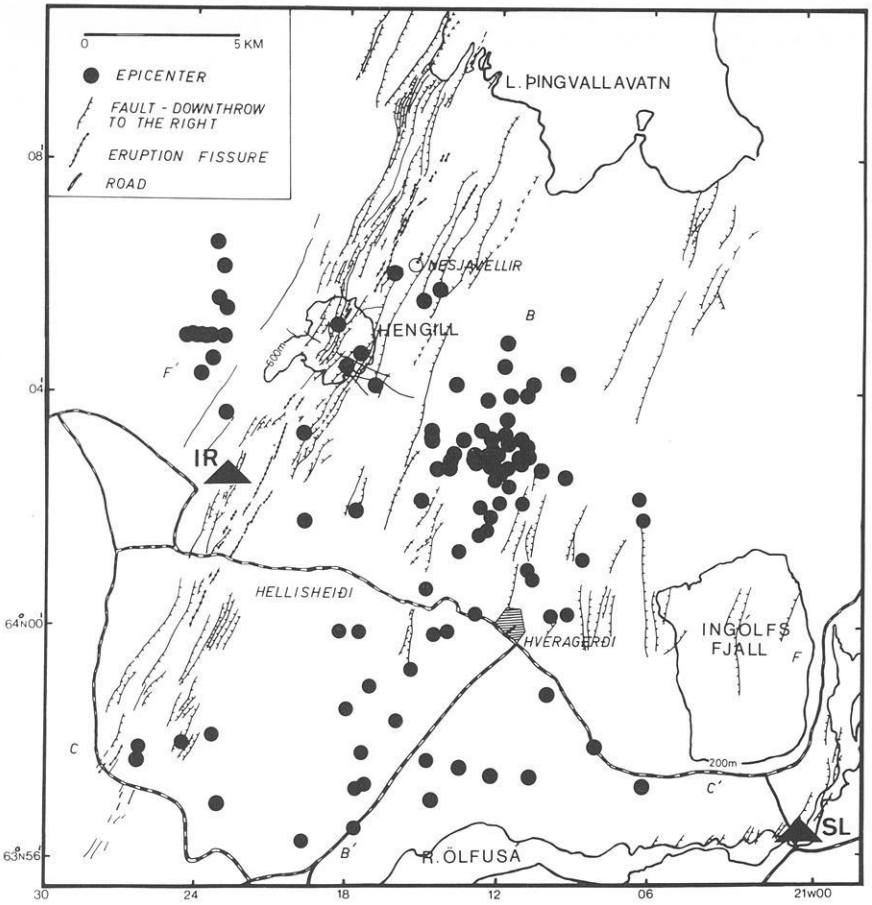

Fig. 2. Map showing the epicenters of 106 events that occurred between August 2, 1974 and November 19, 1978. Faults and fissures compiled from Saemundsson (1967), Eiríksson (1973), Árnason et al. (1969), Jónsson (1978). Seismic stations *IR* and *SL* are marked with *triangles*

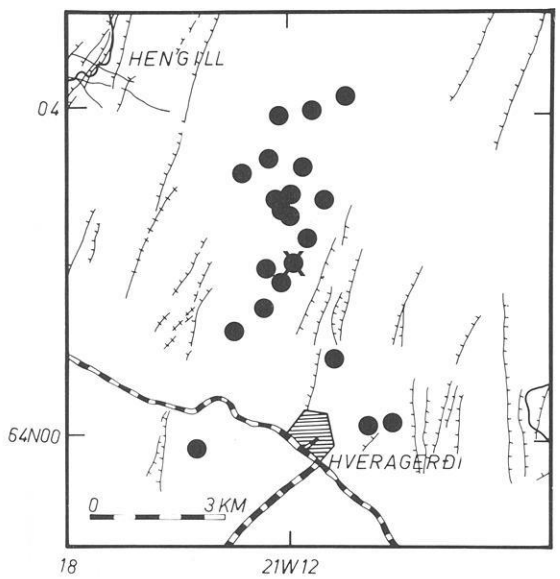

Fig. 3. Map showing the epicenters of 21 events occurring in sequence in February 1977. Symbols as in Fig. 2. Mainshock is marked with X

Björnsson et al., 1977). The geology of the Hengill area has been described in detail by Saemundsson (1967). The surface materials are mostly basaltic pillow lavas and hyaloclastites, erupted under ice. Both intermediate and acid rocks occur also. Several eruption fissures of post-glacial age exist. North of the central volcano the Hengill fault swarm has the structure of nested grabens. An inner graben of 4–5 km width is nested within an outer graben of 15–20 km width. Geological observations in this part of the graben, the Thingvellir graben, indicate that the inner graben has been subsiding at the average rate of 5–8 mm/a during the past 8,000 years. Precision levelling over a 5-year period revealed subsidence at a rate of only 2.5 mm/a (Tryggvason, 1974). The subsidence is hence probably episodic, with most of the movement occurring during short periods of high activity similar to the present activity of the Krafla area. In the volcanic zone of northern Iceland such rifting episodes occur at intervals of 100–150 years (Björnsson et al., 1977), and are intimately related to magmatic processes of central volcanoes. Similar events may have taken place in the Hengill area in the year 1789, when earthquake activity was accompanied by some 60 cm of subsidence in the Thingvellir graben (Thoroddsen, 1899).

The structure and mechanics of the South Iceland seismic zone is not well understood. Stefánsson (1967) described it as a zone of horizontal shear deformation and Ward et al. (1969) and Ward (1971) used the term fracture zone for this area. The epicenters of large, historic earthquakes are arranged within a fairly narrow, E–W trending zone near 64°N (Tryggvason, 1973; Björnsson, 1975), but there is no evidence for a major, E-W striking fault on the surface. Each earthquake appears to be associated with right-lateral movement on northerly striking faults, as evidenced by surface faulting (Tryggvason, 1973) and the shape of the destruction zones (Björnsson, 1975). Individual faults thus appear to be transverse to the epicentral belt of the large earthquakes.

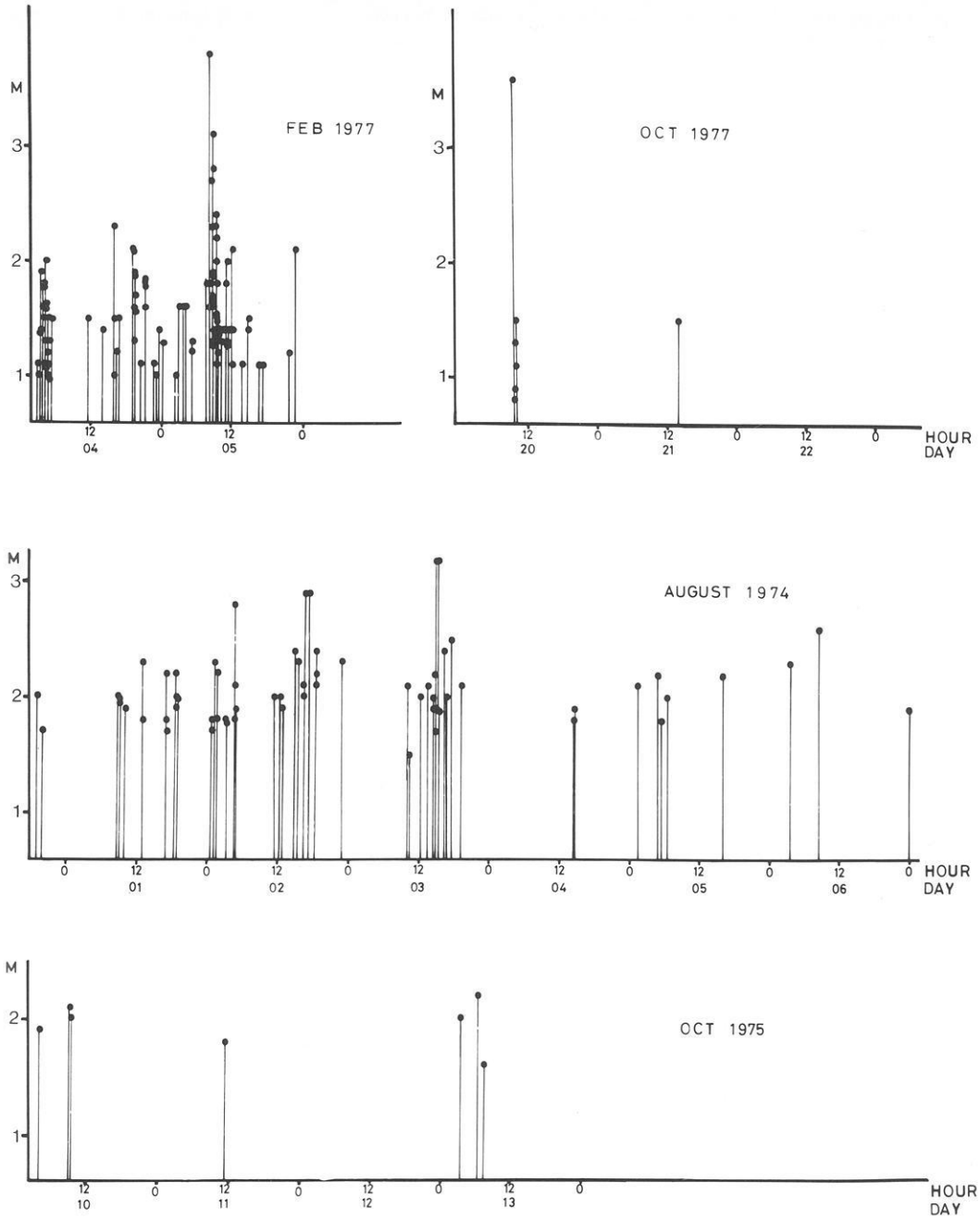

Fig. 4. Magnitudes of all events detected, plotted against time for the earthquake sequences of February 1977, October 1977, August 1974, and October 1975. The magnitude of each event was obtained using both the maximum trace amplitude and the time duration of the event on the seismograms at all calibrated stations which detected the event

Data Collection and Analysis

Seismological data were collected from a network of permanent, short-period seismographs in SW-Iceland (Fig. 1). For a large part of the time, 8 stations were in operation within 80 km of the Hengill-Hellisheidi area. Most of the records are in the form of revolving drum paper records inscribed with pen and ink. Radio time is recorded at all stations, eliminating the necessity for clock corrections. Time resolution is of the order of 0.1 s.

The hypocenters were located using the computer programs HYPO71 (Lee and Lahr, 1972), HYPOELLIPSE (Lahr and Ward, in preparation.) and HYPOINVERSE (Klein, 1978) by minimizing the root mean square of the difference between the calculated and observed travel times. The crustal velocity structure used is an average structure based on seismic refraction data from Pálmason (1971). The hypocentral locations are based mostly on P-wave arrival times, but S-waves were used whenever possible.

Earthquake magnitudes used in this paper are obtained by averaging time duration magnitudes at AR, SL, and VA, and maximum amplitude magnitudes at AR and RK. The duration magnitude scales were found by comparison with the maximum amplitude magnitudes at RK. The comparison was made in the magnitude range 1.8–3.7. The duration magnitude scale was then extrapolated to smaller magnitudes. This procedure is similar to that used by Klein et al. (1977) for earthquakes on the Reykjanes peninsula and was found to provide a reliable estimate of magni-

tude. The detection threshold for earthquakes in the Hengill-Hellisheidi area is near magnitude 1.0, and the set of locatable events is complete above magnitude 2.0.

Spatial Distribution of Seismic Events

All epicenters that could be located with horizontal standard error less than 2.5 km are plotted on the map of Fig. 2. The hypocentral depths appear to be smaller than 10 km, but the error of the depth determinations is large because of the lack of seismic stations in the immediate epicentral area of most of the earthquakes. No evidence has been found for seismic activity deeper than 10 km.

Many of the epicenters are located within a relatively small area about 5 km N of the town Hveragerdi. This cluster of epicenters is elongated in a SSW-NNE direction. This trend is even more pronounced if shorter time intervals are considered. The earthquake sequence of February 1977 (Fig. 3), for example, occurred within the cluster. The mainshock ($M_L = 3.7$) was located near the cluster. The aftershocks then migrated to the NNE and SSW, suggesting bilateral rupture on a NNE striking fault. A total zone length of 8 km was activated during this sequence. The seismic zone defined by the cluster can be traced by the distribution of epicenters farther to the SSW This zone (BB' in Fig. 2) is 30 km long and extends along the eastern border of the Hellisheidi highland.

The alignment of epicenters in Fig. 3 is not an artifact of the location program. The horizontal standard error of the locations is smaller than 2.5 km but for most of the events the error is smaller than 1 km. The error ellipsoid for most of the solutions is nearly spherical.

One further seismic belt is suggested by epicenters in the lowland of the Ölfus district. This is an E-W trending zone at 63°57.5 N (CC' in Fig. 2). This zone is not as well defined as the first one, but its trend suggests that it may be related to the zone of large earthquakes in south Iceland.

The cluster of epicenters west of Hengill belongs to one earthquake swarm that occurred in August 1974 (Fig. 4). This isolated cluster demonstrates how variable the seismicity is, both in space and time. A recording time of 3–4 years is not long enough to reveal all the seismically active elements, even where the activity is high such as in the Hengill-Hellisheidi area. It is noticeable, for example that very few earthquakes occurred in the central part of the Hengill fault swarm, which is the most heavily faulted part of the area.

Time Distribution of Seismic Events

The seismic energy release in the Hengill-Hellisheidi area occurs both in single events and in sequences of events that are related in space and time. Time-magnitude plots of all the largest distinct sequences appear in Fig. 4. It is immediately clear that great variation is displayed in the form of these sequences. Mogi (1963) considers the variation of earthquake sequences in relation to three sequence types, i.e., the mainshock-aftershock (Type 1), foreshock-mainshock-aftershock (Type 2) and the swarm type (Type 3). Complete gradation between all types is found in nature. The form of any sequence is considered to be dependent upon, amongst other things, the tectonic, magmatic and hydrothermal state of the crust (Sykes, 1970). A summary of some suggested associations is given in Table 1 These associations are not exclusive, however, and exceptions are known. Thus, for example, earthquake swarms are known in transform fault zones (Tatham and Savino, 1974; Einarsson, 1976) and normal faulting may occur in a mainshock-aftershock sequence as in the case of the mainshock of the Borgarfjördur earthquakes in West Iceland in 1974 (Einarsson et al., 1977).

Table 1. Physical associations of earthquake sequences

Swarm sequences	Mainshock-aftershock sequences
Inhomogeneity of crust	Homogeneity of crust
Inhomogeneity of stress	Homogeneity of stress
High fluid pressure	Low fluid pressure
Normal faulting	Strike-slip faulting
Short, shallow faults	Long, deep faults
Spreading ridge crest	Transform faults
Areas of recent volcanism	Tectonic earthquakes
Geothermal areas	

Illustrated in Fig. 4 are both typical swarm sequences and mainshock-aftershock sequences. The swarms of August 1974 and October 1975 occurred to the west of Hengill and SW of Hveragerdi respectively. The sequence of February 1977 occurred mostly to the N and W of Hveragerdi and is a foreshock-mainshock-aftershock sequence. The mainshock-aftershock sequence of October 1977 occurred immediately W of Hveragerdi. Thus all three types of sequences occur on the NNE trending epicentral belt (BB') in close proximity to each other. In addition to these larger sequences a continuous background of single events and short sequences is distributed over most of the active area. The wide variety of sequence types may be taken as evidence for large variations in the state of the crust in the Hengill-Hellisheidi area. When more data accumulate it may be possible to use the sequence types as an indicator of the variations in the hydrothermal and tectonic state of the crust on a fine scale.

Discussion

Ward and Björnsson (1971) analyzed seismic data from a small tripartite array, that they operated near Hveragerdi for 11 weeks in 1968. Their epicentral map is in some ways similar to the map presented in this paper. Their map is dominated by the cluster N of Hveragerdi, probably because of the proximity of the array, but the linear trends of epicenters are not clear except that the E-W trend is indicated in the Ölfus lowland. The difference between the results is most likely caused by our longer recording time and the use of a larger seismograph network that encompasses the whole study area. This way the detection capability of the network is more uniform over the area, and the background microearthquake activity that is often found to be associated with high temperature geothermal areas (Ward and Björnsson, 1971) is not as dominating on the epicentral map.

The fault pattern shown in Fig. 2 changes systematically from W to E. In the west the pattern is dominated by the Hengill fault swarm that has a NE-SW trend, but in the southeast part of the area the strike of the faults gradually becomes more northerly. Björnsson et al. (1974) suggested that the faults east of Hengill belonged to the fault swarm of another and older central volcanic complex. It is also possible that the change in strike represents the change in the stress field from the primarily extensional tecto-

nic regime of the Western Volcanic Zone in the west to the strike-slip tectonics of the South Iceland Seismic Zone in the east. This question may be resolved with a focal mechanism study of the earthquakes, which has not yet been possible because of the poor depth resolution of the hypocentral locations obtained so far.

The hydrothermal circulation of the Hengill geothermal area is likely to be affected by the tectonics. The crust in the seismic belts probably has higher permeability and may thus allow water to percolate more freely than the surrounding crust. The concentrations of chlorine, tritium and deuterium in the thermal water indicate that the Hengill area is fed by two deep groundwater systems (Árnason et al., 1969; Árnason, 1976). The water from drill holes near Nesjavellir (Fig. 2) is believed to originate near the Langjökull glacier and this system may extend southerly along the entire length of the Hengill fault swarm. Around Hveragerdi, on the other hand, the deep water has a different deuterium content and may originate about 35 km to the NE. It is noteworthy that the NNE trending epicentral belt separates the Heragerdi system from the other systems. Perhaps the epicentral belt provides a flow channel for one of the deep circulation systems, and then most likely the Hveragerdi system.

Acknowledgements. The authors are grateful to Sveinbjörn Björnsson, Max Wyss, Kristján Saemundsson and Bragi Árnason for their critical reading of the manuscript. Henry Johansen analyzed some of the data from 1976 and 1977. Some of the seismic stations used in this study were built with the support of the Nato Research Grants Programme (Grant no. 715).

References

Árnason, B.: Groundwater systems in Iceland traced by deuterium. Soc. Sci. Isl. Rit **42**, 236, 1976

Árnason, B., Theodórsson, P., Björnsson, S., Saemundsson, K. Hengill, a high temperature thermal area in Iceland. Bull. Volcanol. **33**, 245–260, 1969

Björnsson, A., Saemundsson, K., Einarsson, P., Tryggvason, E., Grönvold, K. Current rifting episode in north Iceland. Nature **266**, 318–323, 1977

Björnsson, A., Tómasson, J., Saemundsson, K.: Hengilssvæðið, staða jarðhitarannsókna vorið 1974, (The Hengill area, the state of geothermal research in the spring of 1974; in Icelandic). Orkustofnun OS JHD **7415**, pp. 9, 1974

Björnsson, S.: Jarðskjálftar á Íslandi. (Earthquakes in Iceland; in Icelandic with English abstract). Náttúrufræðingurinn **45**, 110–133, 1975

Einarsson, P. Relative location of earthquakes within the Tjörnes Fracture Zone. Soc. Sci. Isl., Greinar V, pp. 45–60, 1976

Einarsson, P.: Seismicity and earthquake focal mechanisms along the mid-Atlantic plate boundary between Iceland and the Azores. Tectonophysics **55**, 127–153, 1979

Einarsson, P., Klein, F.W., Björnsson, S. The Borgarfjördur earthquakes of 1974 in West Iceland. Bull. Seismol. Soc. Am. **67**, 187–209, 1977

Eiríksson, J. Jarðlagaskipun ytra Miðsuðurlands, (Stratigraphy of the western part of the South Iceland lowland, in Icelandic). B.S. Thesis, University of Iceland, p. 98, 1973

Jónsson, J.: Jarðfræðikort af Reykjanesskaga, (Geological map of the Reykjanes Peninsula, in Icelandic). National Energy Authority, Reykjavik Report OS JHD 7831, pp. 303, 1978

Klein, F.W.: Hypocenter location program HYPOINVERSE. U.S. Geol. Surv. Open-File Report 78–694, 1978

Klein, F.W., Einarsson, P., Wyss, M.: Microearthquakes on the mid-Atlantic plate boundary on the Reykjanes Peninsula in Iceland. J. Geophys. Res. **78**, 5084–5099, 1973

Klein, F.W., Einarsson, P., Wyss, M. The Reykjanes Peninsula, Iceland, earthquake swarm of September 1972 and its tectonic significance. J. Geophys. Res. **82**, 865–888, 1977

Lee, W.H.K., Lahr, J.C.: HYPO71: A computer program for determining hypocenter, magnitude and first motion pattern of local earthquakes. U.S. Geol. Surv. Open-File Report, 1972

Mogi, K.: Some discussion on aftershocks, foreshocks and earthquake swarms – The fracture of a semi-infinite body caused by an inner stress origin and its relation to the earthquake phenomena, 3. Bull. Earthquake Res. Inst. Tokyo Univ. **41**, 615–658, 1963

Nakamura, K.: En echelon features of Icelandic fissures. Acta Nat. Isl. **2**, 15, 1970

Pálmason, G. Crustal structure of Iceland from explosion seismology. Soc. Sci. Isl., Rit **40**, pp. 187, 1971

Saemundsson, K.: Vulkanismus und Tektonik des Hengill-Gebietes in Südwest-Island. Acta Nat. Isl. **2 (7)**, pp. 109, 1967

Saemundsson, K.: Evolution of the axial rifting zone in northern Iceland and the Tjörnes Fracture Zone. Bull. Geol. Soc. Am. **85**, 495–504, 1974

Saemundsson, K.: Fissure swarms and central volcanoes of the neovolcanic zones of Iceland. Geol. J. Special Issue No. **10**, 415–432, 1978

Stefánsson, R.: Some problems of seismological studies on the Mid-Atlantic Ridge. In: Iceland and Mid-Ocean Ridges, S. Björnsson, ed., Soc. Sci. Isl. **38**, 80–89, 1967

Sykes, L.R. Earthquake swarms and sea-floor spreading. J. Geophys. Res. **75**, 6598–6611, 1970

Tatham, R.H., Savino, J.M. Faulting mechanisms for two oceanic earthquake swarms. J. Geophys. Res. **79**, 2643–2652, 1974

Thoroddsen, Th.: Jarðskjálftar á Suðurlandi (Earthquakes in South Iceland; in Icelandic). Hið íslenska bókmenntafélag, Kaupmannahöfn, pp. 199, 1899

Tryggvason, E.: Measurement of surface deformation in Iceland by precision levelling. J. Geophys. Res. **73**, 7039–7050, 1968

Tryggvason, E. Seismicity, earthquake swarms and plate boundaries in the Iceland region. Bull. Seismol. Soc. Am. **63**, 1327–1348, 1973

Tryggvason, E.: Vertical crustal movements in Iceland. In: Geodynamics of Iceland and the North Atlantic Area, L. Kristjánsson, ed., pp. 241–262, Dordrecht, Holland, Reidel, 1974

Ward, P.L.: New interpretation of the geology of Iceland. Bull. Geol. Soc. Am. **82**, 2991–3012, 1971

Ward, P.L., Björnsson, S. Microearthquakes, swarms and the geothermal areas of Iceland. J. Geophys. Res. **76**, 3953–3982, 1971

Ward, P.L., Pálmason, G., Drake, C.L.: Microearthquakes and the Mid-Atlantic Ridge in Iceland. J. Geophys. Res. **74**, 665–684, 1969

Received April 18, 1979; Revised Version October 9, 1979

J. Geophys. 47, 176–183, 1980

Journal of Geophysics

Rock Stress in an Icelandic Thermal Area, With Implications on Stresses in the Oceanic Lithosphere

B. Voight[1], R. Simon[1], T Thorsteinsson[2], G. Pálmason[2], C. Taylor[3], S.H. Seret Opzoomer-Talma[4], and B.C. Haimson[5]

[1] College of Earth and Mineral Sciences, The Pennsylvania State University, University Park, Pennsylvania 16802, USA
[2] National Energy Authority, Reykjavik, Iceland
[3] 1118 The Colony, Hartsdale, New York, USA
[4] Oranjewoud 625, 8443 G.A. Heerenveen, The Netherlands
[5] University of Wisconsin, Madison, Wisconsin, USA

Abstract. Numerical model analysis of the Reykjavik thermal area in southwest Iceland suggests the possibility of a complex regional stress pattern strongly influenced by thermoelastic effects. The thermal areas are predicted to be domains of relatively high compression, surrounded by zones of approximately radially-diminishing compression and circumferential extension. Model results are compared to data from hydrofracture measurements in southwest Iceland by Haimson and Voight (1977), which suggested a direction of maximum horizontal compression roughly normal to the nearby axial rift zone. Though this regional trend seems supported by additional studies, finite element results presented here suggest that the Reykjavik hydrofracture borehole locations may have been influenced by locally-developed thermoelastic stresses. Predicted stresses and stress orientations for measurement sites are in rather good accord with field measurements. A mechanism for 'locking in' thermoelastic strains and associated stresses is postulated, whereby mineralization in open (thermal) fractures in hot rock prevents these fractures from closing once thermal loading is removed. Old thermal areas may therefore still contain residual stresses on the order of 10^2 bar which reflect paleotemperature fields. Finally, it is asserted that stresses through the upper part of the entire oceanic lithosphere may be dominated by residual, mainly thermal components. If so, intraplate stresses cannot be simply calculated from plate tectonic forces acting on the boundaries of lithosphere plates.

Key words: Iceland – Thermal stress – Residual stress – Plate tectonics – Geothermal – Finite element – Hydrofracturing – Mid-Atlantic Ridge – Ocean lithosphere – Tectonics.

Introduction

Hydrofracturing stress measurements were recently carried out to about 0.4-km depth in two boreholes in Quaternary volcanic rocks in Reykjavik, Iceland, on the flank of the Reykjanes-Langjökull continuation of the Mid-Atlantic Ridge (Figs. 1 and 2, Haimson and Voight, 1977). The measurements indicated for the borehole sites an orientation of σ_{Hmax} approximately perpendicular to the axial rift zone; this orientation contrasts with stress orientation postulated for fissures, high angle faults, and focal mechanism solutions for earthquakes within the nearby axial rift zone of the Reykjanes Peninsula (Haimson and Voight, 1977, cf. Klein et al., 1973, 1977).

Several interpretations were offered as possible explanations of the data. Among these was the following (Haimson and Voight, 1977, p. 172): ' .the possibility of a thermoelastic effect must be raised. It indeed seems likely that a lithospheric plate containing inclusions of abnormally hot rock masses will display an inhomogeneous stress pattern due to the thermoelastic effect (cf. Voight and St. Pierre, 1974). These thermoelastic stresses must be superimposed upon the regional stress field, and their total effect would depend upon the relative magnitudes of each component.

As a highly idealized (plane stress) example we consider here a cylindrical hot inclusion of radius a and uniform temperature T_o in an otherwise cold, unstressed plate. The solution is:

$$\sigma_r = \sigma_\theta = +1/2 E\alpha T_o,\ \sigma_{r\theta} = 0,\ r < a,$$
$$\sigma_r = -\sigma_\theta = +1/2 E\alpha T_o\ (a^2/r^2),\ \sigma_{r\theta} = 0,\ r > a.$$

As a general property of such stress states there is assumed a stress discontinuity across the inclusion surface. Letting $E = 5\times10^5$ bar (cf. Table 1), $\alpha = 8\times10^{-6}\ °C^{-1}$, and $T_o = 100°$ C, we have a uniform value of $\sigma_r = \sigma_\theta = 200$ bar (compression), in the inclusion, and variable σ_r (compression) and σ_θ (tension) in the plates. The latter diminish as $(1/r)^2$; at $r = a$, $\sigma_r = -\sigma_\theta = 200$ bar, at $r = 2a$, $\sigma_r = -\sigma_\theta = 50$ bar, and so forth. The mathematical effect is the same, incidentally, if we start with a uniformly hot plate and nonuniformly cool it (inclusion is cooled to a lesser degree); the latter description more adequately fits the thermal history of Icelandic rocks as discussed previously. The result, which must be interpreted in terms of more or less continuous rather than discontinuous stress fields, is that high values of compression might be expected within thermal anomalies, with radial compression and circumferential tension (diminishing rapidly with radial distance) expected beyond them. Stresses due to overburden pressure and initial conditions must be superimposed upon these predicted thermoelastic changes so that absolute tension might not ordinarily be expected, in addition, actual stress changes should be expected to be less, than theoretical estimates because of rock strength limitations.

Interpretation of the field data in terms of this simple model was not straight-forward, in large part because of the necessity of assumed temperature and stress discontinuities at the inclusion boundary. The boundary of the anomaly in the field is simply not that sharp (Fig. 2). On balance the possibility of some thermoelastic stress influence seemed supported by the available evidence, in any event the hypothesis of a local thermoelastic effect could not be safely rejected (Haimson and Voight, 1977, p. 173). In this paper a more elaborate attempt is made to examine questions of thermoelastic stress. The finite element technique (as discussed e.g. by Voight and Samuelson (1969) and many others; see, Gallagher, 1975) was employed.

0340-062X/80/0047/0176/$01.60

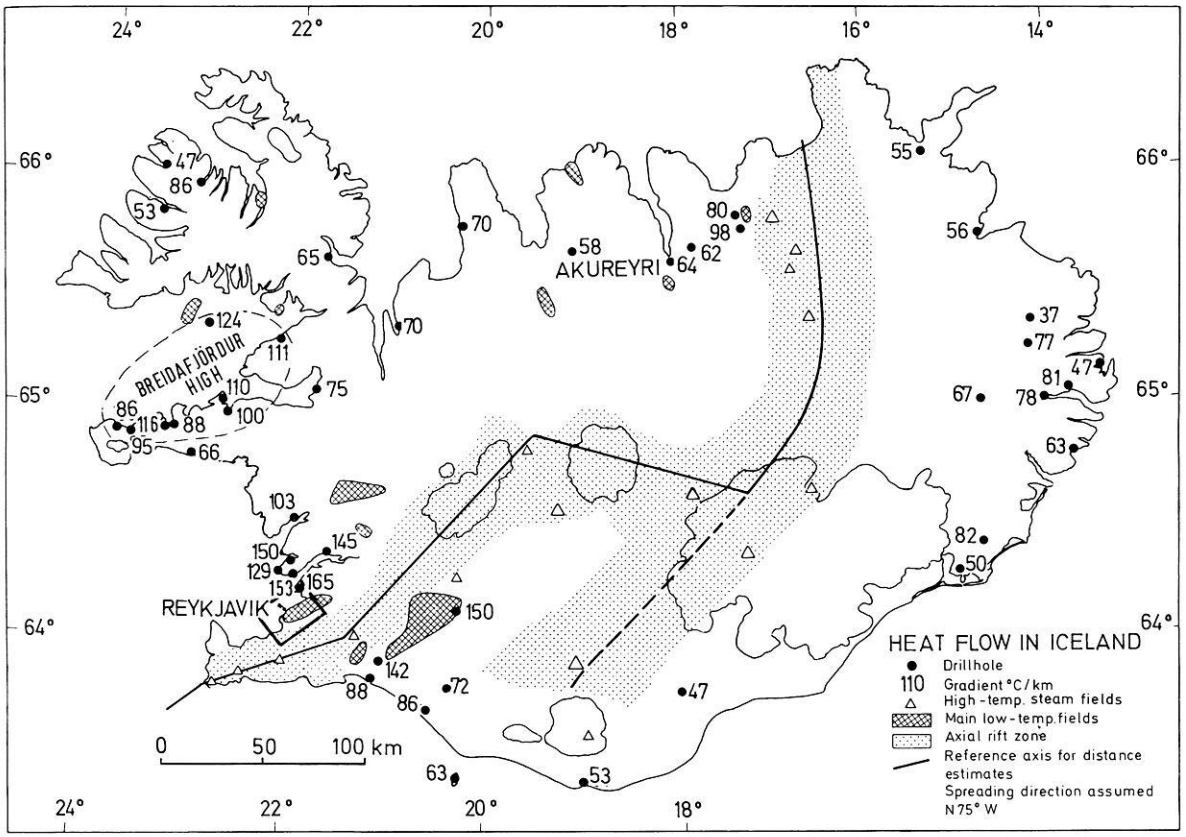

Fig. 1. Map of Iceland (after Pálmason and Saemundsson, 1974), indicating regional distribution of surface temperature gradients. Rectangle near Reykjavik represents map area of Fig. 2. The stippled pattern indicates the active zone of rifting and volcanism

Geometry, Material Properties, Temperature Changes

The area modeled is a rectangle 24×18 km^2, with one long boundary at the approximate edge of the axial rift zone (Fig. 1). The Laugarnes hydrothermal system, the site of the hydrofracture measurements, is located approximately in the center of the finite element model. A grid of 186 nodal points (346 plane stress triangular elements) was constructed, with smaller elements in areas of high temperature gradient. Nodal points were located at stress measurement sites. A reference depth of 300 m was selected, inasmuch as many of the borehole measurements cluster about this depth (Haimson and Voight, 1977, Fig. 8).

The rock types of the Reykjavik area include basalt flows in various stages of alteration, interglacial sediments, hyaloclastites, and local dolerite intrusions; the stress measurements were made in basalt and dolerite. Not unexpectedly, therefore, the associated physical properties cover a fair range (Table 1). For most computer experiments the material was regarded as homogeneous, with a Young's modulus of 4×10^5 bar, Poisson's ratio of 0.25, and coefficient of linear temperature expansion of 5.4×10^{-6} °C^{-1}. However it is recognized that no single set of elastic constants can accurately describe the field situation. The Young's modulus value at any given point in the rock mass seems correct within a factor of about two with respect to measured laboratory values. A fair correspondence of laboratory and field modulus values is expected because most joints are mineralized at this depth. The other property values were assumed. Alternative approaches would have been to (1) vary element properties within the known range, using for example a random number generator (Su et al., 1970), or to (2) specify properties according to the known distribution of specific rock types.

Table 1. Properties of Rock in Reykjavik Area, Iceland, based on laboratory measurements

Density: 2.4–3.0 Mg/m^3
Uniaxial compressive strength: 240–2570 bar
Tensile Strength
Assumed value (1/15 uniaxial compressive strength): 16–170 bar
Laboratory 'hydrofracturing' strength: 21–134 bar
Field 'hydrofracturing' strength: 34–134 bar
Young's modulus: $1.7–8.2 \times 10^5$ bar

Temperature data were based on the detailed surface thermal gradient map of the Reykjavik area (Fig. 2), showing anomalies associated with Laugarnes, Seltjarnarnes, Ellidaár, and Álftanes thermal fields (Pálmason, 1975). Isolines are given in °C/km, and surface gradients as high as 500° C/km are indicated. The surface gradients are not in fact maintained to depths of 1 km and beyond (e.g., Tómasson et al., 1975, Fig. 4), but to 300 m the error in calculated rock temperature seems relatively small, as indicated by drillhole data.

Thermal stresses are due to temperature changes. The simplifying assumption is made that plastic or viscoplastic yielding over geologic time can take place above a given critical temperature, T_p, but that for rock cooled below this reference temperature the crust behaves essentially elastically. Thermoelastic stresses are

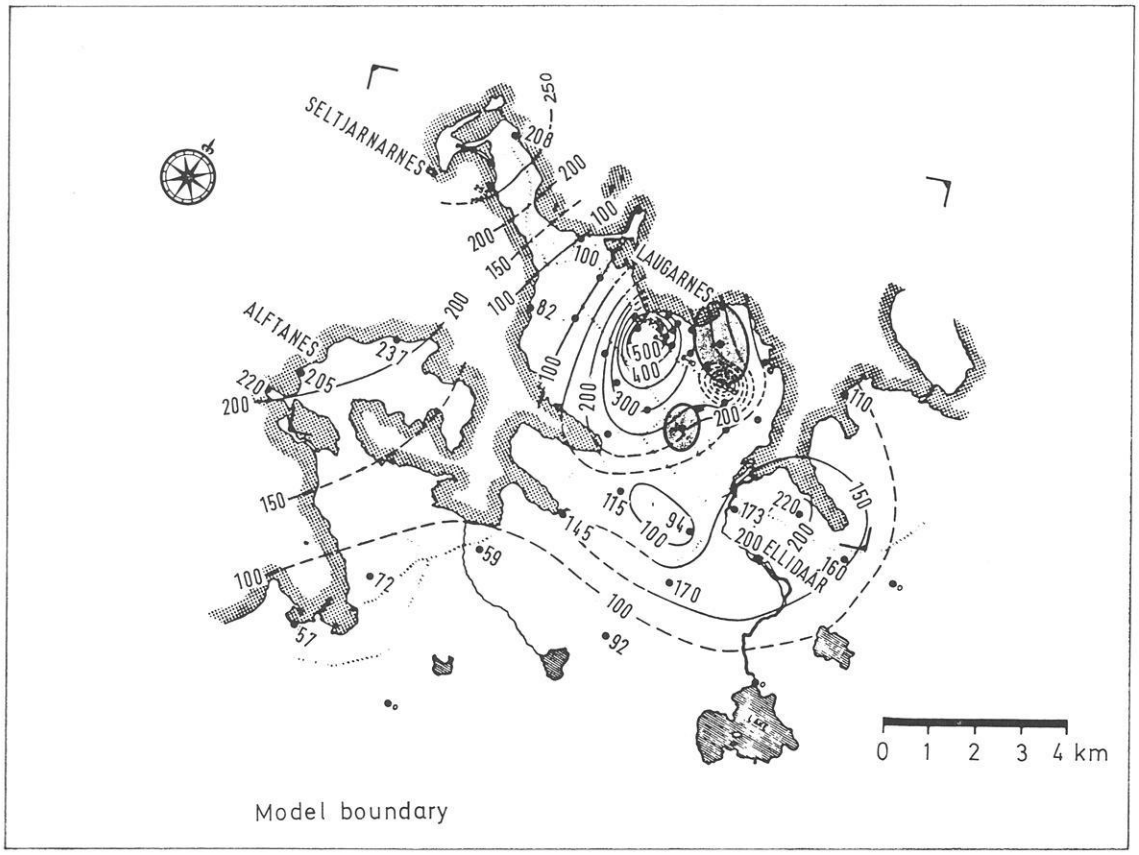

Fig. 2. Thermal gradient map of Reykjavik peninsula and adjacent areas (for location see Fig. 1), showing anomalies associated with Laugarnes, Seltjarnarnes, Ellidaár, and Álftanes fields (after Pálmason, 1975). Isolines in °C/km. Stress ellipses noted for boreholes H18 (the larger) and H32, for about 0.3-km depth (after Haimson and Voight, 1977). Water bodies are patterned. Outer rectangle at model boundaries. Four corners show frame of Figs. 3–6

thus limited to $T < T_p$. Following Turcotte (1974) we assume $T_p =$ 300° C. The temperature change for each element was therefore $T_p - T_{0.3}$, where $T_{0.3}$ is the temperature at the 0.3-km level as estimated from the surface gradient at the element centroid.

Results

If ENE-WSW boundary displacements are restrained (Model I), tensions on the order of 500 bar develop as a consequence of cooling (Fig. 3). The internal stress directions are controlled by the imposed (roller) boundary conditions, with the thermal field variations creating a minor effect. Values of tension are somewhat less (25% or so) over hot spots. The amount of calculated tension is well beyond the tensile strength of the intact rock (by a factor of about 5) and hence also the strength of the rock mass (see e.g. Table 1). Model I therefore is interpreted to predict fracturing of the rock mass more or less perpendicular to the direction of tensile stress, with the principal through-going fractures avoiding the high temperature areas; the tensile stresses would thereby be largely relieved, and the zero-displacement boundary conditions of the original model would be effectively changed to that of boundaries relatively free to displace.

The stresses developed in the model are, of course, proportional to the assumed value of Young's modulus. These stresses could therefore be decreased by assuming a lesser value of Young's modulus. However, because strength and Young's modulus are not truly independent variables, and because the assumed value of Young's modulus is believed to be of the correct order of magnitude, the broad interpretation of Model I as given above would seem justified.

In the next experiment (Model II), lateral boundaries were assumed unstressed (and free to distort), with internal stress depending solely on the distribution of sustained temperature changes. The pattern in plan view is one of strong biaxial compression within the zone of highest vertical temperature gradients, grading outward to a zone of approximately radial compression and circumferential tension (Fig. 4). Qualitatively similar to the thermal inclusion model discussed in the introduction to this paper, this finite element model more adequately treats the stress changes in terms of complex temperature variations observed in the several thermal areas. Stress measurement data for boreholes H18 and H32 are also plotted as ellipses for comparison with theoretically determined values.

The following information was next considered. The total vertical stress σ_v at a depth of 0.3 km is about 84 ± 3 bar, based on known density of overburden. The measured formation pore fluid pressure at this depth is about 24 bar (Haimson and Voight, 1977, Table 3). Thus the effective vertical stress σ'_v (total vertical stress minus pore fluid pressure) can be taken as 60 bar.[1] If the cohesive

[1] The notation σ_i indicates total stresses; with a 'prime', e.g., σ'_i, effective stresses are indicated

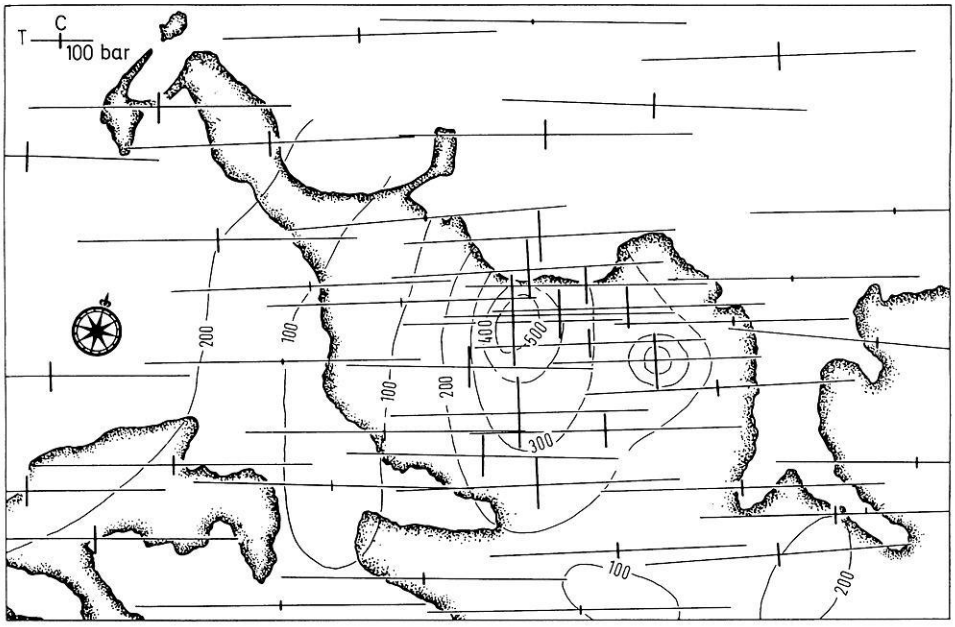

Fig. 3. Horizontal effective stress distribution in the Reykjavik peninsula area (compare Fig. 2 for location and scale) at 0.3-km depth. Model I (ENE-WSW motion restrained at boundaries). Stresses are indicated by *crosses*. Compression *(C)* given by *heavy lines*, tension *(T)* by *thin lines*. Stress scale as indicated for tension line in upper left corner. Surface temperature gradient contours are taken from Fig. 2. The model predicts tension fractures roughly normal to the tensile stresses, with the main fracture zones avoiding the domains of highest temperature

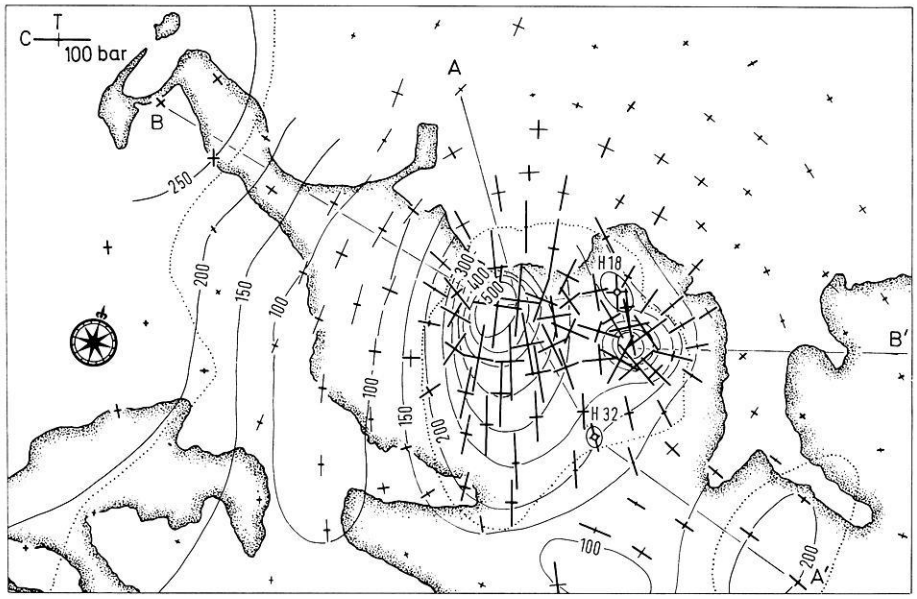

Fig. 4. Horizontal effective stress distribution in the Reykjavik peninsula area (cf. Fig. 2 for location and scale) at 0.3-km depth. Model II (freem, unstressed boundaries). Compression *(C)* given by *heavy lines*, tension *(T)* by *thin lines*. Stress scale as indicated for compression in upper left corner. Surface temperature gradient contours from Fig. 2. Locations of stress profiles *A–A'*, *B–B'* indicated (cf. Figs. 7 and 8). Measured stress ellipses shown at H18 and H32 sites. Ellipse radii indicate magnitude of compression. Ellipse long axis is direction of σ_{Hmax}

resistance is assumed destroyed on marginal faults along the rift zone boundary, the lateral pressure perpendicular to the strike of normal faults at this location (the minimum effective principal stress σ'_3) is assumed to be given by the product of the effective vertical stress and the term $\tan^2(45-{}^1/_2\phi)$, where ϕ = angle of friction, as noted by classical soil mechanics theory. Assuming $\phi = 30°$, the effective lateral boundary stress is 20 bar, acting in a northwest direction (if cohesion >0, $\sigma'_3 < 20$ bar). Boundary stresses in the northeast direction are unknown (as indeed are the appropriate limits of the model 'plate'), but at least at the juncture of the northeast edge of the model with the active rift zone faults, these stresses are inferred as $\geqq 20$ bar.

A third model was therefore considered (Model III), consisting of a flat plate, free to deform at boundaries and subjected to internal thermal loading, with a uniform boundary stress of 20 bar. The solution of Model III is exactly that of Model II (free boundary), except that all principal stress magnitudes are increased by 20 bar. Stress orientations and shear stresses remain unchanged. Therefore, the diagrams of shear stresses and predicted fracture orientations (Figs. 5 and 6) apply exactly to both Models II and III. The diagram of the principal stresses (Fig. 4) is also applicable to both, but for Model III each stress must be increased by a compression of 20 bar. As a result, for Model III a decrease of 20 bar occurs in each of the absolute values of tension indicated in Fig. 4, and a substantial decrease occurs in the area of rock mass subjected to some tensional stress. 'Effective Stress' profiles across the thermal areas are shown in Figs. 7 and 8. The data are for Model II, but the results can be interpreted also for Mo-

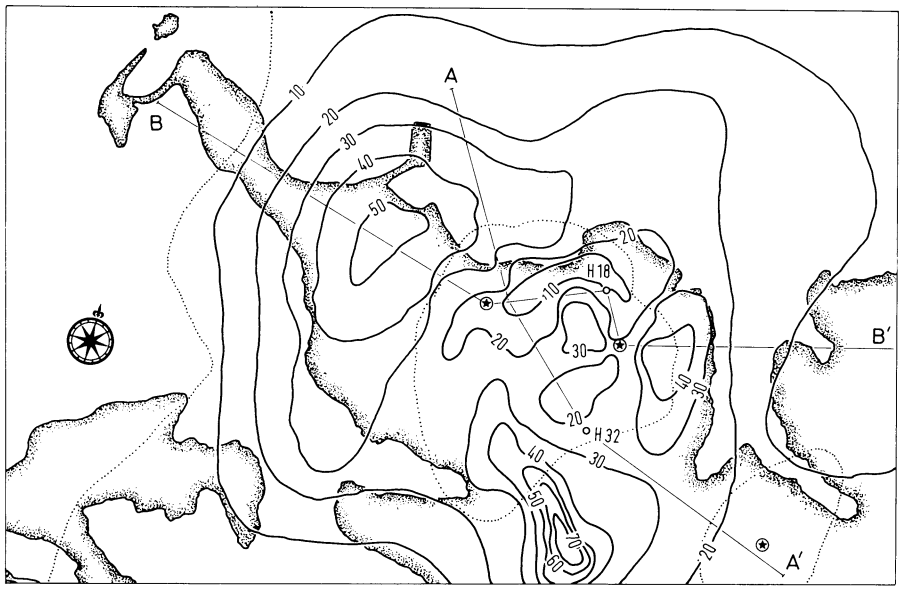

Fig. 5. Horizontal shear stress distribution in the Reykjavik peninsula area at 0.3-km depth (cf. Fig. 2 for location and scale). Models II and III. Shear stress isolines are in bars. Locations of stress profile *A–A′*, *B–B′* indicated (cf. Figs. 7 and 8). *Dotted lines* indicate compression-tension boundaries for Model II. *Stars* denote approximate locations of temperature maxima. Stress measurement sites H18 and H32 are shown

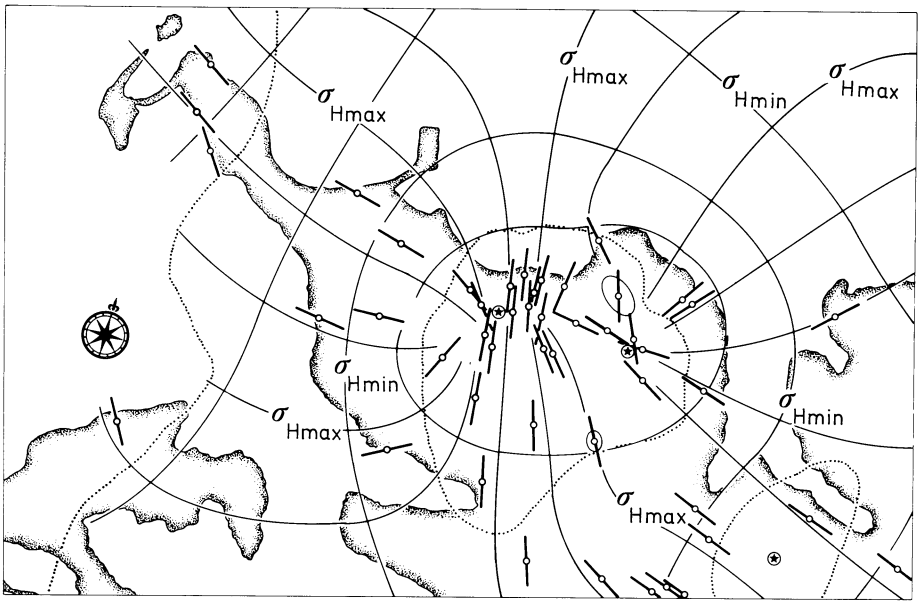

Fig. 6. Horizontal stress trajectories of the Reykjavik peninsula area at 0.3-km depth (cf. Fig. 2 for location and scale). Models II and III. Compression reckoned positive (i.e., σ_{Hmax} is maximum horizontal compression). *Stars, dotted lines* as indicated in Fig. 5. Existing boreholes indicated by *circles, with heavy lines* denoting predicted extension fracture orientations for the borehole sites. Stress ellipses are indicated for the stress measurement sites. The long axes of these ellipses correspond to observed hydrofracture orientations

del III by superposition of 20 bar on the horizontal stresses. The extent to which the stress profiles mirror the temperature gradient profile is clear.

The effective vertical stress is also indicated on the profiles. It appears that over much of the region at this depth, the predicted vertical stress is the greatest effective principal stress (σ_1'), compression reckoned positive. Over the hotter parts of the thermal areas, however, the vertical stress becomes the minimum stress (σ_3'), as the magnitudes of the horizontal stresses become large. Peripheral zones with respect to the hot spots are characterized by $\sigma_v' = \sigma_2'$.

Hydrofracture stress measurement data for boreholes H18 and H32 are also given in Figs. 4, 6, 8, and Table 2, for comparison with theoretical Models II and III. The correspondence of measured values with results of both numerical models is rather striking, both with respect to stress orientation and magnitude. Indeed, the degree of correspondence seems remarkable in view of the large number of simplifying assumptions required. The fit with respect to σ_{Hmin} is better than for σ_{Hmax}, but the measured values of σ_{Hmin} are known to a greater degree of reliability due to the nature of the hydrofracturing technique. No 'backfitting' of Young's moduli was attempted, for example, in order to bring measured and calculated stresses into closer correspondence. On the other hand, the observed correspondence does not guarantee the correctness of the assumed elastic properties, for another set of temperature assumptions, on which the stresses also greatly depend, might easily have been employed.[2] No uniqueness of

[2] The 'correct' field value of Young's modulus might be half of that value indicated by laboratory experiments, whereas the assumed critical temperature T_p might be effectively twice as high. A similar set of predicted stresses might thereby result. The present solution might thus contain an appropriate 'balance' of parametric assumptions even though individual values might be disputed

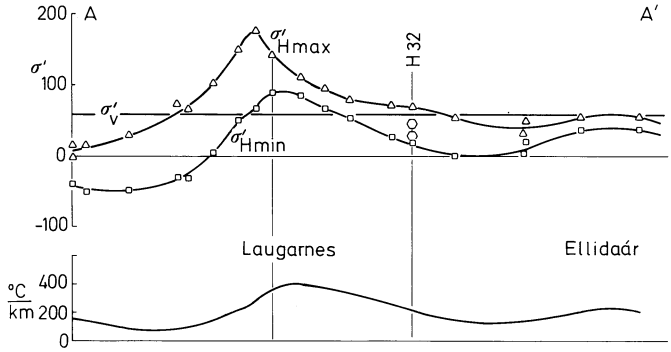

Fig. 7. Effective stress and thermal gradient profiles *A–A'*, crossing Laugarnes and Ellidaár thermal domes (see Figs. 4 and 5 for profile location). Model II (for Model III, add 20 bar to indicated horizontal stresses). Stresses in bar, thermal gradients in °C/km. Note excellent correspondence between stresses and thermal gradients. Measured maximum and minimum horizontal stresses at H32 indicated by octagonal symbols. Note change in orientation in principal stresses as a function of position over the Laugarnes thermal high, $\sigma'_v = \sigma'_3$

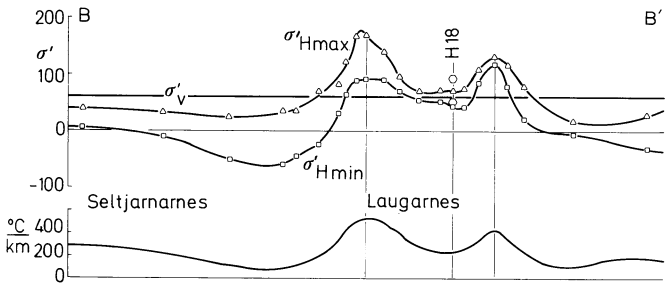

Fig. 8. Effective stress and thermal gradient profiles *B–B'*, from Seltjarnarnes through Laugarnes (see Figs. 4 and 5 for profile location). Explanation as in Fig. 7. Measured horizontal stresses at H18 indicated by octagonal symbols

Table 2. Comparison of Measured and Predicted Effective Stresses

	σ_{Hmax}	σ_{Hmin}	τ_{max}	Direction of σ_{Hmax}
H18				
Measured	94	50	22	N 45 W
Calculated				
Model II	73	43	15	N 16 W
Model III	93	63	15	N 16 W
H32				
Measured	44	29	8	N 25 W
Calculated				
Model II	71	19	26	N 30 W
Model III	91	39	26	N 30 W

Model II implies zero boundary stress
Model III implies a boundary stress of 20 bars on all sides
All stresses given are effective stresses, i.e., total stress minus pore fluid pressure. Total stresses are as given in Haimson and Voight, 1977, Eqs. (4) and (5), p. 168. Fluid pressure of 24 bar assumed for the 0.3 km level (Haimson and Voight, 1977, Table 3)

solution can therefore be claimed, and it is possible that the close agreement in stresses is largely fortuitous. Nonetheless, the hypothesis that thermal gradients are mainly responsible for the observed rock stresses seems greatly strengthened.

Other experiments were conducted in which alternatively, (1) additional boundary loads were applied, (2) internal fissuring was considered, and (3) local changes in Young's modulus were introduced. Results were as follows:

1. With increased compressive boundary stress along one edge, the stress pattern observed was similar to that of Model III except that the directions of maximum compression were somewhat shifted in the direction of the applied boundary load.

2. Internal fissuring, modeled by local reductions in Young's modulus, caused a general decrease in tensional stresses and a decrease in maximum compression, with a shift of the tension-compression boundary toward the strongly heated area. The overall stress pattern remained similar.

3. In the area of H18 higher modulus rocks (dolerite) are known to occur, and thus a portion of the model was specified with a large value of Young's modulus (8×10^5 bar), all other model aspects remaining the same. Higher values of stresses resulted, as anticipated. The general patterns were similar.

For the moment it seems sufficient to note that each of these factors can exert a modifying effect on stress fields on a local scale. More refined experiments are anticipated when additional information on the actual distribution of rocks at depth, fracture distributions and temperatures become available.

Theoretical variations of stress as a function of depth have as yet been incompletely studied. It can, however, be stated that the horizontal stresses approach the vertical (overburden) stress with increasing depth, as T approaches T_p. Near the ground surface, rock temperatures approach a uniform value, and thermoelastic stresses will tend to vanish unless residual stresses reflecting the thermal stress history have previously been 'locked' into the rock mass. This possibility seems a reasonable one, as discussed subsequently.

Discussion

Interpretation of Stresses in the Reykjavik Area

Though the effects of other sources of stress have not been sufficiently analyzed to completely evaluate their significance, comparison of measured with predicted stresses suggests the possibility that the shallow-crust lateral stress field of the Reykjavik area could be dominantly thermoelastic in origin. A complex regional stress pattern is envisaged, inasmuch as the boundary of the thermal area very nearly abuts against the edge of an active portion of the axial rift zone, where trajectories of minimum compression are perpendicular to dip-slip fault and fissure traces and are consistently NW-trending (Fig. 9).

In the paper by Haimson and Voight (1977, pp. 173–183), it was noted that the Reykjavik measurements indicated maximum horizontal compression (i.e., σ_{Hmax}, not necessarily σ_1) roughly normal to the trend of the Reykjanes-Langjökull axial rift zone. This suggested the appropriateness of interpretation in regional terms. Indeed, a new series of stress measurements conducted in 1978 tend to support the concept of systematic reorientation of stress outside rift flanks and σ_{Hmax} realignment roughly normal to the plate boundary (Voight, 1979). But the finite element model results suggest that the two Reykjavik measurement boreholes could have been, by the vicissitudes of fortune, located in areas

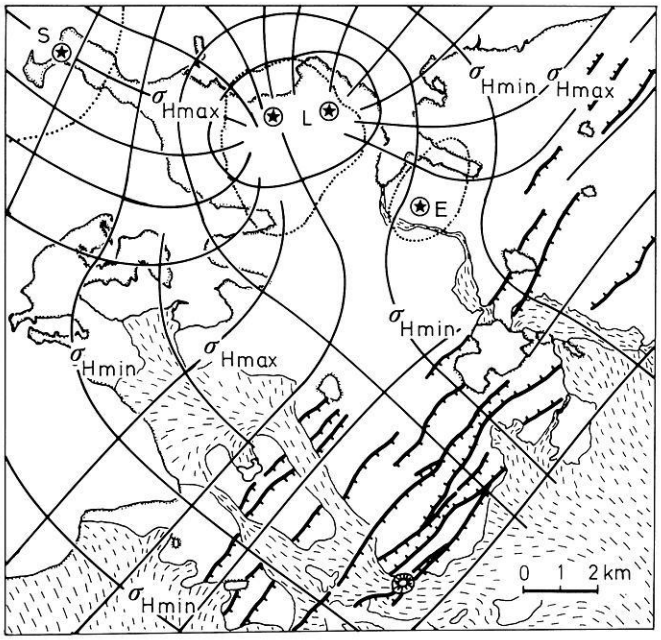

Fig. 9. Inferred regional horizontal stress distribution of Reykjavik and adjacent parts of the axial rift zone, southwest Iceland, partly based on models II and III, and extended to encompass the nearby en-echelon fault zone forming part of the Reykjanes-Langjökull axial rift zone (cf. Fig. 1; Haimson and Voight, 1977, Fig. 2). *Stippled line* at land-sea boundary. *Dashed pattern:* post-glacial lavas. *Circular pattern in the fault zone:* a post-glacial volcano. *Heavy lines with barbs:* faults. *Stars:* approximate centers of thermal areas. *Dotted lines:* compression-tensional boundaries according to Model II. *S:* Seltjarnarnes, *L:* Laugarnes; *E:* Ellidaár

characterized by northwest-trending σ_{Hmax} trajectories. Surrounding these sites the stress patterns could be quite different (Figs. 4 and 9). For example, certain boreholes in the vicinity of the Laugarnes thermal area are located in areas of predicted local northeast-trending σ_{Hmax} trajectories. These boreholes, or others appropriately located, could be used for hydrofracturing stress measurements designed to test the merits of competing hypotheses.

The model could also be further tested by fracture orientation measurements in boreholes stimulated for the purpose of increased productivity. Inflatable open hole injection packers have been used for drill hole stimulation in Iceland since 1967, to depths of 2 km (Tómasson and Thorsteinsson, 1975). Predicted fracture orientations are given by Fig. 6. This diagram, considered together with Figs. 4 and 5, could be useful in designing borehole stimulation programs and in examining the possibility of anisotropic hydraulic conductivity associated with thermally induced rock fracture.

Fracturing should be most intense in areas of high tensile and shear stress at the boundary of (or between) high temperature areas. According to Model III, the most severe fracturing should occur between the Laugarnes and Seltjarnarnes thermal areas, in a relatively narrow belt characterized by high tensile (Fig. 4) and high shear stress (Fig. 5). The predicted orientation of extension fractures is given by Fig. 6, although it is recognised that local shear fracturing may also occur depending upon the specifics of the stress state. Well tests in this area could reflect relatively high fracture permeability, unless the fractures have been rather completely mineralized.

Residual Stresses Associated With Thermal Anomalies?

Some, and perhaps widespread, mineralization of thermally-induced fractures seems likely. The mineralization provides a mechanism for 'locking in' components of the strain system, and hence the stress system, acting within the rock mass at the time of mineralization. These strains, or more precisely a significant portion there of, would remain in the rock mass even if it underwent profound temperature changes. Mineralization simply prevents the fractures from closing once the thermal loading is removed; residual strains and associated stresses can thus be locked within the system (cf. Voight, 1974; Friedman, 1972).

According to this view, old thermal areas may still contain residual stress systems which reflect paleotemperature patterns. Such paleotemperature-caused paleostress patterns may also occur in existing thermal areas, inasmuch as temperature changes have been profound in many parts of such systems. In the Reykjavik area, for example, over 1 km of overburden has been removed, and rock now at the ground surface was at one time characterized by a greatly elevated temperature. The near-surface rock mass may still contain residual stresses on the order of 10^2 bar which reflect paleotemperature conditions. Indeed, it is not yet possible to state the degree to which the subsurface rocks of the Reykjavik area reflect stress patterns due to the present thermal state, as contrasted to residual stresses associated with previous thermal states.

Thermoelastic Effects in 'Oceanic' Lithosphere

Thermoelastic effects within the lithosphere are asserted to occur on several scales; they may be subdivided into several 'kinds' according to the scales on which they operate and the general effects which they produce. The resulting regional stress fields are complex inasmuch as they are influenced by superposition.

Stress due to regional cooling of lithospheric plates (as the plates move away from the axial zone of accretion) includes tension roughly parallel to the axial rift zones. These stresses in turn lead to, or influence, the initiation and propagation of fracture zones and transform faults. Such fractures pass *between* local, smaller-scale thermal areas characterized by locally-high thermally-induced compression as indicated by this paper. Mineralization of fractures could cause residual stresses (strains) on the order of 10^2 bar to be 'locked' into the rocks in the vicinity of these thermal areas. These residual stresses remain even when the temperatures cool to the regional ambient. Such thermally-induced stresses are likely to be present below the ocean floor, in analogy to their occurrence in Iceland.

Basal lithospheric accretion and cooling, on the other hand, causes components of lateral compression to build up regionally in the upper lithosphere, approximately perpendicular to oceanic crust isochrons. These stresses also are residual but on a different (larger) scale than those associated with thermal anomalies. They build up by gradual thickening and cooling of the oceanic lithosphere as it moves away from a ridge crest. New hot material added to the base of the lithosphere cools with time and places the uppermost part of the plate in compression (Sykes and Sbar, 1974). Beyond some critical isochron such compression may be dominant. But at all locations these stresses would be superimposed upon the residual stress systems associated with the local thermal areas. Local variations in accumulated residual stress components may be considerable and could account for the focal

mechanism "maximum compression direction" discrepancies noted for the basal cooling model by Sykes and Sbar (1974, p. 221).

As a consequence, it seems likely that stresses throughout the upper part of *the entire oceanic lithosphere* may be dominated by superposed patterns of residual (mainly thermal) stress components. If so, it would be incorrect to attribute observed intraplate stresses to plate tectonic forces presently acting on the edges and bases of lithospheric plates, as attempted in recent model studies (e.g., Richardson et al., 1976; Voight et al., 1969). Richardson et al. (1976, p. 1848) recognized a need for some caution in this regard, but concluded that 'there are grounds for believing that the effects of such additional stress-producing mechanisms either are minor or can be minimized by scrutiny of the stress observations chosen to compare against the predictions of force models.' This view is too optimistic with respect to the oceanic lithosphere, if our assessment of the Icelandic data is correct.

Acknowledgement. This material is based mainly on work supported by the National Science Foundation under Grant No. EAR 78-12933.

References

Friedman, M.: Residual elastic strain in rocks. Tectonophysics **15**, 297–330, 1972

Gallagher, R.H.: *Finite element Analysis* 420 pp. Englewood Cliffs, NJ: Prentice Hall, 1975

Haimson, B.C., Voight, B. Crustal stress in Iceland. Pure Appl. Geophys. **115**, 153–190, 1977

Klein, F.W., Einarsson, P., Wyss, M. Microearthquakes on the Mid-Atlantic plate boundary on the Reykjanes Peninsula in Iceland. J. Geophys. Res. **78**, 5084–5099, 1973

Klein, F.W., Einarsson, P., Wyss, M.: The Reykjanes Peninsula, Iceland, earthquake swarm of September 1972 and its tectonic significance. J. Geophys. Res. **82**, 865–888, 1977

Pálmason, G. Geophysical methods in geothermal exploration. Proc. 2nd U.N. Symp. Develop. Use Geothermal Resources 1975

Pálmason, G., Saemundsson, K. Iceland in relation to the Mid-Atlantic Ridge. Annu. Rev. Earth Planet. Sci. **2**, 25–50, 1974

Richardson, R.M., Solomon, S.C., Sleep, N.H.: Intraplate stress as an indicator of plate tectonic driving forces. J. Geophys. Res. **81**, 1847–1856, 1976

Su, Y.L., Wang, Y.J., Stefanko, R. Finite element analysis of underground stresses utilizing stochastically simulated material properties. Proc. 11th Symp. Rock. Mech., Soc. Min. Engrs., N.Y pp. 253–266, 1970

Sykes, L.R., Sbar, M.L. Focal mechanism solutions of intraplate earthquakes and stresses in lithosphere. In: Geodynamics of Iceland and North Atlantic Area. L. Kristjansson ed. pp. 207–227. Dordrecht: Reidel, 1974

Tómasson, J., Fridleifsson, I.B., Stefansson, V. A hydrologic model of the flow of thermal water in SW Iceland with a special reference to Reykir and Reykjavik thermal areas. Proc. 2nd U.N. Symp. Develop. Use Geothermal Resources 1975

Tómasson, J., Thorsteinsson, T Use of injection packer for hydrothermal drillhole stimulation in Iceland. Proc. 2nd U.N. Symp. Develop. Use Geothermal Resources 1975

Turcotte, D.L. Are transform faults thermal contraction cracks? J. Geophys. Res. **79**, 2573–2677, 1974

Voight, B. A mechanism of 'locking-in' orogenic stress. Am. J. Sci. **274**, 662–665, 1974

Voight, B.: Structure and stress history of new hydrofracturing stress measurement sites near the 'mid-ocean' plate boundary in Iceland. EOS Trans. Am. Geophys. Union, **60**, 1979

Voight, B., Samuelson, A.C.: On the application of finite-element techniques to problems concerning potential distribution and stress analysis in the earth sciences. Pure Appl. Geophys. **76**, 40–55, 1969

Voight, B., St. Pierre, H.P.B. Stress history and rock stress. Denver: Proc. 3rd Congress, Int. Soc. Rock Mech. 1974

Voight, B., Taylor, J.W., Voight, J.P. Tectonophysical implications of rock stress measurements. Geol. Rundsch. **58**, 655–676, 1969

Received April 30, 1979; Accepted August 10, 1979

Note Added in Proof

Stress measurements at a Hvalfjördur site 20 km north of Reykjavik suggest a NNW direction of $\gamma\sigma_{Hmax}$ (see Haimson, B.C. EOS Trans. Am. Geophys. Union 60, 1979).

J. Geophys. 47, 184–190, 1980

Journal of Geophysics

Crustal and Upper Mantle Structure

A Model of Electrical Resistivity Beneath NE-Iceland, Correlation With Temperature

M. Beblo[1] and A. Björnsson[2]

[1] Institut für Allgemeine und Angewandte Geophysik, Universität München, Theresienstrasse 41, D-8000 München 2, Federal Republic of Germany
[2] National Energy Authority, Laugavegur 116, Reykjavik, Iceland

Abstract. Short period magnetotelluric measurements (15 s–1 h) were made at 19 sites in NE-Iceland, distributed over the neovolcanic zone and the adjoining older Tertiary flood basalt areas. With model-calculations of one- and two-dimensional resistivity distributions a characteristic model was found for the lower crust and upper mantle. Beneath a thin surface layer the resistivity is 100 Ωm except within the active neovolcanic zone where it is 50 Ωm. This layer extends to a layer with low resistivity of 15 Ωm. The low-resistivity layer is about 5 km thick. The depth of its upper boundary increases from 10 km to about 20 km with increasing distance from the rift axis. The resistivity beneath the low-resistivity layer is about 100 Ωm down to at least 100 km. Comparison of field data with laboratory measurements on conductivity at high temperatures indicates that the low-resistivity layer consists of partially molten basalt at a temperature of 1,000°–1,100° C. The underlying layer very probably consists of partially molten ultramafic rocks and is presumably the uppermost part of the mantle beneath Iceland. The basaltic low-resistivity layer is interpreted as the base of the crust formed by upward movement of the basaltic melt fraction from the mantle.

Key words: Magnetotellurics – Iceland – Electrical model – Crust-mantle interface – Temperature – Partial melting.

Introduction

The electrical resistivity of the earth's interior depends strongly on temperature. It is also related to melt fraction and chemical composition. For a known electrical resistivity distribution – obtained, e.g., by magnetotelluric field measurements – it is therefore possible to determine temperature, melt fraction and chemical composition within the earth within certain assumptions.

In 1977 a magnetotelluric field program was carried out in North and East Iceland in cooperation between the university of Munich, Germany, and the National Energy Authority, Iceland. The aim was to investigate vertical and lateral variations of the electrical resistivity. The measurements were made along two profiles: one 260 km long, east-west, 12 magnetotelluric stations, ranging from the Tertiary flood basalts in North Iceland, across the zone of active rifting and present volcanism, to the Tertiary flood basalts in the eastern part of the country; the other, 150 km long, northeast-southwest, more or less along the neovolcanic zone, with 7 magnetotelluric stations (see Fig. 1 for locations).

Mobile magnetotelluric equipment was used consisting of an electrograph, a fluxgate magnetometer and a tape recorder. Two horizontal components of both the magnetic and the electric field were recorded in the period range of 15 s to 1 h for one or two days at each site.

For more detailed information on the experiment and on the general geological situation the reader is referred to Beblo and Björnsson (1978). They presented the preliminary results of the magnetotelluric measurements on the east-west profile. They used one-dimensional model calculations for constructing a resistivity model of the lower crust and upper mantle.

The most significant result of this work was the existence of a low-resistivity layer (15 Ωm) at about 10–20 km depth. Beblo and Björnsson interpreted this layer as caused by partial melting at the base of the crust.

The present paper discusses the results from all 19 magnetotelluric stations, interpreted with one- and two-dimensional model calculations for the resistivity distribution. The computed resistivities are then compared to resistivities determined in the laboratory on different rock types at high temperatures.

The Magnetotelluric Results

The electrical resistivity of the earth can be determined by the magnetotelluric method, which is based on the observation of time-varying magnetic (**B**) and electric (**E**) fields at the earth's surface. The observed time functions $E(t)$ and $B(t)$ are Fourier-transformed into functions of frequency, from which the complex transfer function C_{ij} can be determined.

$$C_{ij}=\frac{1}{i\omega\mu_0}\cdot z_{ij}, \text{ with impedance } z_{ij}=\mu_0\frac{E_i}{B_j}, \quad \omega=\frac{2\pi}{T},$$

SI units, **B** in nT **E** in mV/km, T in s.

Preference Direction of the Electric Field

Important parameters obtained by the magnetotelluric method are the preference direction and the polarization of the induced electrical field. The polarization (axial ratio of polarization ellipse) is a measure of the surface inhomogeneity of the electrical resistivity distribution at the measuring site. The preference direction (direction of major axis of polarization ellipse) is a function of lateral variations of the electric resistivity in a more regional sense. In the case of a two-dimensional structure with low resistivity in higher-resistivity surroundings the preference direction is parallel to the strike inside the anomalous region and perpendicular to

0340-062X/80/0047/0184/$01.40

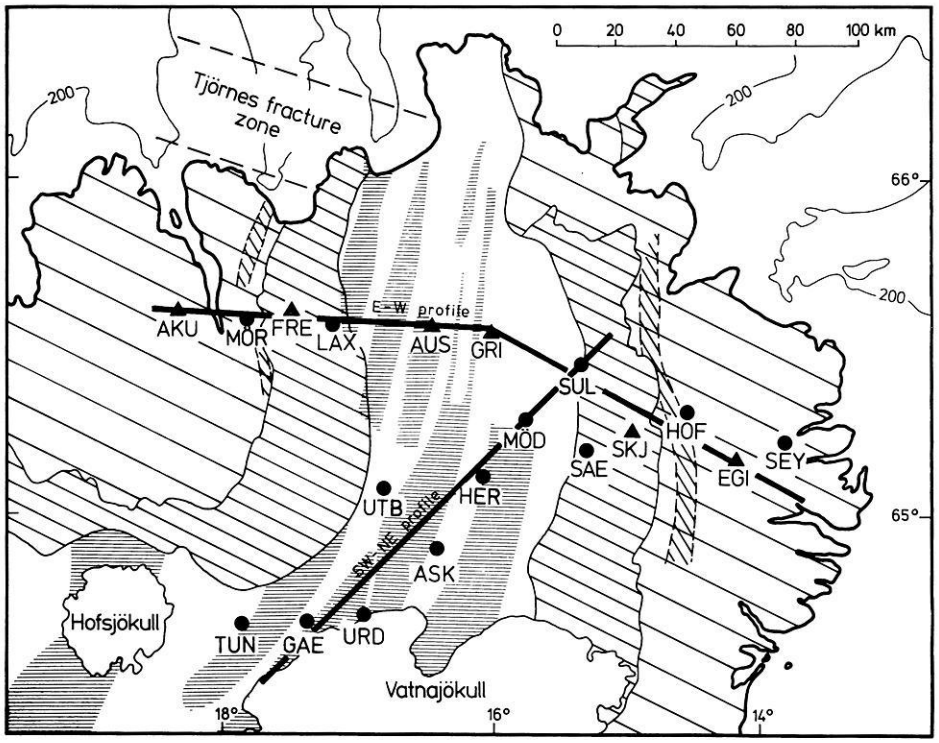

Fig. 1. Simplified geological map of northeast Iceland as redrawn from Saemundsson (1974), showing locations of magnetotelluric measuring stations. Lines are drawn along the two profiles discussed, east-west across the zone of rifting and volcanism, and southwest-northeast along it
Tertiary flood basalt older than 3 m.y.
Quaternary flood basalt 3–0.7 m.y.
Neovolcanic zone younger than 0.7 m.y.
Fissure swarm
Flexured zone
▲ MT-measuring site 15 s–12 h
● MT-measuring site 15 s–1 h

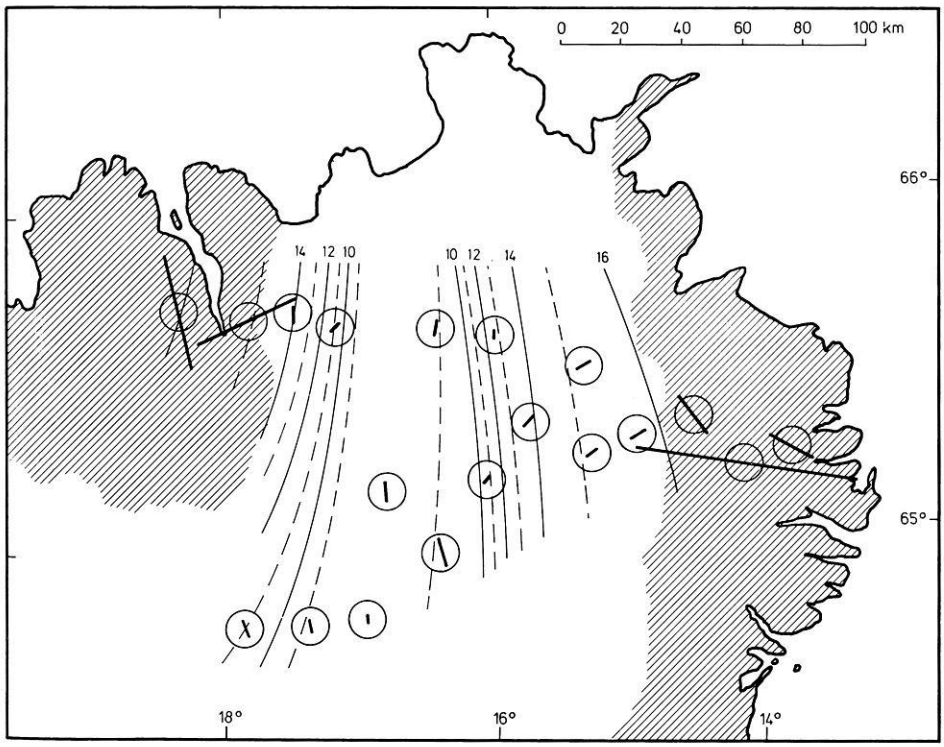

Fig. 2. Preference directions of the induced electrical field for the period range 15–300 s shown by lines in the circles. Depth contour lines of top of the low-resistivity layer; depths in km

the strike outside, an effect of the boundary conditions of the electrical field components at a lateral resistivity contrast.

Figure 2 shows the distribution of the preference direction of the electric field at all magnetotelluric stations for the period range 15 to 300 s. The length of the lines is proportional to the polarization; it should reduce to points for a laterally uniform distribution of resistivity. Within all the Quaternary flood basalt areas and the neovolcanic zone, the short lines indicate small horizontal variations of resistivity. Within the Tertiary flood basalt areas (hatched areas in Fig. 2) there exists a strong horizontal variation of resistivity. The orientation of the preference direction perpendicular to the regional strike outside the Quaternary and the neovolcanic zones and the orientation nearly parallel to the strike inside suggests to us, that within the Quaternary and the

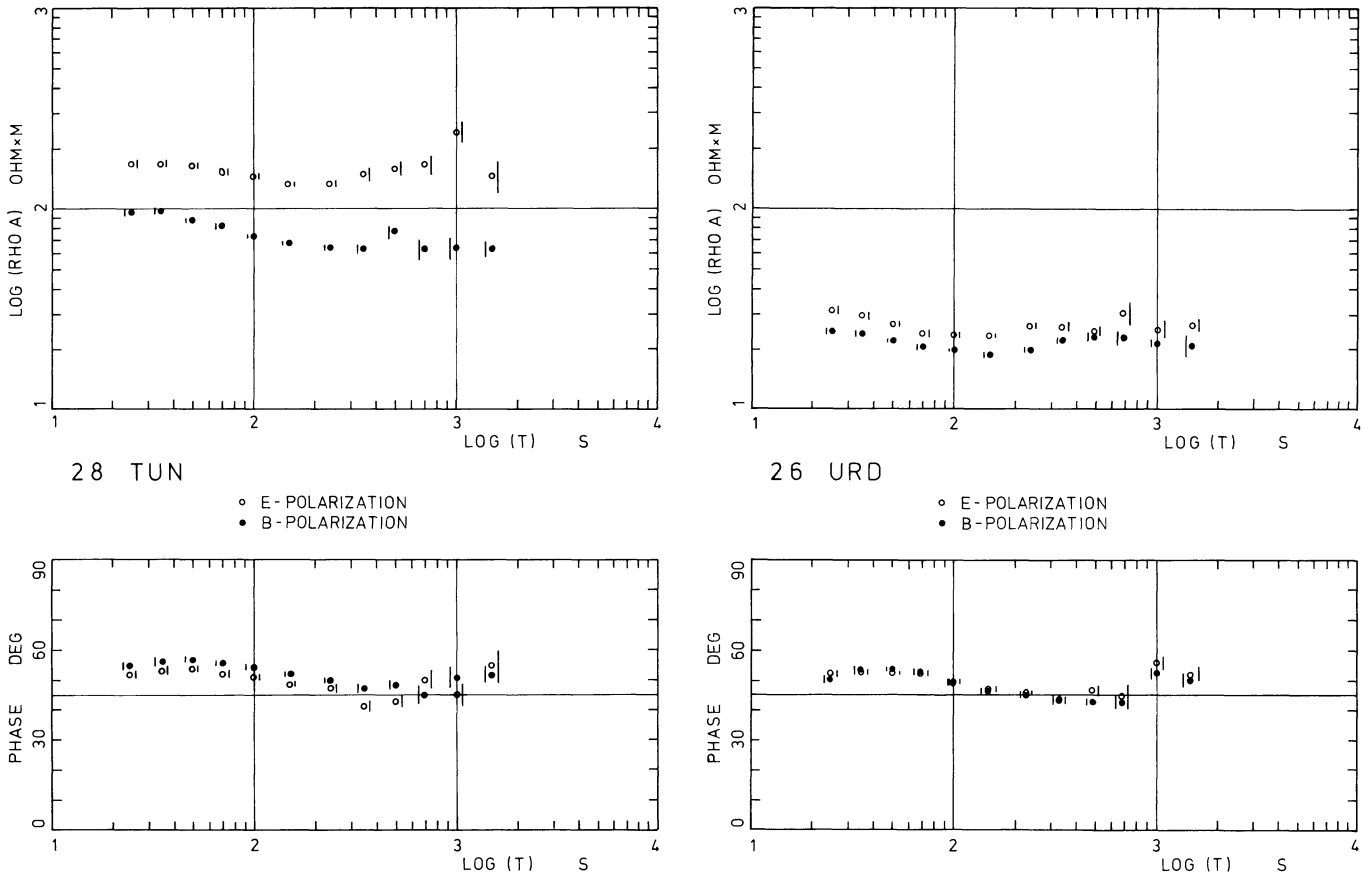

Fig. 3. Apparent resistivities and phase differences (points) and mean square deviations (lines) for the sites *URD* and *TUN*. *E*-and *B*-polarization are nearly identical for *URD*, which implies a one-dimensional resistivity distribution. The difference in *E*- and *B*-polarization at *TUN*, on the other hand, indicates a two- or even three-dimensional resistivity distribution or strong lateral variation in the surface resistivity

neovolcanic regions the surface resistivity is much lower than within the Tertiary basalt areas.

Apparent Resistivities and Phase Differences

Magnetotelluric measurements normally reveal three-dimensional resistivity structures. At the present stage of computer capacities it is not practicable, however, to interpret such structures quantitatively. On the other hand, several methods have been published (e.g., Haak, 1972) for the interpretation of magnetotelluric data in the case of one- or two-dimensional resistivity structures. For a two-dimensional resistivity distribution it is possible to orientate the coordinate system in such a manner, that one axis is parallel and the other perpendicular to the strike of the anomaly. Hence two independent systems of equations are obtained and therefrom two different values for the apparent resistivity ρ_a and phase φ are calculated. The first case means the component of the electric field parallel to the strike (*E*-polarization), the other case means the component perpendicular to the strike (*B*-polarization).

$$\rho_{a_{\parallel}} = \frac{\mu_0 T}{2\pi} |z_{\parallel}|^2, \quad \varphi_{\parallel} = \arg(z_{\parallel}) \quad E\text{-polarization}$$

$$\rho_{a_{\perp}} = \frac{\mu_0 T}{2\pi} |z_{\perp}|^2, \quad \varphi_{\perp} = -\arg(z_{\perp}) \quad B\text{-polarization}$$

ρ in Ωm, φ in degrees.

In the case of a one-dimensional resistivity distribution, both solutions for *E*- and *B*-polarization become identical.

As an example, Fig. 3 shows for the sites Tungnafellsjökull (TUN) and Urdarhals (URD), the calculated values and mean square deviations of the apparent resistivities and phase differences, separately for *E*- and *B*-polarization. The values for the *E*- and *B*-polarization at the site URD are more or less identical, indicating that the resistivity distribution is a function of depth only. At the site TUN polarization of the electrical field is observed, and hence the values for *E*- and *B*-polarization are different. This effect may be caused by a two-dimensional resistivity distribution, or may result from inhomogeneities of surface resistivities (Beblo, 1974). Extremely small deviations of apparent resistivities ρ_a (see Fig. 3) indicate no influences related to an inhomogeneous source field in the observed period range. The ocean effect cannot either be seen in ρ_a, the complete decrease of the ΔZ component of the magnetic field for very long periods (>6 h) (Haak et al., in preparation) supports this.

Model-Calculations

In interpreting magnetotelluric data usually the impedance tensor for model structures is computed and compared to the values obtained from the measurements. The simplest models are one-dimensional, i.e., the resistivity varies only with depth. One-dimensional model-calculations are acceptable, if horizontal variation

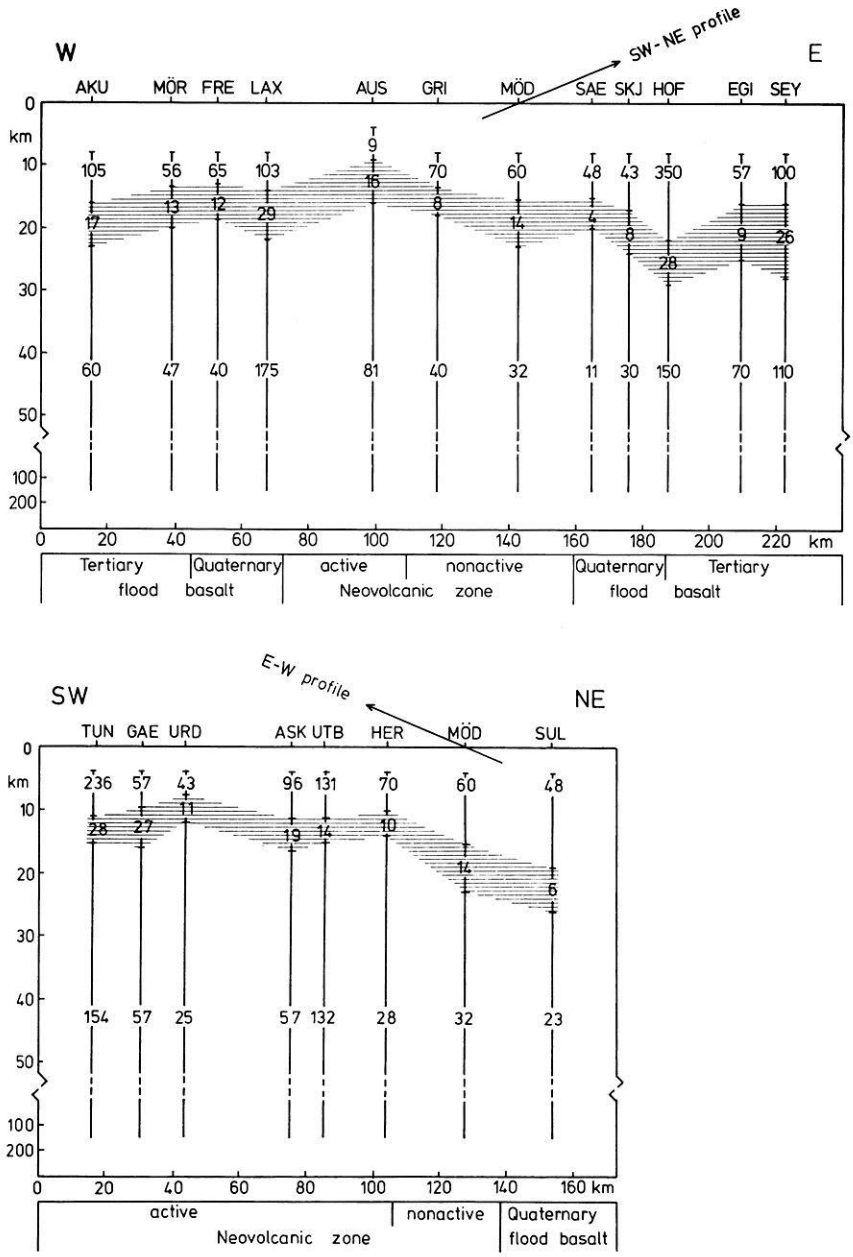

Fig. 4. One-dimensional models of resistivity distribution at all stations, calculated from apparent resistivities and phases of the E-polarization case. The hatched area shows a continuous low resistivity layer with a mean resistivity of 15 Ωm. The numbers indicate resistivities in Ωm, actually computed for each station. For location of sites and profiles see Fig. 1

of resistivity is only weak. From the preference direction (see Fig. 2) this is evident for the measuring sites within the neovolcanic and the Quarternary areas. In the Tertiary areas the preference direction indicates strong horizontal variations in resistivity and one-dimensional model-interpretation is problematic.

However, because of the continuity of the electrical field component parallel to a lateral resistivity contrast, the ρ_a-values of the *E*-polarization case are only weakly influenced by the horizontal near-surface resistivity variations but rather reflect mainly the resistivity variation with depth. Therefore we have used the values of the *E*-polarization for calculating one-dimensional models in the Tertiary areas.

Figure 4 shows the results of the model-calculations for one-dimensional resistivity variation with the depth. For calculating the models we used an inversion method given by Schmucker (1974). For all the stations on both profiles we got the same model type, with the best fit for three-layer models. Although the ρ_a-curves appear extremely flat, the minimum at 100 s and the deviations of the phase from 45° justify at least the use of three-layer models. Models consisting of more than three layers did not show significant improvement in the analyzed period range. Confidence levels computed from the data scatter show model parameter uncertainties less than 10%. Resistivity variations at the surface, which either tend to increase or decrease the resistivity values as a whole in the total period range observed, cause the resistivity values in each layer to vary from station to station but do not weaken the main result. This is stated below.

Beneath the investigated area exists a 5–10 km thick layer with a low resistivity of about 15 Ωm, which is imbedded in layers of higher resistivities. The depth to the low-resistivity layer increases with increasing distance from the spreading axis. Beneath the neovolcanic zone the depth to the well conducting layer is 10 km, but it is about 20 km beneath the Tertiary areas to the east and west. Figure 2 shows smoothed depth contour lines in

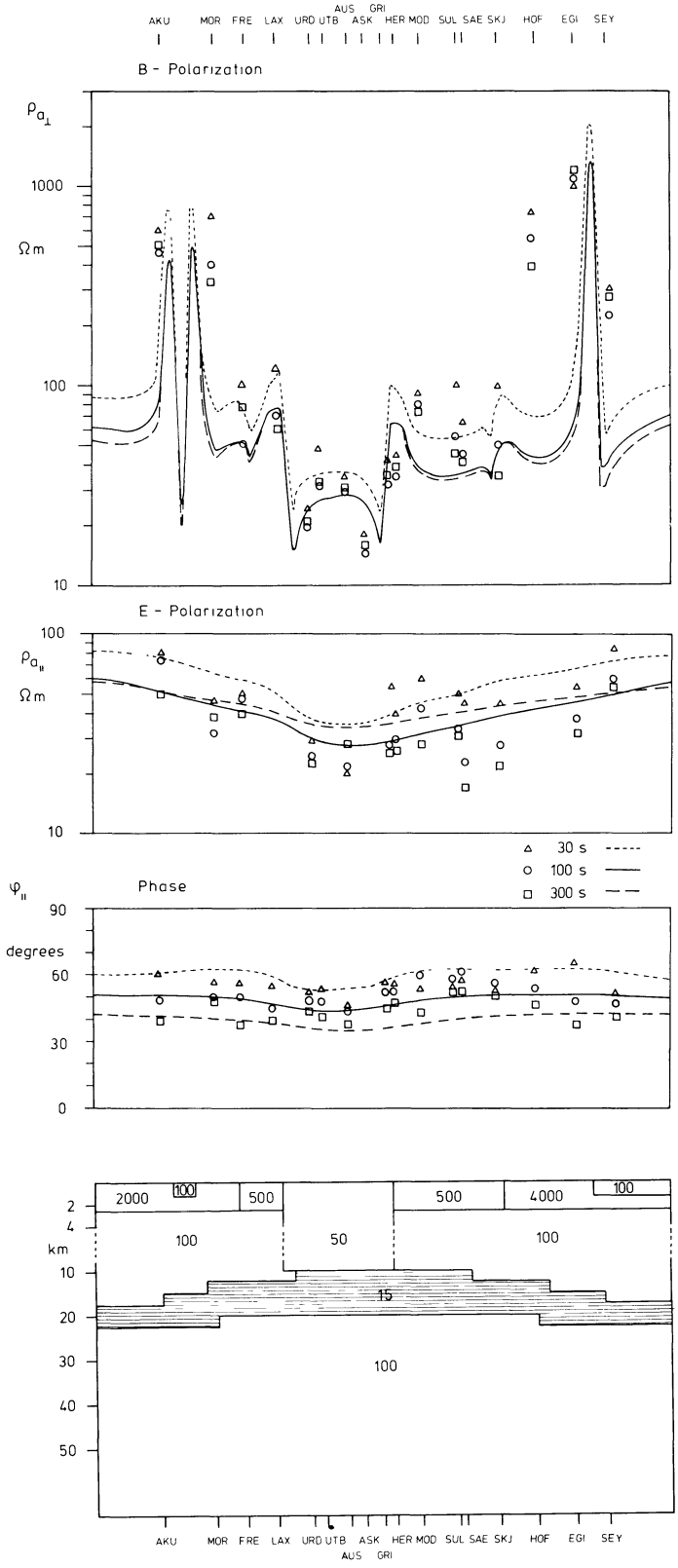

Fig. 5. Two-dimensional model of resistivity distribution beneath east-west profile and computed resistivities and phases for 30, 100, and 300 s. The numbers indicate assumed resistivities in Ωm

km of the top of the low-resistivity layer. The resistivity of the substratum is about 70 Ωm.

Figure 5 shows the results of the model-calculations of a two-dimensional resistivity distribution. The apparent resistivities are shown for both, *B*- and *E*-polarization, the phases are shown for the *E*-polarization case only. For calculating the model curves we used a computer-program by Haak (1978) based on a finite difference method.

The resistivity distribution near the surface has a dominating influence on the *B*-polarization. Hence we formed a near-surface model for the uppermost 2.5 km, based on some resistivity (dipole-dipole) measurements along the profile (Björnsson, 1976). These measurements show high resistivity values for the Tertiary areas (2,000 Ωm in the west, 4,000 Ωm in the east), but much lower resistivities (less than 500 Ωm) within the Quaternary and neovolcanic zones. This near-surface model fits rather well to the *B*-polarization case for all the stations within the Quaternary and the neovolcanic zones. For the Tertiary areas it was not possible to explain the measured values of the *B*-polarization by variation in rock resistivity alone; the computed resistivities are an order of magnitude lower than the observed ones. Therefore we attempted to take into account the influence of the well conducting sea-water in the fjords on both sides of our profile. For the shallow sea-water a resistivity of 100 Ωm has been used according to the model-dimensions. The calculations now show a rather good agreement with the measurements for all the stations over the whole period range. But there remains a deviation which cannot be explained by two-dimensional models and must be caused by three-dimensional local near-surface anomalies (Kemmerle, 1977). This effect can be clearly seen at the site of HOF with calculated $\rho_{a_\perp}$-values an order of magnitude lower than the observed ones. The measuring site of HOF is situated directly in a highly flexured zone near the border of the Tertiary and Quaternary zones (see Fig. 1) which might cause such an effect. A similar, but not as significant deviation can be observed at some other sites, probably caused by near-surface resistivity anomalies as well as by the influence of local topography.

The resistivity distribution at greater depth dominates the *E*-polarization case. Initial guess for two-dimensional model-calculations in greater depth was the result of the one-dimensional model-calculations. These calculations showed a resistivity of about 70 Ωm in the substratum. This resistivity-value fits the *E*-polarization case well, but does not show the weak increase of $\rho_{a_\perp}$ with increasing periods in the *B*-polarization case. A resistivity of 100 Ωm in the substratum gives the observed $\rho_{a_\perp}$-values over the whole period range.

The deviations of the observed $\rho_{a_\parallel}$-values for the *E*-polarization case between adjacent sites are probably produced by small local anomalies of the electrical resistivity near the surface. Such small local anomalies would change the values for the apparent resistivities while the phase difference is obviously not influenced. This can clearly be seen in Fig. 5.

The result of the two-dimensional model-calculations was the following. Below a thin surface layer (2.5 km) the electrical resistivity is 100 Ωm, except within the active part of the neovolcanic zone where the resistivity is 50 Ωm. The layer below has a resistivity of 15 Ωm. The depth to this good conductor increases with distance from the rift axis from 10 km within the neovolcanic zone to about 17 km below the Tertiary basalts. The thickness of the good conductor is 5 km on the eastern and the western side of the profile and about 10 km beneath the Quaternary and the neovolcanic areas. Below the good conductor there is a deep layer with an upper limit of resistivity of 100 Ωm, reaching down

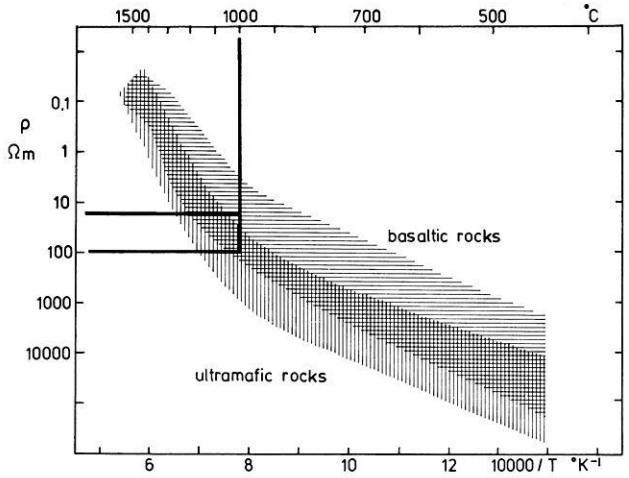

Fig. 6. The electrical resistivity of various basalts and ultramafic rocks as a function of temperature. Redrawn from Haak (1979)

to at least 100 km depth. No exact information can be obtained on the lower boundary of this layer at the present stage, but the deviations of the phase from 45° indicate in the longest periods observed (see Fig. 3) a second good conductor at perhaps 200–300 km depth.

Electrical Resistivity-Temperature

In order to infer the temperature in the lower crust and upper mantle from the resistivity, one must know the dependence of resistivity on temperature for the particular materials of the crust and mantle under the prevailing conditions. In the last few years, a great number of laboratory experiments have been made to investigate the resistivity of different rocks at high temperatures and pressures (for a review see, e.g., Duba, 1976). The most relevant measurements were made on basalts, which are probably the major component of the Icelandic crust. There also exist laboratory measurements on various ultramafic rocks as olivine, which are believed to be the most important component of the upper mantle. Another way to estimate upper mantle resistivity and temperature (done, e.g., by Waff, 1974) is to make theoretical calculations for artificial model-materials, consisting of two different components.

Haak (1979) has given an excellent review of both laboratory experiments and theoretical calculations of electrical resistivity of upper-mantle material. He has collected most of the existing data on basalts and ultramafic rocks. The data scatter considerably and seem to depend strongly on laboratory conditions like oxygen and water fugacities and the measuring technique. Figure 6 is redrawn from Haak (1979) and shows the mean electrical resistivity as a function of temperature for both types of material. There is an overlap in the resistivity distribution of basalts and ultramafic rocks, but it can, nevertheless, be seen that the resistivity of basalt is lower than that of ultramafic rocks at a given temperature by as much as an order of magnitude. For example, the electrical resistivity at 1,000° C is about 15 Ωm for basalts and about 100 Ωm for ultramafic rocks at the same temperature. Figure 6 also shows a significant change in the slopes of the resistivity-temperature curves at about 1,000° C toward lower resistivities above that temperature. This may be caused by the beginning of partial melting.

Discussion

The main result of our investigation is a model of the crust and mantle beneath Iceland, which shows a good conductor at shallow depth. The depth of this layer increases with distance from the rift axis. Since electrical resistivity gives an indication of temperature for a given material, we can discuss the temperatures prevailing in the crust and upper mantle on the basis of the magnetotelluric data; especially the existence or absence of partial melt is in question.

The chemical composition of the lower crust and mantle is not known exactly. But according to most workers it is generally assumed that the crust beneath Iceland consists of basalt and the mantle consists of ultramafic rocks (peridotite). With this assumption we have estimated the temperature by comparing the electrical resistivity inferred from magnetotellurics to the temperature-resistivity curves of Fig. 6.

If the good conductor with a resistivity of 15 Ωm consists of basalt, its temperature should be in the range of 850°–1,200° C with a most likely value near 1,000° C. At this temperature melting begins. Very little can be said about the volume fraction of the melt, but following Shankland and Waff (1977) it could be as much as 10%.

The deeper layer, with a resistivity of about 70–100 Ωm, is believed to be the uppermost mantle, consisting of ultramafic rocks. The corresponding temperature range, according to Fig. 6, is 950°–1,200° C, with a most likely value of about 1,050° C. Some amount of partial basalt melt may be present in a solid olivine matrix. This is supported by seismic observations which indicate anomalously low *P*-wave velocities beneath Iceland (e.g., Tryggvason; 1961; Francis, 1969).

Assuming the 1,000° or 1,100° C isotherm to lie within the good conductor we calculated the mean temperature gradient in the crust (Beblo and Björnsson, 1978). The calculated values showed good agreement with direct temperature gradient measurements in shallow drillholes. The results from the magnetotelluric observations on the SW-NE profile support the earlier interpretation, i.e., a temperature gradient of around 100° C/km in the active zone of rifting and 40°–60° C/km in the Tertiary flood basalt zones to the east and west. No information can be obtained on the temperature gradient in the upper mantle, but the nearly constant resistivity down to 100 km depth indicates a very low temperature gradient for the mantle. This has already been shown by Hermance and Grillot (1974), who found 1° C/km for the temperature gradient within the mantle of SW-Iceland.

It is plausible to interpret the low-resistivity layer to consist of partially molten basalt. This is probably caused by upward movement of lighter basaltic melt through the heavier olivine matrix. The movement causes separation of ultramafic and basaltic material, from which the oceanic crust is generated. A zone of enrichment of partial melt within the oceanic lithosphere has been predicted by Bottinga and Allègre (1976) by theoretical model calculations. They used their result to explain the existence of low-velocity zones near oceanic ridges. Their calculated 1,000° or 1,100° C isotherms are at exactly the depth as our low resistivity layer is. For this depth they predicted a thin zone of enrichment of basaltic composition underlain by ultramafic material. In a recent seismic investigation of Iceland (RRISP-Working Group,

1979) it was found, that the seismic *P*-wave velocity only slightly increases below 10–15 km depth, velocity reversals were not excluded. Also significantly high values of the *P*- to *S*-wave velocity ratio were observed for this depth. Both observations suggest a partially molten state of the mantle beneath Iceland, in good agreement with the magnetotelluric results.

Acknowledgements. The authors are very grateful to Professor Dr. G. Angenheister, Dr. A. Berktold, Dr. V Haak, and Dr. K. Kemmerle for encouragement, support and personal engagement in interpretation and discussion.

References

Beblo, M. Die elektrische Leitfähigkeit unter den Ostalpen, abgeleitet aus magnetotellurischen Messungen längs eines Profiles vom Alpennordrand bis zu den Hohen Tauern. Universität München: Diss. Fak. Geowiss. 1974

Beblo, M., Björnsson, A. Magnetotelluric investigation of the lower crust and upper mantle beneath Iceland. J. Geophys. **45**, 1–16, 1978

Björnsson, A. Electrical resistivity of layer 3 in the Icelandic crust. In: V Greinar ed. pp. 7–23. Reykjavik Societas Scientiarum Islandica 1976

Bottinga, Y., Allègre, C.: Geophysical, petrological and geochemical models of the oceanic lithosphere. Tectonophysics **32**, 9–59, 1976

Duba, A. Are laboratory electrical conductivity data relevant to the Earth? Acta Geodaet. Geophys. Montanist. Acad. Sci. Hung. **11**, 485–495, 1976

Francis, T.J.G. Upper mantle structure along the axis of the Mid-Atlantic Ridge near Iceland. Geophys. J. R. Astron. Soc. **17**, 507–520, 1969

Haak, V Magnetotelluric method The determination of transfer functions in areas with lateral variation of electrical conductivity. Z. Geophys. **38**, 85–102, 1972

Haak, V Interpretations-Verfahren für die Magnetotellurik unter besonderer Berücksichtigung lateral variierender elektrischer Leitfähigkeit im Erdinnern und eines räumlich inhomogenen induzierenden Magnetfeldes. München: Bayerische Adademie der Wissenschaften 1978

Haak, V . Relations between electrical conductivity and petrological parameters of the crust and upper mantle. J. Geomagn. Geoelectr. in press, 1979

Hermance, J.F., Grillot, L.R. Constraints on temperature beneath Iceland from magnetotelluric data. Phys. Earth Planet. Inter **8**, 1–12, 1974

Kemmerle, K. Magnetotellurik am Alpen-Nordrand mit Diskussion der lokalen Effekte und Darstellung einer Einzeleffekt-Auswertung. Universität München: Diss. Fak. Geowiss. 1977

RRISP-Working Group: First results from the Reykjanes Ridge Iceland Seismic Project 1977. Nature **279**, 56–60, 1979

Saemundsson, K. Evolution of the axial rifting zone in northern Iceland and the Tjörnes fracture zone. Bull. Geol. Soc. Am. **85**, 495–504, 1974

Schmucker, U.: Erdmagnetische Tiefensondierung mit langperiodischen Variationen. In: Protokoll DFG-Kolloquium Erdmagn. Tiefensond., A. Berktold, ed.: pp. 313–342. Grafrath-München: 1974

Shankland, T.J., Waff, H.S. Partial melting and electrical conductivity anomalies in the upper mantle. J. Geophys. Res. **82**, 5409–5417, 1977

Tryggvason, E. Arrival times of P-waves and upper mantle structure. Bull. Seismol. Soc. Am. **54**, 727–736, 1961

Waff, H.S.: Theoretical considerations of electrical conductivity in partially molten mantle and implications for geothermometry. J. Geophys. Res. **79**, 4003–4010, 1974

Received April 10, 1979; Revised Version July 6, 1979

J. Geophys. 47, 191–201, 1980

Journal of Geophysics

A Seismic Study of the Rift Zone in Northern Iceland

S.M. Zverev[1], I.V. Litvinenko[2], G. Pálmason[3], G.A. Yaroshevskaya[1], N.N. Osokin[2], M.A. Akhmetjev[4]

[1] Institute of Physics of the Earth, USSR Academy of Sciences, B. Gruzinskaya 10, 123810 Moscow, USSR
[2] Mining Institute, 21 Line 2, 199026 Leningrad, USSR
[3] Orkustofnun, Grensásvegi 9, 108 Reykjavik, Iceland
[4] Geological Institute, USSR Academy of Sciences, Pyzhevsky St., 109017 Moscow, USSR

Abstract. The complex geological-geophysical expedition of the USSR Academy of Sciences jointly with the National Energy Authority (Orkustofnun) of Iceland conducted in 1977 a detailed seismic investigation of the flood basalt and rift zones in northern Iceland, similar to studies in southwestern Iceland. Continuous seismic profiling with 4–6 shot points was carried out across a total length of 90 km. In the flood basalt zone shallow refracting horizons were observed with $V_p = 4.3$–4.5 km/s and tilted toward the rift zone. They closely correspond to dense sheets of flood basalts mapped geologically. Refracting and reflecting horizons at 2 to 12 or 15 km depth are tilted more gently in the same direction. A slight depression filled with neovolcanic formations with $V_p < 3$ km/s exists near the surface in the rift zone. Reflectors with steep tilt can be traced to depths of 15 km. The deepest part of the depression is west of Mývatn in the region of current volcanism and rifting. A seismically homogeneous body without reflectors was detected under this region at 10–15 km depth. On the whole, the structure of the rift zone in northern Iceland is similar to, but more complex than, that of southwestern Iceland.

Key words: Iceland – Active rift zone – Neovolcanic zone – Crustal structure – Seismic profiling.

Introduction

The complex geological-geophysical expedition of the USSR Academy of Sciences jointly with the National Energy Authority of Iceland conducted in 1976–1978 detailed seismic studies in various regions of Iceland; they were aimed at the problems of the origin and development of Iceland. In 1976 and 1977 the structural relationship of the modern rift zone with the adjacent flood basalts was studied. The inner structure of the flood basalts was studied in 1978. The results of the investigation of southwestern Iceland were published by Zverev et al. (1979; 1980). The present paper is the first publication of results obtained in northern Iceland.

Location of Profile and Method of Observation

The investigations were conducted along a profile of about 90 km total length, using the road Akureyri-Mývatn-Grimstadir. The profile starts at Eyjafjördur in the west and runs eastward crossing the river Fnjóská and passing the lakes Ljósavatn, Másvatn, and Mývatn, and ends in the neovolcanic zone at the river Jökulsá á Fjöllum (Fig. 1). The profile crosses the main geological structures of northern Iceland: the flank of the Akureyri anticline, consi-

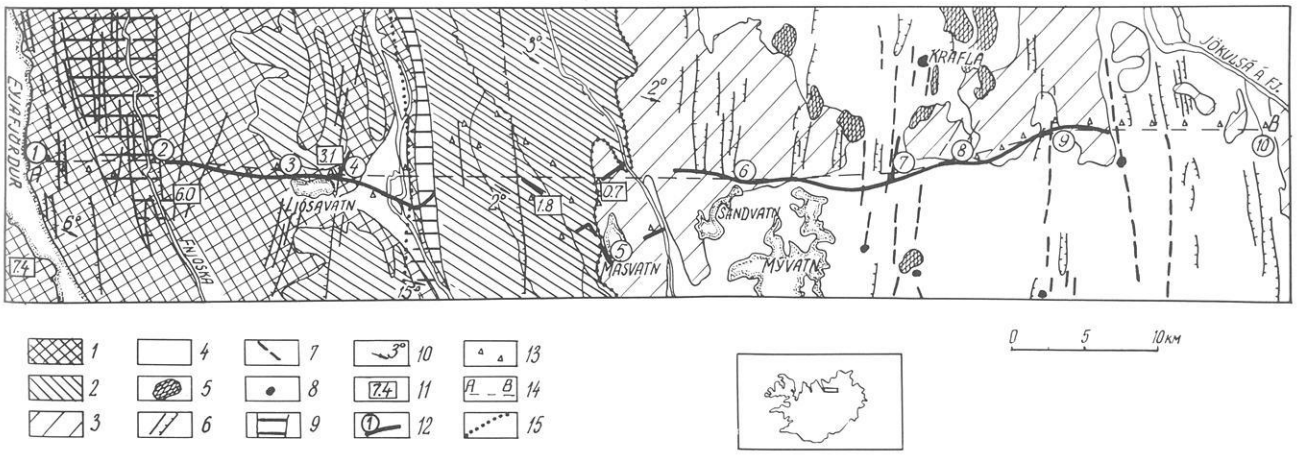

Fig. 1. Schematic geological map of the region under investigation. 1–4: volcanic formations of different ages; 1: Late Miocene-Pliocene (9 to 3 Ma); 2: Late Pliocene-Eopleistocene (3 to 0.7 Ma); 3: Pleistocene (<0.7 Ma); 4: Holocene; 5: dacite and rhyolite; 6: fissures; 7: fissures with Holocene volcanic activity; 8: main Late-Pleistocene and Holocene volcanic vents; 9: flexures; 10: direction and angle of tilt; 11: absolute age of volcanics in Ma; 12: seismic profile with numbers of shot points; 13: positions of automatic stations; 14: geological profile; 15: stratigraphic boundary

0340-062X/80/0047/0191/S02.20

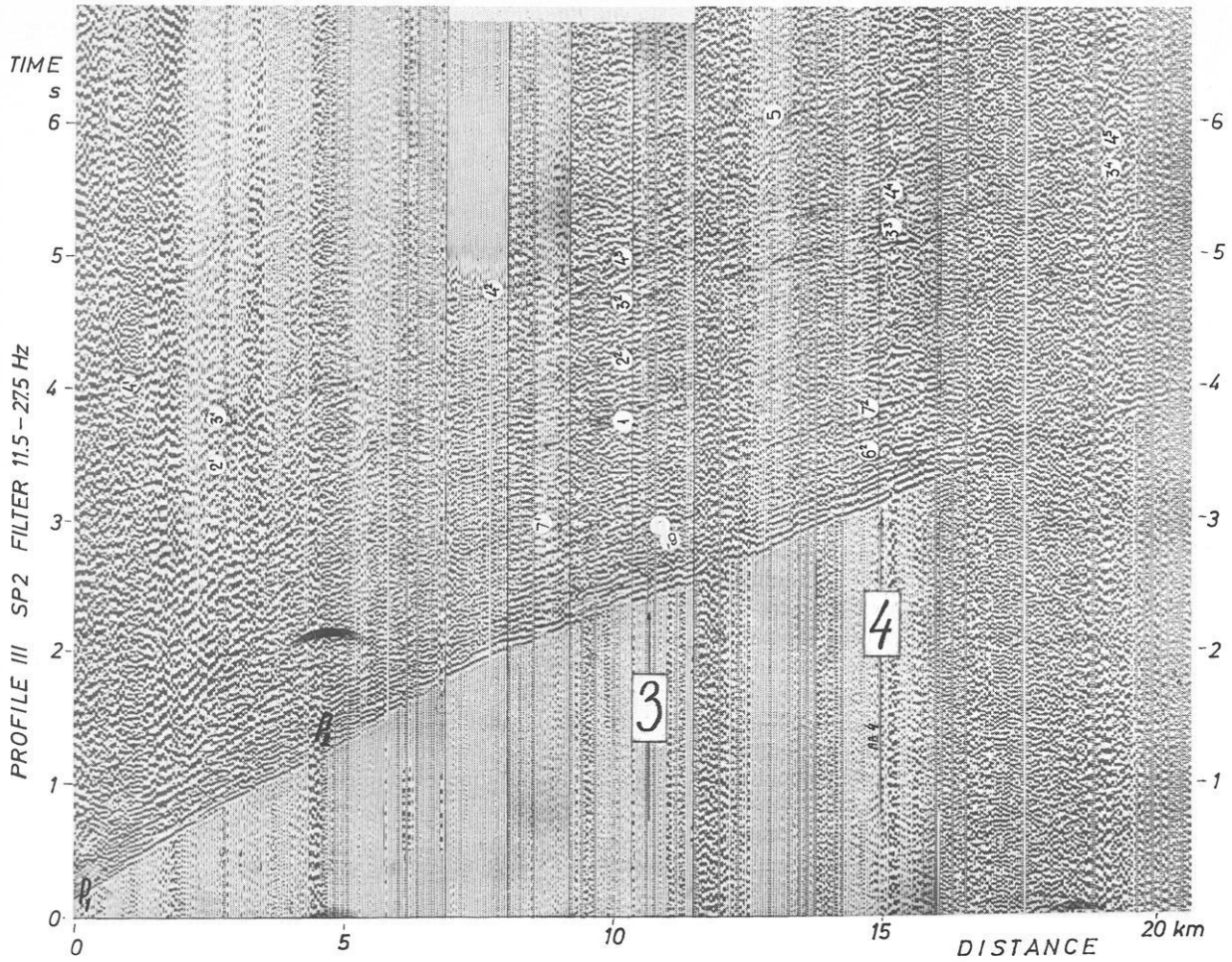

Fig. 2. The record section for SP2; frequency band 11.5–27.5 Hz; big numbers mark shot points, small numbers mark groups of reflected waves

sting of the flood basalt series, 8 or 9 to 3.1 Ma old (Pálmason and Saemundsson, 1974); an outer part of the neovolcanic zone with volcanic ages from 3.1 to 0.7 Ma; and the inner part of the neovolcanic zone with ages less than 0.7 Ma.

The method of observation was largely analogous to the one applied in southwestern Iceland in 1976 (Litvinenko, 1971; Zverev et al., 1979, 1980). On most of the profile continuous profiling was conducted with a multi-channel seismic system, except near Mývatn and Sandvatn where the road strongly deviates from the general profile direction. Here separate soundings were carried out with 2.3 km length each. A small gap in the observations east of Mývatn was caused by high background noise. Different from the work in southwestern Iceland, automatic three-component stations were used in addition to the multi-channel system, to fill the gaps of the continuous profiling and to extend the profile to the east and west (Fig. 1). This allowed us to construct piecewise-continuous travel-time curves for the first arrivals all along the profile.

Two 24-channel seismic refraction recording systems, SMOV-24, were used. The analogue magnetic tape records have a frequency band of 5 to 200 Hz and a dynamic range of 46 db. The geophones, SV-205, have a natural frequency of 5 Hz. Five geophones with a spacing of 50 m along the profile were connected to each channel; each group of geophones is 50 m from the next one; the length of the whole array is 2.3 km.

The automatic stations perform continuous magnetic tape recording in the frequency band of 2 to 30 Hz with a dynamic range of 46 db. Each station contains three-component geophones, SMN-KV, with a natural frequency of 0.5 Hz. The records of both types of instruments were played back on paper with the same band-pass filter setting. The multi-channel records were replayed with a variable-width script on the analogue system 'Ray'.

The shots were fired in a fjord (SP1), in rivers (SP2, 4, 7, 8, 10), in lakes (SP3, 5, 6), and in cavities of lava flows (SP9). The charges varied from several kilograms, when recording was near the shot points, to 120 kg and more, when recording was 40 to 60 km away. Charge sizes were chosen according to depth of water, the placing conditions, and the proximity to populated areas. The conditions at the shot influence the frequency content of the seismic waves (Burkhard and Vees, 1975); lower frequencies were activated by shots in shallow water and in lava cavities, higher frequencies by shots in deeper water. These peculiarities required careful adaptation of the frequency band during playback.

Characteristics of the Seismic Wave Field

The wave field recorded on the northern profile is similar to the one observed in Southwest Iceland (Zverev et al., 1980) in terms

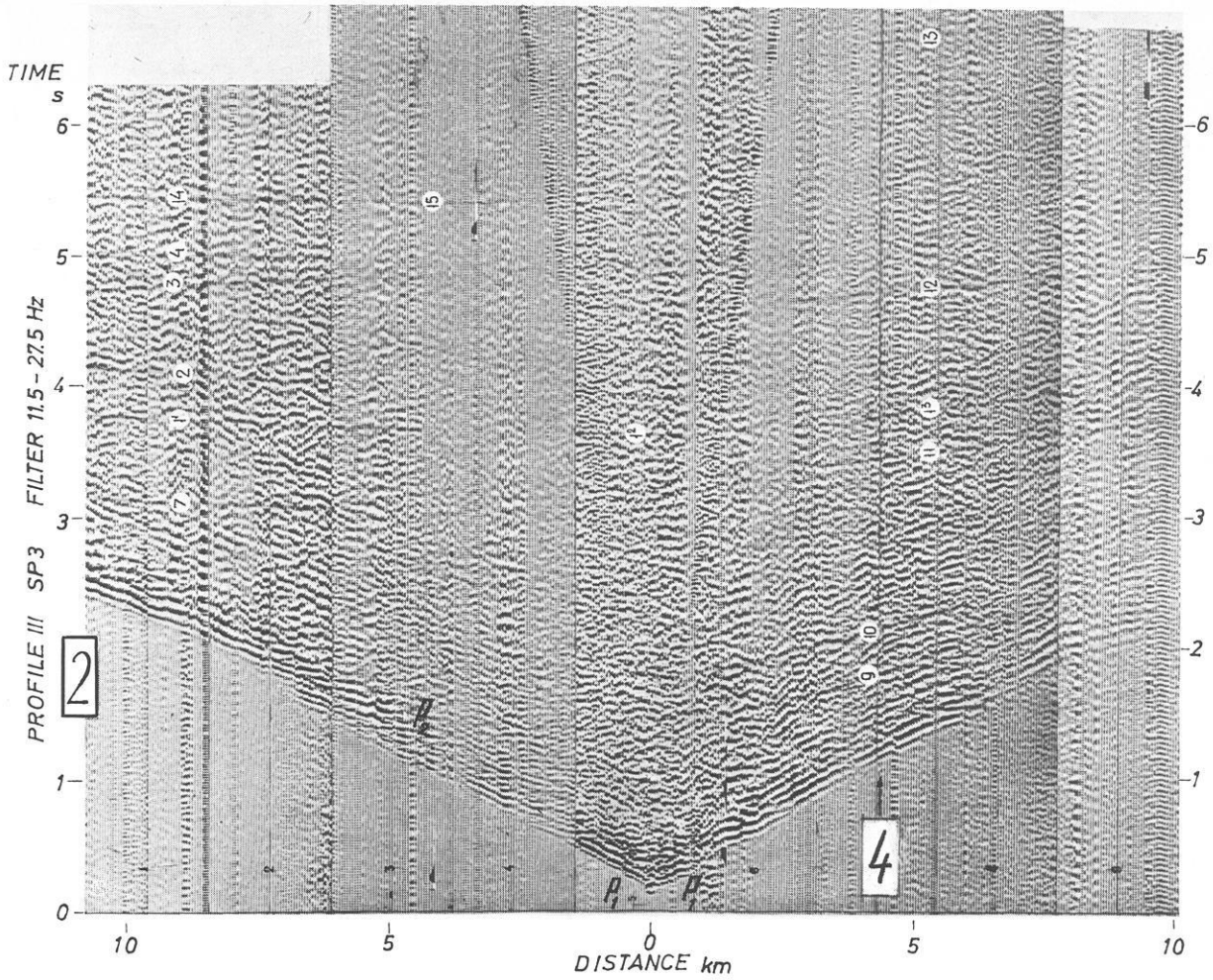

Fig. 3. Record section for SP3; for explanation see Fig. 2

of first-arrival travel-times, range of apparent velocities, characteristic wave forms, etc. Differences in the travel-time curves along the profiles involve more detail in the neovolcanic zone than in the flood basalt region, which might have resulted in data differences. It proved very advantageous that the transition zone could be filled with automatic stations and with isolated multi-channel soundings, because it revealed the nature of the cross-section in this zone.

The most important general features of the wave field are the following (Figs. 2–5):

1. A clear difference of the wave fields in the flood-basalt zone and in the neovolcanic zone both in range of velocities and in travel-times of first arrivals; asymmetry of refracted and reflected wave fields in the flood-basalt region, and symmetry in the neovolcanic zone.

2. In both zones the waves are connected with high-velocity sheets in the upper part of the lava series.

3. Absence of prominent reflections.

4. Considerable disturbances of the wave field by correlatable arrivals with high and even negative apparent velocities of uncertain origin, probably from near-surface faults.

It will be convenient to give a detailed description of the wave field separately for each wave type and each tectonic region.

Characteristics of Refracted Wave Fields

In the flood-basalt region one can distinguish several groups of waves according to their kinematic and dynamic properties (Table 1). Low-velocity waves (1.6–1.8 km/s) are observed near shot points on low-velocity material; its thickness is 30–100 m. A monotonous increase of the apparent velocities with distance is rather typical for the travel-time branches of the P_1 group mostly in the easterly direction (Figs. 2 and 6). These branches, more than 2–3 km long, have closely similar apparent velocities on overlap and attenuate at approximately the same locations. They probably represent waves propagating in high-velocity layers. No parallelism is observed at overlapping travel-time curves in the opposite direction. Waves of this group from various shot points have nearly the same travel-times. The minimum velocities near the shot points are 3.7–3.8 km/s. We interpret these observations to indicate that the flood basalt series is a gradient zone including high-velocity layers.

The change from group P_1 to P_2 in the travel-time diagram is rather clear (see e.g. SP2, Fig. 2). Outside the intersection region, these groups can be traced to the latest arrivals, but in short intervals only (1–2 km) because of disturbance from more intensive waves. The P_2 group corresponds to a rather abrupt boundary.

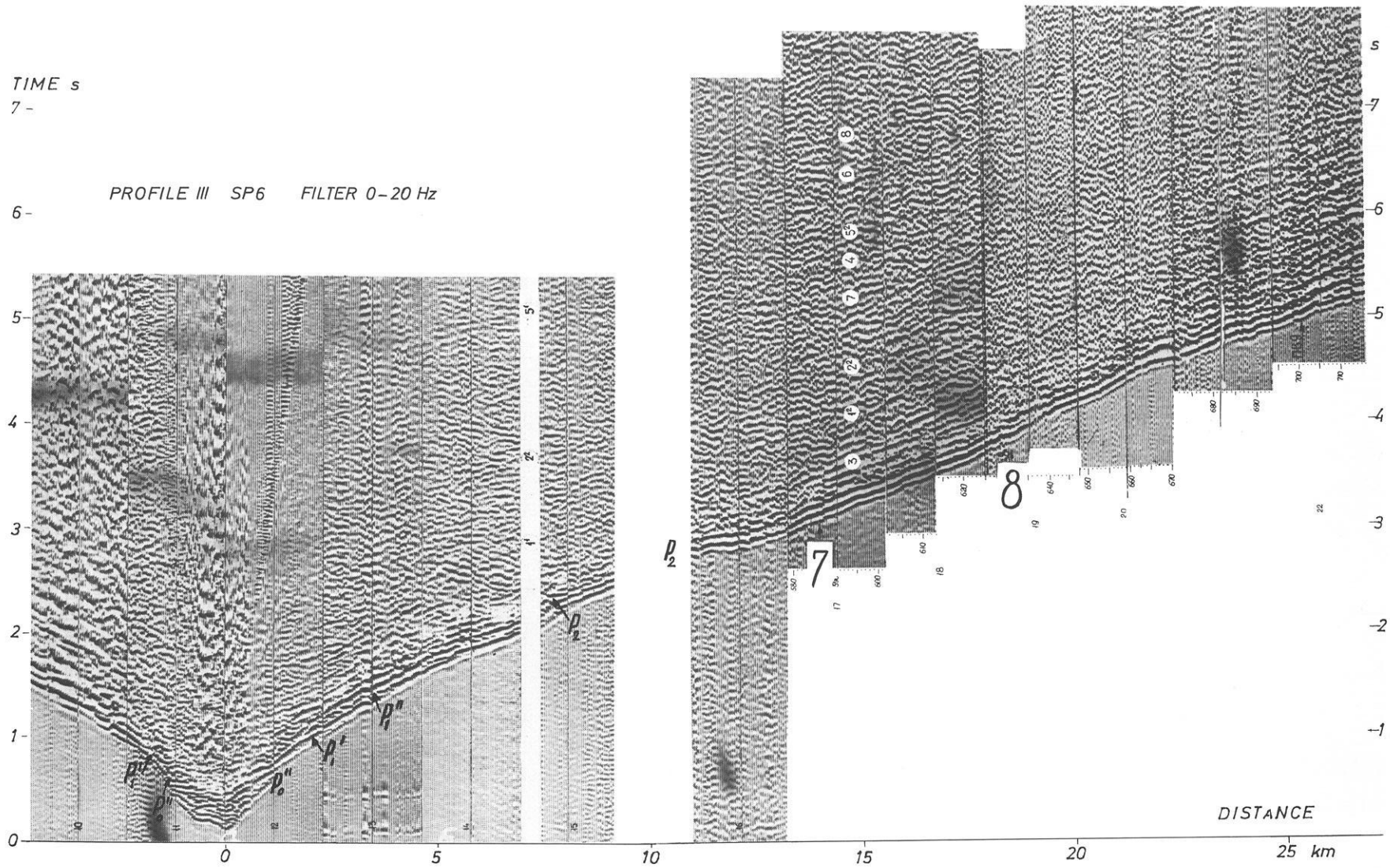

Fig. 4. Record section for SP6; frequency band: 0–20 Hz; for explanation see Fig. 2

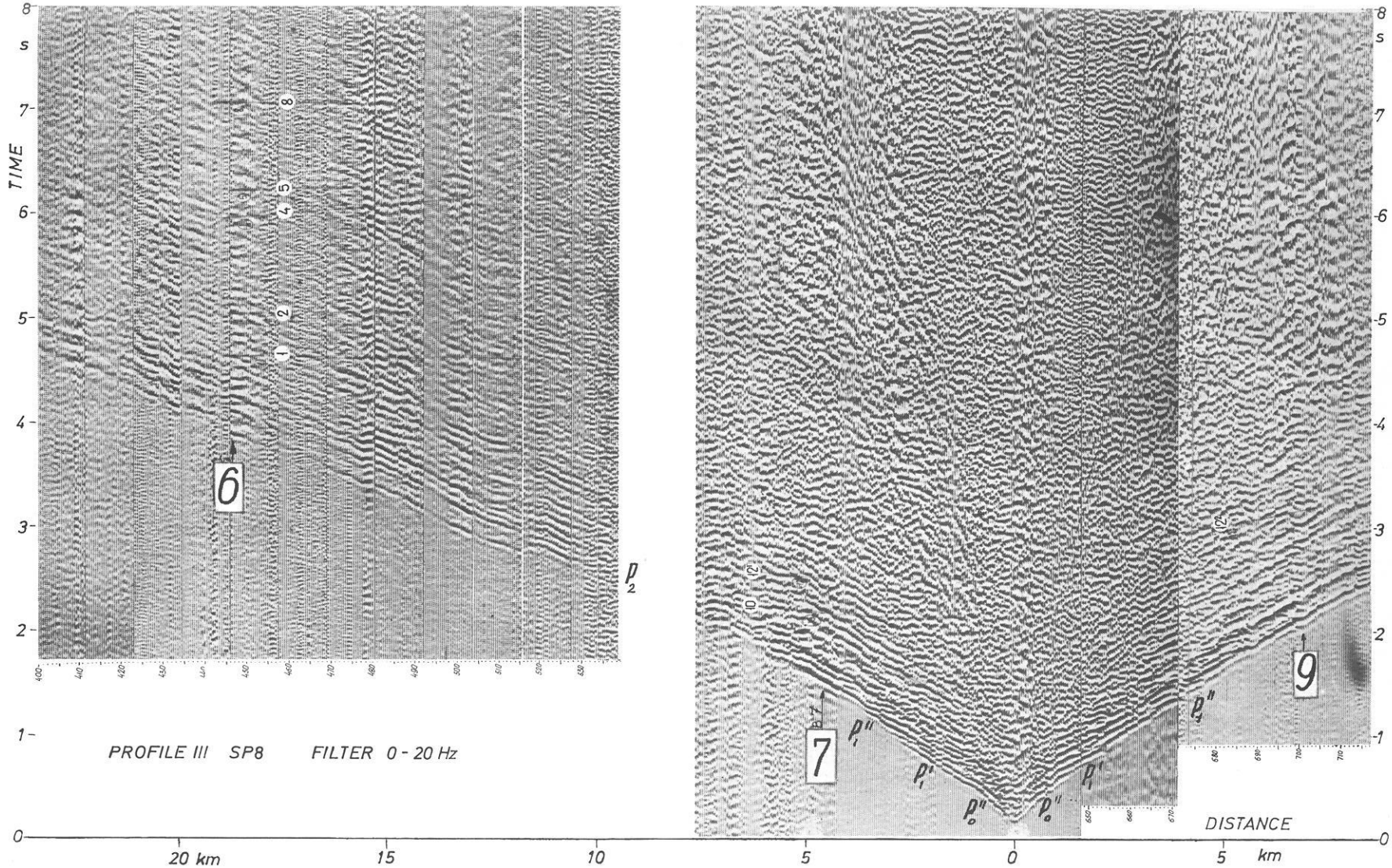

Fig. 5. Record section for SP8; frequency band: 0–20 Hz; for explanation see Fig. 2

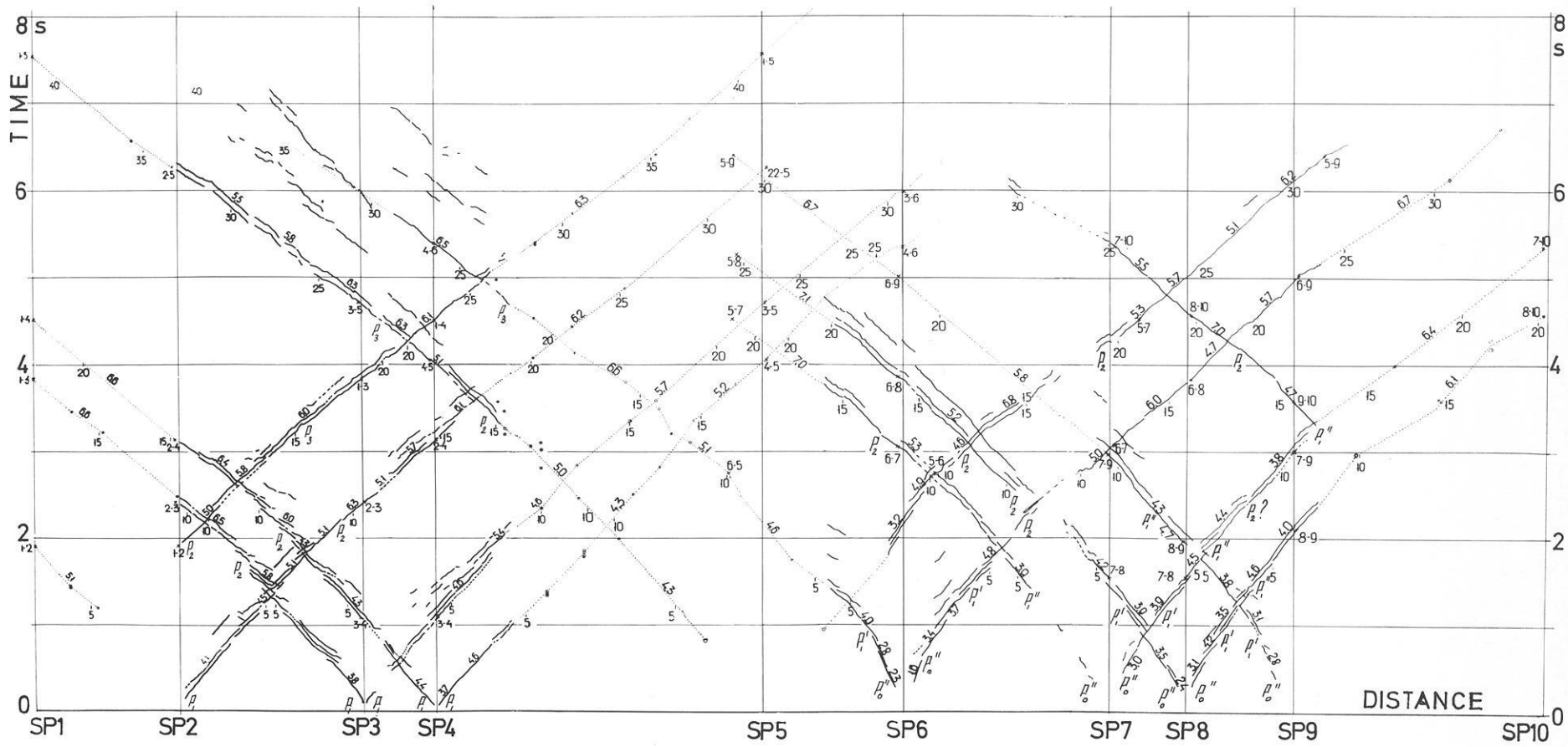

Fig. 6. Travel-time curves of refracted waves. The apparent velocities in km/s are marked at each branch

Table 1. Kinematic and dynamic properties of distinct wave groups

Index of group	V^* (km/s) (average)	Intervals of tracing of the first arrivals (km)	V (km/s) along the boundary	$\bar{V}$ (km/s) till the boundary	Comments
P_1	4.0–4.5	From 0 to 8–9	4.3–4.5	3.7–4	Till 2.5 km 4.0 km/s predominates, below: 4.5–4.7 km/s
P_2	5.5–6.0	To 15–16	5.6–5.7	4.4	
P_3	6.0–7.0	To 35	6.3–6.4	4.8	

Table 2

P_0''	2.8–3.5	From 0.5–1 to 1.5–2.5	3.2	1.9	Near SP $V=1.6$–2.0 km/s
P_1'	3.9–4.0	To 4	4.0	2.3	
P_1''	4.2–4.8	To 8–10	4.5	3.2	
P_2	5.0–7.0	To 30	5.6–5.7	3.7	

The P_2 group is the first arrival at distances from 8 or 10 to 15 km, while looking eastward the corresponding boundary is indicated to dip down; the increase in travel-times is remarkable. The travel-time curves in the only overlapping region (SP3–4 to the left, Fig. 2) demonstrate the existence of a slight velocity gradient in the layer. In contrast to Southwest Iceland, the P_2 group need not be divided into two sub-groups. It is not clear whether this reflects peculiarities of structure or differences in observation.

The change from group P_2 to P_3 is less distinct. P_3 is not clearly curved at greater distance, but it is possible to find a region of interference and a change in sign of the first arrivals. To the east the travel-times are greater than to the west for both groups. The waves are little attenuated and are supposed to be connected with a sharp velocity increase or a gradient zone with small steps.

In the neovolcanic zone the wave field distinctly differs from the one in the flood basalts in the following parameters (Figs. 4–6): (a) greater travel-times, (b) smaller velocities near the shot points, (c) symmetry in the travel-time curves east and west, (d) short segments of waves with $V^*=4.5$ km/s, (e) longer segments of waves with $V^*=6.0$ km/s, (f) absence of waves with $V^*=6.3$–6.5 km/s, as far as observed. The characteristics are summarized in Table 2.

In most cases waves of the P_0'', P_1', and P_1'' groups have no reversed branches of the travel-time curves. They are identified at different shot points by their closely similar apparent velocities and travel-times at the same distances. They quickly attenuate and follow each other with time delays. They are considered to be waves transmitted through layers of constant high velocities within the lava series.

Waves of the P_2 group begin to appear in later arrivals. They have a characteristic stable shape (Fig. 4) and are little attenuated. They can be clearly identified. They overlap in large regions (SP7–8 to the left, SP5–6 to the right). They are essentially parallel, which is surprising in view of their low attenuation.

In the eastern part of the profile (SP9, SP10) one can observe a change of the picture: a decrease of the travel-times and an increase of the recording range for the P_1 group.

In the transition zone, the waves travelling through the flood basalts are seen at ranges smaller than 12 km on the records of the automatic stations (Fig. 7). Later waves arrive with 6.0 km/s and an increase of velocity is found at 18 km distance. The region of traceable waves through the flood basalts with 4.5 km/s is enlarged in the transition zone. Two groups, P_2 and P_3, can be identified. P_2 can be definitely traced through the flood basalts, the transition zone, and the neovolcanic zone by its intensity, velocity, and stability.

Amplitudes were determined on the basis of the records of the automatic stations to define regions with different attenuation. In the flood basalts attenuation is strong along the first few kilometers with $\alpha_{\text{eff}}=4.6\cdot10^{-1}$ km^{-1}, in the range of 8–30 km $\alpha_{\text{eff}}=8\cdot10^{-2}$ km^{-1}, and at greater distances the amplitudes are essentially constant.

A great number of phases with negative apparent velocities and merging with the first arrivals can be traced across distances of one to several kilometers (Figs. 2 and 3); their apparent velocities range from -3 to -6, in rare cases to -10 km/s. The phenomenon is enhanced in the higher frequencies.

Peculiarities of the Reflections

Later arrivals are complex (Figs. 2–5). Low-velocity surface waves of 10–15 Hz can be seen to 2 or 3 km range. They can be suppressed by frequency filtering. Intensive sound waves make correlation of other waves at close range difficult. Many of the later arrivals are longitudinal reflected waves; also present are diffractions, shear waves, and converted waves. The longitudinal reflected waves among the later arrivals can be identified by their kinematic parameters: hyperbolic shape of the travel-time curve, interrelation of reversal and overlap times, etc. In intensity the reflections are usually lower than the first arrivals. Individual phases of the reflections can be traced for shorter distances (to several kilometers), but the groups can be traced across 10–15 km. Frequency filtering often enhances the reflected P-waves.

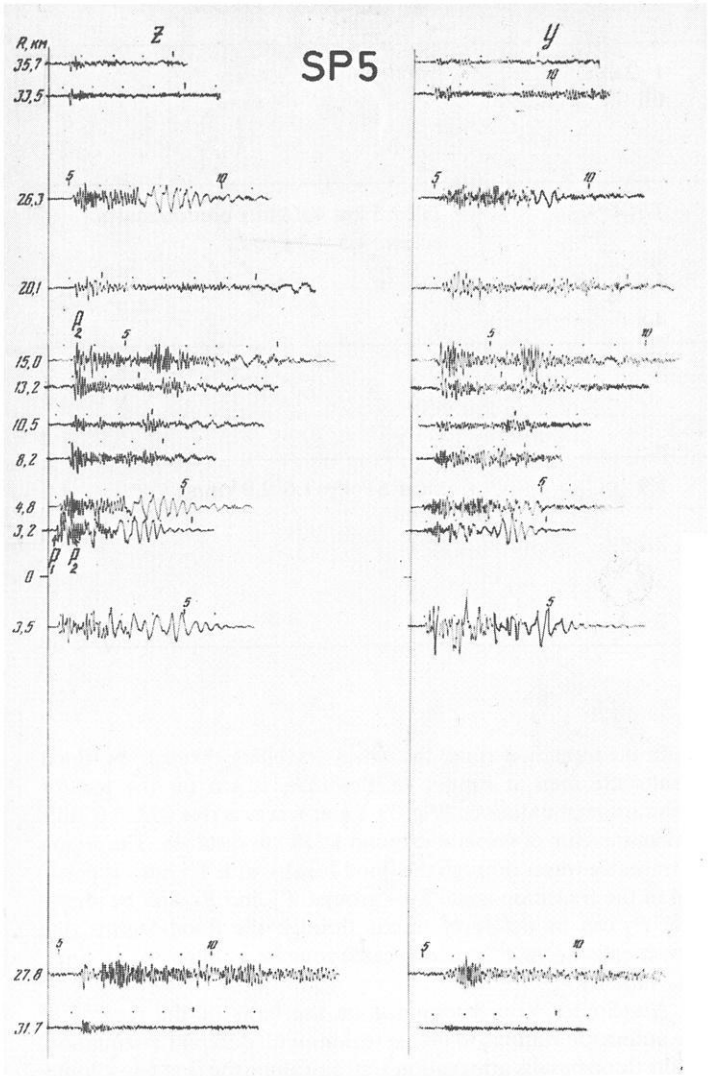

Fig. 7. Record section of automatic stations for SP5 in the frequency band of 5–18 Hz, $V_{red} = 6$ km/s

In the flood basalt region eight groups of reflected waves were found. The wave groups 1, 2, 3, 4, 7 (Figs. 2 and 3) are more clearly expressed than other waves, and all groups have reversed time curves. The former ones represent straight or slightly curved branches, 1–7 km long, from all three shot points, particularly from SP2 (Fig. 2). The later groups identified are numbered on Figs. 2 to 4. Their apparent velocities are greater than those of the first arrivals. Group 6 has a travel-time minimum clearly west of the shot point.

In the neovolcanic zone 12 groups of reflected waves were found on the basis of the reversed branches of the travel-time curves (Figs. 4 and 5). The branches are slightly curved with $V^* =$ 10–12 km/s extending to 15 km.

The ample occurrence of later phases which merge with the first arrivals and have positive or negative apparent velocities was already mentioned. Their travel-time branches are usually straight, sometimes hyperbolic. They are interpreted to be waves reflected from steeply dipping boundaries (>45°) and partly diffractions.

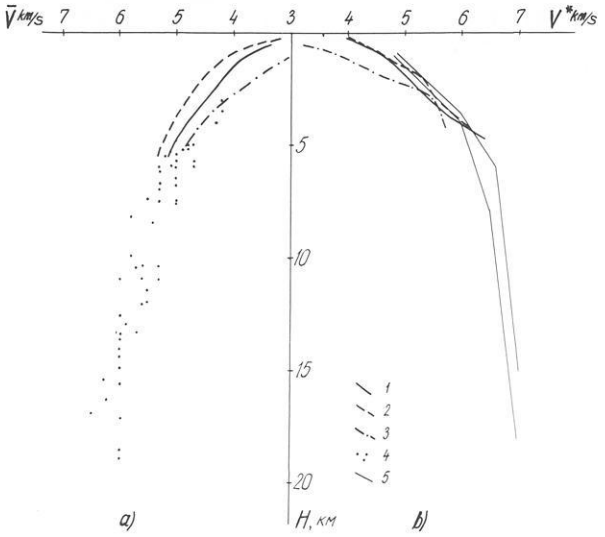

Fig. 8. Apparent (*b*) and average (*a*) velocities, computed from reflected (1–3) and refracted (4) waves. 1: flood basalts, SW-Iceland; 2: flood basalts, NE-Iceland; 3: neovolcanic zone, NE-Iceland; 5: apparent velocities computed from long-range refraction, NE-Iceland (RRISP Working Group, 1980)

Seismic Cross-Sections

The average velocities used in the construction of the cross-section were determined from the refractions and the wide-angle reflections (Fig. 8a). A large scatter is observed for the reflections, and on average, they render lower velocities than the refractions. The apparent velocities which as the first approximation may be regarded as true layer velocities are shown as curve 2 in Fig. 8b; the corresponding velocities from Southwest Iceland (Zverev et al., 1980) are shown for comparison (curve 1). Curve 3 gives the velocities for the neovolcanic zone; they are considerably lower. For comparison, the results from a long-range refraction experiment are presented in curve 5 (RRISP Working Group, 1980; Gebrande et al., 1980). The seismic cross-section shown in Fig. 9 was derived from the refractions and reflections discussed above.

In the flood basalt region, from refraction data, inclined high-velocity layers were constructed from intercept times and apparent velocities with the assumption that group P_1 is a head wave. Two boundaries were established with 4.3 and 4.5 km/s, respectively, and with 8° to 10° dip; the former continues eastward near-horizontally with 4.5 km/s as determined from SP3 and SP4 with the time-field method (Riznichenko, 1946). This method is based on drawing rays and isochrons for the seismic waves. It requires reversed and overlapping travel-time curves; there are no limitations concerning the velocity structure. A boundary with 5.75 km/s (between SP2 and SP3) and 5.65 km/s (between SP2 and SP4) was constructed with the time-field method from group P_2. The travel-time curves between SP1 and SP4 and between SP1 and SP3 give 5.6 km/s for this boundary. The computed depths were in good agreement. A third boundary with 6.3 km/s and 5° to 7° eastward dip was determined with the time-field method for SP1 to SP5.

In the neovolcanic zone, low-velocity refractions have no complete reversed branches in the travel-time curves. Average refractor velocities and intercept times were computed from all travel-time curves and depths were determined iteratively. However, the boun-

daries thus computed must be considered tentative, i.e. only generally representing the depth where the corresponding velocity is reached.

Group P_2 has a travel-time curve to permit a time-field solution for SP6 and SP7 as well as for SP6 and SP8, giving closely similar depths for the 5.7 km/s boundary; it rises slightly towards the center of the neovolcanic zone. The lower boundary is shown approximately as the minimum depth of the velocity isoline of 6.3 km/s, constructed from the ends of the travel-time curves. The data from the automatic stations were used for the construction of velocity isolines only, and the numerical values of the velocities were chosen according to the boundary velocities.

Our cross-section (Fig. 9) is in good agreement with earlier seismic interpretations (Pálmason, 1971,) concerning the upper boundaries; there is some difference in depth and velocity below 2 km. The boundary depths with 5.1–6.8 km/s of Pálmason (1971) clearly depend on the length of the travel-time curves. Due to the detail of observation and to the reverse and overlapping travel-time curves, our section is considered very precise.

The refraction cross-section of the present northern profile (Fig. 9) is similar to the southwestern one (Zverev et al., 1980) in depths and in character of the boundaries in the flood basalt region, but the velocity values are lower in the north (5.7 and 6.3 km/s versus 6.0 and 6.5 km/s).

The construction of the cross-section from the reflections was done in several stages. First, groups of reflections with their vertices were used, nine in the flood basalt zone and 12 in the neovolcanic zone. The shorter reflecting elements were added. Dip vectors were constructed separately using square soundings. Average velocities were chosen such as to give the best agreement between the constructed boundaries. Figure 9 shows that the reflectors constructed from reflection vertices, one-sided branches, and dip vectors are in good agreement.

The reflectors form groups in certain depth intervals (<0.5 km), sometimes up to 5 or 7 km long. The greatest scatter of reflectors occurs at the ends of the profile outside the continuous observations.

On the western flank near SP2, the horizons dip 15°–20° eastward and less further east. This corresponds with the boundaries and velocity isolines from refraction. The steepest dips (up to 40°) occur in the neovolcanic zone under SP6, shallowing again to the velocity contours in the neovolcanic zone.

Discussion of the Results

Our seismic experiment gave more details than earlier work or that in southwestern Iceland (Zverev et al., 1980). Velocity contours, refractors, and reflectors were combined with geological

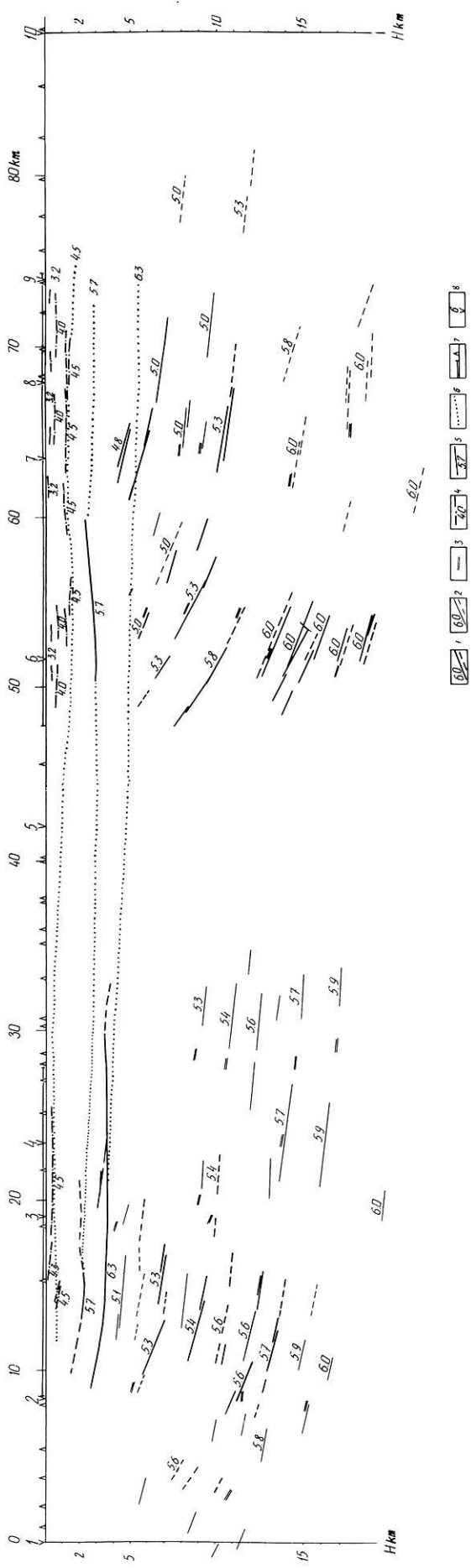

Fig. 9. Seismic cross-section. 1, 2: reflectors, computed from entire travel-time hyperbola (1) or from isolated branches (2); *dashed lines* less reliable; *numbers* indicate average velocities *above* reflectors. 3: Dip of reflectors. 4: Refractors coinciding with geological boundaries. 5: Refractors computed from reversed travel-time curves; *dash-dotted*: from unreversed lines; *numbers* indicate refractor velocities. 6: Velocity contours: 4.5, 5.7, 6.3 km/s. 7: regions of multi-channel coverage and projected positions of automatic stations (Fig. 1). 8: Shot points

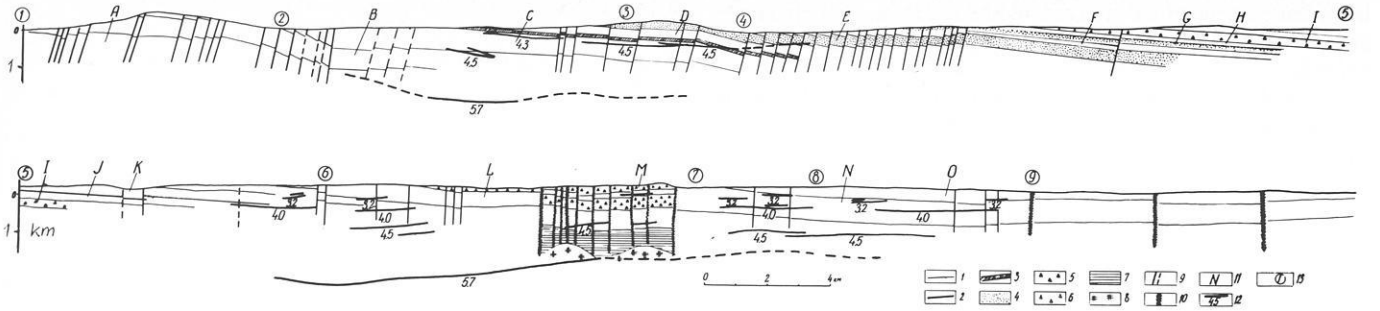

Fig. 10. Geological cross-sections combined with seismic results. 1: lithostratigraphic boundaries; 2: stratigraphic boundaries (3.1 and 0.7 Ma); 3: basalt; 4: basalt alternating with tuffaceous sediments; 5: pyroclastic and glacio-fluviatile formations; 6: agglomerates, volcanic breccias, tuffs; 7: dolerite, gabbro; 8: granophyre; 9: faults; 10: zones of recent volcanism; 11: indices of main subdivisions of the cross-section:

Upper Miocene – Lower Pliocene. A: Porphyrites, olivine basalt, etc.; *B:* aphyric basalt; *C:* aphyric and fine-grained porphyric basalt, porphyrite, dolerite; *D:* basalt, porphyrite, icelandite, tuff, tuffaceous sediments; *E:* basalt, andesite-basalt, series of tuffaceous sediments in top and bottom of layers; *F:* basalt, agglomerate, tuff.

Upper Pliocene – Eopleistocene. G: Tillite, tuffaceous sediments of glacio-fluviatile origin, hyaloclastite; *H:* olivine basalt; *I:* hyaloclastite, tillite; *J:* basalt.

Pleistocene. K, L: Basalt, tillite; *M:* agglomerate, lava breccia, tuff; *N:* basalt, tillite; *O:* late Pliocene and Holocene lava. 12: refractors and corresponding velocities; 13: shot points

observations and published data. The results are a schematic geological map (Fig. 1) and a geological cross-section along the seismic profile (Fig. 10).

Separate seismic waves arise at sharp or gradual changes of physical rock properties. Refractions are generated at velocity increases with depth which may occur in bulk or in thin layers. Reflections originate at discontinuities of acoustic impedance with increasing or decreasing velocities. Reflecting horizons may correspond to contact zones of rocks of different composition or metamorphic grade and to faults, dykes, ets.

The seismic profile crosses the main geological structures of northern Iceland (Fig. 1). The total thickness of the exposed section is estimated 4 000 m. The lower part of the rocks older than 3.1 Ma is 2 500–3 000 m thick and consists predominantly of lava. East of SP3 only one layer of tuffaceous sediments is observed which thickens to the east. In the outer and inner neovolcanic zone the rocks are in almost equal amounts lava, pyroclastites, and tuffaceous sediments mostly of fluvio-glacial origin. Separate series probably have different seismic velocities.

The strip along the profile can be divided into five tectonic regions (Fig. 1). The western-most region includes the eastern slope of the water divide between Eyjafjördur and the river Fnjóská (SP1–2); it is characterized by a monocline composed of flood basalts (Fig. 10) dipping increasingly 5°–6° to 20°–30°. The flexure is accompanied by faults, dykes, and a narrow graben in which the flood basalts have maintained their original flat bedding. The second region between Fnjóská and Skjálfandafljót (SP2–4) is characterized by flat bedding (3°–5° dip) and comparatively rare faults and dykes of northeasterly trend. In the adjoining third region to 7 km east of SP4 there are many faults and dykes of northerly trend. The total throw of the faults from the Akureyri anticline to the edge of the neovolcanic zone is not less than 100–150 m and increases from south to north. The fourth region is also characterized by flat bedding with minor faults and dykes and an increasing proportion of fluvio-glacial formations including large series of pillow lavas, hyaloclastites, and tillites. The fifth region is the inner neovolcanic zone largely built of Pleistocene and Holocene volcanics. Four centers of modern volcanism can be identified: Krafla, Búrfell, Rauduborgir, and Nýjahraun (Figs. 1 and 10). The latter two are crossed by the profile in the east.

On the cross-sections (Figs. 9 and 10) we note the good agreement in the flood basalt zone (the above regions 1 to 3) between the seismic refractors and the geological boundaries near the surface. Near SP3 the 4.3–4.5 km/s horizons exactly coincide with dense basalts (layers C and D, Fig. 10). Near SP4 the 4.5 km/s horizon corresponds to the base of layer E with a large content of low-velocity tuffacious sediments. West of SP3 (Fig. 9) the 4.3–4.5 km/s refractors do not agree with the shape of the velocity contours; the refractors are dense basalt layers while the velocity contours represent the general velocity increase. Commonly in the flood basalt zone, the reflectors parallel the velocity contours and the refractors to great depth as they parallel the shallow geological boundaries. This suggests a long history of invariable flood basalt deposition. Hence the age of the rocks (3 Ma for the 4 000 m exposed section) is expected to increase with depth.

The rift zone is more complicated. The refractors and the 4.5 km/s contour are depressed west of SP7, i.e., east of Mývatn. A second depression occurs east of SP8. These two depressions consist of low-velocity rocks (3.2 and 4.0 km/s refractors). All the above refractors coincide or are parallel to the geological boundaries. The 5.7 km/s contour is slightly arched, culminating at 2.5 km depth under Námafjall on the Krafla fissure swarm (Saemundsson, 1974; 1977; 1978) which currently experiences a rifting episode (Björnsson et al., 1977; 1979; several papers, this volume).

The deeper reflectors in the neovolcanic zone distinctly intersect the refractors. Maximum reflector slopes are 30°–40° (under SP6) decreasing eastward. Two zones with conspicuous absence of deep reflectors occur west of SP7 under the axial depression and under SP9 where the surface layers are also depressed (Figs. 1 and 10). Both are characterized by active fissure swarms. It is suggested that the absence of reflectors is evidence for magma chambers.

The seismic cross-sections in northeastern and southwestern Iceland are very similar. In the flood basalts the near-surface seismic horizons closely correspond to geological layers. Both we-

stern flanks are complex with ancient flexures at Borgarfjördur and Fnjóská, respectively. Near the neovolcanic zones the whole basalt series is slightly tilted toward their centers. The depressions in the neovolcanic zones are filled with low-velocity rocks. Steep dip angles are found to depths of 15 km and more. At the centers of the depression there are active volcanic fissure swarms, below which, at 10–15 km depth, there is evidence for seismically homogeneous bodies which are interpreted to be magma chambers. On the whole the northeastern zone is more complex than the southwestern one.

The spatial continuity of structure from 10–15 km depth to the surface activity of volcanism and rifting is considered by some of the authors to be evidence for temporal continuity of structure and for stability without significant spreading in Iceland. In this view the recent activity is superimposed on ancient crustal structure. Others believe that the spatial continuity indicates a steady-state process (in a time-average sense) of spreading, rifting, and generation of new lithosphere where, however, complications in structure may have arisen from a shifting of the active zone from one location to another.

Acknowledgements. The seismic studies in northern Iceland were carried out in 1977 by the Soviet Geodynamic Expedition of the USSR Academy of Sciences, jointly with the Geothermal Division of the National Energy Authority of Iceland. Great help in the seismic work was rendered by Corresponding Member of the USSR Academy of Sciences, Professor V V Beloussov. Beside the authors, the following Soviet scientists participated in the seismic field work: G.N. Akimov, A.N. Fursov, V V Knjasev, B.I. Kerby, O.A. Kisilev, N.M. Nardov, E.M. Chesnokov (Institute of Physics of the Earth of the USSR Academy of Sciences); Yu.M. Misnik, N.V Kondratjev, A.V Konoplev, V.I. Gatiev (Leningrad Mining Institute); and in geological mapping: A.R. Geptner (Geological Institute, USSR Academy of Sciences). S. Sigurmundsson, G. Petursson, and G. Stefansson were instrumental for the field work. The results were discussed with K. Saemundsson. The Embassy of the USSR in Iceland and the National Research Council of Iceland helped much in the organization of the Expedition's work. We are grateful to all of them.

References

Björnsson, A., Johnsen, G., Sigurdsson, S., Thorbergsson, G., Tryggvason, E.: Rifting of the plate boundary in North Iceland 1975–1978. J. Geophys. Res. **84**, 3029–3038, 1979

Björnsson, A., Saemundsson, K., Einarsson, P., Tryggvason, E., Grönvold, K.: Current rifting episode in North Iceland. Nature **266**, 318–323, 1977

Burkhardt, H., Vees, R.: Explosions in shallow water for deep seismic sounding experiments. J. Geophys. **41**, 463–474, 1975

Gebrande, H., Miller, H., Einarsson, P. Seismic structure of Iceland along RRISP Profile I. J. Geophys. **47**, 239–249, 1980

Litvinenko, I.V.: Seismic methods of studying the complex structure of the upper part of the continental crust. Notes Leningrad Mining Inst. V XI (2), 1971

Pálmason, G. Crustal structure of Iceland from explosion seismology. Soc. Sci. Isl. **40**, 187pp., 1971

Pálmason, G., Saemundsson, K. Iceland in relation to the Mid-Atlantic Ridge. Annu. Rev. Earth. Planet. Sci. **2**, 25–50, 1974

RRISP Working Group: First results from the Reykjanes Ridge Iceland Seismic Project 1977. Nature **279**, 56–60, 1979

RRISP Working Group: Reykjanes Ridge Iceland seismic experiment (RRISP 77). J. Geophys. **47**, 228–238, 1980

Riznichenko, Yu.V Geometrical seismology of stratified media (in Russian). Proc. Inst. Theor Geophys. **II**, 1946

Saemundsson, K.: Evolution of the axial rifting zone in northern Iceland and the Tjörnes fracture zone. Bull. Geol. Soc. Am. **85**, 495–504, 1974

Saemundsson, K. Geological Map of Iceland, Sheet 7. Reykjavik, Mus. Nat. Hist., 1977

Saemundsson, K. Fissure swarms and central volcanoes of the neovolcanic zones of Iceland. Geol. J. Spec. Iss. **10**, 415–432, 1978

Zverev, S.M., Litvinenko, I.V., Pálmason, G., Yaroshevskaya, G.A., Osokin, N.N.: A seismic study of the western rift in southern Iceland (in Russian). Bull. Mosk. O-va ispit. pripodi. otd. geol. (Bull. MOIP), Vol. 54, No. 3, 1979

Zverev, S.M., Litvinenko, L.V., Pálmason, G., Yaroshevskaya, G.A., Osokin, N.N.: A seismic crustal study of the axial rift zone in southwest Iceland. J. Geophys. **47**, 202–210, 1980

Received June 20, 1979; Revised Version August 20, 1979

J. Geophys. 47, 202–210, 1980

Journal of Geophysics

A Seismic Crustal Study of the Axial Rift Zone in Southwest Iceland

S.M. Zverev[1], I.V Litvinenko[2], G. Pálmason[3], G.A. Yaroshevskaya[1], and N.N. Osokin[2]

[1] Institute of the Physics of the Earth, Moscow, USSR
[2] Mining Institute, Leningrad, USSR
[3] National Energy Authority, Reykjavík, Iceland

Abstract. Detailed seismic crustal studies by combined reflection and refraction methods were carried out for the first time in the flood basalts and in the active zone of rifting and volcanism of southwestern Iceland. The observations were carried out along two profiles with a total length of 70 km, with 8 shot points, and with a distance between seismographs of 50 m. The flood basalt series flanking the axial rift zone along the profile line ranges in age from 1 7 to 6.0 Ma at the surface. It is characterized by a general increase in seismic wave velocity with depth, and by the presence of high-velocity layers with V_p=4.3–4.7 km/s, connected with denser lava flows interbedded between lower-velocity rocks. The refracting boundaries in the upper part of the section dip towards the axial rift zone at angles of 8°–9°, which is consistent with the dip of the surface lavas. Less dipping refracting boundaries with velocities of 5.2, 6.0, 6.5 km/s, were found at depths of 2–4 km. Within the axial rift zone the refracting boundaries form a slight depression filled with low-velocity formations (V_p=2–3 km/s). Reflecting horizons with an average length of 1–2 km were found. They are on the whole much less regular than in continental regions with sedimentary deposits. They are generally tilted towards the axial rift zone. Steep dipping elements are traceable to a depth of more than 10 km, the dip decreasing with depth in the flood basalt area. In the axial part of the rift the seismic cross-section outlines a volume, where no reflecting horizons could be detected. This indicates relative homogeneity of physical properties and may point to a magmatic chamber, or a region of partial melting underlying the axis of the zone of rifting and volcanism.

Key words: Iceland – Seismic reflection and refraction profile – Axial rift zone – Magma region.

Introduction

The complex geological – geophysical expedition of the USSR Academy of Sciences jointly with the Icelandic National Energy Authority conducted in 1976 a seismic crustal investigation in southwestern Iceland. The purpose was to study in detail the structure of the upper part of the earth's crust along a line transverse to the active zone of rifting and volcanism, crossing the axial zone as well as the adjacent flank area.

The Tertiary and Quaternary flood basalts comprising the flanks of the axial rift zone in Iceland are known to be almost everywhere tilted towards the axis of the zone. This may be viewed as a vast depression in the flood basalts, partly formed by faulting, and filled with younger volcanic formations (Walker, 1960; Bodvarsson and Walker, 1964; Einarsson, 1965, Pálmason, 1973; Pálmason and Saemundsson, 1974; Beloussov and Milanovsky 1977). Little is known, however, about the detailed deeper structure, since seismic refraction studies (Pálmason, 1971) have limited resolving power, and drillholes have penetrated only to about 3 km depth at the present time (Pálmason et al., 1979).

A mechanism of crustal drift and generation, somewhat analogous to the concept of sea-floor spreading, was proposed by Bodvarsson and Walker (1964) to explain the structure of the Tertiary flood basalts in eastern Iceland. The thermo-mechanical aspects of this process are being studied in more detail by one of the authors of the present paper (Pálmason, 1973, 1980). The generation of new crust is assumed to take place in the axial part of the volcanic rift zone by dykes intruded into the crust and by lavas erupted at the surface. The crust is sagging more or less continually under the weight of new material brought to the surface in volcanic eruptions. One of the objectives of the present study was to try to follow by reflection methods some of the dipping Tertiary and Quaternary lava series from their surface exposures to greater depth in the crust. This might contribute to a better understanding of the processes taking place in the active zone of rifting and volcanism.

Location of Profiles, Methods

The choice of a representative seismic profile locality that would cross the flood basalts as well as the active zone of rifting and volcanism in southwestern Iceland was governed largely by the available roads. The line of seismic observations in 1976 is shown in Fig. 1. It consists of two separate profiles. Profile I extends eastwards from a shot point in Borgarfjördur, about 5 km east of the Borgarfjördur anticlinal axis (Fig. 1), and crosses flood basalts of Miocene-Pliocene age, which near the eastern end are replaced by the younger volcanic rocks of the active zone, especially the lava sheets of the shield volcano Skjaldbreidur. Profile II is located within the active zone of rifting and volcanism where the surface rocks are predominantly postglacial lava sheets and interglacial hyaloclastite ridges. The rocks are broken by young fractures with a mainly northeast-southwest direction. This profile crosses the axial part of the active zone of rifting and volcanism in an oblique direction.

The technique of investigation is characterized by the following features. The profiles followed the available roads and were thus not totally straight, which limited the interpretation possibilities somewhat. The shots were fired in the sea (SP 1), in lakes (SP 2–5)

0340-062X/80/0047/0202/$01.80

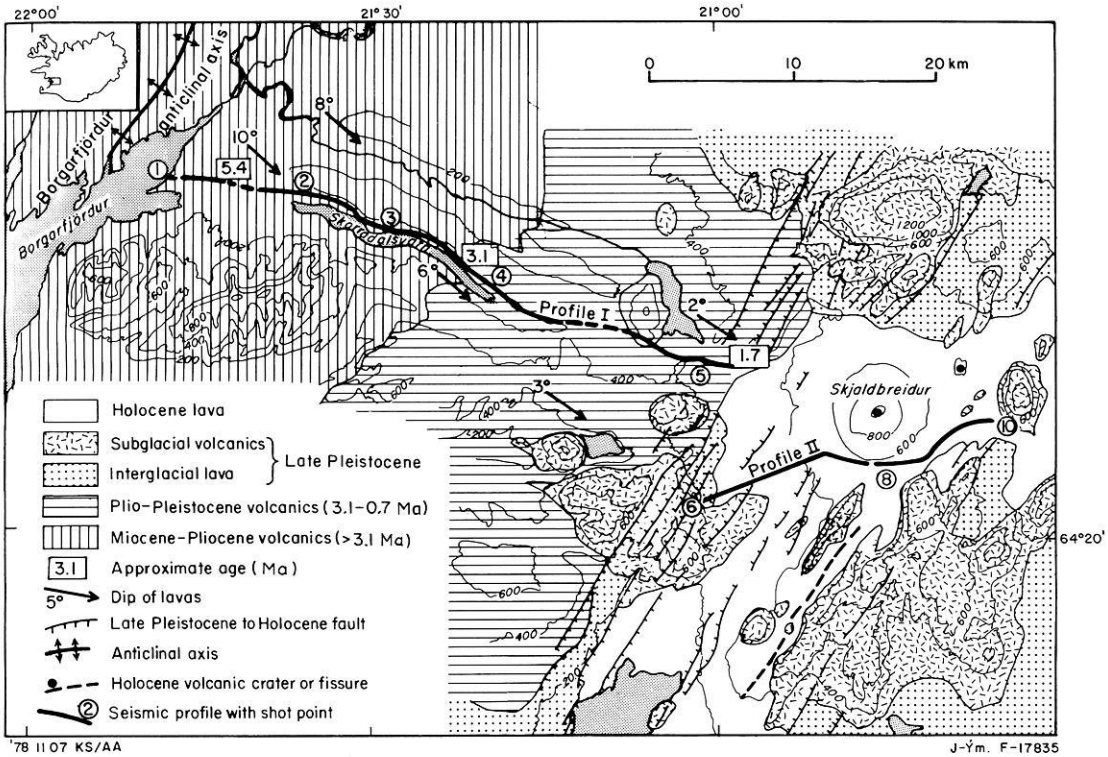

Fig. 1. The location of seismic *Profiles I and II* and the geology of the surrounding area

or in dry pits and cavities of lava flows (SP 8–10). For some of the shot points the charges were limited in size because of proximity to populated areas (SP 1 and especially SP 2–4). The charges for SP 1 were about 150–200 kg, SP 2–4 25 kg, SP 5 50–200 kg, SP 6 150–200 kg, SP 8 250–500 kg, and SP 10 200–400 kg. Shooting conditions were far from optimum in the shallow water basins, open pits, and caves.

Although on the whole the profile measurements were more detailed than in previous seismic investigations in Iceland, they were more of a reconnaissance than a detailed character, if compared with modern seismic exploration surveys. A continuous profiling was used with a distance between the geophones of 50 m. The geophones were usually located on the side of the roads. Two twenty-four channel seismic reflection recording stations of the type SMOV-24 were used. The magnetic tape records were of duration up to 12 or 24 s with a dynamic range of 46 db in the frequency band 5–100 Hz. The geophones had a natural frequency of 10 Hz. The shots were recorded at each recording station from 3 to 6 shot points.

The system of time curves used made it possible to determine twice independently the location of reflecting horizons in the cross-section. At greater depths and on the outermost parts of the profiles the reflecting elements could, however, be traced only for certain ranges of dip. At depths exceeding the length of the time curve only the low-dip boundaries could be traced, while on the outermost parts only the steep ones (Litvinenko, 1971). On Profiles I and II the length of most travel-time curves exceeded 10–15 km. The maximum length reached 45 km, permitting not only the construction of several refracting horizons, but also the identification of reflectors with angles of dip 60°–70° at depths down to 5 km, and at still greater depths of reflectors with lower dip angles.

To identify the useful waves, especially the reflected ones, the field magnetic records were reproduced on special equipment of the types 'Ray' and PSZ-4M. On the record-sections produced, no corrections for elevation, low velocity surface layer, or deviations of the profile from a straight line were introduced, there being insufficient data available for this purpose. In playback the main consideration was given to the frequency filtering of useful signals. In the frequency range above 40 Hz the identification of reflected waves proved to be difficult due to high background noise. At frequencies below 5 Hz the separation of waves was difficult. Experimental tests showed that at distances larger than 15–20 km from the SP the frequency band of 7–14 Hz gave the optimum results and at smaller distances the corresponding frequency band was 10–28 Hz.

The records in the form of conventional seismograms and the above-mentioned record-sections were the basis for the construction of the velocity section, correlating the useful waves and determining the seismic boundaries.

General Features of the Seismic Wave Fields

Examples of wave fields may be seen in the record sections in Figs. 2 and 3. On the whole, the observed picture reveals a complicated medium with little velocity variation. The main features of the wave field are the following:

1. Presence of clear and strong refractions as first arrivals, non-parallel overlapping travel-time curves, difficult separation of waves forming the first arrivals;

2. Short range of observation and little variation in amplitude of later arrivals, lack of dominant reflections;

3. Asymmetry of the travel-time curves of refractions and reflections; in most cases the travel-time minimum of the reflections is displaced from the shot point;

4. Considerable irregularity in the wave field; frequent phases with anomalous velocities join up with the first arrivals and are repeated on reversed and overlapping travel-time curves.

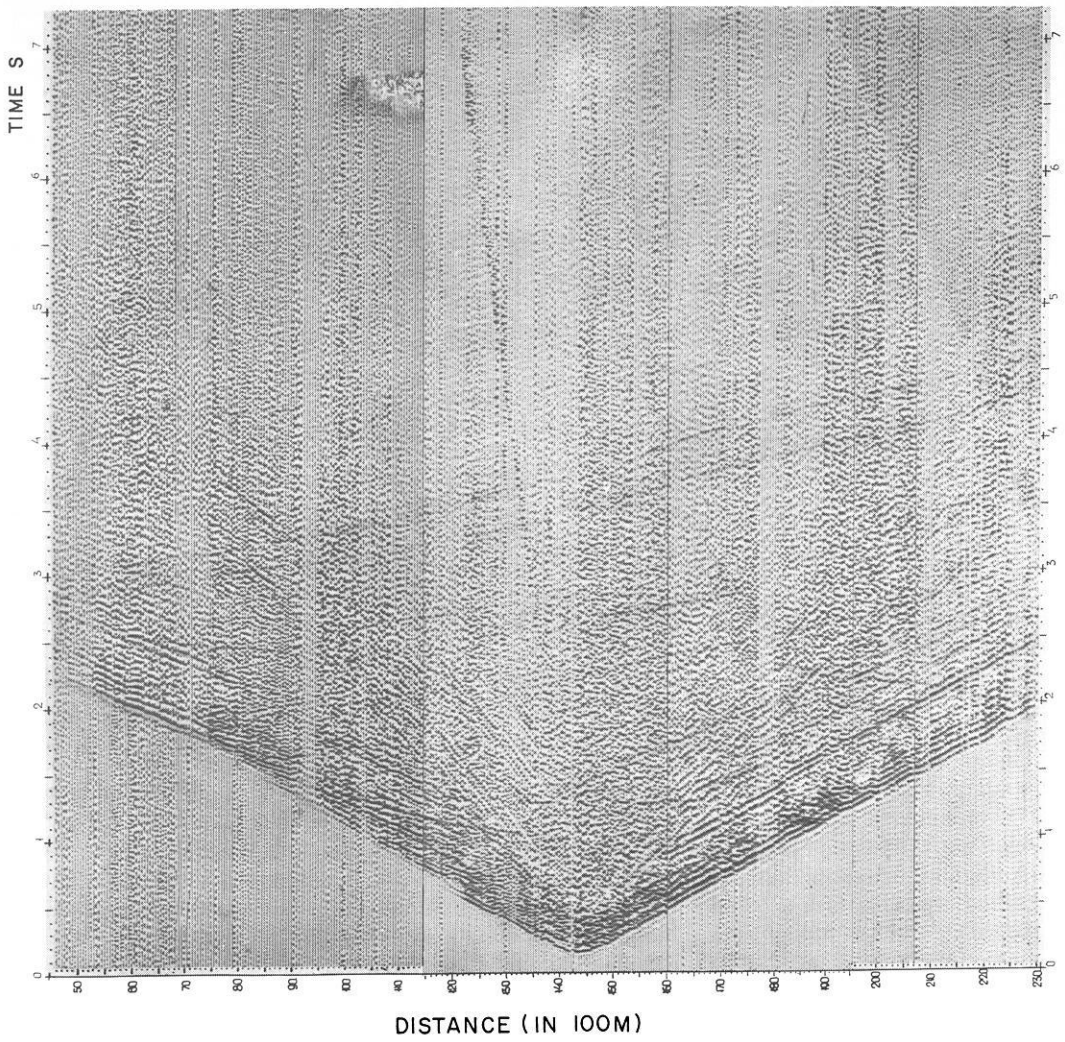

Fig. 2. Record-section in frequency band 9–19 Hz for *SP 3 on Profile I*

Characteristics of Refracted Waves

The refracted waves differ in travel-times and apparent velocities on the two profiles. On Profile I along the flood basalts they are compact oscillations lasting 0.5 s on average (Figs. 2 and 3). Their apparent velocities, V^*, increase from 3 or 4 to 6.5 or 7 km/s (Figs. 4 and 5) in the distance range of 0–40 km. The increase is somewhat gradual indicating the absence of thick layers of constant and strongly contrasting velocities. Overlapping travel-time curves are rarely parallel (Fig. 4) such that distinct wave groups cannot be traced for distances greater than the shot intervals; this means that only refracted and diving waves are observed.

The criteria used in dividing the waves into groups were changes in V^* and wave form. The parameters of the groups are given in Table 1. Small local variations in apparent velocity often make identification difficult. The wave groups P_1 and P_3 are most easily identified. For P_1 a distinct asymmetry with respect to the shot point is found (Fig. 4). To the east V^* gradually increases to 4.4 or 4.6 km/s; the westward branches consist of several high-velocity sections which are highly attenuated. Overlapping travel-time curves terminate at the same locations. This may be explained by a laminated gradient medium with intercalated high-velocity layers. The waves of groups P_2' and P_2'' are traceable over short ranges only and are difficult to distinguish, but their continuation as later arrivals (SP 1, 2, 5; Fig. 4) supports their identification.

A summary of the travel-time curves (Fig. 6) shows that the uppermost part of the section does not change much along the profile. An exception is the area around SP 1 where the travel-times are shorter; the velocities change correspondingly between 2 and 7 km east of SP 1. Generally the travel-times are found to increase from west to east, also for other wave groups, for distances greater than 8 km (Fig. 6); this indicates dip of the refractors toward the neovolcanic zone.

Along Profile II within the active zone of rifting and volcanism, the travel-times are distinctly greater and the near-surface velocities are lower (Figs. 5 and 6). Five different wave groups with velocities from 1.6 to 5.6 km/s are identified (Table 1). The waves with $V^* < 4$ km/s are strongly attenuated and the following ones are separated from the earlier ones by a time interval indicating layers with zero or negative velocity gradients.

Waves propagating in the upper part of the section along Profile I have similar mean apparent velocities as the wave groups P_1'' and P_1''' along Profile II. Waves with lower velocities are absent in Profile I, whereas higher-velocity waves are not found on Profile II; the range of observations is probably too short.

Seismic Cross-Section From Refractions

True and average velocities were determined for the cross-section from the observed refractions with several methods (simplified

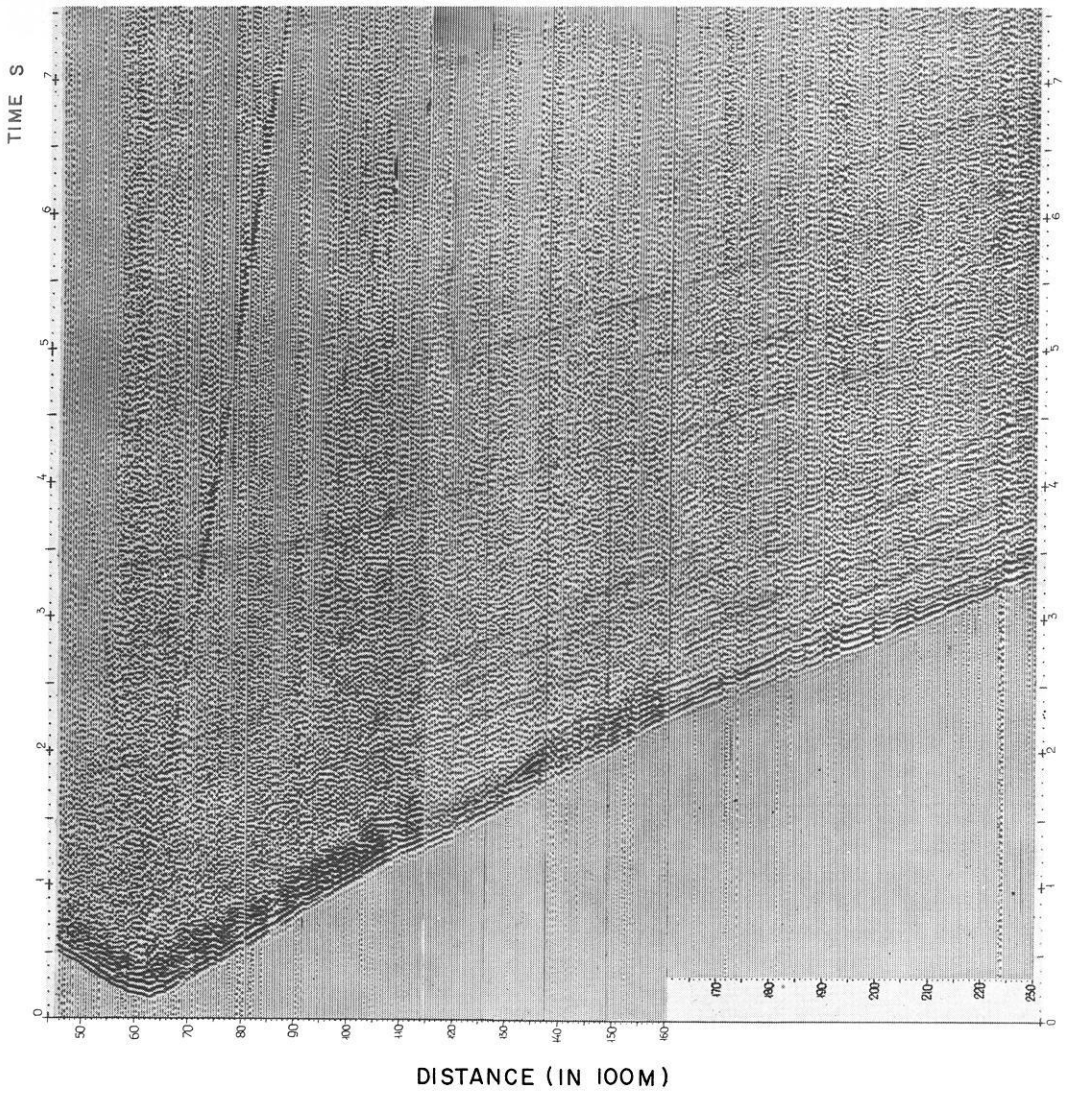

Fig. 3. Record-section in frequency band 9–19 Hz for *SP 2 on Profile I*

Chibisov's (1934) method, intersection-point method, intercept-time method). The average-velocity curves for SP 2–4 of Profile I coincide perfectly (Fig. 7); at SP 5 lower velocities are obtained for 0.5 to 3 km depth; at SP 1 higher values are found. The computed layer velocities agree well with the observed apparent velocities. Owing to less data along Profile II, only one average velocity-depth curve was determined here.

The refractors were computed with various methods. For Profile I, depths and dips were computed with generally known formulae based on apparent velocity V^*, intercept time t_o, average velocity $\bar{V}$, and the values of X and t at both ends of the observation range. The results are given in Table 2. The cross-section (Fig. 8a) shows a complicated structure in the upper part which is considered as a gradient zone. The velocity increases with depth, most strongly in the uppermost 500 m; toward the neovolcanic zone there exist high-velocity intercalations. The boundary velocities are shown in the section (Fig. 8a). The boundaries dip toward the neovolcanic zone with angles of 5°–10° for the flood basalts and 2°–4° at greater depth. At the eastern end of Profile I, the dips slightly decrease.

On Profile II in the neovolcanic zone (Fig. 8b), the boundaries were determined with the intercept-time method and with the time-field method (Riznichenko, 1946). The section has a synclinal structure; the refractors with flood-basalt velocities (4.5–4.7 km/s) regularly dip toward the axis to depths of 3 km, while on Profile I they extend from the surface to about 1.5 km.

Characteristics of the Reflections

Special record-sections were assembled for the identification of reflections (Figs. 2 and 3). Surface waves, shear waves, and diffractions are typical for the sections. Some low-velocity waves join the first phases in certain parts of the profile. Their apparent velocities are practically constant and equal to the velocity of the surface layers (2.5–4 km/s). Diffraction centers seem to occur near the surface usually at fractures, near-surface faults, areas of exposed high-velocity beds, etc.

A large number of wave groups mostly of small intensity are identified in the region where reflections are expected. They can be traced over distances from a few hundred meters to several kilometers. Some have infinite or even negative apparent velocities; they may be reflections from steeply dipping (>45°) boundaries, propagating in a medium with a positive velocity gradient.

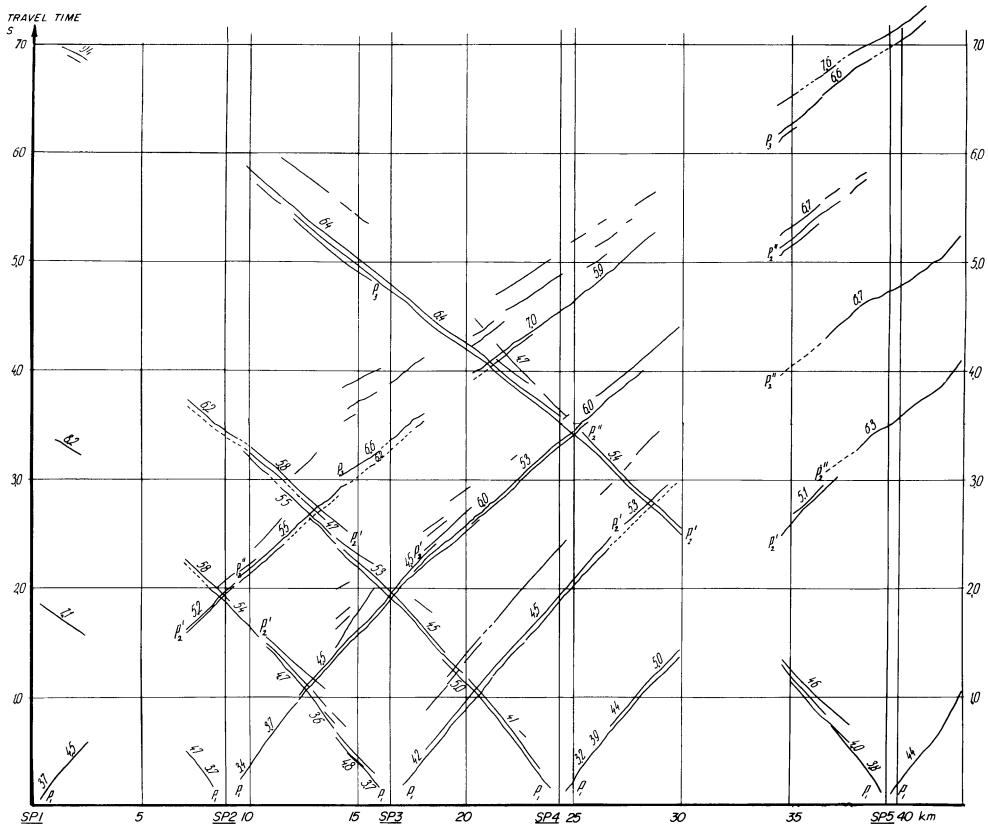

Fig. 4. Travel-time curves of the refracted waves recorded on Profile I

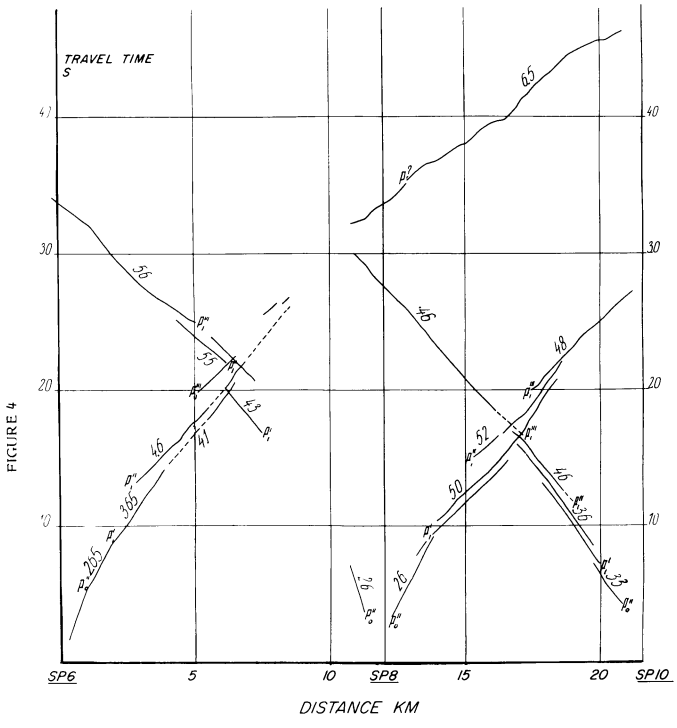

Fig. 5. Travel-time curves of the refracted waves recorded on Profile II

Table 1. Parameters of wave groups

Wave groups	Range of apparent velocities V^* (km/s)	Range of distances (km) for first arrivals
Profile I		
P_1	3.0–4.7	0– 8
P'_2	4.7–5.6	8–12
P''_2	5.6–6.5	12–22
P_3	5.6–7.5	>22
Profile II		
P'_0	1.6–2.0	<1
P''_0	2.6–3.3	1–2
P'_1	3.6–5.0	2–6
P''_1	4.0–5.2	3–7
P'''_1	4.5–5.6	>5

Seismic Cross-Section From Reflections

Correlation of the reflections was carried out in two stages; first, emphasis was placed on tracing correlated waves in reversed sections; second, more intensive phases were identified in unreversed sections. The waves identified in the first stage were the basis for determining the velocity section at greater depth. For that purpose, effective velocities were computed and the corresponding reflecting elements were constructed for all reversed time curves,

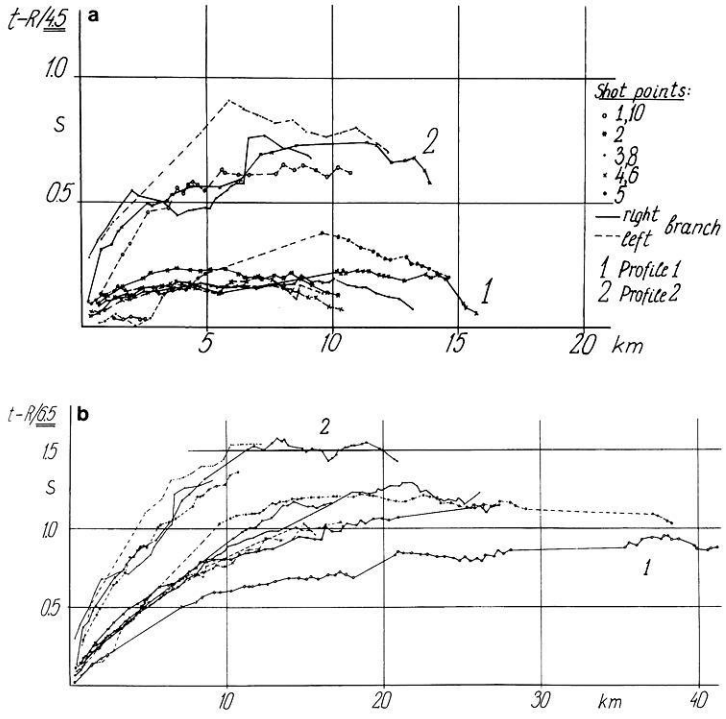

Fig. 6a and b. Travel-times of the first-arrival waves from all shot points on both profiles, with reduction velocities of (**a**) 4.5 km/s and (**b**) 6.5 km/s

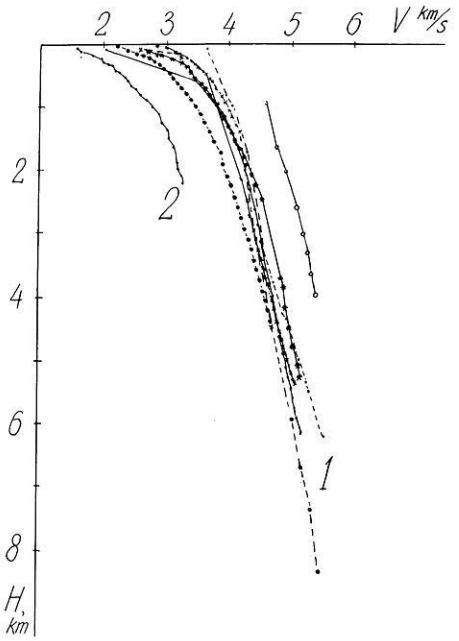

Fig. 7. Average velocities computed from the travel-time curves of refracted waves for different shot points (symbols as in Fig. 6)

then for the unreversed ones. The velocity section derived from the refractions was also taken into account. The reflectors were constructed by conventional methods with the use of reflection times and average velocities above (given in Fig. 8).

Discussion of the Results

The refraction cross-sections (Fig. 8) are in general agreement with previous models (Pálmason, 1971). The present observations give a more detailed picture. Velocities of 3.7 to 4.7 km/s are typical for the Tertiary flood basalts along Profile I, ranging in age from about 6 to 2 Ma. The highest velocities are found in the region of Borgarfjördur in the west, close to the Borgarfjördur anticlinal axis (Fig. 1). Along lake Skorradalsvatn (SP 2–4) the flood basalts are characterized by a general velocity increase with depth. High-velocity layers representing denser lava flows alternate with lower-velocity layers. The seismic layers dip toward the neovolcanic zone at 8°–9° in agreement with the dip of the surface flood basalts. At a depth of 1.5–2.5 km, seismic boundaries have a more gentle dip of up to 3° or 5°. East of Skorradalsvatn, 4.5–4.7 km/s boundaries have been traced, but with large gaps. This suggests a more complex geological structure, although the data are also more scanty.

In the flood basalt region a boundary was determined with a velocity of 6.5 km/s at a depth of 3–4 km. Such a boundary has been found all over Iceland (Pálmason, 1971). It has been suggested that this boundary in Iceland is related to a change in physical conditions in the crust and to a certain grade of metamorphism.

In the flood basalt area of Profile I, it is possible to identify several definite reflecting horizons which dip toward the active volcanic zone. Usually they can be traced from a depth of about 3–4 km, i.e., deeper than the refractor of 6 to 6.5 km/s. Their dip is steep, up to 30° and even more, at depths of 3 to 7 km. At greater depths the dips decrease to 20° and less. The deepest elements are traced to 16 or 20 km with dips not exceeding 10°. The most prominent reflecting horizon, traced under SP 3 at 11 km depth and under SP 2 at 6 km, may be exposed between Borgarfjördur and Skorradalsvatn, where also a change of velocity is found at the surface. East of Skorradalsvatn (SP 4–5) the reflectors are less regular and considerably less steep; this may indicate a more complicated geological structure, but may also be an artefact of the methods used (end of profile, breaks in observations). Diffracting zones are typical for this part, and reflecting elements have very steep dips indicating fractures and lateral structures.

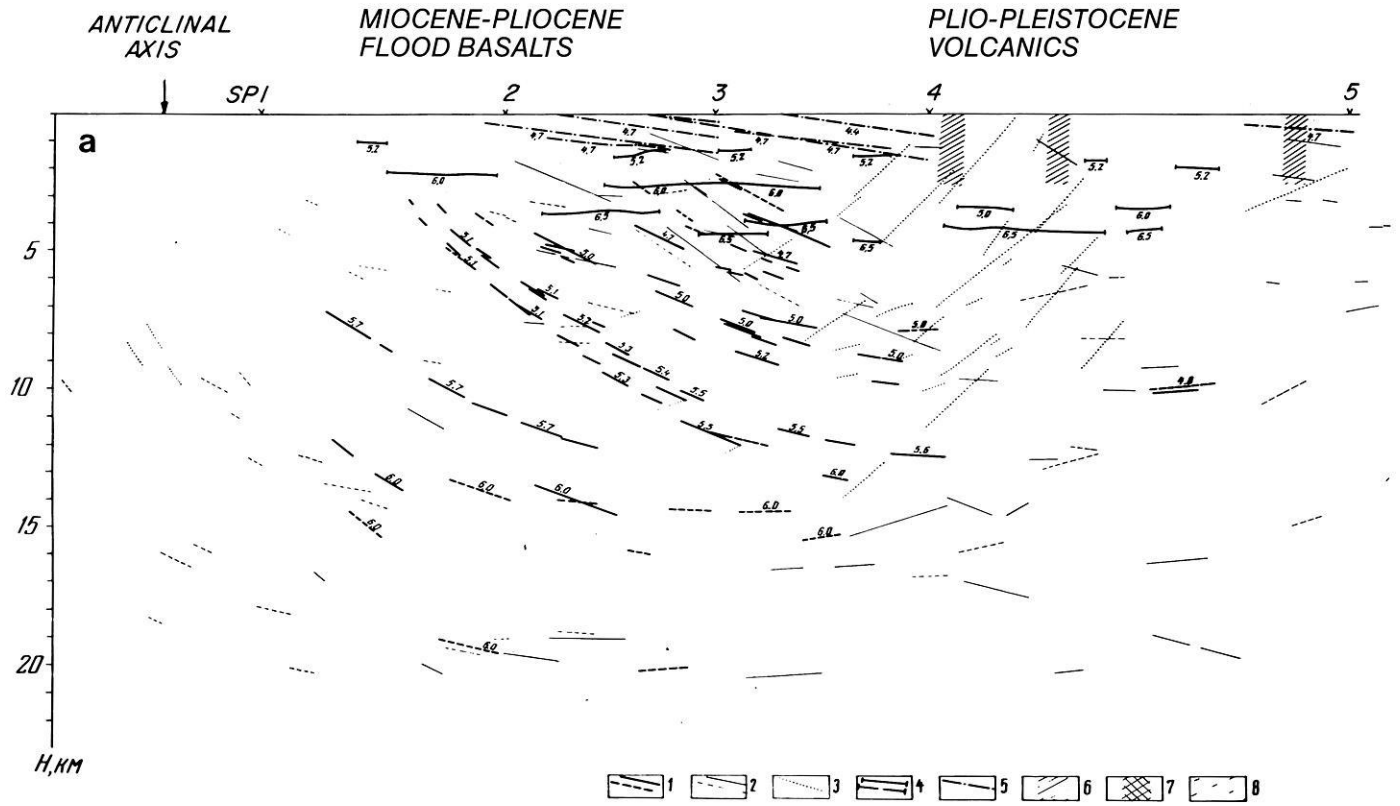

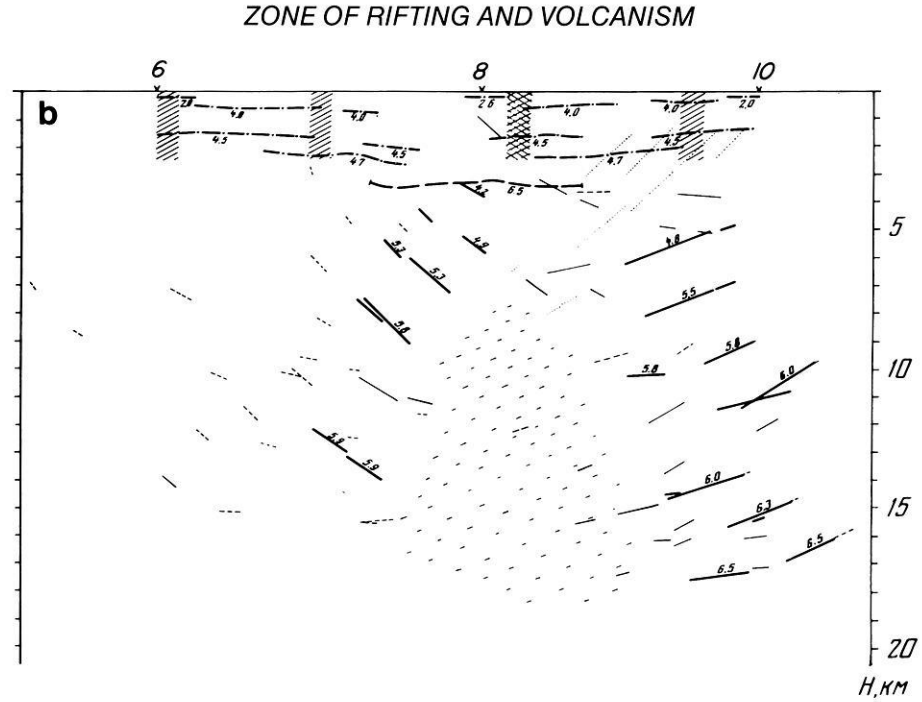

Fig. 8a and b. Seismic cross sections: **a** Profile I and **b** Profile II. *Legend:1* and *2*: reflecting horizons constructed from the travel-time curves, checked in reversal points (*1*) and from single curves (*2*); the *dotted lines* indicate less reliable data; the *numbers* are computed average velocities in overlying section; *3*: steeply dipping reflectors, in some cases probably laterally displaced from section; *4*: refractors constructed from reversed curves (*solid lines*) or single curves (*dashed lines*); the numbers are boundary velocities; *5*: refractors probably connected with geological horizons; *6* and *7*: fracture zones derived from diffraction points and confirmed by geological observations **non**active (*6*) and active (*7*) in Holocene time; *8*: body with homogeneous seismic property, probably a region of melting temperature

In the active volcanic zone the reflecting horizons dip at steep angles of 25°–30° toward the axis near SP 8. This axial region is slightly displaced eastward from that defined by the refractors.

It may be assumed that the reflectors are boundaries between lava flows and other strata in the basalt series, such as compositional boundaries, fault zones, dykes, intrusive sheets, and metamorphic boundaries. The impedance change across these boundaries gives rise to the reflections. The average elastic properties of the rocks in the cross-section, nevertheless, vary only gradually as the result of compaction caused by pressure, heating, and hydro-

Table 2. Boundary parameters (V_b, ϕ, h) computed from single travel-time curves of refracted waves

Number on travel-time curves	Shot point	Distance on record-section (in 100 m)	Input data for computation		Results			
					$\bar{V}$ km/s	V_b km/s	Dip degrees	h km
1	4	91.5–172.5	$t_0 = 0.25$ s $X_k = 5.4$ km	$V^* = 5.0$ km/s	3.7	4.4	8	0.76
2	3	120.5–133.5	$t_0 = 0.1$ s	$V^* = 4.8$ km/s $V^*_{rev} = 4.4$ km/s	3.44	4.6	3.5	0.26
3	4	120.5–149.5	$t_0 = 0.49$ s $V^* = 5.3$ km/s	$t_{ip} = 1.31$ s $X_k = 10.3$ km	3.96 4.0	4.7	9–10	1.6
4	3	85.0–103.5	$V^* = 4.7$ km/s $t_{ip} = 0.68$ s	$X_k = 5.75$ km	3.64 3.62	4.3	8	0.8
5	2 3	131 –148 56.5– 73	$V^* = 4.5$ km/s $V^* = 5.4$ km/s		3.93	 4.7	 7	 1.34
6	5	340 –360	$t_0 = 0.23$ s	$V^* = 4.9$ km/s	3.47	4.6 4.7	4 2.5	0.61 0.59

Computation formulas: $t_{ip} = \frac{2 \cdot h \cdot \cos\phi}{\bar{V} \cdot \cos(i \mp \phi)}$; $t_0 = \frac{2 \cdot h \cdot \cos i}{\bar{V}}$; $V^* = \frac{\bar{V}}{\sin(i \mp \phi)}$

$\tan\phi = \frac{h}{X_k}$; $\sin i = \frac{\bar{V}}{V_b}$

V = Boundary velocity; ϕ = Dip angle; h = Depth

thermal alteration. These processes have a more regional character and lead to more regular refraction than the smaller reflecting elements. The medium containing the reflectors is characterized by velocities of the refracted waves not greater than 7–7.1 km/s, as indicated by the interpretation by G.A. Krasilschikova (personal communication) of a 200 km refraction profile extending our Profiles I and II to the east (W.R. Jacoby, H. Gebrande, and H. Miller, personal communication).

The generalized seismic cross-section of Fig. 8 shows the refracting and the reflecting elements. The faults shown schematically are based on geological data and diffractions. The regular pattern of reflectors in the central part of Profile I (SP 2–4) changes eastward to a complicated zone with more sub-vertical boundaries near the surface and sub-horizontal reflectors at depth.

The axial region of the rift zone is characterized by a depression in the layers with typical flood basalt velocities; the depression is filled with recent low-velocity volcanics. At greater depths reflectors dip steeply toward the axis. In the central part of the active zone, reflecting horizons are absent suggesting homogeneity in physical properties below 8 km depth. This region may be in the state of partial melting or a magma chamber The inclined reflectors on both sides may be intrusive sheets as suggested by Walker (1975) to be important in the lower crust, and as commonly found in the shallow roots of central volcanoes (e.g. Fridleifsson, 1977). The inclined reflectors could also be lavas sagging down above a magma chamber, but it seems unlikely that the deeper reflectors are lavas, since the present rate of volcanism is equivalent to a total lava layer of only some 6–7 km thickness. A similar reasoning may be applied to the deeper reflectors of Profile I along the flood basalts to the west. About 15 km southwest of the suggested magma region was a magneto-telluric station of Hermance and Grillot (1970; 1974); they estimated, on the basis of their observations, that the temperature at 10 km depth should be 800°–1 200° C.

The cross-section of the present study bears a certain resemblance to the crustal structure deduced by Bodvarsson and Walker (1964) on the basis of observations in eastern Iceland. It is also similar to the model of Pálmason (1973, 1980) based on the same data. In particular, these authors predicted the dip of the flood basalts and the presence of a region of partial melting at relatively shallow depth beneath the axial rift zone. These predictions seem to be borne out by the present results.

Acknowledgements. The seismic studies in 1976 were carried out by the Geodynamic Expedition of the USSR Academy of Sciences jointly with the Geothermal Division of the National Energy Authority of Iceland (Orkustofnun). Competent and very helpful assistance in conducting the seismic studies was rendered by Professor V V Beloussov, Corresponding Member of the USSR Academy of Sciences. Beside the authors, the following did the seismic field work. N.V Kondratyev, A.V Konoplev, Y.M. Misnik (Leningrad Mining Institute); N.I. Pavlenkova, V V Knyazev, B.I. Kerby, L.V Nikitin (Institute of Physics of the Earth, USSR Academy of Sciences); an active part was taken by S. Sigurmundsson and G. Petursson (Orkustofnun); much help was rendered by A.A. Krasnov, B.G. Polyak, E.A. Vakin, and V.I. Kononov. E.E. Milanovsky and M.A. Akhmetjev conducted the geological studies of the profiles. K. Saemundsson provided the geological data of Fig. 1. The assistance of all the above colleagues is gratefully acknowledged.

References

Beloussov, V V., Milanovsky, Ye.Ye.. On tectonics and tectonic position of Iceland. Tectonophysics **37**, 25–40, 1977

Bodvarsson, G., Walker, G.P.L.: Crustal drift in Iceland. Geophys. J.R. Astron. Soc. **8**, 285–300, 1964

Chibisov, S.V The interpretation of travel-time curves of elastic waves for plane-layered media (in Russian). J. Geophysic, **4**, (2), 1934

Einarsson, Tr.· Remarks on crustal structure in Iceland. Geophys. J.R. Astron. Soc. **10**, 283–288, 1965

Fridleifsson, I.B. Distribution of large basaltic intrusions in the Icelandic crust and the nature of the layer 2 – layer 3 boundary. Geol. Soc. Am. Bull. **88**, 1689–1693, 1977

Hermance, J.F., Grillot, L.R. Correlation of magnetotelluric, seismic and temperature data from southwest Iceland. J. Geophys. Res. **75**, 6582–6591, 1970

Hermance, J.F., Grillot, L.R.. Constraints on temperatures beneath Iceland from magnetotelluric data. Phys. Earth Planet. Int. **8**, 1–12, 1974

Litvinenko, I.V . Seismic methods of studying the complex structure of the upper part of the continental crust. Notes of the Leningrad Mining Institute, V.XI (2), 1971

Pálmason, G. Crustal structure of Iceland from explosion seismology. Rit 40, Soc. Sci. Islandica, 187 pp., 1971

Pálmason, G.: Kinematics and heat flow in a volcanic rift zone, with application to Iceland. Geophys. J.R. Astron. Soc. **33**, 451–481, 1973

Pálmason, G. A continuum model of crustal generation in Iceland; kinematic aspects. J. Geophys. **47**, 7–18, 1980

Pálmason, G., Arnórsson, S., Fridleifsson, I.B., Kristmannsdóttir, H., Saemundsson, K., Stefansson, V., Steingrímsson, B., Tómasson, J., Kristjánsson, L.· The Iceland crust: Evidence from drillhole data on structure and processes. In. Deep Drilling Results in the Atlantic Ocean: Ocean Crust. M. Talwani, C.G. Harrison, D.E. Hayes eds. Am. Geophys. Union, Maurice Ewing Series **2**, 43–65, 1979

Pálmason, G., Saemundsson, K.· Iceland in relation to the Mid-Atlantic Ridge. Annu. Rev. Earth Planet. Sci. **2**, 25–50, 1974

Riznichenko, Yu.V . Geometrical seismology of stratified media (in Russian). Proc. Inst. Theor. Geophys. II, 1946

Walker, G.P.L.. Zeolite zones and dyke distribution in relation to the structure of the basalts in eastern Iceland. J. Geol. **68**, 515–528, 1960

Walker, G.P.L.: Intrusive sheet swarms and the identity of crustal layer 3 in Iceland. J. Geol. Soc. London **131**, 143–161, 1975

Received March 19, 1979; Revised Version September 26, 1979

J. Geophys. 47, 211–220, 1980

Journal of Geophysics

Seismic Structure of the Icelandic Crust Above Layer Three and the Relation Between Body Wave Velocity and the Alteration of the Basaltic Crust

Ó.G. Flóvenz
Seismological Observatory, University of Bergen, Allegate 41, 5014 Bergen-U, Norway

Abstract. Seismic refraction profiles from Iceland are studied with the aid of synthetic seismograms. The classical layered model of the Icelandic crust is shown to be an unacceptable interpretation of the available data. This is because the layered model does not satisfy the observed amplitude variation. On the other hand, a model which assumes continuously increasing velocity with depth does not contradict the observations and is therefore acceptable although it is not the only possible interpretation. The model represented here shows that the surface value of the *P*-velocity is variable from 2.0 km/s to 5.0 km/s, depending primarily on the degree of metamorphism. The *P*-velocity increases rapidly with depth in the velocity interval 2.0–3.5 km/s followed by an approximately constant gradient of about 0.57 s^{-1} This constant gradient continues down to the 6.5 km/s isovelocity surface below which the *P*-velocity becomes nearly constant. In view of this, it is more reasonable to divide the Icelandic crust into two parts: the upper crust with velocity continuously increasing with depth (corresponding to layers 0, 1, 2 in the layered model) and the lower crust with almost constant velocity (corresponding to layer 3 in the layered model). The depth to the lower crust is variable and depends on how deep the crust is eroded. A typical depth to the lower crust is 5–6 km for an uneroded basalt pile but can be considerable less where the basalt pile is deeply eroded, especially below extinct central volcanoes.

Key words: Seismic refraction – Synthetic seismograms – Poisson's ratio – Amygdale minerals – Crustal structure – Iceland.

Introduction

During the past few decades the classical method in interpreting seismic refraction data has been to assume layers of constant properties and to compute velocities and depth to the boundaries. By this method one has deduced the classical three-layer models of the oceanic and the Icelandic crust.

In the last few years several authors have pointed out the lack of uniqueness in this method. Because of measurement errors, it is not possible to decide whether the travel time curves are slightly curved or made up of straight line segments. It is therefore not possible, by the use of travel time diagrams for first arrivals only, to decide whether the velocity varies continuously with depth or in jumps.

Present address. National Energy Authority, Grensásv. 9, 108 Reykjavík, Iceland

Table 1. Layered seismic structure of the Iceland crust after Pálmason (1963, 1971)

Layer No.	*P*-velocity km/s	*S*-velocity km/s	Poisson's ratio	Density g/cm^3
0	2.75			2.1–2.5
1	4.14	2.34	0.270	2.6
2	5.08	2.78	0.278	2.65
3	6.50	3.53	0.269	2.9
4 (Mantle)	7.20			3.1

Kennett and Orcutt (1976) have applied systematic inversion techniques to marine refraction profiles and they conclude that layer two is a region of strong velocity gradients, while layer three is relatively homogeneous. Lewis (1978) has concluded that the commonly assumed layerd model of the oceanic crust is an artifact of the method of data interpretation.

There is, however, more information than merely first arrivals to be had from a seismogram. By use of secondary arrivals such as wide-angle reflections and amplitude data it should be possible to discriminate to a certain extent between the various models. Use of synthetic seismograms is a powerful tool in such studies.

Båth (1960), Tryggvason and Båth (1961), and Pálmason (1963; 1971) have studied in Icelandic crust by refraction seismology and deduced the layering of the Icelandic crust. Pálmason's work includes studies of more than 80 refraction profiles distributed over Iceland. He concludes that the Icelandic crust consist of four seismic layers underlain by mantle with an anomalously low *P*-wave velocity of 7.2 km/s (Table 1).

Analysis of Seismic Refraction Profiles From Iceland

In order to determine whether or not the Icelandic crust is made up of homogeneous seismic layers, I have used some carefully chosen profiles from Pálmason's (1971) together with one new profile, and have made synthetic seismograms for various models. The profiles have been chosen so that they follow regional geological strike and are not interrupted by central volcanoes. This is done to minimize the possibility of lateral velocity variations in the direction of the profile. The field work and instrumentation involved in these measurements are described by Båth (1960) and Pálmason (1971). It is worth noting here that the recording was made on photographic paper and that the paper velocity was not the same for individual records within the same profile. I

0340-062X/80/0047/0211/$02.00

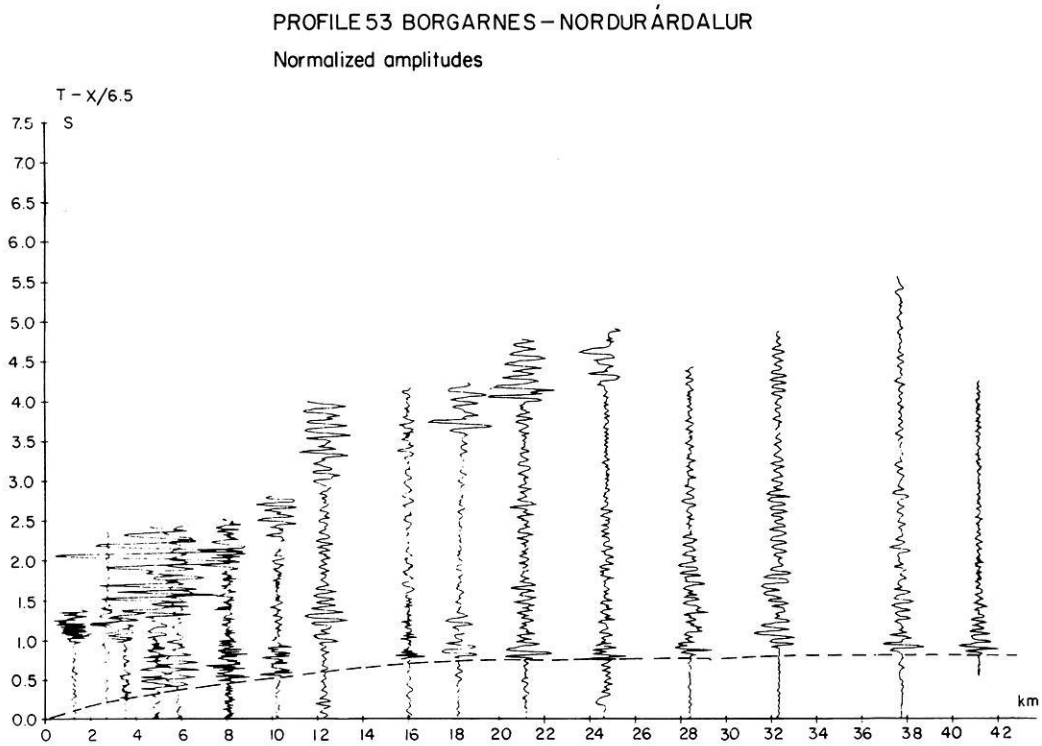

Fig. 1. The seismic record section for Profile 53

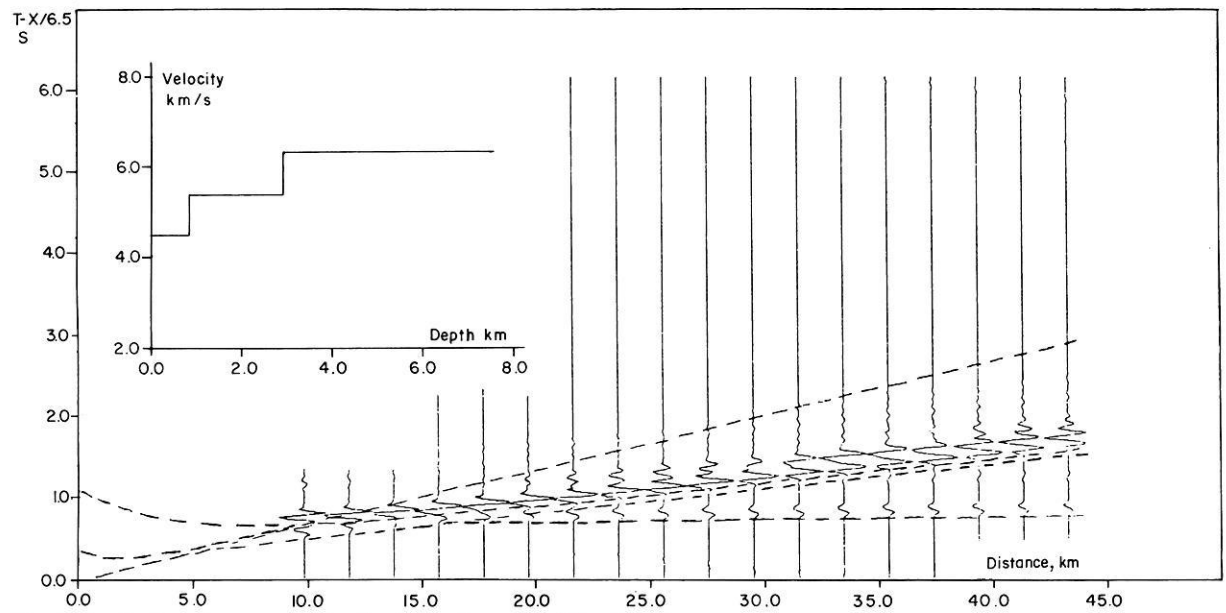

Fig. 2. Synthetic seismograms for the layered model of Profile 53

have therefore digitized the records from the photographic paper and plotted them with aid of a computer. In doing so the seismograms lose some of their characteristics.

For producing synthetic seismograms, I have used a computer program by Mykkeltveit (1978) based on a paper by Fuchs and Müller (1971). I have concentrated mainly on two possibilities: the layered model and a model based on continuously increasing velocity with depth. To deduce the latter model, I have used a computer program by Berge (1976). This program makes use of the Wiechert-Herglotz formula

$$R \cdot \ln\left(\frac{R}{R-z_p}\right) = \frac{1}{\pi}\int_0^{\Delta p} \cosh^{-1}\left(\frac{v_p}{v}\right) d\Delta$$

where R is the radius of the earth, Δp is the distance to the point on the travel-time curve where the apparent velocity is v_p; v_p is the apparent velocity for the ray for which one shall compute the greatest depth of penetration, v is the apparent velocity along the profile and z_p is the maximum depth of penetration of a ray which is recorded in the distance Δp from the shot point.

In computing the synthetic seismograms for a model with continuously increasing velocity with depth, I have assumed the den-

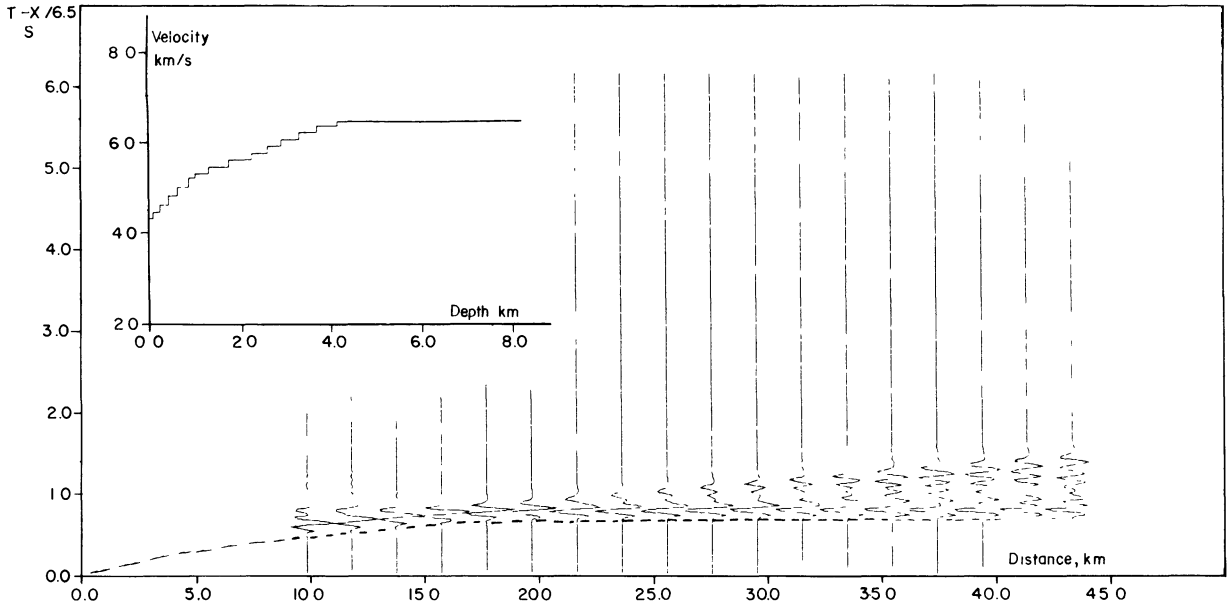

Fig. 3. Synthetic seismograms for a model of Profile 53, based on the Wiechert-Herglotz method

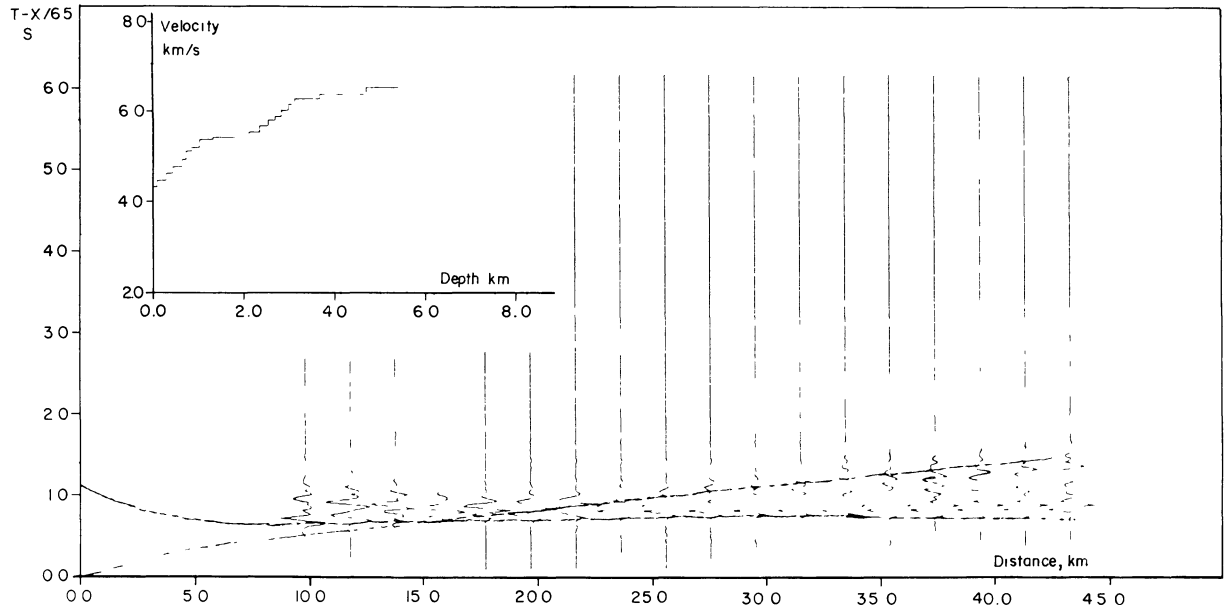

Fig. 4. The same as Fig. 3 except that there is a 0.8-km-thick constant-velocity layer within the upper crust

sity to be 2.60 g/cm^3 for rocks with *P*-velocities around 3.0 km/s, 2.65 g/cm^3 for rocks with velocity 5.0 km/s, 2.90 g/cm^3 for layer three (6.5 km/s) and interpolated linearly between them. These density below Moho is taken to be 3.1 g/cm^3 These values are based on Pálmason's (1971) estimate for the layered model and may be inaccurate. This will, however, not affect the synthetic seismograms seriously because they are not very sensitive to density.

Because of variations in charge size and magnification, and because the geophones were moved between each shot and the attenuation is unknown, I have used mainly synthetic seismograms with normalized amplitudes. It is possible, therefore, to compare the amplitudes within each trace but not to compare individual recordings. I have analysed six seismic refraction profiles from various geological provinces of Iceland. Two of them are described in this paper but the others are discussed in my thesis (Flóvenz, 1979). These two are profiles Nos. 53 and 1 of Pálmason (1971).

Profile 53, Borgarnes – Norðurárdalur, runs northeast from the village Borgarnes in the Tertiary basalt region of western Iceland. The age of the basalt is 6.2–7.0 Ma in Norðurárdalur (McDougall et al., 1977). The shot point is close to the coast. Figure 1 shows the seismic record section. The most characteristic feature of this profile is the relatively large amplitudes of the first arrivals compared with secondary amplitudes and it seems to be difficult to find systematic later arrivals. The travel-time curve for first arrivals can be considered to be composed of either three straight lines or of a curved line from the origin to approximately 6.5 km/s apparent velocity, from where it continues as a straight line. The first mentioned possibility leads to a layered

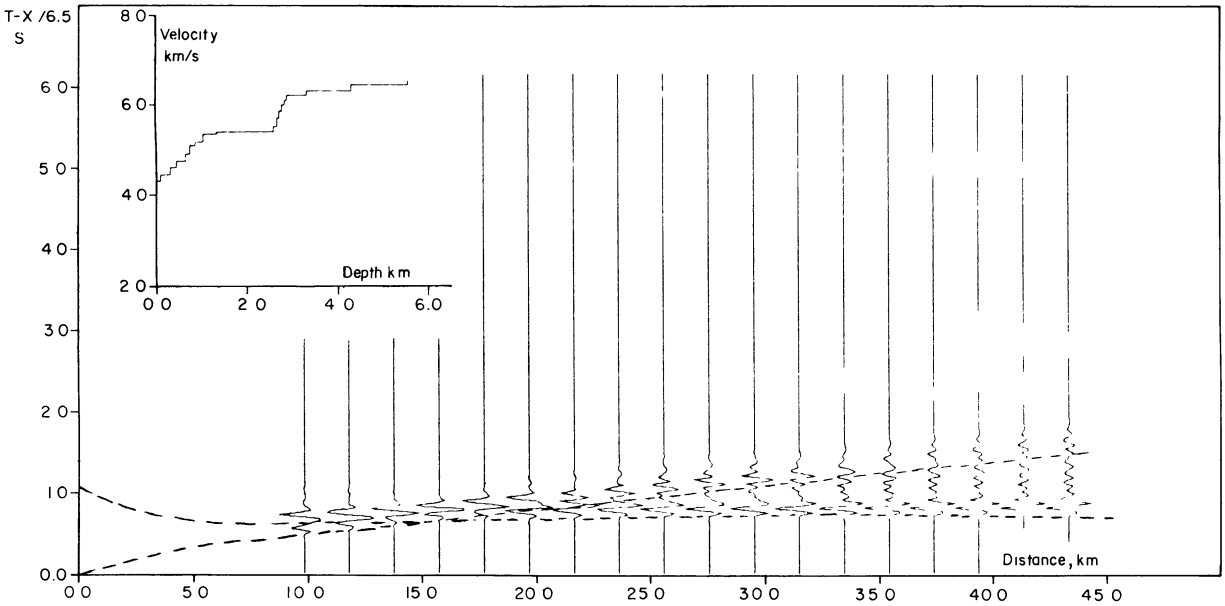

Fig. 5. The same as Fig. 4 but the constant velocity layer is now 1.3 km thick

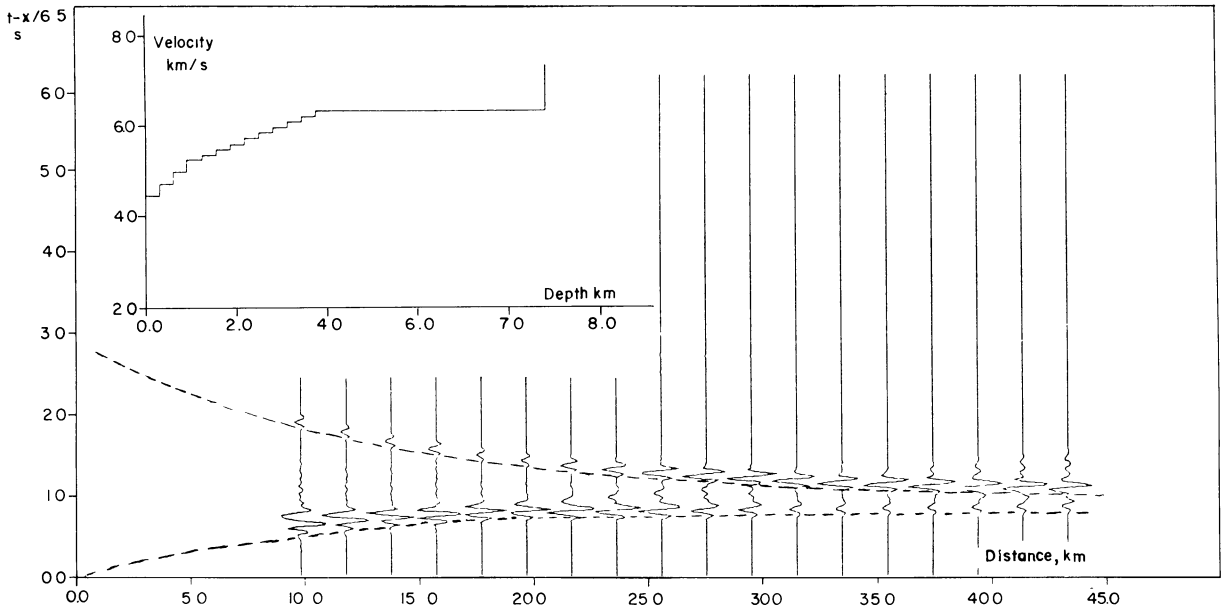

Fig. 6. The same as Fig. 3 except that the Moho is assumed to lie at 9 km depth

model. Figures 2 and 3 show synthetic seismograms for the layered model and a model which assumes continuously increasing velocity with depth.

It is immediately obvious from these figures that the layered model is not an acceptable interpretation of the data. In this model the amplitudes of the waves reflected at wide angles from the layer 2 – layer 3 boundary are much stronger than the refracted ones. These reflections are absent in the observations. On the contrary, the energy is concentrated in the first arrivals for the continuously-increasing velocity model; this bears much more resemblance to the observation.

The travel-time diagram in Fig. 1 is clearly curved at the beginning but over a short interval it approches a straight line with the apparent velocity of 5.4 km/s. It is possible that this part of the curve represents an interval of constant velocity within the crust. Figures 4 and 5 show synthetic seismograms for such models with a 0.8 km and 1.3-km-thick constant velocity layer, respectively. On these seismograms the energy is concentrated in the beginning of each signal just as on the observations. As the constant-velocity layer becomes thicker the velocity gradient between it and layer 3 becomes large enough to give triplication of the travel time curve, resulting in stronger secondary arrivals with an apparent velocity of around 5.5 km/s. As the velocity gradient increases further the amplitude of these secondary arrivals increases and should be detectable in the observations. But the observations do not show such secondary arrivals. It is possible, however that interference with possible bubble pulses can destroy these arrivals.

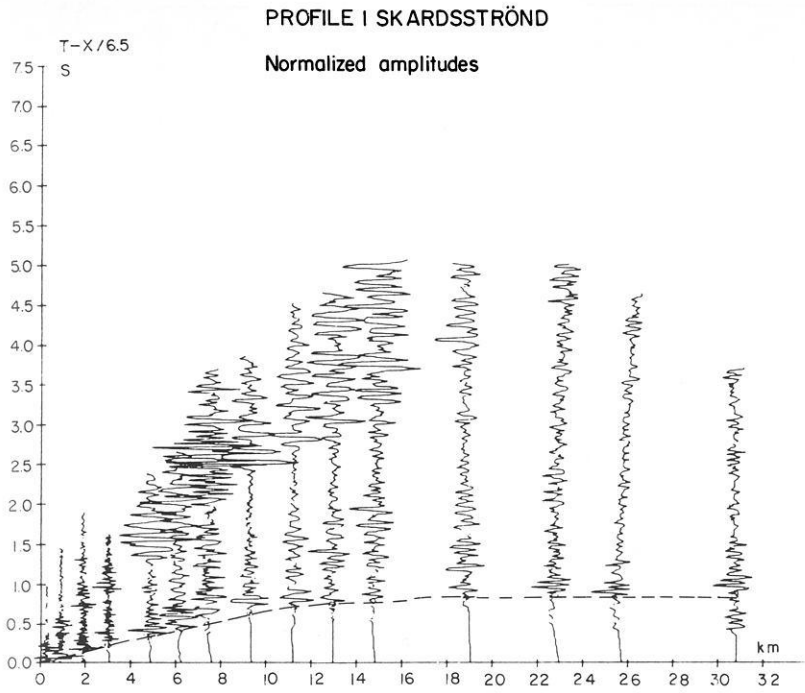

Fig. 7. The seismic record section for Profile 1

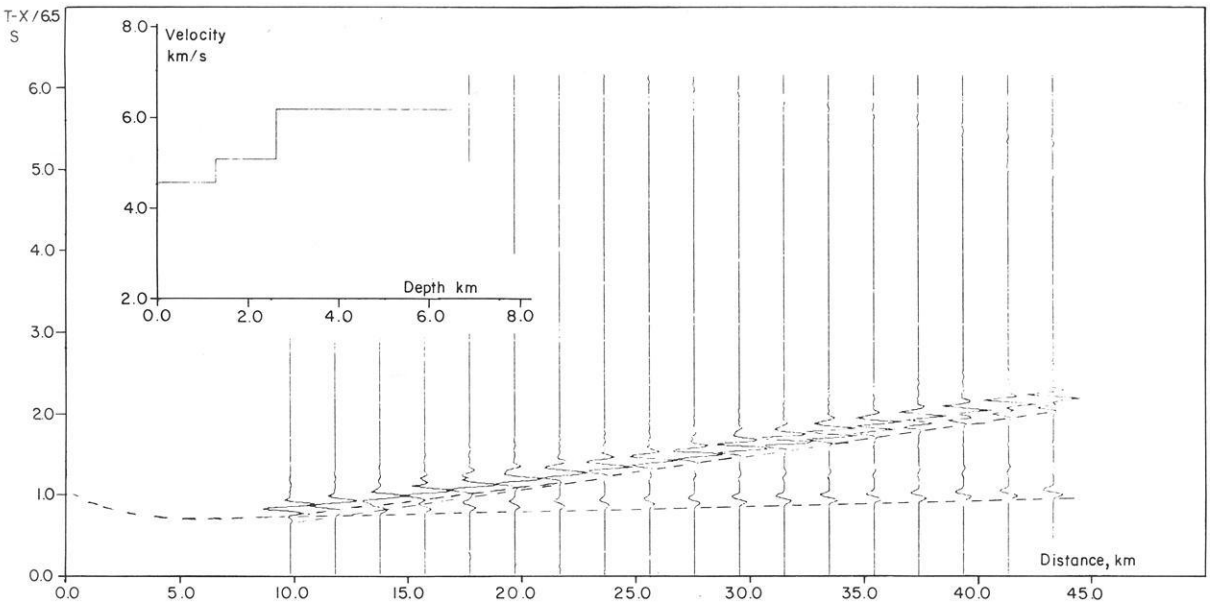

Fig. 8. Synthetic seismograms for the layered model of Profile 1

This profile is too short for recognizing critically refracted waves from the Moho as first arrivals. However, if the Moho discontinuity lies at about 9 km depth as Pálmason (1971) indicates, it is supposed to give rise to wide-angle reflections. Figure 6 shows synthetic seismograms for the model with continuously increasing velocity down to layer three and the Moho discontinuity at 9 km depth. These indicate that wide-angle Moho reflections should be recognizable from around 25 km shot point distance. The observations (Fig. 1) show no such reflections indicating that the Moho must be at a greater depth or be absent as a velocity discontinuity under the profile.

One can therefore conclude from this profile that the velocity increases continuously with depth at least down to the 5.4 km/s isovelocity surface. Below this surface the velocity either takes a constant value over a certain interval and increases after that rapidly to 6.5 km/s in layer 3, or the velocity increases continuously with depth down to layer 3 which seems more likely.

Profile 1 (Skardsströnd) runs northeastwards along the direction of strike on the south coast of Gilsfjörður in western Iceland, a region somewhat older ($\sim$10 Ma) than Borgarfjörður. Figure 7 shows the observations and Figs. 8 and 9 show the synthetic seismograms based on the layered and the continuous-velocity depth models, respectively. As for the previously discussed profile, the amplitudes of the first arrivals are usually the strongest except between 12 and 20 km shot point distance. There is however no regularity to be seen in the secondary arrivals. The synthetic seis-

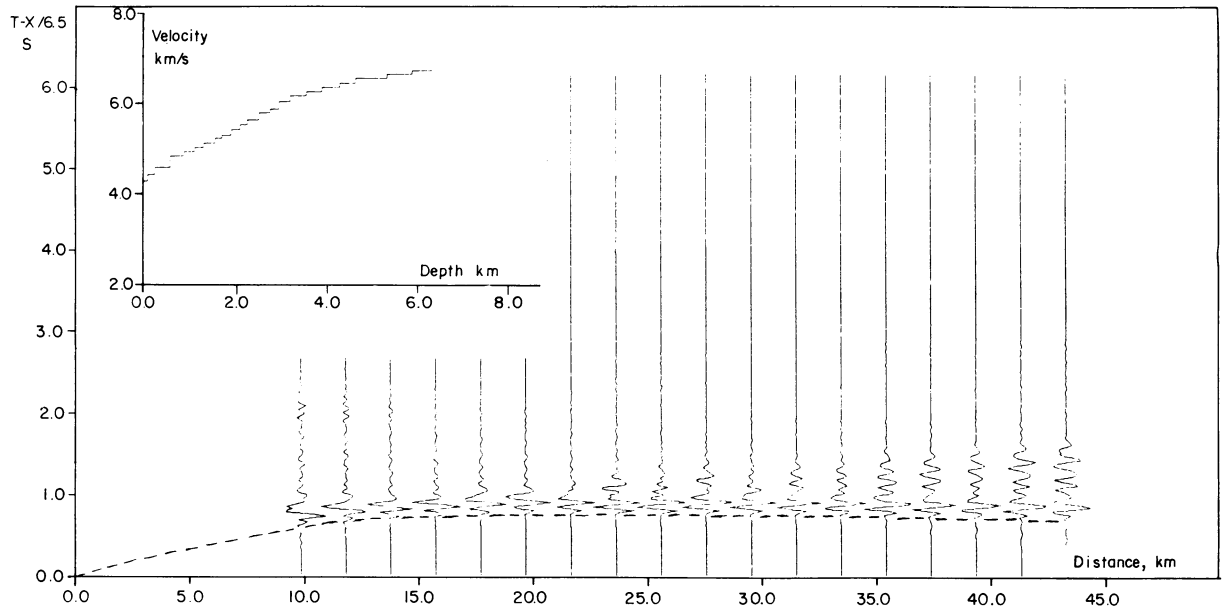

Fig. 9. Synthetic seismograms for a model of Profile 1 which assumes continuously increasing velocity with depth

Table 2. Thicknesses of Zeolite zones in Iceland After Walker (1974)

Types of zeolites	Thickness of each zeolite zone in m
No zeolites	150
Chabasite and thomsonite	450
Analsite	150
Mesolite and scolesite	900
Laumontite	1,400

mograms for the layered model show that a velocity discontinuity between layer two and three should result in much stronger amplitudes for the wide-angle reflections than for the first arrivals. This shows that the layered model is not consistent with the observations. The amplitude distribution for the model which assumes continuously increasing velocity with depth bears more similarity to the observations than the layered model and is therefore the preferable interpretation. It is possible, however, that the velocity can take a constant value over a certain depth interval. The travel-time curve has a fairly constant slope between 5 and 11 km shot point distance with an apparent velocity close to 4.7 km/s. On the basis of these observations alone, it is not possible to prove or disprove the existence of such a constant-velocity layer.

The conclusions that can be drawn from these profiles and the four others which are discussed in my theses (Flóvenz, 1979) are as follows: Both the layered model and the continuously-increasing velocity-depth model do satisfy the travel time curve for first arrivals but the latter better explains the energy distribution in the seismograms. This means that the layered model is generally not an acceptable interpretation of seismic refraction profiles in Iceland. This does not mean, however, that the continuously increasing velocity-depht model is correct, it is only a model that better fits the observations. It is, for instance, possible that the velocity takes a constant value over a limited range of depth. In the six profiles there are no signs of such a constant velocity zone but the available data are not good enough to disprove the existence of constant velocity layers.

In view of the conclusions drawn above, and the fact that these conclusions are based on profiles from all the main geological provinces of Iceland, it is reasonable to re-interpret all the seismic refraction profiles from Iceland by the use of the Wiechert-Herglotz method. This will give a more realistic picture of the Icelandic crust than the layered model. This has been done (Flóvenz, 1979) and the main results are outlined below.

Re-Interpretation of Published Data and the Relationship Between Body Wave Velocity and Alteration of the Basalt

I have re-interpreted about 70 of the 80 profiles described by Pálmason (1971). The position and direction of the profiles are shown on Figs. 1 and 2 of Pálmason (1971). For all these profiles the *P*-velocity distribution has been calculated, and where *S*-waves are available the *S*-wave velocity and Poisson's ratio has been calculated as a function of depth.

The body wave velocities at the surface vary greatly from one profile to another. The lowest *P*-wave velocity in the Icelandic basalt at the surface is slightly more than 2.0 km/s and the highest values are around 5.0 km/s. The surface velocity is lowest in the neovolcanic zone and becomes progressively greater away from it. In most of the profiles the *P*-wave velocity increases very rapidly with depth in the range 2.0 km/s to 3.5 km/s, followed by an approximately constant gradient of about 0.57 s^{-1}. This constant gradient continues down to the 6.5 km/s isovelocity surface below which the velocity becomes nearly constant. The *S*-wave velocity shows similar variations with depth.

The main geological and geophysical structure of Iceland is summarized by Pálmason and Sæmundsson (1974). Pálmason (1973) has calculated the trajectories of a lava element which reaches the surface in the neovolcanic zone. The resultant movement of such an element after it has been cooled on the surface

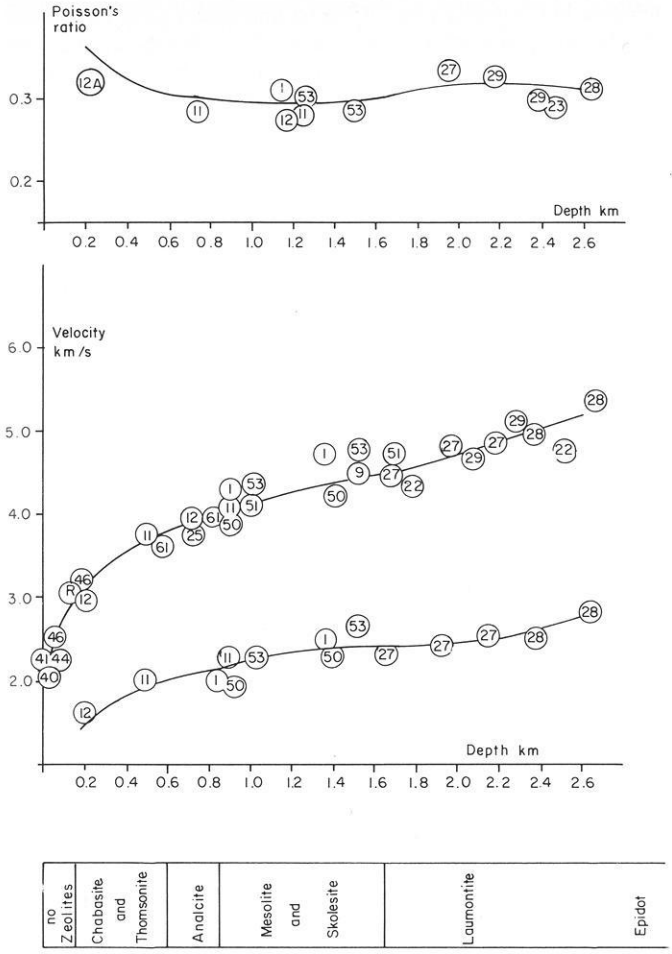

Fig. 10. The *P*- and *S*-wave velocity and Poisson's ratio as function of the alteration of the basalts based on surface values of these parameters. By assuming the thickness of the zeolite zones as given by Walker (1974) and Pálmason et al. (1978) this is equivalent to a plot of *P*- and *S*-wave velocities and Poisson's ratio versus depth in an uneroded basaltic crust, provided that the direct effect of themperature and pressure can be negledted

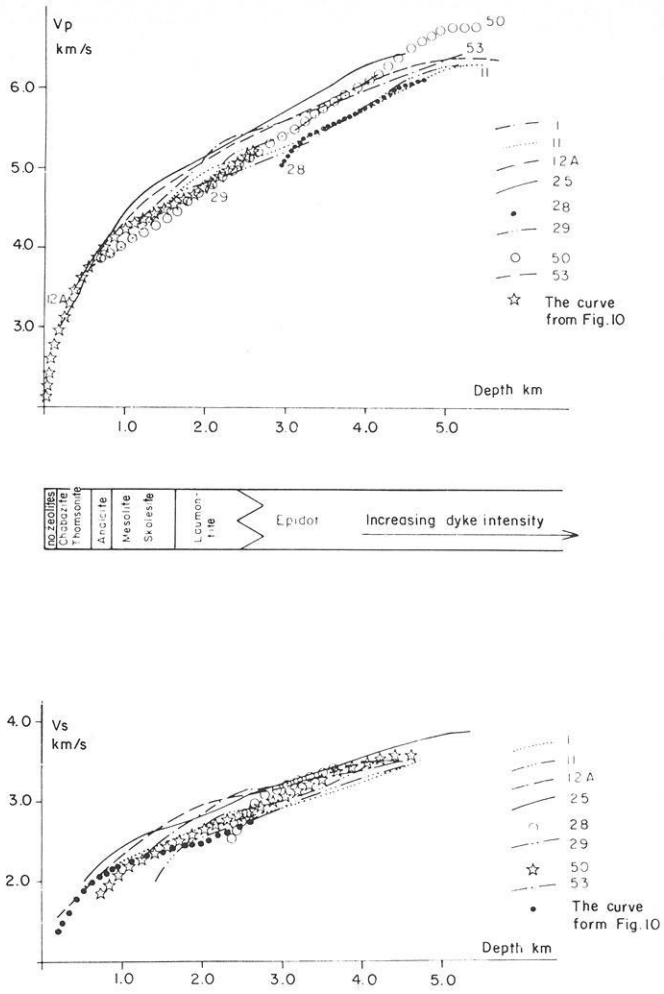

Fig. 11. The *P*- and *S*-wave velocity as function of depth in an uneroded basaltic crust. The figure is based on interpretation of profiles from different geological provinces in Iceland. Each profile is interpretated by the Wiechert-Herglotz method and brought to its relative depth in the uneroded crust as predicted by the zeolite zones. The curve on the *P*-wave figure (*asterixes*) and that one on the *S*-wave figure (*black circles*) are those of Fig. 10

is composed of a downward component of movement as a result of sagging and a lateral component prependicular to the rift zone as a result of ocean-floor spreading. As the lava element subsides it becomes reheated and some metamorphism occurs. As a result of Pleistocene glacial erosion and subsequent uplift due to isostatic adjustment, elements which have been buried down to a depth of 2 km are brought to the surface on both sides of the neovolcanic zone. Walker (1974) has studied the metamorphism produced in this manner in the basalt lavas in eastern Iceland. The low degree of metamorphism in the Icelandic crust is best described in terms of the formation of amygdale minerals. Walker (1974) has calculated the average thickness of the various zeolite zones in the plateau basalt of eastern Iceland (Table 2). Observations from Eyjafjörður in northern Iceland give similar results (Pálmason et al., 1978).

The various degrees of metamorphism near shot points on the seismic refraction profiles can be used to derive a relationship between the low-grade metamophism of the basalt and the body-wave velocity. These results are represented in Fig. 10. The surface is more or less an isotherm and an isobar. The alteration of the basalt should therefore be the only factor which influences the body-wave velocities there. As an example of how the curve is constructed, I take Profile 11. Geological evidence shows that the shot point for this profile is in the lowest part of the chabasite-thomsonite zeolite zone. This corresponds to about 0.5 km depth in the original crust (Table 2). The value of the apparent *P*-wave velocity for the direct wave to the nearest geophones is 3.7 km/s. This represents the *P*-velocity at 0.5 km depth in an uneroded basaltic crust, provided that direct effects of pressure and temperature on the body-wave velocity are small at shallow depts. By use of profiles with shot points in basalt at various stages of alteration it has been possible to construct a typical velocity-depth curve for body waves in the topmost 2.5 km in the Icelandic crust. In addition to the surface values, I have used the value of the velocity at 0.25 km depth from each profile to avoid the possibility of systematic error due to weathering. The use of these values gives the same results as the surface values. It is clear from Fig. 10 that there is no evidence for a discontinuity in the

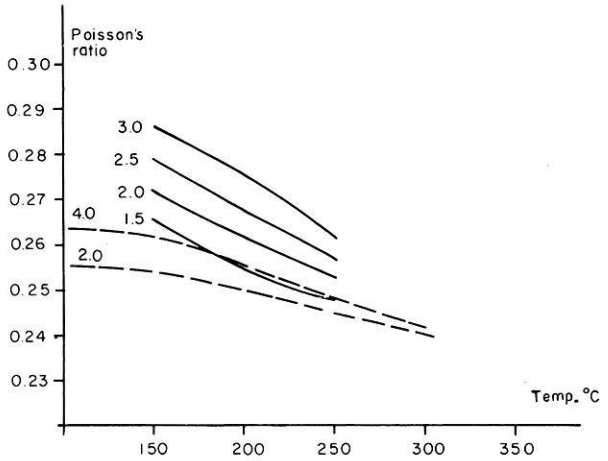

Fig. 12. The relation between Poisson's ratio and temperature for constant depth (pressure) in the Icelandic crust, based on seismic refraction measurements. The *broken lines* are the results of laboratory measurements by Hughes and Maurette (1957)

velocity-depth distribution of *P*- and *S*-waves down to the 5.0 km/s isovelocity surface for *P*-waves and 2.7 km/s for *S*-waves. This curve is constructed without any assumption as to how the velocity varies with depth. It lends firm support to the results abtained above from amplitude studies, namely that the velocity increases continuously with depth at least down to the 5.0 km/s isovelocity surface for *P*-waves.

It is possible to deduce the typical velocity-depth structure for body waves in an uneroded Icelandic basalt crust by taking the velocity-depth curves obtained by the Wiechert-Herglotz method for various profiles and displacing the individual curves to their original positions in the crust as predicted by the zeolites. This has been done in Fig. 11 for eight profiles from various geological provinces in Iceland. The curves overlap and make a narrow velocity-depth band. On the same figure the curve from Fig. 10, based on surface values only, has been plotted. This curve falls within the velocity-depth distribution obtained by use of the Wiechert-Herglotz method an gives almost the same structure. This proves the validity of using the Wiechert-Herglotz method in interpreting seismic refraction profiles from Iceland at least down to the 5.0 km/s surface for *P*-waves. What happens below this surface is not clear but there are no arguments against the idea that the velocity further increases continously with depth to layer 3. This cannot be proved, however, by the available data, and a detailed seismic profile would probably be necessary to demonstrate this.

The Relation Between Poisson's Ratio and Temperature

The body wave velocities in the Icelandic crust depend mostly on the low grade metamorphism but also on temperature and pressure. Varying dyke intensity is also likely to influence the velocities. It is, however, of no importance here because the increasing dyke intensity with depth is incorporated in the curves of body wave velocity with alteration. It is difficult to separate these factors. On the other hand, the Poisson's ratio measured at the surface shows small variations with the alteration in the depth-of-burial-interval 0.5–2.5 km of uneroded basaltic crust. By neglecting these variations it is possible to separate the effects of pressure and temperature by making use of refraction profiles positioned where the thermal gradient has been determined by boreholes. This permits the construction of a curve for Poisson's ratio as a function of temperature for constant pressure (depth). It is done by plotting Poisson's ratio versus depth as determined from the seismic profiles. By marking the temperature taken from extrapolated thermal gradients (from Pálmason et al., 1978) lines of constant temperature can be drawn and the plot can be inverted to give Fig. 12. The values on which Fig. 12 is based are fairly scattered but they do indicate the general trend. By a more accurate determination of this relationship from more detailed seismic measurements it appears to be possible to use seismic refraction measurements to obtain information about the absolute temperature in the Icelandic crust.

Central Volcanoes

The central volcanoes are an important exception to the typical velocity structure described above. As pointed out by Pálmason (1971) layer 3 lies at shallow depths under the roots of the central volcanoes. I have interpreted new seismic refraction data from the Stardalur central volcano near Reykjavík and, reinterpreted similar data from the Vatnsdalur central volcano in north Iceland (Flóvenz, 1979). The velocity seems to increase continuously with depth within the central volcanoes but at a much faster rate then outside, giving layer 3 at shallow dept (up to 1 km). After this velocity is reached, it takes on a constant value. Fan shooting over the Stardalur central volcano shows that the *P*-wave velocity in layer 3 (under the roots of the central volcanoes) is not significantly greater than elsewhere in layer 3. There appears to be a sudden change in velocity between the central volcanoes and their surroundings with much higher velocities inside the central volcanoes than at the same level outside. Thus the central volcanoes appear to act like chimneys through the Icelandic crust.

Division of the Icelandic Crust

In view of the results outlined above, it is reasonable to devide the Icelandic crust into two parts, namely the upper and the lower crust. The upper crust is characterized by continuously increasing velocity with depth from about 2.0 km/s to 6.5 km/s. In the range of 2.0 km/s–3.5 km/s the velocity increases very rapidly with depth but thereafter the velocity-depth gradient decreases and reaches an approximately constant value 0.57 s^{-1} at the 4.0 km/s surface. The lowest velocities correspond to fresh basalt lava at the surface and the rapidly increasing velocity reflects closing of fissures and pores as the basalt becomes buried. The constant velocity depth gradient corresponds to steadily increasing alteration of the basalt and the formation of secondary minerals which fill the pores. Increasing dyke density is also likely to contribute to the increasing velocity downwards. There is a possibility for the occurrence of a constant-velocity layer below the 5.0 km/s isovelocity surface. A possible interpretation of such a layer is that it represents a zone where the dyke intensity is almost constant and epidote is the dominant alteration mineral.

The lower crust (=layer 3) is characterized by a nearly constant body wave velocity and may be equated to layer 3 in the oceanic crust. A map of the depth to layer 3 according to the Wiechert-Herglotz interpretation is given in Fig. 13. The map is inaccurate in some important areas such as mid- and northwest Iceland. Reversal of some of the profiles would help to increase the accu-

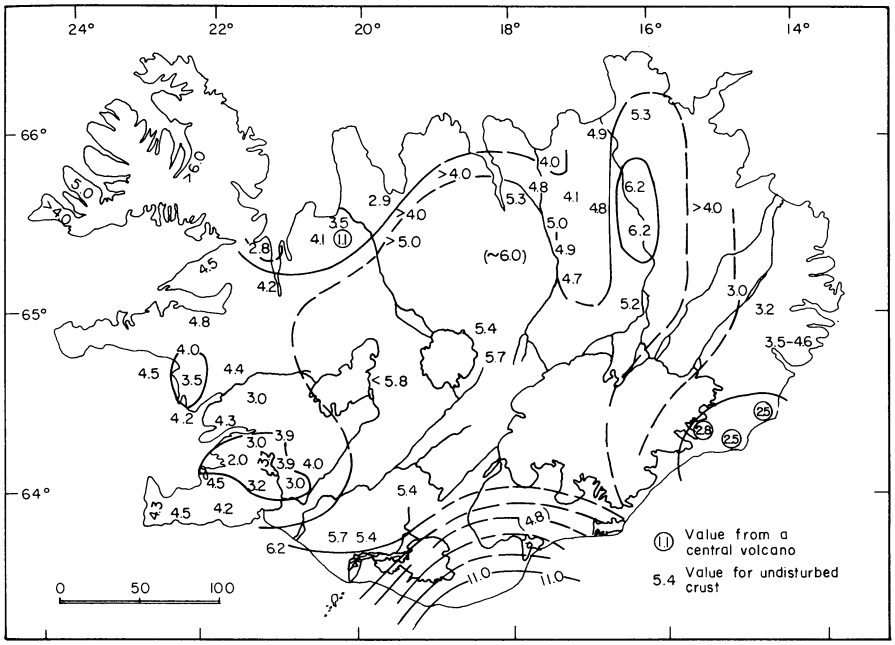

Fig. 13. Depth to the lower crust (layer 3) in Iceland. The velocity is assumed to increase continuously with depth

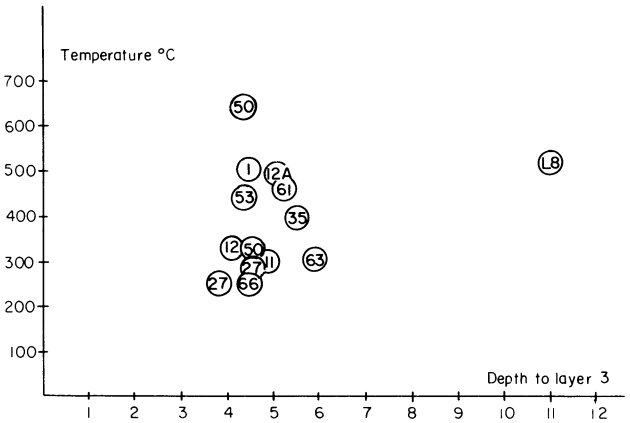

Fig. 14. Temperature at the top of the lower crust (layer 3) as function of depth for profiles outside the neovolcanic zone only. The temperature values are obtained by extrapolating the temperature gradient given by Pálmason et al. (1978) and the depth is taken from Fig. 13

racy of the map. From the map it seems not unlikely that the increasing depth to layer 3 towards the centre of Iceland can contribute to the negative Bouguer anomaly over Iceland. The anomalously great depth to layer 3 around southeast Iceland is not yet understood.

This map can be regarded as giving the maximum depth to the lower crust (correct if the velocity increases continuously with depth) and Pálmason's (1971) map as giving the minimum depth to layer three (correct if the layered model is valid).

The composition of the lower crust is not known, but seismic refraction measurements provide some constraints. The *P*- and *S*-velocities of the lower crust are 6.5 km/s and 3,6 km/s respectively, and Poisson's ratio is 0.28. Extrapolated temperature gradients from Iceland (Pálmason et al., 1978) and the map of the depth to the lower crust can be used to estimate the temperature in layer three. In Fig. 14 the temperature at the top of layer three is plotted versus the depth to the layer for profiles outside the neovolcanic zone. This shows that the top of the lower crust in Iceland lies at 500° C or lower except for one value which may be erroneous (Flóvenz, 1979). Inside the neovolcanic zone the temperature at the top of the lower crust is likly to be still higher. This means that the average temperature of the lower crust is more than 500° C and it is created at much higher temperatures than 500° C.

Acknowledgements. The data used in this paper were provided by the National Energy Authority of Iceland, and interpreted at the University of Bergen, Norway. I am grateful to the personnel of these two institutes for valuable assistance during the work. I want to thank my supervisor Dr. Reidar Kanestrøm for unfailing support throughout the work and Dr. Guðmundur Pálmason for making the data available. Dr. Ronald Steel improved the English text greatly and Dr. Karl Gunnarsson read the paper and made some critical comments.

References

Båth, M.: Crustal structure of Iceland. J. Geophys. Res. **65**, 1793–1807, 1960

Berge, A.M.: Program for beregning av hastighets-dybde fordelingen ut fra gangtidskurva, når hastigheten öker kontinuerkig med dypet. Internal report Seismological Observatory, University of Bergen 1976

Flóvenz,'O.G.: Analyse av refraksjonsseismiske og teleseismiske data fra Island. Cand real thesis, Seismological Observatory, University of Bergen 1979

Fuchs, K., Müller, G.: Computation of synthetic seismograms with the reflectivity method and comparison with observations. Geophys. J. R. Astron. Soc. **23**, 417–433, 1971

Hughes, D.S., Maurette, C.: Variation of elastic wave velocities in basic igneous rocks with pressure and temperature. Geophysics **21**, 23–31, 1957

Kennett, B.L.N., Orcutt, J.A. A comparison of travel time inversions for marine refraction profiles. J. Geophys. Res. **81**, 4061–4070, 1976

Lewis, B.T.R. Evolution of ocean crust velocities. Annu. Rev. Earth Planet. Sci. **6**, 377–404, 1978

McDougall, I., Sæmundsson, K., Jóhannesson, H., Watkins, N.D., Kristjánsson, L. Extension of the geomagnetic polarity time scale to 6.5 m.y. K-Ar dating, geological and paleomagnetic study of a 3500-m lava succession in western Iceland. Bull. Geol. Soc. Am. **88**, 1–15, 1977

Mykkeltveit, S. Computation of synthetic body wave seismograms, theory, program description and application. Internal report, Seismological Observatory, University of Bergen 1978

Pálmason, G. Seismic refraction investigation of the basalt lavas in northern and eastern Iceland. Jökull **13**, 39–60, 1963

Pálmason, G. Crustal structure of Iceland from explosion seismology. Soc. Sci. Isl. **XL**, 1971

Pálmason, G. Kinematics and heat flow in a volcanic rift zone with application to Iceland. Geophys. J. R. Astron. Soc. **33**, 451–481, 1973

Pálmason, G., Arnórsson, S., Fridleifsson, I.B., Kristmannsdóttir, H., Sæmundsson, K., Stefánsson, V., Steingrímsson, B., Tómasson, J. The Icelandic crust. Evidence from drillehole data on structure and process. Second Maurice Ewing Symp., Am. Geophys. Union in press, 1978

Pálmason, G., Sæmundsson, K. Iceland in relation to the Mid-Atlantic Ridge. Annu. Rev. Earth Planet. Sci. **2**, 25–50, 1974

Tryggvason, E., Båth, M. Upper crustal structure of Iceland. J. Geophys. Res. **66**, 1913–1925, 1961

Walker, G.P.L. The structure of eastern Iceland. In. Geodynamics of Iceland and the North Atlantic Area, L. Kristjansson, ed; pp 177–188, Dordrecht. Bosto. Reidel 1974

Received April 30, 1979; Revised Version October 8, 1979

J. Geophys. 47, 221–227, 1980

Journal of Geophysics

Crustal Structure of the Iceland-Faeroe Ridge

M. H. P. Bott and K. Gunnarsson
Department of Geological Sciences, University of Durham, South Road, Durham DH1 3LE, England

Abstract. Knowledge of the crustal structure of the Iceland-Faeroe Ridge is based on results from the North Atlantic Seismic Project of 1972 supplemented by earlier short refraction lines and reflection, gravity and magnetic surveys. The main 5.7 km/s upper crustal layer is locally overlain by lower velocity layers of variable thickness. The upper crust is interpreted as being predominantly basaltic, comprising lavas, regions of pyroclastic rock and intrusives including ring complexes. A 6.7 km/s lower crustal layer underlies the upper crust at a depth of between about 4 and 8 km along the Ridge; this layer is present also beneath the Icelandic shelf but not beneath the Faeroe shelf. A deeper 7.8 km/s refractor interpreted as the Moho occurs at about 30–35 km depth beneath the south-eastern part of the Ridge, shallowing to about 28 km towards the north-western end of it. A significant increase in velocity with depth within the main 6.7 km/s layer has not been detected but may occur, in which case the Moho would be somewhat deeper. The seismic crustal results are consistent with a gravity profile across the Ridge, which indicates approximate Airy isostatic equilibrium. The crust beneath the Ridge, which is of a thickness more typical of the continents than the oceans, is believed to have been formed by sea-floor spreading during the period 55 to 40 Ma ago.

Key words: Iceland-Faeroe Ridge – Crustal structure – Seismic refraction.

1. Introduction

The Iceland-Faeroe Ridge (Fig. 1) forms an upstanding bathymetric feature of NW-SE trend which connects the Iceland Block containing the active spreading centre to the Faeroe Block of probable continental origin. It is about 400 m deep along its smooth crest, and is separated from the Iceland and Faeroe shelves by short, sharp bathymetric scarps. It appears to form the oldest part of the aseismic Icelandic transverse ridge which crosses the north-eastern Atlantic, having originated by seafloor spreading starting about 55 Ma ago during the initial stages of separation of Greenland from the Rockall-Faeroe microcontinent. The shallow bathymetry in relation to the adjacent Norwegian and Reykjanes basins indicates a highly anomalous underlying structure for an oceanic region. Prior to the present investigation, gravity and seismic investigations (Bott et al., 1971) indicated that the elevation of the Ridge probably arises because of an underlying crust with a thickness more like that of continental than oceanic regions. This paper describes the investigation of the anomalous crustal structure of the Ridge by the North Atlantic Seismic Project (NASP) of 1972, incorporating the earlier shorter seismic lines of Bott et al. (1971).

An earlier study of the crustal structure of the Iceland-Faeroe Ridge based on NASP data has been presented by Zverev et al. (1975). They interpreted the crust as being 30–35 km thick in agreement with our interpretation, but they regarded the crust as being in structural continuity with that of the Faeroe Islands in disagreement with us.

2. The North Atlantic Seismic Project

The North Atlantic Seismic Project (NASP) was a sea-to-land explosion seismology crustal refraction investigation of the structure between North Scotland and Iceland taking place in July and early August 1972. Shots were fired at sea from MV *Hawthorn*, these consisting mainly of 300 lb (136 kg) or 600 lb (272 kg) charges of geophex fired along a series of lines shown in Fig. 1 (inset) using long burning fuses. A few 1,200 lb (544 kg) shots were also fired. Most of the shots detonated at about 180 m depth or on the seabed where shallower than this. Of relevance to this paper is the shot line A which stretches from the Faeroe Islands to Iceland and runs along the crest of the Iceland-Faeroe Ridge. About 70 main shots were fired along this line, and a number of smaller shots (23 and 12 kg) were fired in the vicinity of the recording ship *Mikhail Lomonosov* and on the Icelandic shelf. The shots numbered A7 to A38 were situated on the main line along the Iceland-Faeroe Ridge itself and consisted of 600 lb (272 kg) charges, spaced on average at about 10 km interval. A further short subsidiary line of shots was fired on the Ridge to the north-east of the main line along the region of high gravity; this consisted of five 600 lb charges numbered between A75 and A84.

The shots were recorded at seven stations situated on the Faeroe Islands, six of these being provided by Aarhus University in cooperation with Hamburg and Kiel Universities (F1 to F6) and one by Durham University (DU4). A total of fifteen recording stations were situated on Iceland; station M1 was a six-seismometer L-shaped array operated by the National Energy Authority of Iceland and M2 was provided by Lamont-Doherty and operated under the supervision of Dr. P. Einarsson. Station DU5 was provided by Durham University. Stations R1 to R6 were provided by the Institute of the Physics of the Earth, Moscow, and were operated under the supervision of Dr. S.M. Zverev, and stations S1 to S6 along the south coast of Iceland were provided by La-

0340-062X/80/0047/0221/$01.40

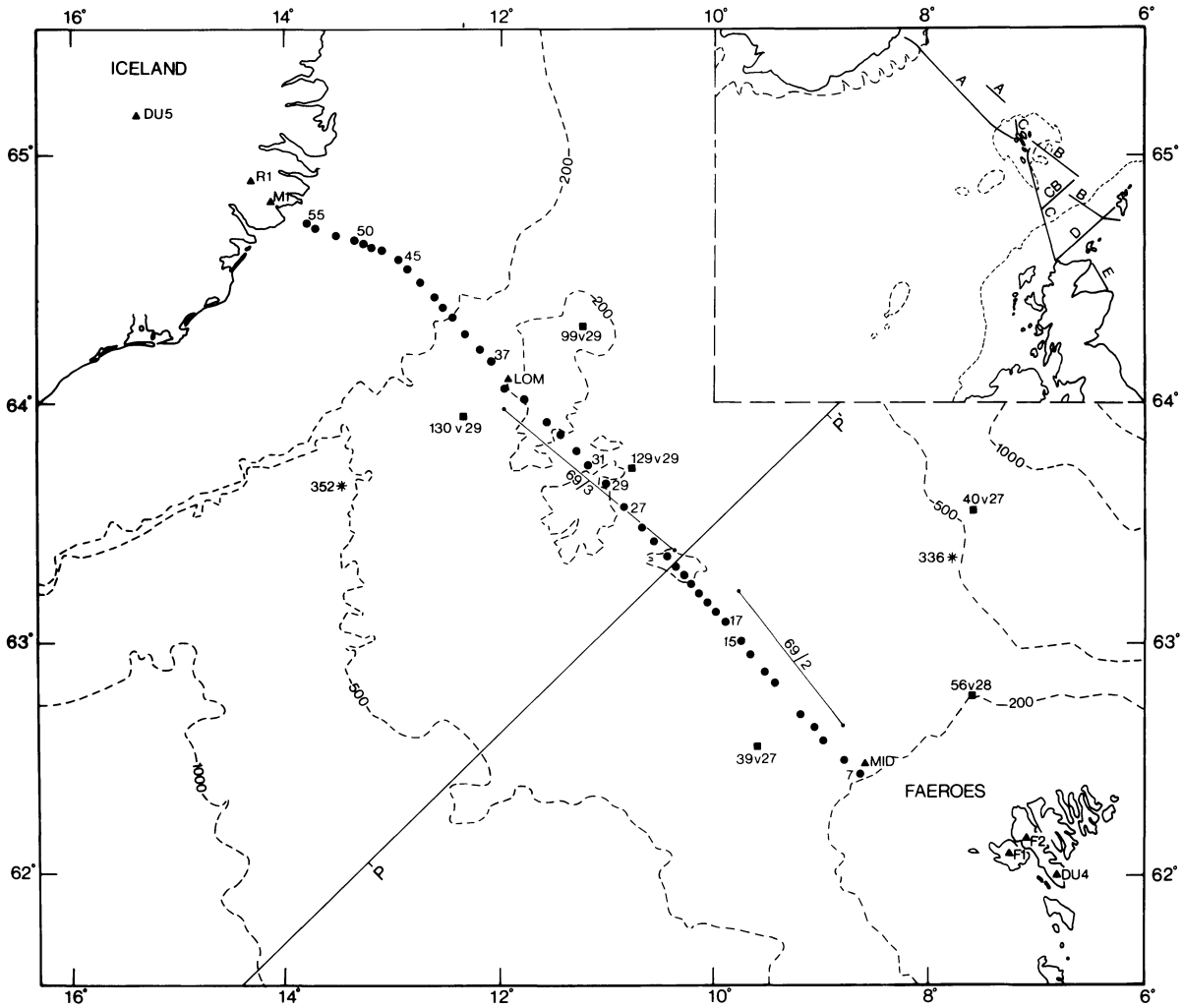

Fig. 1. Map showing shot positions (*solid circles*) and seismic recording stations (*triangles*) used in the determination of crustal structure beneath the Iceland-Faeroe Ridge. *Refraction lines 69/2* and *69/3* are from Bott et al. (1971), sono-buoy refraction lines *99299* etc. from Grønlie and Talwani (1978), and DSDP holes 336 and 352 are shown. Bathymetric depth contours are shown in fathoms, and the overall shot lines of the North Atlantic Seismic Project are shown on inset

mont-Doherty Geological Observatory. Shots were also recorded at sea by the Soviet research vessel *Mikhail Lomonosov* which operated an underwater seismometer station near the north-western end of the line A on the Ridge and by MV *Miranda* which occupied two stations along line A, one of these near the south-eastern end of the Ridge and the other about two-thirds way along it towards the Icelandic shelf.

In this paper we describe an analysis of the crustal structure of the Iceland-Faeroe Ridge based on arrivals from shots A7 to A39 on the Ridge and A40 to A50 on the Iceland shelf. Recordings were used from *Lomonosov* (LOM) and one *Miranda* station (MI(D)) on the ridge, stations DU4, F1, and F2 on the Faeroe Block, and stations M1, R1, and DU5 on Iceland.

3. Upper Crustal Structure

We define the upper crust as the region above the 6.7 km/s main crustal layer which starts at about 7 km depth. This has been studied by reflection profiling, gravity and magnetic surveys, and Leg 38 DSDP drilling. The layering has been investigated by two ship-to-ship refraction lines each of about 100 km length and by sonobuoy refraction lines.

Reflection profiling shows that sediments are thin or absent over most of the smooth crustal region of the Iceland-Faeroe Ridge except in local troughs such as those beneath the scarps at both ends of the Ridge (Johnson and Tanner, 1972; Fleischer et al., 1974; Grønlie and Talwani, 1978). This is borne out by the general presence of conspicuous short wavelength magnetic anomalies indicating that highly magnetic rocks crop out on the seabed or not far beneath it over most of the crestal region (Bott and Ingles, 1972). Some large amplitude circular magnetic anomalies also occur, these probably representing igneous intrusions of ring type occupying the eroded cores of ancient volcanoes (Ingles, 1971). The gravity field over the ridge crest is unusually variable for an apparently oceanic region, with some local anomalies of 20 to 40 mgal amplitude caused by lateral variation of upper crustal density (Bott et al., 1971, Fleischer, 1971, Fleischer et al., 1974). Some regions of gravity low correspond to slight bathymetric depressions. Correlation between gravity anomalies

and medium wavelength magnetic anomalies is also observed, with the magnetic polarity varying from area to area (Bott and Ingles, 1972).

The seismic refraction lines 69/2 and 69/3 of Bott et al. (1971) (Fig. 1) revealed the local presence of one or more low velocity uppermost layers with velocities ranging between 3.2 and 4.6 km/s and a composite thickness locally reaching up to nearly 4 km; elsewhere these layers are thin or absent. The underlying main upper crustal layer yielded an estimated velocity of 5.7 km/s along 69/3 and 5.4 to 5.8 km/s along 69/2. The regions of thick low velocity rocks show correlation with slight bathymetric depressions and low gravity anomalies. The sonobuoy refraction results presented by Grønlie and Talwani (1978) are consistent with this picture.

During Leg 38 of the Deep Sea Drilling Project (Talwani et al., 1976) drilling sites 336 and 352 were situated on opposite flanks of the Iceland-Faeroe Ridge where sediments thicken towards the adjacent Norwegian and Reykjanes basins. At site 336 on the north-eastern flank in 811 m water depth about 30 m of oceanic tholeiitic basalts were penetrated below 515 m of sediment of upper Eocene and later age. The basalts, dated at 40–43 Ma old, show evidence of subaerial erosion indicating that the basement has subsided by at least 1,350 m since formation. At site 352 on the south-eastern flank 122 m of sediment of Oligocene and later age was penetrated but basement was not reached.

The upper crust beneath the Iceland-Faeroe Ridge thus appears to consist of highly magnetic igneous rocks of probable basaltic composition. Pockets of low velocity and low density rocks are best interpreted as regions where pyroclastic rocks (tuffs and agglomerates) predominate. Circular igneous intrusions representing the cores of ancient volcanoes are also found. As evidenced by the subaerially weathered basalt in DSDP hole 336, the crestal region probably stood about 1 km above sea level in early Tertiary time and has subsequently subsided to its present elevation as the underlying lithosphere cooled, as suggested by Bott et al. (1971) and Vogt (1972).

4. Crustal Structure From NASP

The presence of a 6.8 km/s refractor (revised by NASP to 6.7 km/s) beneath the Iceland-Faeroe Ridge at a depth of about 7 km was first detected by refraction line 69/3 (Bott et al., 1971). A short unreversed segment with apparent velocity 7.84 km/s along line 69/2 was originally interpreted tentatively as the head wave from the Moho at about 16 km depth, but the later NASP results presented here indicate that this segment probably represents arrivals from the 6.7 km/s layer where it is dipping. The NASP results indicate the presence of two main crustal refractors beneath the length of the Ridge, the 6.7 km/s refractor representing the top of the main crustal layer, and a 7.8 km/s refractor at about 30 km depth representing the Moho.

The main problem of interpreting the NASP data is that, whereas the shots were fired along the Ridge itself, most of the recording stations were situated on land on the adjacent Iceland and Faeroe Blocks which may lack structural continuity with the Ridge. Fortunately the marine stations occupied by *Lomonosov* and *Miranda* (sites D and E) were situated on the Ridge itself. Under such circumstances, the time-term method can make use of arrivals from the Ridge shots at the stations on Iceland and Faeroe Islands, provided that the travel path to a station beneath an adjacent block from a given refractor beneath the Ridge can be assumed to be identical for all relevant shots.

A serious drawback of the time-term method in crustal seismology is the substantial offset between the surface shot or recording points and the positions where the rays leave the refractor (O'Brien, 1968). This problem is particularly acute for the Moho refractor beneath the Ridge. The dip of the refractor cannot be assumed to be uniform over the cone of critical rays at a surface point, which is of the order of 50 km in radius for Moho arrivals beneath the Iceland-Faeroe Ridge. Thus the variation in time-term along the line cannot be regarded as an accurate indication of variations in depth to the refractor. We have overcome this difficulty by a modification of the time-term method developed by one of us (K.G.). To determine the depth profile of a refractor, we first assume a constant velocity layering above. The refracting interface is then defined in terms of a series of points of specified horizontal location and unknown depths (to be determined). The depths and refractor velocity are determined by iteration from an initial model, using linear inversion at each stage. This method has been applied to the interpretation of first-arrival times from both 6.7 and 7.8 km/s refractors.

The 6.7 km/s Refractor

As a first stage, a time-term solution for the 6.7 km/s layer was obtained using the shots on the Iceland shelf recorded by *Lomonosov* (LOM) and by stations R1 and M1 on Iceland. A well-determined solution UW2 was obtained yielding a refractor velocity of 6.76 ± 0.013 km/s (Fig. 2). The time-terms at LOM and shot A36 were equated to each other, being determined as 0.88 s. The time-terms determined for shots A40 to A50 on the Iceland shelf were found to be about 1.0 s but those for the shots at the NW end of the Ridge are significantly smaller at about 0.7 s.

A separate solution was obtained for the Iceland-Faeroe Ridge itself, using shots between A7 and A31 recorded at MI(D), LOM and land stations F1, F2, and DU4 on the Faeroe Islands (Fig. 2). In order to make the solution unambiguous, it was necessary to assume a time-term value of 0.88 s at LOM as obtained in solution UW2 above (LOM = A36). The approximate validity of this assumption is confirmed by the line 69/3 result and by the determined value at MI(D) being intermediate between values determined for shot points A7 and A8. The results (Fig. 2) show that the time-terms along the Ridge vary between about 1.0 s and 0.5 s, the lower values occurring in the region between shots A13 and A23. The velocity was determined to be 6.73 ± 0.04 km/s. Minus time analysis was used to verify the velocity estimate over short segments of the line.

Variation in delay time (i.e., time-term) to the 6.7 km/s refractor may arise either from lateral variation in the shallow velocity structure, or by variation in depth to the refractor, or both. There is evidence presented by Bott et al. (1971) and Fleischer et al. (1974) to show that much lateral variation does occur, but this is not yet sufficiently well defined along the line to allow for it in constructing a model. We have therefore used the iterative method we have developed to estimate the depth to the 6.7 km/s refractor between MI(D) and LOM assuming that the overlying layer has a constant velocity of 5.0 km/s. The analysis is based on arrivals at LOM, MI(D), F1, F2, and DU4. The resulting shape of the interface (Fig. 3) closely resembles the pattern of time terms, so that the offset is not a serious problem for this relatively shallow refractor This solution yielded an estimated refractor velocity of 6.72 ± 0.05 km/s which does not differ significantly from that obtained by time-term analysis. This interpretation (Fig. 3) shows the refractor shallowing between shots A11

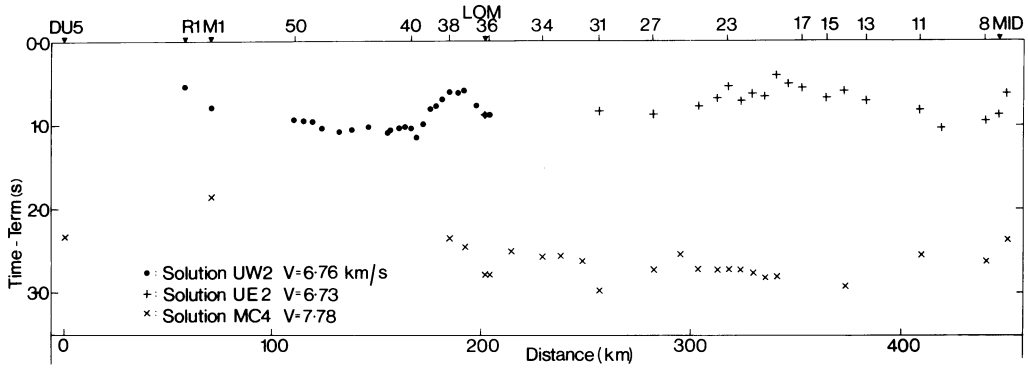

Fig. 2. Results of time-term analyses for line A shots and stations along the Iceland-Faeroe Ridge. Solutions UW2 (Icelandic shelf) and UE2 (Iceland-Faeroe Ridge) are for the 6.7 km/s refractor and solution MC4 for Moho arrivals. For shot and station positions see Fig. 1

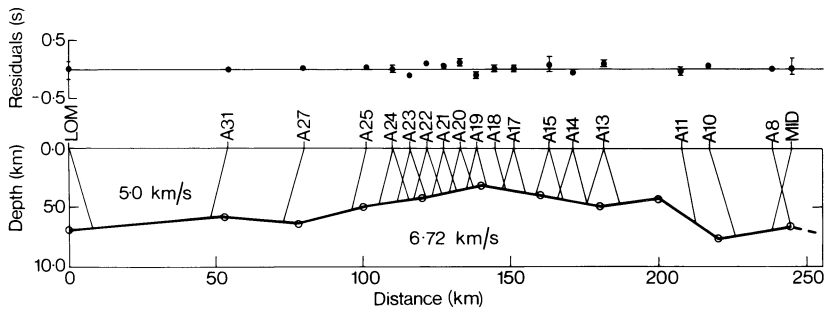

Fig. 3. Interpretation of the depth to the 6.7 km/s refractor beneath the Iceland-Faeroe Ridge along line A, using the iterative refractor mapping method described in the text. The solution uses arrivals at LOM, MI(D), DU4 and F1 but structure is only shown beneath the Ridge itself. Average residuals are shown together with their range where applicable. Ray paths are shown in the upper layer

and A25, and reaching an estimated minimum depth of 3 km beneath shot A19. Between MI(D) and A11 at the south-eastern edge of the Ridge, and between A25 and LOM towards the north-western end, the depth is about 6 to 8 km. North-west of LOM, the depth can be estimated from the time-terms. Between LOM and shot A38 it appears to average about 4 to 5 km. Assuming that the overlying average velocity also applies to the Icelandic shelf, the depth there is estimated to be uniformly about 7.5 km.

The 6.7 km/s layer beneath the Ridge does not give rise to any well-defined pattern of wide-angle reflections, this probably being attributable to inhomogeneity in the overlying layers which may be accentuated because the line perpendicularly crosses the inferred axis of spreading when the Ridge was formed.

It is of interest to note the contrast in structure of the two 'shelf' regions adjacent to the ends of the Ridge. The 6.7 km/s layer appears to be in continuity between the Ridge and the Iceland shelf, although there is an abrupt change in its depth at the boundary. On the other hand, no 6.7 km/s layer has been detected beneath the Faeroe shelf or the Faeroe Islands, the arrivals from the Ridge shots being converted to a lower velocity upper crustal phase at the boundary (Bott et al., 1976).

The Moho

The initial assessment of the Moho beneath the Ridge is based on time-term analysis of relevant arrivals from the Ridge shots (A7 to A38) recorded at F1, F2, and DU4 on Faeroe Islands, DU5 and M1 on Iceland and LOM on the Ridge itself (Fig. 2). The time-terms at LOM and shot A36 were equated to each other. The solution MC4 using 22 shots yielded a velocity of 7.78 ± 0.03 km/s and a mean time-term for the Ridge of 2.7 s. Except for some local scatter, the time-terms do not vary much along the Ridge although the values near the middle of the line (A12 to A25) are marginally higher than those near the ends.

Because of the substantial offset of about 50 km between the rays at the surface and at the Moho, the lateral variation in P_n time terms is not a good indication of variation in depth to the Moho beneath. A better solution can be obtained using our iterative programme to map the interface from the travel times, after correction for the delay above the 6.7 km/s refractor. Analyses were carried out for various combinations of the arrivals at DU5, M1, LOM, F1, and DU4 from shots along the Ridge. The resulting sub-Moho velocity estimates lie between 7.8 and 8.0 km/s and are rather higher than those obtained by time-term analysis. Two of the resulting models are shown in Fig. 4. Both models show the Moho at about 32 to 35 km depth beneath the south-eastern part of the Ridge (A7 to A29) and at a significantly shallower depth of about 25 km beneath the northwestern part of it, but they differ in the emphasis they place on the change in depth of the Moho. Great confidence cannot as yet be placed on this change in depth of the Moho, as it may be partly or wholly an artifact of the complicated structure at depth beneath the junction of the Ridge with the Iceland Block. Confirmation by refraction lines across the length of the Ridge is needed.

A coherent P_mP phase is conspicuously absent from the recordings at LOM, MI(D) and MI(E), although packets of large amplitude arrivals are observed following P_n. It is suggested that the absence of recognisable P_mP branches results from scattering by inhomogeneities in the lower crust or possibly at the Moho. Absence of the P_mP phase removes the possibility of investigation of the Moho in detail or estimation of mean crustal velocity on present evidence.

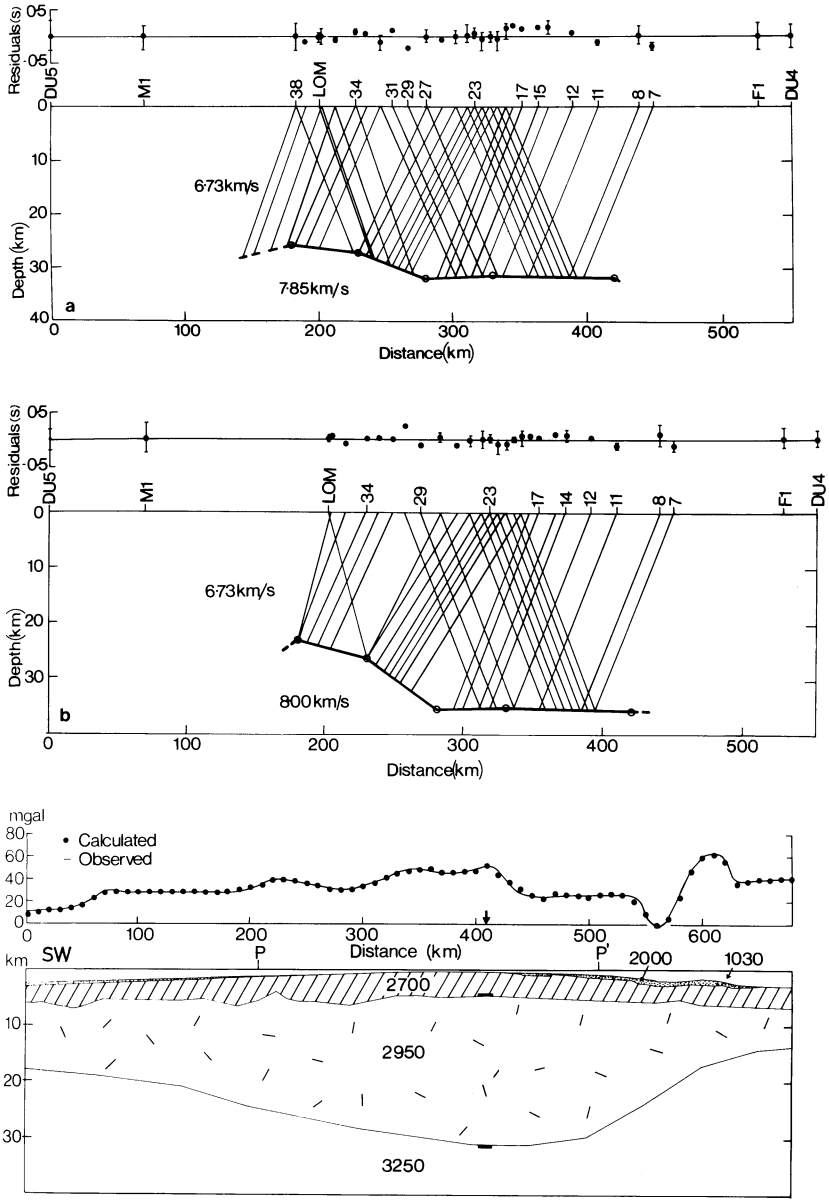

Fig. 4a and b. Interpretations of the depth to the 7.8 km/s Moho refractor beneath the Iceland-Faeroe Ridge using two separate shot-station configurations, including correction for delay in upper crustal layer as shown in Fig. 3. The main distinction between the two models is that the long distance arrivals to station F1 are included in (**a**) but not in (**b**)

Fig. 5. Interpretation of the free air gravity anomaly profile along line PP′ (Fig. 1) and its extension to SW and NE. Densities are shown in kg/m^3 and depth to 6.7 and 7.8 km/s refractors are shown where line A is crossed

5. Gravity Structure Across the Ridge

An earlier gravity interpretation of the structure across the Iceland-Faeroe Ridge from the Norwegian Sea to the Reykjanes Basin was made by Bott et al. (1971). This demonstrated that the Ridge is in approximate isostatic equilibrium in relation to the adjacent ocean basins as a result of a thick underlying crust rather than a low density underlying upper mantle. By assuming a crust-mantle density contrast of 400 kg/m^3 and taking the depth to Moho beneath the Norwegian Sea obtained by Hinz and Moe (1971), the depth to the Moho beneath the Ridge was determined as about 22 km. We now know that this estimate is too low, and therefore we have constructed a more realistic model consistent with the new NASP estimate of crustal thickness beneath the Ridge and incorporating the better evidence on sediment thicknesses now available.

Our new model (Fig. 5) has been constructed on the following basis. Bathymetry and gravity for the whole line and sediment thickness over the crest of the Ridge have been taken from Fleischer et al. (1974). Sediment thicknesses on the flanks of the Ridge have been taken from Grønlie and Talwani (1978) and from individual VEMA profiles. Crustal structure beneath the Ridge is based on the NASP data presented in this paper. In order to produce a sufficiently large change in crustal thickness between the Ridge and the Norwegian Sea to be consistent with the refraction results of Hinz and Moe (1971), a smaller density contrast at the Moho of 300 kg/m^3 had to be used. On this basis, we estimate the Moho to be about 14 km deep at the north-eastern end of the line at the edge of the Norwegian Sea where the water depth is 2.7 km. This is consistent with the estimate of 10 km depth made by Hinz and Moe (1971) in the central part of the Norwegian Sea where the water depth is about 3.6 km. Short-wavelength discrepancies between the observed and calculated profiles have been removed by minor adjustment of the sediment thickness or depth to the 6.7 km/s interface, although these could be equally well attributed to lateral variation in the upper crustal layers.

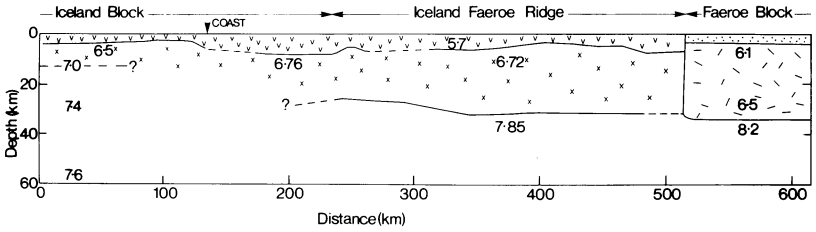

Fig. 6. Interpretation of the crustal structure of the Iceland-Faeroe Ridge along line A and its relationship to the crustal structure of the adjacent Iceland and Faeroe Blocks. The structure beneath Iceland is after Pálmason (1971) and Angenheister et al. (1979) and that beneath the Faeroe Block interpreted as continental crust is after Bott et al. (1976)

The gravity model (Fig. 5) is in good agreement with the available observations. However, there is indication from the work of Haigh (1973) that the upper mantle beneath the Reykjanes Basin is of lower density than that beneath the Norwegian Sea, so that a decrease in upper mantle density towards the south-western end of the line may occur. If so, then the crust towards the south-western end would be thinner than indicated in the model.

6. Conclusions and Discussion

The results from NASP and previous geophysical projects indicate that the main features of crustal structure of the Iceland-Faeroe Ridge are as follows (Fig. 6):

1. Sediments are thin or absent from the crestal region but thicken down the flanks towards the adjacent basins. The 4-to 8-km-thick upper crust above the 6.7 km/s refractor is interpreted as consisting of volcanic rocks which are probably predominantly basaltic. Significant lateral variations seen in short-wavelength gravity, magnetic, and seismic features and in subdued bathymetry may be attributable to regions of thick pyroclastic rocks and to the cores of ancient volcanoes.

2. A 6.7 km/s refractor at 4 to 8 km depth represents the top of the main crustal layer. This layer is apparently shallowest in the region between shots A13 and A24.

3. A well-defined refracted arrival with velocity of about 7.8 km/s is received from the base of the crust. The Moho is estimated to be 30 to 35 km deep beneath the central and south-eastern part of line A along the Ridge, shallowing by a few kilometres beneath the north-western end of it, assuming that the 6.7 km/s velocity remains constant down to the Moho. Lack of coherent wide angle reflections is attributed to scattering in the lower crust along the line which is perpendicular to the direction of the sea-floor spreading axis.

4. The upper crust appears to be similar to that beneath Iceland, with the 6.7 km/s layer apparently continuous between the Ridge and the adjacent Icelandic shelf. In contrast, the 6.7 km/s layer has not been detected beneath the Faeroe Block; 6.7 and 7.8 km/s waves from the Ridge appear to be converted to lower velocity crustal phases at the boundary between Ridge and Faeroe Block, marking a fundamental change in type of crust.

Our interpretation differs from that of Zverev et al. (1975) in the relationship of the Ridge to the adjacent blocks. Zverev et al. (1975) assumed continuity of crustal layering across the whole region. In contrast, we have found evidence for a fundamental change in crust at the boundary between the Ridge and the Faeroe Block. We attribute the relatively high delay times at the land stations on Iceland to lateral reduction in the upper mantle velocity towards central Iceland rather than to deepening of the Moho beneath Iceland.

The Iceland-Faeroe Ridge appears to be underlain by crust of Icelandic type, albeit significantly thicker than that beneath Iceland. We interpret this crust as formed by the sea-floor spreading mechanism as the north-eastern North Atlantic opened since about 55 Ma ago, the Iceland-Faeroe Ridge forming at an early stage in this evolution and Iceland itself forming at a later stage (Bott, 1974). The Icelandic type crust is much thicker than normal oceanic crust (a factor of five thicker beneath the Iceland-Faeroe Ridge, and two to three times thicker beneath Iceland). This is attributed to differentiation of a greater quantity of crustal material from the underlying mantle, possibly as a result of the high underlying temperature at the time of continental splitting and shortly after.

Acknowledgements. This research was supported by the Natural Environment Research Council through research grant GR3/1390 and ship time on MV *Miranda* and MV *Hawthorn*. We are grateful to the officers and crews of these two ships for their contribution to the project. Mr. J.H. Peacock was senior scientist on MV *Miranda* and Dr. J. Sunderland on MV *Hawthorn*. Shot firing was done by Mr. D. Asbery and Mr. G. Wilson. Dr. Gudmundur Pálmason arranged for cooperation in Iceland. Professor S. Björnsson, J. Sveinsson, and E. Hauksson operated the station M1 and Dr. A. Jakobsson acted as coordinator between the recording groups in Iceland and the shooting ship. Stations F1 and F2 were under the supervision of Professor S. Saxov and Dr. U. Casten. Drs. C.H. Boynton, P.K.H. Maguire, and G.K. Westbrook operated stations DU4 and DU5 which were provided by Dr. R.E. Long. Drs. I.P. Kosminskaya and S.M. Zverev kindly provided data. We warmly thank all the above and several others who helped to make the project a success.

References

Angenheister, G., Gebrande, H., Miller, H., Weigel, W., Goldflam, P., Jacoby, W., Pálmason, G.G., Björnsson, S., Einarsson, P., Zverev, S., Loncarevic, B., Solomon, S.: First results from the Reykjanes Ridge Iceland seismic project 1977. Nature (London) **279**, 56–60, 1979

Bott, M.H.P.: Deep structure, evolution and origin of the Icelandic Transverse Ridge. In: Geodynamics of Iceland and the North Atlantic area, L. Kristjansson, ed.: pp. 33–47. Dordrecht: D. Reidel 1974

Bott, M.H.P., Browitt, C.W.A., Stacey, A.P.: The deep structure of the Iceland-Faeroe Ridge. Mar. Geophys. Res. **1**, 328–351, 1971

Bott, M.H.P., Ingles, A.: Matrix methods for joint interpretation of two-dimensional gravity and magnetic anomalies with application to the Iceland-Faeroe Ridge. Geophys. J. Roy. Astron. Soc. **30**, 55–67, 1972

Bott, M.H.P., Nielsen, P.H., Sunderland, J.: Converted *P*-waves originating at the continental margin between the Iceland-Faeroe Ridge and the Faeroe Block. Geophys. J. Roy. Astron. Soc. **44**, 229–238, 1976

Fleischer, U. Gravity surveys over the Reykjanes Ridge and between Iceland and the Faeroe Islands. Mar. Geophys. Res. **1**, 314–327, 1971

Fleischer, U., Holzkamm, F., Vollbrecht, K., Voppel, D.. Die Struktur des Island-Färöer-Rückens aus geophysikalischen Messungen. Dtsch. Hydrogr. Z. **27**, 97–113, 1974

Grønlie, G., Talwani, M.. Geophysical atlas of the Norwegian Greenland Sea. VEMA Research Series IV, Lamont-Doherty Geological Observatory, Palisades, N.Y 1978

Haigh, B.I.R.: North Atlantic oceanic topography and lateral variations in the upper mantle. Geophys. J. R. Astron. Soc. **33**, 405–420, 1973

Hinz, K., Moe, A. Crustal structure in the Norwegian Sea. Nature Phys. Sci. **232**, 187–190, 1971

Ingles, A.D.: The interpretation of magnetic anomalies between Iceland and Scotland. University of Durham Ph. D. Thesis, 152 pp. 1971

Johnson, G.L., Tanner, B. Geophysical observations on the Iceland-Faeroe Ridge. Jökull **21**, 45–52, 1972

O'Brien, P.N.S.: Lake Superior crustal structure – a reinterpretation of the 1963 seismic experiment. J. Geophys. Res. **73**, 2669–2689, 1968

Pálmason, G. Crustal structure of Iceland from explosion seismology. Soc. Sci. Islandica **40**, 187 pp. 1971

Talwani, M., Udintsev, G. et al. Initial Reports of the Deep Sea Drilling Project, Vol. 38, 1256 pp. Washington: U.S. Government Printing Office 1976

Vogt, P.R.: The Faeroe-Iceland-Greenland aseismic ridge and the western boundary undercurrent. Nature (London) **239**, 79–81, 1972

Zverev, S.M., Kosminskaya, I.P., Krasilschikova, G.A., Mikhota, G.G.: Deep structure of Iceland and Iceland-Faeroes-Shetland region from results of seismic studies. Bull. MOIP Otd. Geol. Vol. **L**, No. 3, 99–115, 1975

Received June 26, 1979; Accepted July 16, 1979

J. Geophys. 47, 228–238, 1980

Journal of Geophysics

Reykjanes Ridge Iceland Seismic Experiment (RRISP 77)

RRISP Working Group.

G. Angenheister, H. Gebrande, and H. Miller
Institut für Allgemeine und Angewandte Geophysik
Universität München
Theresienstr 41, D-8000 München 2, Federal Republic of Germany

P. Goldflam and W Weigel
Institut für Geophysik, Universität Hamburg
Bundesstr. 55, D-2000 Hamburg,
Federal Republic of Germany

W.R. Jacoby
Institut für Meteorologie und Geophysik
Universität Frankfurt
Feldbergstr 47, D-6000 Frankfurt, Federal Republic of Germany

G. Pálmason
Orkustofnun (National Energy Authority)
Grensásvegur 9, 108 Reykjavik, Iceland

S. Björnsson and P. Einarsson
Science Institute, University of Iceland
Dunhaga 3, Reykjavik, Iceland

N.I. Pavlenkova and S.M. Zverev
Institute Physics of the Earth, USSR Academy of Sciences
B. Gruzinskaya 10, Moscow, USSR

I.V Litvinenko
Mining Institute, Leningrad University, Leningrad, USSR

B. Loncarevic
Geological Survey of Canada,
Bedford Institute of Oceanography
Box 1006, Dartmouth, N.S., Canada B2Y 4A2

S.C. Solomon
Department of Earth and Planetary Sciences
Massachusetts Institute of Technology
Cambridge, Massachusetts 02139, USA

Abstract. A long-range seismic refraction experiment is described which was realized in 1977 along an 800 km long line across Iceland and along the southeastern flank of Reykjanes Ridge. The main purpose of the experiment was to resolve the structure of the crust and upper mantle to greater depth than previously possible and to study the transition from the oceanic to the Icelandic structure. Shots, both on Iceland and at sea, were recorded by up to 90 stations from Iceland, Germany, and the Soviet Union and by 7 ocean-bottom stations from Germany and Canada. In addition, detailed marine seismic investigations of the Reykjanes Ridge have been carried out from board RV METEOR.

A well developed 10-km-thick oceanic crust and a stratified lower lithosphere with surprisingly high P-wave velocities (up to 8.6 km/s) has been revealed at the 10 Ma isochron on the eastern flank of Reykjanes Ridge. While the Icelandic crust differs from the oceanic one mainly by its greater thickness, the subcrustal structure is fundamentally different. The Icelandic crust is underlain by a low P-wave velocity (7.0 to 7.6 km/s) upper mantle in a state of partial fusion, which is interpreted as a diapiric updoming of the asthenosphere. No indications for continental fragments beneath Iceland could be found. Details of the interpretation are presented in two accompanying papers.

Key words: Iceland – Reykjanes Ridge – Deep seismic sounding – Crust – Lithosphere – Asthenosphere – Anomalous mantle – Partial fusion.

Introduction

As early as 1912, A. Wegener published the hypothesis 'that the Mid-Atlantic Ridge may be the place where during the still progressing expansion of the Atlantic the sea floor is continuously breaking and making room to relatively fluid and high-temperature simatic material rising from the depth' He thereby clearly anticipated a fundamental idea of the modern concepts of sea-floor spreading and plate tectonics.

For the development of these concepts, the North Atlantic and Iceland have again played an important role. The symmetric magnetic anomalies over Reykjanes Ridge (Heirtzler et al. 1966; see also Talwani et al. 1971, Vogt and Avery 1974) have been instrumental for the breakthrough of the sea-floor spreading concept. Radiometric and paleomagnetic analyses of lava successions in Iceland have become an important tool for the refinement and extension of the geomagnetic polarity time scale (McDougal et al. 1976) which is a basic requirement for paleogeographic reconstructions from geomagnetic lineations.

Anomalously low seismic velocities of 7.4 km/s in the topmost mantle first discovered below the Reykjanes ridge (Ewing and Ewing 1959) turned out to be a general property of mid-oceanic ridges and an important constraint for geodynamic and petrogenetic models. They led Ewing and Ewing (1959) to the conclusion that the mid-ocean ridges are built up by rising convection currents which supply basalt magma from the mantle and exert extensional forces on the ridges.

0340-062X/80/0047/0228/$02.00

Anomalous upper mantle velocities below Reykjanes Ridge were later corroborated by refraction seismic investigations of Talwani et al. (1971), Whitmarsh (1971), and Snoek and Goldflam (1978). Values between 7.2 and 7.4 km/s were also observed below Iceland by Båth (1960), Pálmason (1971) and, with a somewhat different interpretation, by Zverev et al. (1976). However, up to now very little information is available on the depth extent and internal structure of the anomalous mantle itself because of the limited range of the earlier seismic profiles.

The RRISP experiment (Reykjanes Ridge Iceland Seismic Project 1977) whose design, technical execution, and main results are described in this paper, was mainly devoted to this problem. Other important questions to which RRISP addresses itself is the structure of the crust and upper mantle beneath Reykjanes Ridge and the transition from the ridge to Iceland, about which nothing is known to date. Such an experiment must provide deep penetration of observable seismic rays and, at the same time, shallow control along the profile. For these reasons the experiment was amphibian with a terrestrial part on Iceland and a marine part on the southeast flank of the northern Reykjanes Ridge. A more detailed description of the two parts is given in the following papers of this volume, paper 2 on the land part, and paper 3 on the marine part. The present paper will be referred to as paper 1

Previous Investigations

Iceland is a unique object of earth science research because it is the world's largest well exposed and accessible segment of a mid-oceanic ridge. It is an excellent platform for the study of deep structure by methods which cannot be applied at all or only at much greater expense in the submerged parts of the ridges. But Iceland also deserves attention on it's own as the culmination of a large-scale anomaly in the North Atlantic. It is situated at the intersection of the spreading Mid-Atlantic Ridge and the aseismic transverse ridges between Baffin Island, Greenland, Iceland and the Faroes. It has been suggested that the transverse ridges have been produced since the break-up of the adjacent continents by a particularly vigorous basaltic volcanism such as is still active in Iceland (Bott et al. 1971, Bott 1974; Nilsen 1978). Spreading in Iceland, though questioned by some (Einarsson 1967; Beloussov 1970; Beloussov and Milanovsky 1976) is now convincingly demonstrated (Pálmason and Saemundson 1974; Saemundson 1978), particularly by the current rifting episode in the Krafla area (Björnsson et al. 1977, 1979; Gerke et al. 1978). Seemingly conflicting observations (Beloussov and Milanovsky 1976) are probably rather the expression of the anomalous situation of this part of the spreading ridge than truly contradicting the spreading concept.

This may be true also for the possible continental affinity of the lower Icelandic crust suggested by Zverev et al. (1976). There is no reason to dismiss this view immediately, since indications for the existence of continental fragments have been found in other parts of the North Atlantic, e.g., at Rockall Plateau (Scrutton 1972; Roberts et al. 1973), the Faeroe Block (Bott et al. 1974) and Jan Mayen Ridge (Gardé 1978). However an opposite interpretation, which more easily fits the sea-floor spreading concept, has been given by Pálmason (1971) according to whom the crust has oceanic affinity with greater thicknesses of individual layers. According to Bott (1974) this type of crust should be termed "Icelandic" rather than "oceanic"

A decision between the conflicting ideas and interpretations may only be reached through knowledge of the upper mantle structure. Anomalous upper mantle velocities have been obtained by refraction studies to date only for the depth range of some 10 to 15 km (Pálmason 1971), but teleseismic travel-time residuals of 1.3 s (Trygvasson 1964; Long and Mitchell 1970) as well as apparent velocities of P-arrivals from Mid-Atlantic-Ridge earthquakes (Francis 1969a) indicate that low velocities may extend down to some 250 km. S-wave travel-time residuals of over 5 s found by Giradin and Poupinet (1974) indicate an even more pronounced S- than P-wave velocity anomaly in the upper mantle below Iceland. Of great importance as they are, travel-time residuals alone cannot be used to resolve details of structure because of their integral nature. Surface wave studies (Tryggvasson 1962; Giradin and Jacoby 1979; Jacoby and Girardin 1980) are subject to similar limitations. Only in combination with the boundary conditions provided by detailed and deeply penetrating refraction seismic investigations, can the above methods be put to full use in developing geodynamic models.

Layout of the Experiment

Figure 1 shows the layout of the whole experiment. The present paper deals mainly with Profile I. The investigations along the marine segment were the central objective of cruise 45/I of RV METEOR. During this cruise three additional lines at sea (Profiles III-V) were shot in order to investigate the evolution with age of the oceanic lithosphere between the ridge crest and our main line. Details of these lines will be published elsewhere.

The main line starts at shot-point A on the southeastern flank of Reykjanes Ridge and runs slightly oblique to magnetic anomaly 5 (approximately 10 Ma), but parallel to the depth contours. It enters Iceland north of Heimaey and lies mostly within the zone of active rifting and volcanism (eastern neovolcanic zone), which is thought to be the continuation of the active spreading axis offset by transform faults south and north of Iceland. North of the central volcano Askja the main line splits into three branches. One continues straight through the Quaternary and Tertiary basalts towards shot-point E (Vopnafjördur), while the second follows the strike of the neovolcanic zone towards shot-point F in the north (Axarfjördur). The third branch is perpendicular to the line A–E in order to provide information on possible lateral variations between the neovolcanic zone and the Tertiary region of the southeast coast. Since the main program could be carried out within 9 days as planned, the remaining days have been used for the observation of an additional profile along the southeast coast (Profile II), which stays completely within the older part of Iceland and which therefore can serve as a reference line.

Different types of recording instruments were used by the different participating groups. The Soviet team used continuously recording refraction stations equipped with three-component seismometers with 2 s natural period (Zverev et al. 1978) at the positions marked by solid inverted triangles. The solid circles in Fig. 1 show positions of recording sites occupied by the German group using a total of 40 seismic stations of MARS 66 type (Berckhemer 1970) and two digitally recording MARS-66-compatible PCM stations (Gebrande et al. 1977). At sea seven refraction instruments were launched and recovered: five anchored telemetric buoy systems of the Institut für Geophysik, Hamburg (Kebe 1971, Weigel et al. 1978) and 2 ocean bottom seismographs (OBS) of Bedford Institute of Oceanography, Dartmouth, Nova Scotia (Sutton et al. 1977; Heffler and Barrett 1979). Their positions are shown in Fig. 1. All systems were provided with bottom hydrophones. In addition each OBS contained one vertical and one horizontal

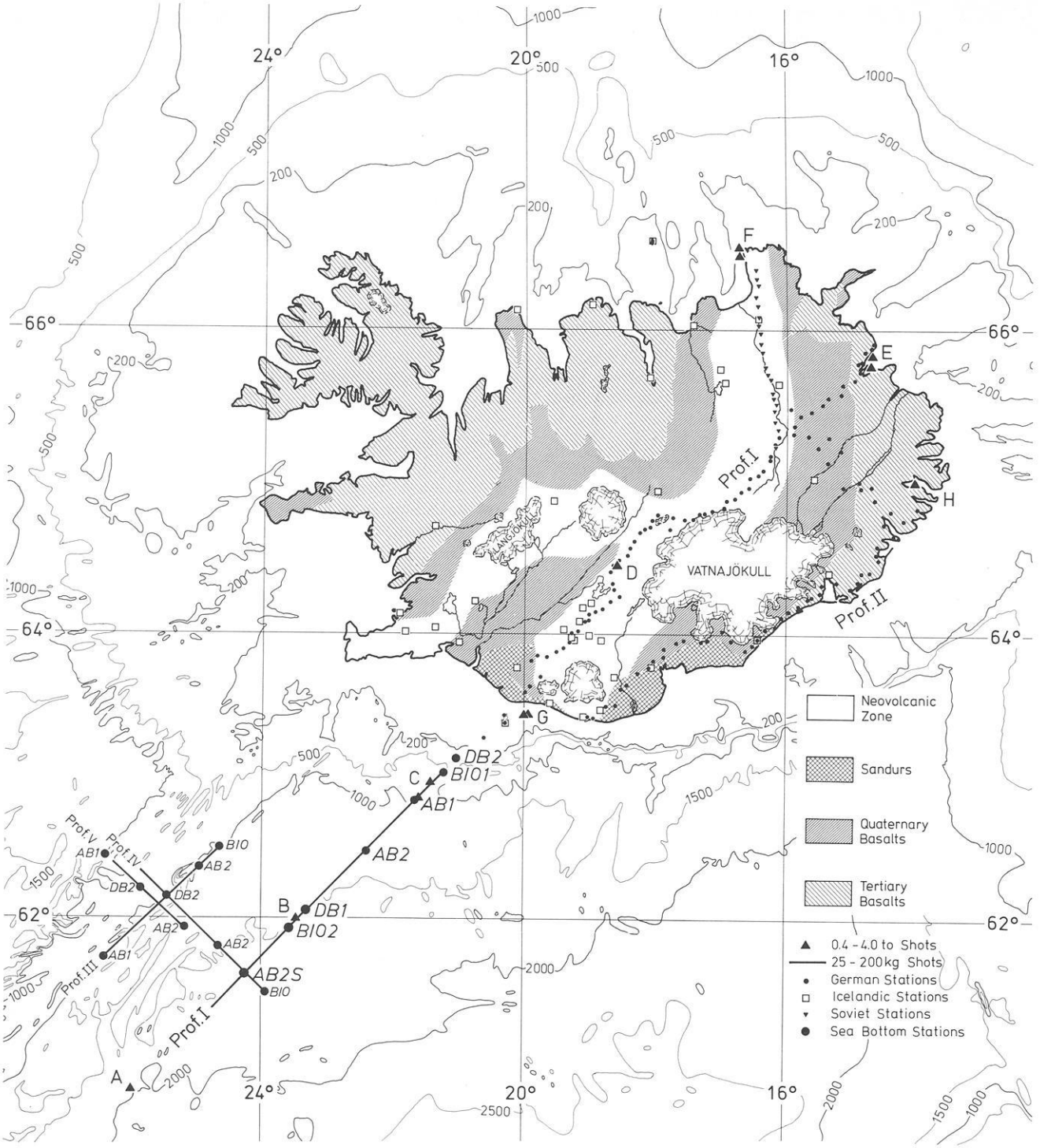

Fig. 1. Simplified geological map of Iceland and bathymetric chart of the surrounding ocean showing shot-points and recording sites of the RRISP 77 project

4.5 Hz seismometer. The principles of the shooting and recording technique at sea are summarized in Fig. 2. Furthermore most of the shots were observed on land by the continuously recording permanent and semipermanent seismic stations of the Icelandic seismological network (Einarsson 1979). Some of these stations were installed especially for the program. Positions are marked as open squares in Fig. 1.

Table 1 gives information on the schedule of the whole experiment and on the large shots fired. The shooting technique varied according to circumstances. At the only land-based shot-point (D) in a shallow lake (Thveraldavatn; depth 17 m) without drainage, the total charge was distributed over a rectangular grid of single 50 kg charges spaced 10 to 20 m apart at the lake bottom; they were fired simultaneously. This shooting technique (Burck-

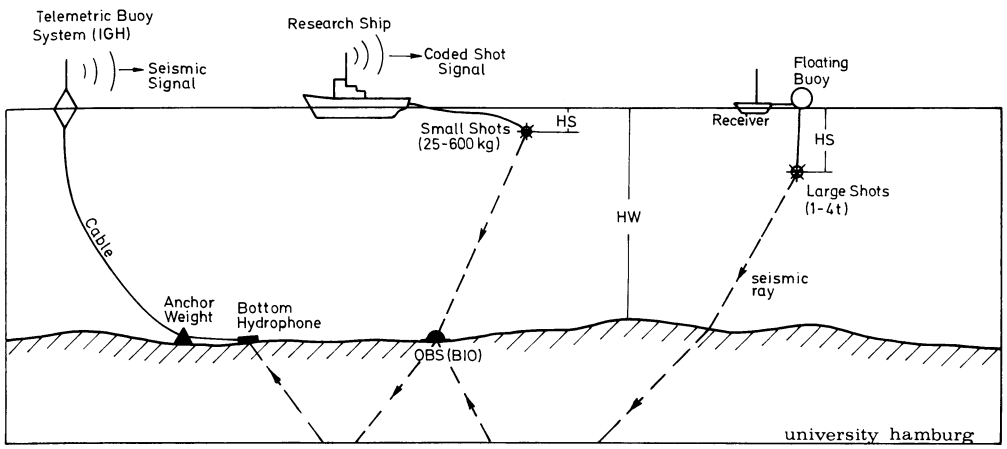

Fig. 2. Shooting and recording technique employed for the marine part of RRISP 77

Table 1. RRISP – Schedule of large shots

Shot no.	Date	Time (GMT)	Longitude west	Latitude north	Charge (kg)		Charge depth (m)	Water depth (m)
C0	12. 7. 77	16–30–00.65	21° 35.9′	62° 51.8′	400		270	1126
C1	14. 7. 77	19–58–02.86	21° 25.0′	62° 58.7′	1000		130	1025
C2	20. 7. 77	10–01–01.78	21° 37.1′	62° 52.0′	1000		130	1117
C3	25. 7. 77	17–01–02.92	21° 35.8′	62° 51.6′	400	single charge	110	1116
B1	15. 7. 77	12–30–36.85	23° 52.9′	61° 59.2′	600		120	1565
B2	17. 7. 77	17–06–22.78	23° 27.4′	61° 59.4′	2000		150	1462
A	18. 7. 77	13–01–04.38	25° 57.8′	60° 43.8′	4000		170	2005
D0	12. 7. 77	18–31–02.79	18° 35.78′	64° 28.33′	500		17	17
D1	15. 7. 77	11–31–02.98	18° 35.78′	64° 28.33′	1000		17	17
D2	18. 7. 77	11–31–02.44	18° 35.78′	64° 28.33′	1000		17	17
E1	19. 7. 77	14–02–10.83	14° 40.93′	65° 50.16′	500		104	104
E2	19. 7. 77	16–02–00.61	14° 42.06′	65° 46.22′	500		110	110
F1	15. 7. 77	15–00–58.42	16° 43.60′	66° 30.16′	500	distributed	115	115
F2	15. 7. 77	17–01–01.60	16° 43.10′	66° 28.15′	500		124	124
F3	17. 7. 77	16–01–02.12	16° 43.10′	66° 27.80′	500		124	124
F4	17. 7. 77	18–01–01.33	16° 43.60′	66° 30.16′	1000		115	115
G1	24. 7. 77	10–01–01.85	20° 00.57′	63° 27.49′	500		110	110
G2	24. 7. 77	11–01–02.85	19° 57.54′	63° 28.15′	500		110	110
H	24. 7. 77	19–01–09.26	14° 02.00′	65° 01.37′	500		113	113

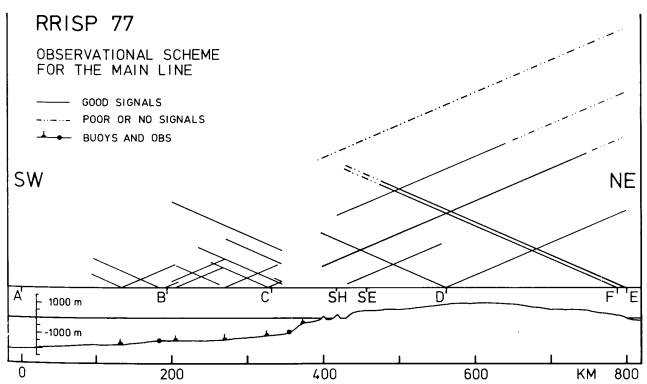

Fig. 3. Simplified diagram showing scheme of observations for the RRISP 77 main profile. Letters *A* to *F* denote shot-points. SH and SE positions of two stations of the Icelandic seismological network. *Solid* and *dot-dashed lines* indicate observational range of sufficient and insufficient signal to noise ratio

hardt and Vees 1975) yielded satisfactory results, even though no optimization with regard to water depth and charge size could be achieved. At the shotpoints close to the coast 500 kg single charges (Soviet TNT and GEOSIT II(TM)) were fired at the sea bottom at optimum depth (110 m), determined by the condition of constructive interference between the gas bubble pulsation and the reverberation of the water layer. Shooting at these points was carried out from small Icelandic fishing vessels rented for that purpose. These shots on the sea bottom were especially valuable, because they radiated not only the expected strong P-waves but also strong S-waves. The shots at points A, B and C were fired from RV METEOR. They were suspended below a buoy at optimum charge depth and detonated by means of a coded radio signal transmitted from the ship. In addition to the large shots, a total of 141 small shots (25–200 kg) spaced 1.8 km apart were fired along the line from receiver BIO1 to south of receiver AB2S (see Fig. 1). These charges were dropped directly from METEOR and detonated by means of a firing line. For the shots fired from METEOR, GEOSIT II(TM) was used as the explosive.

The positions of the buoys, OBS's, and shots at sea were determined by LORAN C and satellite navigation. At the shotpoints close to the coast positioning was done by radar tracking of the coast line, determination of water depth, and photofixes of the shore line. The positions of land stations were determined from aereal photographs and topographic maps on the scale of 1:50000 and 1:100000. In all cases, the accuracy of the positions is estimated to be ± 200 m or better.

Figure 3 gives the scheme of observations along the main line showing the system of reversed and overlapping profiles actually observed. Most of the shots were recorded up to the expected range, but for shot-points A and B energy propagation was not sufficient to cover the whole land line in spite of charges as large as 4 and 2 t. As will be shown later, this is most probably caused by structure and/or absorption rather than by poor shot energy. The two positions SH and SE are locations of two stations of the permanent Icelandic seismological network (Storhöfdi on Heimaey and Selkot at the south coast) which like others have recorded many of the smaller METEOR shots. These recordings were useful in closing the information gap between the marine and the land part.

A combined land-sea experiment of such an extent obviously calls for good communication links between the ship and the land stations. Shooting at sea is highly dependent on weather conditions especially when large charges are to be fired. Therefore the whole schedule is subject to changes and land stations must be informed immediately. During the experiment two headquarters were established, one at Sigalda in the south, the other at Krafla in the north. Both headquarters maintained a permanent shortwave communication link with each other and at Sigalda a strong transmitter (2.5 kW) was used to maintain contact with RV METEOR and also to broadcast news for the observers, who were all equipped with appropriate receivers. During shot-windows Sigalda also transmitted a quarz clock controlled time signal, which could be used as back-up in case the MSF time signal, which was normally recorded, could not be received. Besides our own news broadcasts, information for the observers was also broadcast three times daily by all stations of the Iceland State Broadcasting Service, as shortwave propagation varied very much, but medium and long wave propagation conditions remained fairly constant. This rather elaborate communications set-up was necessary because recording crews consisting of two persons in one four-wheel drive vehicle could not contact the headquarters frequently because of remote and rugged terrain. They were completely self-supporting with respect to food and shelter and were supplied with gasoline whenever tapes were relayed into headquarters. To gain quick information on travel-times and energy propagation, as well as to spot equipment problems, the tapes were played back at headquarters as they came in.

Data

All recordings were digitized for later processing. This was done at the Geophysical Institutes at Karlsruhe (MARS 66 data), Mu-

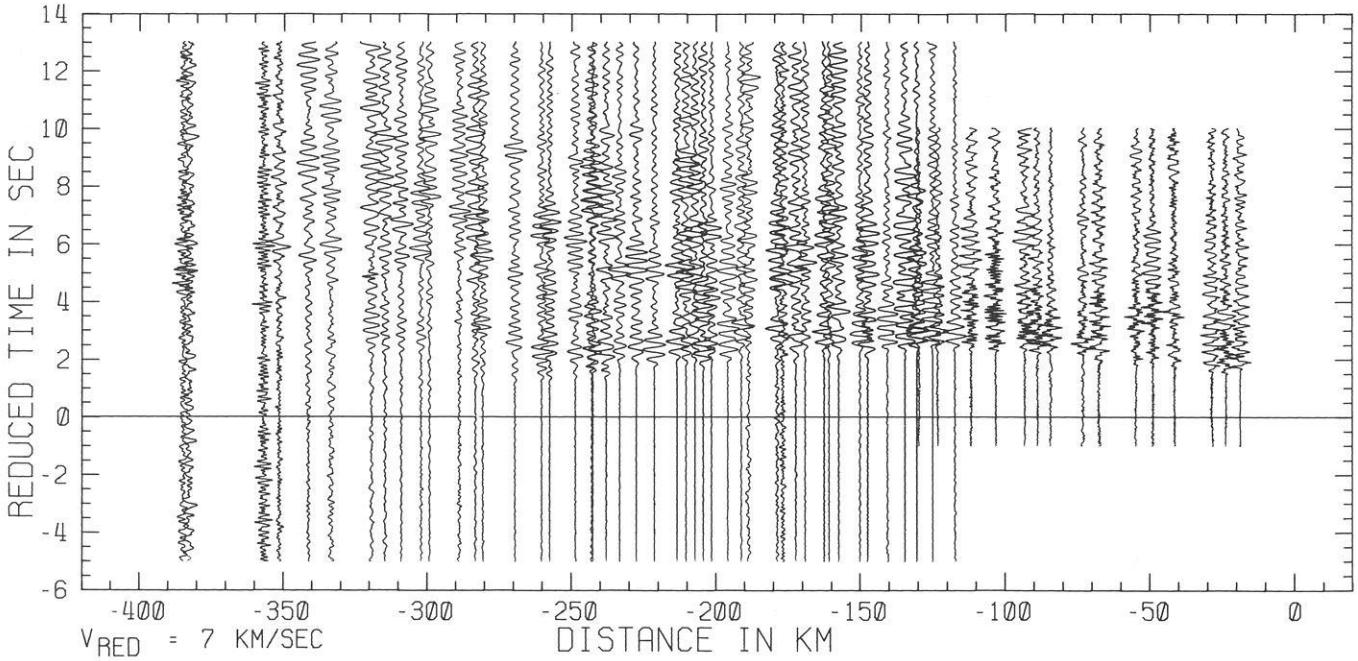

Fig. 4. Record section along the land segment of the main profile; shots F1 and F4, bandpass filtered 1–10 Hz. The section contains records obtained by the Soviet group (0 to 135 km) as well as records obtained by the German group (120 to 390 km). Reduction velocity is 7 km/s

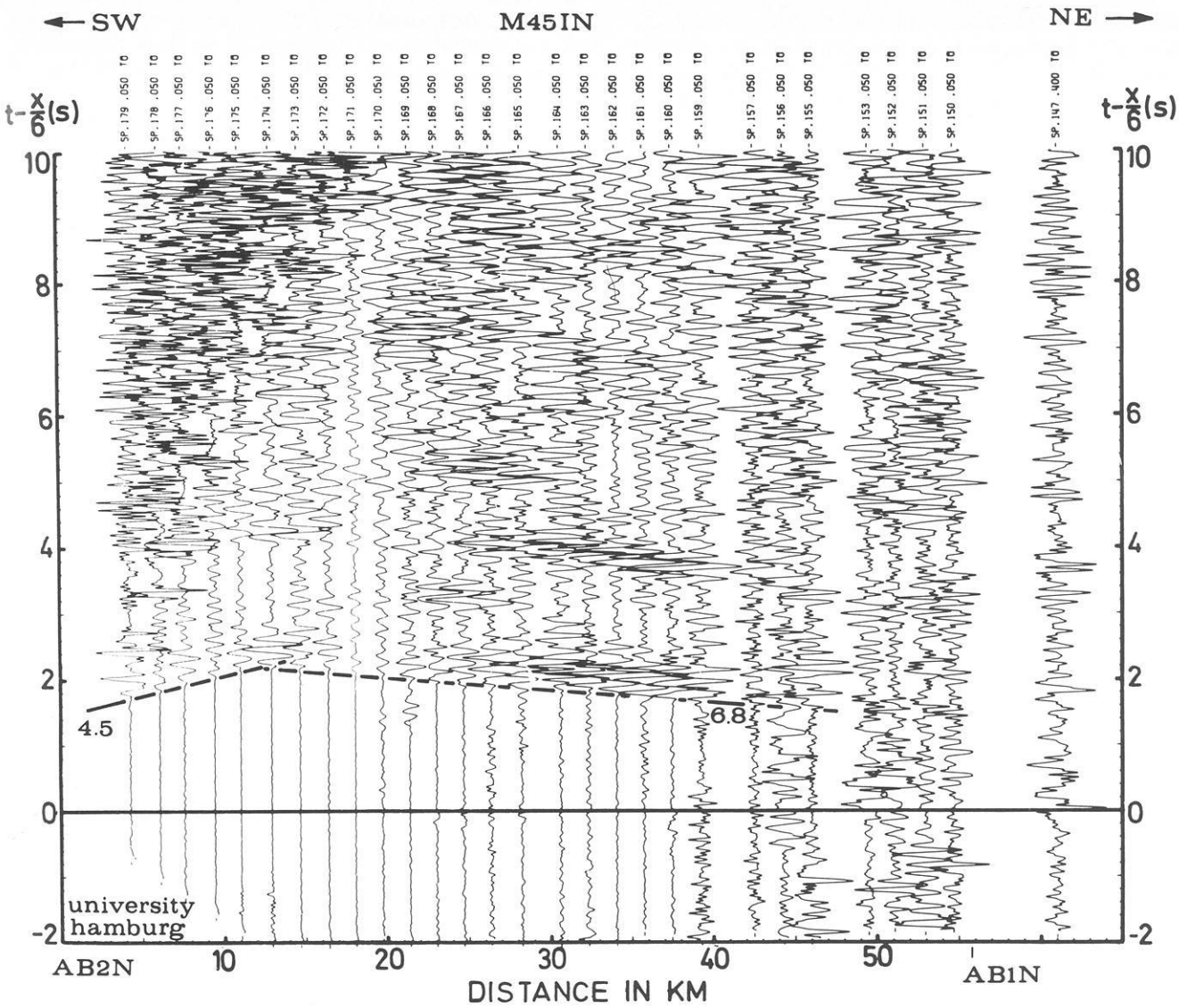

Fig. 5. Marine record section reduced by 6 km/s and bandpass filtered 2–20 Hz. Data were recorded by the ground hydrophone (water depth: 1389 m) of buoy AB2N. Shots were fired along the main line towards the northeast

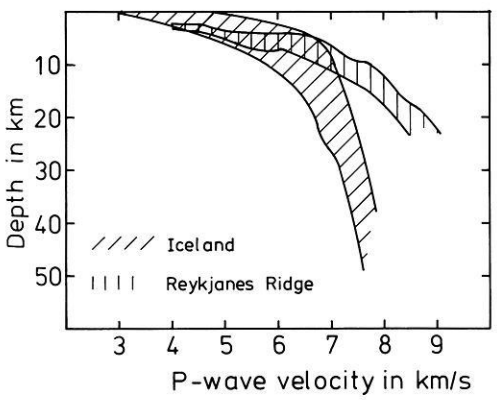

Fig. 6. Extremal bounds on possible velocity-depth distributions beneath Iceland and the southeastern flank of Reykjanes Ridge. The broader region of possible solutions for the land part is indicative of a more heterogeneous velocity distribution

nich (PCM and Soviet data), Hamburg (buoy data), and at Bedford institute (OBS data). The Soviet data were digitized by hand from analog playbacks. The record-sections of Figs. 4 and 5 show examples of the data after some basic processing (digital band-pass filtering). Fig. 4 shows a typical land record-section. It is a compilation of records obtained by the Soviet and German groups from shots F1 and F4, which were fired at the same location but recorded at different recording sites. Reduction velocity is 7 km/s. In the distance range of 120 to 135 km both data sets overlap and one may notice how well they fit.

Each seismogram is normalized with respect to its maximum amplitude and it may be seen that at distances beyond some 240 km the maximum energy within the seismograms is shifted from the first arrival wave train to later times. One may clearly distinguish two different travel-time segments as delineated by first arrivals. The first one with an intercept time of 1.3 s, indicating a thick low-velocity surface layer shows an apparent velocity of 6.8 km/s. At distances greater 120 km, the arrivals can be attributed to another segment with an apparent velocity of 7.2 km/s.

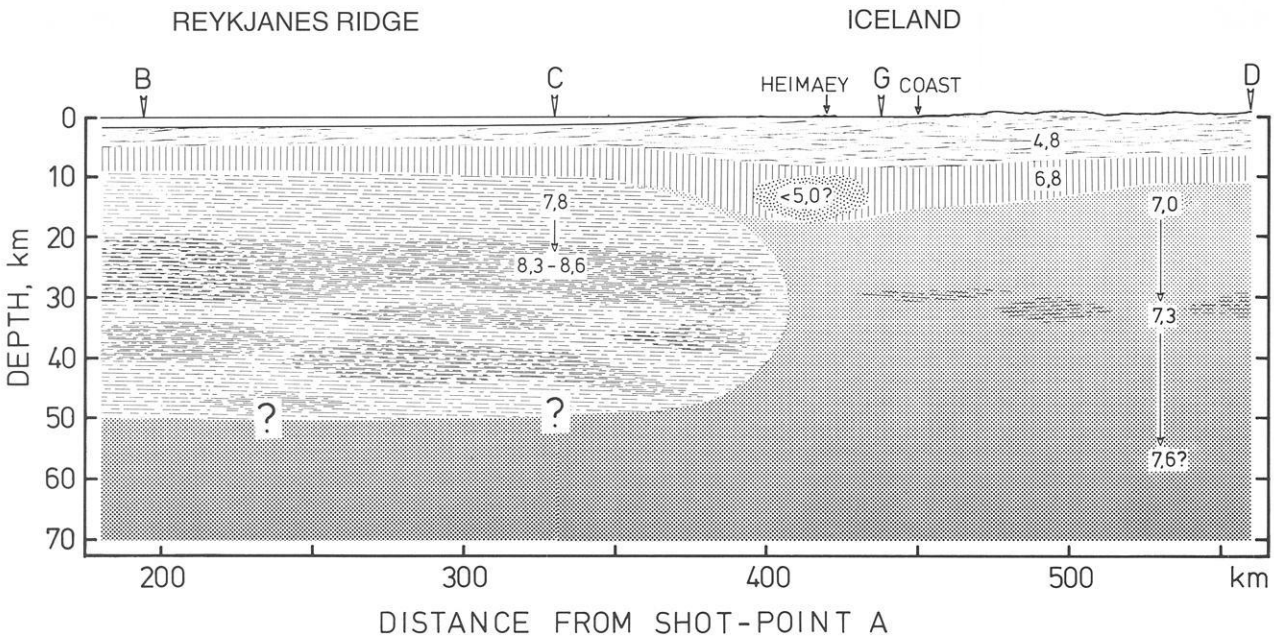

Fig. 7. Generalized crustal and upper-mantle cross section of the central part of RRISP 77 main profile. Letters indicate positions of large shots. Numbers give P-wave velocities in km/s. Crustal layers are continuous across the transition from the ridge to Iceland, whereas there is a drastic change in upper-mantle structure close to the shelf slope, where a well developed oceanic lithosphere beneath Reykjanes Ridge abuts on anomalous upper-mantle material in the state of partial fusion

Both segments can be alternatively correlated as one continuous travel-time curve, indicating velocity gradients rather than discontinuities. The existence of velocity gradients is also suggested by the absence of prominent later arrivals, which could be correlated over some distance and interpreted as reflections or diving waves. This is a salient distinction from seismogram sections obtained in continental areas.

Figure 5 is an example of a record section from the marine part, which (contrary to Fig. 4) has been reduced by 6 km/s. All records were obtained at buoy AB2N from shots along the line towards buoy AB1N. All seismograms were filtered with a pass-band of 2–20 Hz, and are normalized individually with respect to their maximum amplitudes. The section is uncorrected for shot and receiver depths, but nevertheless it gives a good idea of the general character of the marine data. True velocities obtained in combination with the reversed profile (see Fig. 6 in Goldflam et al. 1980) are rather typical for a well developed oceanic crust. The prominent later arrivals parallel to the first ones are multiple reflections from the water surface at the receiver side.

Results

The results presented below are based on most of the data, but only some of the record-sections are shown here, as well as in Gebrande et al. 1980 and Goldflam et al. 1980. As we concentrate here on the general structure, small-scale regional differences will not be discussed.

As a first stage in interpretation, smoothed travel-time curves of the land and marine part were inverted using the tau-p method (Bessonova et al. 1974) and a generalized Wiechert-Herglotz-method. The results are summarized in Fig. 6 with the hatched regions giving the range of possible velocity-depth distributions. In spite of broad bands, a clear difference between the Reykjanes-Ridge flank and Iceland is evident, the marine crust showing a stronger velocity increase with depth. To evaluate the differences in more detail and to obtain the horizontal velocity variations along the main line, extensive ray tracing was performed (see Gebrande et al. 1980; Goldflam et al. 1980).

The main results obtained are shown in Fig. 7. Although generalized, it does show the principal structural trends rather accurately. The different surficial layers have been combined into one with an average velocity of 4.8 km/s. Velocity gradients in this layer are, at least in Iceland, very likely (Flóvenz 1980) but could not be resolved accurately with the receiver spacing of RRISP 77, which was chosen with the aim to obtain structure at greater depth. The necessary crustal control is provided by detailed small-scale seismic refraction work of Pálmason (1971).

Layer 3 is rather homogeneous and continuous from the ocean through Iceland; thus it exists also beneath the neovolcanic zone. The thickness of the crustal layers is generally greater underneath Iceland than under the ocean and their top and bottom show greater relief. Total crustal thickness including the water layer is some 10 km beneath the segment along Reykjanes Ridge, but varies between 15 km in the southeastern and northern, and 10 km in the central section beneath Iceland. Large travel-time residuals for the more distant shots at the recording sites on Heimaey, but normal arrival times for shots G1 and G2, are an indication for the possible existence of a magma chamber in the lower crust beneath Heimaey. This body is shown schematically in Fig. 7 and velocities lower than 5 km/s are attributed to it. A similar body may exist in the area of Askja in northern Iceland (Gebrande et al. 1980).

Below layer 3, fundamental differences in structure exist between the ocean and Iceland. On the marine side we find a velocity of 7.7 to 7.8 km/s which, if interpreted as layer 3b, would be anomalously thick; it is rather attributed to the upper mantle (Golflam et al. 1980). Similar upper-mantle velocities have earlier

been reported by Whitmarsh (1971) for an area 200 km southeast of shot-point A and are also observed beneath the Iceland-Faeroe Ridge (Bott and Gunnarsson 1980). As there is no evidence for velocities of 7.2 to 7.4 km/s as found by Ewing and Ewing (1959) and Talwani et al. (1971) at or near the ridge crest, we must assume a rather well developed oceanic lithosphere. The sub-Moho velocity remains nearly constant down to 15 km but increases continuously at greater depth and reaches values of 8.3 to 8.6 km/s at a depth of about 20 km. This is an important new feature in that area. The 8.3 km/s velocity was observed at OBS BIO1 in the distance range of 90 to 140 km as first arrivals. In the reversed direction even higher velocities were observed at OBS BIO2 in the same distance range. These high velocities are corroborated by records of the Icelandic seismological network at distance ranges of 100 to 180 km. Apparent velocities at stations near the south coast observed from marine shots between points B and C reach values as high as 9 km/s after correction for water depth. This can only partially be explained by interfaces dipping towards Iceland. The data therefore require the existence of P-wave velocities of up to 8.6 km/s or so. These P-wave velocities, however, cannot be constant in the lower lithosphere, because the apparent velocities vary rather irregularly and because the mean S-wave velocities deduced from the inversion of surface waves along the same line are rather low (Jacoby and Girardin 1980). This inhomogeneous velocity distribution is schematically depicted by the darker hatched areas in Fig. 7.

No direct information was obtained on the depth of the lower boundary of the lithosphere below Reykjanes Ridge. However, evidence from surface waves and missing signals from shotpoint A, which must be explained by downward refraction of rays originating from A due to a negative velocity gradient, give a rough idea of the thickness of the lithosphere. The boundary to the asthenosphere was put, somewhat arbitrarily, at a depth of 50 km.

There is no evidence for the continuation of the marine high-velocity lithosphere underneath Iceland. Instead we find velocities increasing from 7 to 7.4 km/s in the same depth range. Only locally, slightly higher velocities may exist (see Gebrande et al. 1980), as symbolized in Fig. 7 by the darker-shaded areas at 30 km depth beneath Iceland. The transition from the high-velocity oceanic lithosphere to the low-velocity upper mantle beneath Iceland is rather abrupt and must occur close to the shelf slope. Although shown here only along the main line, the anomalous upper mantle is not confined to the neovolcanic zone, but extends under all of Iceland. It is also present beneath the older parts of Iceland such as the Tertiary in the east (as shown by Profile II) and west (Båth 1960).

This may account for the rather homogeneous travel-time anomalies (Long and Mitchell 1970). The residuals can be quantitatively explained by our model only if the anomalous mantle extends to depths greater than 100 to 200 km depending upon the velocity gradient assumed below 30 km.

More light on the nature of the anomalous mantle (layer 4 of Pálmason 1971) is shed by the analysis of S-wave propagation through Iceland. As shown by Gebrande et al. (1980) the P to S velocity ratio is 1 76 in the Icelandic crust, which is rather normal for basic material, but reaches values between 1.96 to 2.2 at greater depth. While gabbroic material could marginally account for the observed values at moderate temperatures and pressures (Christensen 1978), this explanation fails in view of the high temperatures (1000–1100°C) at the base of the crust as derived by magnetotelluric (Beblo and Björnsson 1978) and geothermal investigations (Pálmason and Saemundson 1974, Pálmason et al. 1979). The only remaining possibility is partially molten ultrabasic material, as has been suggested earlier by Bott (1965), Pálmason (1971) and Pálmason and Saemundson (1974). As shown by Gebrande et al. (1980) the observed P and S velocities allow a quantitative estimation of the degree of partial fusion. Assuming a mixture of solid peridotite and basaltic melt, we infer a melt concentration greater than 17% at the base of the crust decreasing with increasing depth (see also Beblo and Björnsson 1980). The predominantly ultrabasic composition is the main justification for calling the layer with P-wave velocities from 7.0 to 7.4 km/s 'anomalous mantle' Relying only on the P-wave velocities, it would have been more natural to attribute this depth range to the crust, since similar velocities are widespread in the lowermost crust. In this case the thickness of the Icelandic crust would be about 30 km, the inhomogeneities at this depth range (see Fig. 7) may give some support for such an alternative interpretation. The interpretation as anomalous mantle is largely based on the comparison of the observed seismic wave velocities with laboratory data. Additional laboratory investigations of seismic wave transmission in partially molten rocks would be very important to corroborate or possibly modify our conclusions.

From the extent of the anomalous mantle it may be deduced that partial melting is not confined to the narrow neovolcanic zone but may exist, most likely with local variations in concentration, below the whole island and may be responsible for the high mobility of the Icelandic crust and the existence of active volcanism outside the neovolcanic zones, e.g., at Snaefellsnes and Oraefi. The same conclusion has been reached by Beblo and Björnsson (1978) from the distribution of electrical conductivity derived from magneto-telluric measurements.

Under the seaward continuation of the profile similar partially molten material is obviously absent at shallow depth. However, one may speculate whether the 7.8 km layer might be the marine counterpart of the Icelandic anomalous mantle, but cooler and correspondingly with a smaller melt content. Another possibility would be that this layer is composed of perodotite enriched in a solidified low-melting-point fraction as postulated by the petrogenetic model of Bottinga and Allègre (1976) for the depth range of 10 to 20 km. Unfortunately, since S-waves were not observed on the marine part a decision between both alternatives is not possible.

Another open question is the petrological interpretation of the high upper-mantle velocities (up to 8.6 km/s) underlying the 7.8 km/s layer. Similarly high velocities have been reported for the lower oceanic lithosphere from different areas and by different authors, as has recently been reviewed by Asada and Shimamura (1979). It appears impossible to understand these high velocities in terms of todays knowledge about upper mantle petrology without invoking anisotropy (Green and Liebermann, 1976, Bottinga and Allègre, 1976). The model most favoured for the generation of upper mantle anisotropy is the one proposed by Francis (1969b). According to this model, anisotropy is due to the preferred orientation of the *a* crystallographic axis of olivine parallel to the upper mantle flow lines, induced by plastic deformation, the direction of maximum velocity is therefore expected to be perpendicular to the ridge axis and to the magnetic lineations. This model would require lower velocities in the direction of our main line, contrary to observation. Our results therefore suggest another explanation, namely that the high velocity layer behaves as a transversely isotropic medium with minimum velocity in the vertical axis of symmetry and maximum velocity in horizontal directions. This type of anisotropy is to be expected from the preferred orientation of the *b* crystallographic axis of olivine in the vertical direction and from randomly distributed *a* and *c* axes

in the horizontal plane as is common in cumulate rocks (Christensen 1978). This would imply that the high velocity layer is the product of segregation of olivine from partially molten anomalous mantle rather than being a residual layer formed by depletion in low melting point fraction by rising magma. Another explanation of the upper-mantle velocity distribution, involving Francis-type anisotropy, is discussed by Goldflam et al. (1980). The additional marine profiles (Fig. 1) may resolve this question.

Conclusions

Combined land-sea refraction seismic investigations along an 800 km long line from Reykjanes Ridge to northeast Iceland have revealed the following:

1 Contrary to current opinion, we find a well developed oceanic crust and stratified subcrustal lithosphere already at the 10 Ma isochron (anomaly 5) on the southeastern flank of Reykjanes Ridge.

2. High P-wave velocities of up to 8.6 km/s have been measured parallel to the ridge axis at depths greater than 20 km bearing on possible models of lithospheric evolution.

3. Except for greater thickness and more pronounced lateral variations, the Icelandic crust is very similar to the crust beneath Reykjanes Ridge. Layer 3 can be traced without interruption from the 10 Ma old oceanic crust through Iceland and it exists also beneath the eastern neovolcanic zone, which is supposed to be the present-day active spreading axis.

4. The subcrustal structure below Iceland is fundamentally different from the one below the southeastern flank of Reykjanes Ridge. The Icelandic crust is underlain by low P-wave velocity (7.0 to 7.6 km/s) material down to depths greater than 50 km, which must be interpreted as mantle material in the state of partial fusion. This anomalous mantle seems to form a diapiric updoming of the asthenosphere, much broader than is likely beneath mid-ocean ridges proper. The formation of such an anomaly seems hardly possible without a locally enhanced upwelling convection current, which some might like to call a plume.

5. The transition of the subcrustal structure from Reykjanes Ridge to Iceland takes place within a very narrow zone below the shelf slope. One might speculate whether this sharp boundary is present everywhere around Iceland or whether it is a special feature connected with the Reykjanes Fracture Zone.

Acknowledgements. We thank all, who made this experiment possible. Without the special efforts under often adverse conditions made by the crew of RV METEOR, the observers in the field and the people in the playback centers the experiment would not have been successful. All technical and scientific participants are listed by name in the Appendix. R. Herber, J.M. Misnik, G.G. Petursson, and R. Vees were responsible for the large shots fired. R. Ebel was in charge of communications. St. Sigurmundsson helped in managing the experiment. W Kaminski made his data processing programs available. Orkustofnun and Landsvirkjun provided headquarter facilities at the Sigalda and Krafla power plants. Iceland State Broadcasting Service helped by transmitting special news broadcasts. RRISP 77 was funded through Deutsche Forschungsgemeinschaft, Orkustofnun, Soviet Academy of Sciences, Geological Survey of Canada and National Science Foundation. The National Research Council of Iceland gave permission and support.

Appendix

Participating Institutions (on board RV METEOR)

Institut für Geophysik, Universität Hamburg (IGH)
Deutsches Hydrographisches Institut, Hamburg (DHI)
Institut für Meteorologie und Geophysik, Universität Frankfurt (IGF)
Bedford Institute of Oceanography, Canada (BIO)
Institut für Geophysik, Universität Kiel (IGK)
Massachusetts Institute of Technology, USA (MIT)
Freie und Hansestadt Hamburg, Baubehörde (HHB)
Erprobungsstelle der Bundesmarine, Eckernförde (E 71)

Participating Scientists and Technicians

IGH: M. Eilers, P. Goldflam, M. Hamann, R. Herber, O. Pahl, M. Rahal, H. Richter, and W Weigel. Coordinator for METEOR-Cruise 45
DHI: W Kämmerer
IGF: W Jacoby
BIO: B.D. Loncarevic and D. Heffler
IGK: H.J. Brink
MIT: S. Solomon and S. Richard
HHB: H. Gäbler
E 71 E. Kuthning

Participating Institutions (on Iceland)

Institut für Geophysik, Freie Universität Berlin (B)
Institut für Geophysik, Technische Universität Clausthal (CLZ)
Institut für Meteorologie und Geophysik, Universität Frankfurt (IGF)
Institut für Geophysik, Universität Göttingen (G)
Niedersächsisches Landesamt für Bodenforschung, Hannover (NLfB)
Institut für Geophysik, Universität Karlsruhe (KA)
Institut für Allgemeine und Angewandte Geophysik, Universität München (M)
National Energy Authority (Orkustofnun), Reykjavik (ORK)
Science Institute, University of Iceland, Reykjavik (SCI)
Institute Physics of the Earth, Moscow (IPEM)
Mining Institute, University of Leningrad (MIL)

Participants

B: D. Damaske, R. Ebel, K. Görler, H. Letz, P. Röwer, and H.G. Schütte
CLZ: J. Christiansen, K. Kaiser, and R. Vees
IGF: F. Auer, B. Baier, A. Paulat, H. Reichenberger, H. Schmeling, and P. Temme
G: H.J. Lotz, and E. Klinge
NLfB: C. Behnke, and G. Druivenga
KA: D. Emter, J. Fertig, G. Sattel, J. Schlittenhardt, W Schott, and W. Zürn
M: G. Angenheister, M. Beblo, F. Berktold, W. Brüstle, O. Bühler, H.K. Fuchs, H. Gebrande, V. Haak, K. Kemmerle, H. Miller, W. Pohl, E. Schmedes, U. Strössenreuther, M. Thuringer, M. Will, and P. Zeil

ORK. K. Arnason, H. Eysteinsson, V Gudmunsson, I. Haraldsdottir, M. Magnusson, G. Myrdal, G.G. Petursson, and St. Sigurmundsson
SCI: B. Brandsdottir, P. Einarsson, D. Gunnarsdottir, O. Olafsson, and J. Sveinsson
IPEM. V Akimov, A.N. Fursov, V Knjazev, and S.M. Zverev
MIL: I.V Litvinenko, and J.M. Misnik

References

Asada, T., Shimamura, H.: Long-range refraction experiments in deep ocean. Tectonophysics **56**, 67–82, 1979

Båth, M.: Crustal structure of Iceland. J. Geophys. Res. **65**, 1793–1807, 1960

Beblo, M., Björnsson, A.: Magnetotelluric investigation of the lower crust and upper mantle beneath Iceland. J. Geophys. **45**, 1–16, 1978

Beblo, M., Björnsson, A.: A model of electrical resistivity beneath NE-Iceland, correlation with temperature. J. Geophys. **47**, 184–190, 1980

Beloussov, V V.: Against the hypothesis of ocean-floor spreading. Tectonophysics **9**, 489–511, 1970

Beloussov, V V., Milanovsky, Y Y.: On the tectonics and tectonic position of Iceland. Greinar **5**, 96–120, 1976

Berckhemer, H.: MARS 66 – a magnetic tape recording equipment for deep seismic sounding. Z. Geophysik **36**, 501–518, 1970

Bessonova, E.N., Fishman, V.M., Ryaboyi, V.Z., Sitnikova, G.A.: The tau method for inversion of travel times – I. Deep seismic sounding data. Geophys. J.R. Astron. Soc. **36**, 377–398, 1974

Björnsson, A., Johnsen, G., Sigurdsson, S., Thorburgsson, G., Tryggvason, E.: Rifting of the plate boundary in North Iceland 1975–1978. J. Geophys. Res. **84**, 3029–3038, 1979

Björnsson, A., Saemundsson, K., Einarsson, P., Tryggvason, E., Grönvold, K.: Current rifting episode in north Iceland. Nature **266**, 318–323, 1977

Bott, M.H.P.: The upper mantle beneath Iceland. Geophys. J.R. Astron. Soc. **9**, 275–277, 1965

Bott, M.H.P.: Deep structure, evolution and origin of the Icelandic transverse ridge. In: Geodynamics of Iceland and the North Atlantic Area, L. Kristiansson, ed.: pp. 33–47. Dordrecht: Reidel 1974

Bott, M.H.P., Browitt, C.W.A., Stacey, A.P.: The deep structure of the Iceland-Faeroe Ridge. Marine Geophys. Res. **1**, 328–351, 1971

Bott, M.H.P., Gunnarsson, K.: Crustal structure of the Iceland-Faeroe Ridge. J. Geophys. **47**, 221–227, 1980

Bott, M.H.P., Sunderland, J., Smith, P.J., Casten, U., Saxov, S. Evidence for continental crust beneath the Faeroe Islands. Nature **248**, 202–204, 1974

Bottinga, Y., Allègre, C.: Geophysical, petrological and geochemical models of the oceanic lithosphere. Tectonophysics **32**, 9–59, 1976

Burckhardt, H., Vees, R.: Explosions in shallow water for deep seismic sounding experiments. J. Geophys. **41**, 463–474, 1975

Christensen, N.I.: Ophiolites, seismic velocities and oceanic crustal structure. Tectonophysics **47**, 131–157, 1978

Einarsson, T.: The Icelandic fracture system and the inferred causal stress field. In: Iceland and the Mid-Ocean Ridges, S. Björnsson, ed.: pp. 128–139. Reykjavik: Soc. Sci. Isl. 1967

Einarsson, P.: Travel times recorded at Icelandic seismograph stations during the Reykjanes Ridge Iceland Seismic Project (RRISP). Publ. Sci. Inst. Univ. Iceland, RH-79-10, 1979

Ewing, J., Ewing, M.: Seismic-refraction measurements in the Atlantic Ocean Basin, in the Mediterranean Sea, on the Mid-Atlantic Ridge, and in the Norwegian Sea. Bull. Geol. Soc. Am. **70**, 291–318, 1959

Flóvenz, O.G.: Seismic structure of the Icelandic crust above layer three and the relation between body wave velocity and the alteration of the basaltic crust. J. Geophys. **47**, 211–220, 1980

Francis, T.J.G.: Upper mantle structure along the axis of the Mid-Atlantic Ridge near Iceland. Geophys. J. R. Astron. Soc. **17**, 507–520, 1969a

Francis, T.J.G. Generation of seismic anisotropy in the upper mantle along the mid-oceanic ridges. Nature **221**, 162–165, 1969b

Gardé, S.: Der geologische Aufbau des Jan Mayen Rückens (Nordatlantik) nach seismischen Messungen (abstract). Münster: 38th Ann. Meet. German Geophys. Soc. 1978

Gebrande, H., Miller, H., Einarsson, P.: Seismic structure of Iceland along the RRISP-Profile I. J. Geophys. **47**, 239–249, 1980

Gebrande, H., Miller, H., Schmedes, E.: Digital registrations of aftershocks of the Friuli earthquake 1976. Publ. Inst. Geophys. Polish Acad. Sc. A-6 (117), 75–84, 1977

Gerke, K., Möller, D., Ritter, B.: Geodätische Lagemessungen zur Bestimmung horizontaler Krustenbewegungen in Nordost-Island. Wiss. Arb. Geodät. Photogramm. Kartogr., T.U. Hannover, Nr. 83, 23–33, 1978

Girardin, N., Jacoby, W.R.: Rayleigh wave dispersion along Reykjanes Ridge. Tectonophysics **55**, 155–171, 1979

Girardin, N., Poupinet, G.: Teleseismic S travel-time delay for Mid-Atlantic Ridge earthquakes. Phys. Earth Planet. Inter. **9**, 306–313, 1974

Goldflam, P., Weigel, W., Loncarevic, B.: Seismic structure along RRISP-Profile I on the south-east flank of the Reykjanes Ridge. J. Geophys. **47**, 250–260, 1980

Green, D.H., Liebermann, R.C.: Phase equilibria and elastic properties of a pyrolite model for the oceanic upper mantle. Tectonophysics **32**, 61–92, 1976

Heffler, D.E., Barrett, D.L.: OBS-development at Bedford Institute of Oceanography. Mar. Geophys. Res. **4**, in press, 1979

Heirtzler, J.R., Le Pichon, X., Baron, J.G.: Magnetic anomalies over the Reykjanes Ridge. Deep-Sea Res. **13**, 427–443, 1966

Jacoby, W.R., Girardin, N.: The evolution of the lithosphere at the southeast flank of Reykjanes Ridge from surface wave data. J. Geophys. **47**, 271–277, 1980

Kebe, H.W.: Eine ferngesteuerte Meßboje mit Datenspeicherung für refraktionsseismische Untersuchungen auf See. METEOR-Forsch.-Ergebn., Reihe C, Nr. **6**, 14–20, 1971

Long, R.E., Mitchell, M.G.: Teleseismic P-wave delay time in Iceland. Geophys. J.R. Astron. Soc. **20**, 41–48, 1970

McDougal, I., Watkins, N.D., Walker, G.P.L., Kristjansson, L. Potassium-argon and paleomagnetic analysis of Icelandic lava flows. J. Geophys. Res. **81**, 1505–1512, 1976

Nilsen, T.H.: Lower Tertiary laterite on the Iceland-Faeroe Ridge and the Thulean land bridge. Nature **274**, 786–788, 1978

Pálmason, G.: Crustal structure of Iceland from explosion seismology. Reykjavik: Soc. Sci. Isl. 1971

Pálmason, G., Arnórsson, S., Fridleifsson, I.B., Kristmannsdóttir, H., Saemundsson, K., Stefánsson, V., Steingrimsson, B., Tómasson, J., Kristjansson, L.: The Iceland crust. Evidence from drillhole data on structure and processes. 2nd Maurice Ewing Memorial Symposium. Implications of Deep Drilling Results in the Atlantic Ocean. Washington, D.C. Am. Geophys. Union, in press, 1979

Pálmason, G., Saemundsson, K.: Iceland in relation to the Mid-

Atlantic Ridge. Annu. Rev. Earth Planet. Sci. **2**, 25–50, 1974

Roberts, D.G., Ardus, D.A., Dearnley, R.: Precambrian Rocks drilled on the Rockall Bank. Nature Phys. Sci. **244**, 21–25, 1973

Saemundsson, K.: Fissure swarms and central volcanoes of the neo-volcanic zones of Iceland. Geol. J. Spec. Iss. **10**, 415–432, 1978

Scrutton, R.A. The crustal structure of Rockall Plateau microcontinent. Geophys. J.R. Astron. Soc. **27**, 259–275, 1972

Snoek, M., Goldflam, St.: Crustal structure of the Reykjanes Ridge at 63° N derived from refraction seismic measurements. J. Geophys. **45**, 107–109, 1978

Sutton, G.H., Kasahaza, J., Ichinose, W.N., Byrne, D.A.: Ocean bottom seismograph development of Hawaii Institute of Geophysics. Mar. Geophys. Res. **3**, 153–177, 1977

Talwani, M., Windisch, C.C., Langseth, M.G. Reykjanes Ridge crest: a detailed geophysical survey. J. Geophys. Res. **76**, 473–517, 1971

Tryggvason, E. Crustal structure of Iceland region from dispersion of surface waves. Bull. Seismol. Soc. Am. **52**, 359–388, 1962

Tryggvason, E.: Arrival times of P-waves and upper mantle structure. Bull. Seismol. Soc. Am. **54**, 727–736, 1964

Vogt, P.R., Avery, O.E.: Detailed magnetic surveys in the northeast Atlantic and Labrador Sea. J. Geophys. Res. **79**, 363–389, 1974

Wegener, A. Die Entstehung der Kontinente. Petermanns Geogr. Mitt. **58**, 185–195, 253–256, 305–309, 1912

Weigel, W., Goldflam, P., Hinz, K.: The crustal structure of Concepcion Bank. Mar. Geophys. Res. **3**, 381–392, 1978

Whitmarsh, R.B.: Seismic anisotropy of the uppermost mantle absent beneath the east flank of the Reykjanes Ridge. Bull. Seismol. Soc. Am. **61**, 1351–1368, 1971

Zverev, S.M., Boldyrev, S.A., Bourmin, V Yu., Mironova, V.I. Weak earthquakes in the northern part of the Rift Zone of Iceland. J. Geophys. **44**, 283–296, 1978

Zverev, S.M., Kosminskaya, I.P., Krasilschikova, G.A., Mikhota, G.G.: The crustal structure of Iceland and of the Iceland-Faeroes-Scotland region. Greinar **5**, 74–96, 1976

Received September 3, 1979; Revised Version November 8, 1979

J. Geophys. 47, 239–249, 1980

Journal of Geophysics

Seismic Structure of Iceland Along RRISP-Profile I

H. Gebrande[1], H. Miller[1], and P. Einarsson[2]

[1] Institut für Allgemeine und Angewandte Geophysik, Universität München, Theresienstr. 41, D-8000 München, Federal Republic of Germany

[2] Science Institute, University of Iceland, Dunhaga 3, Reykjavik, Iceland

Abstract. As part of the RRISP 77 combined land-sea refraction seismic experiment, observations were carried out on Iceland itself with special emphasis on resolving the deep structure beneath Iceland and its transition towards the eastern flank of Reykjanes Ridge. The data, interpretational procedures, and results for the land part are described in this paper. A structural model of Iceland is presented which is characterized by a generalized two-layered crust of variable thickness underlain by anomalous mantle with *P*-wave velocities of 7.0 km/s at the base of the crust increasing to 7.4 km/s at 30 km depth. Two regions of relatively low velocity have been identified in the lower crust, possibly indicating zones of high melt concentration. A normal *P*- to *S*-wave velocity ratio of 1.76 is found within the crust, whereas this ratio reaches unusually high values of up to 2.2 in the anomalous mantle. From this and the *P*-wave velocity distribution the amount of partial melt is calculated. The melt content is highest (17%–23%) at the top of the mantle and decreases with increasing depth indicating differentiation processes in the upper mantle. The anomalous mantle is confined to Iceland and a sharp transition exists in the area of the shelf edge where normal oceanic lithosphere replaces the updoming asthenosphere.

Key words: Iceland – Reykjanes Ridge – Deep seismic sounding – Crust – Lithosphere – Asthenosphere – Anomalous mantle – Partial fusion.

Introduction

This is paper 2 of a set of three papers on the Reykjanes Ridge Iceland Seismic Project 1977 (RRISP 77) the general objectives and execution of which have been discussed in paper 1 (RRISP Working Group 1980). The present paper focusses on the deep structure of Iceland and its transition towards the flank of Reykjanes Ridge, while paper 3 (Goldflam et al., 1980) is concerned with the latter itself.

The crustal structure of Iceland has been investigated in considerable detail by a large number of seismic refraction lines which were summarized and homogeneously interpreted by Pálmason (1971, see also Pálmason and Saemundsson, 1974, for a summary). A characteristic layering has been found, resembling the oceanic crust in velocity values, but with greater thickness of individual layers. A surface layer of variable velocity and thickness has been subdivided by Pálmason (1971) into three sub-layers 0, 1, 2, but can also be interpreted as a single layer with *P*-wave velocities changing continuously with depth (Flóvenz, 1980). It is underlain everywhere beneath Iceland by a rather homoseneous layer 3 with a mean *P*-wave velocity of about 6.5 km/s which may be equated with the typical oceanic layer. The depth to layer 3 has been found to be quite variable, usually in the range of 1–5 km but up to 10 km in the southeastern part of Iceland (Pálmason, 1971). Its thickness, as far as known, is usually 4 to 5 km. A simple relationship to the gross geolocical structures (see Fig. 1 of paper 1) is not evident.

The base of layer 3 has been reached only by few of Pálmason's profiles, by one profile of Båth (1960) in the western part of Iceland, and by the NASP observations in northeastern Iceland (Zverev et al., 1976; Bott and Gunnarsson, 1980). Velocities from 7.2 to 7.4 km/s have been attributed to an anomalous mantle by Pálmason (1971) but to the lower crust by Zverev et al. (1976). Combining gravity and refraction seismic data, Zverev et al. (1976) concluded that Iceland may be underlain by a very thick crust of continental affinity and normal upper mantle (with *P*-wave velocities of 8 km/s) at about 50 km depth. A sialic crust underlying Iceland has also been postulated by van Bemmelen (1972) because of the abundance of acidic volcanism and the elevation relative to the Mid-Atlantic Ridge. Beloussov and Milanovsky (1976) have used these and other arguments as evidence against any significant amount of sea-floor spreading in the North Atlantic at the latitude of Iceland, but this reasoning seems not very convincing. Nevertheless, the possible existence of continental fragments beneath Iceland would imply serious complications for the kinematics of sea-floor spreading in the North-Atlantic and earlier paleogeographic reconstructions (Bullard, 1965; Laughton, 1971) would at least have to be modified.

A normal mantle at 50 km depth below Iceland as suggested by Zverev et al. (1976) is in contrast to some seismological observations. Teleseismic travel-time residuals (Tryggvasson, 1964; Long and Mitchell, 1970) as well as apparent velocities from Mid-Atlantic Ridge earthquakes across Iceland (Francis, 1969) have been interpreted as evidence for an anomalous mantle extending to some 240 km depth. On the other hand, Stefánsson (1966) claims that travel-time delays from a large earthquake in Iceland can be better explained with a rather shallow 7.4 km/s layer and a 8.0 to 8.2 km/s layer underneath.

These rather inconsistent results were the incentive for the RRISP experiment. Since the crust was studied in some detail before (Pálmason, 1971), the experiment was mainly designed for the investigation of the so-called anomalous mantle. Large penetration of seismic rays and therefore a long range seismic profile was necessary for this purpose.

As is to be seen from Fig. 1 of paper 1, the line follows for the greater part the trend of the eastern zone of active rifting

0340-062X/80/0047/0239/$02.20

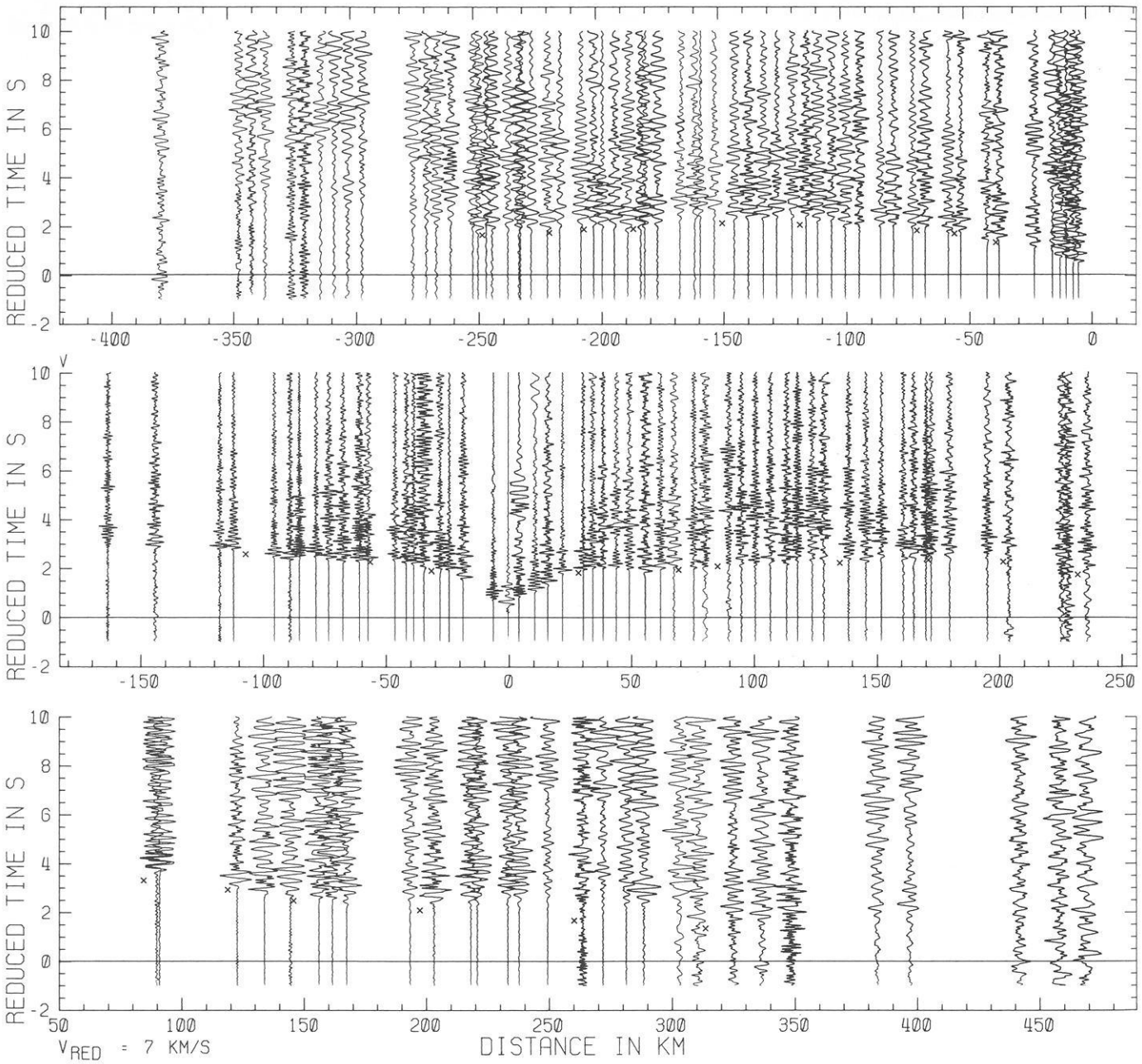

Fig. 1. Record sections from shot-points E, D, and C (from top to bottom). All seismograms are normalized individually to their maximum amplitude within the time interval. Identical stations are on the same vertical line. *Crosses* mark calculated travel-times according to the ray tracing calculations of Fig. 6. Note the delay of the first arrival of the leftmost record of shot C, which is related to a region of very low velocity within the lower crust beneath Heimaey

and volcanism, which for simplicity is called the neovolcanic zone. The reasons for which we chose to observe along this line were the following:

1. This zone is the continuation of the Mid-Atlantic plate boundary, which thus can be studied by land meassurements.

2. Refraction measurements along the strike of geologic units generally provide more reliable velocity information than observations in other directions.

3. Since the eastern neovolcanic zone is offset from the mid-Atlantic spreading axis by the Reykjanes transform fault zone, the combined land-sea experiment enabled us to shoot from the normal oceanic realm into the active spreading zone along its trend. It was felt that by this scheme of observations the effects of absorption could be kept at a minimum because only the land part of the line would lie above possible anomalous mantle. Ray tracing calculations had also shown that the different structural models discussed above would yield significant differences in the characteristics of travel -time curves.

Observations and Interpretation

As the technical part of the experiment has been described to some extent in paper 1 and in RRISP Working Group/Angenhei-

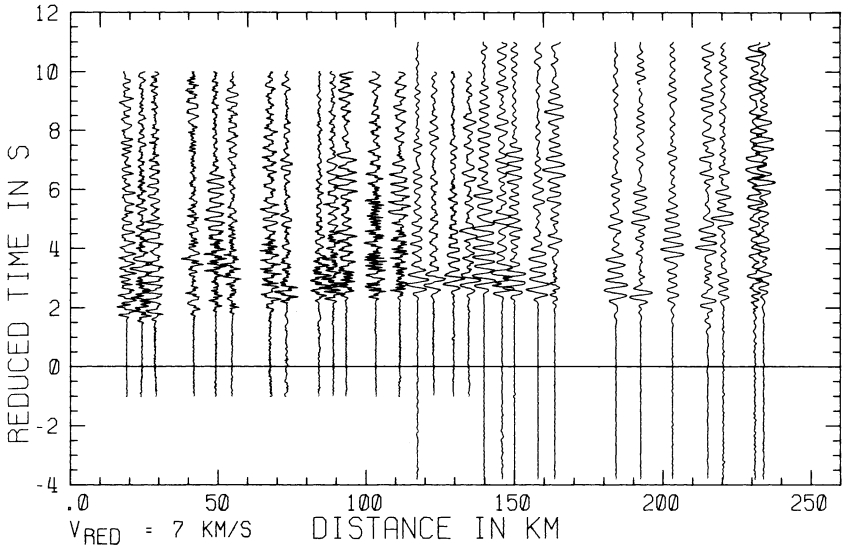

Fig. 2. Record section from shot-point F towards the southeast into the Tertiary basalts. Records starting at a reduced time of −1 s were obtained by the Soviet group, the others by the German group

ster et al. (1979), we can confine ourselves to details of observational results and their evaluation. The record section for shots F (Axarfjördur) through the eastern neovolcanic zone has already been shown in Fig. 4 of paper 1 as a typical example of RRISP data. Figure 1 shows the record section of shot E (Vopnafjördur), D (Thveraldavatn), and C (SW of Surtsey). Reduction velocity is 7 km/s and the sections are arranged in such a way, that seismograms obtained at the same location appear one above the other. Slight deviations from this are caused by the observation taken on a not strictly straight line. One notes that the apparent velocities of the first arrivals are close to and slightly over 7.0 km/s in all sections at distances beyond some 120 km. Whereas for shots D and E, apparent velocities generally increase with distance, they decrease with distance for shot C, which is of particular interest as it suggests the existence of lateral velocity variations. In Fig. 2, the record section for the line from shot-point F towards the southeast coast of Iceland is given. It is very similar in appearance to the record sections of shot-points E and F along the main line, even though the second half lies fully within the Quaternary and Tertiary basalts of East-Iceland, i.e., outside the neovolcanic zone.

In all record sections significant differences can be seen in the first 50 to 100 km, which must be attributed to variations in the crustal layers. The subcrustal structure seems to have no regional differences along the land lines as indicated by the similar apparent velocities observed at distances greater than 100 km. The seismogram sections from Iceland are characterized by the lack of distinct later arrivals. This is in contrast to continental areas, where frequently observed clear later arrivals can be interpreted as overcritical reflections from discontinuities or as diving waves bottoming in zones of strong velocity gradient. A more or less continuously varying velocity distribution is thereby manifested for the Icelandic structure. On the other hand the first onsets, especially at greater observational distance are not impulsive, but rather emergent and there is considerable energy in the later parts of the seismograms. This may be caused by scattered waves from small-scale heterogeneities. Therefore, the small-scale structure may be highly heterogeneous, whereas the deep structure can be characterized by a continuous velocity function when averaged over some wavelengths. With the mean station spacing of

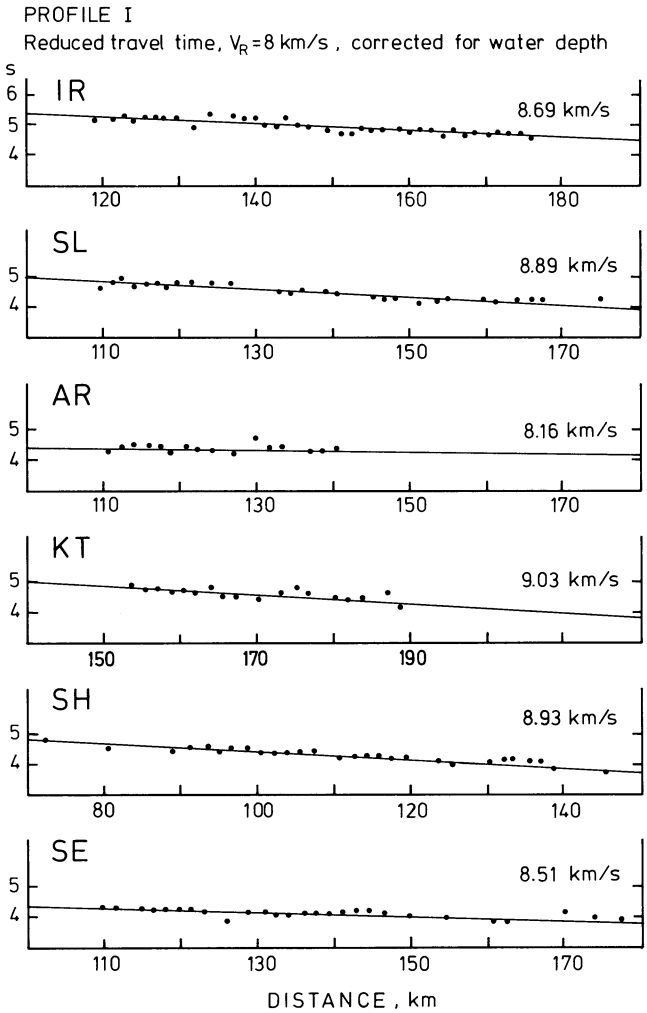

Fig. 3. Travel times from shots on Profile I to stations of the Icelandic seismological network. Travel times are corrected to the ocean bottom. Lines are least-squares fit and numbers give the apparent velocity in km/s

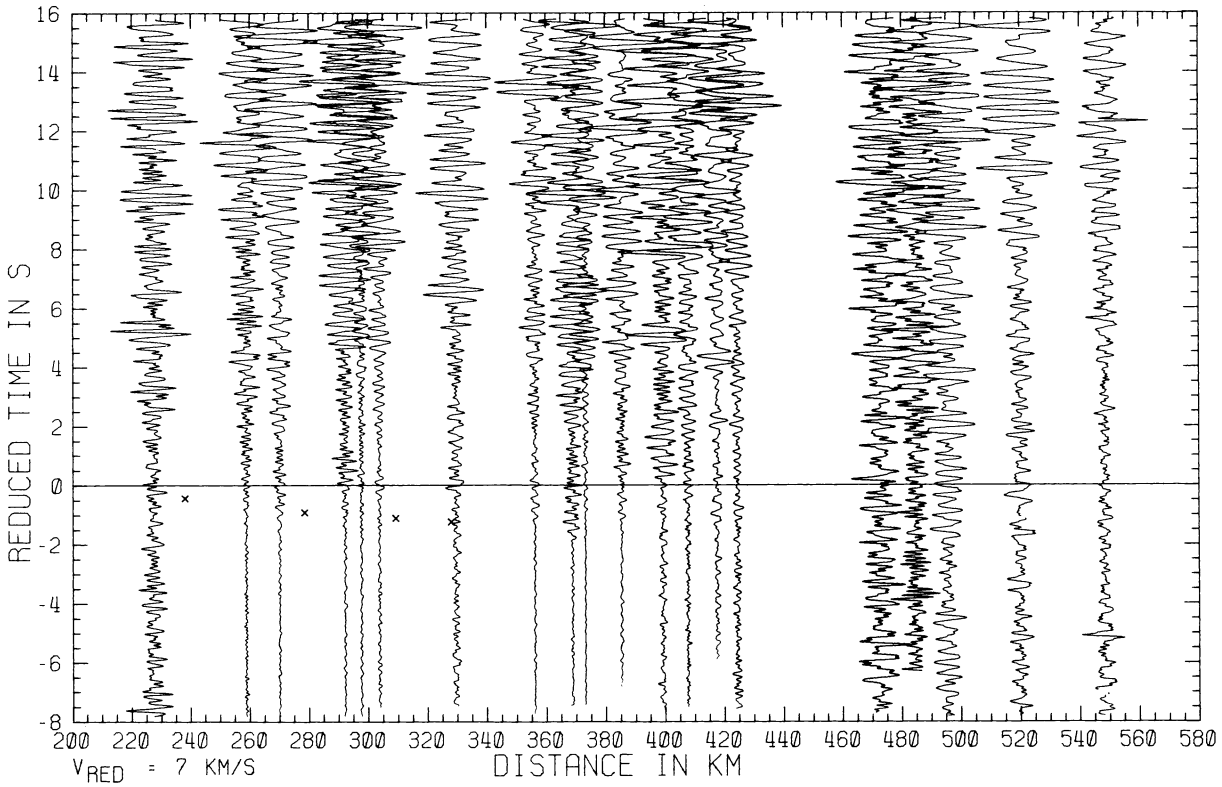

Fig. 4. Record section from shot B, filtered and normalized. The emergent character of the first onset is evident. Main energy within each seismogram begins to arrive at reduced times of some 4 to 5 s. *Crosses* mark calculated travel-times according to the model of Fig. 5

7 km chosen for the RRISP observations it is evident, that we cannot resolve small-scale heterogeneities from the analysis of travel-time data but have to be content with the evaluation of the main features of the deep structure. The lack of overcritical reflections which would give useful information on average velocity, puts further limits on the resolving power of the seimic refraction method.

The only later arrivals which might possibly be correlated over some distance, are found in the record section from shots D towards the northeast (Fig. 1) in the distance range between 90 and 170 km. Reduced travel times are between 4 and 2.5 s and apparent velocity approximately 7.8 km/s. Similar later arrivals are not to be found in the opposite direction from shot D and also not on the reversed line from shotpoint E. This feature may be related to the different frequency content of the D and E signals and may indicate the presence of thin layers of only local extent beneath central Iceland at about 30 km depth. The higher signal frequency content of the D-shots comes from the shooting technique with dispersed charges in shallow water. The dominant frequency of the other shots agrees well with theoretical predictions (Wielandt, 1972) for single charges at optimum depth (see paper 1, Table 1 for further information regarding the shots).

Figure 3 shows travel-time data obtained at some stations of the Icelandic seismological network for the series of small shots at sea between B and C. With the exception of the top two stations IR (IR-Skáli) and SL (Selfoss) all stations shown here lie very close to or on the main line (for location see Einarsson 1979). The travel times have been corrected for water depth at each shot position as follows:

$$t_w = \frac{d}{V_w}(1 - V_w^2/V_n^2)^{\frac{1}{2}} \qquad (1)$$

where d is the water depth, V_w the velocity in water and V_n the velocity in the deepest layer of penetration. Surprisingly high apparent velocities between 8.2 and 9 km/s are calculated from these data. Absolute travel times are greater by 2.0 to 3.0 s as compared to travel times (corrected for water depth) at OBS BI02 in the same distance range (see paper 3). The apparent velocities for individual shots of the same shot series at sea, measured between different stations in Iceland, are much smaller and close to 7.4 km/s. Similar apparent velocities have also been observed along the main line up to distances of about 500 km for the more distant shot-point B. The pertinent record section is shown in Fig. 4. It is an extreme example for the emergent character of the onsets at greater distances and the shift of wave energy to greater travel times, mentioned above. At distances beyond approximately 500 km no onsets can be detected in spite of a rather low ground noise level (on the average 0.3 μm/s in the passband 1 to 10 Hz). The record section of the 4-ton shot at A, which covers the observation range from 420 to 800 km, is not shown here, because no recognizable onsets are to be seen.

The data have been evaluated as follows: First, direct inversion methods were used to find preliminary models, which satisfied the observational data in parts. Thereafter, numerous model calculations with a ray-tracing program by Gebrande (1976) were carried out in order to derive a model for crustal and upper-mantle structure along the main line, that satisfies travel-time data for all shots observed, and includes earlier results (Pálmason, 1971). The model building technique with the necessity of working with a manageable number of model parameters required a certain generalization of the available information for the topmost part of the crust. This was attained by choosing velocities, gradients, and thicknesses in such a way that they give the same transit times as through the more detailed structures given in paper 3

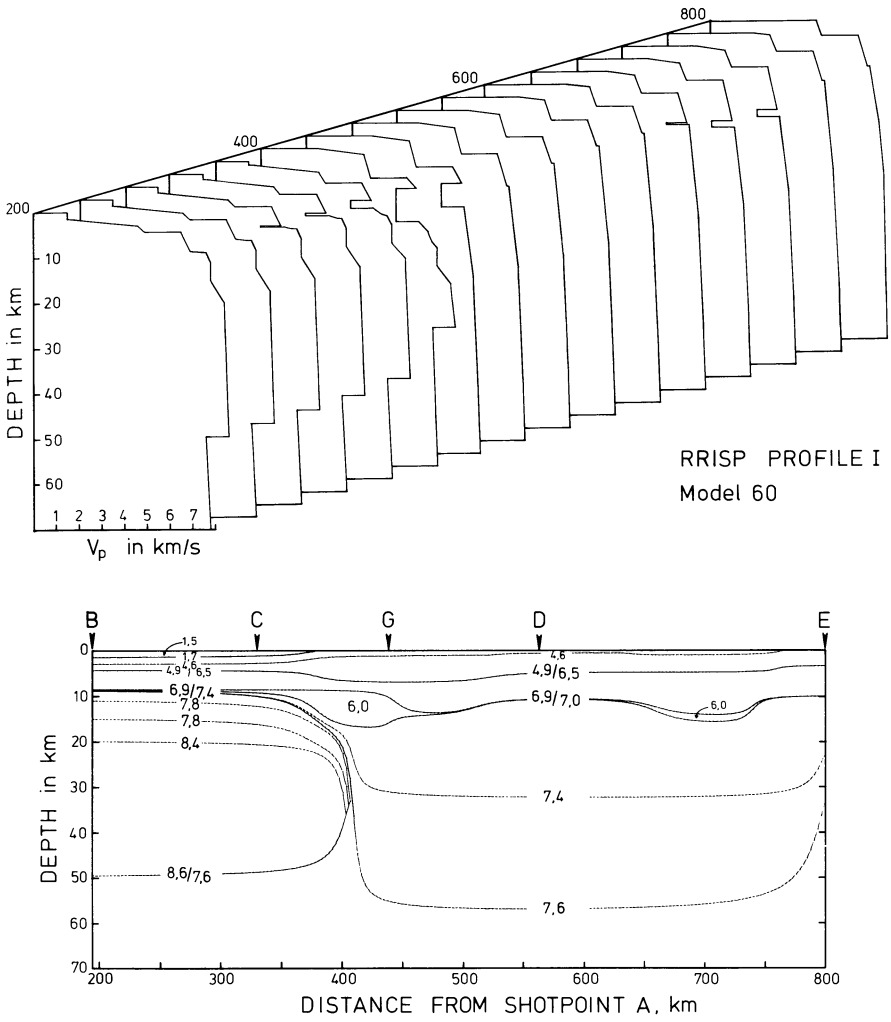

Fig. 5. Crustal and upper-mantle model beneath Iceland and the east flank of Reykjanes Ridge between shot-points B and C. Distances are given from shotpoint A. *Top:* Velocity-depth distributions along RRISP profile I.
Bottom: The model is defined by the velocity isolines and linear vertical interpolation in between. *Numbers* give the velocity at each isoline. The velocity of 6.0 km/s in the two blisters at the base of the crust must be less than 5 km/s to explain observed local travel-time delays

for the marine part and for the land part by Pálmason (1971). His constant-velocity layers 0, 1, 2 have been modelled by two gradient layers. In parts this may even be a better approximation to the real structure.

The lower crust was modelled as a layer with a discontinuous velocity increase at its top to 6.5 km/s and a continuous increase to 6.9 km/s at its base along the whole length of the profile.

The best fitting model derived in this way is shown in Figs. 5 and 6. In the top part of Fig. 5 the velocity-depth structure along the RRISP main line is given in a semi-perspective view and in the lower part it is shown in the form of velocity contours. The model is defined by the velocity contours and linear vertical interpolation in between. As an example of the ray tracing calculations, Fig. 6 shows calculated seismic rays for shotpoints C, D, and E within part of the complete model in order to convey an impression of the sampling of the structures by the seismic rays. Only a few selected rays are shown to keep the figure legible. The calculated travel times are marked as crosses in the record sections of Fig. 1 to give an idea on the degree of fit. Mean deviation is generally less than 0.1 s. In view of the obvious small-scale heterogeneity a better fit would not be very meaningful.

An exceptional large discrepancy between observed and calculated travel-time is found on Heimaey, where a delay of 0.3 s is observed with respect to our model. This discrepancy could be removed by decreasing the velocity in the blister below Heimaey from 6 km/s to less than 5 km/s. The source of this delay cannot lie within the upper crust, since the records of the nearby shots G1, 2 show normal travel-times. If this low velocity is accepted, it may indicate the existence of a zone of relative high degree of partial fusion in the lower crust beneath Heimaey. The horizontal dimensions and the depth of the low velocity body are not well constrained by our data. A similar low-velocity body at the base of the crust is inferred in the northern part of the neovolcanic zone (Askja-Herdubreid).

The base of layer 3 has somewhat arbitrarily been identified with the 6.9 km/s isoline. Contrary to Båth (1960) and Pálmason (1971) we find no pronounced discontinuity to velocities of 7.2 or 7.4 km at that depth range. The small discontinuity from 6.9 to 7.0 km/s present in our model is consistent with the data, but is not an inevitable consequence. We could just as well have a continuous increase in velocity. A more significant change in this depth-range seems to be a reduction of the *P*-wave velocity gradient from about 0.07 to 0.02 s^{-1}. At the moment we will call this zone of low-gradient layer 4 and will show later that it should be identified with anomalous upper mantle.

The crustal layers are continuous across the transition from Iceland to the eastern flank of Reykjanes Ridge and vary only in thickness. Layer 4, on the other hand, is present only beneath Iceland. Beneath Reykjanes Ridge a normal and well developed oceanic crust (paper 3) rests on a layer with a *P*-wave velocity

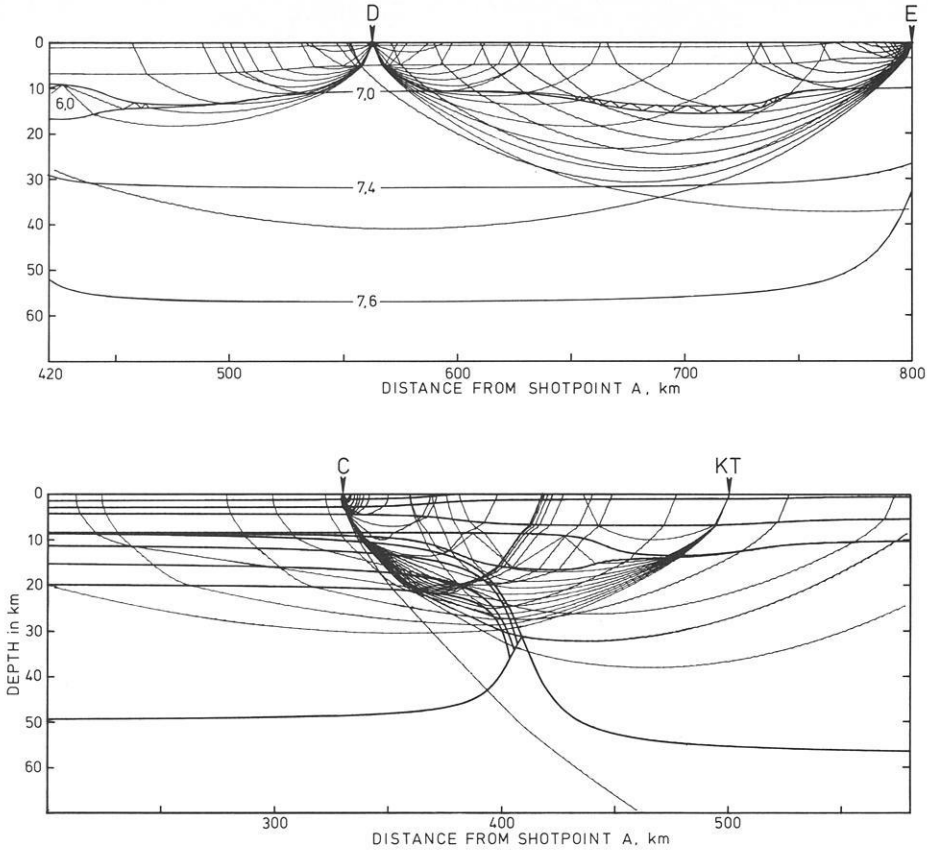

Fig. 6. Some calculated rays through parts of the model of Fig. 5 to give an idea on the sampling of the structures. The calculated travel-times have been plotted into the record sections of Fig. 1.
Top part: Shot-points D and E; *Lower part:* Shot-point C and station KT

of 7.8 km/s followed by a high velocity layer (up to 8.6 km/s) at greater depth. The velocities and the geometry of the transitional part of the model were derived from a combination of the land and OBS data sets by ray tracing. For this purpose the data set recorded at the stations of the Icelandic seismological network was especially useful as it provided reversed information to the OBS data on the marine part.

Looking at the rays for shot-point C (Fig. 6), one may see how the sudden termination of the oceanic lithosphere affects the observed travel times. Particularly evident is the decrease of apparent velocity with increasing distance. Rays bottoming in the high velocity layer of the oceanic lithosphere emerge at distances up to 170 km giving rise to apparent velocities of about 8 km/s, whereas the travel-time segment at greater distance with an apparent velocity of about 7.2 km/s is produced by rays bottoming in layer 4 beneath Iceland. The model structure also explains the observed travel times for shot B as well as for the small shots between B and C recorded on land (see Figs. 4 and 3).

As mentioned above, almost no signal energy could be recorded from the most distant shot A. In our model this is explained by the small thickness of the oceanic lithosphere. The rays sampling the lithosphere emerge south of Iceland, while Iceland itself, with respect to shotpoint A, is situated in a shadow zone caused by the lower velocities in the asthenosphere. Even though lack of signals is a poor means of structural determination, we are quite certain that the lithosphere thickness must be limited, since from the other shot-points we find no evidence of excessively high absorption necessary to reduce signal strength in the manner observed. Because of the negative evidence, the lower boundary of the occeanic lithosphere as shown in the model is by no means certain and was put somewhat arbitrarily at a depth of 50 km.

Although the recorded waves, according to our ray tracing calculations, did not penetrate deeper than some 30 km below Iceland it can be stated, that a continuous layer with *P*-wave velocities around 8 km/s, such as beneath the marine part of the profile cannot exist in the upper 60 km beneath Iceland. This is the result of several ray tracing calculations for models modified accordingly. If an 8 km/s layer or half-space with its top above a depth of 60 km is incorporated in the models, travel-time segments with apparent velocities around 8 km/s arise for which no evidence can be found in the record sections.

It is rather likely that the model presented in Fig. 5 will be subjected to improvements in the future, but we do not expect that the general features of the model will have to be changed. It should be mentioned in passing that the results from Profile II along the southeast coast of Iceland not presented here, corroborate our model and indicate that the structure derived is not only representative for the neovolcanic zone, but for all of Iceland. The details of the model may not be equally accurate in different parts due to different fit of calculated and observed travel times, different coverage of the lines, and different quality of the data, but also due to the principal resolving properties of the refraction seismic method. The reader will judge the accuracy of the model realistically if he keeps in mind, that the refraction seismic method is a good diagnostic for strong positive velocity contrasts. Its resolving power however, is rather weak if, as is the case below Iceland, the velocity gradients are small.

Discussion

The model presented has certain implications for the physical state and the petrology of the material at depth, which we would

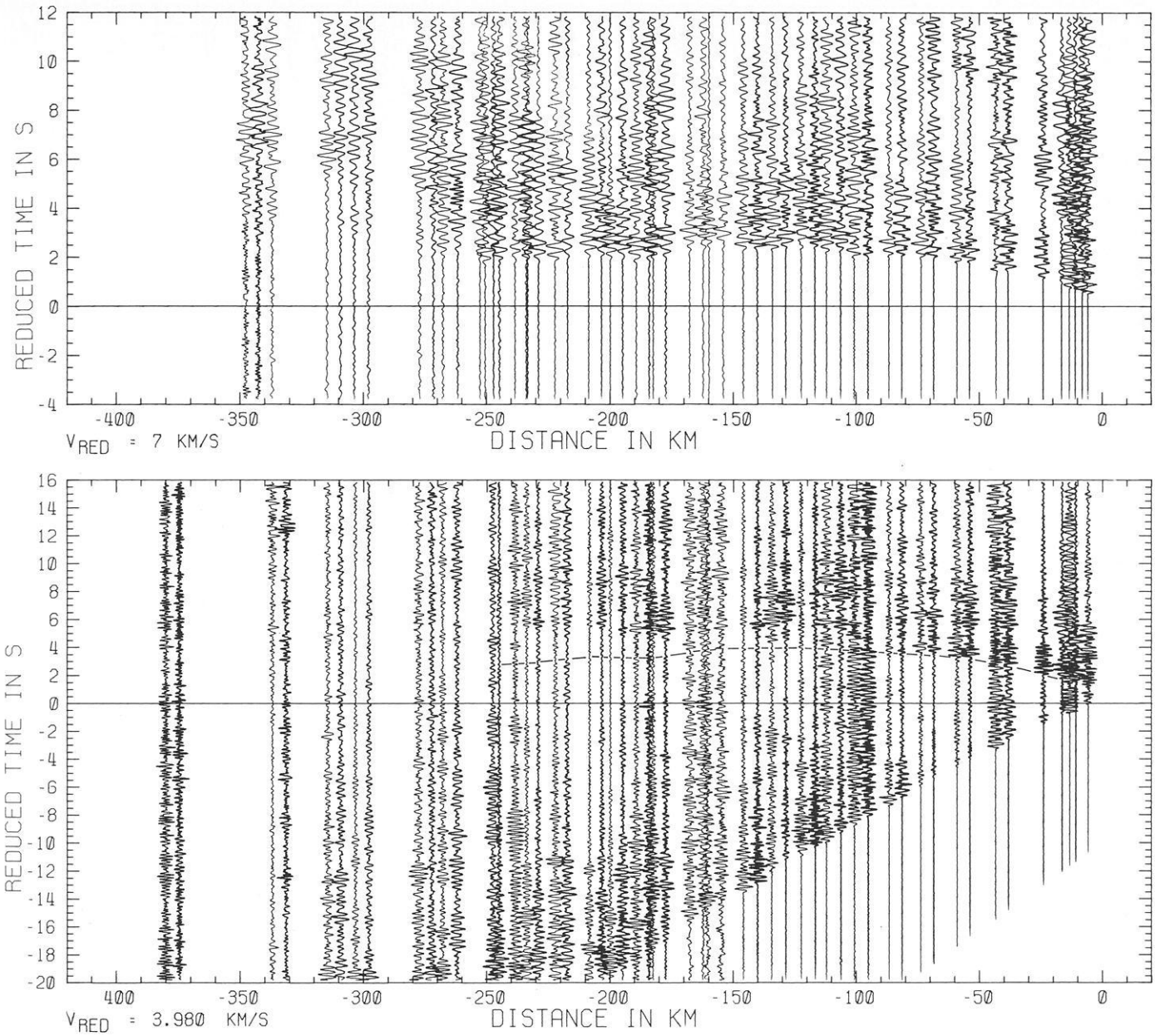

Fig. 7. *Top:* Record section from shotpoint E reduced by 7 km/s. Vertical component seismograms. *Bottom:* Record section from shotpoint E reduced by 3.98 km/s. Horizontal components were used mostly for this section, which shows *P*- and *S*-wave arrivals. Reduction velocity and time axis were chosen such, that *S*-arrivals should be congruent to *P*-arrivals in the top section, if the ratio of *P*- to *S*-wave velocity is 1.76. The *dashed line* gives *S*-arrivals as calculated from the *P*-arrivals with this ratio. The fit is good up to distances of 140 km, beyond which *S*-arrivals become progressively late

like to discuss with special emphasis on layer 4 beneath Iceland. Some conclusions concerning the oceanic lithosphere have already been presented in paper 1.

Additional to the structural information is the *P*- to *S*-wave velocity ratio beneath Iceland determined for shots E and G, which all generated considerable *S*-wave energy. This was not the case for the large shots at sea, which were suspended and not fired on the sea floor. Figures 7 and 8 show the records used. In the upper part of the figures the normal vertical component record sections of shots E and G are shown, reduced by 7 km/s. In the lower part the horizontal component record sections from the same shots are shown but reduced by 3.98 km/s, corresponding to a *P*- to *S*-wave velocity ratio of 1.76. The time axis has been compressed by the same factor. This representation of the data proves particularly useful when one section is laid on top of the other, because deviations from the chosen *P*- to *S*-wave velocity ratio can readily be recognized since *P*- and *S*-arrivals will not be congruent any longer. Since the reader cannot easily do this, for comparison the *P*-wave correlation for shots E has been marked in the corresponding *S*-wave section.

It is quite clear, that beyond distances of 140 km the *P*- to *S*-wave velocity ratio changes to higher values as *S*-arrivals are becoming progressively 'late' with repect to the *P*-arrivals. At the same range, *S*-wave amplitudes decrease in comparison with

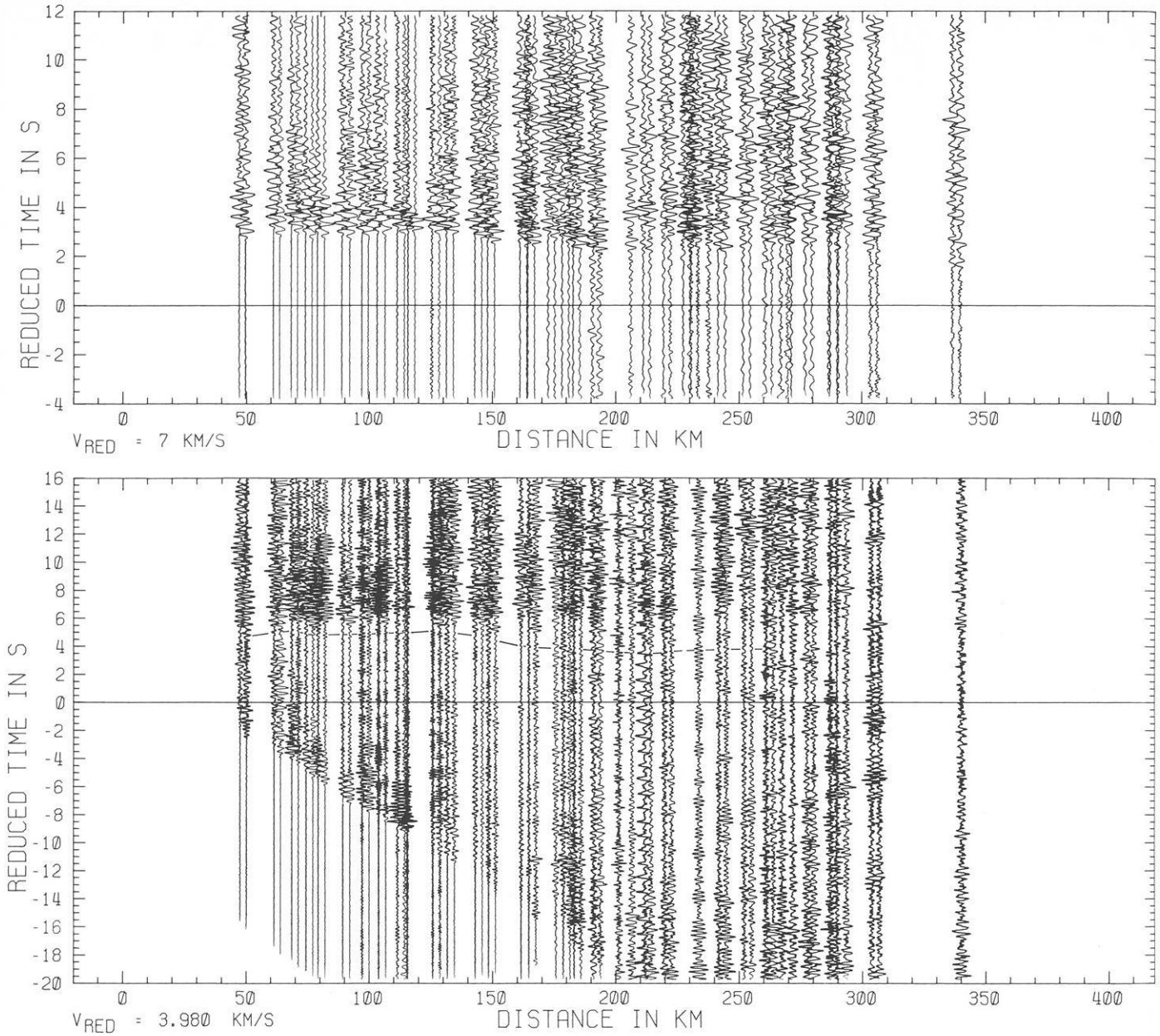

Fig. 8. Same as Fig. 7 but for shots G1 and G2 recorded along the line at the southeast coast

the *P*-wave amplitudes and *S*-wave signals are lost at distances greater than 250 km. It is a rather dramatic amplitude attenuation considering that, e.g., for shots E, the *S*-wave amplitudes are larger than the *P*-amplitudes by at least a factor of 2 at distances between 20 and 130 km (some seismograms are distorted by amplifier saturation).

When looking at the rays from shotpoint E drawn in Fig. 6, one notices that beyond distances of 140 km emergent rays have penetrated the low velocity body mentioned before and have sampled layer 4. We must therefore conclude that at the base of layer 3 a more fundamental change of physical properties takes place than is indicated by the almost negligible change in *P*-wave velocity.

A quantitative evaluation of the *P*- to *S*-wave velocity ratio is given in Fig. 9 where a Wadati diagram for shots E has been plotted. Up to a *P* travel time of 21 s, corresponding to a distance of approx. 140 km, the *P*- to *S*-wave velocity ratio is constant at 1.76. With greater *P*-wave travel-times the slope of the curve reaches values as high as 2.2 with a mean of 1.96.

The knowledge of the change in *P*- to *S*-wave velocity ratio with depth as well as the absolute values help us answering the question how layer 4 should be interpreted. The question, whether the velocity values between 7.0 and 7.4 km/s should be assigned to the crust or upper mantle has been debated extensively in the literature (Båth, 1960; Tryggvason, 1962, 1964; Bott, 1965, 1974; Francis, 1969; Pálmason, 1971; Pálmason and Saemundsson, 1974; Zverev et al., 1976).

In the last decade velocities in the range from 7.0 to 7.7 km/s have more widely been found than assumed previously and are generally assigned to layer 3b of the oceanic crust (e.g., Peterson et al., 1974). Comparison with laboratory measurements of seismic velocities on samples dredged from the ocean floor and taken

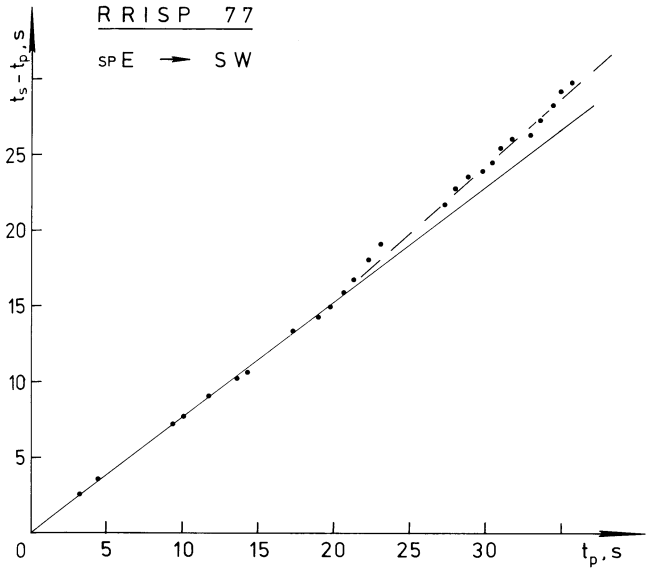

Fig. 9. Wadati plot for shots E1 and E2 along the main line. For P travel-times greater than 21 s the P- to S-wave velocity ratio changes from 1.76 to a mean of 1.96

from ophiolites of presumably oceanic origin shows, that gabbros and metagabbros have about the right velocities at appropriate pressures and moderate temperatures. At the same time, gabbros also exhibit the correct P- to S-wave velocity ratio of 1.9 corresponding to a Poisson's ratio $\sigma = 0.31$ (Christensen and Salisbury, 1975; Kroenke et al., 1976; Christensen, 1978). At temperatures of 1,000° to 1,100° C, such as are indicated beneath Iceland at 10 km to 20 km depth by the geothermal gradient (Pálmason and Saemundsson, 1974) and by magneto-telluric data (Hermance and Grillot, 1970; Beblo and Björnsson, 1978, 1980), the combined influence of pressure and temperature would produce a decrease in the P-wave velocity of gabbroic material of some 1.2 km/s (Kroenke et al., 1976) and this disagrees with the in situ velocities. An additional decrease would result from incipient melting at 1,000° to 1,100° C in the presence of small amounts of water. Therefore gabbroic or other basic material must be discounted as the only or at least principal constituent of layer 4; predominantly ultramafic material must be assumed. It is therefore most natural to attribute layer 4 to the upper mantle. But this is more or less a question of definition. It seems more important to us that, whatever the exact petrological composition of the upper mantle is, a rather large density contrast is to be expected with respect to the normal lower lithosphere beneath Reykjanes Ridge, as long as the material is in the perfect solid state. Taking 7.2 km/s and 8.4 km/s as mean P-wave velocity values for the depth range from 20 to 50 km beneath Iceland and the Reykjanes Ridge (Fig. 5) and a Birch relationship

$$V_P = 3.31\,\rho - 2.55\,(\text{km/s}); \qquad (\rho \text{ in g/cm}^3) \tag{2}$$

as confirmed by Kroenke et al. (1976) for possible lower crust and upper mantle rocks, the density contrast should be some 0.35 g/cm^3. This is reduced to 0.3 g/cm^3 if the relationship given by Christensen and Salisbury (1975) is used. In any case, taking only the depth range of 20 to 50 km into account, this would imply a Bouguer anomaly over Iceland of some −350 mgal, which is about three times the observed value (Einarsson, 1954). This disagreement can be overcome as mentioned by Bott (1965) in a similar context, if the low seismic velocities are mainly attributed to partial fusion. In this case the seimic velocities are relatively much more affected than the density and the usual velocity-density relationship breaks down.

One may now ask, whether quantitiative information on the degree of partial fusion can be extracted from the seismic velocities. This is possible for a simplified model of partially molten material. We assume that it consists of only two phases, a solid phase 1 with properties k_1, μ_1, ρ_1 (bulk modulus, shear modulus, and density) and a liquid phase 2 with properties k_2, $\mu_2 = 0$, ρ_2. With Green and Ringwood (1963) we may identify the solid phase with peridotite and the liquid phase with basaltic melt. We are interested in how the seismic velocities of the inhomogeneous composite material depend upon the properties of the homogeneous phases and the fractional volume of the melt. A solution to this problem should then allow us to determine the melt concentration from the measured seismic velocities, if the properties of the homogeneous phases are known. Unfortunately a unique solution is not possible since the properties of the two-phase material depend in general on the entire 'phase geometry', i.e., the geometry of the phase interfaces. This ambiguity is not removed, if statistical homogeneity is assumed.

Walsh (1968, 1969) has investigated theoretically the special case of isolated melt inclusions in the form of randomly oriented oblate spheroids with minor axes much smaller than major axes. Since melting in polycrystalline material starts at grain boundaries as thin films, this seems to be a good model for incipient melting. It turns out that the elastic moduli of the partially molten material depend not only on the volume concentration c_2 of melt, but also on the aspect ratio α of the inclusions, i.e., the ratio of minor to major diameter d of the oblate spheroids. A smaller aspect ratio of the inclusions requires a much smaller melt content than a larger aspect ratio does, to give same velocity decrease. The velocities therefore cannot be interpreted unambiguously without making assumptions about the aspect ratio. An $\alpha = 0.01$ has been used by several authors. It has however, often been neglected, that the melt content c_2 and the aspect ratio are not independent variables. At a constant aspect ratio, an increase of melt content necessarily requires an increase of the inclusion diameter, which consequently leads to a coalescence of previously isolated inclusions. If this process proceeds too far, the Walsh theory can no longer be applied. It can be shown (Gebrande, in preparation) that with randomly distributed inclusions the fraction of isolated inclusions is less than 90% if $c_2 \leqq \alpha/10$. For $c_2 = \alpha/2$ only 60% of the inclusions can be expected to be isolated. Since α has to be small anyway, the Walsh theory is valid only for rather minimal melt content. It is therefore not possible to apply this theory to the anomalous mantle without violating its inherent assumptions.

For our purpose extremal bounds for bulk and shear moduli k, μ as derived by Hashin and Shtrikman (1963; ref. Hashin 1966) from some elasticity extremum principles are more useful. These bounds can be transformed into bounds for the seismic velocities V_P, V_S and the seismic parameter ϕ. These bounds are the best possible in terms of k_i, μ_i $(i = 1,2)$, and c_2; the velocities of any two-phase material independent of its phase geometry must lie within these bounds. Unfortunately in the case of a solid-fluid mix the bounds for V_P and V_S are rather far apart. This is due to the fact that the lower bound for the shear modulus vanishes. This is physically plausible, since the rigidity of the composite is zero if all solid particles are surrounded by melt. The bounds for the seismic parameter ϕ, and the 'hydrodynamic wave velocity' $\phi^{1/2}$ (Birch 1969) are reasonably close, however. If the P- and S-wave velocities are known, an estimate of the melt content can be derived from these bounds. They are given by:

$$\phi \leqq \frac{1}{\rho}\left\{k_1 + c_2\left(\frac{1}{k_2 - k_1} + 3\frac{1-c_2}{3k_1+4\mu_1}\right)^{-1}\right\} \quad (3)$$

$$\phi \geqq \frac{1}{\rho}\left\{k_2 + (1-c_2)\left(\frac{1}{k_1 - k_2} + \frac{3c_2}{3k_2+4\mu_2}\right)^{-1}\right\} \quad (4)$$

$$\rho = \rho_1 + c_2(\rho_2 - \rho_1). \quad (5)$$

If we assume that the anomalous mantle beneath Iceland is a mixture of the material of the high-velocity layer observed beneath the Reykjanes-Ridge and basaltic melt, we can calculate the extremal bounds according to these formulae. From our model we obtain a *P*-wave velocity of 8.47 km/s in the lower lithosphere at a depth of of 30 km. Correcting for a possible temperature difference of some 200 K between the 10 Ma old Reykjanes Ridge and Iceland at this depth by using a temperature coefficient of

$$(\partial V_p/\partial T)_p = -4 \cdot 10^{-4}\ \mathrm{km/s \cdot K}$$

(Anderson et al. 1972) we obtain a *P*-wave velocity of 8.39 km/s for the solid component. For basaltic melt a *P*-wave velocity of 4.1 km/s is given by Röber and Thyssen (1978). Taking these values and appropriate densities

$$\rho_1 = 3.3\ \mathrm{g/cm^3} \quad \text{and} \quad \rho_2 = 2.76\ \mathrm{g/cm^3} \quad \text{(basalt glass)}$$

the extremal bounds given by the heavy solid lines in Fig. 10 were calculated. The dashed lines are based on values of Birch (1969), who has used the bulk modulus of basalt glass for the melt component. On the other hand, $\phi^{1/2}$ can be calculated from the observed *P*-wave velocity and *P*- to *S*-wave velocity ratio according to

$$\phi^{\frac{1}{2}} = V_p[1 - \tfrac{4}{3}(V_s/V_p)^2]^{\frac{1}{2}}. \quad (6)$$

The corresponding values for the anomalous mantle beneath Iceland have been marked by horizontal lines in Fig. 10. If follows from the theoretical bounds, that the melt content must be between 10% and 16.7% (or 15.5% to 23% for the values of Birch) to explain a *P*-wave velocity of 7.3 km/s and higher values of 17% to 27% are obtained for a *P*-wave velocity of 7.0 km/s. These results seem to reflect a differentiation process in the upper mantle and an enrichment of basaltic melt at the base of the crust. The

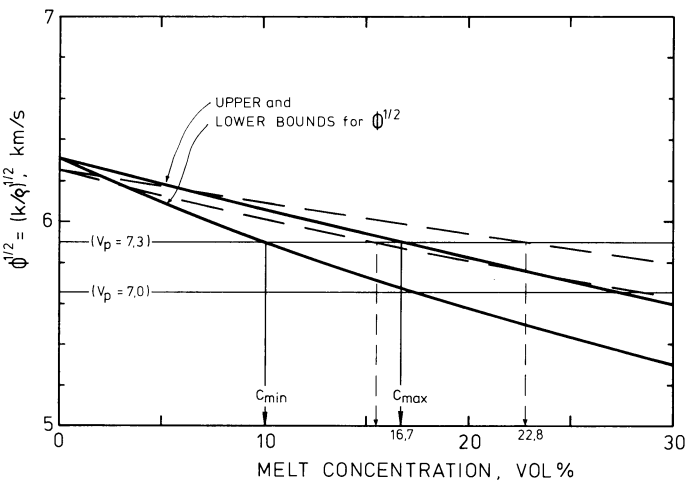

Fig. 10. Upper and lower bounds on the hydrodynamic wave velocity $\Phi^{1/2}$ against melt concentration in a solid-fluid two phase system. The two different bounds (*solid and dashed lines*) are based on different values of elastic parameters

possible existence of local and rather thin reflecting elements at a depth of approximatly 30 km may well be correlated with the decreasing melt content. Taking a melt content of 13% as the average for the depths from 20 to 50 km the mean density difference between Reykjanes-Ridge and Iceland within this depth range becomes 0.07 g/cm^3 according to Eq. (5). This difference is much smaller than expected from a Birch relation for solid rocks; in order to explain the observed gravity anomaly this density anomaly beneath Iceland most likely must extend to depths greater than 50 km. The same conclusion is reached by studying the teleseismic travel-time residuals. The upper 50 km of the model presented in Fig. 5 account only for a travel-time delay of 0.2 s and therefore a much deeper extent of the low-velocity body beneath Iceland must be assumed to explain the 1.4 s delay as observed by Long and Mitchell (1970).

References

Anderson, D.L., Sammis, C., Jordan, T.: Composition of the mantle and core. In: The Nature of the Solid Earth, E.C. Robertson et al., eds.: pp. 41–66. New York: McGraw-Hill 1972

Angenheister, G., Gebrande, H., Miller, H., Weigel, W., Goldflam, P., Jacoby, W., Palmason, G., Björnsson, S., Einarsson, P., Zverev, S., Loncarevic, B., Solomon, S.: First results from the Reykjanes Ridge Iceland Seismic Project 1977. Nature **279**, 56–60, 1979

Båth, M.: Crustal structure of Iceland, J. Geophys. Res. **65**, 1793–1807, 1960

Beblo, M., Björnsson, A.: Magnetotelluric investigation of the lower crust and upper mantle beneath Iceland. J. Geophys. **45**, 1–16, 1978

Beblo, M., Björnsson, A.: A model of electrical resistivity beneath NE-Iceland; Correlation with temperature. J. Geophys. **47**, 184–190, 1980

Beloussov, V.V., Milanovskiy, Y.Y.: On the tectonic and tectonic position of Iceland. Soc. Sci. Islandica, Greinar **5**, 96–120, 1976

Bemmelen, R.W. van: Geodynamic models; an evaluation and a synthesis. Amsterdam: Elsevier 1972

Birch, F.: Density and composition of the upper mantle: first approximation as an olivine layer. In: The Earth's crust and upper mantle, P.J., Hart, ed.: pp. 18–36. Washington: Am. Geophys Union 1969

Bott, M.H.P.: The upper mantle beneath Iceland. Geophys. J. **9**, 275–277, 1965

Bott, M.H.P.: Deep structure, evolution and origin of the Icelandic transverse ridge. In: Geodynamics of Iceland and the North Atlantic Area, L. Kristiansson, ed.: pp. 33–47. Dordrecht: Reidel 1974

Bott, M.H.P., Gunnarsson, K.: Crustal structure of the Iceland-Faeroe Ridge. J. Geophys. **47**, 221–227, 1980

Bullard, E.C., Everett, J.E., Smith, A.G.: The fit of the continents around the Atlantic. Philos. Trans. R. Soc. London, Ser. A: **258**, 41–51, 1965

Christensen, N.I.: Ophiolites, seismic velocities and oceanic crustal structure. Tectonophysics **47**, 131–157, 1978

Christensen, N.I., Salisbury, M.H.: Structure and constitution of the lower oceanic crust. Rev. Geophys. Space Phys. **13**, 57–86, 1976

Einarsson, P.: Travel times recorded at Icelandic seismograph stations during the Reykjanes Ridge Iceland Seismic Project (RRISP). Publ. Sci. Inst. Univ. Iceland RH-79-10, 1979

Einarsson, T.: A survey of gravity in Iceland. Soc. Sci. Islandica **30**, 1954

Flóvenz, O.G.: Seismic structure of the Icelandic crust above layer three and the relation between body wave velocity and the alteration of the basaltic crust. J. Geophys. **47**, 211–220, 1980

Francis, T.J.G.: Upper mantle structure along the axis of the Mid-Atlantic Ridge near Iceland. Geophys. J.R. Astron. Soc. **17**, 507–520, 1969

Gebrande, H.: A seismic-ray tracing method for two-dimensional inhomogenous media. In: Explosion seimology in central Europe, P. Giese, C. Prodehl, A. Stein, eds.: 162–167. Berlin, Heidelberg, New York; Springer 1976

Goldflam, P., Weigel, W., Loncarevic, B.: Seismic structure along RRISP – Profile I on the south-east flank of the Reykjanes Ridge. J. Geophys. **47**, 250–260, 1980

Green, D.H., Ringwood, A.E.: Mineral assemblages in a model mantle composition. J. Geophys. Res. **68**, 937–945, 1963

Hashin, Z.: Elasticity of ceramic systems. In: Ceramic microstructures, R.M. Fulrath, J.A. Pask, eds.: pp. 313–341. New York, London,Sydney: Wiley 1966

Hermance, J.F., Grillot, L.R.: Constraints on temperatures beneath Iceland from magnetotelluric data. Phys. Earth. Planet. Inter. **8**, 1–12, 1974

Kroenke, L.W., Manghnani, M.H., Rai, C.S., Fryer, P., Ramananan-toandro, R.: Elastic properties of selected ophiolitic rocks from Papua New Guinea: nature and composition of the oceanic lower crust and upper mantle. In: The Geophysics of the Pacific Ocean Basin and its Margin, G.H. Sutton, M.H. Manghnani, R. Moberly, eds.: pp. 407–421. Washington: Am. Geophys. Union 1976

Laughton, A.S.: South Labrador Sea and the evolution of the North Atlantic. Nature **232**, 612–617, 1971

Long, R.E., Mitchell, M.G.: Teleseismic P-wave delay time in Iceland. Geophys. J.R. Astron. Soc. **20**, 41–48, 1970

Pálmason, G.: Crustal structure of Iceland from explosion seismology. Reykjavik: Soc. Sci. Islandica **40**, 1971

Pálmason, G., Saemundsson, K.: Iceland in relation to the Mid-Atlantic Ridge. Annu. Rev. Earth Planet. Sci. **2**, 25–50, 1974

Peterson, J.J., Fox, P.J., Schreiber, E.: Newfoundland ophiolites and the geology of the oceanic layer. Nature **247**, 194–196, 1974

Röber, K.R., Thyssen, F.: Messung der Schallgeschwindigkeit beim Übergang fest – flüssig. DFG Kolloquium, Geowissenschaftliche Hochdruckforschung, Bad Honnef pp. 13–14, 1978

RRISP Working Group: Reykjanes Ridge Iceland seismic experiment. J. Geophys. **47**, 228–238, 1980

Stefánsson, R.: Methods of focal mechanism studies with application on two Atlantic earthquakes. Tectonophysics **3**, 210–243, 1966

Tryggvason, E.: Crustal structure of the Iceland region from dispersion of surface waves. Bull. Seismol. Soc. Am. **52**, 359–388, 1962

Tryggvason, E.: Arrival times of P-waves and upper mantle structure. Bull. Seismol. Soc. Am. **54**, 727–736, 1964

Walsh, J.B.: Attenuation in partially melted material. J. Geophys. Res. **73**, 2209–2216, 1968

Walsh, J.B.: New analysis of attenuation in partially melted rock. J. Geophys. Res. **74**, 4333–4337, 1969

Wielandt, E.: Anregung seismischer Wellen durch Unterwasserexplosionen. Diss., Univ. Karlsruhe, 90 pp., 1972

Zverev, S.M., Kosminskaya, I.P., Krasilschikova, G.A., Mikhota, G.G.: The crustal structure of Iceland and of the Iceland-Faeroe-Shetland region. Soc. Sci. Islandica, Greinar **5**, 72–95, 1976

Received September 7, 1979; Revised Version November 14, 1979

J. Geophys. 47, 250–260, 1980

Journal of Geophysics

Seismic Structure Along RRISP – Profile I on the Southeast Flank of the Reykjanes Ridge

P. Goldflam[1], W Weigel[1], and B.D. Loncarevic[2]

[1] Institut für Geophysik, Bundesstr. 55, D-2000 Hamburg 13, Federal Republic of Germany

[2] Geological Survey of Canada, Bedford Institute of Oceanography, Dartmouth, Nova Scotia B2Y 4A2, Canada

Abstract. During the first leg of the 'METEOR-Expedition 45', July 1977, crustal seismic refraction measurements were obtained in the vicinity of the Reykjanes Ridge, south of Iceland. Profile I was located approximately along magnetic lineation anomaly 5 (8.34–9.74 Ma) and was a part of an 800-km-long land-sea seismic experiment. The purpose of the overall experiment was to study the changes in crustal structure of the Ridge near Iceland and to resolve the seismic structure at greater depth than was previously possible by extending the seismic line south of Iceland. At the Mohorovičić discontinuity the velocity increases to 7.7 km/s, a 'typical' low mantle velocity observed frequently in oceanic refraction profiles near ridge crests. A normal upper mantle velocity of 8.2 km/s is observed at a depth greater than 16 km. Reflection profiles show a rough basement topography in the south, becoming smooth towards the north. The results indicate: (i) that a normal oceanic crust is in place within 100 km of an active ridge crest; (ii) that the presence of Iceland has only a second-order effect on the oceanic crust to the south; (iii) that a normal upper-mantle velocity is present underneath a low (7.7 km/s) velocity at the Mohorovičić transition zone; and (iv) that velocity gradients in the lower crust and the upper mantle are consistent with the results of the inversion of time-distance data, but should be confirmed by synthetic seismogram modelling.

Key words: Reykjanes Ridge – Iceland – Seismic structure – Hot spots – Explosion seismology – Anisotropy – Anomalous mantle – Upper mantle – Asthenosphere flow – Mantle plume – Extremal inversion.

1. Introduction

Iceland has fascinated explorers and travellers since the first Norsemen settled there, more than 1,000 years ago. Its rugged volcanic terrain, majestic glaciers and waterfalls, mysterious hot springs and often violent erruptions of lava, all seemed to hold a key to the better understanding of the Earth as a dynamic engine. It is not surprising that the modern research into the nature and structure of the outer rock layers of the Earth, often returned to Iceland and the surrounding ocean for more insight and understanding. The evidence from many directions is presented in this issue. Our paper describes the contribution of the marine program to the Reykjanes Ridge Iceland Seismic Project (RRISP).

Iceland is located astride the Mid-Atlantic Ridge, between latitudes 63° N and 67° N. The edge of Eurasian and North American lithospheric plates (LePichon et al., 1973) is exposed in the neovolcanic zone of Iceland and offers an unparalelled opportunity for study. As a geological feature, Iceland is young: the outpouring of some half a million cubic kilometers of lava occurred within the last 18 Ma (Jakobsson, 1972; Moorbath et al., 1968; Everts et al., 1972). Although Iceland is a part of the Mid-Ocean Ridge system, it differs from a typical cross-section in many important ways: (i) the extensive volcanic activity has created an excess of mass so that it outcrops above the sea surface and forms a 'blister' on the crest of the Mid-Atlantic Ridge; (ii) it is an area of active seismicity and tectonic development; (iii) it is a centre of convective heat flow from the mantel as a postulated 'hot spot'; (iv) the seismic structure indicates a depression of the Moho discontinuity and/or unusually low upper mantle *P*-wave velocity; (v) geochemistry of Icelandic basalts differs from the average composition of mid-ocean ridge basalts (Brooks and Jakobsson 1974). For these and other reasons, Iceland is considered a 'hot spot' (Morgan, 1971) and complicated convection patterns have been postulated to explain its origin (Vogt, 1974).

It is thus accepted that Iceland is an 'anomalous' section of the Mid-Atlantic Ridge but it is not known how far this anomaly extends along the length of the ridge crest. Two transform faults, Tjörness Fracture Zone to the North and Reykjanes Fracture Zone to the south displace the ridge crest through Iceland eastwards. These zones seem to confine the Iceland eruptives but the hot-spot may affect the ridge beyond the fracture zones. The southward extension of the mid-ocean ridge is called Reykjanes Ridge; it is an atypical ridge, probably because of its slow spreading rate (Talwani et al., 1971) and possibly because of the proximity of the hot-spot to the north. Based on an analysis of V-shaped magnetic anomalies (Vogt and Avery 1974) and the distribution of trace elements revealed by geochemical analysis (Schilling, 1973), it has been proposed that some of the lava brought up by the mantle plume under Iceland, finds its way southwards along the ridge axis through hydraulic channeling (Vogt, 1974). In studying the deeper structure of Iceland, it is therefore of great interest to investigate the seismic structure of the surrounding sub-oceanic crust (Bott et al., 1971). The marine seismic experiment, described here, was designed to supplement the land investigations and additionally, to study the uppermost structure of the oceanic lithosphere by extending the length of the seismic refraction Profile I. Data collected along other profiles shown in Fig. 1 will be reported elsewhere.

Long seismic lines at sea are difficult to carry out and only four had been performed prior to the RRISP experiment · two in the Pacific (Asada and Shimamura, 1976, 1979; Orcutt and Dorman, 1977), one in the Atlantic (Steinmetz et al., 1977), and one in the Mediterranean (Hirn et al., 1977). Among the questions

0340-062X/80/0047/0250/$02.20

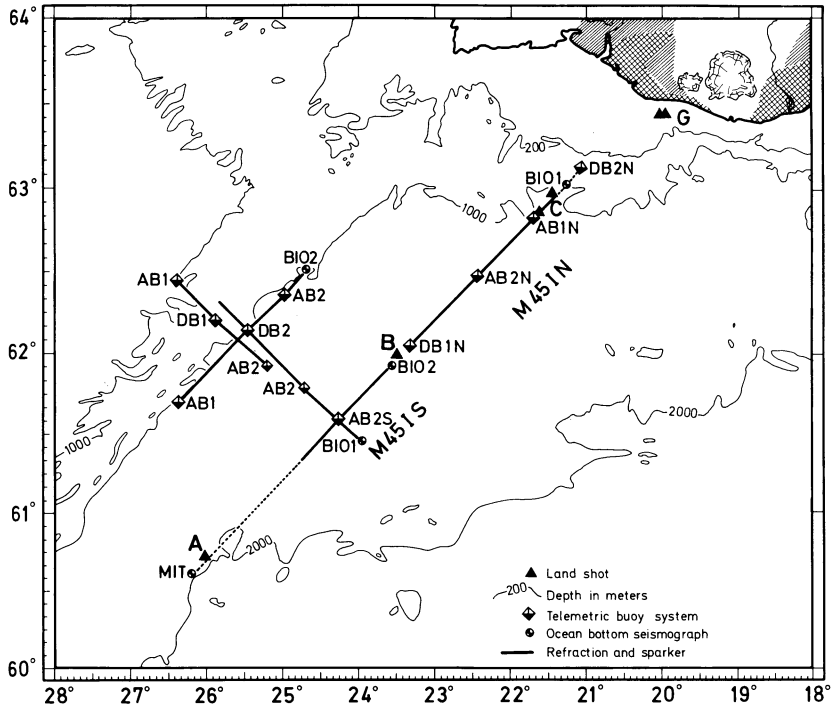

Fig. 1. Geophysical investigations during the METEOR Cruise 45, south of Iceland

posed by these experiments and RRISP were: is there a high-velocity layer 3 B at the base of the crust as shown by Sutton in the Pacific (Sutton et al., 1971) or is there a low velocity zone near the crust-mantel interface (Lewis and Snydsman, 1977); is P-wave velocity in the mantle 'normal', i.e., in the range 8.2 ± 0.2 km/s or is there any anomalously low-velocity mantle away from the axial spreading zone? Is there a velocity gradient in the crustal layers or is a horizontally layered crust an adequate approximation?

The topography of the Reykjanes Ridge is rough in the crestal region and becomes smoother towards the flanks and southwards. The considerable thickness of sediments near the bottom of the continental slope and away from the ridge crest represent an accumulation of erosional material transported from the Iceland Plateau, perhaps by turbidity currents (Fleischer, 1974). The volcanic basement is hidden by a blanket of these sediments and it is not known whether the basement under the flanks is block-faulted and broken up as much as it is near the crest. The structure of the ridge is nearly symmetrical with respect to its axis, and so are the magnetic lineations. The clear correlation of the magnetic stripes in this area confirmed the hypothesis of sea-floor spreading (Vine and Matthews, 1963; Heirtzler et al., 1968). Because of the nature of development of plate boundaries in the North Atlantic, Iceland and Reykjanes Ridge have been the subject of extensive exploration. Gravity and magnetic measurements represent a dense net of observations (Heirtzler et al., 1966; Talwani et al., 1971; Talwani and Eldholm, 1972; Fleischer et al., 1973; Fleischer 1974; Grønlie and Talwani 1978) and reveal a noticeable Bouguer gravity minimum and a high axial magnetic anomaly of over 1,000 *nT*. There is also a substantial body of information regarding the heat flow in the vicinity of the ridge (Talwani and Eldholm, 1977; Grønlie and Talwani, 1978; Bram, 1980; Sclater and Crow, 1979).

In contrast to these extensive geophysical observations, seismic information about the deeper structure of the crust is sparse. The results of early refraction seismic experiments were presented in a compilation by Ewing and Ewing (1959). In this early work usual procedures involved two surface ships. The signal-to-noise ratio was relatively poor and the seismic lines were often too short to detect deeper refractors. About 60 km west of the axis, these authors found a consolidated layer with a compressional wave velocity of 5.7 km/s under local sedimentary troughs of small thickness, and below 6 km depth an anomalous mantle *P*-velocity of about 7.4 km/s. These results only roughly agree with those of Talwani et al. (1971) farther north who found a rise of the material with a similar *P*-velocity (7.4 km/s) from the flank towards the ridge axis. For the crestal area these results correspond to those obtained from earthquake surface wave dispersion observations (Trygvason, 1962). Ariç (1972) presented a crustal section of the west flank of the Reykjanes Ridge from deep reflection seismic results. His depth calculation is based mainly on the *P*-wave velocity structure from the mid-Atlantic Ridge between 0° and 30° N given by Ewing and Ewing (1959) and LePichon et al. (1968). The model calculated shows an extensive body with *P*-velocities varying from 7.3 to 7.7 km/s, underlain by a layer with a velocity of 8.1 km/s. This low-velocity body reaches a depth of 40 km under the crest, and extends about 200 km from the axis. At a distance of about 600 km, this anomalous mantle zone melds into a normal oceanic crust. This interpretation is analogous to the results obtained under Iceland by Zverev et al. (1976). As part of the IPOD/DSDP site surveys (Leg 49, site 409), Snoek and Goldflam (1978) found, at a distance of 18 km from the axis, a high *P*-velocity of 7.9 km/s at a depth of 7 km, a slightly higher velocity than found by Talwani and Eldholm (1977), though still classified an 'anomalous' mantle.

The concept of a mantle plug of lower density and lower *P*-velocity ('anomalous mantle') was introduced by Talwani et al. (1965) as a possible model to explain the observed gravity anomalies across the Mid-Atlantic Ridge. This body extended about 400 km on either side of the median valley and the model was based on the earlier compilation of seismic observations by Ewing and Ewing (1959). From the study of surface wave propagation

Table 1. Type and locations of seismic systems used

System	Latitude (Degree) N	Longitude (Degree) W	Depth (km)	Sensor
M45/IN				
DB2N	63° 7.8′	21° 3.0′	0.366	GHG
BIO1	63° 1.5′	21° 14.1′	0.819	GHG
AB1N	62° 49.8′	21° 40.2′	1.124	GH
AB2N	62° 28.2′	22° 25.2′	1.385	GH
DB1N	62° 2.8′	23° 18.7′	1.542	GH
BIO2	61° 55.0′	23° 34.2′	1.544	GHG
M45/IS				
BIO1	63° 1.5′	21° 14.1′	0.819	GHG
DB1S	62° 2.8′	23° 33.5′	1.439	GH
BIO2	61° 55.0′	23° 34.2′	1.544	GHG
AB2S	61° 35.3′	24° 14.3′	1.605	GH

DB,AB = Digital and analog buoy system, BIO = Ocean bottom seismographs, GH = Ground hydrophones, GHG = Ground hydrophones and geophones

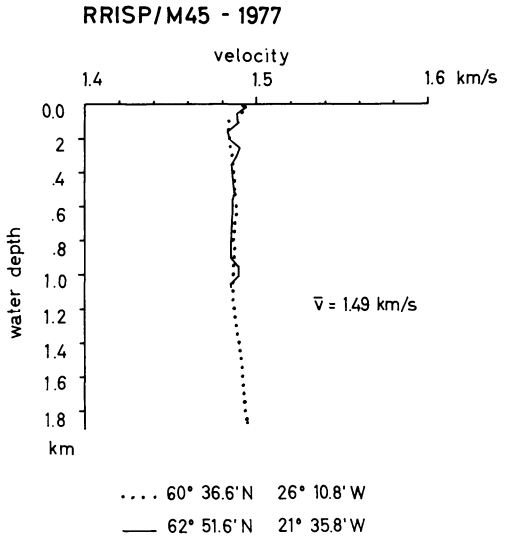

Fig. 2. Sonic log measurements in water at two positions on profile *M45/I*

and teleseimic *P*-delay times (Tryggvason, 1962, 1964; Francis, 1969a, Long and Mitchell, 1970), it was suggested that low-velocity mantle in the vicinity of Iceland may extend to a depth of 150 to 250 km. An examination of the relationship of terrain-corrected Bouguer anomaly to bathymetry within the detailed survey area of the Mid-Atlantic Ridge near 45° N, led Woodside (1972) to suggest that a density deficiency *or* buoyant forces in the upper mantle are responsible for the overall elevation of the crestal mountain region and that the topography of the high-fractured plateau may be partially compensated by undulations of the crust-mantle interface. The search for the low-density, low *P*-velocity mantle under the crestal region and the delineation of the extent of this 'anomalous mantle' away from the ridge has been an objective of much research during the last decade.

Working on Mid-Atlantic Ridge near 45° N, Keen and Tramontini (1970) found the Mohorovičić discontinuity at a mean depth of 7.5 km with a mean velocity of 7.9 km/s for the underlying material. No evidence was found for anomalous mantle material except within the immediate vicinity of the median valley and low *P*-velocities were interpreted as a result of anisotropy. Later work of Fowler (1978) within the same area, re-interpretation of Keen and Tramontini (1970) data by Fowler and Keen (1979), work of Whitmarsh (1975) and Fowler (1976) on the Mid-Atlantic Ridge near 37° N (FAMOUS area), and work of Whitmarsh (1978) and others on the ridge flanks north of the Azores, all confirmed that the crustal structure is more complicated than that described by the standard oceanic model (Raitt, 1963), that a low-density, low *P*-velocity mantle is confined to a narrow axial zone, perhaps not more than a few kilometres wide, and that away from the axis a 'normal' oceanic crust is formed within a few million years.

On the basis of all these results it appeared that Reykjanes Ridge may be different compared to the rest of the Mid-Atlantic Ridge. The question of how it is related to Iceland could only be answered by the knowledge of the deep crustal structure of both Iceland and Reykjanes Ridge. This was the reason for carrying out an 800-km-long refraction profile with 53 mobile and 37 permanent stations on Iceland and 8 stations at sea (consult RRISP Working Group 1980, Gebrande et al., 1980). This combined land/sea profile runs along the eastern flank of the Reykjanes Ridge parallel to the bathymetry contours and somewhat obliquely to magnetic anomaly 5 (8.34–9.74 Ma; LaBrecque et al., 1977), crosses Surtsey and Vestmannaeyjar and continues into the young volcanic zone of Iceland. We present in this paper the results from the sea end of this profile.

2. *Description of the Experiment*

The seismic refraction experiment along the seaward extension of the land profile, called profile M45/I (Fig. 1) was carried out in two parts. Along the 187 km northern section, Profile M45/IN, six seismic receiving systems were launched (Table 1). Four of these were anchored telemetering buoy systems of the Institut für Geophysik, Hamburg (Kebe, 1971, Weigel et al., 1978) and the other two were ocean bottom seismometers (BOBS) of the Bedford Institute of Oceanography, Dartmouth, N.S. (Heffler and Barrett, 1979). All systems included a hydrophone near the sea floor. In addition, BOBS had two geophones (one vertical, one horizontal) but the records from these were too noisy for detailed analysis. The two ocean bottom seismometers, BIO 1 and BIO 2 (Table 1), stayed on the bottom for 14 days and were also used for measurements along the 80-km-long southern section – Profile M45/IS. Along this section, two additional telemetering buoys were anchored, again with sea-floor hydrophones. During the whole seismic experiment, all systems worked satisfactorily except for the buoy DB1S. This buoy drifted 8 km due to unknown reasons, so the results can be used only for qualitative purposes. For the combined land/sea experiment, charges of high explosive GEOSIT II from 25 to 4,000 kg were detonated electrically. In total 141 shots, about 1.8 km apart were fired.

For the determination of the shot and seismic-system coordinates, Loran C and integrated satellite navigation were used, and the raw data were corrected by the method described by Goldflam and Goldflam (1979). Sound velocity in water measurements were carried out at two stations (Fig. 2) and were used to calculate shot to receiver distances. A very weak low-velocity channel appears within the first 100 to 200 m. The mean sound velocity of the sea water remains constant at 1.486 km/s and this value

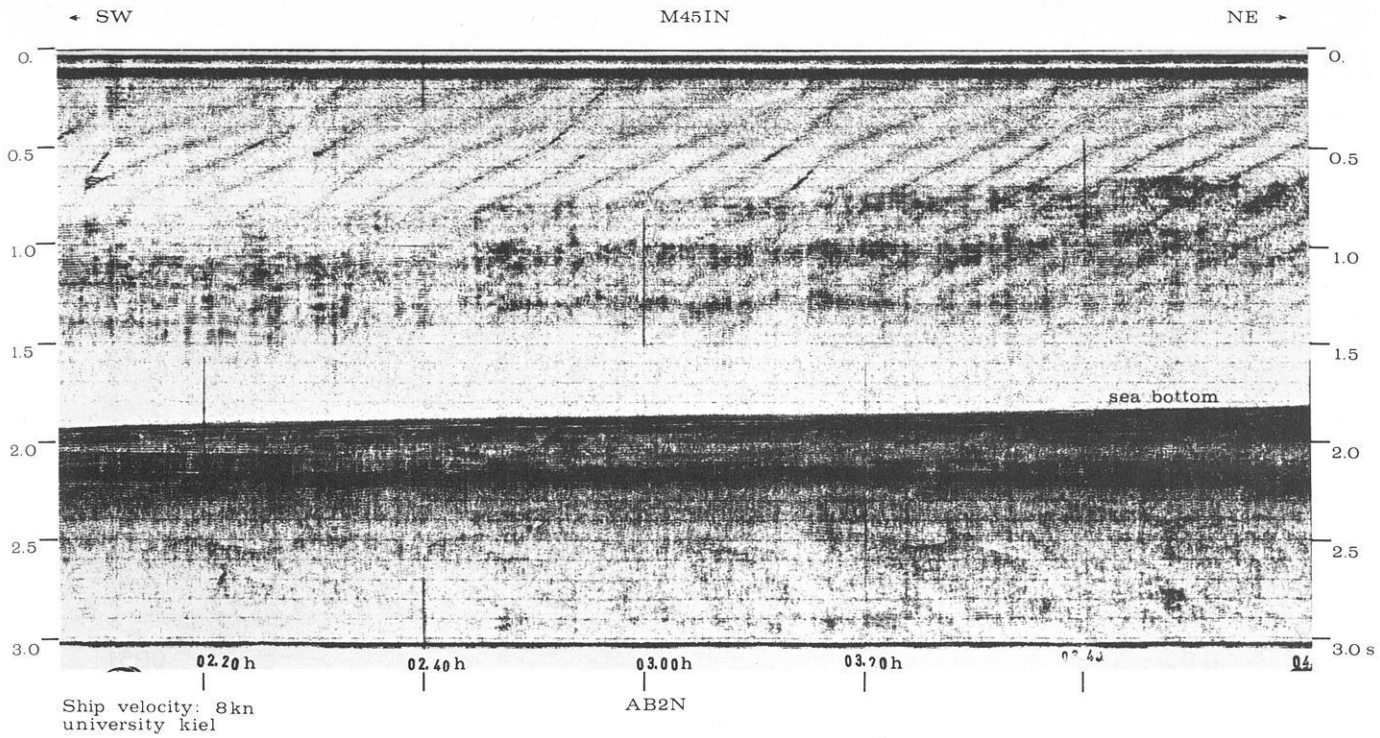

Fig. 3. Sparker results in the area of the buoy AB2N characterized by smooth acoustical basement

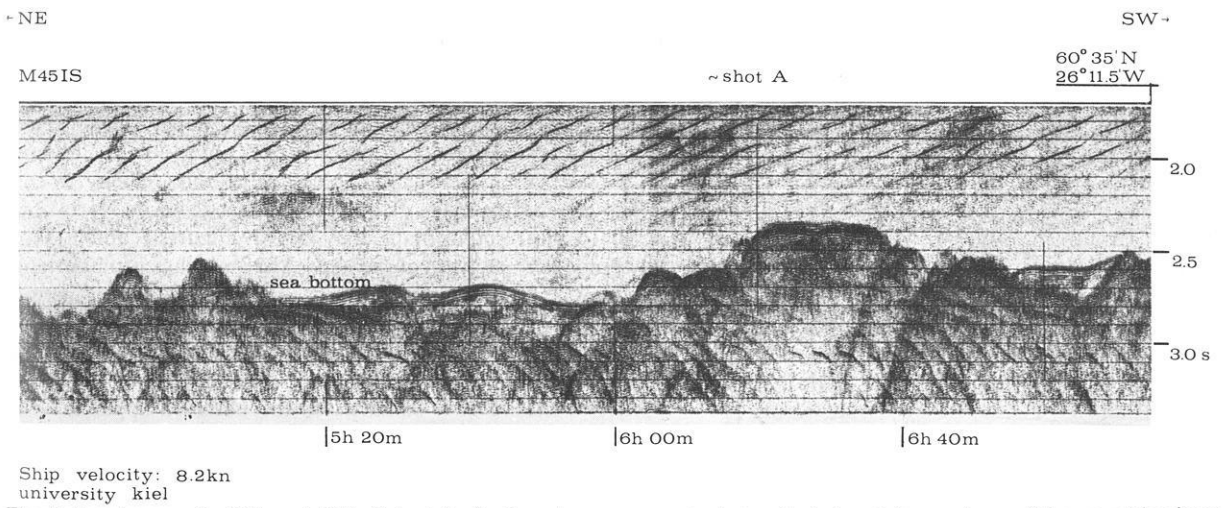

Fig. 4. Sparker results NE and SW of shot A. Sediments are concentrated only in local depressions of the roughly shaped outcropping basement

was used for all calculations. Comparisons of geodetic distances with distances calculated from water-wave arrivals indicate an accuracy of geographical position determination of 200 to 300 m.

To obtain the fine structure of the upper sediments, seismic reflection data using a sparker system were collected along the profile. Over most of the profile we observed smooth acoustic basement and sediment thicknesses up to about 400 m which thin from north to south. In the southern part of the profile, close to shot A, the basement becomes rough (Fig. 4) and the sediments are concentrated only in local depressions between the outcropping basement highs. These features of the basement topography are important for tectonic interpretation of the refraction data (see also RRISP Working Group 1980).

3. The Results

Out of a total of 15 seismogram sections compiled for the interpretation of the refraction observations on Profile M45/I, only four representative examples are presented in this paper in order to save space. The ranges of observations of each system are discussed in RRISP Working Group 1980, (see Fig. 2). All Hamburg seismograms were filtered with a band-pass of 2 to 20 Hz which roughly corresponds to the frequency response of BOBS. The sections are not corrected nor are the arrivals normalized for variations in shot charges. Only the BIO 1 record section is corrected for the attenuation with distance. According to the theory of propagation of head waves (Červeny and Ravindra, 1971), at long ranges

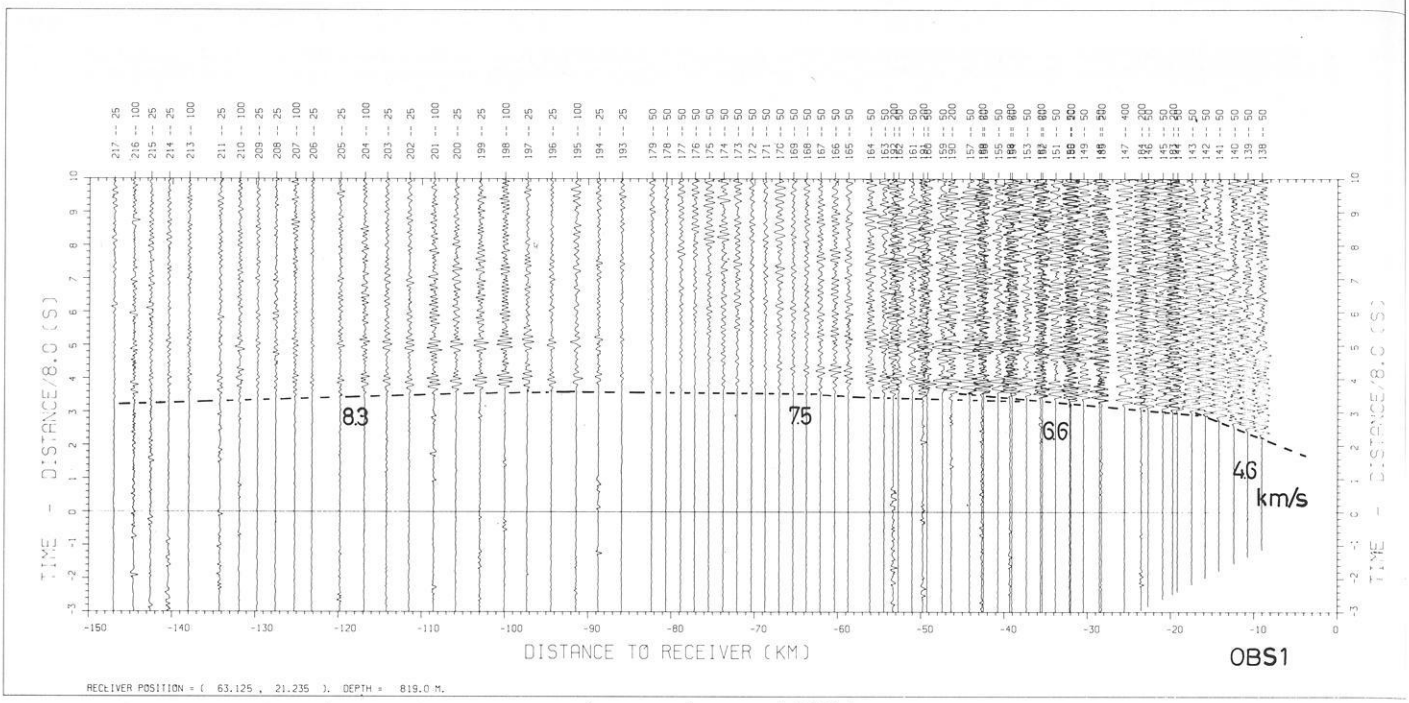

Fig. 5. Seismogram section of the northernmost ocean bottom seismograph BIO 1

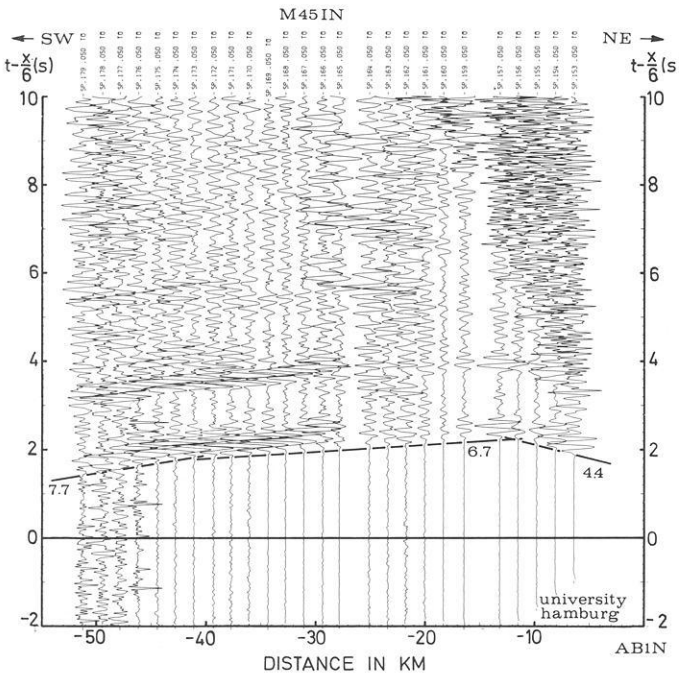

Fig. 6. AB1N seismogram section. Very good phase correlation (supported by clear multiple refraction arrivals)

the first arrival separates from the interference packet by more then the pulse length and so the amplitude decays as r^{-1}. This relationship was used and the constants of proportionality so adjusted that a signal at 120 km range is corrected by a factor of two (i.w., an attenuation of 50% is assumed at that range).

In the illustrations given, the time axis corresponds to the reduced time with a reduction velocity of 6 km/s except for BIO 1 (Fig. 5). Because of long range of observations – almost the whole length of profile M45 I – a reduction velocity of 8 km/s was used for this section. In this seismogram section we can recognize the main horizons which are here characterized by the apparent velocities: $V_{4-}=4.6$; $V_{5-}=6.6$; $V_{6-}=7.5$; and $V_{7-}=8.3$ km/s. Similar results were obtained in the remaining sections, as for example in the reversal part between the buoys AB1N and AB2N (Fig. 6) except that no upper-mantle velocity was observed. The absence of any arrivals indicating the presence of this velocity (V_7) is due to the shorter range of observations on these buoys as compared to the results obtained by BIO 1. Figures 7 and 8 show the seismogram sections of the buoy AB2S which is of importance bacause the apparent velocities V_{4+} and V_{4-} indicate an increase of the true *P*-velocity for this particular layer southwards. This indicates a different crustal constitution in the south as already suggested by the changes in basement morphology.

In Table 2 we have summarized the observed apparent velocities for comparision of the results of all seismic systems. We designate with V_{i+} the apparent velocities of the arrivals originating from shots northeast of the seismic receivers and with V_{i-} those fired southeast of the receiver (Fig. 1). With regard to the horizontal nature of the sediment layer (Fig. 3) and taking into account all the calculated apparent velocities (Table 2), a model was developed to fit the observed travel times on Profile M45/IN by ray-tracing. The velocities at the upper boundaries of the model are as follows: $V_1=1.49$, $V_2=1.6$, $V_3=2.2$, $V_4=4.4$, $V_5=6.7$, $V_6=7.7$, and $V_7=8.2$ km/s. The algorithm used in calculating the ray tracing model required a small velocity gradient in the layers (Gebrande 1976). Similar model calculations along the southern section of this profile (M45/IS) – northeast and southwest of the position of AB2S – show slightly different V_p values for layers 4 to 6 namely: $V_4=4.9$, $V_5=6.5$, and $V_6=7.7$ km.

The extremal inversion of travel time data by the tau-p method (Bessonova et al. 1974; Bessonova et al. 1976; Kennett, 1976) was applied to the data recorded at BIO 1. We find that the model velocities calculated by conventional methods are within the extremal bounds on possible velocity-depth distributions obtained by

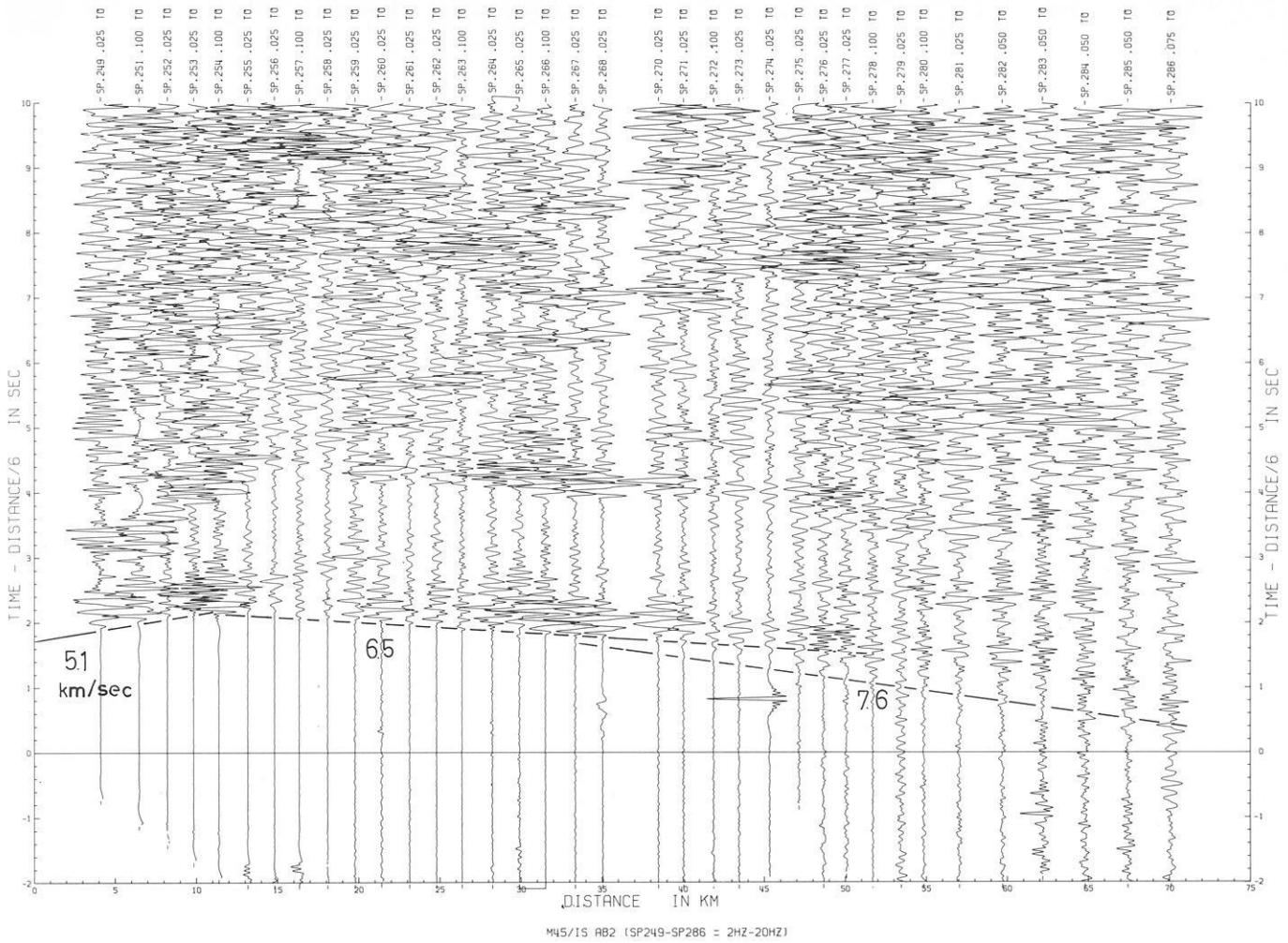

Fig. 7. Results of the observation of the Buoy AB2S on the southern section M45/IS (NNE direction)

the tau-p inversion (Fig. 9). The upper boundary of possible V(z) functions indicates that the transition from 6.7 to 7.7 km/s and from 7.7 to 8.2 km/s layers may be step like. The absence of velocity gradients (i.e., a layered solution) and a presumed absence of 'interference head waves' (Kennett 1977) may account for the low amplitudes of first arrivals at BIO 1 (Fig. 5). The larger amplitudes between 90 and 120 km may be due to a slight positive velocity gradient in the upper mantle. Another explanation for the increased amplitude at greater range is the possible arrival of wide-angle reflections from the mantle boundary *(PnP)*, as observed by Lewis and Snydsman (1977) in the Pacific. For strong reflections, the boundary would have to be sharp and this has implications for petrologic models which may explain our observations as discussed later. These speculations are quite qualitative, however, and should be verified by calculation of synthetic seismograms.

4. Interpretation and Discussion

The main part of the RRISP experiment (see RRISP Working Group 1980; Gebrande et al. 1980) has confirmed the findings of many earlier investigators that the crust under Iceland is 'anomalous'. In contrast, we find under the flanks of the Reykjanes Ridge south of Iceland nearly normal crust, though of greater thickness than elsewhere on mid-ocean ridges. Two aspects of our results deserve further discussion: (i) the absence of strong along-strike changes in crustal thickness as Iceland is approached; and (ii) the nature of 7.7 km/s layer and the transition from 7.7 to 8.2 km/s at a depth of 16 km.

The uppermost (unconsolidated sediment) layer decreases in thickness with distance from the Iceland plateau as is to be expected. This is a surficial phenomenon due to erosion and redistribution of sediments and is not important for understanding deeper structure and tectonic development of the region. Of more interest is the slight increase in the velocity of layer 2 from 4.4 to 4.9 km/s (north to south) and perhaps some thickening southwards. This result needs confirmation from the other seismic lines in the area. These velocities are identical to those of wide-spread basaltic nappes on and around Iceland. Because of the oblique crossing of anomaly 5 by our profile the rocks under the southern portion of Profile M45/I are older and get progressively younger towards the north. Our results would thus suggest an increase in velocity of layer 2 with age. The change (of about 10%) is too large to be explained by compression of basalts and closure of cracks and, if real, may be due to a slight compositional variations in the chemistry of the rocks away from the Iceland plume. Of greater interest, however, is the almost horizontal layering of deeper crustal layers.

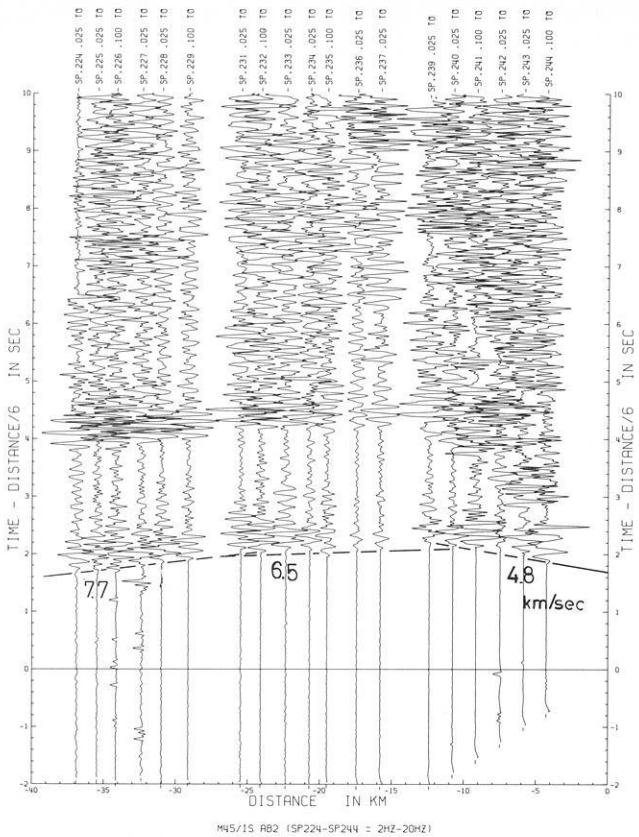

Fig. 8. Results from AB2S to SSW

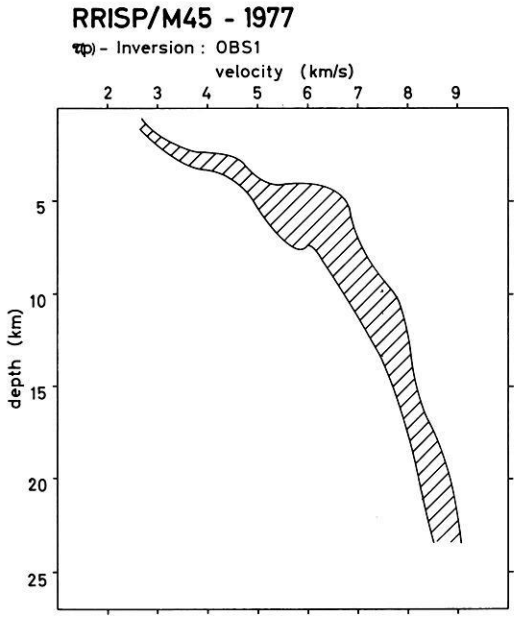

Fig. 9. Extremal bounds for the possible velocity-depth function V(z) obtained by the tau-P inversion applied to the travel time data of the BIO 1

The main crustal layer under Iceland of velocity 6.35 km/s (Pálmason, 1971) to 6.8 km/s (RRISP Working Group 1980) corresponds to the 6.7 km/s layer observed under Profile M45/1 (Fig. 9). The base of this layer under Iceland is at a depth of 8 to 18 km and is underlain by a layer of velocity 7.0 km/s which has a slight positive velocity gradient and may extend to a depth of 150 to 200 km (Tryggvason, 196', 1964; Long and Mitchell, 1970). This is at complete variance with sea observations. The oceanic structure determined under M45/I must come to an abrupt termination just south of the mainland of Iceland, perhaps along the walls of the Reykjanes Fracture Zone. This result places a constraint on the depth of asthenosphere flow outwards from a mantle plume as proposed by Vogt (1974; Vogt and Avery, 1974). This has further implications for search for 'archeo-plumes'. If the anomalous crustal structure is confined to the immediate vicinity of the mantle plume, then traces of ancient plumes will be found only by studying anomalous crustal structures over small areas. Systematic search for ancient or exhausted mantle plumes by seismic refraction techniques is not a practical project at the present time.

A *P*-velocity of 7.7 to 7.9 km/s has been measured frequently at the base of the oceanic crust and interpreted as the crust-mantle or Mohorovičié discontinuity (Wyllie 1971). For example, in an experiment carried out about 200 km southeast from the position of BIO 1, Whitmarsh (1971) found a deep layer of velocity 7.84 km/s at a depth of about 9.5 km. A layer of similar velocity (7.74 km/s, depth 7 km) was detected by Steinmetz et al. (1977) at the eastern flank of the Mid-Atlantic Ridge north of the Azores. Measurments on the younger crust of faster spreading ridges in the Pacific have also found similar velocities: 7.3 to 7.9 km/s near the Explorer Ridge (Malecek and Clowes 1978) and 7.5 to 8.2 km/s (age dependent) on the Cocos Plate (Lewis and Snydsman 1979). None of these experiments reported a further sharp increase in *P*-velocity at a greater depth as we observed under M45/I. This is significant and can be explained in several ways. (i) The 7.7 to 8.2 km/s transition is widespread but has not been observed

Table 2. Observed apparent *P*-velocities in km/s

Observed to SW				Shot point	Buoy	Shot point	Observed to NE				
$\bar{v}_{4-}$	$\bar{v}_{5-}$	$\bar{v}_{6-}$	$\bar{v}_{7-}$				$\bar{v}_{3+}$	$\bar{v}_{4+}$	$\bar{v}_{5+}$	$\bar{v}_{6+}$	$\bar{v}_{7+}$
		7.7		138–146	DB2 N						
4.6	6.6	7.5	8.3	138–217	BIO 1						
4.4	6.7	7.7		153–179	AB1 N	138–148		4.6	6.8		
	6.7	7.7		199–220	AB2 N	147–179		4.5	6.8		
					DB1 N	169–219		5.0	6.9	7.4	
	6.7			252–283	DB1 S						
4.9		7.6		224–277	BIO 2	147–278	2.1	4.9	6.7	7.5	8.3
4.8	6.7	7.7		224–244	AB2 S	249–286		5.1	6.5	7.6	

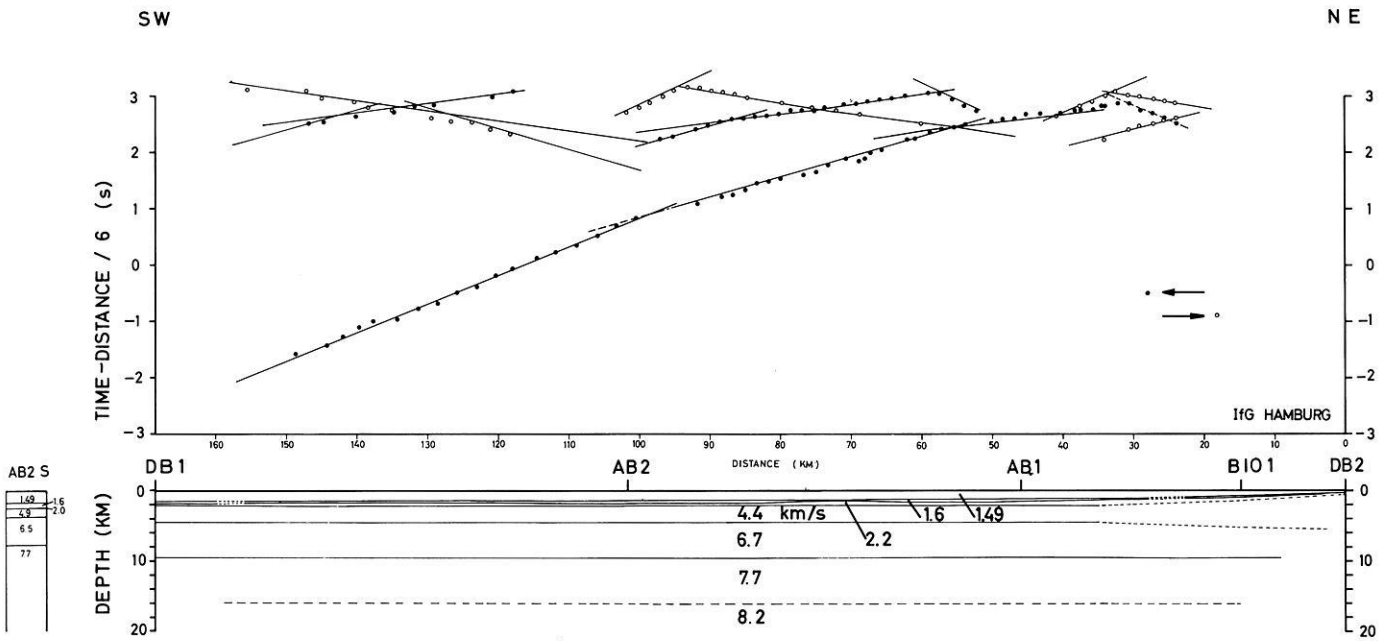

Fig. 10. Crustal model of the eastern flank of the Reykjanes Ridges calculated by means of the ray tracing theory *(bottom)*. Upper part: calculated *(solid lines)* and observed *(symbols)* travel time

elsewhere because of insufficient length of profiles (typically less than 100 km); (ii) this transition is widespread and normally at a greater depth; peculiar conditions under Reykjanes Ridge (elevated temperatures? asthenosphere flow?) make it possible to observe the transition there; and (iii) the transition is a special feature of Reykjanes Ridge. As will be seen from the subsequent discussion, we favour explanation (iii) allowing that (ii) also may be possible. The correct choice depends on a plausible explanation of the 7.7 to 8.2 km/s transition. We offer here one explanation based on anisotropy. We also note that there are other possible explanations based on phase transitions in different petrologic models proposed for the composition of the lower crust and the upper mantle.

The anisotropy in seismic velocity measurements is a measure of dependence of elastic parameters on the direction of propagation of *P*-waves. As was originally shown by Birch (1960, 1961), the strong variation of compressional wave velocity with propagation direction in ultramafic rocks is related to prefered orientation of olivine. At temperatures less then 1,000° C an low strain rates over a geological time scale, olivine crystals may be aligned in the direction of maximum compressional velocity (a crystallographic axis) parallel to the principal glide plane (Francis 1969b). Measurements on single crystals of olivine by Verma (1960) detected velocities of 9.87, 7.73, and 8.65 km/s in the *a*, *b*, and *c* crystallographic directions, with intermediate velocities possible in intermediate directions. Recent detailed measurements on field samples from the ophiolite complex of western Newfoundland by Christensen and Salisbury (1979) have confirmed this range of variations on a suit of rocks presumed to represent an upthrust and exposed section of the oceanic mantle.

In several marine seismic refraction experiments where anisotropy was detected, the variation in velocity is of the order of 5 to 8% with the direction of minimum usually perpendicular to the direction of spreading (Raitt et al. 1969, 1971; Keen and Tramontini 1970, Keen and Barrett 1971, Lewis and Snydsman 1979). All of these experiments were performed relatively close to the spreading axis, on crust less than 12 Ma old. On the flanks of Reykjanes ridge, on crust 35 Ma old, careful experiment by Whitmarsh (1971) failed to measure anisotropy. Lewis and Snydsman (1979) have shown that on a fast-spreading ridge (4.4 cm/a half spreading rate on Cocos plate) the anisotropy decreases from 0.6 km/s to 0.3 km/s within the first 10 Ma of lithospheric plate development. It is thus possible that Whitmarsh's experiment was too far from the spreading axis and his results do not preclude the possibility that our observation of 7.7 km/s layer represents mantle with low velocity due to anisotropy. [Our additional lines in the area (Fig. 1) may resolve this question. Unfortunately there are problems with the data reduction and we cannot report the results from these lines at the present time.]

In the deepest layer observed in this experiment the velocity increases from 7.7 km/s to 8.2 km/s. This range of the *P*-velocity change is of the same magnitude as the change that could be caused by anisotropy due to a prefered orientation of olivine crystals. We therefore wish to consider a model in which the uppermost part of the mantle is composed of petrologically uniform material but with a change in *P*-velocity with depth due to rheological causes.

We could envisage a couple of forces acting on the uppermost lithosphere, perhaps over different time scales. The first, and perhaps dominant, force is the driving force of the ocean-floor spreading. This causes strain and the minimum of *P*-velocity would be parallel to the Reykjanes Ridge axis. This would be the 7.7 km/s velocity observed along our profile M45/I. The orientation of the crystals which gives this low velocity could be 'frozen-in' early in the cooling stage of the lithosphere development.

At depth, another force may be acting according to the hypothesis of outward flow from a mantle plume as developed by Vogt and Avery (1974). If there is a significant flow at depth away from Iceland parallel to the direction of, and under, the Reykjanes Ridge, then the temperature and viscous stress may

be sufficient to re-orient the olivine crystals along their gliding planes. The maximum *P*-velocity in this depth range would be in the direction of flow, i.e., parallel to the ridge crest. This would be the observed 8.2 km/s velocity.

The transition between 7.7 km/s and 8.2 km/s could be gradual or sharp, depending on the actual mechanism of olivine crystal re-orientation. If the temperature gradient and stress field are uniform, the crystals may be reoriented gradually and all the intermediate velocities between 7.7 and 8.2 km/s would be present along our profile. On the other hand, if there is a 'stickiness threshold' which must be reached before the plastic deformation begins and the crystals start to re-orient, and if, once this threshold is reached, the reorientation proceeds until the alignment in the new direction is completed, then the change from 7.7 to 8.2 km/s could be quite sharp. Synthetic seismograms may discriminate between the models with sharp and gradual transitions between 7.7 and 8.2 km/s and we intend to make these calculations in the near future. Incidentally, the couple produced by the spreading in the southeasterly direction and the asthenosphere flow in the southwesterly direction, may explain the highly developed en echelon fracturing of the ridge crest (Laughton et al., 1979).

Finally, we want to comment on the possibility that the decrease of velocity from 8.2 to 7.7 km/s is due to petrological changes in the upper mantle, the most likely candidate being serpentinization of the ultramafics at the base of the crust. Serpentinization was recognized as an important process in the development of the lower crust by Hess (1955). Geophysical consequences of serpentinization are a decrease in seismic velocity (Christensen 1966) and an increase in volume. To explain the observed change in *P*-velocity the degree of serpentinization would not have to be great, perhaps 10 to 15%. This is consistent with observations that in most ophiolite suites, the lowermost section of ultramafics is serpentinized (Clague and Straley, 1977). The volume expansion could provide the upward thrust to maintain the crest of the Reykjanes Ridge at a high elevation and thus explain the remarkable absence of an isostatic gravity anomaly compared to other cross-sections of the Mid-Atlantic Ridge (Cochran, 1979). Serpentinization, however, requires water, and it is difficult to envisage hydrothermal circulation to the depth of 10 to 16 km (Lister 1974; Fehn and Cathles 1979). Elevated temperatures at the bottom of the crust in the neighbourhood of the hot spot would prevent the serpentinization reaction above 450° C even if water was present. For these reasons we reject the serpentinization hypothesis and suggest vertical anisotropy as an explanation of our observations.

Acknowledgements. We wish to express particular gratitude to our colleagues M. Hamann, R. Herber, O. Pahl, and H. Richter, as well as the captain and the crew of the RV 'METEOR', whose efforts made the experiment possible. W.R. Jacoby invited the Canadian group to the experiment. We also whish to acknowledge the assistance of D.E. Heffler, designer of Bedford Institute of Oceanography Bottom Seismometers (BOBS), who participated in the Expedition METEOR/45. Constructive criticism of an earlier draft by C.E. Keen helped us clarify a number of points in this paper. The financial support for the RRISP Experiment was provided by the Deutsche Forschungsgemeinschaft and the Geological Survey of Canada.

References

Ariç, K.: Der Krustenaufbau und die Tiefenstruktur des Reykjanes-Rückens, südwestlich von Island, nach reflexions-seismischen Messungen. Ergänzgsh. Dtsch. Hydrogr. Z. Reihe A: **11**, 1972

Asada, T Shimamura, H. Observations of earthquakes and explosions at the bottom of the western Pacific: Structure of oceanic lithosphere revealed by Longshot Experiment. Am. Geophys. Union, Geophys. Monogr. **19**, 135, 1976

Asada, T., Shimanura, H.: Long-range refraction experiments in deep ocean. Tectonophysics **56**, 67–82 1979

Bessonova, E.N., Fishman, V.M., Ryaboyi, V.Z., Sitnikova, G.A. The tau method for inversion of travel times – I. Deep seismic sounding data. Geophys. J.R. Astron. Soc. **36**, 377–398, 1974

Bessonova, E.N., Fishman, V.M., Shnirman, M.G., Sitnikova, G.A. The tau method for inversion of travel times – II. Earthquake data. Geophys. J.R. Astron. Soc. **46**, 87–108, 1976

Birch, F.: The velocity of compressional waves in rocks to 10 kbars, 1. J. Geophys. Res. **65**, 1083–1102, 1960

Birch, F. The velocity of compressional waves in rocks to 10 Kilobars, 2. J. Geophys. Res. **66**, 2199–2224, 1961

Bott, M.H.P., Browitt, C.W.A., Stacey, A.P. The deep structure of the Iceland Faeroe Ridge. Mar. Geophys. Res. **1**, 328–351, 1971

Bram, K. New heat flow observations on the Reykjanes Ridge. J. Geophysics **47**, 86–90, 1980

Brooks, C.K., Jakobsson, S.P.: Petrochemistry of the volcanic rocks of the North Atlantic Ridge system. In: *Geodynamics of Iceland and the North Atlantic Area,* L. Kristjansson, ed. pp. 139–154. Dordrecht. Reidel 1974

Červeny, V., Ravindra, R. *Theory of Seismic Head Waves.* Toronto: University of Toronto Press 1971

Christensen, N.I.: Elasticity of ultrabasic rocks. J. Geophys. Res. **71**, 5921–5931, 1966

Christensen, N.I., Salisbury, M.H. Seismic anisotropy of the oceanic upper mantle: Evidence from the Bay of Islands ophiolite complex. J. Geophys. Res. **84**, 4601–4609, 1979

Clague, D.A., Straley, P.F.: Petrologic nature of the oceanic Moho. Geology **5**, 133–136, 1977

Cochran, J.R. An analysis of isostasy in the world's oceans: 2. Midocean ridge crests. J. Geophys. Res. **84**, 4713–4729, 1979

Everts, P., Koerfer, L.E., Schwarzbach, M.: Neue K/Ar-Datierungen isländischer Basalte. Neues Jahrb. Geol. Palaentol. Abh. 280–284, 1972

Ewing, J., Ewing, M.: Seismic refraction measurements in the Atlantic Ocean basins, in the Mediterranean Sea, on the Mid-Atlantic Ridge, and in the Norwegian Sea. Bull. Geol. Soc. Am. **70**, 291, 1959

Fehn, U., Cathles, L.M.: Hydrothermal convection at slow-spreading mid-ocean ridges. Tectonophysics **55**, 239–260, 1979

Fleischer, U. The Reykjanes Ridge - a summary of geophysical data. In: *Geodynamics of Iceland and the North Atlantic Area,* L. Kristjansson, ed.: pp. 17–31. Dordrecht. Reidel 1974

Fleischer, U., Korschunow, A., Schulz, G. Eine gravimetrische und erdmagnetische Vermessung des südlichen Reykjanes-Rückens mit dem Forschungsschiff METEOR. Meteor Forschungsergebn. Reihe C: **13**, *64*, 1973

Fowler, C.M.R. Crustal structure of the Mid-Atlantic Ridge crest at 37° N. Geophys. J.R. Astron. Soc. **47**, 459–491, 1976

Fowler, C.M.R. The Mid-Atlantic Ridge: structure at 45° N. Geophys. J.R. Astron. Soc. **54**, 167–183, 1978

Fowler, C.M.R., Keen, C.E.: Oceanic crustal structure – Mid-Atlantic Ridge at 45° N. Geophys. J.R. Astron. Soc. **56**, 219–226, 1979

Francis, T.J.G. Upper mantle structure along the axis of the Mid-Atlantic Ridge near Iceland. Geophys. J.R. Astron. Soc. **17**, 507–520, 1969a

Francis, T.J.G. Generation of seismic anisotropy in the upper mantle along the mid-oceanic ridges. Nature **221**, 162–165, 1969b

Gebrande, H. A seismic ray tracing method for two-dimensional inhomogeneous media. – In: *Explosion Seismology in Central Europe*. P. Giese, C. Prodehl, A. Stein, eds. pp. 162–167, Berlin, Heidelberg, New York: Springer 1976

Gebrande, H., Miller, H., Einarsson, P.: Seismic structure of Iceland along RRISP-Profile I. J. Geophys. **47**, 239–249, 1980

Goldflam, P., Goldflam, S. Ein Verfahren zur digitalen Verarbeitung und Korrektur von Navigationsdaten (Abstr.) Kiel. Dtsch. Geophys. Ges., 1979

Grønlie, G., Talwani, H. Geophysical Atlas of the Norwegian Greenland Sea. VEMA Research Series IV, Lamont-Doherty Geological Observatory, Palisades, N.Y., L-D60 Contribution No. 2652, 1978

Heffler, D.E., Barrett, D.L.: OBS development at Bedford Institute of Oceanography. Mar. Geophys. Res. **4**, in press, 1979

Heirtzler, J.R., LePichon, X., Baron, J.G. Magnetic anomalies over the Reykjanes Ridge. Deep-Sea Res. **13**, 427–443, 1966

Heirtzler, J.R., Dickson, G.O., Pitman, W.C., Herron, E., LePichon, X. Marine magnetic anomalies and the geomagnetic timescale. J. Geophys. Res. **73**, 2119–2136, 1968

Hess, H.H. Serpentines, orogeny and epirogeny. In: Crust of the Earth, A. Poldervaart, ed. Geol. Soc. Am. Spec. Pap. **62**, 391–408, 1955

Hirn, A., Steinmetz, L., Sapin, M. A long range seismic profile in the western Mediterranean Basin: structure of the upper mantle. Ann. Geophys. **33**, 373–384, 1977

Jakobsson, S.P. Chemistry and distribution pattern of recent basaltic rocks in Iceland. Lithos **5**, 365–386, 1972

Kebe, H.W. Eine ferngesteuerte Meßboje mit Datenspeicherung für refraktionsseismische Untersuchungen auf See. Meteor Forschungsergebn. Reihe C: **6**, 14–20, 1971

Keen, C.E., Barrett, D.L. A measurement of seismic anistropy [sic] in the northeast Pacific. Can. J. Earth Sci. **8**, 1056–1064, 1971

Keen, C.E., Tramontini, C. A seismic refraction survey on the Mid-Atlantic Ridge. Geophys. J.R. Astron. Soc. **20**, 473–491, 1970

Kennett, B.L.N. A comparison of travel-time inversions. Geophys. J.R. Astron. Soc. **44**, 517–536, 1976

Kennett, B.L.N. Towards a more detailed seismic picture of the oceanic crust and mantle. Mar. Geophys. Res. **3**, 7–42, 1977

LaBrecque, J.L., Kent, D.V., Cande, S.C. Revised magnetic polarity time scale for Late Cretaceous and Cenozoic time. Geology **5**, 330–335, 1977

Laughton, A.S., Searle, R.C., Roberts, D.G. The Reykjanes Ridge crest and the transition between its rifted and non-rifted regions. Tectonophysics **55**, 173–177, 1979

LePichon, X., Ewing, J., Houtz, R.E. Deep sea sediment velocity determination made while reflection profiling. J. Geophys. Res. **73**, 2597–2614, 1968

LePichon, X., Francheteau, J., Bonnin, J. *Plate tectonics*. 300 pp. Amsterdam: Elsevier, 1973

Lewis, B.T.R., Snydsman, W.E.: Evidence for a low velocity layer at the base of the oceanic crust. Nature **277**, 340–344, 1977

Lewis, B.T.R., Snydsman, W.E. Fine structure of the lower oceanic crust on the Cocos Plate. Tectonophysics **55**, 87–105, 1979

Lister, C.R.B. On the penetration of water into hot rock. Geophys. J.R. Astron. Soc. **39**, 465–509, 1974

Long, R.E., Mitchell, M.G.: Teleseismic P-wave delay time in Iceland. Geophys. J.R. Astron. Soc. **20**, 41–48, 1970

Malecek, S.J., Clowes, R.M.: Crustal structure near Explorer Ridge from a marine deep seismic sounding survey. J. Geophys. Res. **83**, 5899–5912, 1978

Moorbath, S., Sigurdsson, H., Goodwin, R. K-Ar ages of the oldest exposed rocks in Iceland. Earth Planet. Sci. Lett. **4**, 197–205, 1968

Morgan, W.J. Convection plumes in the lower mantle. Nature **230**, 42–43, 1971

Orcutt, J.A., Dorman, L.M. An oceanic long range explosion experiment. J. Geophys. **43**, 257–263, 1977

Pálmason, G. Crustal structure of Iceland from explosion seismology. Reykjavik. Soc. Sci. Isl. Rit **40**, 187, 1971

Raitt, R.W. The crustal rocks, In *The sea,* vol. 3, M.N. Hill ed., pp. 85–102. New York Wiley 1963

Raitt, R.W., Shor, G.G. Jr., Francis, T.J.G., Morris, G.B. Anisotropy of the Pacific upper mantle. J. Geophys. Res. **74**, 3095–3109, 1969

Raitt, R.W., Shor, G.G., Morris, G.B., Kirk, H.K. Mantle anisotropy in the Pacific Ocean. Tectonophysics **12**, 173–186, 1971

RRISP Working Group: Reykjanes Ridge Iceland seismic experiment (RRISP 77). J. Geophys. **47**, 228–238, 1980

Schilling, J.G. Iceland mantle plume existence and influence along the Reykjanes Ridge: I. Geochemical evidence. Nature **242**, 565–569, 1973

Sclater, J.G., Crow, J.: A heat flow survey at anomaly 13 on the Reykjanes Ridge: A critical test of the relation between heat flow and age. J. Geophys. Res. **84**, 1593–1602, 1979

Snoek, M., Goldflam, St. Crustal structure of the Reykjanes Ridge at 63° N derived from refraction seismic measurements. J. Geophys. **45**, 107–109, 1978

Steinmetz, L., Whitmarsh, R.B., Moreira, V.S. Upper mantle structure beneath the Mid-Atlantic Ridge north of the Azores based on observations of compressional waves. Geophys. J.R. Astron. Soc. **50**, 353–380, 1977

Sutton, G.H., Maynard, G.L., Hussong, D.M.: Wide-spread occurrence of a high-velocity basal crustal layer in the Pacific crust found with repetitive sources and sonobuoys. Am Geophys. Union, Geophys. Monogr. **14**, 193–209, 1971

Talwani, M., LePichon, X., Ewing, M.: Crustal Structure of the mid-ocean ridges, 2. computed model from gravity and seismic reflection data. J. Geophys. Res. **70**, 341–352, 1965

Talwani, M., Eldholm, O. The continental margin off Norway: A geophysical study. Geol. Soc. Am. Bull. **83**, 3575–3608, 1972

Talwani, M., Eldholm, O. Evolution of the Norwegian-Greenland Sea. Geol. Soc. Am. Bull. **88**, 969–999, 1977

Talwani, M., Windish, C., Langseth, M. Reykjanes Ridge crest A detailed geophysical study. J. Geophys. Res. **76**, 473–517, 1971

Tryggvason, E. Crustal structure of Iceland region from dispersion of surface waves. Bull. Seismol. Soc. Am. **52**, 359–388, 1962

Tryggvason, E. Arrival times of P-waves and upper mantle structure. Seismol. Soc. Am. Bull. **54**, 727–736, 1964

Verma, R.K.: Elasticity of some high density crystals. J. Geophys. Res. **65**, 757–766, 1960

Vine, F., Matthews, D.H. Magnetic anomalies over oceanic ridges. Nature **199**, 947–949, 1963

Vogt, P.R. Asthenosphere motion recorded by the ocean floor south of Iceland. Earth Planet. Sci. Lett. **13**, 153–160, 1971

Vogt, P.R.: The Iceland phenomenon: Imprints of a hot spot on the ocean crust, and implications for flow below the plates. In: *Geodynamics of Iceland and the North Atlantic Area.* L. Kristjansson, ed. pp. 105–126. Dordrecht: Reidel 1974

Vogt, P.R., Avery, O.E.: Detailed magnetic surveys in the northeast Atlantic and Labrador Sea. J. Geophys. Res. **79**, 363–389, 1974

Weigel, W., Goldflam, P., Hinz, K.: The crustal structure of Concepcion Bank. Marine Geophys. Res. **3**, 381–392, 1978

Whitmarsh, R.B. Seismic anisotropy of the uppermost mantle absent beneath the east flank of the Reykjanes Ridge. Bull. Seismol. Soc. Am. **61**, 1351–1368, 1971

Whitmarsh, R.B. Axial intrusion zone beneath the median valley of the Mid-Atlantic Ridge at 37° N detected by explosion seismology. Geophys. J.R. Astron. Soc. **42**, 189–215, 1975

Whitmarsh, R.B.: Seismic refraction studies of the upper igneous crust in the North Atlantic and porosity estimates for layer 2. Earth Planet. Sci. Lett. **37**, 451–464, 1978

Woodside, J.M.: The Mid-Atlantic Ridge near 45° N. XX. The gravity field. Can. J. Earth Sci. **9**, 942–959, 1972

Wyllie, J.P.: *The Dynamic Earth.* 416 pp. New York: Wiley 1971

Zverev, S.M., Kosminskaya, J.P., Krasilstchikova, G.A., Mikhota, G.G. The crustal structure of Iceland and the Iceland-Faeroe-Shetland region. Greinar **5**, 72–95, 1976

Received July 5, 1979; Revised Version November 7, 1979

J. Geophys. 47, 261–264, 1980

Journal of Geophysics

Crustal Development of the Reykjanes Ridge From Seismic Refraction

A.W.H. Bunch
Department of Goedesy and Geophysics, Madingley Rise, Madingley Road, Cambridge CB3 OEZ, England

Abstract. A seismic refraction experiment was carried out on the Reykjanes Ridge at approximately 60° N 30° W to determine the detailed seismic structure of the crust and the way in which this structure changes with age. Three 120-km-long overlapping split reversed profiles were shot over crust of ages 0, 3, and 9 Ma on the Eastern flank of the ridge. The data gathered were first analysed using travel-time analysis, these structures were then refined by modelling the experimental waveforms with synthetic seismograms. The detailed structures obtained indicate that with increasing age the 4.6 km/s layer thins and the crust with velocities 6.6 to 7.1 km/s thickens and increases its mean velocity. The velocity of the deepest layer seen increases with age, 7.1 km/s at 0 Ma and 8.2 km/s at 9 Ma, the vertical transition to this velocity being modelled best by a velocity gradient (0.66 km/s/km).

Key words: Reykjanes ridge – Crustal ageing – Mid Atlantic Ridge – Seismic refraction.

Introduction

During the summer of 1977 Cambridge University carried out a seismic experiment on the Reykjanes Ridge, at approximately 60° N 30° W, (Fig. 1), the position chosen marks the south-western limit of the section of the Reykjanes Ridge with no median valley and at this latitude the ridge breaks up into sections whose axes lie obliquely to the overall spreading axis of the ridge (Shih et al., 1978). The Reykjanes Ridge north-east of 59° 30′ N also exhibits a lower level of seismicity, less than a quarter of the activity of the ridge further south-west (Francis, 1973).

The experiment was designed with two aims:

(i) To determine a detailed crustal structure for this section of the ridge.

(ii) To investigate the way in which the seismic crustal structure changes with age.

Three refraction lines were shot parallel to the ridge axis over crust of approximate ages 0, 3, and 9 Ma, these ages corresponding to the crest of the ridge, the foot of the central triangular section of the ridge, and the edge of a raised plateau bordering the ridge. The lines shot were 120 km long 'overlapping-split reserved' profiles with a maximum shot receiver range of 70 km. On each line between four and five receivers (free floating recording sonobuoys) were used and up to 33 shots detonated. In addition, to determine the sediment thickness, normal incidence reflection profiles were shot, using a Geomechanique array, over the 3 and 9 Ma refraction lines, but none over the ridge axis, as previous work (Ruddiman, 1972) indicated that there was no sedimentary cover.

Travel-Time Analysis

Good quality amplitude data were obtained from all the shots at all the receivers. The first arrival times were picked from unfiltered digital record sections, the correlations being facilitated by using filtered record sections. The arrival times were corrected for the varying sedimentary thicknesses and water depths below shot and receivers. The timing corrections made for variations in the water depth were calculated assuming that all sub-basement interfaces lay parallel to the basement topography (Kennett and Orcutt, 1976). This assumption is common for marine refraction work and is usually justified in areas where the basement relief exhibits only gentle undulations, as on the 0 and 9 Ma profiles. On the 3 Ma profile the basement topography was rough and any assumption, when calculating the water depth correction, would be hard to justify for the data collected. An alternative assumption would be that all the basement topography was due to variations in thickness of the shallowest seismic layer, all sub-

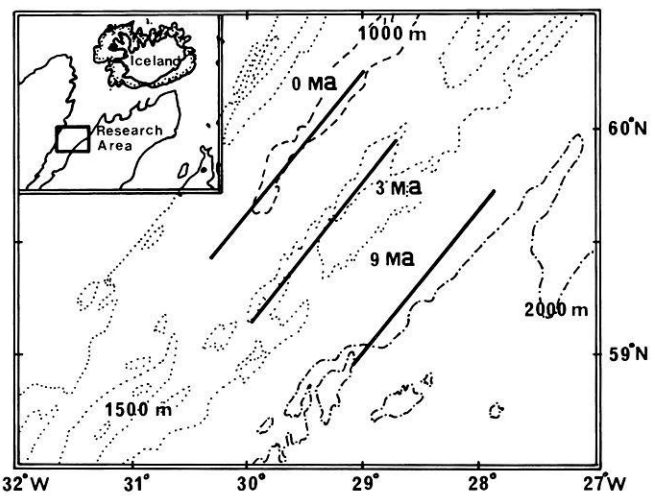

Fig. 1. Chart showing location of the three refraction profiles (*solid lines*) described in the text. The profiles were shot over crust of approximate ages 0, 3, and 9 Ma. Contours at 500 m intervals are given (Shih et al., 1978). The position of the research area relative to Iceland is shown in the *inset*

0340-062X/80/0047/0261/$01.00

basement interfaces being flat. These two different approaches in calculating the water depth correction give rise to differences of 0.040 s for the timing corrections of the data gathered, this error being of the same magnitude as the errors on the arrival time data in the travel-time analysis. However, no correlation was found between these travel-time errors and the calculated water depth corrections which suggests that the assumption used was appropriate.

The arrival times from all the sonobuoys could be combined from both the 0 and 9 Ma profiles giving a high data density. On the 3 Ma line poor control on the water depth below four of the five sonobuoys made it necessary to determine time delays which would make it possible to overlay the arrival times. For each profile the combined arrivals were then split into groups, each representing one 'refractor'. An indication of the ranges at which to split the data was found by examining the behaviour with range of:

(i) The waveform of the first arrival wave-group (taking into account change due to variations of shot size).

(ii) The peak to peak amplitude of the first arrival wave-group.

The shape and amplitude of the first arrival wave-packet showed marked changes over a narrow range band, e.g., at 25 km for the 0 Ma profile Fig. 3 and 4. These ranges, 'cross-over' ranges, were taken as indicating a change in the nature of the seismic arrivals as the changes could not be accounted for by variations of shot size. Using these 'cross-over' ranges as a guide, the arrivals were assigned to the various groups, the arrivals coming from ranges near to, less than 5 km, the 'cross-over' ranges being assigned to groups with the aid of time-distance plots of all the arrivals. Least-squares lines were fitted to the data groups and from the results the structures shown in Fig. 2 were calculated.

The velocity-depth bounds shown in Fig. 2 were derived from the 'tau' technique of Bessonova et al. (1974) with the modifications of Kennett and Orcutt (1976). The first arrival groups gave only a patchy tau-p curve which was completed using the method of parallelograms (Keilis-Borok, 1971). The completed bounds were then inverted into velocity-depth bounds using the Herglotz-Wiechert integral. On the 3 Ma profile, due to the poor quality data, the arrivals were not divided up into groups when forming the tau-p curve. Thus the velocity-depth bounds for this profile are broader and show less structure. The velocity-depth bounds found from the 'tau' technique are useful in that they give a guide for alterations to the first arrival structure when matching the amplitude-distance behavior of seismograms.

Surface Structure

The structure of the top 2 km of the crust was determined from data gathered when recovering the sonobuoys using a 1,000 in.^{3} air-gun as sound source. In addition to the refraction data gathered in this way, wide angle reflections were seen coming from an interface below the basement. On all three profiles these reflections were interpreted as coming from the base of the layer with velocity 4.6 km/s. These reflections were only seen over a narrow range window, the amplitude rising and falling sharply. This amplitude-distance behavior (Červený and Zahrandnik, 1972) suggests that a velocity gradient underlies the 4.6 km/s layer. On the 3 Ma line, where the data density was highest, the seismic structure from the travel-time data modelled the crust at the base of the 4.6 km/s layer with thin layers, this being an equivalent representation of a velocity gradient in terms of constant velocity layers.

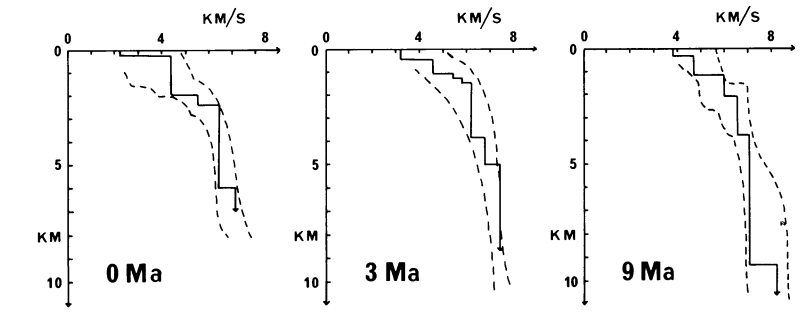

Fig. 2. The seismic velocity-depth structures (*solid lines*) calculated from the travel-times measured for the three refraction profiles. The *broken lines* are the velocity-depth bounds as calculated from the 'tau' technique (Bessonova et al., 1974)

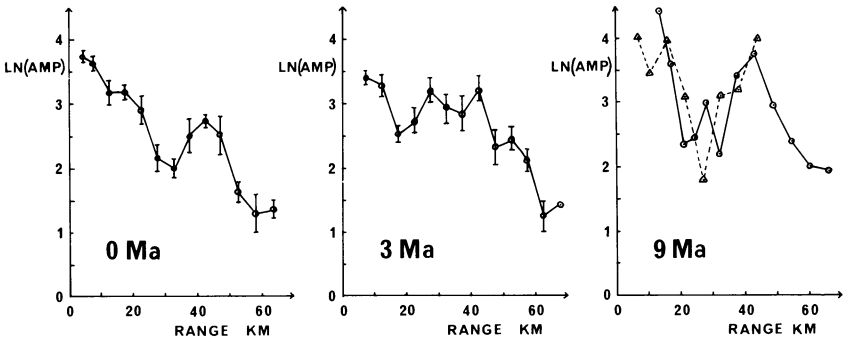

Fig. 3. Average amplitude-distance curves for the three refraction profiles. The amplitude is the peak to peak amplitude of the first arrival wave-group, the scale being arbitary. For the 0 and 3 Ma profiles the data from all buoys have been combined and averaged over 5 km range bins. The mean amplitude of each range bin is plotted together with the standard error in the mean. At both ends of the 3 Ma line the four shots furthest from the receivers gave anomalously low amplitudes, either due to lateral crustal variations or incomplete charge detonation. In this figure these amplitudes have been corrected for the latter effect. For the 9 Ma profile the results from only one sonobuoy are plotted, as the data from the other buoys were either noisy or incomplete. The *solid line* is for the section of the profile shot from the SW into the buoy and the *broken line* corresponds to shots NE of the buoys

Amplitude and Waveform Analysis

In order to define the general characteristics common to record-sections from all of the sonobuoys for a profile, average amplitude-distance curves were calculated for each profile. The amplitude plotted in Fig. 3 is the peak to peak amplitude of the first arrival wave-group. It can be seen that at certain ranges there are marked changes of amplitude and the position and magnitude of these changes were used as a descriminant when modelling the experimental records with synthetic seismograms.

All the modelling of the seismic record sections was completed using the reflectivity method (Fuchs and Müller, 1971; Kennett, 1975). For each profile, a synthetic record section was first computed for the travel-time structure. This structure was then altered by the addition of new layers in an attempt to improve the match of the amplitude behaviour between the synthetic and experimental record-sections. The changes in the velocity-depth structure were made so as to maintain the intercept times of the refractors seen as first arrivals.

On the 0 Ma line the travel-time velocity-depth structure was altered mainly by changes in the structure below 3.5 km depth. Layers of velocities 6.8, 6.6, and 6.8 km/s were included to increase the amplitude present at less than 25 km range and produce the correct drop in amplitude at 25 km (Fig. 3). The low-velocity zone was required to achieve the correct range to the amplitude peak at around 40 km. To increase the sharpness of this amplitude peak the 7.1 km/s interface was exchanged for a velocity gradient of 0.6 km/s/km. A comparison of the experimental and synthetic record sections is made in Fig. 4.

Two changes were made to the travel-time structure for the 9 Ma profile. The first alteration was the inclusion of a 6.9 km/s layer above the 7.1 km/s layer. This layer was included to increase the amplitude at less than 17 km range and decrease the amplitude at 25 km. The amplitude contrast was further improved by exchanging the 6.6 to 6.9 km/s interface to a velocity gradient. The second modification was to change the 7.1 to 8.2 km/s interface to a 0.66 km/s/km velocity gradient. This sharpened the amplitude peak of the synthetic seismograms at 40 km range, as seen on the experimental records (Fig. 5).

The data from the 3 Ma profile were of a poorer quality and thus the final structure obtained is not as well controlled as for the 0 and 9 Ma profiles. Anomalously low amplitudes on both ends of the profile from the four charges most distant from the receivers make it difficult to define the velocity structure below 6.5 km depth. However changes were made in the travel-time velocity-depth model to improve the match between the experimental and synthetic record sections of which the best solution is shown in Fig. 6.

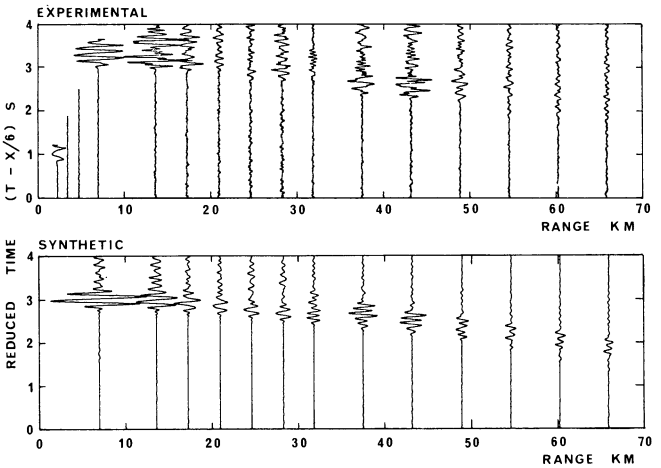

Fig. 5. Synthetic seismograms calculated for the final velocity depth structure proposed for the 9 Ma profile together with some of the experimental data. The experimental records have been scaled for range and varying charge weights, the same scaling for range being applied to the synthetic records

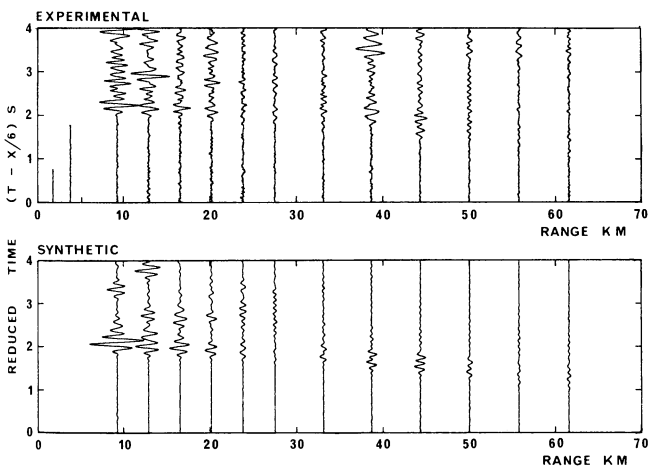

Fig. 4. Synthetic seismograms for the final velocity-depth structure proposed for the 0 Ma profile together with some of the experimental data. The experimental seismograms have been scaled for range and varying charge weight, the same scaling for range being used for the synthetic records. The energy delayed approximately 1 s from the first arrival corresponds to the sea-water multiple

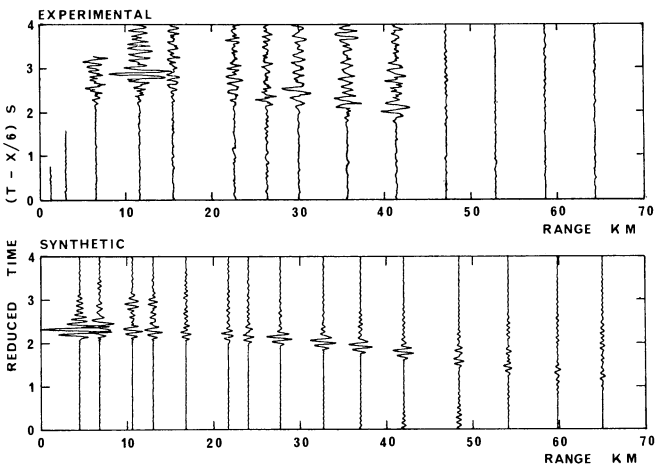

Fig. 6. Synthetic seismograms for the final velocity-depth structure proposed for the 3 Ma profile together with some of the experimental data. The experimental records have been scaled for range and varying charge weights, the same scaling for range being applied to the synthetic records. The anomolously low amplitudes beyond 45 km range may be due either to lateral changes in the crust along the profile or incomplete shot detonation. The amplitudes shown are scaled as if these shots fired completely

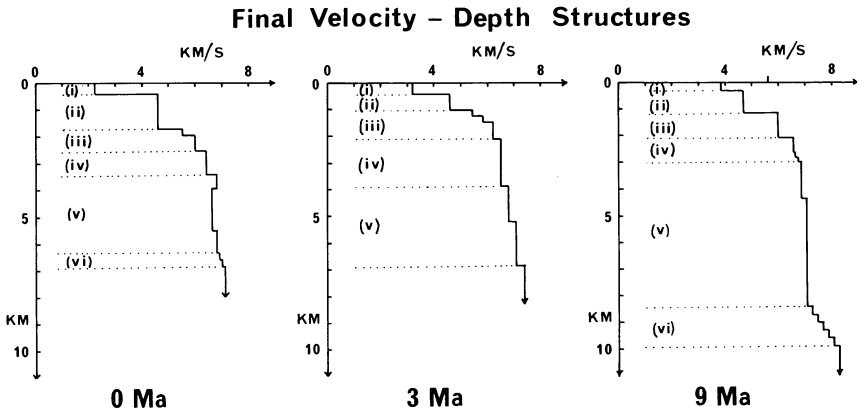

Fig. 7. The final velocity-depth structures proposed for the three refraction profiles. The Roman numerals correspond to the sections of the conclusions

Conclusions

The final velocity depth structures obtained for the three refraction profiles are shown in Fig. 7. Several conclusions may be made about the change in seismic structure with age. The trends with increasing age are:

(i) The sea-floor refraction velocity increases from 2.2 km/s at the ridge axis to 3.8 km/s for crust 9 Ma, these velocities being obtained from the air-gun observations.

(ii) The 4.6 to 4.7 km/s layer thins by 0.5 km in 9 Ma, but its velocity remains relatively constant.

(iii) The 5.4 to 6.2 km/s layers become shallower, though their combined thickness and mean velocity remain relatively constant. Wide-angle reflections from the base of the 4.6 km/s layer would indicate that this is a region of a velocity gradient rather than a constant velocity layer.

(iv) The 6.4 to 6.6 km/s layer also becomes shallower and its thickness appears relatively constant.

(v) The layers with velocities between 6.6 and 7.2 km/s increase their mean velocity and thickness. At the ridge axis a slight low velocity zone is present, velocity 6.6 km/s, below a 6.8 km/s lid. Away from the ridge the velocity increases and at 9 Ma this region has a mild velocity increase with depth.

(vi) The transition to the highest velocity measured is best modelled by a velocity gradient rather than a first-order discontinuity, the velocity gradient being approximately 0.66 km/s/km.

The structures obtained are relatively smooth structures. This suggests that the seismic model of the oceanic crust should be seen more as a smooth velocity-depth profile with changing velocity gradients rather than as a model of constant-velocity layers.

A more detailed discussion of the analysis and conclusions from this experiment may be found in Bunch and Kennett (1979).

Acknowledgements. I should like to thank the Master and crew of RRS Shackleton and everybody who helped at sea. T.J.G. Francis and the members of Blacknest aboard were of great help in carrying out the experiment. A. Claydon, M. Mason and R. Theobald were very helpful in building and maintaining the equipment used. I also thank C.M.R. Fowler, B.L.N. Kennett, K.E. Louden, and D.H. Matthews for their help in the experiment and in discussions of its analysis. This work was supported by a Shell studentship and by a NERC grant GR/3/1651.

References

Bessonova, E.N., Fishman, V.M., Ryaboyi, V.Z., Sitnikova, G.A.: The Tau method for inversion of travel-times – I. Deep seismic sounding data. Geophys. J. R. Astron. Soc. **36**, 377–398, 1974

Bunch, A.W.H., Kennett, B.L.N.: The crustal structure of the Reykjanes Ridge at 59° 30′ N. Geophys. J. R. Astron. Soc. in press, 1979

Červený, V., Zahrandnik, J.: Amplitude-Distance curves of seismic body waves in the neighbourhood of critical points and caustics – a comparison. Z. Geophys. **38**, 499–516, 1972

Francis, T.J.G.: The seismicity of the Reykjanes Ridge. Earth Planet. Sci. Lett. **18**, 119–123, 1973

Fuchs, K., Müller, G.: Computation of synthetic seismograms with the reflectivity method and comparison with observations. Geophys. J. R. Astron. Soc. **23**, 417–433, 1971

Keilis-Borok, V.J.: The inverse problem of seismology. In: Proceedings of the International School of Physics 'Enrico Fermi', course L, Mantle and Core in Planetary Physics, J. Coulomb and M. Caputo, eds.: pp. 242–274. New York: Academic Press, 1971

Kennett, B.L.N.: The effects of attenuation on seismograms. Bull. Seismol. Soc. Am. **65**, 1643–1651, 1975

Kennett, B.L.N., Orcutt, J.A.: A comparison of travel-time inversions for marine refraction profiles. J. Geophys. Res. **81**, 4061–4070, 1976

Ruddiman, W.F.: Sediment redistribution on the Reykjanes ridge: Seismic evidence. Bull. Geol. Soc. Am. **83**, 2039–2062, 1972

Shih, J.S.F., Atwater, T., McNutt, M.: A near-bottom geophysical traverse of the Reykjanes Ridge. Earth Planet. Sci. Lett. **39**, 75–83, 1978

Received April 6, 1979; Revised Version July 16, 1979

J. Geophys. 47, 265–270, 1980

Journal of Geophysics

Reykjanes Ridge Crest Studied by Surface Waves With an Earthquake-Pair Technique

C.E. Keen[1], A. Fricker[1], M.J. Keen[1], and L. Blinn[2]

[1] Atlantic Geoscience Centre, Geological Survey of Canada, Bedford Institute of Oceanography, Dartmouth, Nova Scotia, Canada
[2] Department of Oceanography, Dalhousie University, Halifax, Nova Scotia, Canada

Abstract. Dispersion of surface waves generated by earthquakes beneath the Reykjanes Ridge is used to find a model for the shear-wave velocity as a function of depth beneath a young crestal region. The Reykjanes Ridge and the WWSSN observatory AKU in Iceland lie close to a great circle, so it is possible to separate dispersion generated by paths on the Ridge itself from the total dispersion, which includes the effects of Iceland, using an adaptation of the station-to-station technique. As there are no pairs of stations, pairs of earthquakes are used; cross-correlation and filtering of the surface wave trains yields the travel times between earthquakes – and so the group velocities – at different periods. The observed dispersion of Love waves and Rayleigh waves seen over two paths along the Ridge are modelled using Backus-Gilbert inversion techniques, varying shear-wave velocities with depth. The periods used are 6 to 18 s (Love) and 6 to 37 s (Rayleigh). Velocities in the crust (to 6.45 km) are fixed from seismic refraction observations. Model velocities below this increase to 4.3 km/s at 20 km, reflecting a high-velocity lid, and decrease to 4.0 km/s by 40–50 km, reflecting the low-velocity zone. The base of this zone is not seen because the periods used are not sufficiently long, but it must lie below 100 km. This model can be interpreted in terms of a zone of partial melting only a few tens of kilometres wide below the high-velocity lid; a density model based upon this feature can account for the observed gravity field.

Key words: Reykjanes Ridge crest – Surface wave dispersion upper-mantle structure – Gravity.

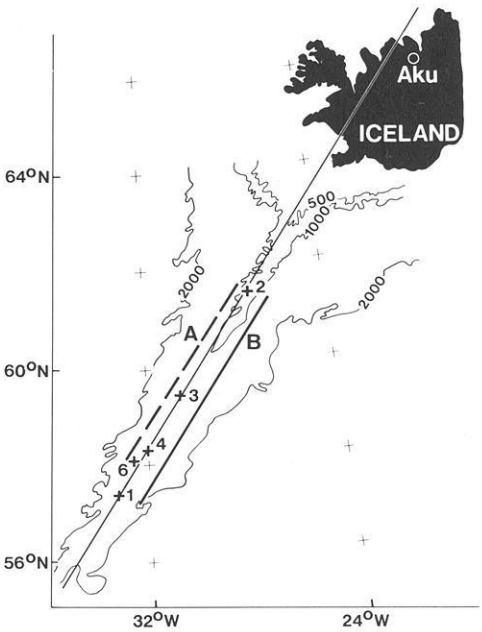

Fig. 1. The Reykjanes Ridge and Iceland. Bathymetric contours are in metres. Path *A* lies between events 2 in the north and 4 and 6 in the south; path *B* lies between events 2 and 1. The *long solid line* shows the great-circle path along the Ridge

Introduction

Studies of the crust and mantle of crestal regions of mid-ocean ridges are important because new lithosphere forms beneath such regions, and an understanding of the processes of lithosphere formation requires a knowledge of the physical properties underneath the ridge crests. Some experiments, such as long-range refraction experiments, are difficult or expensive to do; observations of heat-flow near crestal regions may be difficult to obtain, or hard to interpret (Sclater et al., 1976). Deductions from dispersion of surface waves may be ambiguous because of the geometrical relationships between sources and receivers, the paths crossing oceanic provinces belonging to a great range of ages; consequently a path which is restricted to a region of uniform age with uniform properties along the path, would be valuable (Forsyth, 1975). Earthquakes along the Reykjanes Ridge, recorded at the WWSSN station AKU in northern Iceland provide such a path beneath the crestal region of a mid-ocean ridge (Fig. 1). In this report we describe how surface waves travelling along this path lead us to shear-wave velocities within young crust and mantle.

We need to determine group velocity as a function of period for Rayleigh or Love waves or both, but one of the two methods most commonly used renders results difficult to interpret, the other cannot be applied. If there is a single source and a single station present interpretation techniques require that the earth between is laterally homogeneous. This would clearly be an improper assumption to make because most of Iceland lies between the Reykjanes Ridge and AKU. Paths of more restricted length – and so, hopefully, with more laterally uniform properties beneath – can often be obtained by using two stations with a single source beyond the line joining the two stations. Dispersion caused by the earth between the source and the closer station is, in essence, 'subtracted' from the dispersion observed at the farther station, leaving only the dispersion caused by the earth between the stations (Landisman et al., 1969). However, there is only one station along the path Reykjanes Ridge–Iceland, and so instead of using pairs

0340-062X/80/0047/0265/$01.20

of stations we restrict the path lengths over which we measure dispersion to the Rekjanes Ridge itself by choosing pairs of earthquakes. The Ridge and AKU bear a convenient geometrical relationship one to another, so that pairs can be chosen which lie on a great circle from AKU. The effect of the earthquake closer to AKU is 'subtracted' from the effect of the earthquake farther from AKU to leave the dispersion due only to the earth beneath the path between the earthquakes. In principle, this should yield results identical to the more usual 'pure-path' techniques, but in this case we obtain group velocities between sources, instead of stations.

Figure 1 shows the locations of earthquake sources used in this study, in relation to the position of AKU. Each source location is the site of more than one event, usually a main shock followed by a sequence of aftershocks, so that a number of dispersion curves can be obtained for the same path. This allows mean dispersion curves to be calculated and errors to be estimated. The data have been divided between two paths, A and B, where the events at location 2 are common to both (Fig. 1). This division into two paths was made because (a) the paths are somewhat different, and (b) it yields some assessment of the effects of different source mechanisms. Since shear velocities have been estimated independently along each path this allows some estimate of the validity of the method to be made.

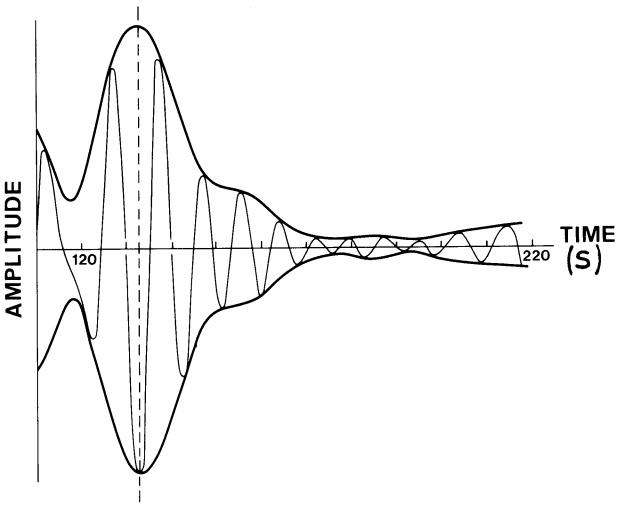

Fig. 2. The filtered cross-correlogram for the pair 2A–4D, vertical component. Central filter period 9.9 s, event-to-event distance 436.6 km. The peak in the envelope at 132 s gives the group arrival time of signal energy at the central filter period

Analysis of Data

Our concern is to determine group velocities of surface waves generated by an earthquake as a function of period for a segment of a ridge crest. We can then compare these (experimental) velocities with the (theoretical) values generated from a model, and so obtain estimates of the model parameters which control the model group velocities – in this case, shear-wave velocity as a function of depth. Consequently we need to find the travel time of phases over a range of periods between two points on the ridge crest, knowing the distance between them.

Briefly, we obtain the Fourier transform of a pair of seismograms, $f_1(t)$, $f_2(t)$, generated by a source at either end of Path A or B (Fig. 1) and received at AKU. Cross-multiplication in the frequency domain, the equivalent of cross-correlation in the time domain, gives the phase difference as a function of frequency between the seismograms and removes the effect of the propagation paths lying between the station and the event closest to it. The cross-correlated spectrum is filtered using the Gaussian filter

$$G(\omega) = A\, e^{-a(\omega-\omega_0)^2}$$

centred at frequency ω_0 for which we seek the group velocity. The advantage of this filter is that it gives the optimum resolution of both time (or group velocity) and frequency (Robinson, 1967). Here the parameter, a, was chosen to give equal fractional uncertainty in both group velocity and period (Fricker, 1971). Inverse Fourier transformation of the filtered signal allows the arrival time of the energy centred on ω_0 to be obtained. Figure 2 shows an example of a typical filtered and inverse-transformed cross-correlogram. The envelope's peak defines the group arrival time centred on ω_0.

Nine earthquakes from the four locations, 1, 2, 4, and 6, were chosen from all occurring on the Reykjanes Ridge between March, 1962 and March, 1972 with body wave magnitudes $m_b > 4.7$ (Table 1). Their reported depths are the reference depth of 33 km, not the actual depths, likely to be in the range of 5 (or less) to 10 km (Weidner and Aki, 1973).

The records of all components were photo-enlarged three times, and digitized with a D-MAC pencil follower at intervals of approximately 1.5 s (and all maxima and minima); cubic spline iterpolation was used to give evenly spaced data points at 0.75 s. The digitized seismograms were windowed, and the spectra found using a fast Fourier Transform algorithm; these spectra were corrected for the instrument response at AKU. The Rayleigh and Love modes were resolved using the horizontal and vertical components. In the case of Love waves the horizontal motion normal to the wave path (assumed to be the great circle path) was found from the east-west and north-south spectra; in the case of Rayleigh waves we usually used only the vertical spectra, because of higher noise levels associated with the horizontal spectra (so that the enhancement of signal to noise anticipated using horizontal components along the wave path together with the vertical component could not be realized).

The events were set in pairs, so that each event from one site could be cross-correlated with all events at a second site. This led to ten dispersion curves along path A, and four along path B, corresponding to events 2 and 4, 2 and 6 (Path A) and 2 and 1 (Path B) (Tables 1 and 2). The spectral records, resolved for Rayleigh and Love modes, were then cross-multiplied and filtered as described already. Group velocities were found for periods of 6 to 37 s for fundamental Rayleigh mode and 6 to 18 s for fundamental Love mode, the limits being selected on the basis of digitizing interval, signal energy, and the wavelengths at long periods – which become comparable to path length.

Because there are a number of pairs of earthquakes for each path, we can calculate mean values and standard errors of the group velocities at each period. The methods used are described only briefly here; details are given in Fricker (1971, 1976). The errors leading to differences in values of velocity are of two sorts. Errors common to all periods in one dispersion curve lead to general differences in 'level' between curves of velocity versus period for the different earthquake pairs, and are due to: mislocation of earthquakes; error in origin time; fault zones of finite length; and long-term drift in instrument response not seen in calibration. These errors can be partly removed by 'sliding' together the velocity-period curves using as criteria for adjustment

Table 1. Earthquake sources

No.	Date	Time	Lat. °N	Long. °W	m_b	Azimuth°	Dist km
1A 1972	June 19	06:00:51.1±0.99	57.37±0.033	33.43±0.036	5.0	228.3	1,227.9
1B 1972	June 19	12:14:27.0±0.96	57.39±0.029	33.38±0.031	4.8	228.2	1,224.3
2A 1966	May 05	15:25:12.5≡0.21	61.49±0.040	27.40±0.048	4.7	228.8	655.9
2B 1966	May 05	15:52:40.9±0.15	61.45±0.031	27.49±0.040	4.9	228.9	662.4
4A 1969	September 20	00:56:52 ±1.3	58.27±0.054	32.15±0.054	4.9	228.1	1,102.1
4B 1969	September 20	01:07:41 ±1.1	58.29±0.043	32.03±0.046	5.0	227.8	1,096.2
4C 1969	September 20	01:03:07 ±1.2	58.19±0.044	32.05±0.046	5.1	227.6	1,106.0
4D 1969	September 20	05:08:57.8±12	58.35±0.029	32.08±0.030	5.6	228.2	1,092.5
6A 1968	September 14	01:38:42.6±0.28	58.08±0.061	32.64±0.060	5.1	228.6	1,136.1

Notes: These data have been taken from the Bulletin of the International Seismological Centre, Edinburgh, Scotland. Distances to AKU were calculated using a spheroidal earth. Azimuths are the great-circle directions from the station towards the event

Table 2. Earthquake pairs for paths A and B

Pair	Path length (km)	Azimuth°
	Path A	
2A–4A (1)	446.2	228.5
2A–4B (2)	440.3	228.3
2A–4C (3)	450.1	228.2
2A–4D (4)	436.6	228.5
2B–4A (6)	439.7	228.5
2B–4B (7)	433.8	228.4
2B–4C (8)	443.6	228.2
2B–4D (9)	430.1	228.5
2A–6A (5)	480.2	228.7
2B–6A (10)	473.7	228.8
	Path B	
2A–1A (1)	572.0	228.6
2A–1B (2)	568.5	228.5
2B–1A (3)	565.5	228.6
2B–1B (4)	561.9	228.6

Note: Numbers in brackets are those shown in Figs. 3 and 4

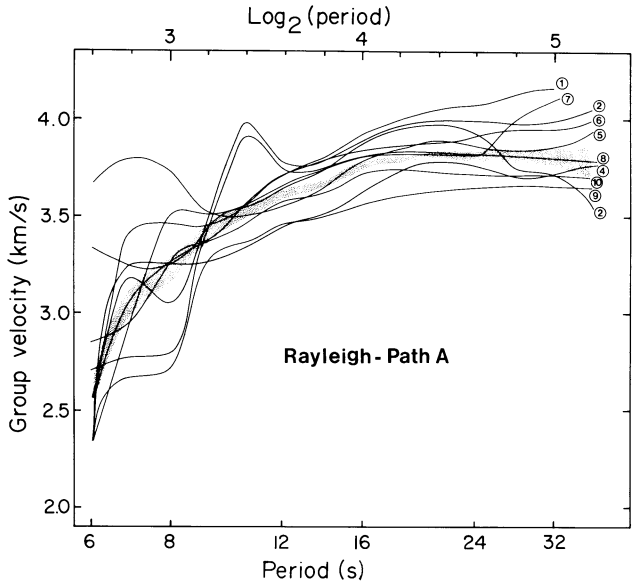

Fig. 3. Group velocity versus period for *Path A, Rayleigh.* The *solid curves* show the observations for different pairs. *Each number* designates a particular pair, given in Table 2.The shading encompasses one standard error on each side of the mean curve (see text). Observations made at increments of 0.2 on the log scale

the condition that the mean overall remains unchanged, and by seeing that the standard errors are minimized (in the least-squares sense). The errors which remain are random and due to: digitization; source mechanism; and noise. In addition, 'structural' effects between sources – sloping interfaces, for example – and interference by higher mode Love waves may make interpretation difficult. The second type of errors are random errors and lead to 'wiggles' in the curves, not necessarily coherent from one curve to another. It is from these that the standard errors used here have been calculated.

The mean group velocity at any period is calculated after the errors common to all periods from each curve, as described above, are removed in the following way (Fricker, 1976). The arrival time at a particular period will be in error because of contamination by noise and the effects of the filter used to isolate the period. Consequently weights are assigned to each value on a group velocity versus period curve which are functions of filter parameter, period, and the signal to noise ratio. These weights give value to each point on a curve inversely proportional to the likely error in travel-time, which can be calculated (in terms of the factors mentioned). Means and standard errors are calculated from the weighted values of travel time (in essence, reciprocals of group velocity). The standard errors themselves should not fluctuate markedly from period to period, and are smoothed using a binomial smoothing scheme. These smoothed standard errors, due only to random errors, are used when modelling. The curves of mean group velocity versus period should themselves vary smoothly from period to period, and so are smoothed (and interpolated) by cubic spline smoothing. The periods at which group velocities were determined are shown on Figs. 3 and 4.

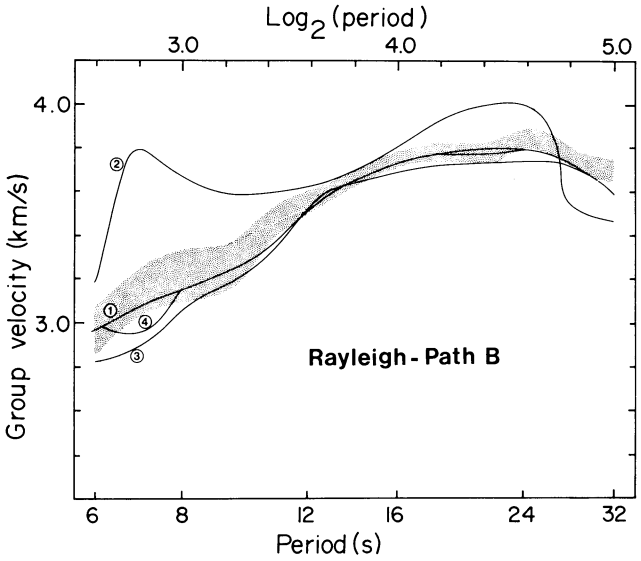

Fig. 4. Group velocity versus period for *Path B, Rayleigh.* The *solid curves* show the observations for different pairs. *Each number* designates a particular pair, given in Table 2.The shading encompasses one standard error on each side of the mean curve (see text). Observations made at increments of 0.2 on the log scale

Figures 3 and 4 show the Rayleigh wave group velocity curves before any corrections for errors and smoothing have been applied as well as the band of values falling within one standard error unit of the mean, calculated as described above. Note that the fluctuation in the individual group velocity curves has been strongly reduced in the final curves and that the standard errors are appreciably less than those which might be estimated from the scatter of the individual curves. The differences between the standard errors shown and those which might seem intuitively reasonable, which are about five times greater, are due partly to the weighting of the individual curves. However, the standard errors shown are probably underestimates. The justification for the use of these smaller errors is that the linearized inversion scheme applied to the data to obtain a shear-velocity model becomes unstable if larger errors are used, and hence the use of the smaller error estimates represents a compromise between obtaining a model by means of the inversion technique and the need to rely on modelling techniques which give no estimates of the precision and resolution of the final models. The latter would be necessary if larger errors were used.

The weakest link in the method of analysis applied here is that the behaviour of all the source functions is assumed to be the same and hence no corrections have been made for the effect of the source function and the phase as a function of frequency. While all the earthquakes are located on the Reykjanes Ridge crest, away from known fracture zones, and hence may have similar focal mechanisms representative of normal faulting, the effects of small differences in fault plane orientation and dip on the data has not been established, mainly because most of the earthquakes were not large enough to obtain reliable fault plane solutions. In addition, variations in velocity perpendicular to the ridge crest causing lateral refraction of the propagating waves have not been considered here. These effects, while important, would not in our opinion, change the basic results of the study but they should be considered in any further studies of this type.

Modelling

Models of shear velocity as a function of depth were obtained from the dispersion data, using linear inversion techniques (Backus and Gilbert, 1970). The use of these methods for surface wave studies has been described by Wiggins (1972) and specific details of the computations used in this study are given by Fricker (1976). The linear inversion method gives us both models which fit the data to within specified error limits and also estimates of the uncertainties of the models.

Theoretical data are calculated using Haskell's (1953) matrix formulation which approximates the elastic properties of the real earth by a stack of horizontal layers, each with uniform compressional and shear-wave velocities and density. The values of these parameters are varied iteratively until all the theoretical data calculated from a particular model agree with the observations to within predetermined error limits, usually one standard deviation. For rapid digital computation, the Haskell matrices have been modified as described by Schwab and Knopoff (1970), among others.

If we start with an initial model which is close to the desired model, the required changes in the parameters necessary to bring the theoretical data, calculated from the model, into agreement with the observations may be estimated by the size of the partial derivatives of the theoretical data parameters with respect to the model parameters.

The derivatives with respect to shear-wave velocities are much larger than those of compressional wave velocity or density. Variations of V_p and ρ affect the final model by an order of magnitude less than V_s. Thus V_p and ρ were not varied in producing the final models but were held at fixed values corresponding to the initial model. This starting model, as stated above, must be sufficiently close to the final result that the partial derivatives are valid indicators of the adjustments needed in the model to fit the data. Thus a certain amount of trial and error modelling is required before proceeding to the final inversion. In this study, we found that the calculated group velocities are very sensitive to water depth and the thickness of the first crustal layer. This problem was overcome by constraining the shear-wave velocities of the upper crustal layers to be in reasonable accord with the compressional wave data for the Reykjanes Ridge described by Talwani et al. (1971), and by setting the water depth at 1.62 km – a reasonable mean value for paths used. Trygvasson (1962) has shown that the effects of sloping water interfaces on Rayleigh wave dispersion curves are small at periods greater than 8 s; Love waves are of course not affected at all. In addition, the group velocities at the periods considered here have no bearing on the model below 150 km. Therefore the shear velocity was held constant at 4.33 km/s below this depth. The parameters which have been fixed during inversion are shown in Table 3; we see here that shear velocity was allowed to vary during inversion in eleven layers between depths of 6.45 km and 150 km.

Wiggins (1972) showed that for real data a limited number of model parameters can be determined if a certain degree of precision of these parameters is desired. As in other linear inverse problems a compromise must be reached between a detailed model which is poorly defined, with large uncertainties in some of the parameters, and a model which includes less detail but which is accurate to a predetermined acceptable level. This is the trade-off between resolution and precision.

The surface wave inversion method involves the solution of a set of equations using least squares minimization of the difference between theoretical and observed data (Wiggins, 1972). Thus a desired level of accuracy, the standard error of the problem, σ,

Table 3. Fixed parameters used in inversion

Depth to top of layer km	Density gm/cm^3	V_p km/s	V_s km/s
0.00	1.03	1.50	0.0000
1.62	2.84	4.20	2.1554
2.32	2.84	5.81	2.6096
3.31	2.84	6.53	3.0994
4.88	3.00	6.53	3.6752
6.45	3.20	7.20	
8.40	3.30	8.00	
9.55	3.30	8.00	
15.00	3.30	8.00	Inversion
25.00	3.30	8.00	
35.00	3.30	8.00	Parameters
40.00	3.30	8.00	
60.00	3.20	7.20	
80.00	3.20	7.20	
100.00	3.20	7.20	
125.00	3.20	7.20	
150.00	3.30	8.00	4.3300

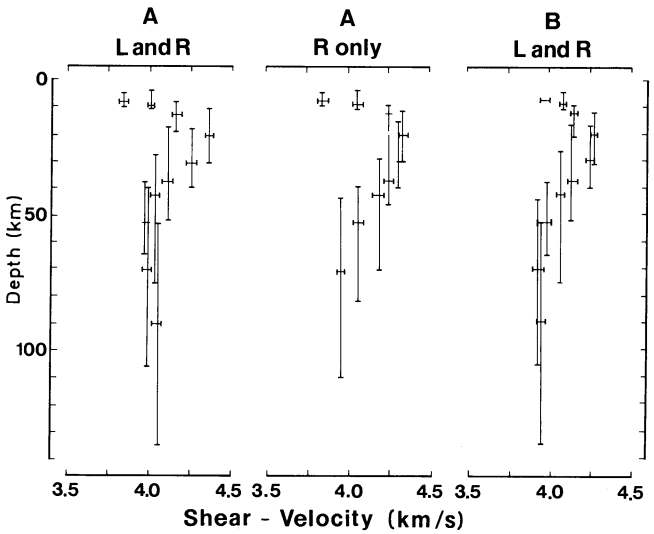

Fig. 5. Shear-velocity against depth for *Path A Love and Rayleigh (left), Rayleigh only (middle),* and *Path B Love and Rayleigh (right). Horizontal bars* give standard errors in velocity, vertical bars give the spread in depth

can be set. In this case a relative standard error of 0.01 was chosen which allows us to determine only three or four independent model parameters. This may be compared to the five parameters obtained by Forsyth (1975) for surface wave data in the Pacific. We attempted to fit both Love and Rayleigh wave data combined and Rayleigh wave data alone. Similar models were obtained in both cases, with the model data falling within about one standard error of the observations. In the case of Path A, it was not possible to obtain a really satisfactory fit to the combined Rayleigh and Love wave data, possibly because the fundamental Love mode was contaminated with higher mode interference. However, the model obtained, shown in Fig. 5, is in agreement with the other models.

The shear-velocity models are presented in Fig. 5. The horizontal bars represent the standard errors in the shear-wave velocities and the vertical bars, the depth resolution of these determinations. The resolution kernels (Backus and Gilbert, 1970) were generally compact, having a high value in only one layer. However, some degree of non-compactness was observed for the deeper layers.

A visual comparison of the shear velocity curve for Paths A and B (Fig. 5) shows no significant differences between them. At shallow depths, the shear velocity increases with depth reaching 4.3 km/s at 20 km. The velocity then decreases to about 4.0 km/s between 40 and 50 km. Below this, the resolution is not sufficient to define the base of this low-velocity zone.

Discussion

Our models showing shear-wave velocity as a function of depth are similar to those of others who have concerned themselves with young lithosphere and asthenosphere. Forsyth (1977) for example, points out that in the age range 0–5 Ma the high-velocity lid will have a velocity of 4.3 km/s, and a thickness of 30 km (or less); we see the same velocity, and his depth to the base of the lid is compatible with the marked decrease in velocity below 30–40 km demanded by our models. The velocity below this, 4.0 km/s, also agrees with Forsyth's (1977) conclusions. These similarities are significant, because the two paths we have used lie wholly along the crest of a ridge, uncontaminated by dispersion caused by other structural elements, inevitable if dispersion is measured using an earthquake-station pair, (because of the locations of the stations). This would not necessarily be true of a study such as the very interesting one of Jacoby and Girardin (1980).

The model of a low-velocity zone below 30–40 km is also in agreement with the conclusions of Solomon and Julian (1974), who, in a study of focal mechanisms of earthquakes on ridges (including one from the Reykjanes Ridge), suggested that a zone of anomalously low compressional wave velocity lay beneath the crests. They attributed this to the existence of a region of partial melting.

We have no information on the lateral extent of the low-velocity zone from our surface wave study; we can, however, model its equivalent roughly in terms of density variations, using gravity data, and compare the gravity field which would result with the observations of Talwani et al. (1971). This is done in Fig. 6; we have not tried to model lateral changes in density in the lithosphere and asthenosphere (which would be predicted by the lateral changes in shear-wave velocity suggested by Forsyth, 1977), nor are the density contrasts shown obtained from the shear-velocity models presented here, but were arbitrarily chosen. We show in Fig. 7 how our suggestion of a relatively narrow asthenospheric wedge beneath the ridge crest compares with other models.

The apparent lack of agreement near the crestal zone is hardly surprising. Parker and Oldenburg's (1973) model assumed heat to be transported by conduction, with no additional cooling by hydrothermal circulation; in their surface wave study Leeds et al. (1974) assumed that the shear-wave velocity in the high-velocity lid was 4.6 km/s (rather than 4.3 km/s near the crests) so that they could model the change in thickness of the lid with age.

It is gratifying that the technique using earthquake-pairs is in such good agreement with the studied of Forsyth (1977), and Solomon and Julian (1974). The method could perhaps be extended with profit to seek variations in velocity-depth models

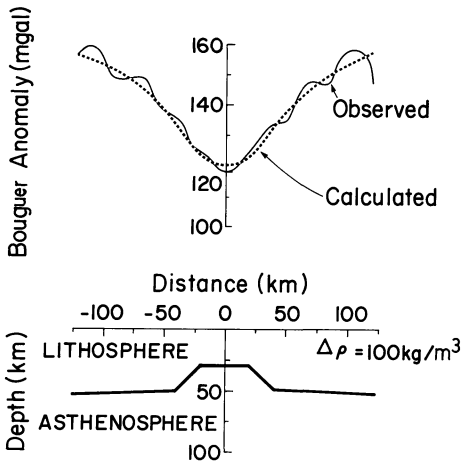

Fig. 6. The observed Bouguer anomaly across the Reykjanes Ridge (from Talwani et al. (1971) and the anomaly corresponding to the model beneath

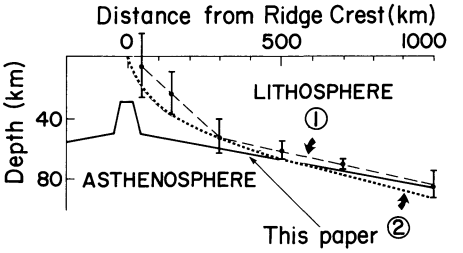

Fig. 7. Some models of the Reykjanes Ridge. The model corresponding to the density model of Fig. 6 is shown solid. *Model 1* is that derived from the surface wave study by Leeds et al. (1974) (who fixed the shear-wave velocities; see text) the vertical bars are their error limits; *Model 2* is Parker and Oldenburg's (1973) (who assumed heat transfer by conduction only; see text)

along ridge crests, seeking regional variations along particular ridges, and variations with rates of spreading. We should perhaps point out that although sophistication in modelling has been achieved using Backus-Gilbert inversion techniques, nevertheless, as they are usually applied in studies with surface waves, no account is taken of anisotropy, or lateral inhomogeneities – which in crestal regions must be significant.

Acknowledgements. We thank the National Research Council of Canada for support, and Christopher Garrett and Lynn Smith for aid. Louis Blinn and Aubrey Fricker received scholarships from Dalhousie University. Comments on the paper from D. Forsyth, R. Falconer, C. Beaumont, and S. Srivastava were most helpful.

References

Backus, G.E., Gilbert, J.F.: Uniqueness in the inversion of inaccurate gross earth data. Philos. Trans. R. Soc. London, Ser. A: **266**, 123–192, 1970

Forsyth, D.W.: The early structural evolution and anisotropy of the oceanic upper mantle. Geophys. J.R. Astron. Soc. **43**, 103–162, 1975

Forsyth, D.W . The evolution of the upper mantle beneath mid-ocean ridges. Tectonophysics **38**, 89–118, 1977

Fricker, A. A development of surface wave analysis and interpretation in the Canadian Shield. Unpublished M.Sc. Thesis, Dalhousie University, 1971

Fricker, A. Crustal models from seismic surface waves. Unpublished Ph.D. Thesis, Dalhousie University, 1976

Haskell, N.A.: Dispersion of surface waves in multilayered media. Bull. Seismol. Soc. Am. **43**, 17–29, 1953

Jacoby, W.R., Girardin, N. The evolution of the lithosphere at the southeast flank of Reykjanes Ridge from surface wave data. J. Geophys. **47**, 271–277, 1980

Landisman, M., Dziewonski, A., Sato, Y : Recent improvements in the analysis of seismic surface wave observations. Geophys. J. Astron. Soc. **17**, 369–403, 1969

Leeds, A., Knopoff, L., Kausel, E. Variations of upper-mantle structure under the Pacific Ocean. Science **186**, 141–143, 1974

Parker, R., Oldenburg, D.: Thermal model of ocean ridges. Nature Phys. Sci. **242**, 137–139, 1973

Robinson, E.A.· Statistical communication and detection. London: Griffin, 357 pp, 1967

Schwab, F.L., Knopoff, L. Surface wave dispersion computations, Bull. Seismol. Soc. Am. **60**, 321–344, 1970

Sclater, J.G., Crowe, J., Anderson, R.N. On the reliability of oceanic heat-flow averages. J. Geophys. Res. **81**, 2997–3007, 1976

Solomon, S.C., Julian, B.: Seismic constraints on ocean ridge mantle structure: anomalous fault plane solutions from first motions. Geophys. J. R. Astron. Soc. **38**, 265–285, 1974

Talwani, M.C., Windisch, C.C., Langseth, M.G.· Reykjanes Ridge crest· a detailed geophysical study. J. Geophys. Res. **76**, 473–517, 1971

Trygvasson, E. Crustal structure of the Iceland region from dispersion of surface waves. Bull. Seismol. Soc. Am. **52**, 359–388, 1962

Weidner, D., Aki, K.: Focal depth and mechanism of mid-oceanic ridge earthquakes. J. Geophys. Res. **78**, 1818–1831, 1973

Wiggins, R.A. The general linear inverse problem: implication of surface waves and free oscillations for earth structure. Rev. Geophys. **10**, 251–285, 1972

Received April 5, 1979; Revised Version August 31, 1979

J. Geophys. 47, 271–277, 1980

Journal of Geophysics

The Evolution of the Lithosphere at the Southeast Flank of Reykjanes Ridge From Surface Wave Data

W.R. Jacoby[1] and N. Girardin[2]

[1] Institut für Meteorologie und Geophysik, Universität Frankfurt, Feldbergstr. 47, D-6000 Frankfurt a.M. 1, Federal Republic of Germany

[2] Institute de Physique du Globe, 4, Place Jussieu, F-75230 Paris, Cedex 05, France

Abstract. Rayleigh wave group velocities for 15–40-s periods have been measured along paths parallel to the Reykjanes Ridge axis. They have traversed age slices of lithosphere between 0 and 20 Ma. Three groups of dispersion curves can be distinguished mainly on the basis of their shapes: for age slices 0–3, 6–8, and 10–20 Ma. The latter group of curves has also a significantly higher average level. Since the group velocity determinations at individual periods for anyone earthquake are not statistically independent, but the individual curves of each group are rather shifted along the velocity scale, we know their average shape better than their average level. This allows a fairly detailed resolution of vertical structure in the evolving lithosphere, particularly of S wave velocity, but only less precise information about the evolution of the absolute S velocities. Modelling has been carried out with the usual assumption of horizontal layering. A low-velocity layer with top at about 60 km depth develops with age as the lid increases its S velocities. One of the most interesting results is the suggestion of a low-velocity zone between 20 and 30 km depth; it is not yet clearly evident at 0–3 Ma age, it is distinct at 6–8 Ma age, and it appears to decay again for older age. The interpretation involves extensive melting of a peridotite mantle beneath the ridge axis; while upward segregation of melt and its drainage in the volcanic zone forms the crust, some melt may be trapped below the young thin cool lid after a few million years of age. A depleted lower high-velocity layer is left behind; it forms the lower lithosphere. Such a process will produce a chemically layered lithosphere which may be also evident at greater ages.

Key words: Lithosphere evolution – Rayleigh wave dispersion – Reykjanes Ridge.

Introduction

Rayleigh wave group velocities are used in this study to learn more about the development of the lithosphere as it is generated at the Reykjanes Ridge axis. Surface waves from earthquakes at the Charlie-Gibbs fracture zone and the southern Reykjanes Ridge travel nearly parallel to the ridge axis to the WWSSN station of Akureyri (AKU) in Northern Iceland. They sample different age slices of the lithosphere (Fig. 1).

The present paper is an extension of an earlier one (Girardin and Jacoby 1979; henceforth called 'paper I') where we treated the same data from a somewhat different point of view. Treating each group velocity determination at any period for any earthquake as statistically independent led to rather wide error bounds. We could distinguish only two groups of dispersion curves for paths through 0–8 and 10–20 Ma old lithosphere. We then attempted to interpret them with the aid of theoretical dispersion curves computed for horizontally layered models where we varied systematically three parameters and accepted all models which gave dispersion curves within the wide error bounds. We could not resolve much vertical structure. All we could detect about lithosphere evolution from 0–8 to 10–20 Ma was an increase in average S velocity in the upper 60 km from 4.2 or 4.3 km/s (and no obvious low-velocity layer) to 4.5 or 4.6 km/s (with a significant low-velocity layer underneath).

The reason for extending the study is that it is justified to look at the data accuracy more optimistically than in paper I, if one does not take the individual group velocity determinations as statistically independent. As shown below, the shapes of the dispersion curves are, actually, better known and one can, in fact, distinguish three groups by lithospheric age of the paths (through 0–3, 6–8, and 10–20 Ma old lithosphere). Consequently vertical structure and evolution with age can be resolved in more detail. This in turn sheds new light on thermodynamic and petrologic models of the evolving lithosphere at the Reykjanes Ridge.

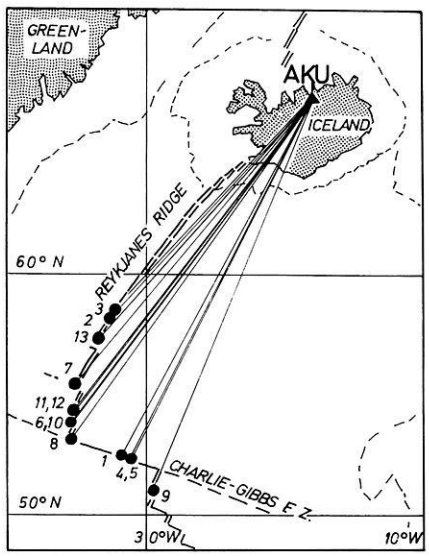

Fig. 1. Map of North Atlantic showing earthquake epicentres and station used (AKU), as well as great circle paths of Rayleigh waves between them

0340-062X/80/0047/0271/$01.40

Table 1. Earthquake parameters

No.	Date	Origin time	Coordinates (degrees)	Depth (km)	Distance (degrees)	*N*
1	July 3, 1965	02 22 18.2	52.73N 32.05W	30	14.8	107
2	September 20, 1969	00 56 52.0	58.19N 32.05W	36	9.9	83
3	September 20, 1969	01 07 42.1	58.29N 32.03W	61	9.9	113
4	September 24, 1969	03 58 58.0	52.61N 32.01W	28	14.9	162
5	September 24, 1969	04 20 51.3	52.64N 31.83W	18	14.8	172
6	January 31, 1970	16 35 03.9	53.77N 35.51W	33	14.7	143
7	April 26, 1970	06 39 54.0	55.55N 35.18W	59	13.1	130
8	August 23, 1970	11 07 18.8	53.11N 35.14W	33	15.2	128
9	September 18, 1970	16 12 08.0	51.03N 29.56W	43	15.8	189
10	September 8, 1971	20 32 30.0	53.93N 35.31W	27	14.6	89
11	April 3, 1972	18 52 59.8	54.28N 35.14W	32	14.2	242
12	April 3, 1972	20 36 22.2	54.33N 35.20W	13	14.2	247
13	June 19, 1972	06 00 51.1	57.37N 33.43W	37	11.1	169

N is the number of stations reporting for epicenter determination

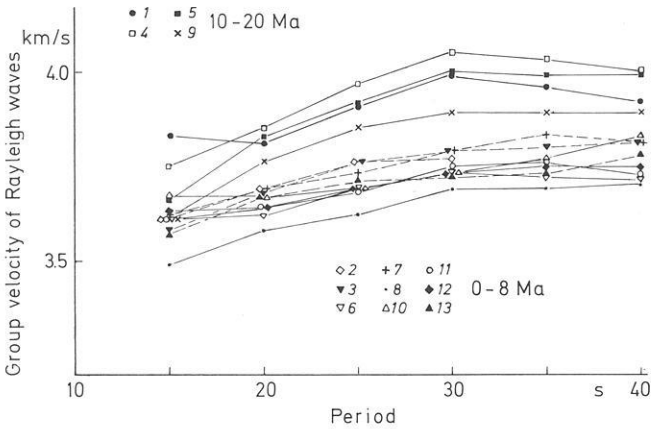

Fig. 2. Rayleigh wave group velocities measured for the 13 earthquakes shown in Fig. 1, plotted versus period (after paper I)

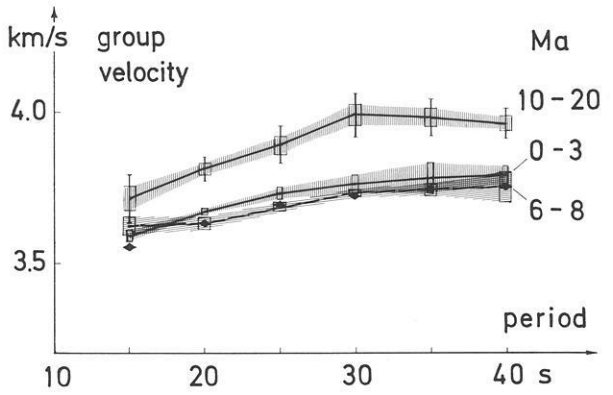

Fig. 3. Group velocities averaged for three age groups. Hatched bands correspond to the error bounds chosen for modelling

Data

Before coming to the new analysis we must briefly repeat from paper I the essential facts about the data used. Table 1 presents the earthquakes, their locations are shown in Fig. 1. The ages of the oceanic paths are taken from Heirtzler et al. (1966, 1968) and Talwani et al. (1971). The long-period records of AKU were digitized, the vertical component was analized by multiple filtering (Dzievonski et al. 1969); the group velocities for each earthquake were computed from the arrival times of maximum energy in a moving frequency window (corrected for instrumental group delay) and the source time and distance.

The results are shown in Fig. 2. All individual dispersion curves essentially rise in the 15 to 40 s period range from 3.7 to 4 km/s (10–20 Ma paths) or from 3.6 to 3.8 km/s (0–8 Ma paths); they group at two different velocity levels. In the 'older' group all curves are very similar (with one exception at 15 s) rising monotonously to 30 s and then levelling off or actually dropping. If the curves are shifted along the velocity axis they can be made to fit quite closely. There are several ways of doing this, but with only four dispersion curves at hand, it hardly matters which way is taken to estimate the best average shape. We have simply taken the arithmetic mean at each period; for the error bounds as related to shape only, we have taken half the standard deviation at each period (Fig. 3), implying that over 80% of it is related to uncertainty of velocity level.

The 'younger' group of Fig. 2 of nine dispersion curves for the age slice 0–8 Ma does not show, at first glance, much more structure than a nearly linear increase with period. Examining the curves more carefully, one notices, however, two sub-groups with different shapes; they are marked in Fig. 2 by dashed lines and by solid lines and correspond to the age slices 0–3 and 6–8 Ma, respectively. Again we have estimated their average shapes by taking the arithmetic mean at each period (Fig. 3). The standard error bands at each period are rather narrow; although they comprise both the scatter in level and random errors at each period, we accept the standard errors as the error bounds for later modelling. These error bounds do not overlap for the two sub-groups between 20 and 30 s period, but it would be difficult to argue on this basis for a very significant difference in velocity level. In shape, however, the difference appears to be more significant at the lower period end with the 0–3 Ma curve rising monotonously

and the 6–8 Ma curve showing a clear dip if not a weak actual minimum at 20 s.

For the assessment of the significance of the data it is important to discuss briefly the errors of the group velocity determinations. For more details the reader is referred to paper I. Errors of the earthquake source parameters, particularly latitude, depth, and origin time will mainly shift the dispersion curves along the velocity axis, a type of scatter in fact observed. The focal depths given in Table 1 (from ISC) are probably in most cases too great (Weidner and Aki 1973); if this is so, the group velocities, particularly for the 0–3 Ma age slice, could be lower by 1%, or so, than given in Figs. 2 and 3; this would reduce the difference in level between the 0–3 and the 6–8 Ma groups. Very small focal depths also lessen the uncertainty of initial phase which is independent from frequency for any focal mechanism at zero depth. We have, nevertheless refrained from using phase velocities which could still be critically affected by the unknown initial phase related to the unknown focal mechanisms.

There are other effects hampering the interpretation. The possibility of lateral refraction along paths particularly near the ridge axis cannot be dismissed, although the polarization at AKU is close to theoretical. The result will be one of smearing out the effects of evolution with lithospheric age and thus will make us rather underestimate than overestimate them. The same can be said about the fact that the paths to some extent intersect the lithospheric isochrons and that the precise age is not everywhere known.

More serious is the uncertain influence of Iceland itself on the group velocities since the waves traverse significant distances through it. In paper I we could, however, show that the influence is not too critical to our study. (1) It is not very large in the period range considered. (2) It does not strongly depend on the various Iceland models we had tested. (3) It does not strongly depend on the different oceanic paths which closely converge on AKU in Iceland. (4) The influence does, however, subdue rather than enhance the differences between the dispersion curves for the different age groups; this last point is perhaps the most important one, because if we use the observed Rayleigh wave group velocities of paper I without the 'Iceland correction' we are not in danger of overestimating the variations related to lithospheric evolution.

Table 2. Top parts of models for Rayleigh wave group velocity computations: water depths and crustal structures

Age slice (Ma)	Depth (km)	*P* velocity (km/s)	*S* velocity (km/s)	Density (g/cm³)
0–3	0.0	1.52	0.0	1.03
		1.52	0.0	1.03
	0.9			
		2.8	1.6	2.7
		3.9	2.3	2.8
	2.3			
		4.9	3.2	2.9
	5.0	5.9	4.0	3.0
6–8	0.0	1.52	0.0	1.03
		1.52	0.0	1.03
	1.5			
		1.65	1.0	2.0
		1.65	1.0	2.0
	1.6			
		3.7	2.15	2.7
		5.3	3.1	2.8
	3.3			
		6.1	3.5	2.9
	5.5	7.3	4.1	3.0
10–20	0.0	1.52	0.0	1.03
		1.52	0.0	1.03
	2.3			
		1.65	1.0	2.0
		1.65	1.0	2.0
	2.5			
		4.7	2.7	2.6
		4.7	2.7	2.6
	4.5			
		6.3	3.6	2.9
	6.5	6.3	3.6	2.9

Velocities and densities vary linearly from top to bottom of layers

Shear Velocity Structure of Reykjanes Ridge

We use simple methods for the interpretation of the data. The uncertainties discussed in the two previous paragraphs really have to do with our incapability of modelling surface wave propagation through a complex three-dimensional structure. For the computation of theoretical dispersion curves we had to assume horizontally layered models for the three different age slices. We know that this is a very crude approximation to reality. We must, however, also economize; the kind of data we have does not warrant the application of more sophisticated cumbersome methods which would resolve more details only in connection with much more precise data.

We repeat that we are not worried about the fact that the use of horizontally layered models will 'smear out' the real lateral variation of structure with lithospheric age; so will the neglect of the influence of Iceland. We must, however, worry about unpredictable effects of the simple modelling and keep this in mind until better modelling becomes available. We warn the reader to remain aware of this.

We believe that the interesting variations of vertical structure which we do see are not grossly wrong and that they give us hints to the thermodynamic and petrologic processes involved in lithosphere generation.

In modelling we have constrained water depth and crustal structure. Table 2 states our assumptions for the three age groups; they are mainly based on *P* velocities found by Talwani et al. (1971) for the NW flank of Reykjanes Ridge, supplemented by recent results of the RRISP Working Group (1979) on the SE flank. As average structures they are not without uncertainty; To investigate what an effect an error in crustal structure and water depth may have on the theoretical dispersion curves, we did some of the model computations twice: 1. with the 'correct' water and crust of Table 2 (e.g. with the 0–3 Ma water/crust for a 0–3 Ma mantle model) and 2. with the 'wrong' one (i.e., with the 6–8 Ma water/crust for a 0–3 Ma mantle model and vice versa); the effect in the period range considered is largely one of shifting the dispersion curves.

In modelling the 0–3 and 6–8 Ma structures we also held the *S* velocity below 70 km fixed at 4.1 km/s, indicated by a heavy

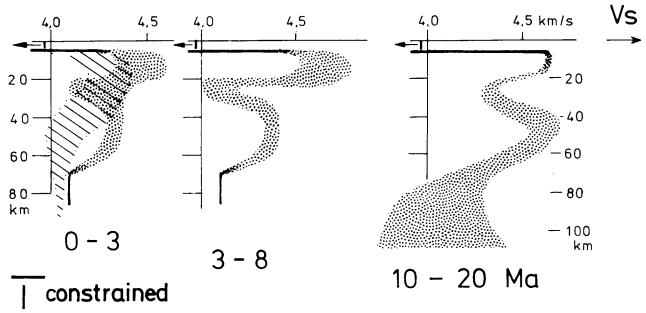

Fig. 4. Range of models found for the three age slices. *Each of the shaded areas* encompasses several models for which dispersion curves have been computed to fall within the error bounds of Fig. 3; wavelengths of vertical S velocity variation in the models has generally been held above 20 km. Regions of velocity-depth functions held fixed during modelling shown by *heavy lines*. Hatched model area in the 0–3 Ma slice is taken from Keen et al. (this volume) for comparison

line in Fig. 4 giving the modelling results. In the 10–20 Ma models the S velocities below 70 km depth were allowed to vary (Fig. 4); this will be discussed below.

The P velocities in the upper mantle were assumed to be linked to the S velocities with Poisson's ratios between 0.25 and 0.3; the densities were computed with Birch's (1960, 1961) velocity-density relationship. The effect of these assumptions on the results is only slight.

The method and the program used for computing the theoretical dispersion curves are due to Derr (1967). The program gives the eigenfunctions of spherical earth models for specified modes and thence the phase and group velocities of Rayleigh and/or Love waves.

In searching for models which give dispersion curves within the error bounds of Fig. 3, we were guided by the models presented in paper I; they had been found by a systematic search of three parameters for only two average dispersion curves (0–8 and 10–20 Ma) with wide error bounds. For the present study we used the traditional manual search by trial and error. We were, however, not content with a single acceptable model for each age group but rather repeated the search many times from different starting points. In modelling we attempted to avoid unresolvable detail by allowing the S velocity to vary only with 'vertical wavelengths' greater than 10 or 20 km, keeping in mind the trade-off between the uncertainty of average velocity determination and the (vertical) averaging distance (Backus and Gilbert 1968), but we did not strictly apply inversion theory.

The results of our search for the three age groups are presented in Fig. 4. Instead of showing the individual S velocity-depth models we found to be compatible with the observations, we only show the bands comprising all models. This does not mean that a velocity-depth function which takes an arbitrary course through such a band will necessarily give an acceptable dispersion curve; a function meandering through the band has, however, a good chance. We cannot claim that we have fully explored the extremes of the model space, but we have attempted to carefully investigate those features which appeared important to us. These are mainly the upper low-velocity layer in the 20 to 30 km depth range, particularly for the 6–8 and 10–20 Ma age slices, and the depth to the deeper and broader low-velocity layer which is commonly associated with the asthenosphere (tested mainly for 10–20 Ma).

We attempted to find models (6–8, 10–20 Ma) without an upper low-velocity channel but we were not successful, particularly if we constrained the uppermost mantle S velocities to be >4.4 km/s, according to the S_n velocities found by Hart and Press (1973). Without a high top velocity and a channel the computed dispersion curves are convex upward at the low period end; introduction of this feature brings about the correct shape. From this point of view the upper low-velocity layer must be significant in the 6–8 Ma slice to produce the dip in the dispersion curve at 20 s period. Although we found this feature without fixing the topmost mantle velocity, we probably need this constraint because other parameters as water depth and crustal structure are not known precisely enough. This uncertainty does, in fact, cause the large models scatter at shallow depth for 0–3 and 6–8 Ma (Fig. 4).

We also searched systematically for the depth to the top of the deeper, i.e., 'asthenospheric' low-velocity layer whose bottom we cannot 'see'. Attempts to place the top as shallow as 50 km or as deep as 90 km failed; the significant velocity decrease occurs at a depth of 60 or 70 km in agreement with Press (1970), Haigh (1973), and Forsyth (1977), among others. The wide scatter of the models for 10–20 Ma in this depth range reflecting the lack of resolution from 15–40 s data leaves us sufficient confidence in the 60 to 70 km top of the 'asthenosphere'. The small scatter in the 0–3 and 6–8 Ma models at depth is, of course, the result of fixing the channel velocity and of avoiding drastic short-wavelength variations directly above.

The development of the models (Fig. 4) in steps from 0–3 to 6–8 and 10–20 Ma involves a rise of the upper-lid velocity by about 0.2 km/s and the upper channel becoming pronounced at 6–8 Ma and perhaps weakening thereafter. The S velocity of the lower high-velocity layer clearly increases in the third stage. The bottom of this lower layer becomes more pronounced but its depth does not significantly change. A square-root age growth of lithospheric thickness (Parker and Oldenburg 1973) is not evident but, because the age span of our data is too short, we cannot really test this. For the 0–20 Ma span a more complicated nature of the lithospheric growth is, however, suggested. The definition of the lithosphere as one high-velocity lid may break down if both channels are 'weak' mechanically. Alternatively, if the upper lid forms the 'strong' lithosphere of about 20-km thickness for the first few million years, there may be an abrupt thickness increase at about 10 Ma of age.

A Model for Lithosphere Generated at Reykjanes Ridge

In the following discussion we attempt to give a plausible explanation for the S velocity structure presented above. The model is largely based on work by Forsyth (1977), Green and Lieberman (1976), Bottinga (1974), Bottinga and Allègre (1976) and others. We assume a predominantly peridotitic upper mantle or one that is chemically a mixture of peridotite and tholeiite basalt (Ringwood 1966) with small traces of water and adopt Green and Liebermann's (1976, Fig. 1) phase diagram for $\leqq 0.4\%$ H_2O content and $CO_2 \ll H_2O$ (Fig. 5). In Fig. 5 we also show Forsyth's (1977) geotherms (long-dashed lines) computed for a cooling half-space with heat sources in the upper 300 km. The lithosphere in this model represents a thermal boundary layer. In the age range of interest, however, there is little difference between this and the cooling slab model (e.g. McKenzie 1967, Sclater and Francheteau 1970) if equivalent boundary conditions are chosen. The solidi are then mapped into the cooling lithosphere shown in Fig. 6 as stippled bands; also shown are average S velocities in four depth intervals and three age zones taken from Fig. 4.

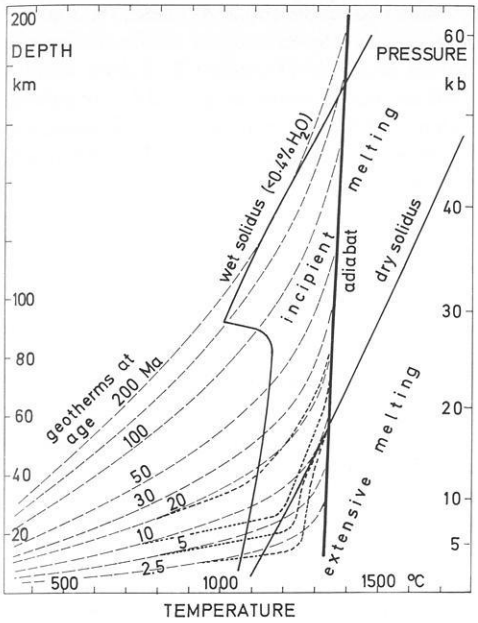

Fig. 5. Phase diagram of peridotite with 0.4% of water after Green and Liebermann (1976); geotherms after Forsyth (1977): *long-dashed lines;* qualitatively drawn distortions of geotherms, caused by two-phase convection: *short-dashed lines*

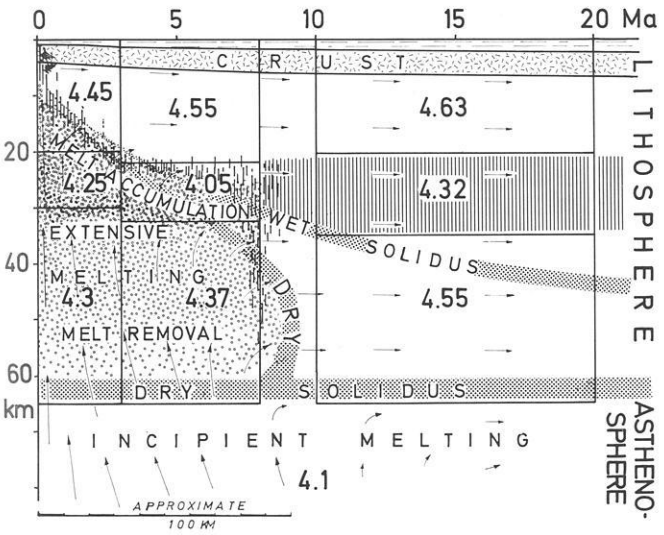

Fig. 6. Cartoon of the structure of Reykjanes Ridge based on theoretical geotherms (Forsyth 1977) and peridotite phase diagram with traces of water (Green and Liebermann 1976). *Heavy numbers* are average model *S* velocities in km/s for depth ranges shown (taken from Fig. 4). Solidi of conduction solution (Forsyth 1977): *dotted bands;* distortions of solidi by two-phase convection: bands of irregular *vertical lines. Arrows* depict flow lines qualitatively, their lengths approximately depict the flow velocities). See text for further discussion

If we now compare on Fig. 6 our *S* velocities with the solidi (stippled) taken from Forsyth, we find a fairly good agreement except in the region of the top low-velocity layer between 20 and 30 km depth at ages beyond 5 Ma or so. This suggests to us that the model for the young lithosphere should be somewhat modified. While Forsyth argued only for melt removal from, and depletion of, the lower lithosphere (to explain its apparently rapid thickening till 10 Ma, or so, and its constant thickness thereafter), we propose that we also 'see' melt accumulation near the top, forming the 20 to 30 km low-velocity zone after a few million years of cooling of the uppermost lithosphere forming a kind of 'magma-tight' lid. Melt depletion at depth and accumulation higher up might be looked upon as two-phase convection described by Frank (1968). As a consequence the geotherms would be distorted (as intuitively sketched by the short-dashed lines in Fig. 5) and so would the solidi. The resulting chemical differentiation would, however, make the application of the solidi problematical for parts of the structure. The low-velocity layer beyond 10 Ma would probably decay or could be frozen into the lithosphere as its chemical layering.

The essential features of the above picture were, in fact, predicted by quantitative petrological model calculations of Bottinga (1974), Bottinga and Allègre (1976) and Steinmetz et al. (1976). For a ridge with a half-spreading rate of 1 cm/a their models display a similar region where melt is concentrated between 20 and 30 or 40 km depth and between 10 and 50 km from the axis. The small amount of melt will cause a distinct low-velocity layer; the *S* velocity structure predicted is thus quite similar to the one we found. The distortion of the geotherms with respect to the conduction solution is also similar to the one we only guessed (Fig. 5). The upper low *P* velocity layer of Steinmetz et al. (1976) is at a slightly shallower depth than our *S* velocity channel. The physical reason for the 'asthenospheric upwelling model' of Bottinga and colleagues doing the trick explaining the *upper* low-velocity layer seems to be that it includes the two-phase convection of melt advancing from a residue.

Complimentary evidence for the top low-velocity layer has recently been presented by Yu and Mitchell (1979) who used regionalized group and phase velocities of Rayleigh and Love waves to deduce mantle shear velocities for Pacific Plate age slices of 0–20, 20–50, 50–100, and > 100 Ma. They found a 'lithospheric' low-velocity layer in the same depth range, but at older ages (20–50 Ma) than we found; they state that its existence still must be scrutinized.

Most explosion seismic studies at ocean ridges (e.g. Orcutt et al. 1976; Steinmetz et al. 1976; and many others) did not reach sufficient depth. Steinmetz et al. (1976), for a profile along the 9 Ma isochron west of the Azores, report a high velocity layer at 30 km depth which might correspond to the bottom of our proposed channel. A long-range refraction experiment along the SE flank of Reykjanes Ridge and across Iceland (RRISP Working Group, 1979; this volume; Gebrande et al., this volume) gave indirect evidence of a 'lithospheric' low-velocity channel; very low-amplitude first arrivals on Iceland from marine shots at > 200 and 400 km distance may be interpreted as indicating the shadow zone corresponding to it.

Support for an initially very thin lithosphere comes from a study of topography and gravity near the Mid-Atlantic Ridge axis (McKenzie and Bowin 1976) suggesting that the elastically bending part of the lithosphere to some distance from the ridge axis is only about 10 km thick. The value is expected to be lower than the seismic thickness. The mushroom shaped low-density body under Reykjanes Ridge of Talwani et al. (1965) also resembles our velocity model.

Further seismological support, though only in a gross sense, may be taken from the *Q* structure of the southern Reykjanes Ridge proposed by Solomon (1973) and from its *S* velocity structure assumed by Solomon and Julian (1971) to explain anomalous

fault-plane solutions. In an even cruder sense, support for low mantle velocities and partial melting below the ridge comes from the travel time residuals in the Reykjanes Ridge Iceland area for *P* waves (Francis 1969) and *S* waves (Girardin and Poupinet 1974; Duschenes and Solomon 1977).

Conclusions

Surface wave dispersion data have been interpreted to indicate a peculiar *S* velocity structure of Reykjanes Ridge with a 'lithospheric' low-velocity zone which comes into being at some distance from the axis and may then decay again. The surface wave evidence may not be totally convincing by itself, but additional seismological constraints make the interpretation plausible. The structure has then been explained by a thermodynamic-petrological model in line with Bottinga's (1974) and its extensions.

The model would, in principle, be expected to apply to all spreading ridges; but it is, of course, quite possible that the structure of Reykjanes Ridge is unique, related to the closeness of the hot spot of Iceland (Vogt and Johnson 1975). We shall, nevertheless, conclude this paper by sketching a cartoon of how we envisage the formation of the lithosphere (at Reykjanes Ridge).

Mantle material is assumed to rise adiabatically from great depth beneath the ridge axis. The mantle solidus is probably depressed to a certain extent (to the wet solidus) by water activity; the amount of partial melting will depend on the quantity of water present (Bottinga and Allègre 1978; Wyllie 1971). Thus, the material passes through a region between the wet and dry solidi in which incipient melting will occur; the melt fraction is probably too small to lead to extensive gravitational upward filtering. Above the dry solidus at ~ 60 km, melting becomes extensive, the fraction increases, and the melt will begin to buoyantly rise more rapidly through the crystal mush than the bulk moves. At depth, melt removal and crystal accumulation will prevail; this part will 'dry out' Higher up, melt will accumulate; this part will be enriched in volatiles, magma chambers will form and will tend to spill out, predominantly at thr ridge axis to form the chemically distinct crust.

The shape of the barriers to this process of two-phase convention is determined by the geotherms intersecting the wet and dry solidi. In the zone of depletion the dry solidus will mark the boundary between the 'fluid' rising asthenosphere and the 'solid' lithosphere; the wet solidus will be irrelevant here. The temperature will be lower than in the conduction case. At shallower levels where melt accumulates it will probably be the wet solidus that is important. The temperature will be higher than in the conduction case. A thin lid will nevertheless form by cooling and this will help trapping and concentrating the melt, the lid may not be perfectly magma-tight as suggested by volcanoes off the ridge axis. The effect of these processes will be to widen the rising column of asthenosphere at shallow depth and perhaps to narrow it at depth, as illustrated by Fig. 6. A mushroom shape will develop as is familiar from diapiric structures. The physical reasons, however, are quite different in both cases. In diapirs it is the bulk that spreads laterally at high levels; in our model of rising asthenosphere it is the light melt which moves faster and more steeply than the bulk before it accumulates. The resulting density structure is quite similar. But as the lithosphere spreads as a whole (in contrast to diapiric processes) it will be chemically layered. Future experiments may test this feature.

Further thorough research is needed to verify, or to decide against, our model of lithosphere generation.

Acknowledgements. Critical comments by Y Bottinga, R. Gaulon, K. v. Gehlen, S. Gregersen, S. Müller, and D. Forsyth who read an earlier version of this paper were helpful. T. Kurita supplied his version of the surface wave computer program. Computing facilities at the University of Frankfurt were used. Financial support by Deutsche Forschungsgemeinschaft grant Ja 258/6 is acknowledged. We are grateful to all of them.

References

Backus, G.E., Gilbert, F.. The resolving power of gross earth data. Geophys. J. R. Astron. Soc. **16**, 169–205, 1968

Birch, F.: The velocity of compressional waves in rocks to 10 kbars, 1. J. Geophys. Res. **65**, 1083–1102, 1960

Birch, F.· The velocity of compressional waves in rocks to 10 kbars, 2. J. Geophys. Res. **66**, 2199–2224, 1961

Bottinga, Y Thermal aspects of sea-floor spreading, and the nature of the sub-oceanic lithosphere. Tectonophysics **21**, 15–38, 1974

Bottinga, Y., Allègre, C.· Geophysical, petrological, and geochemical models of the oceanic lithosphere. Tectonophysics **32**, 9–59, 1976

Bottinga, Y., Allègre, C.J.. Partial melting under spreading ridges. Philos. Trans. R. Soc. London. Ser. A: **288**, 501–525, 1978

Derr, J.S.. A comparison of free oscillations of oceanic and continental earth models. Bull. Seismol. Soc. Am. **57**, 1047–1061, 1967

Duschenes, J.D., Solomon, S.C.. Shear wave travel time residuals from oceanic earthquakes and the evolution of oceanic lithosphere. J. Geophys. Res. **82**, 1985–2000, 1977

Dziewonski, A., Bloch, S., Landisman, H.: A technique for the analysis of transient seismic signals. Bull. Seismol. Soc. Am. **59**, 421–444, 1969

Forsyth, D.W.. The evolution of the upper mantle beneath mid-ocean ridges. Tectonophysics **38**, 89–118, 1977

Francis, T.J.G.. Upper mantle structure along the axis of the mid-Atlantic ridge near Iceland. Geophys. J. R. Astron. Soc. **17**, 507–520, 1969

Frank, F.C. Two-component flow model for convection in the earth's mantle. Nature **220**, 350–352, 1968

Gebrande, H., Miller, H., Einarsson, P. Seismic structure of Iceland along RRISP profile I. J. Geophys. **47**, 239–249, 1980

Girardin, N., Jacoby, W.R. Rayleigh wave dispersion along Reykjanes Ridge. Tectonophysics **55**, 155–177, 1979

Girardin, N., Poupinet, G. Teleseismic S travel-time delay for mid-Atlantic ridge earthquakes. Phys. Earth Planet. Inter. **9**, 306–313, 1974

Green, D.H., Liebermann, R.C. Phase equilibria and elastic properties of a pyrolite model for the oceanic upper mantle. Tectonophysics **32**, 61–92, 1976

Haigh, B.I.R. North Atlantic oceanic topography and lateral variations in the upper mantle. Geophys. J. R. Astron. Soc. **33**, 405–420, 1973

Hart, R.S., Press, F. Sn velocities and the composition of the lithosphere in the regionalized Atlantic. J. Geophys. Res. **78**, 407–411, 1973

Heirtzler, J.R., Dickson, G.O., Herron, E.M., Pitman, W.C., LePichon, X.· Magnetic anomalies, geomagnetic field reversals, and motions of the ocean floor and continents. J. Geophys. Res. **73**, 2119–2136, 1968

Heirtzler, J.R., LePichon, X., Baron, J.G.· Magnetic anomalies over the Reykjanes Ridge. Deep-Sea Res. **13**, 427–443, 1966

Keen, C.E., Fricker, A., Keen, M.J., Blinn, L.: Reykjanes Ridge crest studied by surface waves with the an earthquake-pair technique. J. Geophys. **47**, 265–270, 1980

McKenzie, D.P.: Some remarks on heat flow and gravity anomalies. J. Geophys. Res. **72**, 6261–6273, 1967

McKenzie, D.P., Bowin, C.: The relationship between bathymetry and gravity in the Atlantic ocean. J. Geophys. Res. **81**, 1903–1915, 1976

Orcutt, J.A., Kennett, B.L.N., Dorman, L.M.: Structure of the east Pacific rise from an ocean bottom seismometer survey. Geophys. J. R. Astron. Soc. **45**, 305–320, 1976

Parker, R.L., Oldenburg, D.W.: Thermal model of ocean ridges. Nature Phys. Sci. **242**, 137–139, 1973

Press, F.: Earth models consistent with geophysical data. Phys. Earth Planet Sci. Inter. **3**, 3–22, 1970

Ringwood, A.E.: Mineralogy of the mantle. In: Advances in earth science, P.M., Hurley, ed.: pp. 357–399. Cambridge, Mass. M.I.T. Press, 1966

RRISP Working Group: First results from Reykjanes Ridge Iceland Seismic Project 1977. Nature **279**, 56–60, 1979

Sclater, J.G., Francheteau, J.: The implications of terrestrial heat flow observations on current tectonic and geochemical models of the crust and upper mantle of the earth. Geophys. J. R. Astron. Soc. **20**, 493–509, 1970

Solomon, S.C.: Shear wave attenuation and melting beneath the mid-Atlantic ridge. J. Geophys. Res. **78**, 6044–6059, 1973

Solomon, S.C., Julian, B.R.: Seismic constraints on ocean-ridge mantle structure: anomalous fault plane solutions from first motions. Geophys. J. R. Astron. Soc. **38**, 265–285, 1971

Steinmetz, L., Whitmarsh, R.B., Moreira, V.S.: Upper mantle structure beneath the mid-Atlantic ridge north of the Azores based on observations of compressional waves. Geophys. J. R. Astron. Soc. **50**, 353–380, 1976

Talwani, M., LePichon, X., Ewing, M.: Crustal structure of the mid-ocean ridges, 2, computed model from gravity and seismic refraction data. J. Geophys. Res. **70**, 341–352, 1965

Talwani, M., Windisch, C.C., Langseth, M.G.: Reykjanes Ridge crest: a detailed geophysical study. J. Geophys. Res. **76**, 473–517, 1971

Vogt, P.R., Johnson, G.L.: Transform faults and longitudinal flow below the midoceanic ridge. J. Geophys. Res. **80**, 1399–1428, 1975

Weidner, D.J., Aki, K.: Focal depth and mechanism of mid-ocean ridge earthquakes. J. Geophys. Res. **78**, 1818–1831, 1973

Wyllie, P.J.: Role of water in magma generation and initiation of diapiric uprise in the mantle. J. Geophys. Res. **76**, 1328–1338, 1971

Yu, G.K., Mitchell, B.J.: Regionalized shear velocity models of the Pacific upper mantle from observed Love and Rayleigh wave dispersion. Geophys. J. R. Astron. Soc. **57**, 311–341, 1979

Received June 15, 1979; Revised Version September 10, 1979